

Palaeozoic Palaeomagnetism of South-Eastern Australia: Implications for the APW path of Gondwana

*Inaugural-Dissertation
zur Erlangung des Doktorgrades
der Fakultät für Geowissenschaften der
Ludwig – Maximilians – Universität München*

vorgelegt von
Christian Vérard
Januar 2004

Dissertation eingereicht: 30. Januar 2004

Erster Berichterstatter: Dr. Jennifer TAIT

Zweiter Berichterstatter: Prof. Dr. Valerian BACHTADSE

Tag der mündlichen Prüfung: 02. Juni 2004.

Abstract

The drift history of Gondwana following the break-up of Rodinia (or perhaps Pannotia) to the amalgamation into Pangaea has great implications in many disciplines in Earth sciences, but remains largely unknown. Among the apparent polar wander (APW) paths published for Gondwana in the last few decades, large discrepancies exist (sometimes up to thousands of kilometres). The mid Palaeozoic segment of the APW path is particularly problematic, and two primary schools of thought arise. Some authors favour a Silurian – Devonian loop in their APW path passing through southern South America (on a reconstruction of Gondwana), whereas others draw a path directly through Africa during this period. The main controversy stems essentially from whether or not palaeomagnetic data from eastern Australia are incorporated in order to compensate for the lack of mid Palaeozoic data. Determining whether the terranes of the Southern Tasmanides are (para-)autochthonous or allochthonous in origin is therefore of crucial importance and a matter of intense debate. The aim of the work presented herein is to palaeomagnetically define the positions of these terranes throughout the Palaeozoic in order to better constrain the complex tectonic history of this region and to help clarifying the APW path of Gondwana.

The construction of an APW path is discussed herein. An attempt is made to determine whether only “objective” criteria can be employed to select data used to draw an APW path. However, it is shown that the palaeomagnetic database has not enough entries. Subjective data selection must be introduced leading to two end-members: the X-type and the Y-type, thought to be best illustrated by the X-path proposed by Bachtadse & Briden (1991) and the Y-path proposed by Schmidt *et al.* (1990). These two models are, therefore, used in the discussion of the results obtained for this study.

The Southern Tasmanides had a complex tectonic history with several orogenic events throughout the Palaeozoic. The sampling coverage carried out for this study comprises fifty localities (289 sites, 1576 cores, 3969 specimens; see table 1, pages 54-55) distributed along an east-west transect across most of the subdivisions of the Southern Tasmanides. The sampled localities are gathered in three main areas: the Broken Hill area, the Mount Bowen area, and the Molong area, which are situated where no published palaeomagnetic studies were previously available providing, therefore, new information. Sampling and laboratory procedures have been carried out using standard techniques. In particular, detailed stepwise thermal demagnetisation, principal component analysis, anisotropy of magnetic susceptibility and rock magnetic measurements have been systematically employed.

The routine measurement of the anisotropy of magnetic susceptibility allowed drawing the first maps of the magnetic fabrics throughout the region. A strong correlation between the magnetic fabrics and the main tectonic structures corroborates the existence of cross-structures (E-W) in the Southern Tasmanides.

The directions of magnetisation obtained yielded much information, despite poor quality. The effects of weathering are deep, intense and widespread. For example, most of the samples from the Mount Arrowsmith Formation (localities ARR & ARO) and the Funeral Creek Limestone (FUN) in the Broken Hill area (western New South Wales) are totally remagnetised, as

well as some from the Mitchell Formation (MIT) in the Molong area (eastern New South Wales). Secondary magnetisations are also largely responsible for the bad results obtained in most of the fifty localities studied. Intermediate directions of magnetisation are common and often result in significant data scattering, as illustrated for instance by results from the Kandie Tank Limestone (KAN; Broken Hill area) or the Ambone and Ural Volcanics (HOP, BOW, SHE; Mount Bowen area). In general, it has not been possible to precise the remagnetisation process leading to those scattering.

Nevertheless, a major remagnetisation event, probably thermo-chemical in origin, has been also recognised. This event is thought to be Oligocene in age and triggered by changes in geothermal gradient prior to the onset of hot spot volcanism in the Molong area. The existence of Jurassic overprints are also suggested, in particular in the Broken Hill area, possibly in association of intrusion of mafic dykes.

All other magnetic components described herein are considered Palaeozoic in age, but further constraints on age are very difficult to establish since field tests are most often not significant. Palaeopoles obtained from three localities, however, are believed to correspond to primary magnetisations. The pole from the Late Cambrian Cupala Creek Formation (CUP), confirmed by a positive unconformity test, implies that this zone can be regarded fixed relative to the craton since the Late Cambrian. In the Early Devonian Mount Daubeny Formation (DAU), the applied fold test, contact test and conglomerate test indicate the primary origin of the magnetisation carried by haematite. The corresponding pole (DAU) is, however, significantly distinct from the VGP deduced from the Early Devonian Ural Volcanics (MER) showing that at least one of the two localities has been rotated. The MER pole agrees with the remagnetisation pole associated with the Cupala Creek Formation, and favours the X-type of APW path proposed by Bachtadse & Briden (1991) for Gondwana. The outcome of this agreement contradicts the Y-type path and the existence of a Silurian – Devonian loop mainly anchored on the Early Devonian Snowy River Volcanics pole obtained by Schmidt *et al.* (1987). Invocation of terrane rotation, arising possibly from a pull-apart basin, may explain the discrepancy between the pole from Mount Daubeny Formation and the X-path.

The most significant finding of this study is the widespread terrane rotation. This conclusion is based upon the inability of intermediate directions of magnetisation, alternate APW path for Gondwana, true polar wander or non-dipole field contribution to correctly explain the distribution of these new data. Consequently, one has to admit that block translation and rotation occurred in the Southern Tasmanides in the first half of the Palaeozoic Era and perhaps up to the Early Carboniferous.

A possible scenario concerning the tectonic arrangement of blocks in the Southern Tasmanides is presented in conclusion. This palinspastic model involves block translation in the Siluro-Devonian, and rotation in the Early and more probably Middle Devonian, with late tectonic displacements and rotations in the South-Western Belt of the Lachlan Orogen in the Late Devonian to Early Carboniferous.

Key words: Palaeomagnetism, apparent polar wander paths, Gondwana, Southern Tasmanides, Lachlan and Delamerian Orogens, New South Wales, Australia, Palaeozoic reconstruction.

Zusammenfassung

Die Geschichte der Kontinentaldrift Gondwanas seit dem Aufbrechen Rodinias (oder vielleicht Pannotias) bis zur Angliederung an Pangea hat zwar bedeutende Auswirkungen auf viele Teildisziplinen der Geowissenschaften, ist aber weitestgehend unbekannt. Bei den scheinbaren Polwanderungskurven (SPWK), die in den letzten Jahren publiziert worden sind, gibt es große Abweichungen (mehr als tausend Kilometer). Besonders problematisch ist das Segment der SPWK während des mittleren Paläozoikums. Zwei deutliche Interpretationen dieses Segments werden in der wissenschaftlichen Literatur kontrovers diskutiert. Einige Autoren favorisieren eine SPWK, die während des Silurs und Devons in einem Bogen um das südliche Südamerika verläuft (in einer Rekonstruktion Gondwanas in afrikanischen Koordinaten), wohingegen andere Autoren die Kurve für diesen Zeitraum direkt durch Afrika zeichnen. Der Hauptunterschied zwischen diesen beiden Modellen beruht auf der zugrundeliegenden Auswahl der paläomagnetischen Daten, insbesondere ob Ergebnisse aus Ost-Australien in die Analyse mit einbezogen werden oder nicht. Dies ist von besonderer Bedeutung, da gerade für das mittlere Paläozoikum äußerst wenige Daten zur Verfügung stehen. Ausschlaggebend ist darüberhinaus die Frage, ob die Terranes der südlichen Tasmaniden (para-)autochthon oder allochthon sind. Das Ziel dieser Arbeit ist die paläomagnetische Bestimmung der Positionen dieser Terranes während des Paläozoikums, um die tektonische Entwicklung dieser komplexen Region besser zu verstehen, und somit Klarheit in den Verlauf der SPWK zu bringen.

Das Verfahren zur Erstellung einer SPWK wird in Kapitel 2 dieser Arbeit diskutiert. Dazu wird untersucht, ob „objektive“ Kriterien bei der Datenauswahl für den SPWK-Verlauf ausreichend sind. Allerdings zeigt sich, daß für eine derartige Analyse zu wenig Eintragungen in der paläomagnetischen Datenbank vorliegen. Daher muß eine „subjektive“ Selektion durchgeführt werden. Dies führt zu zwei unterschiedlichen Gruppen von Ergebnissen: dem X- und Y-Typ der SPWK Gondwanas. Am besten wird der X-Typ durch die Kurve von Bachtadse und Briden (1991), der Y-Typ durch die Kurve von Schmidt *et al.* (1990) dargestellt. Diese beiden Möglichkeiten werden für die Diskussion der Ergebnisse dieser Studie verwendet.

Die südlichen Tasmaniden haben eine komplexe tektonische Geschichte mit mehreren orogenen Phasen während des Paläozoikums. Die Proben für diesen Teil der Arbeit stammen von fünfzig Lokalitäten (289 Probenlokationen, 1576 Kerne, 3969 Einzelproben; siehe Tabelle 1, S. 54-55), entlang eines Ost-West-Profiles durch die südlichen Tasmaniden. Zu den beprobten Einheiten lagen bisher keine veröffentlichten paläomagnetischen Untersuchungen vor. Drei Beprobungsgebiete können unterschieden werden: das Broken Hill Region, das Mount Bowen Region und das Molong Region. Bei Beprobung und Laboruntersuchung wurden paläomagnetische Standardtechniken angewendet. Insbesondere wurden folgende Untersuchungen systematisch durchgeführt: detaillierte thermische Entmagnetisierung und Analyse der Richtungskomponenten sowie Messung der Anisotropie der magnetischen Suszeptibilität und der gesteinsmagnetischen Eigenschaften.

Anhand der Anisotropie der magnetischen Suszeptibilität konnte eine Karte des magnetischen Gefüges der Region erstellt werden. Neben der starken Korrelation des magnetischen Gefüges mit den charakteristischen tektonischen Strukturen (N-S) der Region zeigen die Daten auch die Existenz von ost-west gerichteten Störungen.

Die oftmals sehr komplexen Magnetisierungsrichtungen liefern wertvolle Informationen. Die beprobten Gesteine sind generell stark und tiefgreifend verwittert. So sind beispielsweise die Proben von der Mount Arrowsmith Formation (Lokalitäten ARR & ARO) und die Kalksteine des Funeral Creeks (FUN) in der Region von Broken Hill (westliches New South Wales) vollständig remagnetisiert. Dies gilt auch für einige Proben von der Mitchell Formation in der Region von Molong (östliches New South Wales). Starke sekundäre Überprägungen der Magnetisierung werden auch bei den Proben der übrigen Lokalitäten beobachtet. Nicht immer war es möglich die verschiedenen Remanenzkomponenten eindeutig zu isolieren. Dies führt zu einer starken Streuung der Richtungen, wie es unter anderem bei den Lokalitäten der Kandie Tank Kalksteine (KAN, Broken Hill) oder der Ambone und Ural Vulkaniten (HOP, BOW, SHE, Mount Bowen) der Fall ist. All diese Remagnetsierungen können nicht einem einzelnen Remagnetisierungsprozess zugeordnet werden.

In einigen Fällen allerdings zeigen die Überprägungen konsistente Richtungen. Diese Remagnetisierung ist wahrscheinlich thermo-chemischen Ursprungs und wurde im Oligozän erworben. Man nimmt an, daß sie durch Veränderung des geothermischen Gradienten vor dem Einsetzen des Hotspot Vulkanismus in der Region von Molong ausgelöst wurde. Die Existenz jurassischer Überprägungen, besonders in der Region von Broken Hill, kann auf die Intrusion mafischer Gänge zurückgeführt werden.

Alle anderen in dieser Arbeit beschriebenen Magnetisierungskomponenten werden als Remanenzen paläozoischen Alters interpretiert. Eine genauere zeitliche Einordnung des Remanenzenerwerbs dieser Komponenten gestaltet sich schwierig da die paläomagnetischen Tests oft insignifikante Ergebnisse liefern. Die Resultate von drei Lokalitäten werden allerdings als primäre paläozoische Magnetisierungen betrachtet. Der Paläopol der spätkambrischen Cupala Creek Formation (CUP) ist durch einen positiven Diskordanz Test verifiziert. Dieser Paläopol belegt, daß sich diese Region relativ zu dem Kraton seit dem späten Kambrium nicht bewegt hat. Die charakteristische Magnetisierung der frühdevonischen Mount Daubeny Formation (DAU) wird von Hämatit getragen. Sowohl der Faltestest als auch der Kontakt- und Konglomeratstest zeigen das diese Magnetisierungs-komponente primär ist. Der sich ergebende Paläopol weicht allerdings signifikant von dem virtuelle geomagnetische Pol (VGP) der frühdevonischen Ural Vulkanite (MER) ab. Es muß daher eine relative Rotation der beiden Einheiten gegeneinander angenommen werden. Der MER Pol ist konsistent mit dem remagnetisierten Pol der Cupala Creek Formation und unterstützt die Hypothese von Bachtadse und Briden (1991) einer SPWK des X-Typs für Gondwana. Der silurische-devonische Bogen in der SPWK nach dem Y-Typ, der hauptsächlich auf den Daten der devonische Vulkanite des Snowy Rivers (Schmidt et al., 1987) basiert, kann daher ausgeschlossen werden. Die Abweichung des Pols der Mount Daubeny Formation vom Pfad des X-Typs kann mit einer Terranrotation, möglicherweise in Folge der Bildung eines „Pull-Apart-Basins“, erklärt werden.

Das Hauptergebniss dieser Arbeit ist der Nachweis verbreiteter Rotationen der einzelnen Terrane der südlichen Tasmaniden. Die meisten der beobachteten Paläopole können weder durch die Verwendung der zwei konkurrierenden SPWK-Modelle noch durch andere Effekte wie „True-Polar-Wander“ oder Nicht-Dipol Anteile des Erdmagnetfeldes erklärt werden. Nur unter Annahme von Blocktranslationen und -rotationen in der ersten Hälfte des Paläozoikums, oder auch bis in das frühe Karbon, lassen sich die Beobachtungen in Einklang bringen.

Ein Szenario für die Verteilung der einzelnen Terrane in den südlichen Tasmaniden wird in Kapitel 8 entwickelt. Dieses paläogeographische Modell beinhaltet Blocktranslationen im Silur/Devon. Rotation treten in diesem Modell im frühen bis mittleren Devon auf. Spätere tektonische Verschiebungen und Rotationen im südwestlichen Gürtel des Lachlan Orogens sind demnach vom späten Devon bis zum frühen Karbon zu beobachten.

Kennwörter: Paläomagnetismus, scheinbaren Polarwanderungskurven, Gondwana, Südliche Tasmaniden, Lachlan und Delamerian Orogen, New South Wales, Australien, Paläozoische Paläogeographie.

Résumé

L'histoire de la dérive du Gondwana, depuis sa séparation de Rodinia (ou peut-être de Pannotia) jusqu'à son incorporation dans la Pangée, a d'importantes implications dans plusieurs disciplines des Sciences de la Terre, mais reste largement inconnue. Parmi les courbes de dérive apparente du pôle (CDAP) publiées ces dernières décennies, de grandes disparités existent (supérieures à plusieurs milliers de kilomètres). La configuration du milieu du Paléozoïque est particulièrement problématique, mais il apparaît que deux principales écoles de pensée émergent. Certains auteurs préfèrent une boucle siluro-dévonienne dans leur CDAP passant par le sud de l'Amérique du Sud (pour une reconstruction du Gondwana dans les coordonnées de l'Afrique), tandis que d'autres dessinent pour cette même période un chemin coupant directement à travers l'Afrique. Cette controverse majeure est essentiellement liée à la possibilité d'utiliser des données paléomagnétiques provenant de l'Australie orientale pour pallier au manque de données paléomagnétiques d'âge mi-Paléozoïque. Déterminer si les écailles crustales (« terranes ») des Tasmanides méridionales sont (para-)autochtones ou allochtones se révèle donc crucial et le sujet d'un intense débat. Le but de ce travail est ainsi de définir au mieux les positions de ces écailles crustales tout au long du Paléozoïque afin de mieux contraindre l'histoire tectonique complexe de cette région et aussi de préciser la CDAP du Gondwana.

La construction d'une CDAP est ici discutée. Il a été tenté de déterminer si des critères « objectifs » uniquement pouvaient être utilisés dans la sélection de données servant à tracer une CDAP. Il en ressort néanmoins que la base de données paléomagnétiques n'a pas suffisamment d'entrées. Une sélection subjective des données doit être introduite, et ceci conduit à l'obtention de deux types de solution : le type « X » et le type « Y », dont les meilleurs représentants sont considérés être le chemin « X » proposé par Bachtadse & Briden (1991) et le chemin « Y » proposé par Schmidt *et al.* (1990). Ces deux modèles sont ainsi utilisés pour discuter les résultats obtenus dans cette étude.

Les Tasmanides méridionales ont eu une histoire tectonique complexe tout au long du Paléozoïque comportant plusieurs événements orogéniques. L'échantillonnage effectué pour cette étude comprend cinquante localités (289 sites, 1576 carottes, 3969 spécimens ; voir table 1, pages 54-55) distribuées le long d'un transect Est – Ouest recoupant la majeure partie des subdivisions des Tasmanides méridionales. Ces localités peuvent être réunies en trois zones principales : la zone de Broken Hill, la zone du Mont Bowen, et la zone de Molong. Elles sont situées là où aucune autre étude paléomagnétique n'était alors disponible et fournissent donc de nouvelles informations. Les méthodes d'échantillonnage sur le terrain et traitement en laboratoire sont conformes aux techniques standards utilisées en paléomagnétisme. En particulier, la désaimantation thermique progressive détaillée, l'analyse des composantes principales, les mesures d'anisotropie de susceptibilité magnétique et de magnétisme des roches ont été systématiquement employées.

La mesure en routine de l'anisotropie de susceptibilité magnétique a permis en outre l'établissement des premières cartes de la fabrique magnétique dans cette région. La forte corrélation entre les fabriques magnétiques et les principales structures tectoniques corroborent l'existence de structures transverses (E-O) dans les Tasmanides méridionales.

Les directions d'aimantations obtenues ont apportées beaucoup d'information malgré leur mauvaise qualité. Les effets de l'altération sont profonds, intenses et largement répandus.

Par exemple, l'essentiel des échantillons de la Formation du Mont Arrowsmith (localités ARR & ARO) et ceux des calcaires du Ruisseau Funeral (FUN) dans la zone de Broken Hill (Ouest de la Nouvelle Galles du Sud) est entièrement ré-aimanté, tout comme certains échantillons de la Formation Mitchell (MIT) dans la zone de Molong (Est de la Nouvelle Galles du Sud). Les aimantations secondaires sont aussi largement responsables des mauvais résultats obtenus dans la majeure partie des cinquante localités étudiées. Des directions intermédiaires d'aimantation sont communes et provoquent souvent une importante dispersion des données comme c'est le cas par exemple pour les calcaires de Kandie Tank (KAN ; zone de Broken Hill) ou pour les roches volcaniques d'Ambone ou de l'Oural (HOP, BOW, SHE ; zone du Mont Bowen). Il n'a généralement pas été possible de préciser les processus de réaimantation occasionnant ces dispersions.

Une réaimantation majeure, en revanche, probablement d'origine thermo-chimique, a pu être reconnue. Elle est considérée être d'âge Oligocène et déclenchée par des changements dans le gradient géothermique précédant la mise en place du volcanisme de point chaud dans la zone de Molong. De plus, l'existence de ré-aimantations jurassiques est suggérée, en particulier pour la zone de Broken Hill, peut-être en association avec des intrusions de filons mafiques.

Les autres composantes paléomagnétiques définies sont considérées comme étant d'âge Paléozoïque mais il est extrêmement difficile de contraindre plus précisément leurs âges puisque la plupart des tests paléomagnétiques ne sont pas significatifs. Toutefois, les paléopôles obtenus à partir de trois localités sont interprétés comme correspondant à des aimantations primaires. Le pôle obtenu dans la formation du Ruisseau Cupala du Cambrien Supérieur (CUP), confirmé par l'obtention d'un test positif d'inconformité, implique que cet endroit s'est comporté de manière semblable au craton depuis le Cambrien Supérieur. Dans la formation dévonienne inférieure du Mont Daubeny (DAU), le test du pli, le test du contact, et le test du conglomérat indiquent que l'aimantation portée par l'hématite est d'origine primaire. Le pôle correspondant (DAU) est malgré tout clairement distinct du PGV déduit des roches volcaniques dévoniennes inférieures de l'Oural (MER), montrant que l'une des deux localités au moins a été pivotée par la suite. Ce dernier pôle est en accord avec le pôle correspondant à la direction d'aimantation secondaire dans la Formation du Ruisseau Cupala et est en faveur d'une CDAP de type « X » comme celle proposée par Bachtadse & Briden (1991) pour le Gondwana. Quoiqu'il en soit, cela met sérieusement en doute les chemins de type « Y » et contredit l'existence d'une boucle siluro-dévonienne essentiellement ancrée sur le pôle dévonien inférieur obtenu par Schmidt *et al.* (1987) dans les roches volcaniques de la Rivière Enneigée. Une rotation d'échelle crustale peut être invoquée pour expliquer le désaccord entre le pôle de la Formation du Mont Daubeny et le chemin « X » puisque cette formation pourrait se trouver en fait un bassin en pull-apart.

D'une façon générale, l'existence de rotation d'échelles crustales est le résultat le plus significatif de cette étude. Cette conclusion découle du fait que des directions intermédiaires d'aimantation, une autre forme de CDAP pour le Gondwana, ou même une contribution significative de dérive « vraie » des pôles ou de champ non-dipôle ne peuvent expliquer de manière satisfaisante la distribution des paléopôles obtenus dans cette région. Par conséquence, il doit être admis que des rotations et des translations de blocs se sont produites dans les Tasmanides méridionales pendant la première moitié de l'Ere Paléozoïque et peut-être jusqu'au Carbonifère Inférieur.

Un scénario possible concernant la mise en place des blocs dans les Tasmanides méridionales est ainsi présenté en conclusion. Il comporte la translation de blocs au Silurien – Dévonien, et leurs rotations au Dévonien Inférieur ou plus probablement au Dévonien Moyen, avec des mouvements et rotations tectoniques tardives dans la chaîne méridiono-occidentale de l'orogène Lachlan entre le Dévonien Supérieur et le Carbonifère Inférieur.

Mots clefs : Paléomagnétisme, courbes de dérive apparente du pôle, Gondwana, Tasmanides méridionales, orogènes Lachlan et Délamérienne, Nouvelle Galles du Sud, Australie, reconstruction Paléozoïque.

Contents

Abstracts – English.....	I
German.....	III
French.....	V
Contents.....	VII
List of photos.....	XI
List of figures.....	XI
List of tables.....	XIV
Acknowledgements.....	XV
 Chapter 1. Presentation and problematic: implications for the history of Gondwana.....	 1
1.1. Introduction.....	1
1.1.1. Problematic.....	1
❖ Aim of the project.....	2
1.1.2. Structure of this work.....	2
1.1.3. Geological time scale.....	3
1.2. Shape of Gondwana.....	5
1.2.1. The Gondwana continent.....	5
1.2.2. The reconstruction of Gondwana.....	6
1.3. Geological history of Gondwana.....	7
1.3.1. Assembly of Gondwana.....	7
1.3.2. Palaeozoic evolution of Gondwana.....	8
1.3.3. Incorporation of Gondwana in Pangea, and its Jurassic break-up.....	10
Summary of chapter 1.....	11
 Chapter 2. Apparent Polar Wander Path for Gondwana.....	 12
2.1. Previously published APW paths for Gondwana.....	12
2.2. The problem of reference data.....	15
2.3. Palaeomagnetic database.....	16
2.3.1. Data from Gondwana.....	16
2.3.2. Analysis per period.....	17
2.4. APW paths based on “objective” data selection.....	21
2.4.1. Research of objective criteria for data selection.....	21
2.4.2. Calculation of APW paths according to selection levels.....	22
2.4.3. Significance of these APW paths.....	26
2.5. Comparison of APW paths obtained by mean pole positions and by density peak position.....	27
2.5.1. Synthetic APW path from mean pole positions.....	27
2.5.2. Density contours.....	28
2.6. Alternative approach: APW path from Small Circles Fit.....	29
2.7. Mesozoic and Cainozoic APW path for Australia.....	30
2.8. Conclusions about the APW path for Australia-Gondwana.....	31
Summary of chapter 2.....	33

Chapter 3: Tectonic history of Australia.....	34
3.1. Physical presentation of Australia.....	34
3.2. The Tasmanides in Australia.....	36
3.3. Phanerozoic history of the Southern Tasmanides.....	37
3.3.1. The Delamerian Orogeny	37
3.3.2. The Lachlan Orogeny	37
3.3.3. The New England Orogeny	41
3.3.4. Other Mesozoic and Cainozoic events affecting New South Wales	42
3.4. Geological framework of south-eastern Australia.....	43
3.5. Models for the geodynamic evolution of the Tasmanides.....	44
Summary of chapter 3.....	46
Chapter 4. Methodology, sampling and previous studies.....	47
4.1. Methodology.....	47
4.1.1. Sampling procedures	47
4.1.2. Laboratory procedures	48
4.2. Anisotropy of Magnetic Susceptibility (AMS) and contribution to structural control.....	49
4.3. Sampling coverage: rocks and localities targeted.....	50
4.3.1. Rejected palaeomagnetic results	51
4.3.2. Palaeomagnetic results presented	54
4.4. Previous palaeomagnetic studies in New South Wales.....	57
4.4.1. Post-Lachlan Orogeny data	58
4.4.2. Ordovician to Devonian data	58
4.4.3. Cambrian data	59
Summary of chapter 4.....	61
Chapter 5. Palaeomagnetic results from the Broken Hill area.....	62
5.1. Presentation of the Broken Hill area.....	62
5.1.1. Sampling coverage	62
5.1.2. Geological features	62
5.2. The Mount Arrowsmith Property (ARR & ARO).....	64
5.2.1. Presentation	64
5.2.2. Anisotropy of magnetic susceptibility	65
5.2.3. Rock magnetism for the dolomites of Mt Arrowsmith	67
5.2.4. Palaeomagnetic results for the dolomites of Mt Arrowsmith	67
5.3. The Funeral Creek Limestone (FUN).....	69
5.3.1. Presentation	69
5.3.2. Anisotropy of magnetic susceptibility	69
5.3.3. Rock magnetism	71
5.3.4. Palaeomagnetic results	71
5.4. The Cupala Creek sandstones (CUP).....	73
5.3.1. Presentation	73
5.3.2. Anisotropy of magnetic susceptibility	74
5.3.3. Rock magnetism	75
5.3.4. Palaeomagnetic results	76
5.5. The Kandie Tank Limestone (KAN) and the Gum Creek sandstones (GUM).....	82
5.5.1. Presentation	82
5.5.2. Anisotropy of magnetic susceptibility	83
5.5.3. Rock magnetism	84
5.5.4. Palaeomagnetic results	85
5.6. The Mount Daubeny Formation (DAU).....	87
5.6.1. Presentation	87

5.6.2. Anisotropy of magnetic susceptibility	88
5.6.3. Rock magnetism	90
5.6.4. Palaeomagnetic result	91
5.7. The Mount Daubeny Formation from the Churinga Property (CHU).....	97
5.7.1. Presentation	97
5.7.2. Anisotropy of magnetic susceptibility	97
5.7.3. Rock magnetism	98
5.7.4. Palaeomagnetic results	99
5.8. Rhyolitic to dacitic intrusions – The Sisters (SIS).....	102
5.8.1. Presentation	102
5.8.2. Anisotropy of magnetic susceptibility	103
5.8.3. Rock magnetism	104
5.8.4. Palaeomagnetic results	104
5.9. Conclusions about the Broken Hill area.....	108
5.9.1. Palaeomagnetic results	108
5.9.2. Regional magnetic fabric	108
Summary of chapter 5.....	110
Chapter 6. Palaeomagnetic results from the Mount Bowen area.....	111
6.1. Presentation of the Mount Bowen area.....	111
6.1.1. Sampling coverage	111
6.1.2. Geological features	111
6.2. The Gundaroo sandstones from the Bulgoo Property (BUL).....	113
6.2.1. Presentation	113
6.2.2. Anisotropy of magnetic susceptibility	113
6.2.3. Rock magnetism	114
6.2.4. Palaeomagnetic results	115
6.3. The Ambone Volcanics from Mount Hope (HOP).....	118
6.3.1. Presentation	118
6.3.2. Anisotropy of magnetic susceptibility	119
6.3.3. Rock magnetism	120
6.3.4. Palaeomagnetic results	121
6.4. The Ural Volcanics (localities BOW, TAR, SHE, MER).....	122
6.4.1. Presentation	122
6.4.2. Anisotropy of magnetic susceptibility	124
6.4.3. Rock magnetism	128
6.4.4. Palaeomagnetic results	129
6.5. Conclusions about the Mount Bowen area.....	134
6.5.1. Palaeomagnetic results	134
6.5.2. Regional magnetic fabric	135
Summary of chapter 6.....	137
Chapter 7. Palaeomagnetic results from the Molong area.....	138
7.1. Presentation of the Molong area.....	138
7.1.1. Sampling coverage	138
7.1.2. Geological features	140
7.2. Tertiary overprint.....	141
7.2.1. Presentation and rock magnetism	141
7.2.2. Palaeomagnetic results	142
7.3. The Ordovician Oakdale Formation (WIN-O) and the Silurian Nandillyan Formation (WIN-S) from the Winchester Property (WIN).....	143
7.3.1. Presentation	143

7.3.2. Anisotropy of magnetic susceptibility	144
7.3.3. Rock magnetism	147
7.3.4. Palaeomagnetic results	148
7.4. The Mitchell Formation (MIT).....	152
7.4.1. Presentation	152
7.4.2. Anisotropy of magnetic susceptibility	152
7.4.3. Rock magnetism	153
7.4.4. Palaeomagnetic results	154
7.5. The Fairbridge Volcanics (OAK).....	157
7.5.1. Presentation	157
7.5.2. Anisotropy of magnetic susceptibility	157
7.5.3. Rock magnetism	159
7.5.4. Palaeomagnetic results	159
7.6. The Bowan Park Limestone Subgroup from the Quondong quarry (QUO).....	162
7.6.1. Presentation	162
7.6.2. Anisotropy of magnetic susceptibility	162
7.6.3. Rock magnetism	163
7.6.4. Palaeomagnetic results	165
7.7. The Yuranigh Limestone Member (YUR).....	169
7.7.1. Presentation	169
7.7.2. Anisotropy of magnetic susceptibility	169
7.7.3. Rock magnetism	170
7.7.4. Palaeomagnetic results	171
7.8. The Cliefden Caves Limestone from the Little Boonderoo Property (BOO).....	173
7.8.1. Presentation	173
7.8.2. Anisotropy of magnetic susceptibility	174
7.8.3. Rock magnetism	175
7.8.4. Palaeomagnetic results	176
7.9. Conclusions about the Molong area.....	180
7.9.1. Palaeomagnetic results	180
7.9.2. Regional magnetic fabric	181
Summary of chapter 7.....	183
Chapter 8. Discussion and conclusions.....	184
8.1. Summary of the presented results.....	184
8.2. Signification and reliability of the presented results.....	185
8.2.1. Three key localities	185
8.2.2. Other results	187
8.3. Palaeoreconstruction based on key localities.....	187
8.3.1. Hypothesis 1: data favour the X-path	188
8.3.2. Hypothesis 2: data favour the Small Circles Fit path	188
8.3.3. Synthetic hypothesis	189
8.4. Palaeoreconstruction based on all results.....	190
8.4.1. Localities from the southern Molong area	190
8.4.2. Localities from the northern Molong area	192
8.4.3. Localities from the Mt Bowen and Broken Hill areas	194
8.5. Conclusions.....	196
References.....	202
Annexe I.....	210
Annexe II.....	215
Lebensfauf (Curriculum Vitae).....	217

List of photos

Photo 1: Rock sampling using a portable water-cooled drilling machine.....	60
Photo 2: Ordovician and Late Cambrian rocks at the Mt Arrowsmith Property (ARO & ARR).....	64
Photo 3: Sub-vertical beds of Middle – Late Cambrian dolomites of the Wydjah Formation	64
Photo 4: Late Cambrian limestone near the Funeral Creek in the vicinity of Pulgamurtie (FUN)	69
Photo 5: View from the Late Cambrian Cupala Creek Formation (CUP)	73
Photos 6: Basal conglomerate and sandstones of the Mt Daubeny Formation, and mafic dykes intruding the sandstones at the top of the section (DAU)	87
Photo 7: Meter-scale fold in the Mt Daubeny Formation of the Churinga Property (CHU)	97
Photo 8: One of the Sisters – a sill of rhyolitic rocks form a hill in the vicinity of the Wertago Property (SIS)	102
Photo 10: Columnar jointings of the latest Praghian Ambone Volcanics near Mt Hope township (HOP).....	119
Photo 11: View from the top of Mount Bowen (BOW)	123
Photo 12: Abandoned quarry at Shepherds Hill (SHE)	123
Photo 13: Leaning polygonal columnar jointings in the small quarry at the Merri Abba Property (MER)	124
Photo 14: Kangaroos hopping over the Silurian Nandillyan Limestone of the Winchester Property (WIN).....	144
Photos 15: Sub-vertical beds and grain size finning-up and determining the facing in the volcanoclastics sandstones from the Fairbridge Volcanics (OAK)	157

List of figures

Figure 1.1: X- and Y- APW paths for Gondwana proposed by Morel & Irving (1978).....	2
Figure 1.2: Changing views of the Late Neoproterozoic to earliest Ordovician time, after Bowring & Erwin (1998)	3
Figure 1.3: Geological time scale used in this work	4
Figure 1.4: Present-day world map showing the distribution of the fragments from Greater Gondwana	5
Figure 1.5: Different reconstructions of Gondwana (focussed on the “southern” side)	7
Figures 1.6: Digital isochrones and uncertainties in the age of the ocean floor; after Müller <i>et al.</i> (1997)	9
Figure 2.1: Eleven published APW paths for Gondwana for Palaeozoic times.....	13-14
Figures 2.2: World map showing locations of palaeomagnetic studies in Greater Gondwana	17
Figures 2.3: World map showing poles of base level selection from the palaeomagnetic database (version 4.4)	18
Figures 2.4: Relative proportion of data coming from suspect “orange” regions only and from cratonic “green” region only in the selection of data given in table I (Annexe I)	18
Figure 2.5: Comparison of results obtained by mean direction and by density contours on a simulated dataset	19
Figure 2.6: Age averages per period and their standard deviations for selected data	19
Figure 2.7: Mean pole positions per period for data coming from suspect “orange” regions only and from cratonic “green” regions only; density peaks are also represented	20
Figure 2.8: Frequency – period histogram for the quality of palaeomagnetic poles from Gondwana	22
Figures 2.9: Frequency – age histogram showing the provenance of palaeomagnetic poles of base level selection from “green & orange” regions; and from “green” regions only	23
Figure 2.10: Shape of the triangular sliding window used to calculate APW paths	22
Figure 2.11: APW path of Gondwana; and corresponding directions plotted on a stereogram for the Base Level	24
Figure 2.12: APW paths of Gondwana; and corresponding directions plotted on a stereogram for the Low Level	24
Figure 2.13: APW paths of Gondwana; and corresponding directions plotted on a stereogram for the Middle Level	25
Figure 2.14: APW paths of Gondwana; and corresponding directions plotted on a stereogram for the High Level	25
Figure 2.15: Comparison between mean values and density peaks obtained on a synthetic level of selection	28
Figure 2.16: APW path obtained by fitting small circles on data of “green” regions only	29
Figures 2.17: APW path for Australia-Gondwana; and corresponding directions plotted on a stereogram	31
Figure 2.18: The two schools of thought about the shape of the APW path for Gondwana. The X-path after Bachtadse & Briden (1991) and the Y-path after Schmidt <i>et al.</i> (1990)	32
Figures 3.1: Topographic map; and Aeromagnetic map of Australia.....	35
Figure 3.2: Main entities of Australia	35
Figure 3.3: The “outcropping Australia”, redrawn and modified after Veevers (2001)	36
Figures 3.4: Extension of orogenic events for the Delamerian Orogeny and the Early Silurian event of the Lachlan Orogeny, after Fergusson & Coney (1992); and after Veevers (2001)	38
Figures 3.5: Extension of the Siluro-Devonian event, after Fergusson & Coney (1992); and after Veevers (2001)	39
Figures 3.6: Extension of the Middle Devonian event, after Fergusson & Coney (1992); and after Veevers (2001)	40
Figures 3.7: Extension of the Early Carboniferous event, after Fergusson & Coney (1992); and after Veevers (2001)	41
Figures 3.8: Age of oceanic crust; and half-spreading rates in mm/year around Australia, after Müller <i>et al.</i> (1997)	42
Figure 3.9: Main geological subdivisions of south-eastern Australia used in this work, after Glen (1992)	43

Figures 3.10: Model of the geodynamic evolution of the Southern Tasmanides, after Gray & Foster (1997)	45
Figure 3.11: Palinspastic map of Eastern Gondwana before Late Silurian time, after Glen <i>et al.</i> (1992-b)	45
Figure 4.1: Position of localities sampled for this work and shown in table 1.....	51
Figures 4.2: Example of thermal demagnetisation from sample BOG1-2A	55
Figures 4.3: Example of thermal demagnetisation from sample BOG3-2A	55
Figures 4.4: Example of thermal demagnetisation from sample BOG5-5B	56
Figure 4.5: Corresponding directions of magnetisation for the locality “BOG”	56
Figure 4.6: Sampling localities from the Cooma & Narooma area	54
Figure 4.7: Comparison between sampling coverages obtained for this work and previous palaeomagnetic studies	57
Figure 4.8: Published poles coming from the Southern Tasmanides (except from the New England Orogen)	59
Figure 5.1: Inset recalling the position of the Broken Hill area in the Southern Tasmanides.....	62
Figure 5.2: Simplified geological map of the Broken Hill area, situating the studied localities	63
Figures 5.3: AMS parameters, Flinn-type; and $\{T\}$ vs. $\{P_j\}$ diagrams for locality ARR.....	65
Figures 5.4: Orientations of the principal axes of magnetic susceptibility for localities ARO & ARR	66
Figures 5.5: Example of rock magnetic measurements in the dolomites (ARR), specimen ARR5-5	67
Figures 5.6: Example of palaeomagnetic results obtained by thermal demagnetisation in the dolomites (ARR)	68
Figures 5.7: Single components and overall mean directions from the dolomites (ARR)	69
Figures 5.8: AMS parameters, Flinn-type; and $\{T\}$ vs. $\{P_j\}$ diagrams for locality FUN.....	70
Figures 5.9: Orientations of the principal axes of magnetic susceptibility for locality FUN	70
Figures 5.10: Example of rock magnetic measurements in the limestone (FUN), specimen FUN3-3	71
Figures 5.11: Example of palaeomagnetic results obtained by thermal demagnetisation in the limestone (FUN)	72
Figures 5.12: Single components and overall mean directions from the limestone (FUN)	73
Figures 5.13: AMS parameters, Flinn-type; and $\{T\}$ vs. $\{P_j\}$ diagrams for locality CUP.....	74
Figures 5.14: Orientations of the principal axes of magnetic susceptibility for locality CUP	75
Figures 5.15: Example of rock magnetic measurements in the sandstones (CUP), specimen CUP3-3	76
Figures 5.16: Examples of palaeomagnetic results obtained by thermal demagnetisation in the sandstones (CUP)	77
Figures 5.17: Example of palaeomagnetic results obtained by thermal demagnetisation for the Unconformity Test	78
Figures 5.18: Site mean and overall mean directions for mid temperature and the high temperature components in the Cupala Creek Formation (CUP) and in the underlying rocks (Unconformity Test)	79
Figure 5.19: Corresponding palaeopoles in Australian coordinates	81
Figures 5.20: AMS parameters, Flinn-type; and $\{T\}$ vs. $\{P_j\}$ diagrams for locality KAN.....	83
Figures 5.21: Orientations of the principal axes of magnetic susceptibility for locality KAN	83
Figures 5.22: AMS parameters, Flinn-type; and $\{T\}$ vs. $\{P_j\}$ diagrams for locality GUM	84
Figures 5.23: Orientations of the principal axes of magnetic susceptibility for locality GUM	84
Figures 5.24: Example of rock magnetic measurements in the sandstones (GUM), specimen GUM3-3	85
Figures 5.25: Example of palaeomagnetic results obtained by thermal demagnetisation in the limestone (KAN)	86
Figures 5.26: Example of palaeomagnetic results obtained by thermal demagnetisation in the sandstones (GUM)	86
Figures 5.27: Single components and overall mean directions <i>in situ</i> from localities GUM and KAN	87
Figure 5.28: Sketch showing the geometry of the syncline of the Mt Daubeny Formation.....	88
Figures 5.29: AMS parameters, Flinn-type; and $\{T\}$ vs. $\{P_j\}$ diagrams for locality DAU	89
Figures 5.30: Orientations of the principal axes of magnetic susceptibility for locality DAU	89
Figures 5.31: Example of rock magnetic measurements in the sandstones (DAU), specimen DAU3-3	90
Figures 5.32: Example of rock magnetic measurements from a volcanic pebble of the basal conglomerate (DAU) Conglomerate Test, specimen DAU1-16	90
Figures 5.33: Example of rock magnetic measurements from the mafic dykes, which intrude the top of the sampled section (DAU); Contact Test, specimen DAU7-15	91
Figures 5.34: Examples of palaeomagnetic results obtained by thermal demagnetisation in the sandstones (DAU)	92
Figures 5.35: Example of palaeomagnetic results obtained by thermal demagnetisation in the mafic dykes	92
Figures 5.36: Site mean and overall mean directions for components M & H in the sandstones of the Mt Daubeny Formation (DAU)	93
Figures 5.37: Single components and overall mean directions <i>in situ</i> for the Conglomerate Test; and for the Contact Test performed at locality (DAU)	94
Figure 5.38: Corresponding palaeopoles in Australian coordinates	97
Figures 5.39: AMS parameters, Flinn-type; and $\{T\}$ vs. $\{P_j\}$ diagrams for locality CHU.....	98
Figures 5.40: Orientations of the principal axes of magnetic susceptibility for locality CHU	98
Figures 5.41: Example of rock magnetic measurements in the sandstones (CHU), specimen CHU2-5	99
Figures 5.42: Examples of palaeomagnetic results obtained by thermal demagnetisation in the sandstones (CHU)	100
Figures 5.43: Site mean and overall mean directions for components M & H in the Mt Daubeny Formation of the Churinga Property (CHU)	101
Figure 5.44: Corresponding palaeopoles in Australian coordinates	102
Figures 5.45: AMS parameters, Flinn-type; and $\{T\}$ vs. $\{P_j\}$ diagrams for locality SIS.....	103
Figures 5.46: Orientations of the principal axes of magnetic susceptibility for locality SIS	103

Figures 5.47: Example of rock magnetic measurements in the rhyolites (SIS), specimen SIS2-4	104
Figures 5.48: Examples of palaeomagnetic results showing only component M by thermal demagnetisation (SIS)	105
Figures 5.49: Examples of palaeomagnetic results showing components M & H by thermal demagnetisation (SIS)	105
Figures 5.50: Single components and overall mean directions for components M & H in the rhyolites of the Sisters intruding the Mt Daubeny Formation (SIS)	106
Figure 5.51: Corresponding palaeopoles in Australian coordinates	107
Figure 5.52: Regional magnetic fabric of the Broken Hill area.....	109
Figure 6.1: Inset recalling the position of the Mount Bowen area in the Southern Tasmanides.....	111
Figure 6.2: Simplified geological map of the Mount Bowen area, situating the studied localities	112
Figures 6.3: AMS parameters, Flinn-type; and $\{T\}$ vs. $\{P_j\}$ diagrams for locality BUL.....	113
Figures 6.4: Orientations of the principal axes of magnetic susceptibility for locality BUL	114
Figures 6.5: First example of rock magnetic measurements in the sandstones (BUL), specimen BUL3-3	114
Figures 6.6: Second example of rock magnetic measurements in the sandstones (BUL), specimen BUL7-1	115
Figures 6.7: Example of palaeomagnetic results showing a useless high temperature magnetic signal obtained by thermal demagnetisation in the sandstones (BUL)	116
Figures 6.8: Example of palaeomagnetic results showing an interesting high temperature magnetic signal obtained by thermal demagnetisation in the sandstones (BUL)	116
Figures 6.9: Single components and overall mean directions from the sandstones (BUL)	117
Figure 6.10: Corresponding palaeopoles in Australian coordinates	118
Figures 6.11: AMS parameters, Flinn-type; and $\{T\}$ vs. $\{P_j\}$ diagrams for locality HOP.....	119
Figures 6.12: Orientations of the principal axes of magnetic susceptibility for locality HOP	120
Figures 6.13: Example of rock magnetic measurements in the volcanics (HOP), specimen HOP3-3	120
Figures 6.14: Example of palaeomagnetic results obtained by thermal demagnetisation in the volcanics (HOP)	121
Figures 6.15: Single components and overall mean directions from the Ambone Volcanics (HOP)	122
Figures 6.16: AMS parameters, Flinn-type; and $\{T\}$ vs. $\{P_j\}$ diagrams for locality BOW.....	124
Figures 6.17: Orientations of the principal axes of magnetic susceptibility for locality BOW	125
Figures 6.18: AMS parameters, Flinn-type; and $\{T\}$ vs. $\{P_j\}$ diagrams for locality SHE	125
Figures 6.19: Orientations of the principal axes of magnetic susceptibility for locality SHE	126
Figure 6.20: Sketch map of the Shepherds Hill quarry with numbers referring to drilled sites	126
Figures 6.21: AMS parameters, Flinn-type; and $\{T\}$ vs. $\{P_j\}$ diagrams for locality MER	127
Figures 6.22: Orientations of the principal axes of magnetic susceptibility for locality MER	127
Figures 6.23: Example of rock magnetic measurements in the volcanics (MER), specimen MER3-1	128
Figures 6.24: First example of palaeomagnetic results showing a noisy magnetic signal at high temperatures obtained by thermal demagnetisation in the volcanics (SHE; Site-03)	129
Figures 6.25: Second example of palaeomagnetic results showing a more coherent magnetic signal at high temperatures obtained by thermal demagnetisation in the volcanics (SHE; Site-01)	130
Figures 6.26: Example of palaeomagnetic results obtained by thermal demagnetisation in the volcanics (MER)	130
Figures 6.27: Single components and overall mean directions from the Ural Volcanics (SHE)	133
Figures 6.28: Site mean and overall mean directions for components C_{MT} & C_{HT} from the Ural Volcanics (MER)	133
Figure 6.29: Corresponding palaeopoles in Australian coordinates	134
Figure 6.30: Regional magnetic fabric of the Mount Bowen area.....	136
Figure 7.1: Inset recalling the position of the Molong area in the Southern Tasmanides.....	138
Figure 7.2: Simplified geological map of the Molong area, situating the studied localities	139
Figures 7.3: Example of rock magnetic measurements identifying the presence of pyrrhotite, specimen GRO1-5.....	141
Figures 7.4: Tertiary overprint: regional overall mean direction; and corresponding palaeopole in Australian coordinates, for components C_p carried by pyrrhotite	142
Figure 7.5: Possible regional extent of the occurrence of components C_p carried by pyrrhotite	143
Figures 7.6: AMS parameters, Flinn-type; and $\{T\}$ vs. $\{P_j\}$ diagrams for locality WIN-O.....	144
Figures 7.7: AMS parameters, Flinn-type; and $\{T\}$ vs. $\{P_j\}$ diagrams for locality WIN-S	145
Figures 7.8: Orientations of the principal axes of magnetic susceptibility for locality WIN (WIN-O & WIN-S)	146
Figures 7.9: Example of rock magnetic measurements in the turbidites (WIN-O), specimen WIN4-3	147
Figures 7.10: Example of rock magnetic measurements in the limestone (WIN-S), specimen WIN7-5	148
Figures 7.11: Example of palaeomagnetic results obtained by thermal demagnetisation in the turbidites (WIN-O)	149
Figures 7.12: Example of palaeomagnetic results obtained by thermal demagnetisation in the limestone (WIN-S)	149
Figures 7.13: Site mean and overall mean directions for components C_p , C_{HT-O} & C_{HT-S} from the turbidites and limestone of the Winchester Property (WIN)	150
Figure 7.14: Corresponding palaeopoles in Australian coordinates	151
Figures 7.15: AMS parameters, Flinn-type; and $\{T\}$ vs. $\{P_j\}$ diagrams for locality MIT.....	152
Figures 7.16: Orientations of the principal axes of magnetic susceptibility for locality MIT	153
Figures 7.17: Example of rock magnetic measurements in the volcaniclastics (MIT), specimen MIT2-3	153
Figures 7.18: First example of palaeomagnetic results, showing a clear component C_{HT} distinct from the present-day field, obtained by thermal demagnetisation in the volcaniclastics (MIT)	155

Figures 7.19: Second example of palaeomagnetic results, showing a component C_{HT} being merged with the present-day field, obtained by thermal demagnetisation in the volcaniclastics (MIT)	155
Figures 7.20: Site mean and overall mean directions for components C_P & C_{HT} from the Mitchell Formation	156
Figure 7.21: Corresponding palaeopoles in Australian coordinates	156
Figures 7.22: AMS parameters, Flinn-type; and $\{T\}$ vs. $\{P_j\}$ diagrams for locality OAK	158
Figures 7.23: Orientations of the principal axes of magnetic susceptibility for locality OAK	158
Figures 7.24: Example of rock magnetic measurements in the volcaniclastics (OAK), specimen OAK3-1	159
Figures 7.25: Example of palaeomagnetic results obtained by thermal demagnetisation in the volcaniclastics (OAK)	160
Figures 7.26: Single components and overall mean directions for components C_1 , C_2 & C_3 from the volcaniclastic rocks of the Fairbridge Volcanics	161
Figure 7.27: Corresponding palaeopoles in Australian coordinates	162
Figures 7.28: AMS parameters, Flinn-type; and $\{T\}$ vs. $\{P_j\}$ diagrams for locality QUO	163
Figures 7.29: Orientations of the principal axes of magnetic susceptibility for locality QUO	163
Figures 7.30: First example of rock magnetic measurements in the limestone (QUO), specimen QUO8-1	164
Figures 7.31: Second example of rock magnetic measurements in the limestone (QUO), specimen QUO12-1	164
Figures 7.32: First example of palaeomagnetic results, showing a component C_{EW} obtained by thermal demagnetisation in the limestone (QUO; specimen QUO8-1D)	166
Figures 7.33: Second example of palaeomagnetic results, showing a component C_{NS} obtained by thermal demagnetisation in the limestone (QUO; specimen QUO12-1D)	166
Figures 7.34: Single components and overall mean directions for components C_P , C_{EW} & C_{NS} from the Bowan Park Limestone of the Quondong quarry	167
Figure 7.35: Corresponding palaeopoles in Australian coordinates	168
Figures 7.36: AMS parameters, Flinn-type; and $\{T\}$ vs. $\{P_j\}$ diagrams for locality YUR	169
Figures 7.37: Orientations of the principal axes of magnetic susceptibility for locality YUR	170
Figures 7.38: Example of rock magnetic measurements in the limestone (YUR), specimen YUR3-1	170
Figures 7.39: Example of palaeomagnetic results obtained by thermal demagnetisation in the limestone (YUR)	171
Figures 7.40: Single components and overall mean directions for components C_S from the Yuranigh Limestone Member, and compared with components C_{EW} of locality QUO	172
Figure 7.41: Corresponding palaeopoles in Australian coordinates	173
Figures 7.42: AMS parameters, Flinn-type; and $\{T\}$ vs. $\{P_j\}$ diagrams for locality BOO	174
Figures 7.43: Orientations of the principal axes of magnetic susceptibility for locality BOO	174
Figures 7.44: Example of rock magnetic measurements in the limestone (BOO), specimen BOO1-1	175
Figures 7.45: Example of palaeomagnetic results obtained by thermal demagnetisation in the limestone (BOO)	176
Figures 7.46: Site mean and overall mean directions for components C_P & C_M from the Cliefden Caves Limestone	178
Figures 7.47: Comparison between the directions obtained at locality BOO and results reported by Goleby (1980)	179
Figure 7.48: Corresponding palaeopoles in Australian coordinates	180
Figure 7.49: Regional magnetic fabric of the Molong area	182
Figure 8.1: Palaeopoles presented in the previous chapters and shown on a reconstruction of Gondwana in African coordinates	184
Figure 8.2: Poles of the three key localities used to anchor the different following hypotheses	187
Figure 8.3: Hypothesis based on key localities only (CUP, DAU, MER, and SRV, CV, HG, WPF)	189
Figure 8.4: Localities from the southern Molong area (BOO, QUO, YUR)	191
Figure 8.5: Localities from the northern Molong area (MIT, OAK)	192
Figure 8.6: Localities from the Mount Bowen and Broken Hill areas (BUL, CHU)	194
Figure 8.7: Reconstruction of the Australia-Antarctica-New Zealand region at anomaly M0, after Müller <i>et al.</i> (2001)	196
Figures 8.8: Ordovician; and Silurian palaeogeographic reconstruction of Gondwana	197
Figures 8.9: Early Devonian palinspatic reconstruction	198
Figures 8.10: late Early to Middle Devonian palinspatic reconstruction	199
Figures 8.11: Late Devonian palinspatic reconstruction	199
Figures 8.12: Early Carboniferous palinspatic reconstruction	200

List of Tables

Table 1: List of sampling localities	52-53
Table 2: List of localities in the Cooma – Narooma area	54
Table 3: List of localities in the Broken Hill area	62
Table 4: Site mean directions and overall mean directions for locality CUP	80
Table 5: Corresponding palaeopoles for the Cupala Creek Formation (CUP)	80
Table 6: Comparable published Late Cambrian palaeopoles for Gondwana	81
Table 7: Site mean directions and overall mean directions for locality DAU	95
Table 8: Corresponding palaeopoles for the Mount Daubeny Formation (DAU)	96

Table 9: Comparable published Silurian – Early Devonian palaeopoles for Gondwana	96
Table 10: Site mean directions and overall mean directions for locality CHU	100
Table 11: Corresponding palaeopoles for the Mount Daubeny Formation (CHU)	102
Table 12: Overall mean directions obtained from single specimen orientations for locality SIS	107
Table 13: Corresponding palaeopoles for the Sisters (SIS)	107
Table 14: List of localities in the Mount Bowen area.....	111
Table 15: Overall mean directions obtained from single specimen orientations for locality BUL	117
Table 16: Corresponding palaeopoles for the Gundaroo sandstones (BUL)	118
Table 17: Overall mean directions obtained from single specimen orientations for locality HOP	122
Table 18: Overall mean directions obtained from single specimen orientations for locality SHE	132
Table 19: Site mean directions and overall mean directions for locality MER	132
Table 20: Corresponding palaeopoles for the Ural Volcanics (SHE & MER)	134
Table 21: List of localities in the Molong area.....	138 & 140
Table 22: Overall mean directions per locality obtained from component C _p	142
Table 23: Site mean directions and overall mean directions for locality WIN	151
Table 24: Corresponding palaeopoles for locality WIN	151
Table 25: Site mean directions and overall mean directions for locality MIT	154
Table 26: Corresponding palaeopoles for the Mitchell Formation (MIT)	157
Table 27: Site mean directions and overall mean directions for locality OAK	161
Table 28: Corresponding palaeopoles for the Fairbridge Volcanics (OAK)	162
Table 29: Site mean directions and overall mean directions for locality QUO	167
Table 30: Corresponding palaeopoles for the Bowan Park Limestone Subgroup (QUO)	169
Table 31: Site mean directions and overall mean directions for locality YUR	172
Table 32: Corresponding palaeopoles for the Yuranigh Limestone Member (YUR)	173
Table 33: Site mean directions and overall mean directions for locality BOO	177
Table 34: Overall mean directions for several localities studied by Goleby (1980)	177
Table 35: Corresponding palaeopoles for the Cliefden Caves Limestone Subgroup (BOO)	180
Table 36: Localities presented in the previous chapters and corresponding palaeopoles.....	185



Acknowledgements

I cannot thank everyone who helped me for these work. Nevertheless, I just would like to thank Jennifer Tait for taking me in, Richard Glen and Ian Percival for their precious help and advices both in Sydney and on the field, and Kingsley Mills, for sharing his enormous knowledge of the Broken Hill area. I am also indebted to Peter Buckley and Roger Cameron, and in particular to Kate Bulls who transmitted me much information and comments. My two field assistants, Adam Wadsworth and Kari Anderson, have probably suffered a lot carrying water for me, but I think we had very good time together. Phil Schmidt, Valerian Bachtadse, Nikolai Petersen and Heinrich Soffel were very helpful for their remarks and comments all along these years. Thank you very much also to everyone who read, corrected, commented, and advised me for this thesis, in particular Kari Anderson and Phil Schmidt who spent of lot of time for me.

Finally, I just would like to say thank you to all my friends and family for their support.

Chapter 1

Introduction and problematic: implications for the history of Gondwana

1.1. Introduction

1.1.1. Problematic

Palaeogeographic reconstruction has great implications for many disciplines in Earth sciences. It is in particular of paramount importance for our understanding of Earth dynamic processes, palaeoclimate and palaeoenvironment evolution, and biodiversification. Recognition of sea floor magnetic anomalies was one of the major arguments for the outcome of the plate tectonic theory, and are now largely used for Cainozoic and Mesozoic reconstruction together with palaeomagnetism. Palaeomagnetic records are the best tools to witness block or continent's movement through time and are used to define apparent polar wander (APW) paths.

The beginning of the Palaeozoic Era saw an “explosion of life”, the causes of which remain one of the key enigmas in geosciences. The position of continents at this time and the associated palaeoenvironments probably played a major role in this event. However, the palaeoposition of Gondwana – a huge landmass that encompassed the two thirds of the present-day continents – is still largely unknown for most of the Palaeozoic times. There is indeed too few high quality palaeomagnetic data to track precisely Gondwana's movement through time and sea floor magnetic anomalies are not available as the oldest oceanic crust on Earth is Early Jurassic in age.

However, several APW paths for Gondwana have been tentatively published since about 30 years. They are all very different but from a general point of view, two schools of thought arise from them. On a reconstruction of Gondwana in African coordinates (held fixed), some authors draw a quite direct path through Africa between the Ordovician and Carboniferous times. This is rather in agreement with the “classic” X-path (figure 1.1) proposed by Morel & Irving (1978). Some other authors involve in particular a Siluro-Devonian loop reaching southern Chile and better corresponding to the Y-path of Morel & Irving (1978).

The difference of shape between these two cases is not only important for palaeogeography but has also implications for Earth dynamic. The loop in the Y-path model implies drift rates for Gondwana in the order of 40 to 60 cm/year. Such rates are not known on Earth, even in back-arc basins. If a continent as big as Gondwana moved with that speed, internal Earth mechanisms were probably much different in the Early Palaeozoic. On the other hand, most of the data used to draw this Siluro-Devonian loop come from the Tasmanides of eastern

Australia. This region is made up of terranes and their relation with the core of Gondwana is unclear. Some authors suggest they are (para-)autochthonous and are therefore representative of cratonic Gondwana. Others argue they are allochthonous, which means that their drift history is distinct from Gondwana and then, the use of palaeomagnetic data from this region must be prohibited to draw the APW path of Gondwana.

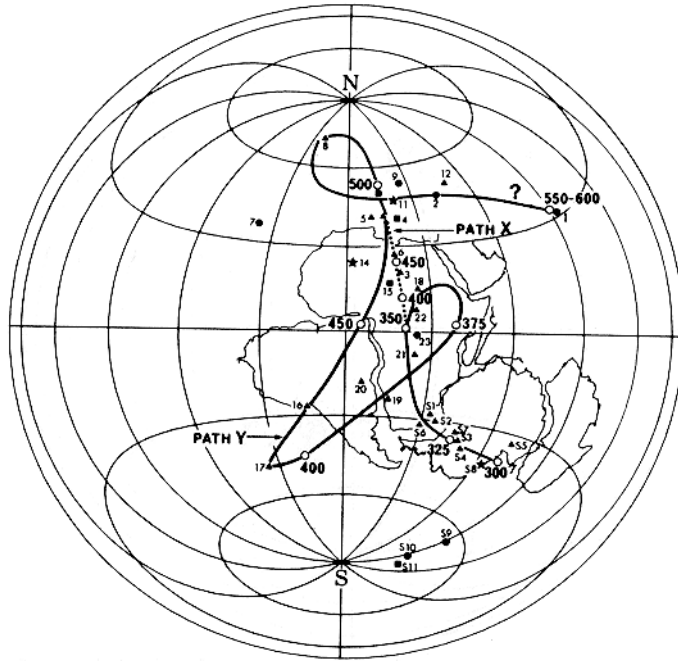


Figure 1.1: X- (dashed line) and Y- (solid line) apparent polar wander paths (APWPs) for Gondwana proposed by Morel & Irving (1978). It illustrates the main controversy still under debate concerning the existence or not of a Siluro-Devonian loop.

The upright triangles are poles from Australia, squares from Antarctica, stars from South America, and circles from Africa. Calibration points are shown as open circles and labelled in millions of years (in bold). Reader is referred to the original paper concerning the data used (numbers).

The palaeomagnetic poles are drawn on the reconstruction of Smith & Hallam (1970).

❖ Aim of the project:

The tectonic history of the Tasmanides is consequently a keystone in the determination of the APW path of Gondwana. The aim of this project is thus to constrain the Early – Middle Palaeozoic palaeogeography of south-eastern Australia using palaeomagnetism in order to refine the drift history of Gondwana and to help understanding the formation of the Southern Tasmanides.

1.1.2. Structure of this work

This thesis is structured as follows. The following section recalls some geological knowledge about the history of Gondwana from its assembly to its dislocation. Some previously published APW paths are discussed and their differences are analysed using the palaeomagnetic database (McElhinny & Lock, 1996; Version 4.4 maintained on-line by Pisarevsky, 2003).

Australia is briefly presented and the main tectonic events that have affected the Southern Tasmanides are shown. They underline the complex tectonic history of the region and explain divergences in opinion about the origin of terranes. These events are also important for a palaeomagnetic study, as they may be responsible of remagnetisations. Previous palaeomagnetic studies carried out in this sector are analysed and compared to the sampling coverage obtained for this work.

Localities sampled can be grouped in three main areas and a chapter is devoted to each of them showing results for anisotropy of magnetic susceptibility, rock magnetic analysis and palaeomagnetism of selected localities. Rocks sampled are indeed often very poorly exposed and in addition they often show a strong degree of weathering. Consequently, most of the rocks sampled are actually revealed unsuitable for relevant palaeomagnetic purposes and only a few are presented herein.

To conclude, the last chapter gives some hypotheses deduced from our results and some tentative palinspastic reconstructions are shown to illustrate this.

For clarity purposes, a summary of the main points developed is provided at the end of each chapter (except chapter of discussion and conclusion).

1.1.3. Geological time scale

The Palaeozoic time scale has strongly varied in the last few decades, in particular for Cambrian and Ordovician periods.

Figure 1.2 shows changing views of Late Neoproterozoic to Early Ordovician time. About a decade ago, it became evident that most of the published age data on the Cambrian were irrelevant because they were based on Rb-Sr ages that deviated from the true values and gave ages that were up to 50 Ma too old. And a number of recent ages created remarkable changes in the age assignment. A diagrammatic summary of biostratigraphically and geochronologically well constraint samples of Late Vendian and Cambrian ages was provided by Bowring & Erwin (1998).

Hence, ages and epochs are employed and incorporated in the geological time scale used in this thesis (figure 1.3). The rest of the geological time scale is based on that of the Geological Society of America, 1999 [Compilers: Palmer & Geissman].

Australia has a specific time subdivision for Early Palaeozoic. Here (figure 1.3), only subdivisions for the Ordovician will be used, and references to international ages follow that of Veevers (2000).

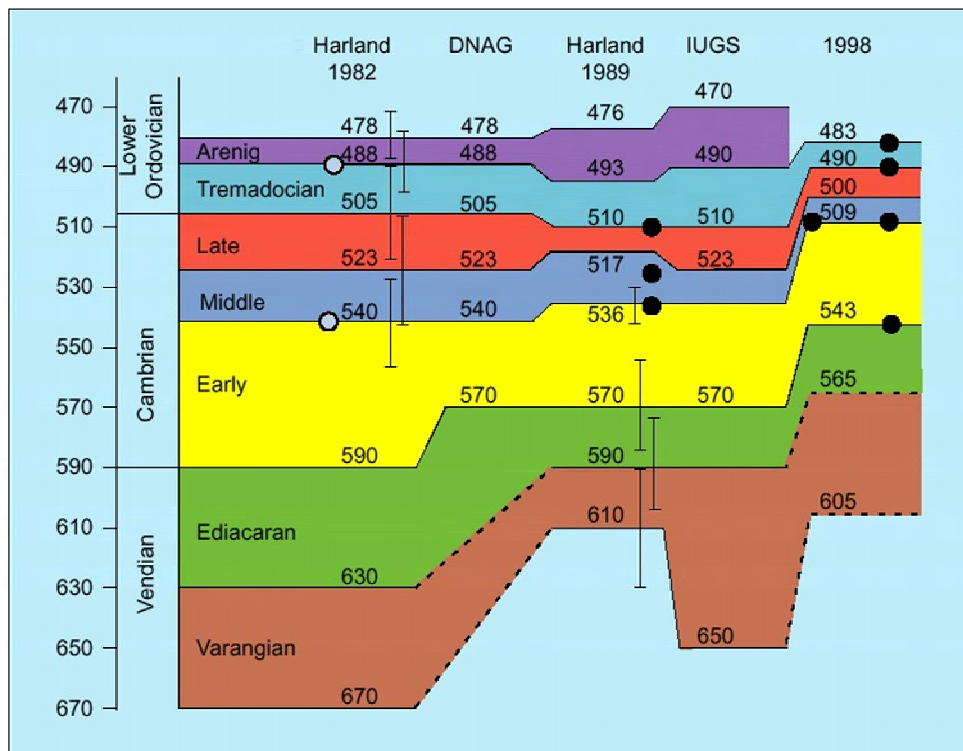
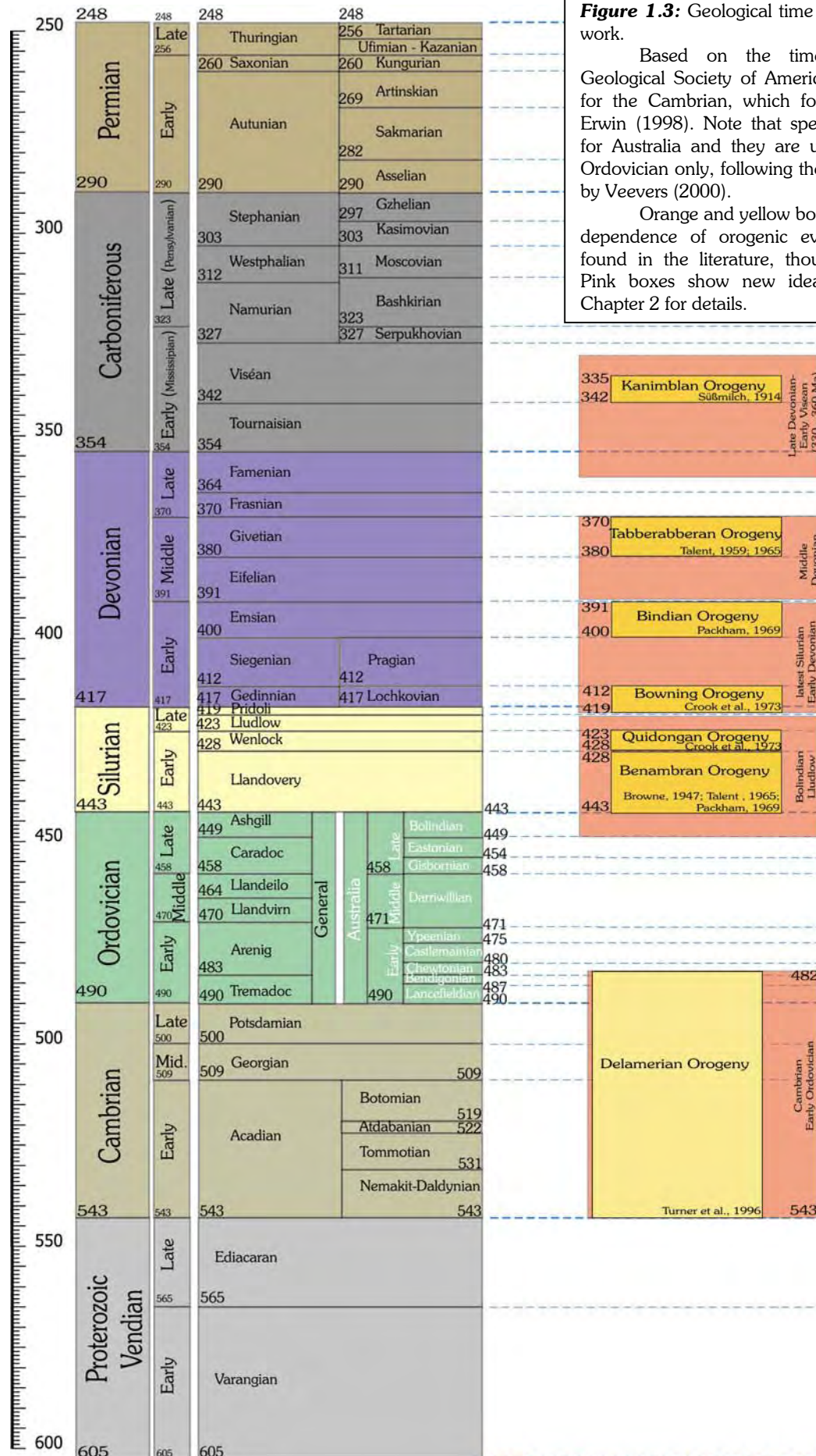


Figure 1.2: Changing views of Late Neoproterozoic to earliest Ordovician time. The estimated boundary dates are shown from Harland *et al.* (1982), the Decade of North American Geology (DNAG) in 1983, Harland *et al.* (1990), the International Union of Geological Sciences (IUGS) in 1989, and Bowring & Erwin (1998).

The open circles represent poorly constrained geochronologic tie-points and the black circles better-constrained tie-points. Error bars are shown for Harland *et al.* time scales.

Note that the subdivisions of the Late Neoproterozoic have not been firmly established.

After Bowring & Erwin (1998) and references therein.



1.2. Shape of Gondwana

1.2.1. The Gondwana continent

Du Toit (1937) presented detailed evidence that the southern continents had once been united but had been subsequently dispersed. He produced the first plausible maps of Gondwana that closely resemble currently accepted views of its original shape. Even if he considered **Wegener** as the originator of the theory of continent drift (**Wegener**, 1912; and his book, 1915, translated in English in 1924), he reported that **Neumayr** visualised a continuous continent extending from South America to Africa and even North-East India as early as 1887. Moreover, it is the Austrian **Eduard Suess** in 1885 that conferred on the mass the name of Gondwana-Land. Gondwana is derived from Sanskrit and means literally the forest [Land] of the Gonds – a people from the Dekkan region in North India. Gondwana is therefore used here instead of the longer term Gondwanaland.

Gondwana was a huge continent that comprised about two thirds of the present-day continents on Earth. Its constituents are difficult to list in a concise way, since they depend on what time period is considered. Indeed, the shape of Gondwana evolved continuously from its amalgamation to its disintegration, in particular on its margins. However, three groups of constituents can be considered: the major fragments, the intra-Gondwana fragments and the peri-Gondwana fragments. They form all together the so-called Greater Gondwana.

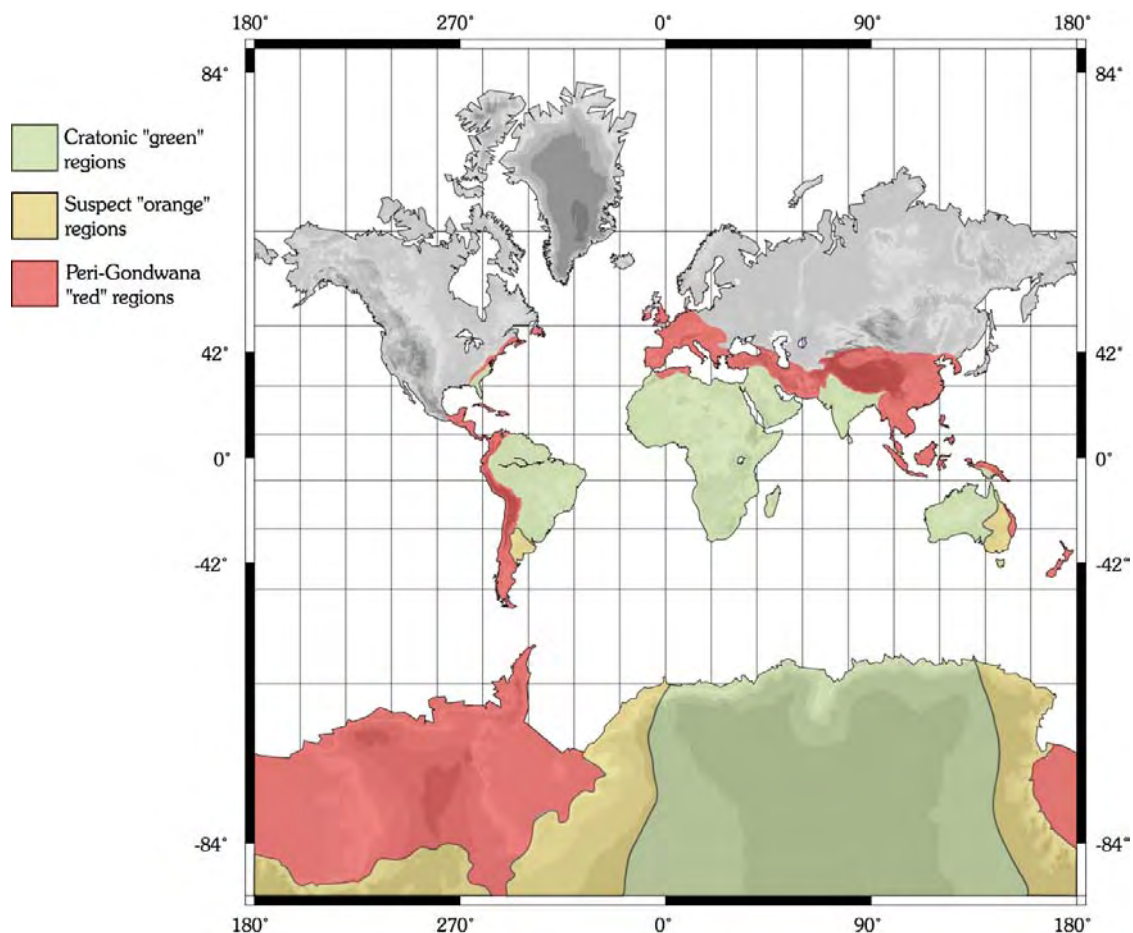


Figure 1.4: Present-day world map showing in colours fragments above sea-level that have belonged at some time to Greater Gondwana. In **red**, peri-Gondwana fragments, which should be discarded for the determination of the APWP of Gondwana. In **green**, the craton of Gondwana. In **orange**, “suspect” regions concerning the representation of Gondwana. Mercator projection.

Major fragments include the present-day South America, Africa, Arabia, Madagascar, India, Australia and Antarctica. They form the core of Gondwana. Other fragments are small continental pieces, which were situated between major fragments (intra-Gondwana fragments) or surrounding them (peri-Gondwana fragments). Seychelles Islands or Sri Lanka, for instance, can be considered as such intra-Gondwana fragments. Peri-Gondwana fragments are difficult to name because some rifted off and some amalgamated to Gondwana throughout the Palaeozoic Era. However, they can all be regarded as microplates surrounding the core of Gondwana.

It is not clear whether East Australia (Tasmanides), West Antarctica (Transantarctic Mountains) and south South America (Patagonia), which are composed of terranes, may be considered as part of the core or as peri-Gondwana fragments (see below).

In determining the drift history of Gondwana using palaeomagnetic data, results obtained from peri-Gondwana fragments are not representative and should be discarded (shown in red in figure 1.4). Unfortunately, data from the craton of Gondwana (in green in figure 1.4) are scarce and often contradictory, especially for the Silurian and Devonian times. That is the reason why knowing whether “suspect” regions (in orange in figure 1.4) are representative of the craton and subsequently whether the use of palaeomagnetic data from these regions is valid for Gondwana, is of crucial importance for the determination of the APW path.

1.2.2. Reconstruction of Gondwana

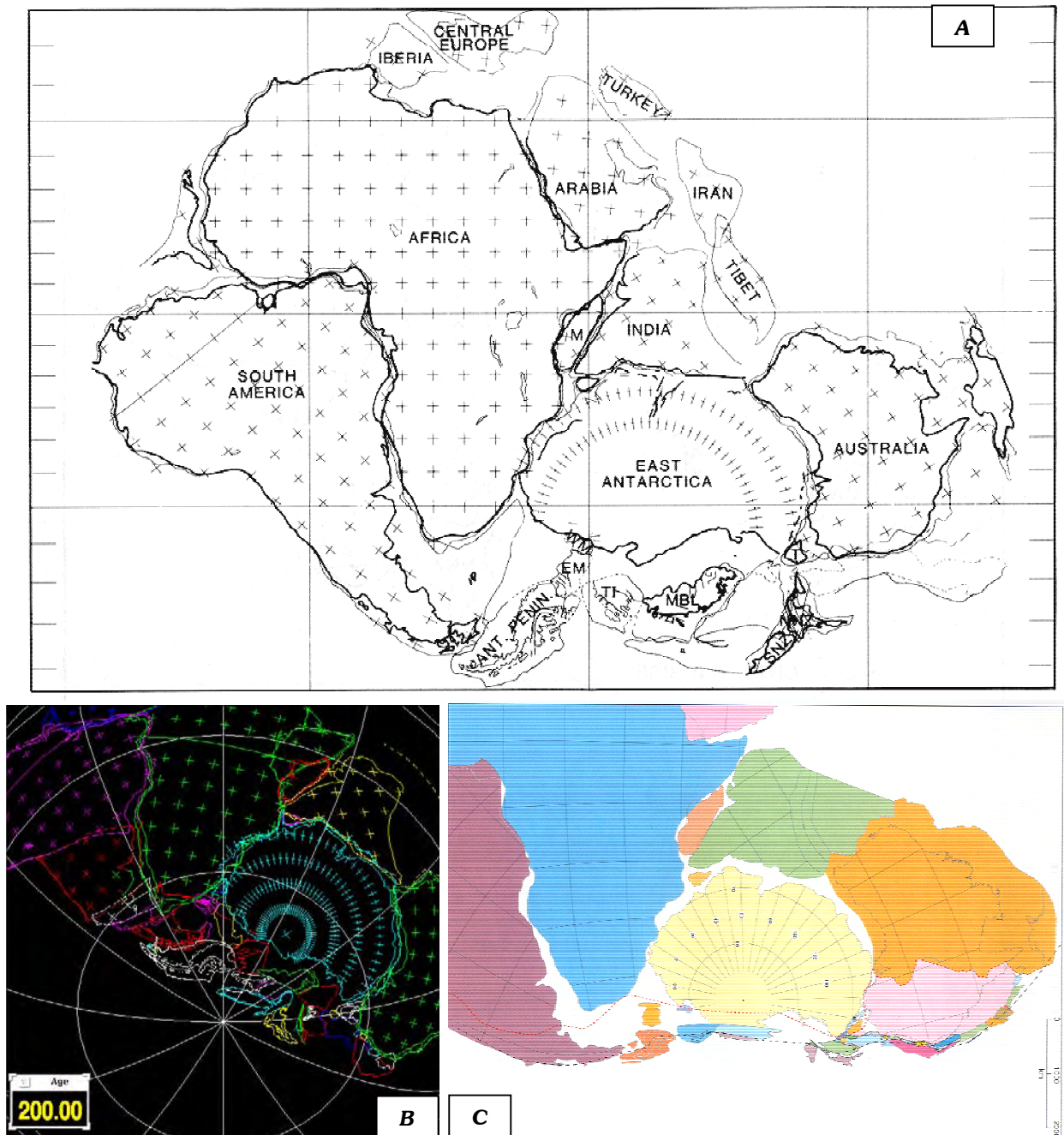
In the last few decades, several reconstructions have been proposed, such as that of Smith & Hallam (1970). Nevertheless, the inside fit of Gondwana was a matter of debate. In particular, the positions of Madagascar, Sri Lanka and Antarctica relative to Africa were problematic. Now, reconstructions favour the fit of Lawver & Scotese (1987; figure 1.5-A), as discussed for instance, by Rakotosolof (1999). However, as noticed by Lawver & Scotese (1987) themselves, their fit is not fundamentally different from the fit proposed by DuToit (1937).

The discussion is currently more focused on peri-Gondwana fragments. As far as this work is concerned, special attention is given to the configuration in the sector of Australia, Antarctica and New Zealand. In the fit of Lawver & Scotese (1987), the “southern” margin is not well established and it leaves major gaps between fragments (figure 1.5-A). Other reconstructions have been therefore proposed in order to refine the palaeogeography of this zone, and two suggestions are shown here (figures 1.5-B & C) for comparison.

The position of North and South New Zealand at the beginning of the Mesozoic in particular, relative to Australia and Antarctica, clearly illustrates these differences and are of great importance to the palaeogeography of the Tasmanides. South New Zealand lies more to the “South” (oceanwards) in Lawver & Scotese’s reconstruction than in reconstructions by Gahagan *et al.* (1999; figure 1.5-B is an image produced for the “PLATES Project”; but the corresponding paper is from Lawver *et al.*, 1999) and by Veevers (2001; figure 1.5-C). In the fit of Gahagan *et al.* (1999), South New Zealand (block in blue) is closer to the craton and has lower latitude than North New Zealand (in yellow). Note also that South America is not considered as a single entity. In the fit of Veevers (2001), New Zealand is put in another position. It must be mentioned that all peri-Gondwana fragments along the Pacific margin have been narrowed in order to account for present-day crustal extension.

The position of Tasmania differs as well. In the fit of Lawver & Scotese (1987) as well as that of Veevers (2001), Tasmania lies North of Victoria Land in Antarctica, whereas Gahagan *et al.* (1999) places it more to the “East” (oceanwards). Such representations are very important for the correlations made between the Tasmanides of Australia and the Transantarctic Mountains of Antarctica (see for instance Borg & DePaolo, 1991).

However, all these reconstructions still leave gaps and overlaps.



Figures 1.5: Different reconstructions of Gondwana (focused on the “southern” side).

A: In the fit of Lawver & Scotese (1987); WM is Whitmore Mountains, EM: Ellsworth Mountains, TI: Thurston Island block, NNZ: northern New Zealand, SNZ: southern New Zealand attached to Campbell Plateau, M: Madagascar, T: Tasmania; South New Zealand lies more to the “south” (oceanward) relative to North New Zealand than in other reconstructions. **B:** In the fit of Gahagan *et al.* (1999); South New Zealand (block in blue) is closer to the craton and has lower latitude than North New Zealand (in yellow). Note also that South America is not considered as a single entity. **C:** In the fit of Veevers (2001); here, New Zealand has another position. It must be mentioned that all peri-Gondwana fragments along the Pacific margin have been narrowed in order to account for present-day crustal extension.

1.3. Geological history of Gondwana

1.3.1. Assembly of Gondwana

The idea of the existence of a Meso-Neoproterozoic supercontinent, Rodinia (McMenamin & McMenamin, 1990), has renewed interest in Precambrian continental

reconstruction, since the hypothesis of a SWEAT connection (Southwest USA – East Antarctica) by Moores (1991). Although Jefferson (1978) already proposed that western Laurentia was flanked in the Late Proterozoic by the eastern margin of Australian and Antarctic cratons corresponding to the Transantarctic Mountains, the SWEAT connection hypothesis has been especially bolstered by Dalziel (1991), who provided a computer reconstruction of the supercontinent. Rodinia is thought to have formed at about 1100 Ma on the basis of linkage of truncated Grenvillian orogenies. Its existence is also supported by palaeomagnetic data (Powell *et al.*, 1993; Torsvik *et al.*, 1996; Meert & Van der Voo, 1997; Weil *et al.*, 1998). Break-up of Rodinia, which began at about 725-750 Ma, and the assembly of Gondwana still remains a problem.

Hoffmann (1991) suggested that Gondwana formed by rotation of a part of Rodinia (*i.e.* the Kalahari craton, Madagascar, Sri Lanka, India, Antarctica and Australia) around an Euler pole located in the Weddell Sea, and by collision against the other side of Rodinia (*i.e.* the Congo, West Africa and Amazonia cratons) during the Pan-African Orogeny. Hence, Dalziel (1992-a) postulated the existence of a second short-lived supercontinent, now called Pannotia, where Laurentia is juxtaposed to western South America. It is supported by near-simultaneous initiation of thermal subsidence in the mid-Atlantic region of North America and in north-western Argentina, faunal similarities between the Appalachian and Andean margin, and some palaeomagnetic data (see Dalziel, 1992-a and references therein).

Nonetheless, Wilson *et al.* (1997) have particularly outlined the complex history of the assembly of Gondwana. They emphasized the large age range of tectonism, syntectonic plutonism and/or granulite development in Pan-African belts. They also questioned major plate motions between the Congo and Kalahari blocks, and argued that Gondwana was not a stable, rigid entity up to the Mid-Late Cambrian, as ages of tectonism range from 650 to 500 Ma, or even 450 Ma in the Damara belt of southwestern Africa.

Therefore, most authors now consider the final assembly of Gondwana to have occurred between 500 and 580 Ma (522 ± 13 Ma for Powell *et al.*, 1993; 530 Ma for Meert & Van der Voo, 1997; ~ 550 Ma for Weil *et al.*, 1998; 580 Ma for Smith, 1999; and ~ 550 Ma for Torsvik *et al.*, 2001-a). This casts, of course, a doubt on the existence of Pannotia, as the consolidation of Gondwana may have occurred after Laurentia broke apart.

1.3.2. Palaeozoic evolution of Gondwana

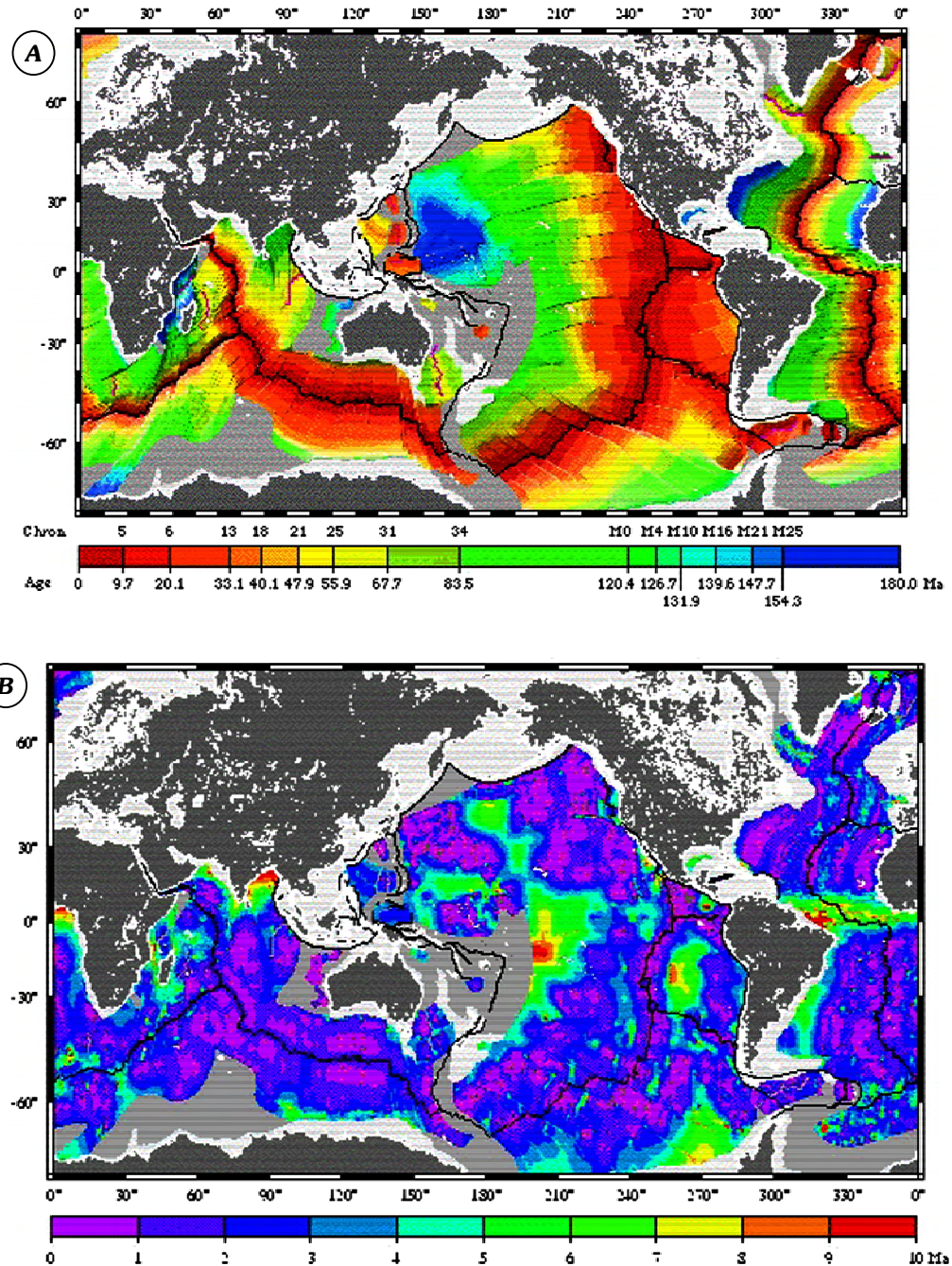
The “north-eastern” peri-Gondwana fragments belonged to Gondwana in the Early Palaeozoic (Burrett *et al.*, 1990; Cocks & Fortrey, 1990; Pedder & Oliver, 1990; Finney & Xu, 1990), but began to break off in the Ordovician. North and South China had highly endemic continental fish faunas from the Silurian through to the Early-Middle Devonian, indicating prolonged isolation of these terranes (Burrett *et al.*, 1990). Nevertheless, the timing and drift history for north-eastern peri-Gondwana fragments is still very poorly known.

Avalonia rifted away from the north-west margin of Gondwana in the Early Ordovician. By the Middle Ordovician, the faunas of Avalonia were more similar to those of Baltica than Gondwana (Cocks & Fortrey, 1990) or Bohemia, Armorica and Morocco (Havliček, 1989). The fate of the European massifs is as yet not well established, although palaeomagnetic data clearly indicate that Armorica and Bohemia were at high latitudes together with Gondwana and Avalonia during the Early Ordovician (Perroud *et al.*, 1984; Torsvik *et al.*, 1993; Tait *et al.*, 1994). However, palaeomagnetic data from Bohemia (Tait *et al.*, 1995) show that this microcontinent rifted off Gondwana during mid Ordovician times, although Robardet (2003) questioned the existence of an Armorica microplate on the basis of palaeobiogeographical data. This may suggest that Armorica, Bohemia and Avalonia had disparate drift-histories as already suggested by Torsvik *et al.* (1996; p.248).

The history of amalgamation of terranes along the palaeo-Pacific margin is complex and not well-understood yet. The type of geological setting, however, is probably comparable to the

formation of the Tasmanides of eastern Australia that will be detailed in the following chapter (see also Stump, 1987; Dalziel & Pankhurst, 1987 and reference therein; Borg & DePaolo, 1991; Coney, 1992; Grunow, 1995; Grunow & Encarnación, 2000).

As explained in the introduction, the absolute motion of the core of Gondwana is itself a matter of controversial debate. The APW path for Gondwana is discussed thereafter.



Figures 1.6-A: Digital isochrones of the ocean floor. Each colour refers to interval between magnetic anomalies.

B: Uncertainties in the age of the ocean floor. Note that the majority of errors is smaller than 3 Ma, and rarely exceeds 5 Ma. The motion of major tectonic plates relative one another is thus well-constrained.

After Müller *et al.*, 1997.

1.3.3. Incorporation of Gondwana in Pangea, and its Jurassic break-up

Plate reconstruction is facilitated by sea floor spreading, which allows for major plates at least, quite precise positioning up to 180 Ma, the age of the oldest oceanic crust (Müller *et al.*, 1997; figures 1.6). This yields to the Pangea configuration of Wegener (1912, 1915) and Bullard *et al.* (1965). This configuration later became known as Pangea A (Morel & Irving, 1981).

However, palaeomagnetic data for Permian to Triassic times are in disagreement with this configuration. Torsvik *et al.* (2001-b) concluded that northern Pangea must have changed systematically between about 214 and 170 Ma. That is the reason why other configurations have been proposed, such as the Pangea B configuration of Morel & Irving (1981). The transition from Pangea A to Pangea B configurations, and other Pangeas (A2, C or D), were examined by Smith & Livermore (1991), who argued that the transition could be accomplished theoretically only by invoking a Pangea transform zone between Laurussia and Gondwana. However, this transform zone has not been confirmed by geological observations.

Alternatively, Smith (1999) suggested that this mismatch between the APW paths of Laurentia and Gondwana in Permian times might also be due to inaccurate interpretation (*e.g.* structural control, age control, overprinting, etc...) in palaeomagnetic data. He speculated that some rocks, especially from passive margins or in the vicinity of orogenic belts, may have been partially or completely remagnetised. Including a significant numbers of remagnetised poles would yield an APW path being significantly in error.

Recently, Van der Voo & Torsvik (2001) and Torsvik & Van der Voo (2002) provocatively proposed to solve this problem by taking into account long-term contributions from non-dipole fields, in particular octupole fields. The fact that the contribution of non-dipole fields may have significantly varied through time is very plausible, but no evidence substantiates this hypothesis against the geomagnetic axial dipole (GAD) field assumption. This recent proposition is therefore regarded with scepticism by most of the scientific community. The validity of palaeomagnetic data however, needs to be confirmed by other methods and in particular, geological observations.

The break-up of Gondwana – within Pangea – occurred in the Middle Jurassic and is recorded by age of oceanic crust. Although the oldest oceanic crust found within Pangea lies in the North Atlantic Ocean, Gondwana itself split in two nearly simultaneously with the Indian Ocean opening, separated Madagascar and Antarctica from Africa (see crust represented in blue on figure 1.6-A; after Müller *et al.*, 1997). Recognition of magnetic anomaly in the ocean floor allows determining quite precisely (see figure 1.6-B) the movement of tectonic plates relative one to another. This will be used in this work to help defining the APW path for Australia from 200 Ma to present (see next Chapter).

Summary of chapter 1

The shape of the Gondwana apparent polar wander (APW) path remains a great matter of debate, especially concerning the existence or not of a Silurian – Devonian loop as illustrated by the X and Y paths of Morel & Irving (1978). This loop is mostly based on poles coming from the Tasmanides of eastern Australia, and as noticed by Van der Voo (1993), this region is made up of “suspect” terranes. Indeed, the question remains open as to whether these terranes had already accreted the Australian craton in the Early Palaeozoic (*i.e.* no displacement or rotation occurred relative to the craton since then) so they can be considered as (para-) autochthonous or whether they must be regarded as allochthonous. Thus the reliability of using palaeomagnetic data from this region to construct an APW path for Gondwana remains unresolved.

❖ Aim of the project:

The aim of this project is therefore to constrain the Early – Middle Palaeozoic palaeogeography of the south-eastern Australia through a palaeomagnetic study in order to refine the drift history of Gondwana and the formation of the Tasmanides.

The assembly of the core of Gondwana apparently occurred at the boundary between the Neoproterozoic and the Palaeozoic. Peri-Gondwana fragments can be regarded as microplates that drifted off or amalgamated to the craton of Gondwana throughout the Palaeozoic Era, although their specific tectonic evolution is still largely unknown. At the end of the Palaeozoic, Gondwana collided to Laurasia to form Pangea. The break-up of Gondwana – within Pangea – is better constrained thanks to recordings of sea floor magnetic anomalies. However, the exact configuration of Gondwana just before the Mesozoic sea floor spreading remains unclear, in particular concerning peri-Gondwana fragments and the zone comprised between Australia, Antarctica and New Zealand.

Chapter 2

Apparent Polar Wander Path for Gondwana

Understanding the tectonic history of Gondwana involves determining its formation, its drift history, and its disintegration. The drift history concerns in particular palaeomagnetism, and many apparent polar wander (APW) paths have been published over the past few decades. Some, shown and discussed below, lead to very contradictory conclusions about the movement of this continent. Their differences are mainly based upon subjective data selection. That is why an attempt is made herein to determine whether a selection as objective as possible can lead to a significant improvement.

2.1. Previously published APW paths for Gondwana

Among the number of paths that have been published for Gondwana for Palaeozoic times, eleven have been redrawn and are compared herein (figures 2.1).

The first work considered (because it is the oldest of these eleven and best illustrates the two schools of thought on the shape of the path for Gondwana) is the APW path set out by Morel & Irving in 1978 (red path in figure 2.1-A). This path actually offers alternatives: an X-path running directly through Africa (dashed line) for mid Palaeozoic times, or a Y-path involving a loop passing by offshore Chile (solid line). These two options stem from whether the palaeomagnetic data from the Tasmanides are included or not. It is striking to see that this controversy has persisted since then, and that basically, the same controversy over these two options is still debated in recent papers (see below).

In 1990, a set of APW paths was published in a special edition of the Geological Society of London (McKerrow & Scotese). Three of them shown here are very similar to the Y-path of Morel & Irving (1978). Bachtadse & Briden drew a smooth path (pink path in figure 2.1-B), using a spherical smoothed spline algorithm. They show that their path implies a minimal drift rate of 23 cm/year to account for the Siluro-Devonian hairpin. This extremely high drift rate is of course similar for any analogous paths, and is actually even lower than most of them. It leads to the open question: is it plausible for such a landmass, comprising two thirds of the continents of the Earth to drift at such a high rate? Indeed, paths from Kent & Van der Voo and Schmidt *et al.* (brown and orange respectively in figure 2.1-B) show a palaeopole near Tunisia in the Ordovician (+35° to +40° in latitude), and a Silurian pole to the south of South America (-50° to -60°).



Figure 2.1-C: APW paths after Scotese & Barrett (1990); Bachtadse & Briden (1991); Grunow (1999); and Smith (1999).

Same projection and legend as in figure 2.1-A.

Legend :

- Bachtadse & Briden, 1991
- Grunow, 1999
- Scotese & Barrett, 1990
- Smith, 1999

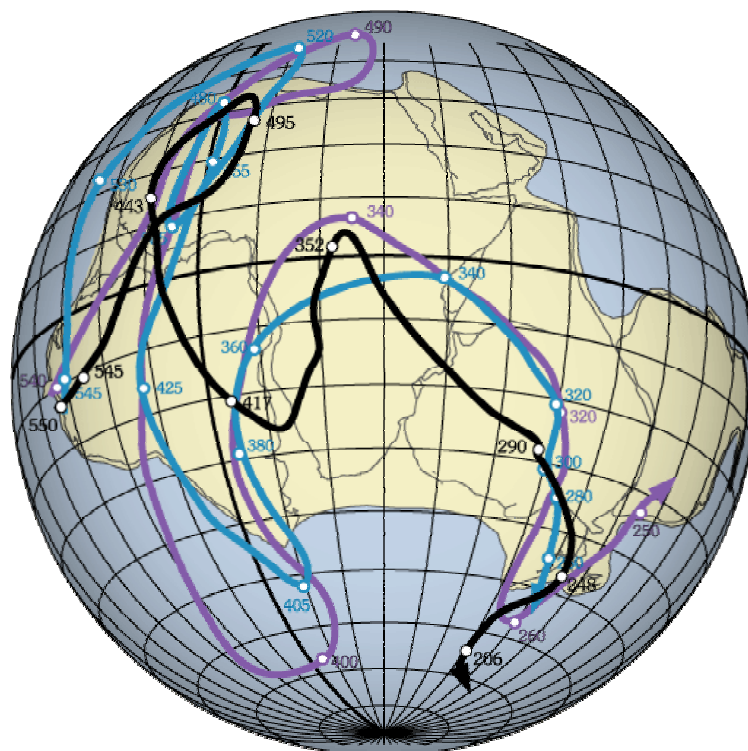


Figure 2.1-D: APW paths after Li & Powell (2001); McEhlinny *et al.* (2003); and Torsvik & Van der Voo (2002).

Same projection and legend as in figure 2.1-A.

Legend :

- Li & Powell, 2001
- McEhlinny *et al.*, 2003
- Torsvik & Van der Voo, 2002

Smith (1999) drew his path using an uncommon but interesting approach to select poles. Usually, authors tend to use data with a quality as high as possible. On the contrary, Smith used all available palaeomagnetic data for Gondwana (except those having a deviation larger than 40° to the mean pole) including untested poles, and gave two main justifications for this. First, he considers that low quality data do include a real signal. And secondly, even if the dataset may have a much larger scatter, deviation to the mean pole will be then averaged.

The controversy about data from the Tasmanides led Bachtadse & Briden (1991) to propose a new path (light brown in figure 2.1-C). This path, obtained by using a spline method, is

the one, which is the most easterly positioned from the eleven presented here and also the closest to the classic X-path of Morel & Irving (1978). The Cambro-Ordovician segment is analogous to other paths (such as Schmidt *et al.*, 1990 for example), but the Early – Mid Palaeozoic path runs directly through Africa. They mainly anchored their path on the palaeomagnetic results they then just obtained from the Gilif Hills Volcanics in Sudan (Bachtadse & Briden, 1991), and suggested that data from the Tasmanides could have been rotated or remagnetised. They involved in particular a Carboniferous hairpin to account for Australian data such as results from the Hervey Group (Li *et al.*, 1988) or from the Worange Point Formation (Thrupp *et al.*, 1991), which they considered as possibly overprinted, despite the positive fold tests.

Finally, three more paths, published in the last few years, include again a Siluro-Devonian hairpin. Li & Powell's path (2001) shows the most drastic movement between $+50^\circ$ at 490 Ma and nearly -70° at 400 Ma (violet path in figure 2.1-D). The path proposed by McElhinny *et al.* (2003) adds a "small" loop in West Africa during the Late Cambrian – Early Ordovician (blue path in figure 2.1-D). These paths imply very complex movement of the continent and the highest drift rates proposed.

The path of Torsvik & Van der Voo (2002) is more reasonable in terms of drift rates (black path in figure 2.1-D). It has been calculated using a spherical spline method, and excludes data from the Tasmanides.

As a conclusion, every path is very different from one another, even if two main types of shape can be distinguished. Pole positions may differ in the order of thousands of kilometres. This divergence is essentially related to how poles are selected.

2.2. The problem of reference data

The aim of this work is to test for the existence or not of terrane rotations and/or movements in the southern Tasmanides relative to the craton of Gondwana, and subsequently to help refining the APW path for Gondwana. One of Van der Voo's criteria (1988, 1993) to assess the quality of a palaeomagnetic datum is that there is no resemblance to palaeopoles of any younger ages. Reference data are thus needed in parallel with field tests to recognise possible remagnetisation. But what reference data, *i.e.* what APW path should be considered? How can terrane rotation be detected?

The best solution is probably to compare coeval data obtained within the Tasmanides. If they do not show the same pole position, one of the localities, or perhaps both of them, must have been rotated and/or displaced. It will be shown in the following chapters however that rocks of equivalent age and suitable for palaeomagnetic purposes are not easy to find. In addition, the magnetisations in rocks studied are very complex, and most of the results are affected by remagnetisations. The age of magnetisations is hence not well constrained and the existence of terrane rotation/movement is difficult to establish since possibilities are numerous. A possible reference path is therefore needed. Three different approaches can be suggested.

- The first approach consists in using only palaeomagnetic data, for which one has a good knowledge of the methodology and laboratory used, and a good knowledge of the geology of the studied localities. One can argue then for the relevance of these data and propose an APW path consistent with the favoured hypotheses. This approach was apparently that of McElhinny *et al.* (2003) for instance, but has the strong disadvantage to be very subjective and to merely ignore other data that could contradict the retained data used. Consequently, the credibility of the APW path obtained can be questioned.

- The second approach is to consider all available data and to argue for each of them possible reasons for the discrepancy observed in the entire dataset (*e.g.* existence of tectonic rotation or misinterpreted structural control, remagnetisation or overlap of components

contributing to obtaining intermediate direction of magnetisation, etc...). This approach is of course also subjective. However, it is believed here that this process leads to end up with the two schools of thought concerning the Palaeozoic APW path for Gondwana, that are the X- and Y-type proposed by Morel & Irving (1978). It is beyond the scope of this thesis to discuss the validity of each single datum from the database, but it is considered that the two best representatives of these end-members are the X-path of Bachtadse & Briden (1991) and the Y-path of Schmidt *et al.* (1990).

- The third approach intends to be as objective as possible. In this case, all available data are selected, perhaps filtered according to statistical parameters (number of data, κ parameter, radius of the confidence cone, etc...) and the best solution is determined using a smoothing method. This technique is objective since data are only discriminated from a statistical point of view, and data showing a significant deviation from the mean can be regarded as erroneous. This was apparently the thought process of Smith (1999) and to a certain extent that of Torsvik & Van der Voo (2002) to discuss the possible influence of non-dipole field. The two APW paths proposed by these authors are however different from one another, and the following sections will bear upon a discussion of the validity of the third approach. By looking at several methods, it will be shown that this process is simply not adapted for Gondwana given the critical paucity of palaeomagnetic data in particular of Mid Palaeozoic age.

2.3. Palaeomagnetic database

2.3.1. Data from Gondwana

To better understand the discrepancies in APW paths, it is thus necessary to refer back to the original palaeomagnetic data. For this purpose, the I.A.G.A palaeomagnetic database (version 4.4 – Pisarevsky, 2003; first version from McElhinny & Lock, 1996) has been used. The aim of this paragraph is to try to establish what data could represent Gondwana and where do the discrepancies in the dataset come from, but it is not to discuss the quality of every single data of this database.

The first step is to select all available Palaeozoic – Early Mesozoic poles (200 – 545 Ma) for Greater Gondwana, as described in §.1.2.1 (see Chapter 1, and figure 1.4). Poles provided by the database and considered to represent primary magnetisations are selected, and their site locations are plotted on a world map (figure 2.2; same map as figure 1.4). The upper age of 200 Ma is chosen since continental drift from 200 Ma to present can be modelled (see §.2.7, below).

The following step of selection consists of discarding poles coming from the disturbed margins of Gondwana (shown in red in figure 2.2). This geographical selection is justified by the fact that possible rotation in orogenic belts could not be recognised as, precisely, “reference” data from the craton are not established.

Palaeopoles calculated from the selected palaeomagnetic database (Annexe I; and figure 2.2) have been rotated into African coordinates (figure 2.3; rotation parameters of Royer *et al.*, 1992). The problem of their polarity is subjective but in most cases, one common polarity can be easily adopted, and is here chosen to match those used in previously published APW paths (see §.2.1 above). Nevertheless, pole positions are still very scattered. In particular, some Cambrian and Silurian data are widely separated from the mean poles calculated for the same period. They are shown with a red border on the map (figure 2.3). For the sake of objectivity, however, these data are not discarded, because they have the same likelihood to represent the “true” palaeopole for Gondwana as the others. Because their polarity to represent the South Pole is a matter of debate, the two possible polarities for these particular data have been tested for four levels of selection described below.

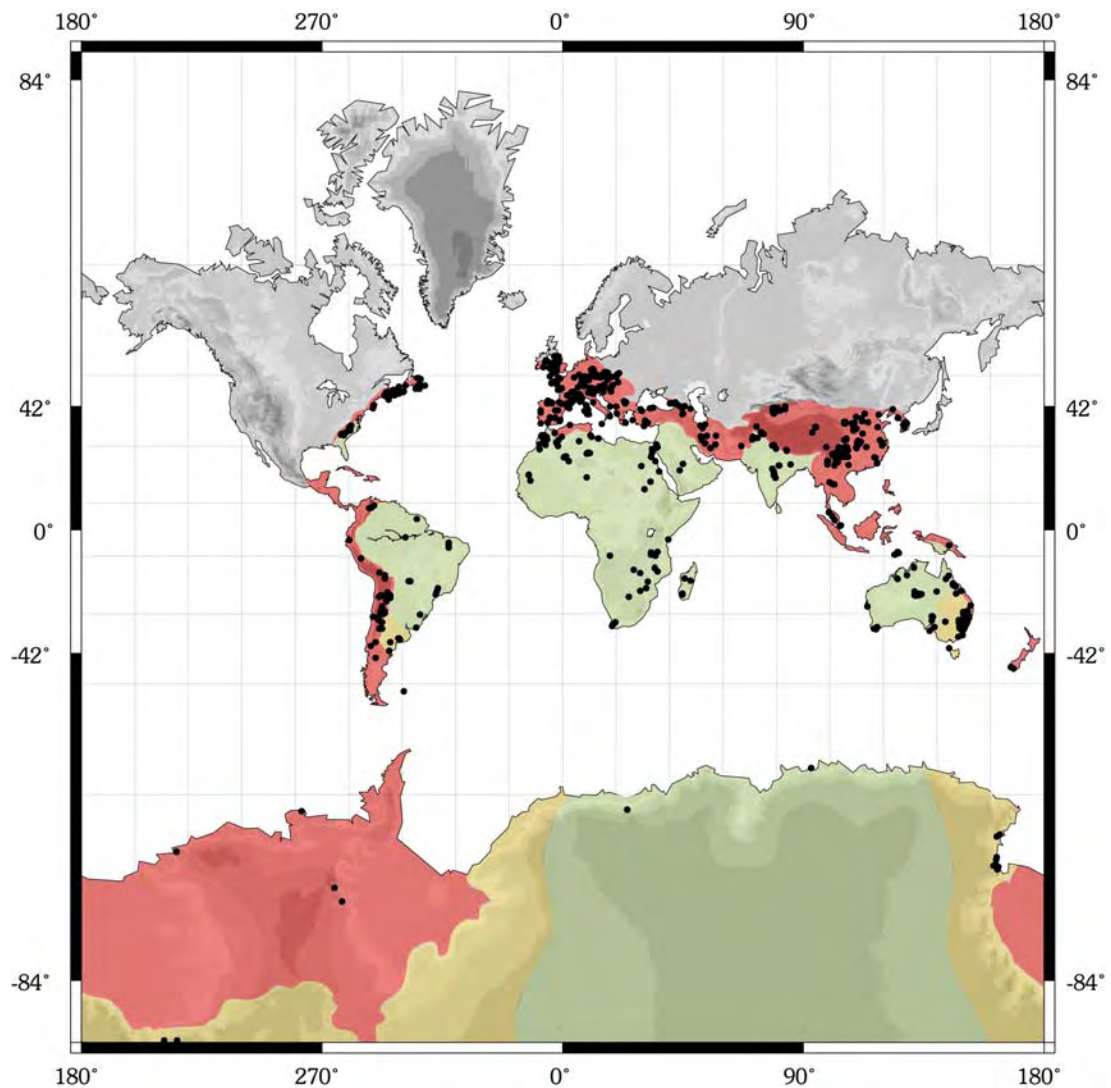


Figure 2.2: World map showing locations of palaeomagnetic studies in greater Gondwana, which have yielded primary magnetisations. In green, craton; red: orogenic zones, and in orange: controversial regions (same map as in figure 1.4). Mercator projection.

2.3.2. Analysis per period

One of the conclusions that can be drawn from the published APW paths (§.2.1) is that none are clearly superior and that the possibility of using data coming from suspect “orange” regions is of crucial importance. Moreover, their relative proportion is important for Mid Palaeozoic times (figure 2.4).

Is it possible at this level already (by looking at the scale of geological periods) to distinguish differences between data coming from the cratonic “green” and the suspect “orange” regions? As a corollary, is it possible to suspect already terranes rotation?

This can be investigated by looking at the mean pole per period for “green” regions only and for “orange” regions only. Nevertheless, as illustrated by simulated data (figures 2.5), a couple of erroneous poles can easily lead to deviate the mean pole and to obtain a very large cone at the 95% confidence level (here larger than 30°). Such results are usually not considered further as it is regarded as not significant. This is not the case when density contours are used (figure 2.5-B).

- Mean poles approach

Distinguishing data coming from the “green” and the “orange” regions can be illustrated with the example of Devonian data.

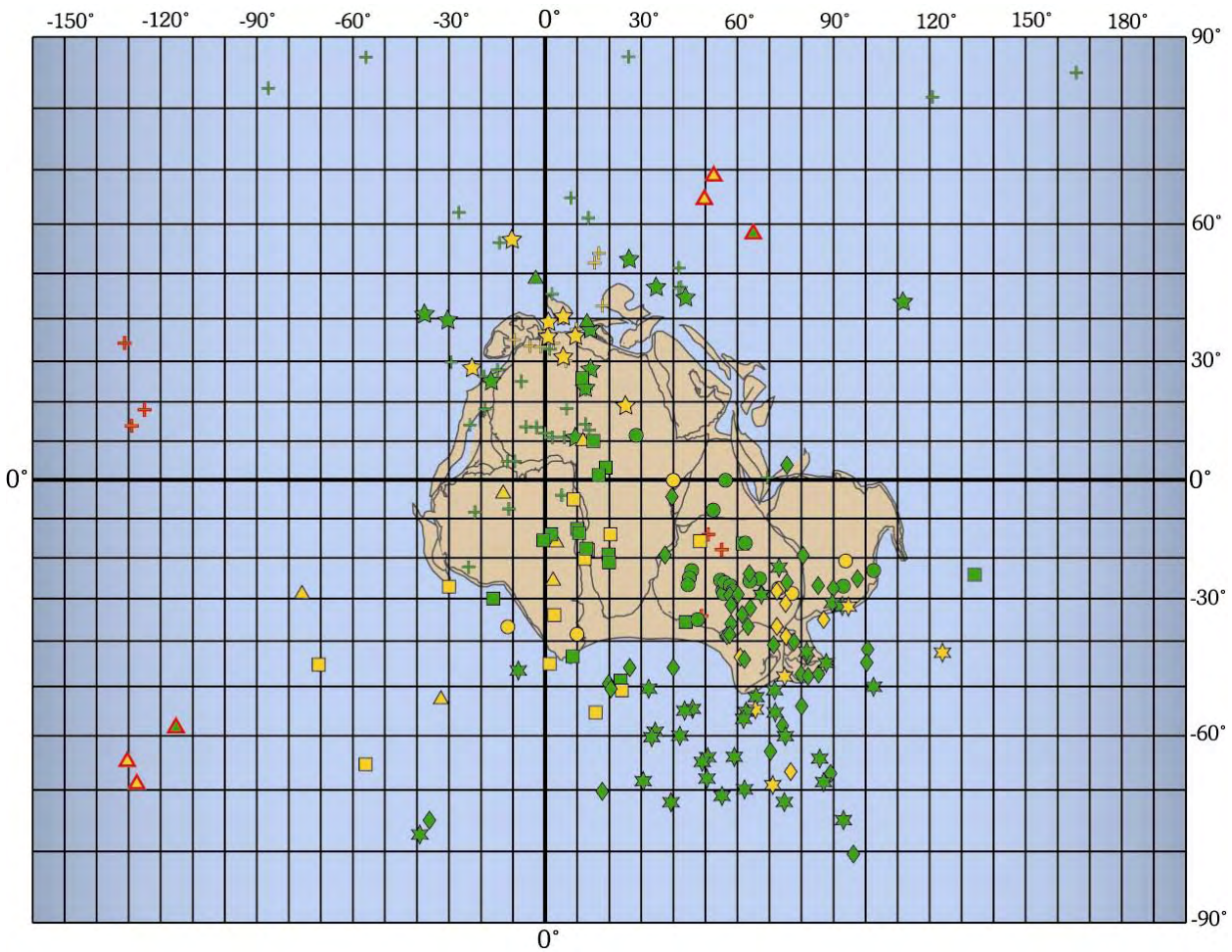


Figure 2.3: World map showing poles from the palaeomagnetic database (version 4.4; 2003) retained after the base level selection described below in §.2.4.1 (see list of poles in Annexe I). **Crosses:** Cambrian poles; **stars** (5 branches): Ordovician poles; **triangles:** Silurian poles; **squares:** Devonian poles; **circles:** Carboniferous poles; **diamonds:** Permian poles; **stars** (6 branches): Triassic and Hettangian (200 – 248 Ma) poles. Green symbols represents data coming from cratonic “green” regions; orange symbols, data from suspect “orange” regions. Symbols with a red contour are plotted twice in regard with their two possible polarities. Data presented on a reconstruction of Gondwana in African coordinates. Mercator projection.

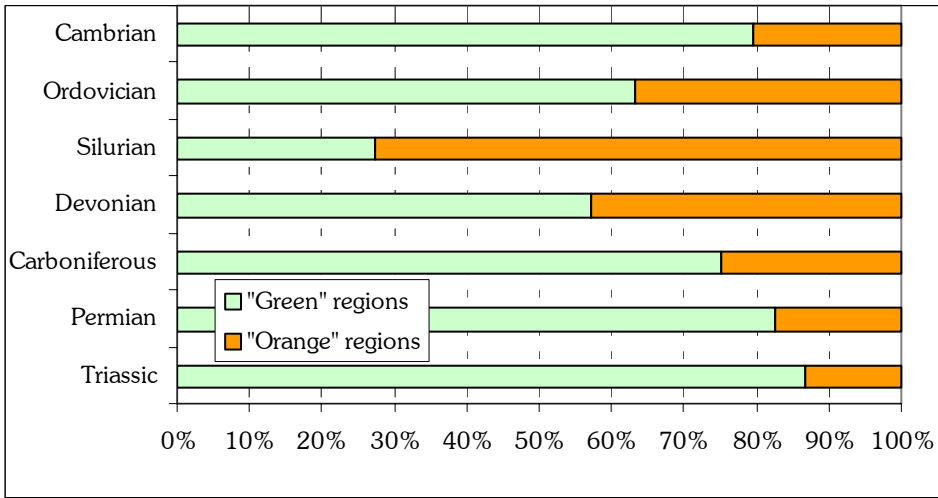
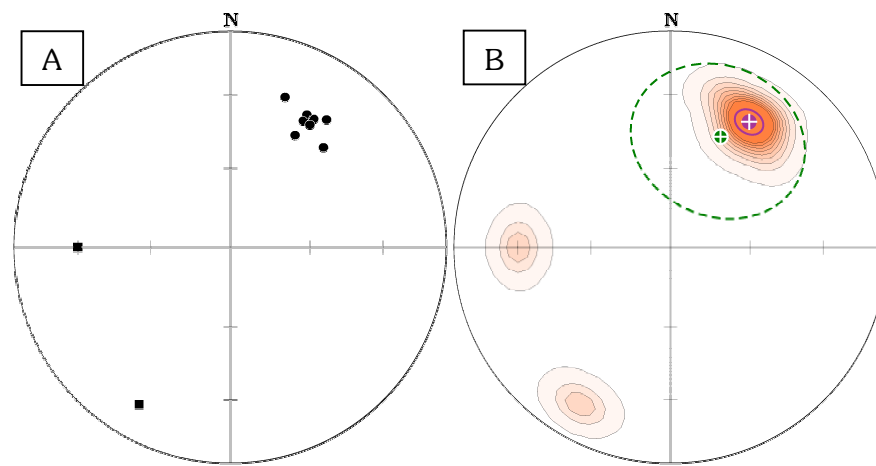


Figure 2.4: Relative proportion of data coming from suspect “orange” regions only and from cratonic “green” regions only in the selection data given in table I, Annexe I (NB: “Triassic” includes the Hettangian: 200 – 248 Ma).

Indeed, the distribution of data from “orange” regions looks, simply visually, slightly more grouped to the south-west than data from the “green” regions (looking only at squares in figure 2.3). These data might not be comparable as they could simply reflect a younger and an

older part of the Devonian segment of the APW path. However, this is not the case as the age averages per periode (note again that the “Triassic” actually includes the Hettangian: 200 – 248 Ma) are equal within their standard deviation (figure 2.6). When mean poles coming only from suspect “orange” regions or only from cratonic “green” regions are plotted per period on a map (figure 2.7), the “orange” Devonian pole does indeed plot more to the south-west than the “green” one, but the two cones calculated at the 95% confidence level are overlapping. This difference appears thus to be not statistically significant. On the other hand, the two cones have a large radius ($>16,0^\circ$). This entails that any conclusion would be rather speculative. Similarly, it would be speculative to draw any conclusion for the Silurian, while confidence cones are extremely large (about 50° , and even $>180^\circ$ for the alternate polarity with data from cratonic “green” regions: blue path).

It must be noticed in addition that mean poles from suspect “orange” data only and cratonic “green” data only for the Permian also look distinct. From a statistical point of view, their confidence cones are not separated but tangent. This problem probably stems from the fact that the “orange” mean pole is calculated from too few and scattered data, but may also reflect problems encounter for the latest Paleozoic reconstruction of Pangea.



Figures 2.5: Comparison of results obtained by mean direction and by density contours on a simulated scattered dataset.

A- Simulated data considered; squares are erroneous data.

B- the mean direction (**green dot** with white cross) is deviated from the mean direction obtained if the two erroneous data are discarded (**violet dot** with white cross), and the corresponding 95% confidence cone (**dashed green**) is large ($>30^\circ$). Conversely, the density contours (**orange**) agrees well with the mean direction without erroneous data (**violet**).

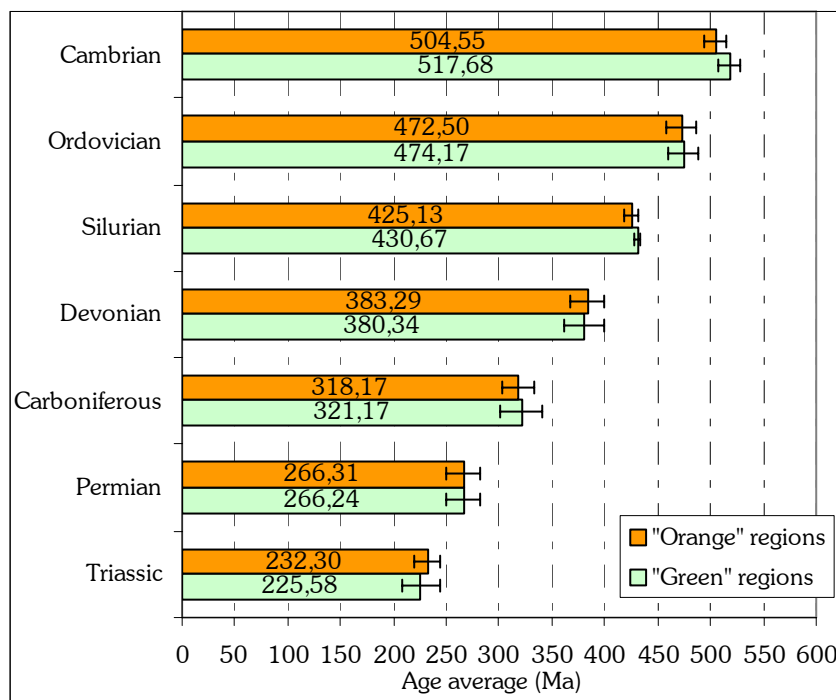


Figure 2.6: Age averages per period and their standard deviations (error bars) for selected data from “orange” and “green” regions only. It shows that data are comparable per period as they represent the same segment of time on the APW path (NB: “Triassic” includes the Hettangian: 200 – 248 Ma).

- Density peak approach

Even if mean poles may be deviated due to scattering, calculation of density contours shows a quite identical peak density for the Permian. Similarly, density peak positions from “green” and from “orange” regions are analogous.

However, the position of density peak is also particularly subject to inaccuracy when the number of data is insufficient, because two data simply closer one another by chance may then form the highest density.

Nevertheless, a good agreement between position of peak density and mean pole could be used as a good indication for the accuracy of the APW path. It is for instance very not the case for the Silurian with both polarities (figure 2.7).

- Conclusion

Hence, it seems that there is no significant difference between the two datasets is visible when viewed on a scale of the geological period.

As expected from the presentation of some published APW paths for Gondwana, major discrepancies in palaeopole positions range from Late Ordovician to Early Carboniferous in age. However, the statistical quality of all these data is not equivalent, and can be evaluated from a relative objective point of view.

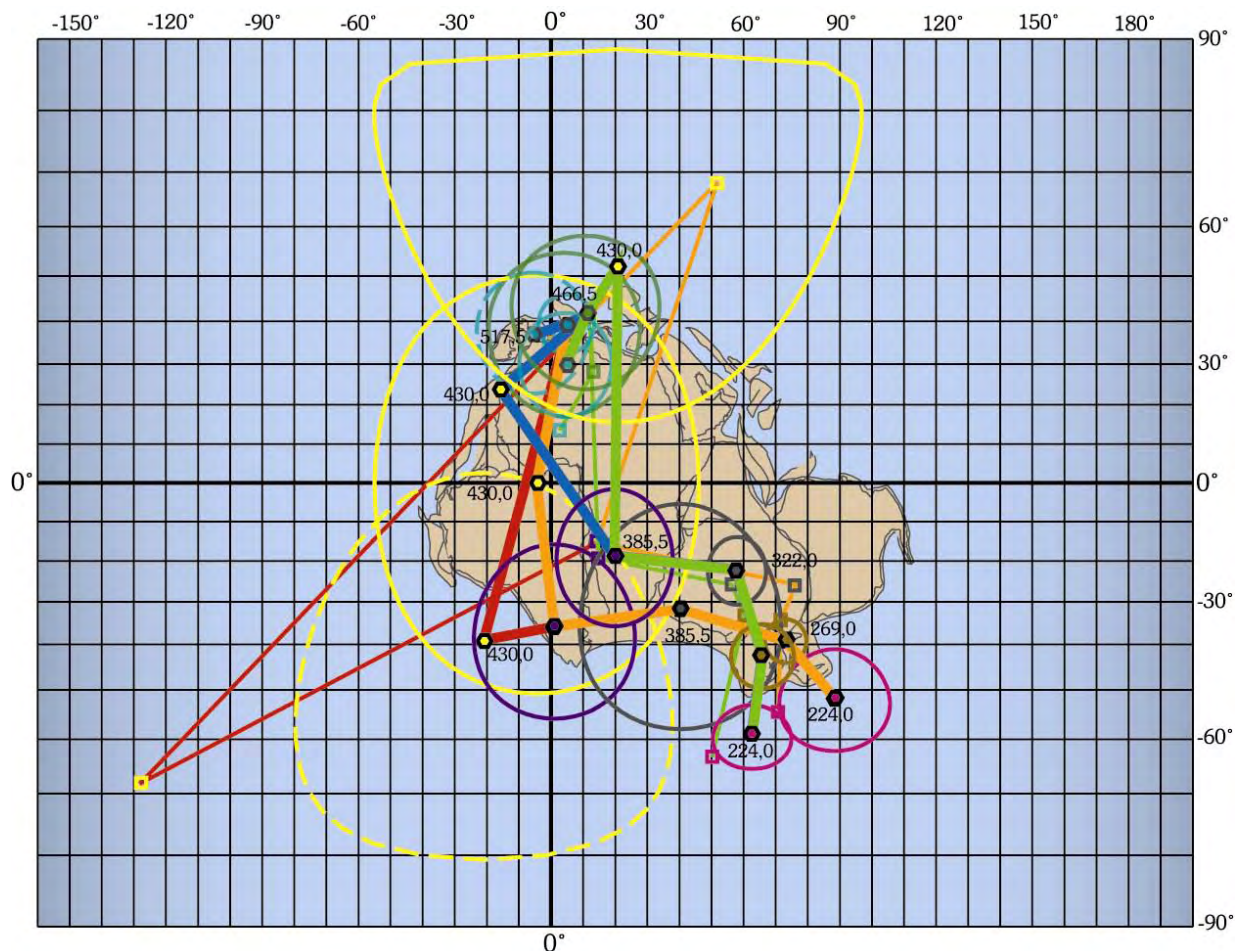


Figure 2.7: Mean pole positions per period (**hexagones**) for data coming only from suspect “orange” regions: orange path (red: alternate polarities); or only from cratonic “green” regions: green path (blue: alternate polarities). Thin lines represent paths calculated from density peaks (**squares**). Numbers are age averages for each period. Cones given at the 95% confidence level are shown with different colour for each period. **Pink:** Triassic (including Hettangian; i.e. 200 – 248 Ma); **brown:** Permian; **black:** Carboniferous; violet: Devonian; **yellow:** Silurian (confidence cone shown with dashed line for alternate polarities, but not shown for the blue path as it exceeds 180°); **green:** Ordovician; **turquoise:** Cambrian (dashed line: alternate polarities). On a reconstruction of Gondwana in African coordinates; Mercator projection.

2.4. APW paths based on “objective” data selection

2.4.1. Research of objective criteria for data selection

One of main reasons for the discrepancy between published APW paths for Gondwana is the way that data are selected and the differences in statistical significance. Van der Voo (1988, 1993) proposed seven objective criteria to assess the quality of palaeomagnetic data, resulting in the determination of a quality factor Q. These criteria are:

- 1- A well-determined rock age and a presumption that magnetisation is the same age.
- 2- Sufficient number of samples such as:
 - $N \geq 24$ (where N is the number of samples)
 - $\kappa \geq 10$ (where κ is the precision parameter; Fisher, 1953)
 - $\alpha_{95} \leq 16,0^\circ$ (where α_{95} is the radius of the cone at the 95% confidence level).
- 3- Adequate demagnetisation that demonstrably includes vectors subtraction.
- 4- Field tests that constrain the age of magnetisation.
- 5- Structural control, and tectonic coherence with craton of block involved.
- 6- Presence of reversals.
- 7- No resemblance to palaeopoles of younger age (by more than a period).

Nevertheless, it is believed here that the earlier criteria are more important than those later. Thus, four levels of selection are proposed below to account for this order:

- The “**base**” level examines all data provided by the database. This corresponds to satisfying only criterion 1 of Van der Voo (1993): presumption that rock age and magnetisation age is the same.
- The “**low**” level considers data having satisfied statistical parameters, and adequate demagnetisation. This corresponds to select in the database (I.A.G.A, 2002; McElhinny & Lock, 1996) data having a quality factor, “Demagcode” ≥ 3 ; a number of samples, $N \geq 24$; a Fisherian parameter, $\kappa \geq 10$; and a radius of the cone at the 95% confidence level, $\alpha_{95} \leq 16,0^\circ$. It is equivalent then to satisfying the three first Van der Voo’s criteria.
- The “**mid**” level adds a good age control. The age is here simply regarded as the average between the “low age” and “high age” given in the database, and the uncertainty, as the difference between the age limit and the average. The uncertainty is viewed as acceptable for this level when it does not exceed 15 Ma (i.e. age ± 15 Ma). This limit has been arbitrarily chosen, but is in the time order of an epoch (i.e. ~ 30 Ma).
- The “**high**” level accepts only data from the “mid” level having at least one positive field test (fold test, conglomerate test, contact test, reversal test).

These four levels are established in order to make selection as objective as possible. The overall dataset between 200 and 545 Ma for Gondwana is poor since:

- with data from “**green**” regions only, the base level includes 159 data, 70 for the low level, 46 for the mid level, and 14 only the high level.
- with data from both “**green & orange**” regions, the base level includes 215 data, 101 for the low level, 72 for the mid level, and 25 for the high level.

The distribution per period (figure 2.8) of the number of data from both “green” and “orange” regions is particularly demonstrative of the lack of data for Mid Palaeozoic times. It is striking to see, however, that the Mid Palaeozoic contains both the smallest number of data of “base level” (Silurian), and the highest number of data of “high” level (Devonian).

Moreover, besides the low number of Mid Palaeozoic data, most of them come from the Tasmanides, an “orange” region. Histograms, showing the provenance of data of base level coming from “green” regions only (figure 2.9-A) and from “green & orange” regions (figure 2.9-B), illustrate this problem. In addition, as soon as the low level is considered, no data from the craton (“green”) exists for the Silurian (410 – 440 Ma) anymore.

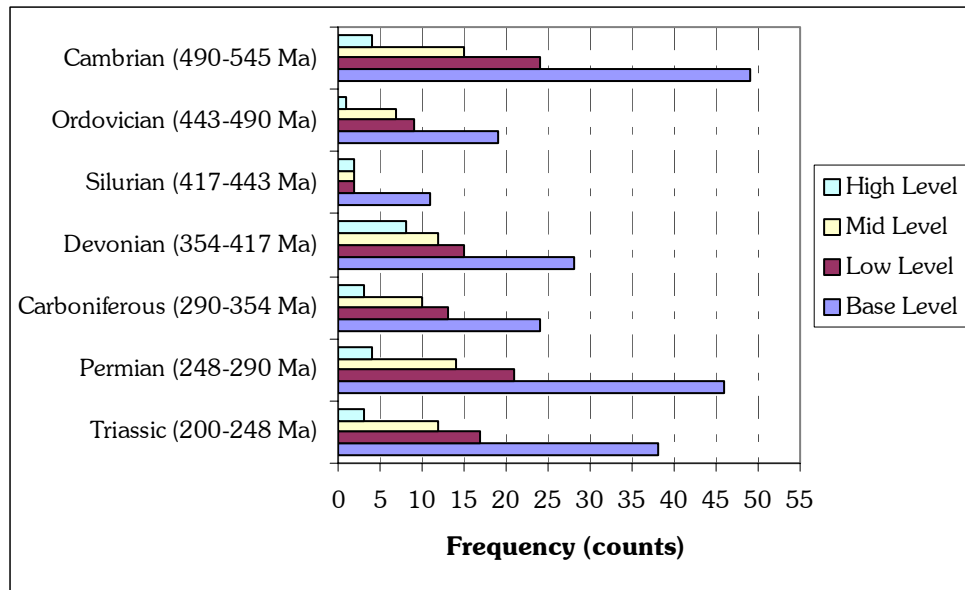


Figure 2.8: Frequency – period histogram showing the quality of palaeomagnetic poles from both “green” & “orange” regions from Gondwana. Note that Triassic times include the Hettangian (i.e. 200 – 248 Ma).

2.4.2. Calculation of APW paths according to selection levels

APW paths have been calculated every 5 Ma using a triangular sliding window of 50 Ma for each level of selection. The two possible polarities have been tested for the Silurian and Cambrian ambiguous data. This shape of sliding window (figure 2.10) is easy to apply, and avoids border effects by contrast to rectangular windows for instance. It is especially important when the number of data is low, like in the Mid Palaeozoic.

APW paths obtained for the four levels are shown below (figures 2.11 to 2.14). The corresponding directions (in the Australian coordinates, at the locality of Molong, New South Wales; Long: 150°; lat: -33°) are drawn on stereograms.

- **APW path with base-level selection**

The APW paths obtained with data satisfying the base-level selection are shown in orange when data includes suspect “orange” regions, and in green when only cratonic “green” regions are represented (figure 2.11). Paths obtained using the alternate polarities of Cambrian and Silurian ambiguous data are shown in red and blue respectively.

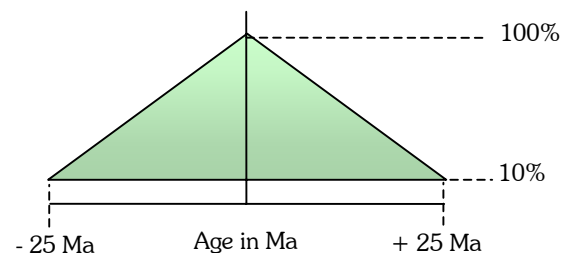


Figure 2.10: Shape of the triangular sliding window used to calculate APW paths.

The results are quite similar from 200 to 370 Ma. For Cambrian times, the main difference comes from the polarity used but not from inclusion or not of data from “orange” regions. By contrast, the question of which one of both polarities is used and where data come from plays a major role on paths for Mid Palaeozoic times. At 425 Ma for example, poles obtained may lie anywhere between Peru and Madagascar, a difference of some 6000 kilometres.

However, the general shape of the orange path including “orange” data better resembles that of Torsvik & Van der Voo (2002) whereas the red path using the alternate polarity is closer to that of Smith (1999) for the Early and Mid Palaeozoic. The position of the pole at 550 Ma in southern Mali is in any cases more similar to that of Smith (1999) than that of Torsvik and Van der Voo (2002).

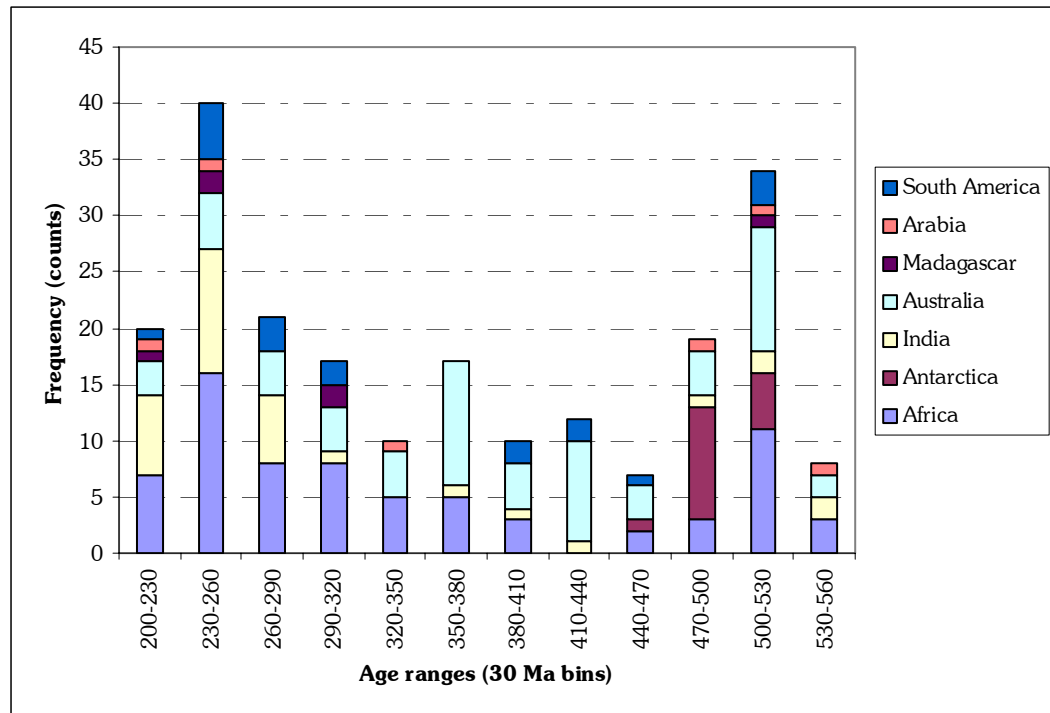


Figure 2.9-A: Frequency – age histogram showing the provenance of palaeomagnetic poles of base-level selection from “green & orange” regions of Gondwana.

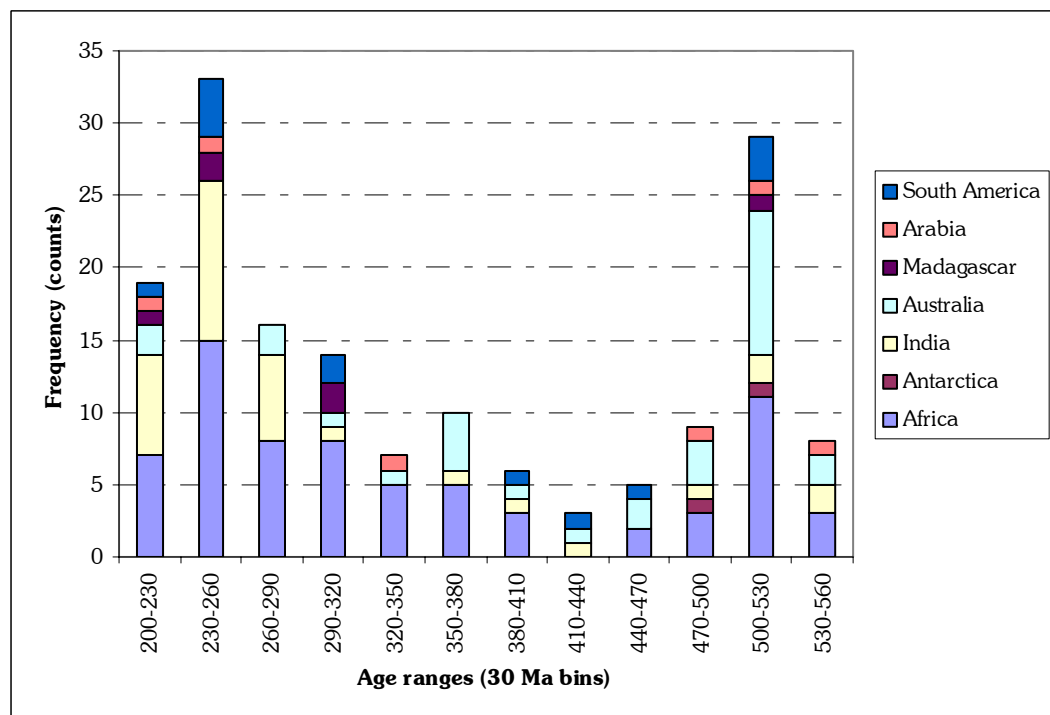
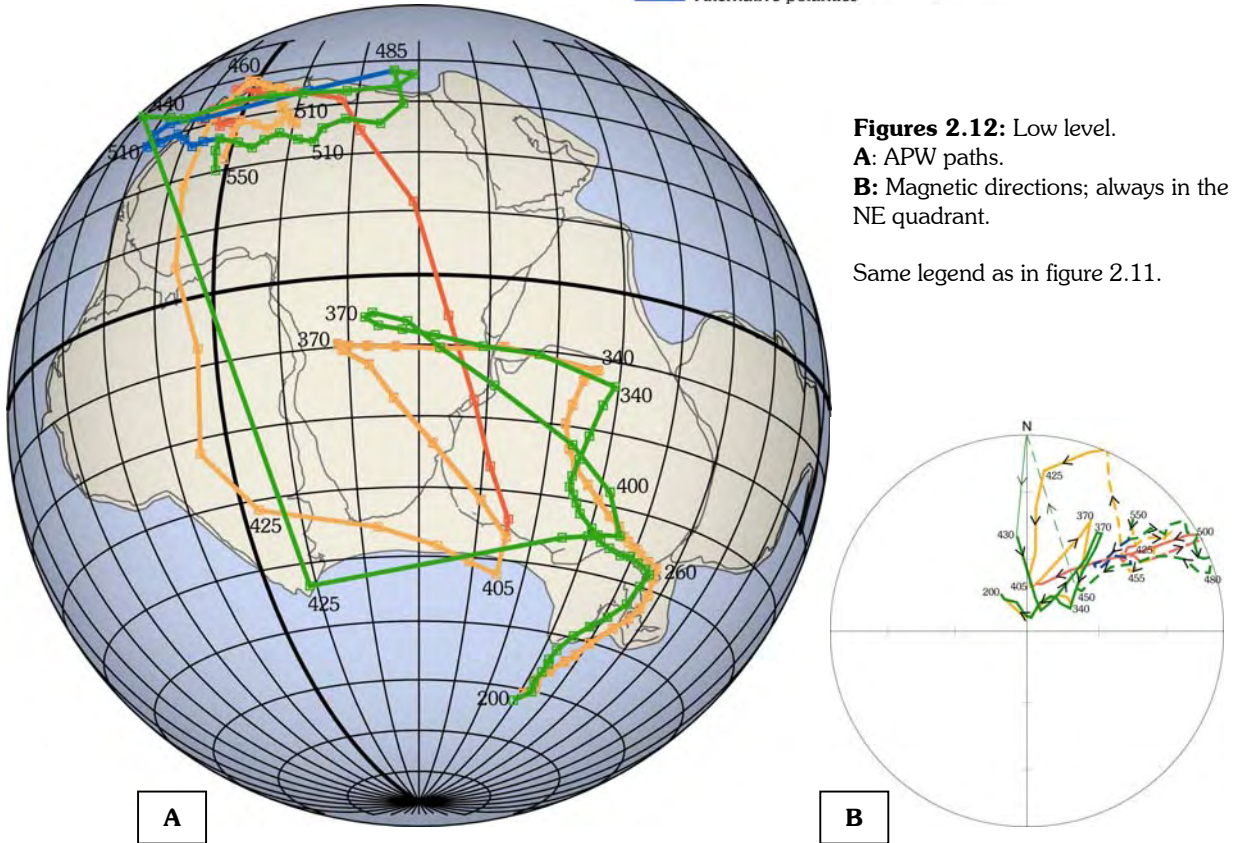
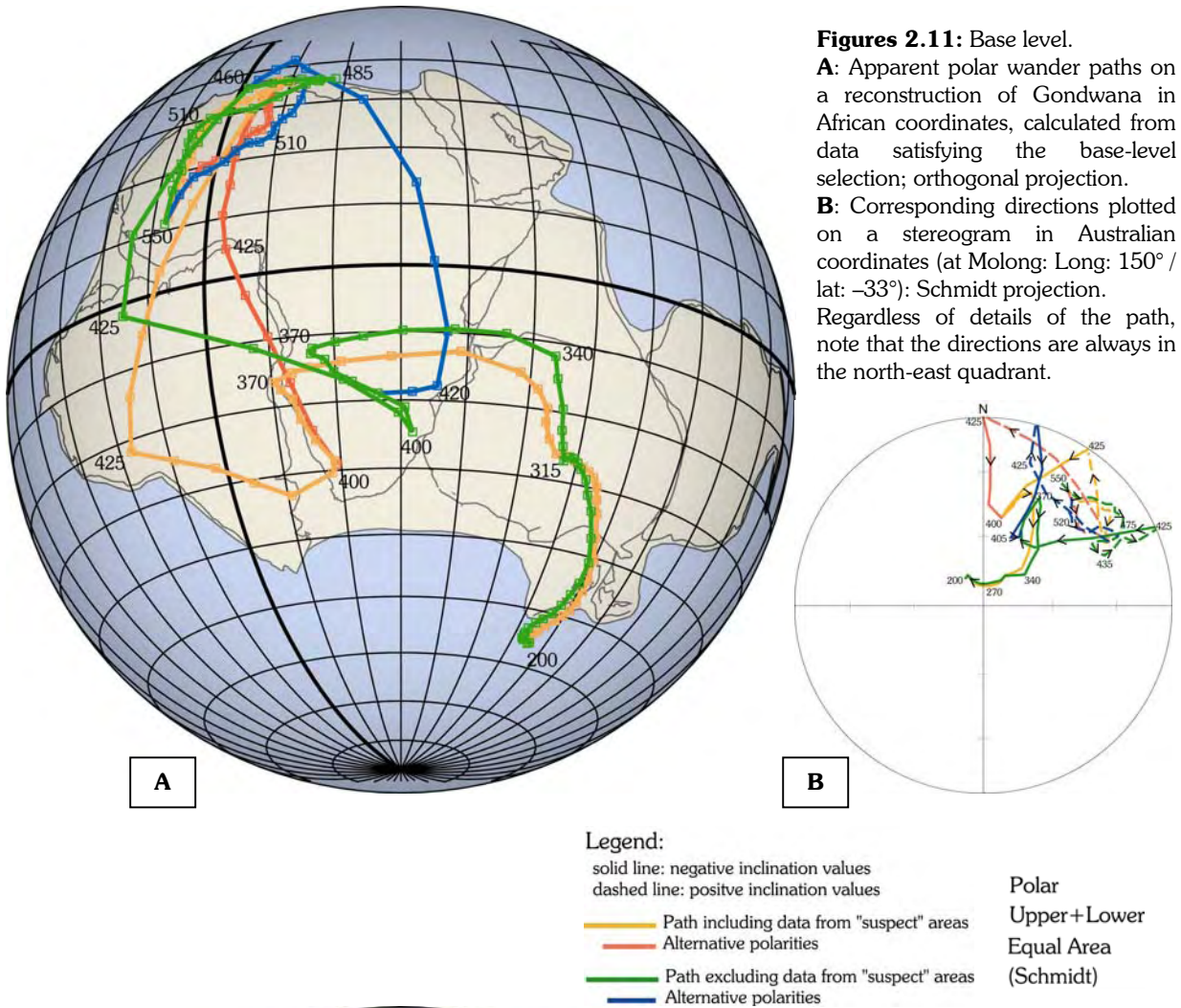
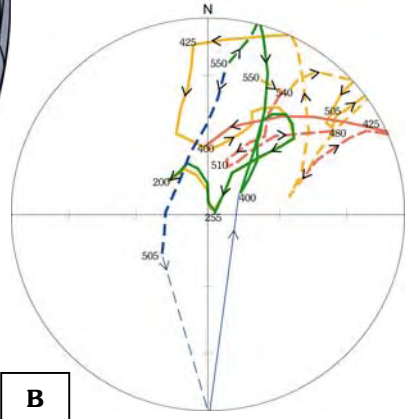
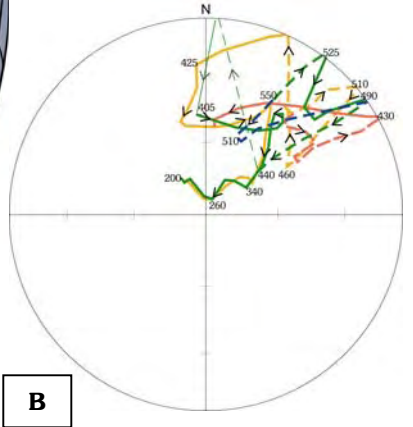


Figure 2.9-B: Frequency – age histogram showing the provenance of palaeomagnetic poles of base-level selection from “green” regions only of Gondwana.

- **APW path with low-level selection**

When only data satisfying the low level are selected, the APW paths (figure 2.12) have a very different shape for the Early and Mid Palaeozoic, but remain relatively similar for time period between 200 and 370 Ma. Uncertainty of the polarity for the Silurian only concerns paths including data from “orange” regions since such data from “green” regions have been discarded. The 550 Ma pole is moved forward to northern Mali relative to the base-level paths.





The difference between alternative polarities is more pronounced, and discrepancies appear between orange (or red) and green (or blue) paths. The Mid Palaeozoic paths are still very different according to the different choices. Poles at 425 Ma are placed either more to the south of South America or in Sudan. No data from “green” regions exist anymore between 425 and 440 Ma

- **APW path with mid-level selection**

Paths drawn with data from the mid-level selection (figure 2.13) are still in good agreement from 200 to 370 Ma. Nevertheless, the discrepancy increases for Cambrian times. The Mid Palaeozoic gap for the green path also increases with a lack of data between 400 and 450 Ma. The 425 Ma pole is either in central South America (orange path) or in Libya (red path).

- **APW path with high-level selection**

Between 200 and 370 Ma, the green and orange paths (figure 2.14) are still similar one to another, but differ significantly from paths of lower level selections. On the other hand, the green and blue paths are drastically changed because of the lack of Early and Mid Palaeozoic data. However, the position of the pole at 550 Ma is closer to positions proposed by Schmidt *et al.* (1990), Li & Powell (2001), McEhlinny *et al.* (2003) or Torsvik & Van der Voo (2002). The orange path involves a larger Siluro-Devonian loop nearly reaching -60° in latitude, and from this point of view, more similar to paths of the 1990's. On the alternate red path, the 425 Ma pole is situated somewhere in Zaire, position which surprisingly recalls the X-path of Morel & Irving (1978).

2.4.3. Significance of these APW paths

Although the real shape of the Palaeozoic APW path for Gondwana is unknown, the path obtained using high-level data and coming only from the cratonic “green” regions seems to be very unlikely. This is obviously paradoxical. Indeed, these data are supposed to be the best representative of palaeopositions of Gondwana. It seems then that what is gained in precision with a high-level selection, is lost in accuracy of the path.

Reasons for this paradox stem from the fact that the level of selection considered takes merely palaeomagnetic statistical parameters into account. However, even when these parameters reflect high level of confidence for a datum, scattering may still persists due to:

- misinterpretation of structural control, in particular at regional scale. Imprecise correction of conical or complex folds may also lead to erroneous paleopole positions (see for instance Pueyo *et al.*, 2003).
- misinterpretation of the age of the rocks. It must be kept in mind in addition, that the uncertainty on the age of the rock is very important because the 16° limit accepted for a confidence cone drawn around a palaeomagnetic result is exceeded simply with an age uncertainty superior to 17,8 Ma at a polar drift rate of 10 cm/year.
- misinterpretation of the age of magnetisation. This age is theoretically constrained by field tests, but a large time interval can exist between the age of the rock and the age of magnetisation. On the other hand, it is still possible that confusion between primary magnetisation and overprint occur although a positive fold test has been obtained.

It appears that this reason must be invoked, for example, for the “ambiguous” Cambrian data (cross with red contour in figure 2.3) from the Sidi-Said Maachou Volcanics (Khattach *et al.*, 1995). Most of the other Cambrian plot in North-West Africa or northern South America (in African coordinates) whereas this datum plot in Antarctica. It better corresponds to the position of Carboniferous data. Hence, the fold test seems to have been erroneously interpreted as positive, and this result might represent a Carboniferous magnetisation.

It is believed also that some results reported by Goleby (1980) from the Lachlan Orogen and similar to some obtained for this study are also erroneous (see Chapter 3 & 5). It is indeed thought that positive fold tests have been obtained by mixing Palaeozoic magnetisation with present-day or recent overprint. The improvement in clustering of the directions of magnetisation by tilt correction is interpreted as coincidental.

The suspicious reliability of those last data is clear, but such error potentially exists for any entries in the database. A sufficient number of data must be therefore maintained to average out data scattering whatever the level of selection considered.

Since the increasing level of selection discards palaeomagnetically erroneous data but decreases drastically their number, all the paths calculated above are to a certain extent equivocal.

However, an important results from these APW paths, is the fact that almost all directions of magnetisation (at the locality of Molong; Long.150° / lat.-33°) for the Palaeozoic lie in the North-East quadrant of a stereogram with negative values for the Mid – Late Palaeozoic and positive for the early Palaeozoic (except with high level data from “green” regions only). It will be shown in the following chapters that most of the palaeomagnetic results obtained for this study do not plot in that quadrant.

2.5. Comparison of APW paths obtained by mean pole positions and by density peak positions

2.5.1. Synthetic APW path from mean pole positions

If objectivity is to be maintained, a compromise must found in data selection. It can be stated from the previous APW paths that:

- 1- The number of data in the database is too low. For example, only 7 data exist between 440 and 470 Ma (figure 2.9-A), although data from suspect “orange” regions are included. Smith’s approach (1999), consisting in using all the available data in order to average scattering, is interesting but is not valid with the current database.
- 2- As errors cannot be averaged using Smith’s approach, data of base level at least have to be discarded, since they do not have a sufficient statistical significance. In addition, it is considered that the maximum radius for the confidence cone must be 16° (see Van der Voo, 1993; and references therein). With a reasonable drift rate of 10 cm/year, an age uncertainty of ± 20 Ma already surpasses 1779 km – i.e. 16° – of “acceptable” error. In other words, the uncertainty of ± 15 Ma chosen for the mid level selection here is less than an equivalent error of 16° when the drift rate is slower than 11,8 cm/year. By comparison, the oft chosen uncertainty of ± 25 Ma reaches this limit for a rate of 7,1 cm/year. Thus, data with large age uncertainty have to be discarded as well, to maintain a consistent statistical significance, and the low level of selection has not enough constraints on data quality. However, it is difficult to choose a limit as age uncertainty usually increases with older ages.
- 3- High level data are not better grouped as data satisfying lower levels of selection. This means that the high level of selection is probably necessary, but not sufficient to affirm that data are of high quality. Therefore, because of the low number of data of this level, the large scattering and temporal gaps obtained, confidence cones are so large that it prevents any conclusive interpretations.

In conclusion, if the maximum objectivity is to be maintained in data selection, the mid-level selection appears to be the best compromise between statistical significance and sufficient number of data. A limit of age uncertainty of ± 15 Ma however, is perhaps too strict and discards data, which could probably be really representative of the APW path for Gondwana. A linear increase of uncertainty limit from ± 15 Ma to ± 25 Ma in data selection can be conceived in order to account for the general tendency that, the older the rocks are, the larger the age uncertainty is.

From this alternative selection, a synthetic APW path has been calculated every 5 Ma (figure 2.15) using the triangular sliding window presented above (figure 2.10). The shapes of the orange path and the green path are relatively similar to one another and also to the

APW path proposed by Torsvik & Van der Voo (2002), which has been produced in an analogous manner. Nevertheless, the associated cones calculated at the 95% confidence level are in general too large to be conclusive, and the envelope is shown only when it does not exceed 30°.

2.5.2. Density contours

It has been shown (figure 2.5) that erroneous data may induce a large deviation of the mean value, whereas density peaks (calculated from density contours computed here with a Gaussian model; $K=100$) are expected to be less influenced. In addition, agreement between density peaks and mean values is interpreted as a good indication for the accuracy of the pole position obtained.

This idea has been tested by comparing the mean values and the density peaks obtained from the alternative selection of data (figure 2.15).

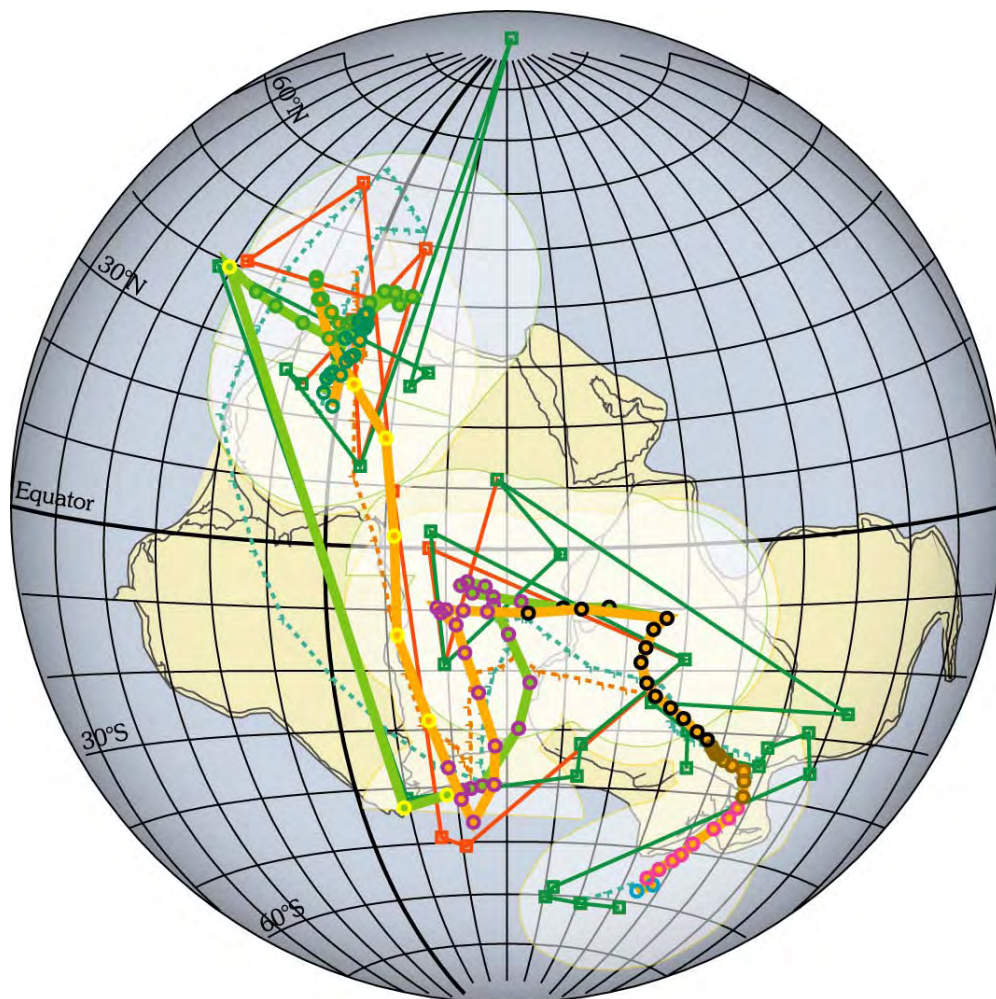


Figure 2.15: Comparison between mean values and density peaks obtained on a synthetic level of selection. APW paths obtained from data of both “orange” & “green” regions (orange path) and only from “green regions (green path).

Dots correspond to mean poles calculated every 5 Ma, and the envelop of their confidence cones (α_{95}) is shown, except when they exceed 30°. Their colour represent different periods: **blue**: Hettangian; **pink**: Triassic; **brown**: Permian; **black**: Carboniferous; **violet**: Devonian; **yellow**: Silurian; **green**: Ordovician; and **turquoise**: Cambrian.

Squares are positions of peak density every 5 Ma. Dashed lines with **plus** shown every 5 Ma correspond to smooth paths calculated from peak density positions.

In African coordinates; grid spacing: 10°, heavy lines at lat.0° and Long.0°; Schmidt projection.

Unfortunately, comparison between APW paths obtained from mean values and from density peaks shows that a lot of density peaks are quite away from the mean values, and the paths are much more scattered. Again, this result probably stems from the fact that

palaeomagnetic data are not clustered enough. Indeed, most of the peaks are actually calculated on two or three data only – perhaps simply closer one another by chance – even if the number of data bracketed by the window is larger.

However, smoothing the paths obtained by density peaks with the triangular window yields a good match between density peaks and mean values for Late Palaeozoic times. Large difference remains whether data from “orange” regions are included or not for the Early – Mid Palaeozoic. Nevertheless, such smoothing corresponds to encountering the problem as the one found with mean values, *i.e.* deviating the peak density position.

2.6. Alternative approach: APW path from Small Circles Fit

It appears very difficult to determine a sufficiently reliable APW path for Gondwana using a smoothing method (here, a triangular sliding window) on data selected with “objective” criteria only (at least, as objective as possible). It shows also that the palaeomagnetic dataset contains currently not enough accurate data to choose this way between the X-type and the Y-type shapes for the APW path for Gondwana given the huge cones obtained at the 95% confidence level.

Consequently, a different approach should be found. One may consist in assuming that motion of continent does not fundamentally vary during a certain period of time. It is indeed difficult to conceive that a continent as large as Gondwana had many complex movements implying many small loops for its APW paths. A rough approximation consists therefore in determining the best small circle that fit the data. This method becomes of course subjective, as a period of standstill position of the Euler pole must be arbitrarily defined.

On the basis of shapes of the published APW paths (§.2.1 above, and figures 2.1), four periods are chosen: a ~Late Proterozoic-Cambrian (570-500 Ma), an ~Early Palaeozoic (490-390 Ma), a ~Late Palaeozoic (390-230 Ma), and an ~Early Mesozoic (230-175 Ma) periods of time.

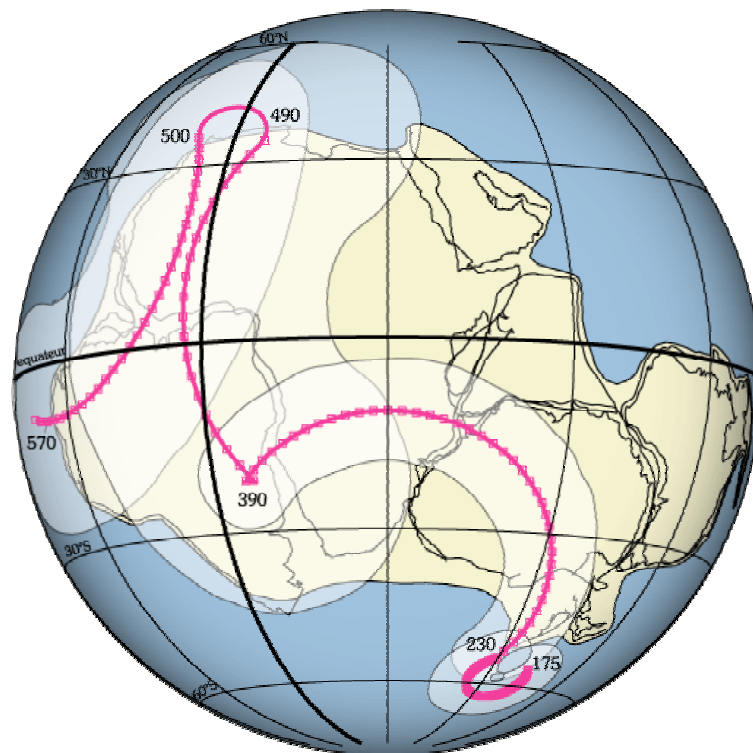


Figure 2.16: APW path obtained by fitting small circles on data from cratonic “green” regions only. Each square corresponds to a rotation of 5° around the Euler poles for the following period:

- **570 – 500 Ma:** $P_{E\text{Long}}.324,80^\circ$ / $P_{E\text{lat}}.19,70^\circ$ ($\alpha_{95}=18,0^\circ$; $\theta=28,4^\circ$; $APDR=10,96\pm 6,27$ cm/year).
- **490 – 390 Ma:** $P_{E\text{Long}}.036,10^\circ$ / $P_{E\text{lat}}.05,80^\circ$ ($\alpha_{95}=23,8^\circ$; $\theta=39,4^\circ$; $APDR=6,70\pm 3,29$ cm/year).
- **390 – 230 Ma:** $P_{E\text{Long}}.030,00^\circ$ / $P_{E\text{lat}}.-37,20^\circ$ ($\alpha_{95}=8,0^\circ$; $\theta=26,1^\circ$; $APDR=5,96\pm 1,69$ cm/year).
- **230 – 175 Ma:** $P_{E\text{Long}}.063,90^\circ$ / $P_{E\text{lat}}.-58,20^\circ$ ($\alpha_{95}=5,9^\circ$; $\theta=5,0^\circ$; $APDR=4,67\pm 5,07$ cm/year).

$P_{E\text{Long}}$ and $P_{E\text{lat}}$ are the longitude and latitude of the Euler pole; α_{95} is cone calculated at the 95% confidence level around the rotation axis; θ , the angular opening of the cone to draw the small circles; and APDR, the apparent polar drift rate. Orthogonal projection.

The changes in apparent drift direction might be associated with some postulated geological events, such as: the end of amalgamation of Gondwana and/or the break-up of

Rodinia/Pannotia in the Cambrian (see §.1.3.1; Chapter 1), the Caledonian Orogeny and the possible “soft” collision between Laurentia and Gondwana in the Devonian (see for instance Dalziel *et al.*, 1999; Young *et al.*, 2000; McKerrow *et al.*, 2000), and the Hercynian Orogeny and formation of Pangea in the Late Carboniferous – Permian. These associations are obviously largely speculative, but can be similarly called upon for the changes in the general direction of apparent polar drift for the published APW paths presented above (§.2.1).

A selection similar to that presented in §.2.5.1 (the “synthetic” selection) has been done on a slightly larger dataset. Indeed, a reasonable small circle was rather difficult to obtain for the Cambrian. Data selection has been then extended to the Late Neoproterozoic (up to 570 Ma), and for similar reason, in the Jurassic (down to 175 Ma). All data come from cratonic “green” regions only. Four positions of Euler poles with their associated 95% confidence cones have been calculated, and an average of the apparent drift rate of the pole can be evaluated for every periods of time.

The general pattern for this path (figure 2.16) looks a good possible alternative to APW paths previously shown. Moreover, almost every published paths shown in §.2.1 lie within the envelop of the confidence cones obtained from the small circles fit.

This kind of fit however has to be regarded with much caution. The corresponding drift rates for a locality situated at 90° from the pole (*i.e.* the maximum relative drift values) are $23,03 \pm 1,13$ cm/year, $10,56 \pm 0,90$ cm/year, $13,55 \pm 0,13$ cm/year, and $53,58 \pm 0,28$ cm/year for the four periods of times, *i.e.* 570-500, 490-390, 390-230, and 230-175 Ma, respectively. The latter drift rate seems unrealistic even if the path pattern looks reasonable. It illustrates that a kink is probably necessary in this segment. Hence, subjective limits must be fixed concerning the duration of more or less standstill position of the Euler poles on the one hand, but also concerning the age (and apparent polar position) when the APW path trend changes in direction on the other hand.

In conclusion, pole positions for Gondwana may correspond to these small circles fits within their envelopes confidence but the detail of the path is likely to be incorrect and therefore movements deduced from Euler poles would be misinterpreted.

2.7. Mesozoic and Cainozoic APW path for Australia

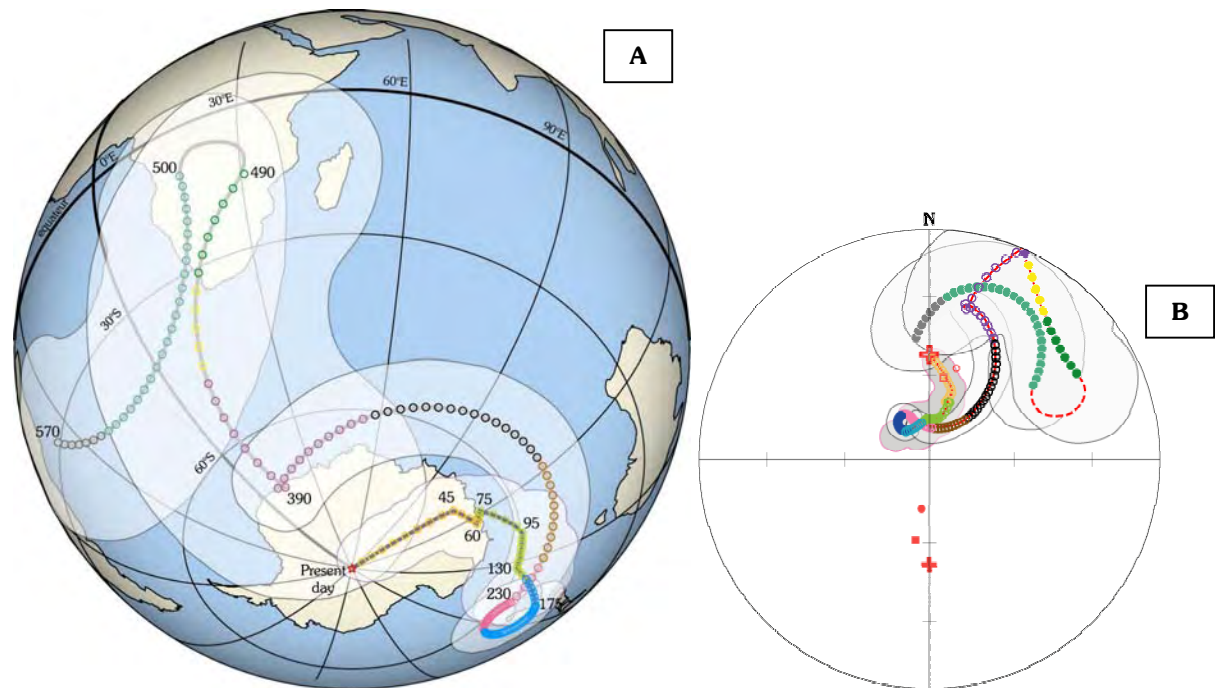
As shown in figures 1.6 (§.1.3.3; Chapter 1), the movements of tectonic plates relative to one another are well-constrained. Controversy bears upon motions relative to a reference frame. Usually, this reference frame is deduced from hotspots considered fixed (for instance Besse & Courtillot, 1991), but recent studies argue this not the case, at least for some of them (DiVenere & Kent, 1999; and Courtillot *et al.*, 2003, who propose however, that three types of hotspots can be distinguished on Earth, among which some can be considered as fixed). Errors however, can be regarded as small, in particular compared to those for the Palaeozoic (see confidence cones given by Besse & Courtillot, 1991).

The Global Isochron Chart of Royer *et al.* (1992) has been used to rotate precisely Australia in its corresponding palaeopositions and data have been interpolated between chrons in order to draw an APW path every 5 Ma from 0 to 200 Ma.

This path is shown in Australian coordinates (figure 2.17-A) associated with the “path-pattern” deduced from the small circles approach for easier general overview. The corresponding magnetic direction expected at the locality of Molong, New South Wales (Long.150°/lat.-33°) is also presented (figure 2.17-B).

An important conclusion when results for Cainozoic-Mesozoic and for Palaeozoic are combined is that pole positions from the Permian to the Cretaceous cannot be distinguished given the overlap of the 95% confidence cones. It must be also noticed that 1- as the largest majority of directions of magnetisation shown in figures 2.11 to 2.14, every points for the

Palaeozoic drawn from the small circles fit approach plot in the North-East quadrant of the stereogram, and 2- it seems that all directions for poles older than mid Carboniferous have an inclination value lower than 60° (i.e. $[-60^\circ; +60^\circ]$), whereas all younger directions have a steeper inclination value, except for the present-day and Neogene.



Figures 2.17: **A-** APW path for Australia from 0 to 175 Ma and prolonged by the “path-pattern” from 175 to 570 Ma deduced from small circles fit. In Australian coordinates; orthogonal projection. **B-** Corresponding magnetic directions plotted on a stereogram for the locality of Molong, New South Wales (Long.150°/lat.-33°); Schmidt equal area projection. Open (closed) red cross represents the magnetic direction corresponding to the geographic North (South) pole (D.000°/I.-52,4°); open (closed) red square, the present-day North (South) dipole field (D.009,7°/I.-60,6°); and open (closed) red circle, direction for the true North (South) magnetic pole (North pole: D.016,4°/I.-56,1°; South pole: D.188,6°/I.+72,2°).

Red symbols correspond to present-day pole position or magnetic direction; **orange** for Cainozoic; **light green** for Cretaceous; **blue** for Jurassic (beyond 175 Ma, data are calculated from small circle fits, and results are shown in darker blue on the stereogram); **pink** for Triassic; **brown** for Permian; **black** for Carboniferous; **violet** for Devonian; **yellow** for Silurian; **dark green** for Ordovician; **turquoise** for Cambrian; and **grey** for Late Neoproterozoic. For the path deduced from small circles, ages are assigned given a regular drift rate between the ages taken as limit for standstill positions of Euler poles. White and grey shaded areas correspond to envelopes of the 95% confidence cones.

2.8. Conclusions about the APW path for Australia-Gondwana

As a conclusion, having looked at various methods of defining the path objectively, it appears that the data are not satisfyingly discriminating when only objective criteria of selection are used. This problem cannot be satisfyingly overcome by changing the method used to draw APW path and stems merely from the crucial lack of Palaeozoic data for Gondwana.

Consequently, as long as the number of data in the database is so low, the best solution to determine an APW path is probably to adopt a subjective way to select data, which implies to discuss the quality of every single data used. It is believed that such work leads to produce either the X- or Y-type APW paths. The two best examples are probably the X-type path proposed by Bachtadse & Briden (1991) and the Y-type path of Schmidt *et al.* (1990).

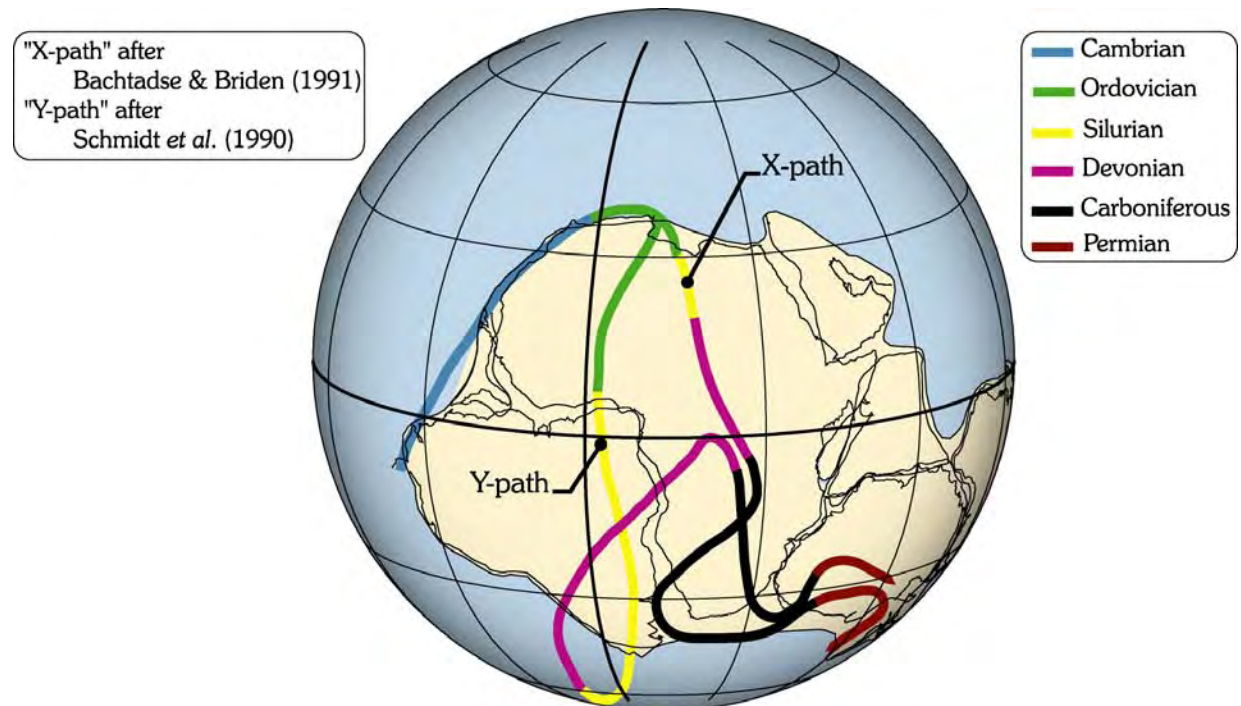


Figure 2.18: The two schools of thought about the shape of the APW path for Gondwana. The X-path, here after Bachtadse & Briden (1991), runs more or less directly through Africa during the mid Palaeozoic. The Y-path, after Schmidt *et al.* (1990), involves a Siluro-Devonian loop mainly based on palaeomagnetic data from the Lachlan Orogen. Ages of the segments of these paths are colour coded. Reconstruction of Gondwana in African coordinates; orthogonal projection.

Applying a method such as a sliding window to a dataset will always give a result, and can even yield relatively reasonable statistical values (e.g. confidence cones). This does not mean that results are directly acceptable. It has been shown here that “high quality” data in particular have a great scattering due to factors (intermediate direction of magnetisation, age of magnetisation, structural control and in particular block/terrane rotation, etc...), which cannot yet be objectively discriminated from the palaeomagnetic database. Thus, precision does not mean accuracy, and subjectivity must be introduced in data selection. It implies that the APW path proposed by Smith (1999), and to certain extent, that of Torsvik & Van der Voo (2002) are probably not selective enough, since they use the larger number of “acceptable” data available.

Nevertheless, although the Small Circle Fit is a subjective approach since periods of standstill position of Euler poles must be defined, it is also a relatively objective method compared to others, which is much less sensitive to data scattering. This means that it is a rough but possibly a good approximation of palaeopole positions. It is however relatively in contradiction with published APW path such as that of McElhinny *et al.* (2003; figure 2.4-C), which involves rapid changes in drift direction (see the Late Cambrian – Early Ordovician hairpin).

The definition of zones, where palaeopole positions for Gondwana can be expected, is necessary both to be able to speak about possible terrane displacement and/or rotation and to recognise probable remagnetisations. By obtaining a 95% confidence envelope with the Small Circle Fit approach, which in addition encompasses most of the published APW paths shown above, makes the definition of such zone possible.

Hence, in order to prevent favouring *a priori* one or the other type of path, palaeomagnetic results obtained for this study will be shown first in parallel with the Mesozoic – Cainozoic and the Small Circles Fit path as defined in §.2.6 (figures 2.17) merely for comparison purposes. Concerning the discussion and conclusions about the origin of the terranes and the palaeogeography of the southern Tasmanides however, the X- and Y-paths (figure 2.18) representing the two schools of thought about the shape of the APW path for Gondwana will be used.

Summary of chapter 2

Understanding the tectonic evolution of the southern Tasmanides of Australia and detecting possible terrane displacement and/or rotation is a rather difficult task without any reference path for Gondwana. Many were published in the last few decades, and some are presented herein. What distinguishes them is basically the approach used to select palaeomagnetic data upon which they are based.

- The first approach is very subjective since it consists in using only palaeomagnetic data, for which one has a good knowledge. The credibility of the APW path obtained can be questioned, since it usually ignores information yielded by other studies.
- The second approach is to consider all available data and to argue for each of them possible reasons for the discrepancy observed in the entire dataset. This approach is of course also subjective. However, it is believed here that this process leads to end up with the two schools of thought concerning the Palaeozoic APW path for Gondwana, *i.e.* the X-path of Bachtadse & Briden (1991) and the Y-path of Schmidt *et al.* (1990).
- The third approach intends to be as objective as possible. In this case, all available data are selected, perhaps automatically filtered, and the best solution is determined using a smoothing method.

These approaches are briefly discussed and an attempt is made herein to assess whether a selection as objective as possible can lead to a significant improvement.

By looking at several methods, it is shown that this process is simply not adapted for Gondwana given the critical paucity of palaeomagnetic data in particular of Mid Palaeozoic age. Nevertheless, the definition of zones, where palaeopole positions for Gondwana can be expected, is necessary both to be able to speak about possible terrane displacement and/or rotation and to recognise probable remagnetisation. This is made possible by obtaining a confidence envelope with a Small Circle Fit approach, which also encompasses most of the published APW paths previously presented. In addition, the Global Isochron Chart of Royer *et al.* (1992) and its reference frame has been used to rotate precisely Australia in its corresponding palaeopositions and data have been interpolated between chrons in order to draw an APW path every 5 Ma from 0 to 200 Ma. An important conclusion with the path obtained for the whole Phanerozoic is that, on a stereographic projection, 1) all points for the Palaeozoic drawn from the small circles fit approach plot in the North-East quadrant of the stereogram, and 2) it seems that all directions for poles older than mid-Carboniferous have an inclination value lower than 60° (*i.e.* [-60°; +60°]), whereas all younger directions have a steeper inclination value, except for the present-day and Neogene.

In order to prevent favouring *a priori* the X- or Y-type of path, palaeomagnetic results obtained for this study will be shown first in parallel with this Phanerozoic path simply for comparison purposes. Concerning the discussion and conclusions about the origin of the terranes and the palaeogeography of the southern Tasmanides however, the X- and Y-paths representing the two schools of thought about the shape of the APW path for Gondwana will be used.

Chapter 3

Tectonic history of Australia

3.1. Physical presentation of Australia

Australia can be divided into two main parts, already visible on a topographic map (figure 3.1-A). The two western thirds constitutes the craton, mainly Precambrian in age. It is anomalously thick (see for instance Scheibner, 1996) and elevated as it commonly reaches 900 m or more in altitude. The eastern third is believed to have a Palaeozoic basement, and corresponds to the Tasmanides (or Tasman Fold Belt System). A mountain range relief, the Great Dividing Range, lies along the coast. Its highest point, Mount Kosciusko, reaches 2230 meters, which can be viewed as also anomalously high given the age of formation of the Tasmanides (see below). By contrast, west of this range, exists a wide zone of low-lands, even being below the sea level in the north of the Flinders Ranges in Southern Australia. These two parts are also clearly visible on an aeromagnetic image (AGCRC, 2001), where the craton is represented by rough colours and the Tasmanides, by smooth colours (figure 3.1-B). It must be noticed also that the craton is cross-cut by major faults (figure 3.1-B). The mainly Carboniferous Alice Spring Orogeny of Central Australia – a poorly understood intraplate orogeny – takes place along such major faults.

The boundary between these two parts is called the Tasman Line. This line is considered to delimit the Proterozoic rocks of the craton to the West from the Palaeozoic rocks of the Tasmanides to the East. In detail, drawing this line on the field is very difficult as Proterozoic and Palaeozoic outcrops are scattered over this zone. This has resulted in different shapes of the Tasman Line according to different authors. However, in general, the line runs from the Kangaroo Island to the south, along the Flinders Ranges, back to the west in the Sturt and the Simpson deserts, extents to the north-west around the Cloncurry Plateau, and to the north to the York Peninsula (see figure 3.2; see in particular Scheibner, 1996 and also the recent paper of Direen & Crawford, 2003).

Field work has been concentrated in the state of New South Wales in collaboration with Richard Glen, Ian Percival, and Kingsley Mills from the Geological Survey of New South Wales. Sampling has being focused on Early and Middle Palaeozoic rocks of the Tasmanides. These rocks are often poorly exposed but however, more accessible in areas of higher relief (figure 3.3).

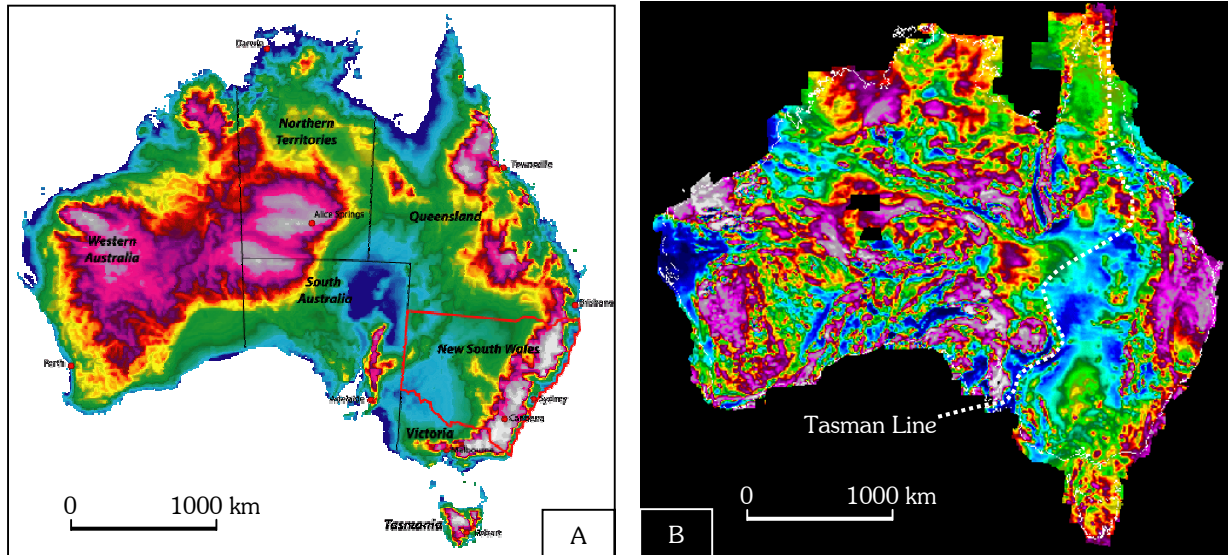


Figure 3.1-A: Topographic map of Australia showing the high-elevated craton to the West (in purple [700-800 m], pink [800-900 m], grey [900-1000 m] and white [>1000 m]), the low-lands of South Australia (in dark blue [<100 m]) to the North of the Flinders Ranges, and the Tasmanides corresponding to the third eastern part of Australia including the Great Dividing Range along the coast. We focused our work in New South Wales, here outlined in red.
B: Aeromagnetic image of Australia (from the ACGRC, 2001). The rough colours on the western two third of Australia correspond to the craton. This image shows clearly major faults cross-cutting it. East of the Tasman line, coloration is smoother and corresponds to the Tasmanides.

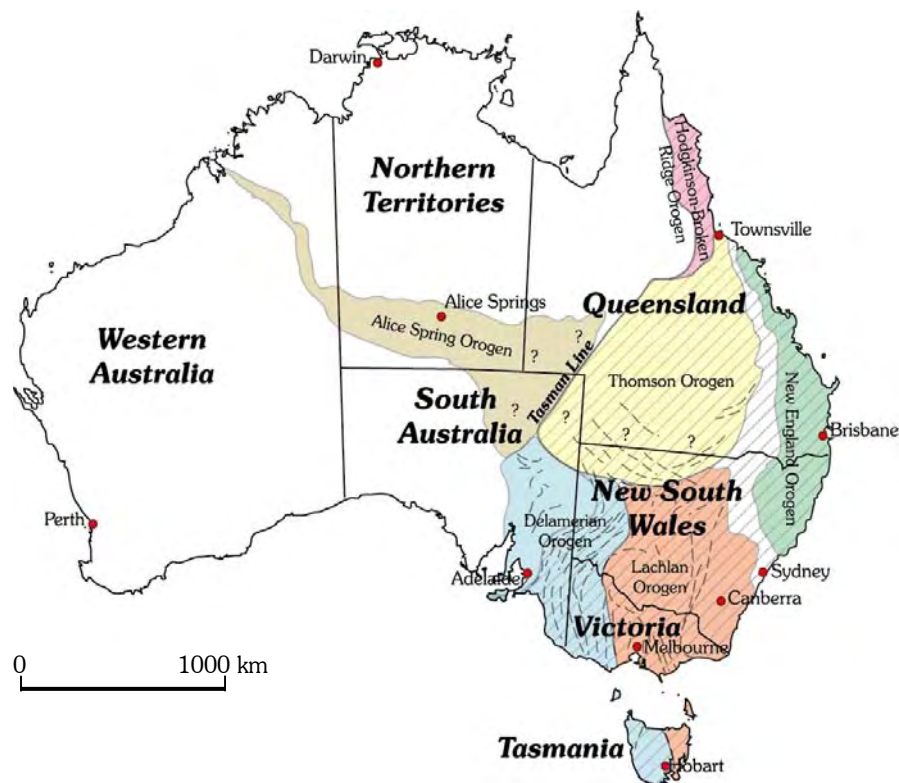


Figure 3.2: Main entities of Australia. The Tasman Line separates the craton to the West (white) from the Tasmanides to the East (hatched line). The craton is cross-cut by faults along which the mainly Carboniferous Alice Spring Orogeny (brown) took place. Its south-eastern corner is also deformed by the Cambrian Delamerian Orogeny. The Tasmanides are divided in three main parts: the Delamerian Orogen (blue); the Lachlan Orogen (red) and its possible northern continuation, the Thomson (yellow) and the Hodgkinson – Broken Ridge (pink) orogens; and the New England Orogen (green). The Thomson Orogen is mainly inferred from interpretations of trends (dashed lines) in gravity and aeromagnetic images. The boundary between the New England Orogen and the rest of the Tasmanides is not clearly defined because it is covered by the Permo-Triassic Sydney – Bowen Basin (hatched white).

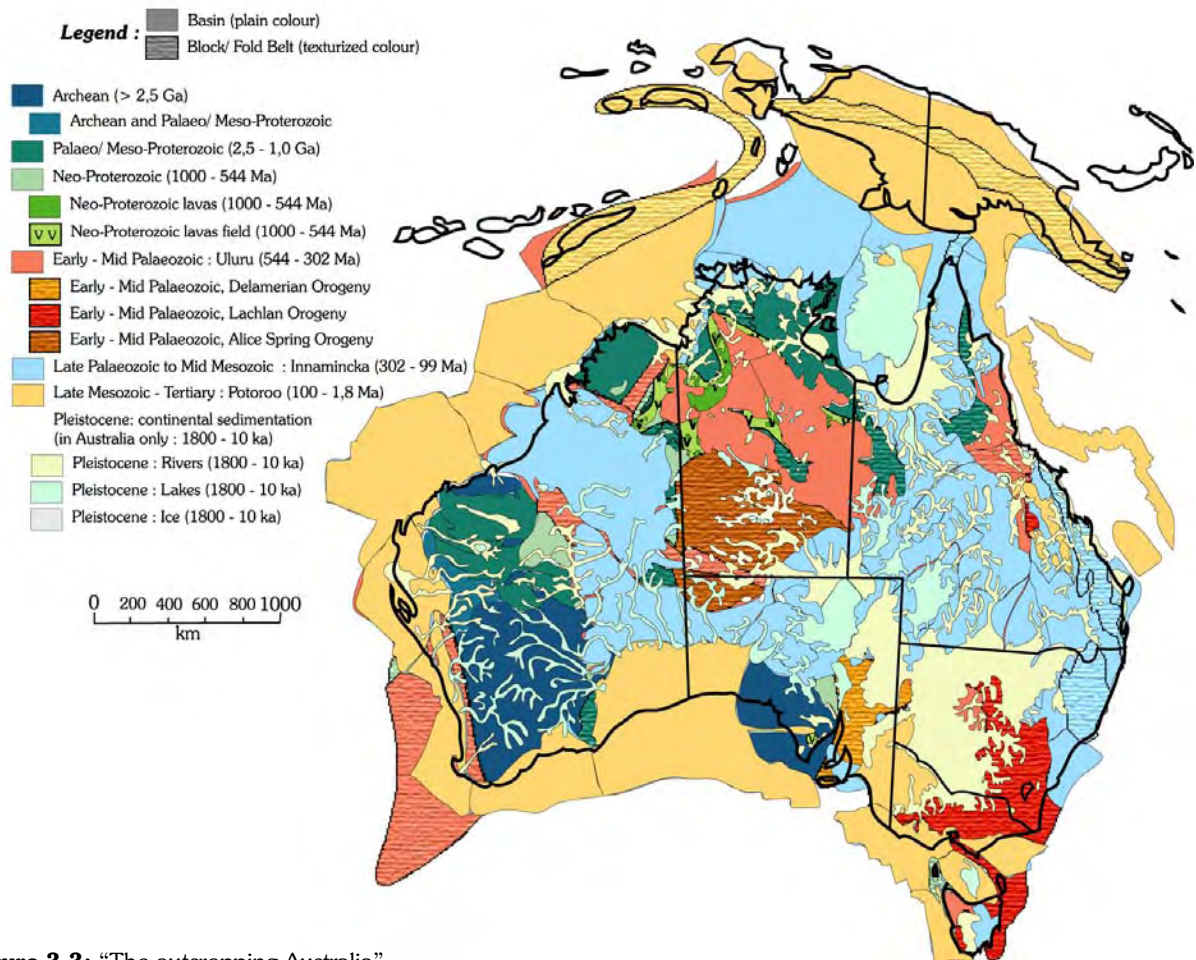


Figure 3.3: “The outcropping Australia”.

Map of blocks and basins outcropping in Australia and Papua-New Guinea. Note in particular the difficulty to correlate the tectono-stratigraphy of the Lachlan Orogen (in rasterised red) with the Delamerian Orogen (in rasterised orange) in New South Wales, and even more with its possible northern continuation, the Thomson and the Hodgkinson-Broken Ridge orogens, in Queensland.

Redrawn and modified after Veevers (2001).

3.2. The Tasmanides in Australia

The Tasmanides (or Tasman Fold Belt System) can be described with three main entities (Figure 3.2) mainly based on pre-Permian rock association. To the West, the Adelaide Fold Belt and the Kanmantoo Fold Belt have been deformed by the same orogenic event, and can be gathered in the Delamerian Orogen (Glen, 1992). In the center, the Tasmanides comprise the Lachlan Orogen (or Lachlan Fold Belt), as well as its possible northward continuation, the Thompson Orogen and even the Hodgkinson – Broken River Orogen (or fold belts). Finally, the third entity to the East is called the New England Orogen (or New England Fold Belt).

Nota bene: the term “orogen” is here favoured rather than “fold belt” following Glen (1992).

Actually, the boundaries of these orogenies are difficult to determine, because the Tasmanides are basically exposed where relieves are (compare figure 3.3 to figure 3.1-A), the rest being hidden by Mesozoic and Cainozoic cover. It explains also why geophysical methods (magnetic imagery, gravimetry, seismic, etc...) have been extensively used to help mapping the Tasmanides. Consequently, interpretations are often matter of debate, and subdivisions and correlations frequently vary from one author to another.

3.3. Phanerozoic history of the Southern Tasmanides

Several Palaeozoic orogenic events affected south-eastern Australia, and they are used to define the different structural domains of the Tasmanides. The temporal and spatial extent of these events, however, varies among authors. To illustrate this problem, two versions are shown herein: one from Fergusson & Coney (1992) who show relatively restricted zones affected by orogenic events, the second from Veevers (2000 & 2001) who represents them quite extended. It must be noticed that several indications represented on the figures redrawn after Veevers (2001), are not discussed in this work. Readers are referred to the original publications for further information.

3.3.1. The Delamerian Orogeny

The oldest Palaeozoic deformations are recorded in the West, and correspond to the Delamerian Orogeny (Turner *et al.*, 1996). This orogen has a well-defined western edge, the Torrens Hinge Zone in South Australia. But the position and nature of the boundary between the Delamerian and Lachlan orogens is still subject of much discussion.

In New South Wales, the Broken Hill Block, the Bancannia Trough, the Wertago terrane and the Kayrunnera terrane have undergone Cambrian to Early Ordovician folding, thrusting and some metamorphism. This means that the Delamerian Orogeny has affected the whole Broken Hill area (introduced in Chapter 4, figure 4.7; and presented in Chapter 5).

In Victoria, the extension to the East of the Delamerian Orogeny is not well constrained. Veevers (2001) shows a Delamerian event encompassing the Glenelg River Complex, the Stavely terrane and the Stawell terrane (figure 3.4-C). This is similar to previous model, such as that of Glen (1992) who extended the Delamerian Orogeny to the Avocat fault. By contrast, Fergusson & Conney (1992) or Gray & Foster (1997) restricted the orogen to the Glenelg River Complex only (figure 3.4-A).

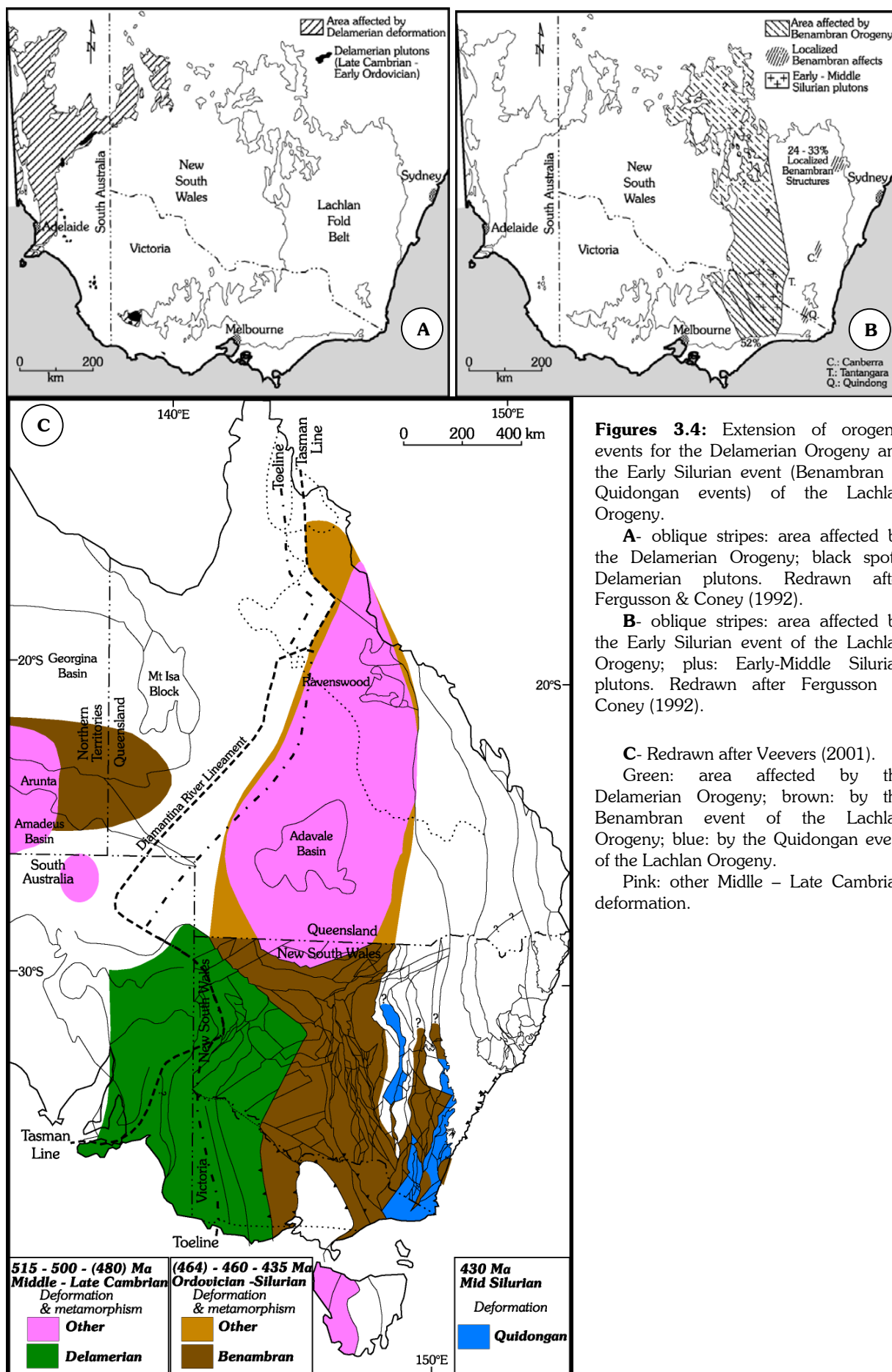
The Delamerian Orogeny has also been extended to the Ross Orogen in Antarctica. Indeed, good correlation seems to exist between the Glenelg River Complex, the Stavely and Stawell terranes in Australia, and the Wilson, Bowers and Robertston Bay terranes in Antarctica, respectively (Stump *et al.*, 1986; Borg & DePaolo, 1991). New evidences, however, link also the Stawell terrane to terranes in the East and belonging to the Lachlan Orogen (Korsch *et al.*, 2002; Glen, *personal communication*, 2002; Willman *et al.*, 2002). Further work is needed in both Australia and Antarctica to better define the boundary between these two orogens.

The geochemical analysis of greenstone belts in Antarctica, Victoria, and New South Wales reveals composition associated to subduction zone. Although the present-day westward thrust vergence, the direction of subduction is not clearly established.

However, the collisional event leading to the Delamerian Orogeny itself appears to be relatively short (~10-20 Ma) and may be centred about 510 Ma ago, at least in the Broken Hill area (Mills, *personal communication*, 2002).

3.3.2. The Lachlan Orogeny

Within the Lachlan Orogen, a number of different deformation events have been recognised. Nevertheless, there is still a controversy on whether these events are distinct as usually described in the literature, or whether it corresponds to one continuous phenomenon with several pulses.



a) – Early Silurian event

In the literature, the first recording of deformation is called the Benambran event (Talent, 1965), and can be found surprisingly in the Wagga-Omeo Zone, situated in the middle of the Lachlan Orogen. Tight folds, thrusts, syn-tectonic pluton emplacement and high temperature – low pressure metamorphism occurred all over the Wagga-Omeo Zone, and in a certain extent in the Howqua and Tabberabbera zones (figures 3.4-B & 3.4-C). As pointed out by Gray & Foster (1997) however, even if the Benambran event is usually considered as Llandoveryan, the tightest fossil control brackets it between Bolindian (Late Ordovician) and Llundlow.

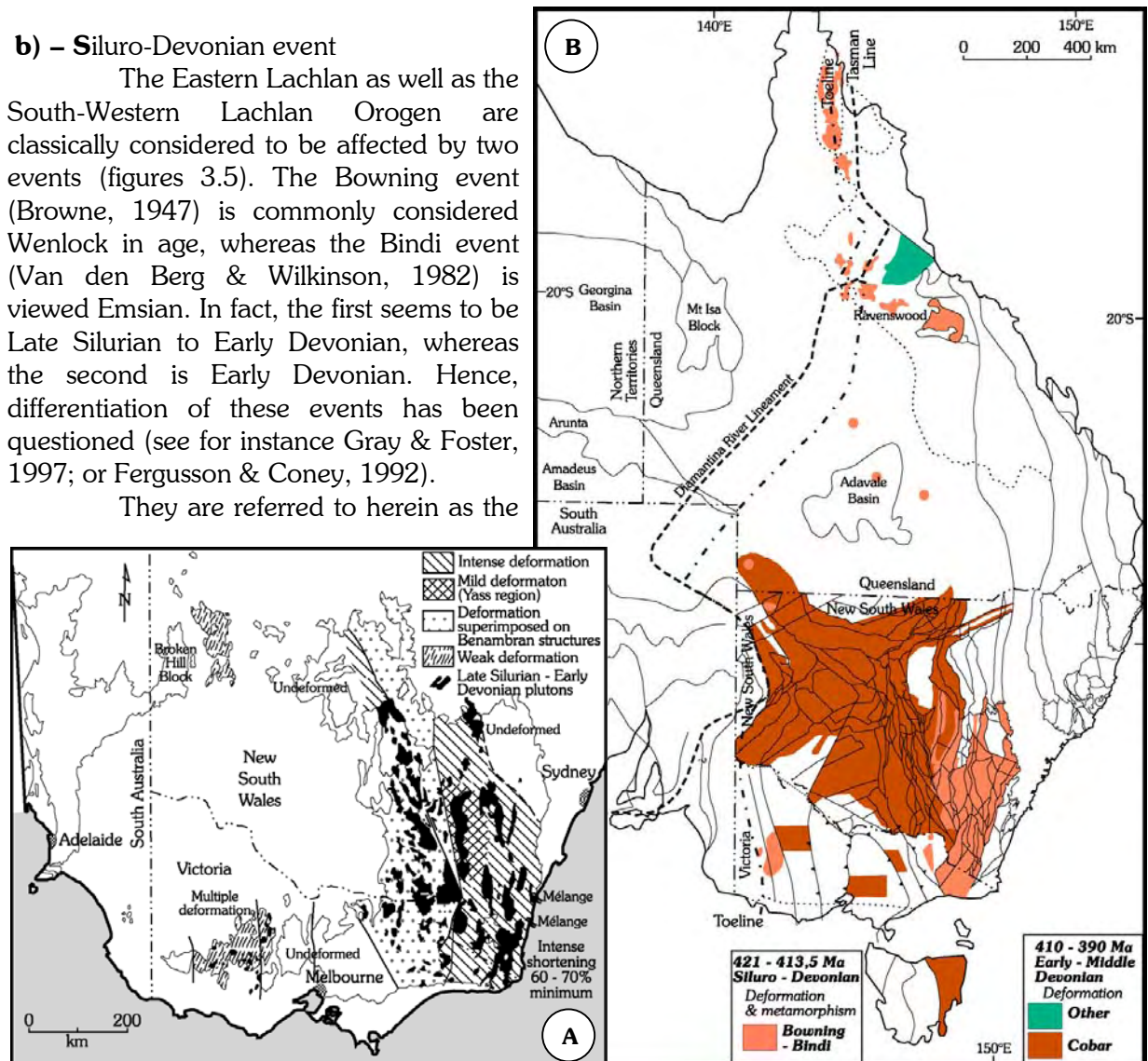
The Quidongan event (Crook *et al.*, 1973) describes deformation in compression more concentrated in the South-East of the Lachlan Orogen. This event, clearly determined near Quidong (New South Wales), is centered in the Wenlock. Nevertheless, the North-East Lachlan Orogen apparently experienced extensional tectonism, which led to split the Ordovician Macquarie Arc in several volcanic belts (see §.3.4; and figure 3.9, below). However, regionally, deformations range from Late Llandovery to the Late Wenlock/Llundlow, and cannot be distinguished from the Benambran event. That is why the Quidongan event is often merely considered as the continuation of the Benambran event.

Hence, for simplicity, both the Benambran and Quidongan events will be refer here to as the Early Silurian event.

b) – Siluro-Devonian event

The Eastern Lachlan as well as the South-Western Lachlan Orogen are classically considered to be affected by two events (figures 3.5). The Bowning event (Browne, 1947) is commonly considered Wenlock in age, whereas the Bindi event (Van den Berg & Wilkinson, 1982) is viewed Emsian. In fact, the first seems to be Late Silurian to Early Devonian, whereas the second is Early Devonian. Hence, differentiation of these events has been questioned (see for instance Gray & Foster, 1997; or Fergusson & Coney, 1992).

They are referred to herein as the



Figures 3.5: Extension of the Siluro-Devonian event (Bowing & Bindi events). **A-** Redrawn after Fergusson & Coney (1992). **B-** Redrawn after Veevers (2001).

Siluro-Devonian event.

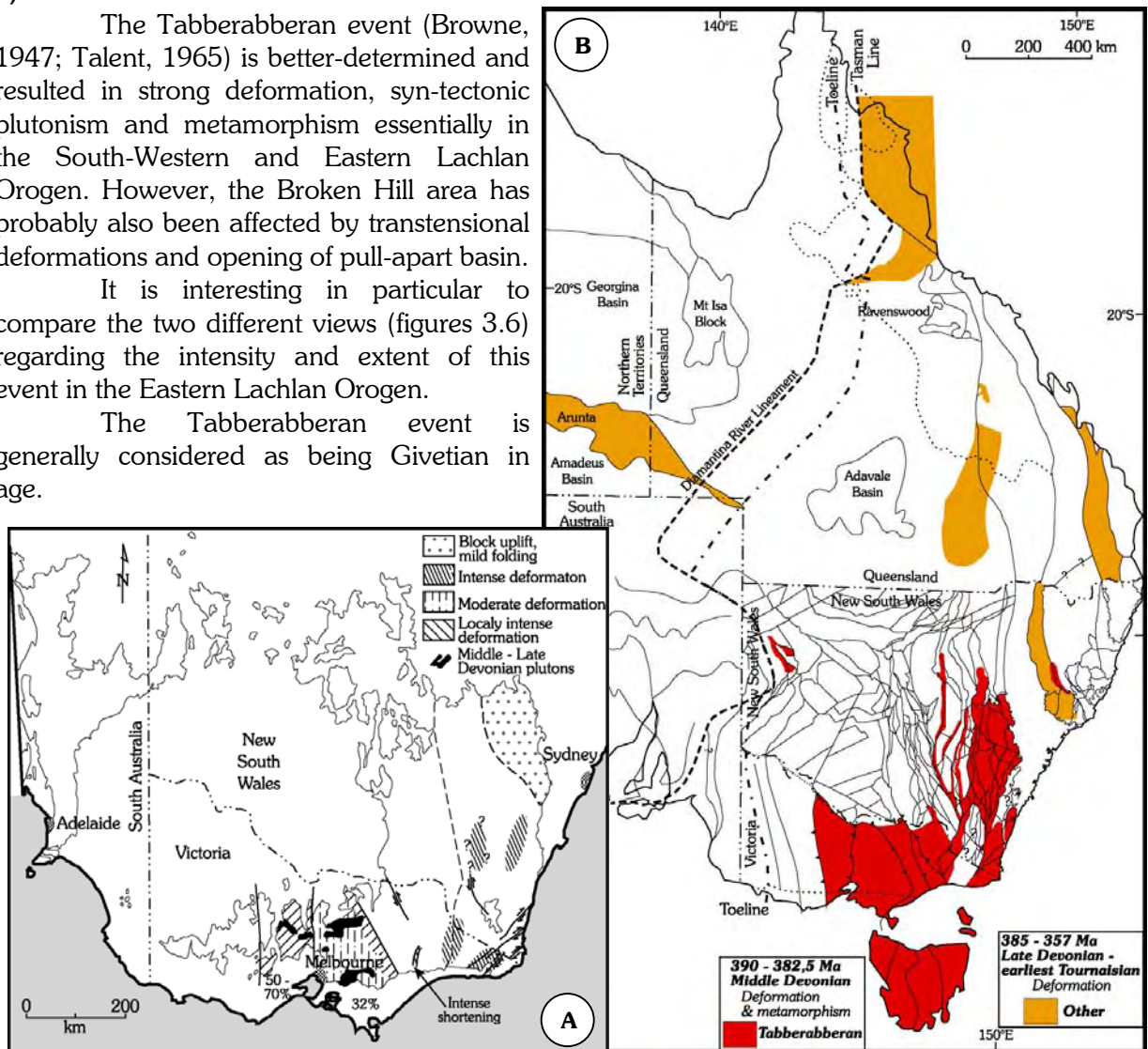
It is interesting to point out here also that this deformation corresponds to the Tahua Orogeny in New Zealand.

c) – Middle Devonian Tabberabberan event

The Tabberabberan event (Browne, 1947; Talent, 1965) is better-determined and resulted in strong deformation, syn-tectonic plutonism and metamorphism essentially in the South-Western and Eastern Lachlan Orogen. However, the Broken Hill area has probably also been affected by transtensional deformations and opening of pull-apart basin.

It is interesting in particular to compare the two different views (figures 3.6) regarding the intensity and extent of this event in the Eastern Lachlan Orogen.

The Tabberabberan event is generally considered as being Givetian in age.



Figures 3.6: Extension of the Middle Devonian event (Tabberabberan event). **A-** Redrawn after Fergusson & Coney (1992). **B-** Redrawn after Veevers (2001).

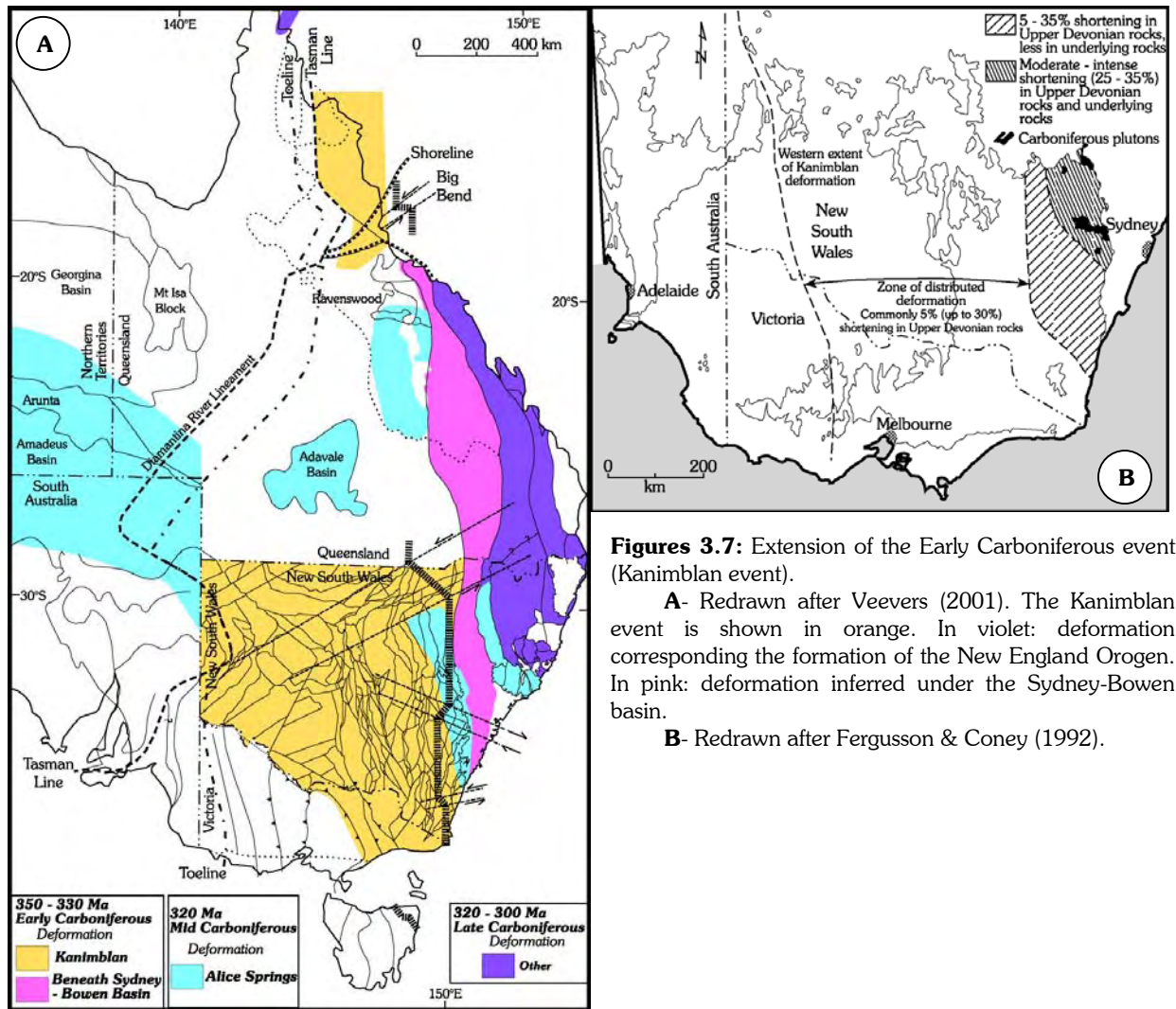
Compare in particular in the two cases the extent and intensity of this event in the Eastern Lachlan Orogen.

d) – Early Carboniferous Kanimblan event

The Early Carboniferous Kanimblan event (Süßmilch, 1914) resulted in widespread deformation throughout the Lachlan Orogen (figures 3.7) involving many fault reactivations. Its age is usually considered as Early Viséan, and it was the final Palaeozoic orogenic event in the Tasmanides. However, it is poorly understood, but is thought to be related to the beginning of the accretion of the New England Orogen to the East.

The upper age limit is given by the Carboniferous I-type granitoids of the eastern Lachlan Orogen, which are not affected by deformation.

Nonetheless, coeval fault reactivation in western New South Wales indicates probable link with the Carboniferous Alice Spring Orogeny of central Australia as well.



Figures 3.7: Extension of the Early Carboniferous event (Kanimblan event).

A- Redrawn after Veevers (2001). The Kanimblan event is shown in orange. In violet: deformation corresponding the formation of the New England Orogen. In pink: deformation inferred under the Sydney-Bowen basin.

B- Redrawn after Fergusson & Coney (1992).

3.3.3. The New England Orogeny

Three approximately north-northwest-trending belts can be identified in the pre-Jurassic rocks of north-eastern New South Wales.

Almost undeformed paralic and nonmarine sedimentary rocks of Permian and Triassic age unconformably overlap the Lachlan rocks and comprise the Sydney and Bowen basins. They are bounded eastward, mainly along east-dipping thrusts, by the Tamworth Belt, the western subdivision of the mostly Devonian to Permian New England Orogen.

The Tamworth Belt is dominated by volcanic arc and volcanoclastic arc margin basins fill of Devonian and Carboniferous age, overlain by Early Permian strata. These rocks are only mildly deformed and granitoids are unusual and confined to the eastern part of the belt.

Immediately to the east of the Tamworth Belt are highly deformed Middle to Late stratified rocks of the Tablelands Complex of the New England Orogen. The older (Silurian – Carboniferous) stratified rocks comprise an accretionary subduction complex whereas the younger (Early Permian) accumulated in a rift basin. The Tablelands Complex was the site of widespread granite emplacement in the latest Carboniferous to Triassic.

The major orogenic event in the New England Orogen occurred in the Late Permian to Triassic, the effects of which decreased rapidly southwest into the Sydney-Bowen basin (see Collins, 1991; Korsch *et al.*, 1992; Jenkins *et al.*, 2002; and Klootwijk, 2002; Geeve *et al.*, 2002). This region is thus clearly not stable before this time, and has been discarded in this study.

3.3.4. Other Mesozoic and Cainozoic events affecting New South Wales

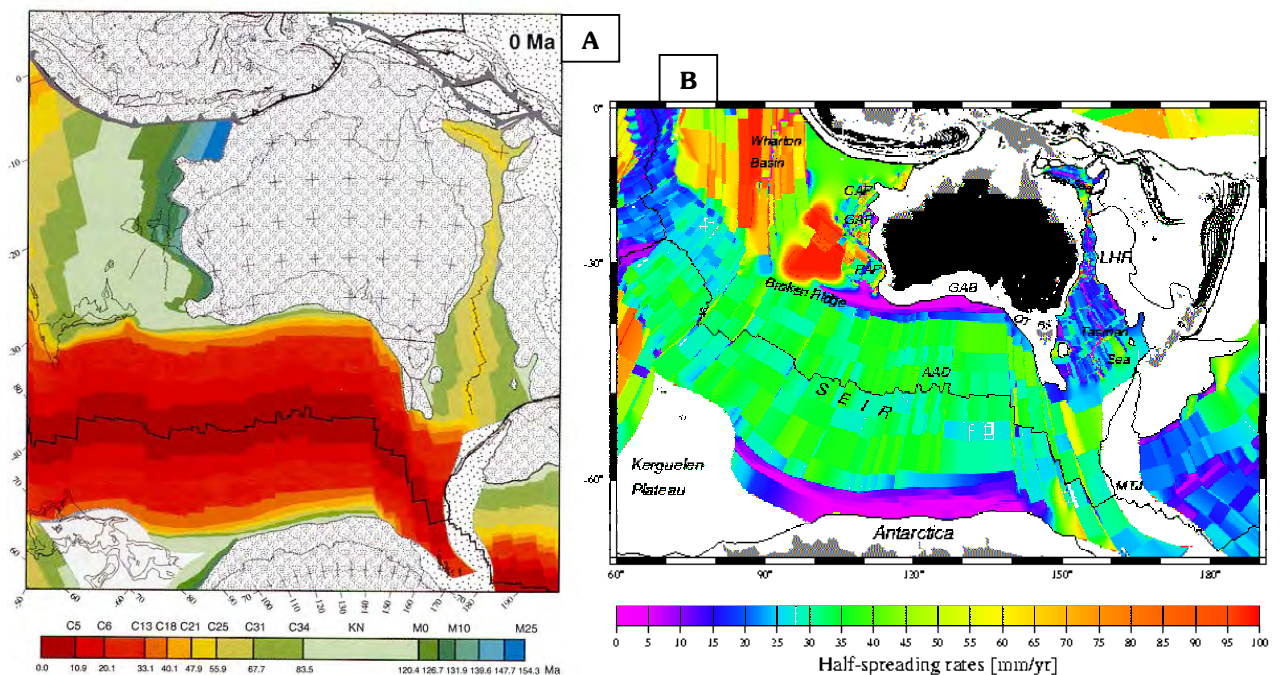
Following the Kanimblan event, the Lachlan Orogen underwent however a number of geological events, predominantly thermal, which are of course, possible causes for remagnetisations.

Scattered volcanics of Triassic to Early Jurassic age are present in south-eastern Australia, and according to Veevers (2000), they appear to be linked to the Jurassic flood volcanism in southern South America and to tholeiitic basalt activity in southern Africa, Antarctica and Tasmania. Dyke intrusions of probably this age are also visible in the Broken Hill area. If this magmatism is as widespread as suggested by Veevers, remagnetisation of that age can be expected all over the Tasmanides.

The separation between Australia and Antarctica probably changed the geothermal gradient in the Tasmanides. The rifting between the two continent began at 154,3 Ma, mainly with strike-slip faulting (Müller *et al.*, 2000). The rift-to-drift transition (figure 3.8-A) is marked by the recognition of the first sea floor magnetic anomaly C34 (83,5 Ma), but spreading rates (figure 3.8-B) remained very low (about 1 cm/yr) until anomaly C13 (33,1 Ma) when it accelerated to a rate of about 4 cm/yr.

The opening of the Tasman Sea is coeval with this separation as anomaly C34 can be identified also East of Tasmania (Gaina *et al.*, 1998). This opening develops mainly from South to North and isolated the Lord Howe Rise and Challenger Plateau already at Chron 33 (73 Ma) and the Dampier Rise at about Chron 27 (61 Ma). Only the western South Tasman Rise continued to move southward after Chron 24 (52 Ma), and joined the eastern South Tasman Rise at approximately 40 Ma after about 120 km of strike-slip motion. With this exception, a reconstruction at 52 Ma shows the present-day tectonic configuration of the Tasman Sea.

Late Tertiary and Quaternary hot spot volcanism affected New South Wales and Victoria. In the Molong area, the Tertiary volcanics comprise mainly basalts lavas and plugs with subordinates trachytic intrusives, lavas and pyroclastics together with minor alkali rhyolite. Isotopic age dating indicates these volcanics range in age from Late Eocene to Late Miocene (Pogson & Watkins, 1998).



Figures 3.8- **A:** Age of oceanic crust between Australia and Antarctica and in the Tasman Sea from sea floor magnetic anomalies, after Müller *et al.*, 2000. **B:** Half-spreading rates in mm/year deduced from magnetic anomalies, after Müller *et al.*, 1997.

Rate of erosion during the Mesozoic and Cainozoic was thought to be low (Glen, 1988; Blevin *et al.*, 1996; Collins, 1991).

Still, O'Sullivan *et al.* (2000-b), on the base of fission track data as well as palaeomagnetic recording, argue for two major denudation events from the Carboniferous in the Parkes area (*i.e.* the Molong area). The first is a Middle Permian to Middle Triassic cooling event that is related to the New England Orogeny. The second is a kilometre-scale and rapid denudation in the Tertiary, about 60 to 40 Ma ago. Fission track and $\text{Ar}^{40}\text{-Ar}^{39}$ dating studies have been also carried out in Tasmania and around the Mt Kosciuszko area, and lead to the same conclusions (O'Sullivan *et al.*, 1996; O'Sullivan *et al.*, 2000-a).

3.4. Geological framework of south-eastern Australia

Albeit discrepancies in delimitations, all authors define three main entities in the southern Tasmanides on the basis of orogenic events. Each of them is in turn subdivided into belts and terranes (or zones).

In New South Wales alone, Scheibner (1996) describes up to 196 terranes. However, for sake of clarity, it will be simply referred to orogens and belts, which subdivide the Lachlan Orogen only. Names of terranes will be used only where sampling has been carried out.

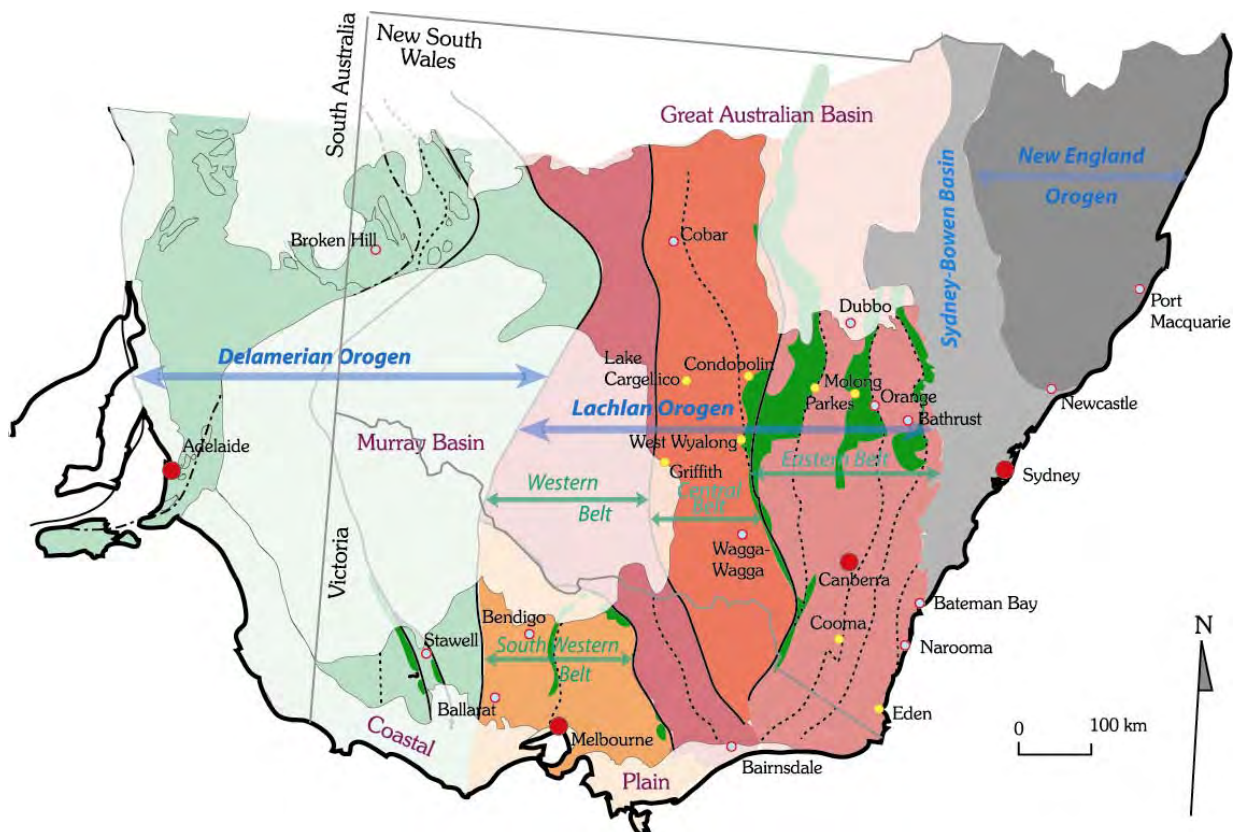


Figure 3.9: Main geological subdivisions of south-eastern Australia used in this work, after Glen (1992).

The Tasmanides are composed of three orogens: the Delamerian, the Lachlan and the New England Orogens. Each of them is subdivided in several belts, themselves made up of numerous zones (or terranes). The Lachlan Orogen in particular, comprises the Western, the South-Western, the Central and the Eastern belts. Green areas correspond to Cambro-Ordovician Volcanic Arcs present in Western Victoria and in particular in Eastern Lachlan Orogen. The Permian – Triassic Sydney-Bowen Basin and the Mesozoic – Cainozoic Great Australian Basin, Murray Basin and Coastal Plain Basin hide the most part of south-eastern Australia, and consequently, obscure the relationship between the different components of the southern Tasmanides.

The geological framework used in this thesis (figure 3.9) follows that of Glen (1992). In addition to fault-bounded subdivisions, an interesting feature is the presence of Cambrian – Ordovician “green-stone” belts. Some are present in the Delamerian Orogen and in the South-Western Lachlan Orogen in Victoria, but the largest extent seems to correspond to the Ordovician Macquarie Volcanic Arcs of Eastern Lachlan Orogen. These rocks are related to a west-dipping subduction zone (e.g. Glen, 1992; Gray *et al.*, 1997), which would have split the Macquarie arc in three in the Early Silurian (cf. §.3.3.2.a.), but apparently not its southern continuation, the Kiandra Volcanic Belt at the boundary between the Central and the Eastern Lachlan Orogen. This implies that an East – West structural zone, not shown here (figure 3.9), could exist.

3.5. Models for the geodynamic evolution of the Tasmanides

A number of various models for the geodynamic evolution of the Tasmanides have been proposed. These can broadly be divided into two schools of thought.

For the first one, deformations occurred in the Lachlan Orogen from the Early Silurian (see §.3.3.2.a.). This means that, even if these terranes were previously allochthonous, they were at least already amalgamated from that time on. Moreover, as the Delemarian Orogeny is Cambrian, it is possible that the Lachlan Orogen amalgamated as one block together with the Kanmantoo Fold Belt (i.e. East part of the Delamerian Orogen) against the proto-margin of Gondwana. Elements of the Tasmanides are hence considered to have been (para-) autochthonous to the Australian craton throughout the most of the Palaeozoic (Schmidt & Morris, 1977; Morel & Irving, 1978; Goleby, 1980; Schmidt *et al.*, 1986, and 1987; Hargraves *et al.*, 1987; Van Houten & Hargraves, 1987; Van der Voo, 1988; Offler *et al.*, 1998). According to these models, any subduction zones must have lain outboard of the present-day eastern margin of Australia probably from the Cambrian. Consequently, palaeomagnetic data from these regions are representative of the craton of Gondwana from the Palaeozoic. This implies however, that no palaeomagnetically detectable movements or rotations occurred in the Tasmanides since then.

Alternatively, other models describe the Tasmanides as an amalgamation of multiple allochthonous microcontinents against the proto-margin of Gondwana (Embleton *et al.*, 1974; McElhinny & Embleton, 1974; Perroud *et al.*, 1984; Veevers, 1984; Livermore *et al.*, 1985; Scotese *et al.*, 1985 ; Leitch & Scheibner, 1987 ; Powell *et al.*, 1990).

Two models implying an allochthonous origin are briefly shown here as examples. The first appeals multiple subduction zones whereas the second more specifically implies tear-zones.

The first, from Gray & Foster (1997), involves three subduction zones (figures 3.10) to take into account the vergences of thrusting and diachronism of deformation over the southern Tasmanides. The western subduction is west-dipping and corresponds now to the Stavely – Lake Wintlow suture of Victoria. The two eastern subduction zones are facing one another and can explain the high temperature – low pressure metamorphism of the Central Lachlan Orogen. This model is attracting but does not account for stratigraphic similarities between the Melbourne Zone in the South-Western Belt and terranes of the Eastern Belt of the Lachlan Orogen.

The second model is the basis for a palinspastic map after Glen *et al.* (1992-b) before Late Silurian time (figure 3.11). It represents the elements of the southern Tasmanides as microcontinents, which have amalgamated against the proto-margin of Gondwana, following a west-directed subduction that led to the Delamerian Orogeny. After Late Silurian time, the Bendigot-Ballararat, Melbourne and East Tasmania Zones in particular have been displaced towards

the North-West mostly with strike-slip movement. This microcontinent indented between the Victorian Microcontinent and the Delamerian Orogen to form the Southern Belt of the Lachlan Orogen. This hypothesis provides a good solution to explain why the deformation migrates roughly from West to East and jump back in the South-Western Belt during the Middle Devonian Tabberabberan event on the one hand, and on the other hand, places the South-Western Belts elements as south prolongation of terranes from the Eastern Belt to take account for stratigraphic similarities between these two parts of the southern Tasmanides.

Figures 3.10: Model of the geodynamic evolution of the southern Tasmanides after Gray & Foster (1997).

A: Palinspastic map at the Early Silurian time.

B: Cross-section showing the three subduction zones, where the two eastern ones are facing one another.

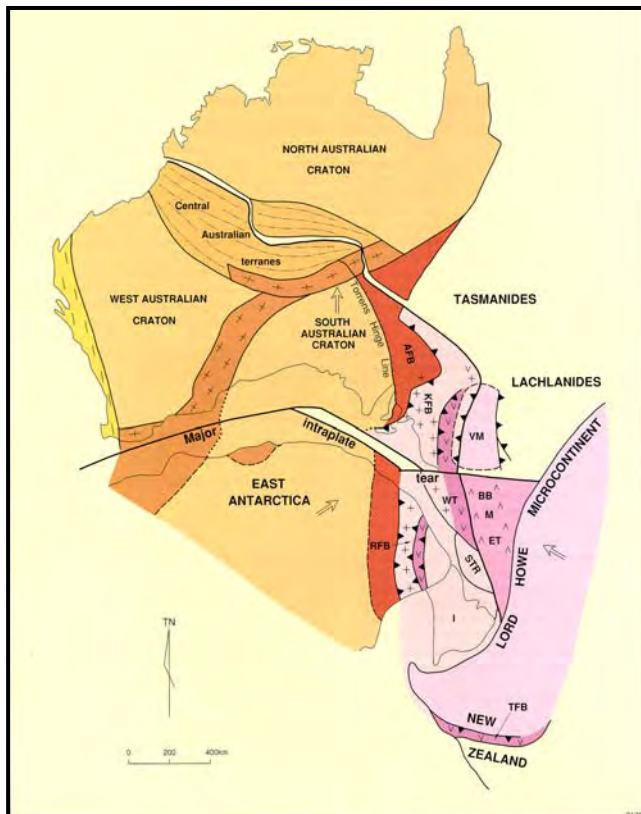
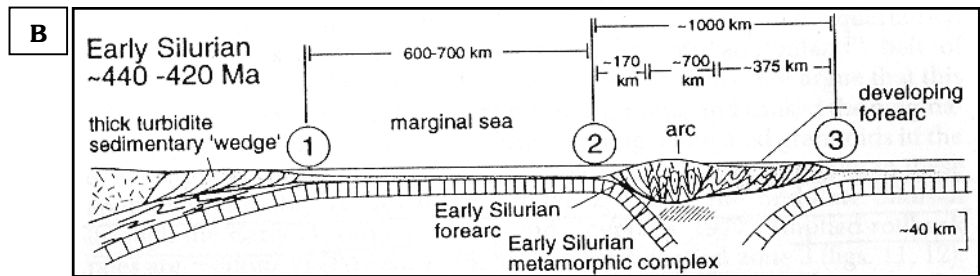
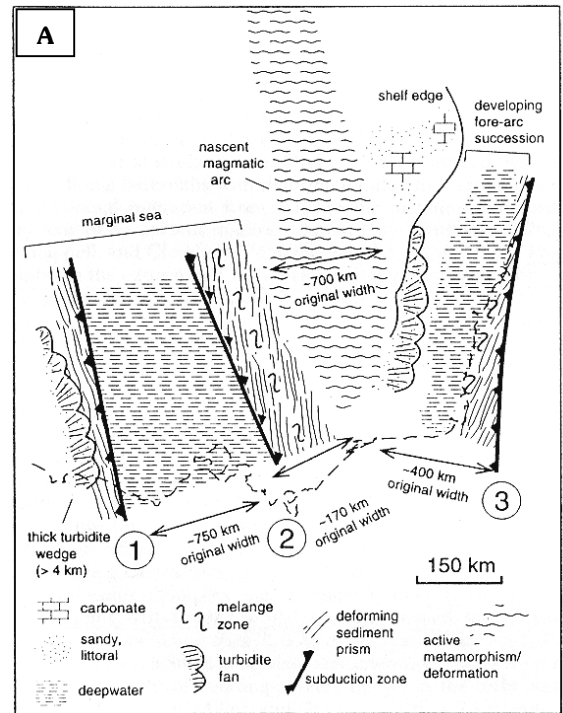


Figure 3.11: Palinspastic map of Eastern Gondwana before Late Silurian time, after Glen *et al.* (1992-b).

AFB: Adelaide Fold Belt; **KFB:** Kanmantoo Fold Belt; **VM:** Victorian Microcontinent; **WT:** Western Tasmania; **ET:** Eastern Tasmania; **M:** Melbourne Zone; **BB:** Bendigo-Ballarat Zone; **STR:** South Tasman Rise; **RFB:** Ross Fold Belt; **I:** Iselin; **TFB:** Tahua Fold Belt.

Summary of chapter 3

The Tasmanides constitute the eastern third of Australia. It is made up in its southern part, of three main entities: the Delamerian, the Lachlan, and the New England Orogens. Delimitation of these orogens is based on orogenic events they underwent during their Phanerozoic history. The Delamerian Orogeny is a tectonic event that affected the western side of New South Wales and Victoria mainly during the Cambrian. The Lachlan Orogen formed after four main orogenic events: the Early Silurian (Benambran & Quidongan), the Siluro-Devonian (Bowling & Bindi), the Middle Devonian Tabberabberan and the Early Carboniferous Kanimblan events. The New England Orogeny affected the most north-eastern part of New South Wales and culminated in the Late Permian to Triassic. It formed in the Late Palaeozoic an active margin with accretionary complex and was not stable until the Early Mesozoic. That is why this area has been discarded in this study.

Although the last orogenic event is Early Carboniferous, our study areas may have been affected by other geological events, predominantly thermal, since the Mesozoic and Cainozoic. These events can be also responsible of remagnetisations.

Despite good evidences on the geological history, the geodynamic evolution of the southern Tasmanides is still poorly established, and broadly two schools of thought divide the scientific community. Authors who present the Tasmanides as (para-) autochthonous with respect to the Australian craton throughout the Palaeozoic, and place any subduction zones outboard the present-day eastern margin of Australia. And others who consider the Tasmanides as an amalgamation of fragments of allochthonous origin.

Chapter 4

Methodology, sampling and previous studies

4.1. Methodology

4.1.1. Sampling procedure

Sampling localities were targeted in particular in collaboration with Ian Percival (palaeontologist), and Richard Glen and Kingsley Mills from the Geological Survey of New South Wales. They were chosen in order to have the best possible age control on the rock, to focus predominantly on fine-grained formation, to avoid units affected by metamorphism (such as the Hill End Trough in the Molong area, for instance [see map in figure 7.2, Chapter 7], where metamorphism is believed to have reached biotite grade; Barron, 1998) or by penetrative cleavage. The aspect and topography of the outcrop were naturally taken into account as well since deep weathering and/or lightning effects are common in Australia.

Sampling was carried out using a gasoline-powered water-cooled portable drilling machine (see photo 1 at the end of the chapter). Typically, a minimum of five sites per locality, each of them containing a minimum of five cores per site, were collected. Whenever possible, samples were separated by several metres and each site, by about a hundred metres in order to clearly average secular variations (see, for example, discussion in Collinson, 1983; Soffel, 1991; or Butler, 1992). The size of a locality is then in the order of a kilometre. The main reason for such a scale is that samples are collected in a region made up of terranes. This means that the tectonic behaviour can be completely different from one terrane to another, and that a good structural control is only possible at rather small scale. This is particularly of great importance in the Tasmanides where plunging fold axis and/or conical folds are common.

A core is between 5 and 25 cm long and has the standard diameter of 25 mm. It yields one to six standard cylindrical specimens (i.e. 25 mm x 22 mm, corresponding to a ratio $R_{\text{Height/Length}}=0,88$; this ratio being the closest approximation to a sphere. See discussion in Collinson (1983), and references therein [pages 213 to 218]). Cores were oriented in the field using both sun and magnetic compasses. Data from the magnetic compass have been systematically used since no deviation with the sun compass has been detected. All directional data have been corrected from the local declination, which ranges from 8,9° in the Broken Hill area in the West to 12,1° in the Molong area in the East (see figure 4.7, below). All data herein are given relative to the “true” North.

4.1.2. Laboratory procedures

Measurements of the anisotropy of magnetic susceptibility (AMS) have been performed on one specimen from every core using a “KLY-2” Kappabridge magnetic susceptibility meter (15 positions).

Many parameters have been calculated in order to determine the shape of the ellipsoid of magnetic susceptibility (Flinn, 1962, 1965-a and 1965-b; Jelinek, 1981; Khan, 1962), and to try to have an indication about the degree of strain (Parés & Van der Pluijm, 2002). When necessary, bootstrap analysis (Tauxe, 1998) were conducted to determine the orientation of the three main axes of magnetic susceptibility, but generally, single specimen axes, plotted together with density contours (Gaussian counting model with K=100) to better visualise both data scattering and grouping, is enough to obtain the broad orientation of the ellipsoid (see §.4.2, below).

At least one specimen per locality has been used as pilot sample, and demagnetised using alternating field (AF) techniques. The very large majority showed the presence of high coercivity minerals resistant to complete demagnetisation, and often related to weathering effect. All other specimens (one per core) have been therefore thermally demagnetised and measured using a 2G Cryogenic Magnetometer in the shielded room of the laboratory of the Ludwig-Maximilians-University (LMU) in Munich, Germany. In routine, detailed stepwise demagnetisation (~ 23 steps) has been carried out, and susceptibility, measured at each step of heating using a “Minikappa” KLF-3 magnetic susceptibility meter, allowed monitoring mineralogical changes during the heating process.

Vector subtraction, standard principal component analysis and/or great circle analysis (Kirschvink, 1980), and field tests have been performed using the PALMAG program developed at the University of Munich. For every result, many statistic parameters are calculated (angular standard deviation δ ; angular variance s ; etc), but only the precision parameter κ (the best approximation of a finite sample set of directions) and the cone calculated at the 95% confidence level α_{95} (Fisher, 1953) will be given. They are obtained as follows:

$$\kappa = \frac{N-1}{N-R} \quad \text{Where, N is the number of specimens}$$

$$R \text{ is the resultant vector: } R = ((\sum x)^2 + (\sum y)^2 + (\sum z)^2)^{1/2}.$$

$$\alpha_{(p)} = \arccos \left(1 - \left(\frac{N-R}{R} \right) \cdot \left(\frac{1}{1-p} \right)^{\left(\frac{1}{N-1} \right)^{-1}} \right) \quad \text{with p, the probability (e.g. 95%).}$$

Fold tests performed in routine are that of McElhinny (1964) and McFadden (1990), but for specific localities, the fold test of Enkin & Watson (1996) and bootstrap analysis of Tauxe (1998) have been also employed to account for changes in statistical distribution after bedding correction. Indeed, some localities show relatively complex geometries and fold tests used in routine are not valid in such cases.

In many cases, however, the bedding is not changing enough over the locality to obtain a significant fold test, neither it is when stepwise unfolding is used (systematically tested with the PALMAG program). Nevertheless, it seems that the bedding correction improves (or on the contrary worsens) data clustering. Although such results are not statistically reliable and interpretations cannot be directly based on them, it is interesting to evaluate whether magnetisation has a better chance to be acquired before or after folding. Thus, calculating at which level of confidence the classic fold test (McElhinny, 1964) becomes positive may give an interesting indication. This is done using the F-Distribution Function:

$$F(F) = \int_0^F \frac{\Gamma\left(\frac{m+n}{2}\right)}{\Gamma\left(\frac{m}{2}\right) \cdot \Gamma\left(\frac{n}{2}\right)} \cdot m^{\frac{m}{2}} \cdot n^{\frac{n}{2}} \cdot x^{\frac{m}{2}-1} \cdot (n+mx)^{-\frac{m+n}{2}} dx$$

Where the Gamma Function is defined by,

$$\Gamma(n) = \int_0^{\infty} t^{n-1} e^{-t} dt \quad \text{with, } n > 0.$$

This can be simplified by finding when:

$$\frac{1}{\beta_{inv}((1-p), (N-1), (N-1))} - 1 \leq \{\kappa - ratio\}$$

Where, β_{inv} is the Beta Inverse Function

p, the probability

N, the number of samples

κ -ratio, the ratio of the κ parameter calculated *in situ* divided by the κ obtained after bedding correction.

Samples from each locality have been also subjected to rock magnetic measurements using the variable frequency translation balances (VFTB) operating in the laboratory of Munich. Isothermal Remanence Magnetisation (IRM), backfield curves, thermomagnetic curves and hysteresis properties have been determined and analysed using the VFTB-Analyser 1.8 software package also developed in Munich. Although samples are often weak for instruments, the general characteristic still can be seen and information wangled despite noise.

4.2. Anisotropy of Magnetic Susceptibility (AMS) and contribution to structural control

Inaccurate structural control is probably one of the major causes of obtaining palaeomagnetic results significantly in error. A recent study (Pueyo *et al.*, 2003) shows again the consequences of such incorrect tectonic correction in palaeomagnetism. They notably argued that erroneous correction could lead to an apparent rotation of up to 28°.

In the Tasmanides, folding may be complex and in particular, conical folds can be common. Where samples have been collected however, folds are revealed to be comparable to cylindrical folds, albeit often with a plunging axis.

Anisotropy of magnetic susceptibility can be used as an independent indicator to check the credibility of the bedding correction employed.

Besides this, what is usually unknown in the Tasmanides, is the degree of internal strain in rocks. It has been demonstrated that ductile strain results in development magnetic carriers preferred orientations, which necessarily induces some deviations of the natural remanent magnetisation (Cogné, 1987).

It, therefore, appears necessary to complete the statistical argument about the time of acquisition of magnetisation relative to folding, with a discussion of the total lack of strain.

The study of anisotropy of magnetic susceptibility, since it reflects the preferred orientation of magnetic minerals, is probably the best argument in this discussion.

The directional variability of induced magnetisation in a weak magnetic field is what is named the anisotropy of magnetic susceptibility (AMS). Weak field magnetisation is a linear function of field strength and is written as:

$$\begin{cases} M_1 = k_{11}.H_1 + k_{12}.H_2 + k_{13}.H_3 \\ M_2 = k_{21}.H_1 + k_{22}.H_2 + k_{23}.H_3 \\ M_3 = k_{31}.H_1 + k_{32}.H_2 + k_{33}.H_3 \end{cases} \quad \text{or, } M_i = k_{ij}.H_j \text{ with } i, j = 1, 2, 3.$$

Where, M_i : Cartesian coordinates of induced magnetisation vector.

H_i : Cartesian coordinates of magnetic field vector.

k_{ij} : second order symmetrical Cartesian tensor, the AMS tensor. This tensor has three real eigenvalues: k_1, k_2, k_3 , the principal susceptibilities.

An ellipsoid of magnetic susceptibility has therefore three main axes, K_{max} (maximum), K_{int} (intermediate), K_{min} (minimum), which lengths reflect the principal susceptibilities k_1, k_2, k_3 .

Following Hrouda (1982), causes for AMS are generally summarised as follows:

- 1- Shape alignment of ferromagnetic grains.
- 2- Lattice alignment of crystals with magnetocrystalline anisotropy.
- 3- Magnetic domain alignment.
- 4- Stringing together of magnetic grains.
- 5- Stress-induced anisotropy.
- 6- Exchange anisotropy.

Among them, AMS in natural rocks is considered as being mainly controlled by causes [1] and [2]. Measuring AMS in a rock thus yields an estimation of its fabric, and this can be used as a structural tool for almost all rock types.

Several parameters have been proposed to estimate the shape of the ellipsoid of magnetic susceptibility and to evaluate the degree of internal deformation (Flinn, 1962, 1965-a, 1965-b; Kahn, 1962; Rees, 1966; Parés & Van der Pluijm, 2002).

Two diagrams will be systematically presented here with the orientation of the three main axes of magnetic susceptibility to illustrate this estimation. The first is a Flinn-type diagram showing the magnetic lineation $\{L\}$ versus the magnetic foliation $\{P\}$ to define the shape of the ellipsoid (Flinn, 1962, 1965-a, 1965-b; Hrouda, 1982), where:

$$\begin{cases} L = K_1 / K_2 \\ P = K_2 / K_3 \end{cases}$$

The second shows the shape parameter $\{T\}$ versus the degree of anisotropy $\{P_j\}$ (Jelinek, 1981; Hrouda, 1982), where:

$$T = \frac{\ln(K_2) - \ln(K_3)}{\ln(K_1) - \ln(K_3)}$$

$$P_j = \exp(\sqrt{2((\ln(K_1) - nm)^2 + (\ln(K_2) - nm)^2 + (\ln(K_3) - nm)^2)})$$

$$\text{with, } nm = \frac{\ln(K_1) + \ln(K_2) + \ln(K_3)}{3}$$

The Königsberger ratio (Königsberger, 1938) is also systematically checked since it can be regarded as an indicator for lightning effects, which are frequently observed in Australian rocks (Schmidt, *personal communication*).

Some remarks concerning the regional magnetic fabric observed in every area will be given at the end of each following chapter.

4.3. Sampling coverage: rocks and localities targeted

Three field trips have been organised over three years. The first target area was the Ordovician Macquarie Volcanic Arc in the Eastern Belt of the Lachlan Orogen. The aim of this trip was to collect samples pre-dating the orogenic events (the first orogenic event being Silurian; see Chapter 3), and to try to determine whether this arc was adjacent to the cratonic part of Gondwana (*i.e.* more or less its present-day relative position), or whether it represented an island arc isolated far offshore mainland Gondwana. The second trip targeted again some rocks in the Eastern Belt, but focused on rocks from the Delamerian Orogen in far western New South Wales, where terranes are considered to be (para-) autochthonous since the Early Ordovician (end of the

Delamerian Orogeny). Finally, the last field trip was devoted to complete our sampling coverage over the rather East-West transect drawn across the Tasmanides of New South Wales.

A list of the 50 localities (289 sites, 1576 cores, 3969 specimens), where samples were collected, is provided in table 1. Their positions are indicated on a simplified geological map presented below (figure 4.1).

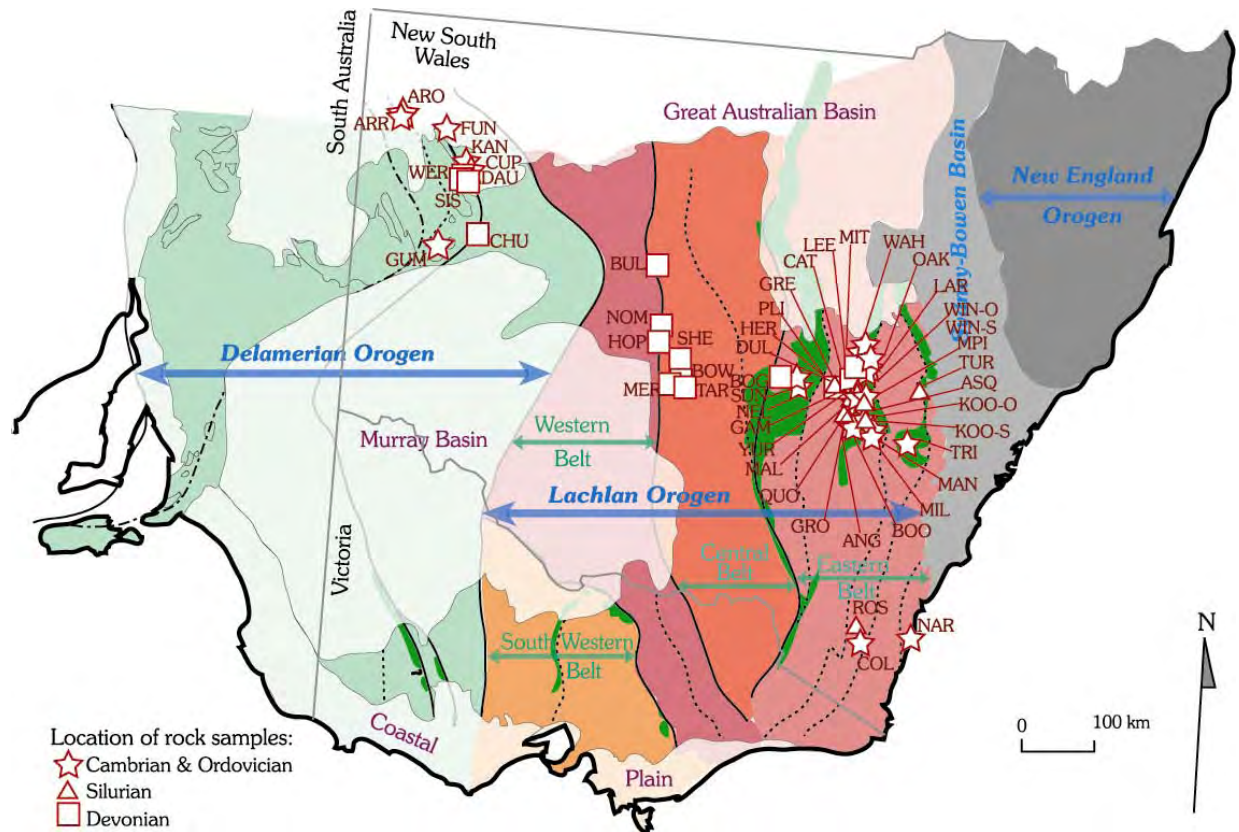


Figure 4.1: Position of localities sampled for this work and shown in table 1 (mnemonics are the same). Stars represent sampling in Cambrian-Ordovician rocks; triangles, in Silurian rocks; and squares, in Devonian rocks. The map of the southern Tasmanides is the same as the one presented in Chapter 3 (§.3.4), figure 3.9.

A large number of localities is concentrated in the vicinity of the Ordovician Macquarie Volcanic Arc of the Eastern Lachlan Orogen, but in general, sampling has been carried out in order to define a sort of transect across the different entities of the southern Tasmanides of New South Wales.

4.3.1. Rejected palaeomagnetic results

Among the localities studied, a large amount was revealed to be not suitable for palaeomagnetic purposes. One example is given here with the locality “BOG” as it is very representative of results obtained for this study.

Ten sites (53 cores) have been collected over a large syncline of white-pink silicified fine-grained sandstone in the vicinity of Bogan Gate. These rocks belong to the Cudelbar Sandstone Member of the Hervey Group, and are early Late Famennian in age (Duggan *et al.*, 1999).

A large majority of samples reveals coherent demagnetisation behaviour, either with one main component (figures 4.2) or two (figures 4.3), after removal of a low temperature component (up to 80°C in figure 4.2, and to 120°C in figure 4.3), which direction usually corresponds to the present-day field. The first component can be clearly identified up to 575°C (close to the Curie temperature of magnetite), and the second, when it exists, is entirely removed above 650 – 680°C (figures 4.2). It is probably carried by haematite and results from oxidation. Some other specimens show a completely noisy magnetic signal (figures 4.4) that cannot be interpreted at all.

Table 1: List of sampling localities

Mnem.	Area	Localisation	Group	Formation	N	B	Age sampled
ANG	M.A	West Canowindra	Cabonne Gp	Angullong Fm	38	7	Bolindian
ARO	BH.A	Mt Arrowsmith, Pincally	Ordovician Fms	Tabita Fm	15	3	Early Ordovician
ARR	BH.A	Mt Arrowsmith, Pincally	Mid-Late Cambrian Fms	Pincally & Wydjah Fms	5+37	1+7	Mid – Late Cambrian
ASQ	M.A	East Cudal	Mumbil Gp	Mirrabooka Fm	15	3	Wenlock - Llandovery
BOG	M.A	Bogan Gates	Hervey Gp	Cudgelbar Sandstone Mb	53	10	Mid Famennian
BOO	M.A	East Canowindra	Barrajin Gp	Cliefden Caves Limestone sGp	47	9	Eastonian
BOW	MB.A	SW Lake Cargellico	Rast Gp	Ural Volcanics	29	6	424 ± 6 Ma (SHRIMP)
BUL	MB.A	South Cobar	Winduck Gp	Gundaroo Sandstone	39	7	Late Pragian
CAT	M.A	North Molong	Catombal Gp	Black Shale & Ganangle sGp	43	9	Late Devonian
CHU	BH.A	South Barrier Hwy, Churinga	probably Mt Daubeny Fm	probably Mt Daubeny Fm	28	5	Gedinnian (?)
COL	Cooma	West Numerala	Adaminaby Gp	undifferentiated	35	5	Early Ordovician
CUP	BH.A	East Wertago	probably Kayrunnera Gp	Cupala Creek Fm	37+10	7+1	Late Cambrian
DAU	BH.A	Wertago	Mt Daubeny Fm	Mt Daubeny Fm	18+14+46	1+2+7	Gedinnian
DUL	M.A	SW Manildra	Dulladerly Volcanics	undifferentiated	25	5	Givetian
FUN	BH.A	Pulgarmurrie	probably Kayrunnera Gp	unnamed Cambro-Ordovician rocks	30	6	Late Cambrian – Ordovician
GAM	M.A	Molong	Cabonne Gp	Reedy Creek Limestone	51	10	Eastonian – 1
GRE	M.A	Manildra	Grega Gp	undifferentiated	17	3	Early Gedinnian
GRO	M.A	NW Canowindra	Cudal Gp	Gospel Oak Shale	26	5	Early Wenlock
GUM	BH.A	South Barrier Hwy, Bilpa	Scopes Ranges Redbeds	Scopes Ranges Redbeds	10	2	Late Cambrian – Ordovician
HER	M.A	West Cudal	Hervey Gp	Mandagery & Kadina Fms	31	6	Frasnian – Early Famennian
HOP	MB.A	Mt Hope	Mt Hope Gp	Ambone Volcanics	30	6	latest Pragian
KAN	BH.A	NE Wertago	probably Kayrunnera Gp	Kandie Tank Limestone	30	6	Late Cambrian
KOO-O	M.A	Four Mile Creek, South Orange	Cabonne Gp	Angullong Fm	5	1	Bolindian – 2
KOO-S	M.A	Four Mile Creek, South Orange	Ashburnia Gp	undifferentiated	10	2	Mid Llandovery
LAR	M.A	North Molong	Kenilworth Gp	Fairbridge Volcanics	9	2	Darriwillian – Gisbornian
LEE	M.A	North Molong	Catombal Gp	Canangle sGp	25	5	Famennian
MAL	M.A	Cudal, Malachi Hill	Barrajin Gp	Bowan Park Limestone sGp	42	8	Eastonian
MAN	M.A	South Mandurama	Kenilworth Gp	Coombing Fm	28	5	Darriwillian – Gisbornian
MER	MB.A	SW Lake Cargellico	Rast Gp	Ural Volcanics	30	6	413 ± 5 Ma (SHRIMP)
MIL	M.A	North Lake Wyangala	Adaminaby Gp	undifferentiated	26	5	Yapeenian – Darriwillian

Abbreviations: Mt: Mount; Hwy: Highway; Lm: Limestone; Mb: Member; Fm: Formation; sGp: subgroup; Gp: Group.

M.A: the Molong area; **MB.A:** the Mount Bowen area; **BH.A:** the Broken Hill area.

N: number of cores; **B:** number of sites. Sums correspond to sampling in different lithologies.

Table 1: List of sampling localities (continued)

Mnem.	Area	Localisation	Group	Formation	N	B	Age sampled
MIT	M.A	Mitchell Hwy, North Molong	Hensleigh Gp	Mitchell Fm	36	7	Bendigonian
MPI	M.A	Mitchell Hwy, South Molong	Kenilworth Gp	Fairbridge Volcanics	33	5	Darriwillian – Gisbornian
NAR	Narooma	Narooma	Wagonga Gp	Narooma Chert & Argillites	12	2	Early Lancefieldian & Darriwillian – 4
NEL	M.A	West Parkes	Goonumbla Volcanics	Gunningbland Shale Mb and Lm & Goonumbla Volcanics	40+21+15	8+4+3	Gisbornian – Eastonian
NOM	MB.A	North Mt Hope	Mt Hope Gp	Nombiginni Volcanics	28	5	Mid – Late Praguian
OAK	M.A	NE Molong	Kenilworth Gp	Fairbridge Volcanics (Formerly Oakdale Fm)	69	13	Gisbornian
PLI	M.A	SW Manildra	Hervey Gp	Mandagery & Kadina Fms	45	9	Frasnian – Early Famennian
QUO	M.A	North Cargo	Barrajin Gp	Bowan Park Limestone sGp	70	14	Eastonian
ROS	Cooma	North Cooma	Yahny Gp	Ryrie Sandstone	6	1	Llandovery
SHE	MB.A	NW Lake Cargellico	Rast Gp	Ural Volcanics	35	7	410 ± 8 Ma (SHRIMP)
SIS	BH.A	Wertago	Early – Mid Devonian intrusions	Rhyolitic intrusions	24	5	Early – Middle Devonian
SUN	M.A	West Parkes	Goonumbla Volcanics	Goonumbla Limestone Mb	15	3	Darriwillian – 4 – Eastonian
TAR	MB.A	SW Lake Cargellico	Rast Gp	Ural Volcanics	4	1	414 ± 3 Ma (SHRIMP)
TRI	M.A	Rockeley	Kenilworth Gp	Triangle Creek Fm	10	2	Darriwillian
TUR	M.A	Two Miles Creek, Sofala	ungrouped Silurian Fms	Pipers Flat Fm	5	1	Llandovery
WAH	M.A	Wahringa, South Dubbo	Cabonne Gp	Wahringa Limestone Mb	49	9	Darriwillian – 4 – Gisbornian – 1
WER	BH.A	Wertago	Mt Daubeny Fm	Mt Daubeny Fm	26	5	Gedinnian
WIN-O	M.A	East Molong	Cabonne Gp	Oakdale Fm	25	5	Eastonian – Bolindian
WIN-S	M.A	East Molong	Mumbil Gp	Nandilyan Fm	25	5	Wentlock
YUR	M.A	South Molong	Kenilworth Gp	Yuranigh Limestone Mb	10+4	2+1	Gisbornian

Abbreviations: Mt: Mount; Hwy: Highway; Lm: Limestone; Mb: Member; Fm: Formation; sGp: subgroup; Gp: Group.

M.A: the Molong area; **MB.A:** the Mount Bowen area; **BH.A:** the Broken Hill area.

N: number of cores; **B:** number of sites.

However, from the directions of magnetisation having a stable magnetic signal, no relevant overall mean direction can be obtained since the directions are totally randomised (figure 4.5).

Reasons for this kind of results may be multiple. First, the intensity of magnetisation is rather weak. For most of them however, the problem stems from the combination of relatively large grain size of magnetic particles, strong weathering effects and/or possible lightning effects, overlap of magnetisation spectra due to multiple phases of remagnetisation (probably often associated with fluid migration), and strain effects sometimes visible with developing cleavage.

This is representative of results obtained in many localities studied but rejected for discussion or interpretation concerning magnetisation or tectonic events in the Southern Tasmanides.

4.3.2. Palaeomagnetic results presented

Results presented in the following chapters have not necessarily a direct significance, but may give indications in terms of magnetic events or palaeogeography. Those that are shown, have simply a consistent magnetic behaviour, which can be compared to others.

For sake of clarity, they will be always presented as follow:

- Analysis of AMS in order to assess the degree of internal strain, to determine the magnetic fabric and usually the associated petrofabric, and to check the consistence of the bedding control.
- Presentation of rock magnetic measurements of one specimen in order to help defining the main magnetic carriers. Magnetisations however, are in general complex, and carriers are multiple. These measurements, associated with determination of unblocking temperature spectra, usually yield only indications about the possible nature of a magnetic carrier.
- Example of thermal demagnetisation and determination of the principal components of magnetisation.
- Interpretations of the mean directions in terms of geological history of the locality and if possible, in terms of palaeogeography. Paleapole positions and palaeogeographic reconstructions are drawn using GMap (Version 2002; Torsvik & Smethrust, 1999).

Sampling carried out for this work can be grouped in three main areas (figure 4.7): the Broken Hill area to the West, the Mount Bowen area in the centre, and the Molong area to the East. Results will be then presented in the following chapters according to this geographical distribution.

A fourth area, the Cooma – Narooma area, only concerns pilot investigations. Localities, listed in table 2, yielded irrelevant results, and consequently won't be further considered.

Table 2: List of localities in the Cooma – Narooma area

Mnemonics	Names coming from	Location (Long. /lat.)
COL	Collins Road	149,3278 / -36,1876
NAR	Narooma	150,1275 / -36,2107
ROS	Rose Valley Road	149,2248 / -36,1441

These localities are presented in table 1 (Same mnemonics).

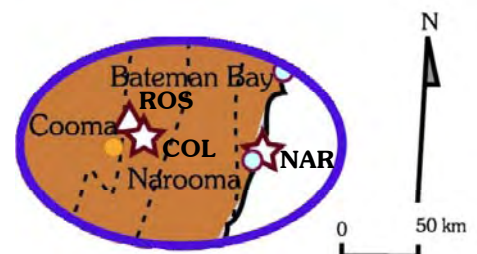
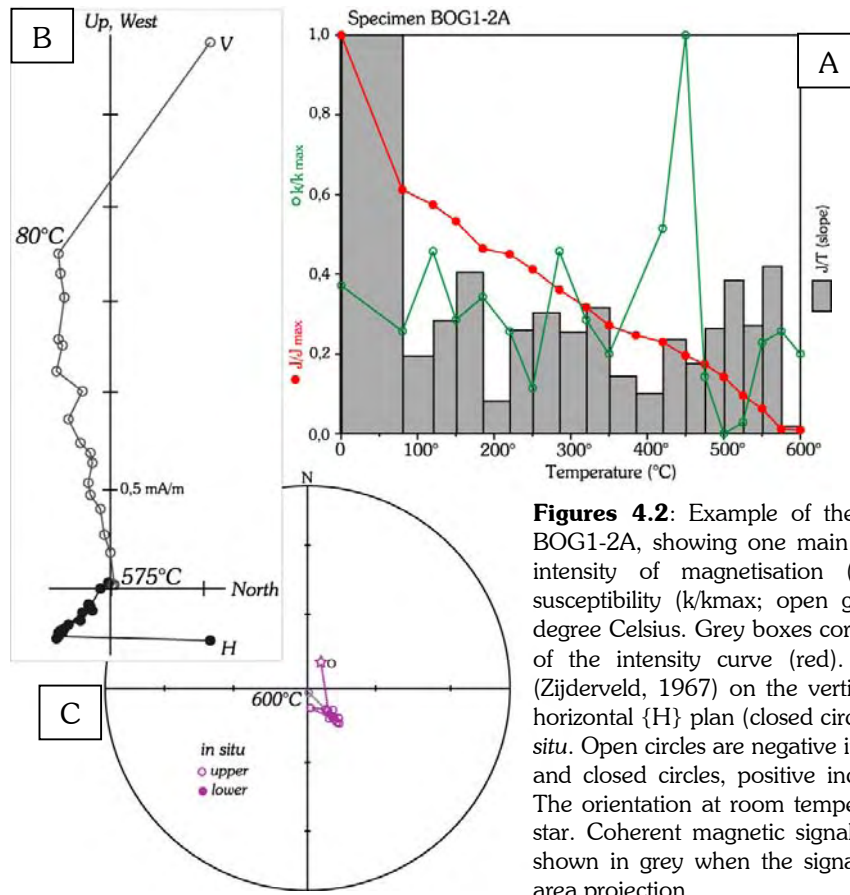
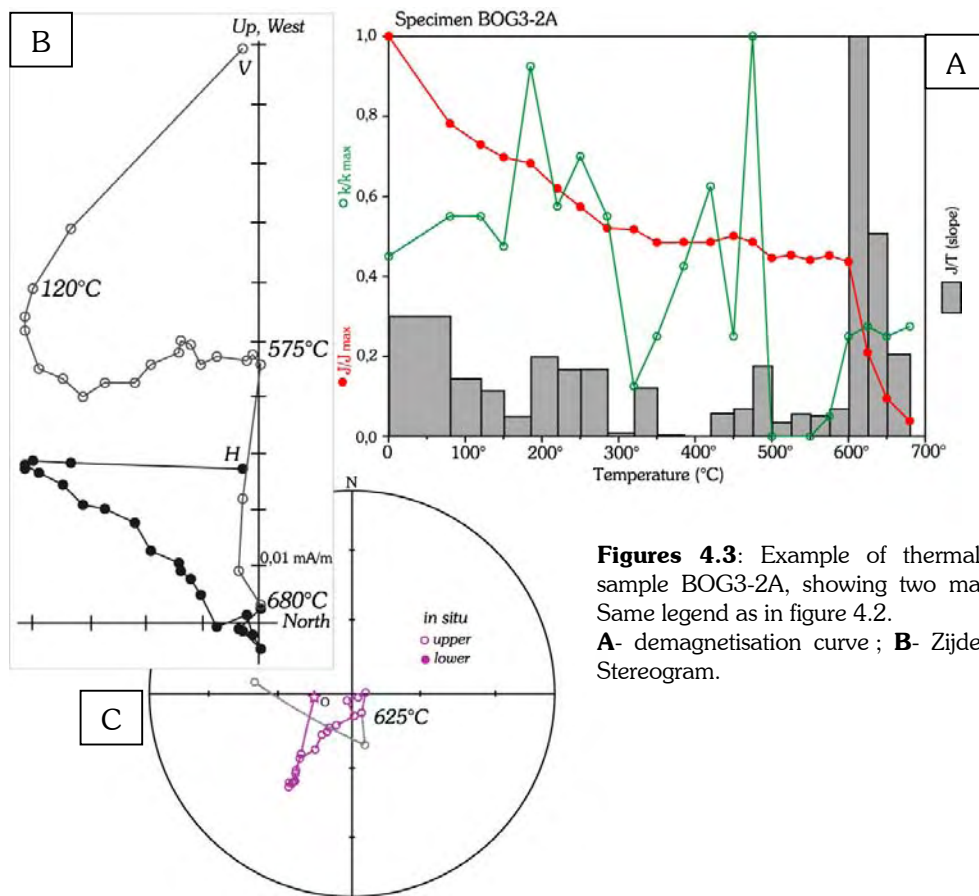


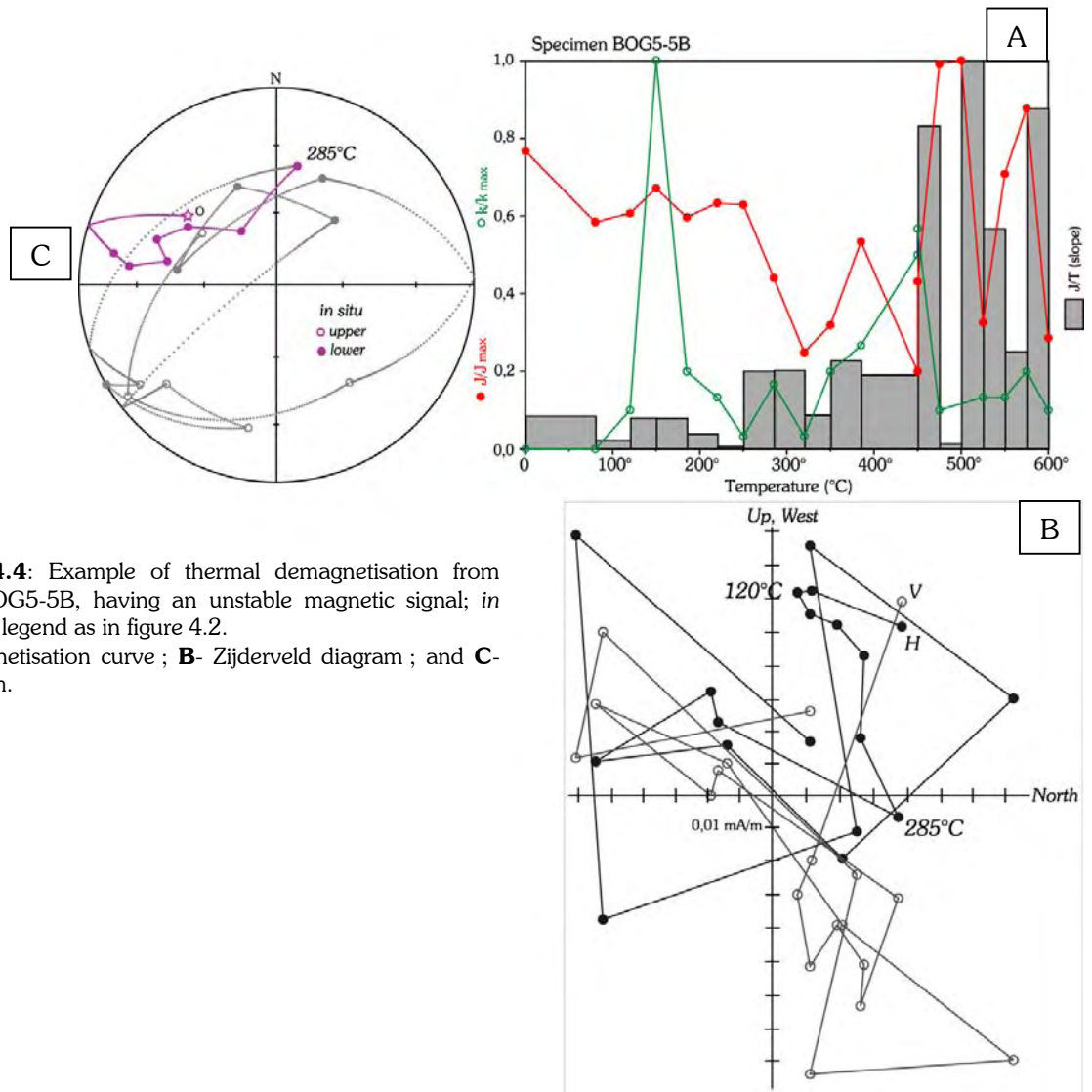
Figure 4.6: Sampling localities from the Cooma & Narooma area. No simplified geological map is shown, but just a sketch corresponding to the Cooma area of figure 4.7 (see below).



Figures 4.2: Example of thermal demagnetisation from sample BOG1-2A, showing one main component; *in situ*. **A-** Normalised intensity of magnetisation (J/J_{max} ; closed red circles) and susceptibility (k/k_{max} ; open green circles) versus temperature in degree Celsius. Grey boxes correspond to the first derivative (slope) of the intensity curve (red). **B-** Orthogonal projection, *in situ* (Zijderveld, 1967) on the vertical {V} plan (open circles) and the horizontal {H} plan (closed circles). **C-** Stereographic projection, *in situ*. Open circles are negative inclination values (upper hemisphere) and closed circles, positive inclination values (lower hemisphere). The orientation at room temperature (origin {O}) is shown with a star. Coherent magnetic signal is represented in violet, while it is shown in grey when the signal becomes unstable. Schmidt equal area projection.



Figures 4.3: Example of thermal demagnetisation from sample BOG3-2A, showing two main components; *in situ*. Same legend as in figure 4.2. **A-** demagnetisation curve ; **B-** Zijderveld diagram ; and **C-** Stereogram.



Figures 4.4: Example of thermal demagnetisation from sample BOG5-5B, having an unstable magnetic signal; *in situ*. Same legend as in figure 4.2.

A- demagnetisation curve ; **B-** Zijderveld diagram ; and **C-** Stereogram.

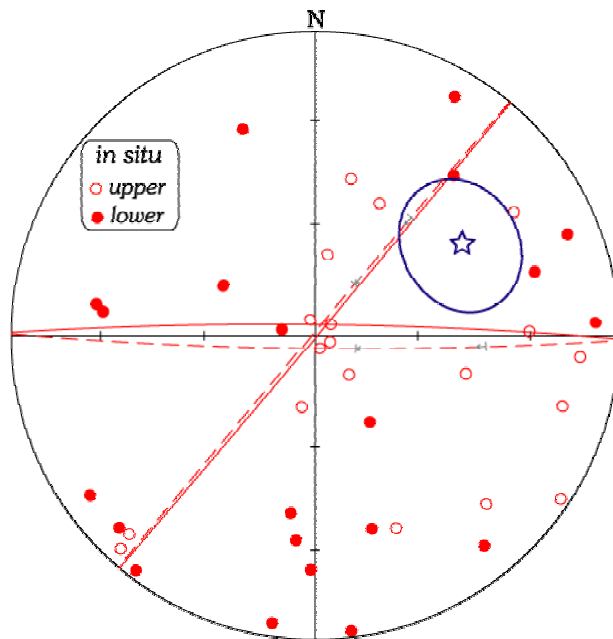


Figure 4.5: Corresponding directions of magnetisation for the locality "BOG".

Red circles are directions of single sample component considered as having a stable magnetic signal. The orientations obtained for the locality, however, are randomised (see text); **open circles**, negative inclination values (upper hemisphere); **closed circles**, positive inclination values (lower hemisphere).

The **star** represents the mean direction with its associated 95% confidence cone, but it is of course, not relevant.

4.4. Previous palaeomagnetic studies in New South Wales

Several palaeomagnetic studies have been already conducted in the southern Tasmanides, but most of them are located either in the Eastern Lachlan Orogen, Sydney-Bowen Basin and New England Orogen, or in the Delamerian Orogen (figure 4.7; and Annexe II). By contrast, samples have been collected along a roughly East-West transect for this study. Data from the New England Orogen are not considered as this orogen was not stable until the end of the Palaeozoic or the beginning of the Mesozoic (see Chapter 3; §.3.3.3).

When the data are selected according to criteria explained in Chapter 2 (§.2.4.1), more than half of them do not satisfy more than the “base level” of selection (See Annexe II). This is due to the fact that a lot of data are quite old and the demagnetisation procedure is not sufficiently reliable (“Demagcode”=2 only). Some, however, are rejected because of their too low number of samples or because of their unsatisfactory statistical parameters, although the demagnetisation procedure seems correct (“Demagcode”=3 or 4). The 17 data left are presented briefly below and plotted together with the APW path for Gondwana based on small circle fit (figure 4.8). As discussed in Chapter 2 (§.2.6; figures 2.16 & 2.17), this path is only indicative and recalled for comparison purposes only. Data must be also compared with mean directions per period, as shown in Chapter 2 (§.2.3.2; and figure 2.7).

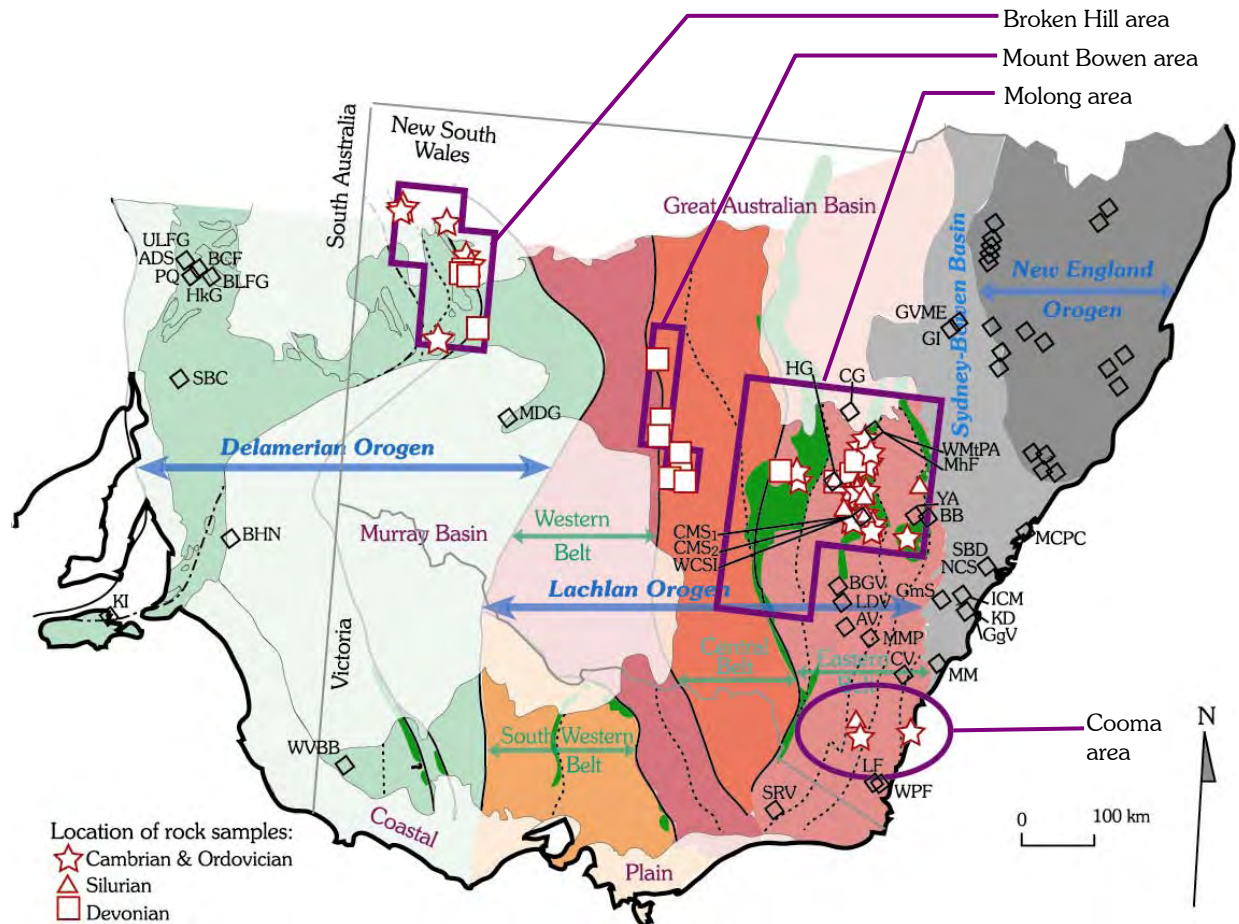


Figure 4.7: Comparison between sampling coverages obtained for this work and previous palaeomagnetic studies in the Southern Tasmanides.

Localities, which are shown as in figure 4.1 and correspond to table 1, can be grouped in three areas: the Broken Hill area (West), the Mt Bowen area (centre) and the Molong area (East); the Cooma – Narooma area is not considered further as it concerns only pilot investigations. They can be compared to previous palaeomagnetic studies (black diamonds), which are more restricted to the East or to the far West. Data corresponding to the mnemonics are listed in Annexe II (not for the New England Orogen; see text).

4.4.1. “Post-Lachlan Orogeny” data

The two Jurassic data (Sydney Basin Dykes [SBD] and Kiama Dykes [KD]; Annexe II, figure 4.8) are in good agreement one another and also with other data from Gondwana. The New England Orogen is indeed fully cratonised, but it means in particular that the Jurassic volcanism (that Veevers (2000) links to tholeiitic activity in Antarctica and South Africa) and the Cretaceous opening of the Tasman Sea did not apparently triggered a widespread remagnetisation event.

This is not the case however for the two Triassic data (Munmorah conglomerate & Patonga claystone [MCPC] and Milton Monzonite [MM] ; Annexe II, figure 4.8), which are clearly distinct one another and also about 30 to 60° East of the Triassic mean direction for Gondwana (see Chapter 2; §.2.3, figure 2.7). This may signify that these directions of magnetisation have perhaps been partly overprinted or affected by internal strain. However, although the New England Orogeny was still active, block rotation in the Sydney Basin is unlikely. Moreover, the Late Permian data from the Gerringong Volcanics [GgV] (cf. Annexe II, figure 4.8) does not appear to be fundamentally distinct from other poles from Gondwana (§.2.3, figure 2.7).

The mid Carboniferous Bathurst Batholiths [BB] (cf. Annexe II, figure 4.8) are coeval with the onset of the New England Orogeny and were probably emplaced along a fracture zone. On the field, these rocks show porphyroblasts of plagioclase, and are often deeply weathered and relatively strongly cleaved. This may be a reason why the corresponding palaeopole appears slightly apart from the mean pole for the Carboniferous, even if its 95% confidence cone overlap the confidence envelop drawn around the Small Circle Fit path (figure 4.8). Large grain size of magnetic particles associated with weathering effects and strain may have deviated the mean direction of magnetisation from this locality.

4.4.2. Ordovician to Devonian data

All data satisfying at least the “low” level selection and ranging from Ordovician to Devonian come from the Eastern Lachlan Orogen (Annexe II and figure 4.7). Three of them, the Early Silurian the Cowra Trough – Molong High Sediments [CMS₁] of Goleby (1980), the Early Devonian Snowy River Volcanics [SRV] of Schmidt *et al.* (1987), and the Givetian Comerong Volcanics [CV] of Schmidt *et al.* (1986), have been largely used to fulfil the Silurian – Devonian hiatus in the APW path for Gondwana due to the lack of data.

Goleby (1980) made the most extensive and interesting work in the Molong area and collected 384 cores from 22 formations for his Master of Science. Nevertheless, his conclusions are questionable. His Silurian palaeopole for example is based in particular upon the Belubula Shale, which conformably overlies the Ghost Hill Formation. Graptolites suggest that both formations are Wenlock to Ludlow in age. However, after bedding correction, the overall mean direction for the Belubula Shale is D.003,5°/I.-10,6° (N=19; $\kappa=52,4$ / $\alpha_{95}=4,7^\circ$) whereas it is D.196,7°/I.-22,8° (N=27; $\kappa=37,2$ / $\alpha_{95}=4,6^\circ$) in the Ghost Hill Formation. It means that these two directions, which have clearly distinct 95% confidence cones, are still separated by over 30° when corrected from bedding orientation. It is suspicious then to try to combine these data at regional scale. In addition, the direction of magnetisation for the Belubula Shale is very close to the present-day field orientation *in situ*. Hence, this direction may not be primary, although the κ parameter goes from $\kappa=30,3$ *in situ* to $\kappa=117,4$ after bedding correction, which makes the classic fold test (McElhinny, 1964) overcoming the 99,9% confidence level (with N=19). This positive fold test is therefore interpreted to be coincidental but may in addition results from a strong bias introduced in the calculation, because it seems that several specimens from the same core (*i.e.* with the same orientation) have been used. This problem may also exist for other results published by Goleby (1980), in particular for the Ordovician Molong High Formation [MhF] pole, which lies at higher latitude than other data (in African coordinates; figure 4.8), even if their respective 95% confidence cones still overlap in general.



Figure 4.8: Published poles (**stars**) coming from the Southern Tasmanides (except from the New England Orogen), and satisfying at least the “low” level selection. Mnemonics refers to Annexe II.

APW path (**squares**) for Australia from 0 to 175 Ma and prolonged by the “path-pattern” from 175 to 570 Ma deduced from small circle fit is shown for comparison purposes.

Red corresponds to present-day pole position; **light orange** for Neogene; **darker orange** for Palaeogene; **light green** for Cretaceous; **blue** for Jurassic (beyond 175 Ma, data are calculated from small circle fits); **pink** for Triassic; **brown** for Permian; **black** for Carboniferous; **violet** for Devonian; **yellow** for Silurian; **dark green** for Ordovician; **turquoise** for Cambrian; and **grey** for Late Neoproterozoic. For the path deduced from small circles, ages are assigned given a regular drift rate between the ages taken as limit for standstill positions of Euler poles. White and grey shaded areas correspond to envelopes of the 95% confidence cones. See Chapter 2 (§2.6.2) for details.

In African coordinates; orthogonal projection.

The Early Devonian pole from the Snowy River Volcanics (Schmidt *et al.*, 1987) is very good in term of statistical significance. The positive fold test is also convincing, and that is why many authors have used this result as a key-pole for the APW path of Gondwana. Nevertheless, the Early Devonian corresponds to the strongest orogenic event in the Eastern Lachlan Orogen. In addition, a bending in magnetic and fault patterns relative to the general North-South trend is visible on aeromagnetic images and geological map (figure 4.7) in the south of the Eastern Lachlan Orogen, close to the Snowy River Volcanics. It is not impossible then that terrane rotation occurred, even if this region may not be necessarily allochthonous. This only way to overcome this problem is to acquire reliable data of same age from another region. The conclusions are identical for the Givetian Comerong Volcanics (Schmidt *et al.*, 1986).

The Frasnian – Famennian Hervey Group studied by Li *et al.* (1988) is situated in the Molong area (figure 4.7). It consists of red and white quartzitic sandstones and minor red siltstone, which are predominantly alluvial with depositional environment fluctuating between braided (mixed load) and meandering (suspended load) fluvial systems (Pogson & Watkins, 1998). These terranes, if allochthonous, are then fully accreted to Gondwana, but their tight-folding and sometimes strong cleavage show that the region was still tectonically active. The general trend for fold axes is North-South suggesting an East-West direction of compression, but locally, fold trend may be very different like to the South-West of Manildra where it is NW-SE. This may results from a local specific strain orientation or from block rotation. Moreover, on the field, many meso-scale folds (about 10-20 meters) are quite significantly conical. Li *et al.* (1988), however, do not mention peculiar bedding correction of their data. It is possible thus, that part of their results have a incorrect structural control, and this may explain why the corresponding pole (figure 4.8) tends to be closer to the equator than many others like the Worange Point Formation [WPF] of Thrupp *et al.* (1991) although their 95% confidence cones are largely overlapping.

4.4.3. Cambrian data

Every Cambrian data come from palaeomagnetic studies located in the Flinders Ranges of South Australia, except one obtained in North-West Tasmania [NW Tas; not shown in figure 4.7] by Li *et al.* (1997). The late Early Cambrian Basal Lake Frome Group [BLFG] and Billy Creek Formation [BCF], and the early Early Cambrian Hawker Group [HkG]

have been published by Klootwijk (1980). The Tasmanian pole and the two late Early Cambrian poles have overlapping confidence cones but define however a track consistent with their age and sub-parallel to path obtained by Small Circle Fit and within its confidence envelop (figure 4.8).

From this point of view, the Hawker Group pole appears to be shifted to the North as it could be expected closer to South America (on the reconstruction of Gondwana; figure 4.8). Indeed, world-wide, there are 28 Ediacaran data (543 to 565 Ma) among which only 9 belongs to Gondwana (considering cratonic “green” & suspect “orange” regions; see Chapter 2, §.2.3 and figure 2.2): 3 from Africa, 4 from Australia, and 2 from South America. They all plot West of these Cambrian data, and the three best (satisfying the “high” level of selection described in Chapter 2; §.2.4.1) lie on the vicinity of the coast of Equator, *i.e.* close to the Small Circle Fit path for Late Neoproterozoic (figure 4.8). The APW path for Gondwana is therefore much more complicated if the Hawker Group pole is introduced between the Ediacaran and the other Cambrian poles, whereas it looks quite simple (similar in shape to the Small Circle Fit path) if this data is ignored.

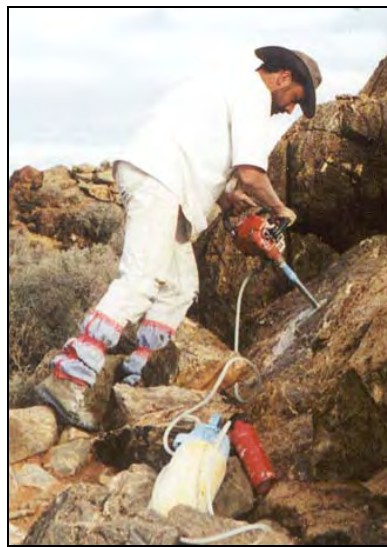


Photo 1: Rock sampling using a portable water-cooled drilling machine.

Summary of chapter 4

Localities have been chosen in the attempt to define a broadly East-West transect across the Tasmanides of New South Wales. Interest is here focused on Early – Mid Palaeozoic rocks and three areas could have been distinguished. The Molong area focuses on rocks from the Eastern Belt of the Lachlan Orogen, and especially on the Ordovician Macquarie Volcanic Arc. The Mount Bowen area is situated at the boundary between the Central and the Western Belt of the Lachlan Orogen, and the Broken Hill area, within the Delamerian Orogen in the North-East corner of New South Wales. A fourth area groups some pilot investigations that have been carried out to the south, in the region of Cooma and in the Narooma Zone.

Rocks from 50 localities (289 sites, 1576 cores, 3969 specimens; see table 1) have been collected, treated and analysed carefully using standard procedures. Bedding orientation and fold geometry have been in particular carefully studied to take into account the complexity of the structures commonly observed in the field. In addition, AMS measurements have been systematically carried out to determine magnetic fabrics and degree of internal strain, but also to control the bedding orientations. The Königsberger ratio is also systematically calculated and used as indicator regarding the possibility of lightning strikes. Rock magnetic measurements using the VFTBs housed at the laboratory of Munich were also performed to assess the magnetic mineralogy of the samples. In many cases, the intensity is revealed very weak and reaches the limit of the instruments, but still, general features can be recognised in spite of a noisy signal. All magnetic measurements have been conducted at the laboratory of the Ludwig-Maximilians-Universität in Munich, Germany.

Only some results of the 50 localities are presented in the following chapters, because magnetic signals are often not adequate for interpretations. The main causes are probably the relatively weak magnetic signal often measured, the high degree of weathering, and a complex magnetisation history. However, some are believed to be sufficiently representative to give interesting palaeomagnetic information. Moreover, sampling has been carried out where almost no palaeomagnetic study was before available. Ordovician to Devonian results from the Southern Tasmanides have been largely used to draw the APW path of Gondwana, but some of them appear to have low level of quality.

Chapter 5

Palaeomagnetic results from the Broken Hill area

5.1. Presentation of the Broken Hill area

5.1.1. Sampling coverage

Localities studied in far western New South Wales can be gathered in an area, covered by the 1:250 000 Koonenberry pre-Permian Interpretation Map (Stevens *et al.*, 2000), and which is referred here as to the Broken Hill area (figure 5.1).

These localities are listed in table 3 (and table 1 in Chapter 4; §.4.3), and plotted on a simplified geological map (figure 5.2) redrawn after that of Stevens *et al.* (2000). Six out of ten are located along the Koonenberry fault, either in the Mt Daubeny Basin in the Wertago terrane West of the fault, or in the Kayrunnera terrane East of it. Rock samples are rather Late Cambrian or Early – Mid Devonian. The only clear Early Ordovician rocks are found nearby the Arrowsmith Property, in the North – West corner of the map. Only two localities (GUM & CHU) could have been drilled south of the apparent bending in fault trend (see below).

5.1.2. Geological features

The simplified map mainly focuses on the Wertago terrane situated between the Bynguano fault to the East and the Koonenberry fault to the West.

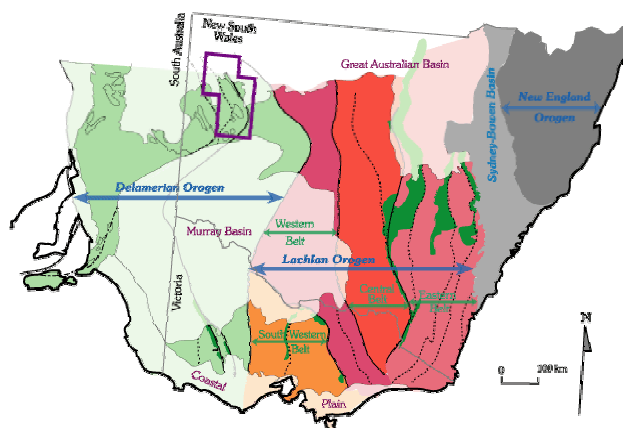


Figure 5.1: Inset recalls the position the Broken Hill area in the Southern Tasmanides as presented on the map of figure 4.7 (Chapter 4). The corresponding simplified geological map is shown in figure 5.2.

Table 3: List of localities in the Broken Hill area

Mnemonics	Names coming from	Location (Long. /lat.)
ARO	Arrowsmith property	141,5993 / -30,1760
ARR	Arrowsmith property	141,5993 / -30,1760
CHU	Churinga property	142,7671 / -31,7033
CUP	Cupala Creek Formation	142,6717 / -30,9295
DAU	Mt Daubeny Formation	142,6281 / -30,9652
FUN	Funeral Creek Formation	142,2074 / -30,3819
GUM	Gum Creek Formation	142,3563 / -31,8647
KAN	Kandie Tank Limestone	142,5911 / -30,8500
SIS	The Sisters (rhyolite)	142,6281 / -30,9652
WER	Wertago property	142,6417 / -30,9963

Mnemonics refer to table 1, Chapter 4; §.4.3.

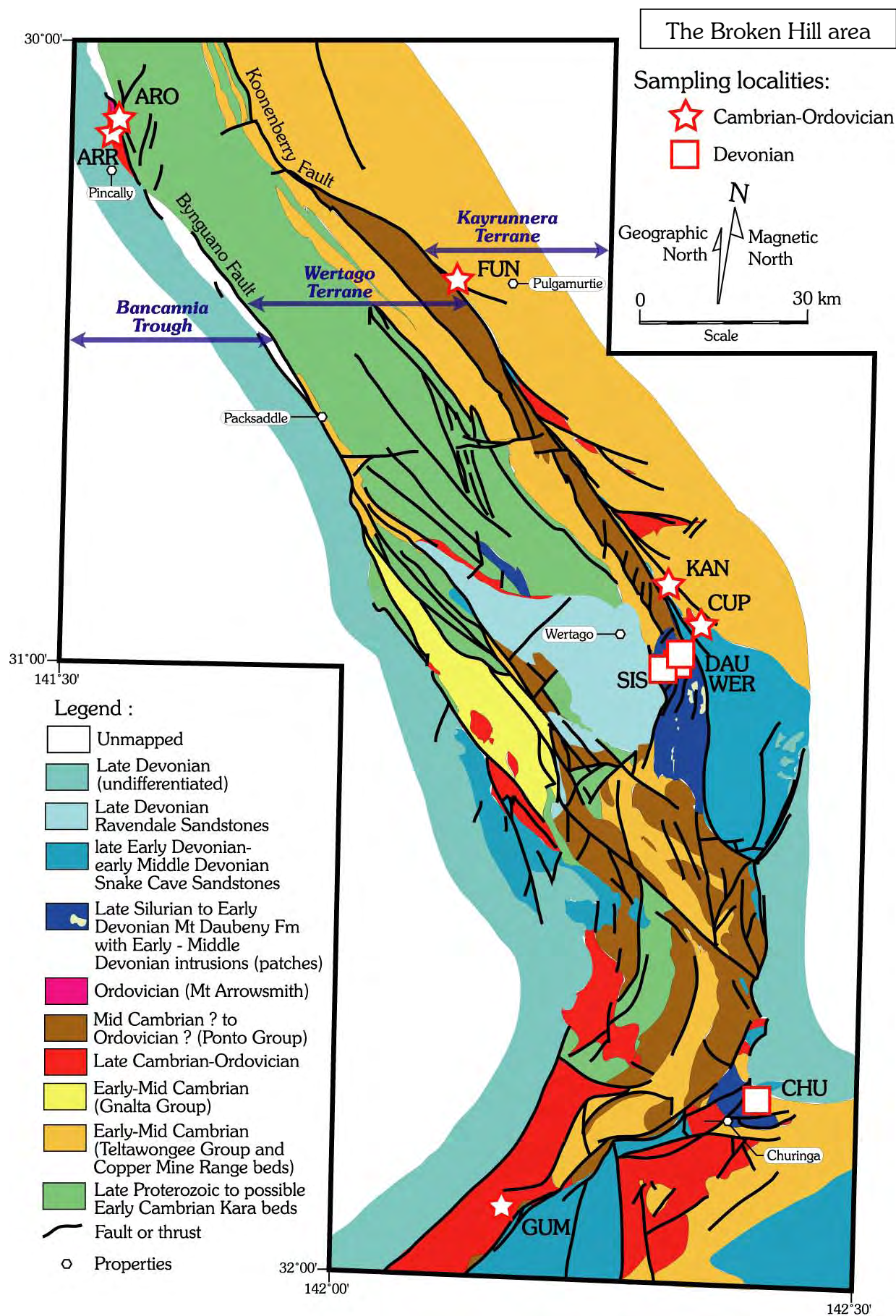


Figure 5.2: Simplified geological map of the Broken Hill area, showing localities studied (see also table 3). Map redrawn after the 1:250 000 pre-Permian Koonenberry interpretation map of Stevens *et al.* (2000).

The striking feature of this map is the change from the NNW fault trend of the northern two thirds of the map to the NNE trend in the southern third. The trend of the cleavage shows also a $\sim 120^\circ$ change in direction from North to South (Mills, *personal communication*, 2001). Whether this trend just expresses compression against a protruding crustal block, or indicates relative block rotation, is not known.

Early-Mid Cambrian rocks have been tightly folded during the Delamerian Orogeny. This tectonic event seems to be centered around 510 Ma and probably lasted not much longer than ~ 10 -20 Ma (Mills, *personal communication*, 2001). On the contrary, Late Cambrian and Ordovician rocks only show mild deformation. Nevertheless, strike-slip faulting occurred at least along the Koonenberry fault. First, with a dextral movement leading to the opening of the Mt Daubeny pull-apart basin in the Silurian(?) and Early Devonian, then, with a sinistral movement involving structural inversion in the Early-Mid Devonian and probably in the Carboniferous in relation with the Alice Spring Orogeny of central Australia.

5.2. The Mount Arrowsmith Property (ARR & ARO)

5.2.1. Presentation



The localities ARR and ARO belong to the Mount Arrowsmith Property, East of Pincally, in the NE corner of the map (figure 5.2). Three formations have been drilled: one site in the Middle Cambrian grey shale and siltstone of the Pincally Formation, seven in the Middle – Late Cambrian dolomites of the Wydjah Formation, and three in the Ordovician red sandstone of the Tabita Formation.

The dolomites (photo 3) uncomfortably overlie the Middle Cambrian siltstones, which are poorly exposed because most of it is covered by a sand dune. The top of the Cambrian rocks is probably bounded by a fault running along a ridge of quartzite (photo 2). This quartzite seems to reappear on a second ridge to the East (right hand side of photo 2), and this may define a syncline, wherein the only clear Ordovician rocks of the Broken Hill area are found (Percival, *personal communication*, 2001).



Photo 2 (top)- Syncline of Ordovician rocks of the Mt Arrowsmith Property delimited by two ridges of quartzite. To the West (left hand side), the Middle – Late Cambrian Wydjah Formation seems to be bounded by a fault running along the quartzite. Geologists in centre of the picture give the scale.

Photo 3 (bottom)- Sub-vertical beds of Middle – Late Cambrian dolomites of the Wydjah Formation. The sample orienter gives the scale of these beds.

Fifteen cores (3 sites) have been collected in the Ordovician sandstone, locality ARO (just East of the western ridge of quartzite on photo 2), thirty-seven cores in the dolomites and five in the siltstone (1+7 sites) of the Middle – Late Cambrian Pincally & Wydjah formations, locality ARR. Rock magnetic and palaeomagnetic results will be shown just for the dolomites (see below).

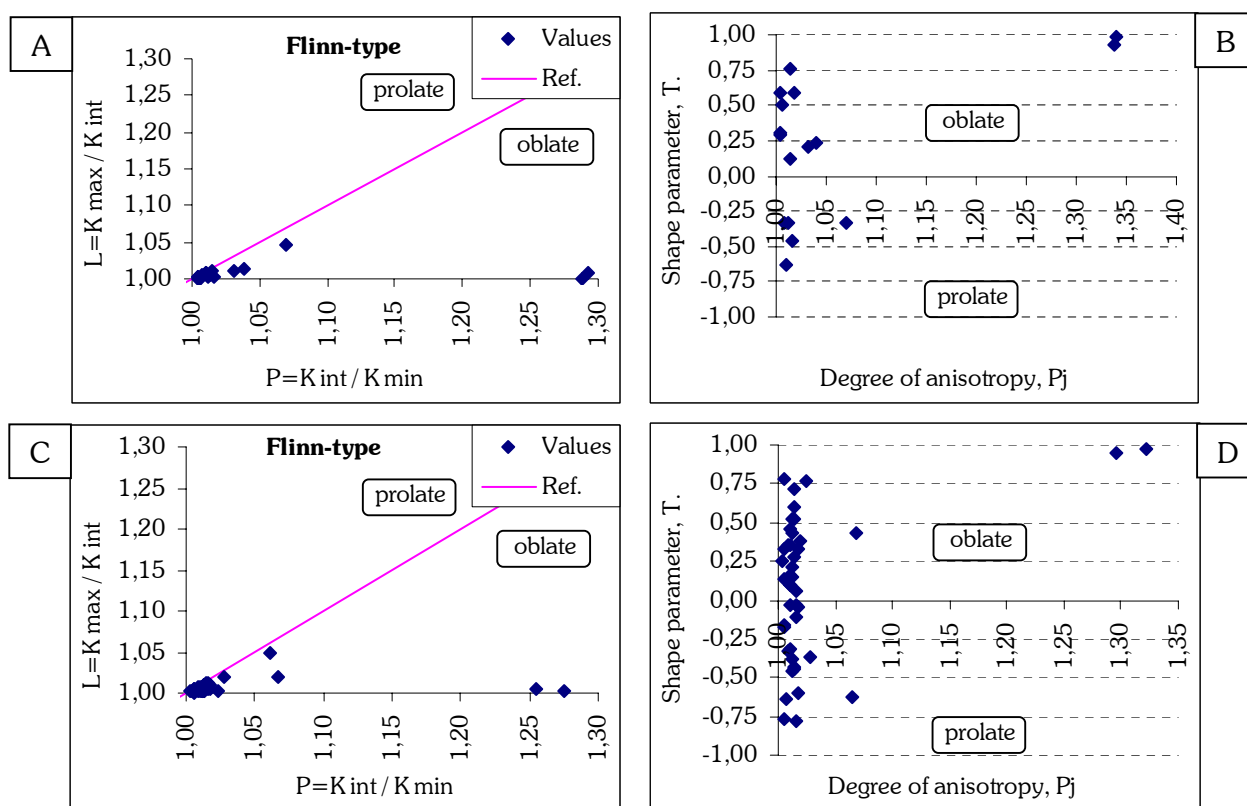
5.2.2. Anisotropy of magnetic susceptibility (AMS)

The AMS parameters show that (except for two data having high degree of susceptibility probably due to environmental magnetic perturbation during data acquisition), the degree of anisotropy in both the Cambrian and Ordovician rocks is low (figures 5.3) with P_j about 1,02 in average. In both cases, the shape parameter $\{T\}$ tends to have a positive value, which expresses a slight oblate shape of the ellipsoid of magnetic susceptibility (figures 5.3-B & D). The Flinn-type diagrams (figures 5.3-A & C) confirm this as all points plot in the oblate side.

It can, therefore, be concluded that these rocks have not undergone penetrative deformation and that internal strain can be neglected in the localities ARR and ARO.

The Königsberger ratio Q_K (Königsberger, 1938) in the dolomites equals $3,09 \pm 4,40$ in average (with standard deviation) at room temperature (written @RT) and drops down to $0,48 \pm 0,87$ after heating to 80°C (written @ 80°C). This change seems to be caused by the presence of important viscous magnetisation at low temperatures (shown by demagnetisation procedure below). No direct information about the grain size can be drawn because of multiple magnetic carriers but it appears that lightning effects can be discarded.

The susceptibility prior to heat treatment of these dolomites ranges from $3,4 \cdot 10^{-5}$ to $1,8 \cdot 10^{-4}$ SI.



Figures 5.3: **A-** Flinn-type diagram (Flinn, 1962, 1965-a, 1965-b) and **B-** $\{T\}$ versus $\{P_j\}$ diagram (Jelinek, 1981; Hrouda, 1982) for the Ordovician red sandstone of locality ARO; **C-** Flinn-type diagram and **D-** $\{T\}$ vs $\{P_j\}$ diagram for the Middle – Late Cambrian rocks of the locality ARR.

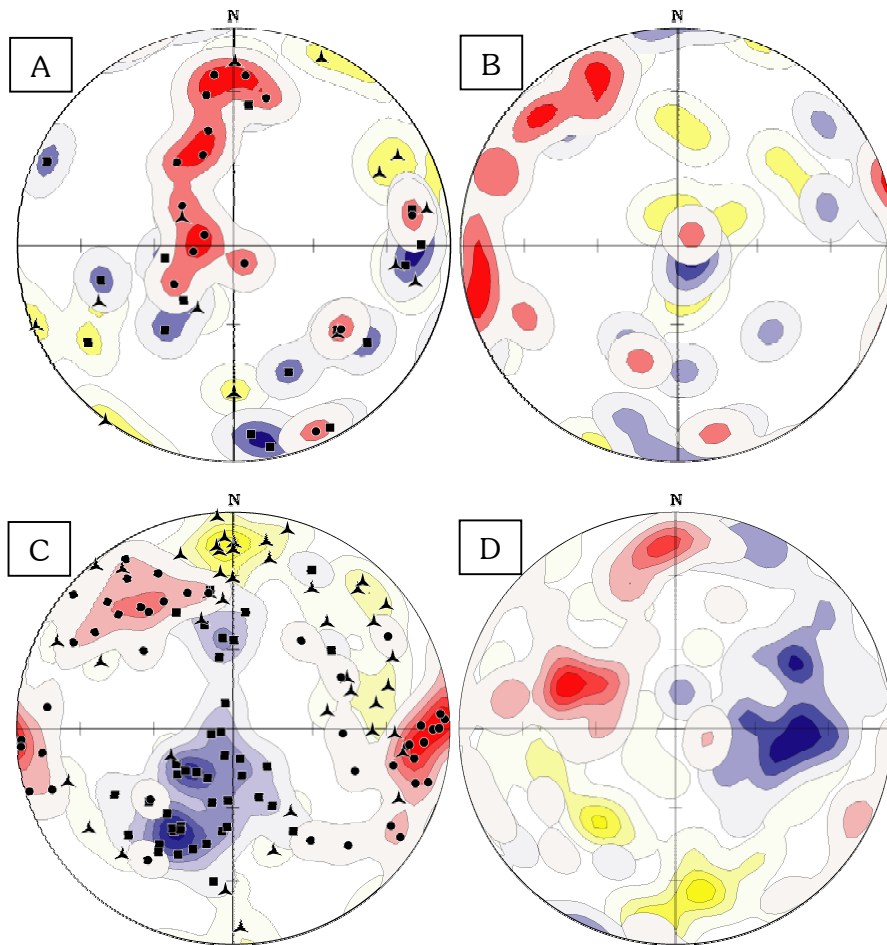


Figure 5.4: Orientations of the principal axes of magnetic susceptibility for localities ARO and ARR.

Locality **ARO**, Ordovician sandstone, **A-** *in situ* and **B-** after bedding correction.

Locality **ARR**, Middle – Late Cambrian Pincally & Wydjah formations, **C-** *in situ* and **D-** after bedding correction.

Kmax (**squares**) and associated density contours (**blue**); Kint (**triangles**), and **yellow** density contours; Kmin (**dots**), and **red** density contours. For sake of clarity, data points are only drawn *in situ*.

Stereographic projection, Schmidt equal area, lower hemisphere; density contours with Gaussian counting model, K=100.

The orientations of the principal axes of magnetic susceptibility are relatively scattered (figures 5.4). This is probably related to the weak degree of anisotropy.

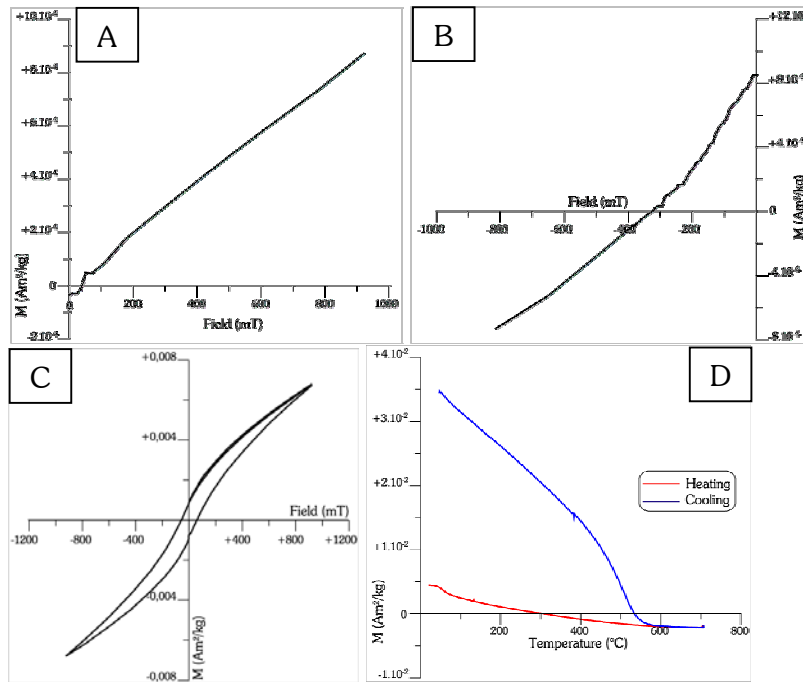
In the Ordovician rocks (ARO) however, the majority of Kmin axes *in situ* tends to be aligned from the vertical to a northern shallow position (figure 5.4-A), whereas they become E-W to NW-SE after bedding correction. By contrast, in the Middle – Late Cambrian rocks (ARR), a clear E-W direction and a more vague NW-SE direction are visible for the Kmin axes. After bedding correction, the E-W direction becomes oblique and the NW-SE adopts a northern shallow position. A sub-vertical magnetic fabric acquired after folding (figure 5.4-A) is hardly conceivable from tectonic strain and this feature should have been recorded prior to folding.

There are several possibilities for the origin of these magnetic fabrics:

1. Both magnetic fabrics have been first acquired prior to folding (thus, stereograms after bedding correction). They show that Ordovician rocks moved westerly over Cambrian rocks (East dipping thrust) during an E-W compression recorded in ARO. A N-S compression overprinted both fabrics after folding, being sufficiently strong to position Kmin in a northern shallow orientation for ARO (figure 5.4-A) but not for ARR (figure 5.4-C) where Kint show these orientations.
2. The magnetic fabric shows an E-W compression, perhaps changing to NW-SE (or inversely), that occurred after folding of the Cambrian rocks, but prior to folding of Ordovician rocks.
3. An E-W compression is recorded before folding in Ordovician rocks and after in Cambrian rocks, and then a N-S compression occurred, after both folding, positioning Kmin in a northern shallow orientation and not strong enough to overprint the magnetic fabric in the Cambrian rocks as Kint show the northern shallow orientation. Same story as [1] but no thrust, and the magnetic fabric in ARR only stems from post-folding recording.

However, the orientations of the principal axes of magnetic susceptibility are too scattered, and any firm conclusions from these results can be considered as over-interpretation.

5.2.3. Rock magnetism for the dolomites of Mt Arrowsmith



Figures 5.5: Example of rock magnetic measurements in the dolomites of the Wydjah Formation (locality ARR): specimen ARR5-5.

A- IRM curve; **B-** Back field curve (coercivity); **C-** Hysteresis properties; and **D-** IST curve, in red while heating and in blue while cooling ($B=535$ mT).

$H_C=93,3$ mT; $H_{CR}=325,2$ mT.

$M_S=210,1 \cdot 10^{-5}$ Am²/kg; $M_{RS}=80,6 \cdot 10^{-5}$ Am²/kg.

One example of rock magnetic measurements performed on a specimen of dolomite of the Wydjah Formation is shown here (figures 5.5).

The IRM and back field curves show clearly the presence of strong coercivity minerals as both curves are not saturated (figures 5.5-A & B). The IST curve (figure 5.5-D) decrease almost linearly up to 700°C while heating. This shape is close to paramagnetic behaviour, which is confirmed by the slope of the hysteresis curve (figure 5.5-C). The IST curve reveals also that an important amount of magnetite is formed while cooling.

These curves are difficult to interpret. It can be suggested however that the high coercivity stems from the presence of goethite, as a slight decrease is visible around 70°-80°C (also

visible in the remanence; see below), but not from hematite as no magnetisation appears to exist above 600°C. The paramagnetic behaviour could be due to the presence of siderite or some phyllosilicates, which can also explain the new formation of magnetite. Magnetite however, is probably present already at room temperature. Negative values by 600°-700°C are mainly due to the diamagnetic contribution of calcite.

5.2.4. Palaeomagnetic results for the dolomites of Mt Arrowsmith

Palaeomagnetic results are shown only for the dolomites of the Wydjah Formation, because of the number of samples collected on the one hand, but also because results obtained from the Cambrian Pincally Formation and from the Ordovician Tabita Formation can be considered as randomised.

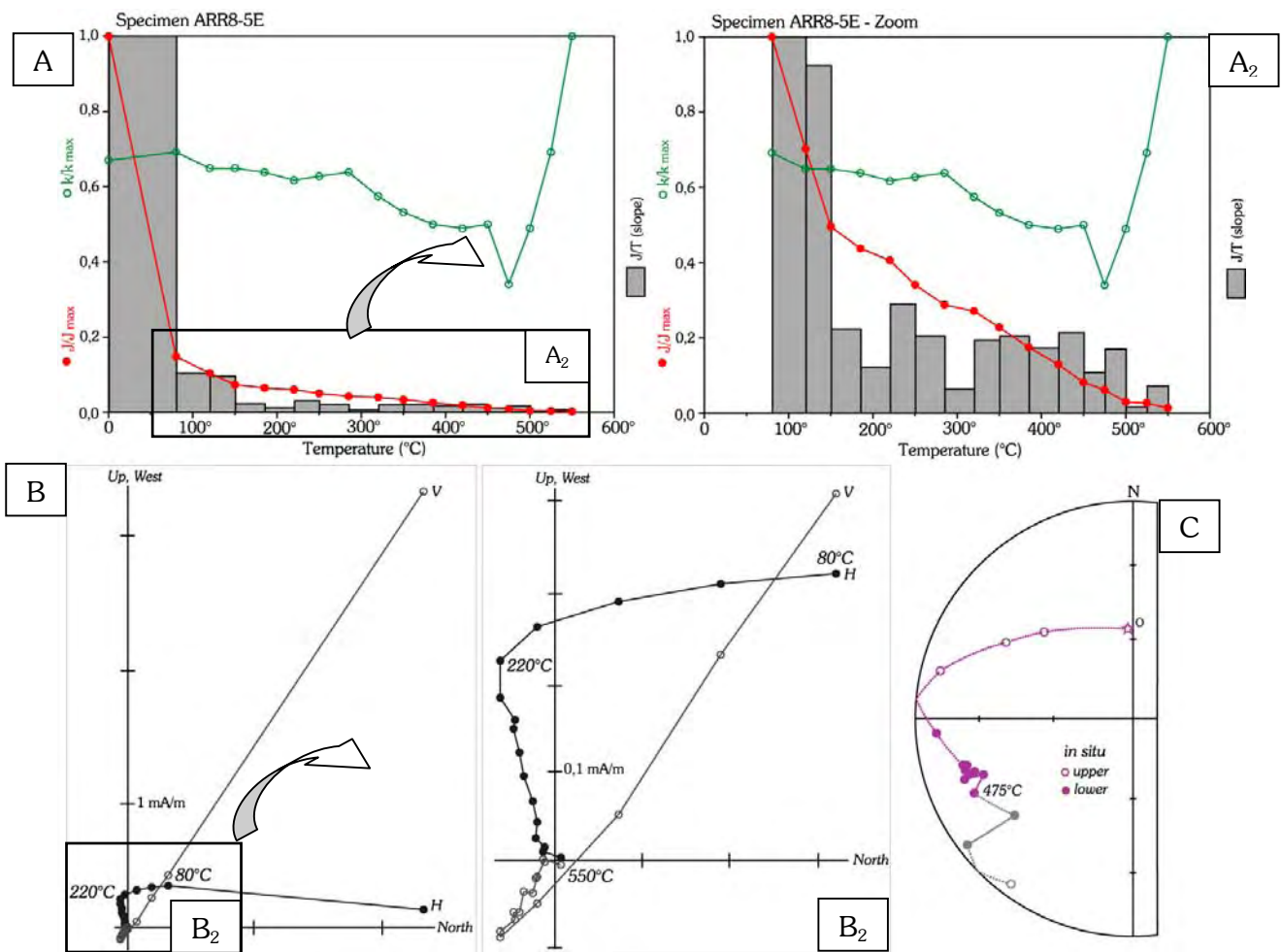
- Demagnetisation

The 37 specimens have been thermally demagnetised. The example shown here (figures 5.6) is representative of the locality as a strong viscous magnetisation carries more than 80% of the remanence below 80°C. This is in agreement with the existence of goethite as suggested by rock magnetic measurements. The first component C_1 , however, persists up to 220°C, proving that goethite is not the only magnetic carrier of C_1 . Nevertheless, other carriers of C_1 remain unidentified. A second component, C_2 , is demagnetised from 220° to 500°-550°C and appears to be mainly carried by magnetite.

- Interpretation

The low temperature components C_1 (red squares in figure 5.7) correspond clearly to the present-day field and the overall mean direction is oriented $D.359,4^\circ/I.-57,4^\circ$ ($N=28$; $R=27,4$; $\alpha_{95}=4,3^\circ$; $\kappa=41,7$; *in situ*).

When single specimen components C_2 are plotted on a stereogram (figure 5.7), they are distributed on a great circle, which has a pole oriented $D.001^\circ/I.+43^\circ$ ($\alpha_{95}=10,1^\circ$). The overall mean direction for these components has therefore no signification (and is consequently not shown in figure 5.7), but the density contours shows a peak directed $D.185,2^\circ/I.+52,0^\circ$, *in situ*. This is of reverse polarity from the present-day field (positive reversal test classified C from components C_1 and the density peak of components C_2). Hence, although components are defined from clear segments on Zijderveld diagrams, this distribution probably illustrates the strong weathering that affects Australian rocks.



Figures 5.6: Example of palaeomagnetic results obtained by thermal demagnetisation from the dolomites of the Wydjah Formation (locality ARR). Intensity of $NRM@RT=4,04$ mA/m; $NRM@80^\circ C=6,01 \cdot 10^{-1}$ mA/m.

A- Demagnetisation curve showing on Y-axis the normalized (J/J_{max}) intensity in red, and in green, the normalized susceptibility (k/k_{max}) versus temperature in degree Celsius on the X-axis. Boxes are the first derivative (J/T) of the thermal demagnetisation curve (*i.e.* slope of the red line). **A₂-** Zoom on the inset shown on A. **B-** Orthogonal projection (Zijderveld, 1967) of the resultant vector *in situ* during demagnetisation, with open circles, projection on the vertical plane [V], and closed circles, projection on the horizontal plane [H]. **B₂-** Zoom on the inset shown on B. **C-** "Schmidt" equal area polar projection of *in situ* orientations of the resultant vector of magnetisation during heating. The origin [O] measured at room temperature is shown with a star. Coherent magnetic signal is drawn in violet, while it is represented in grey when it becomes unstable. Open circles are negative inclination values (upper hemisphere); closed circles, positive inclination values (lower hemisphere).

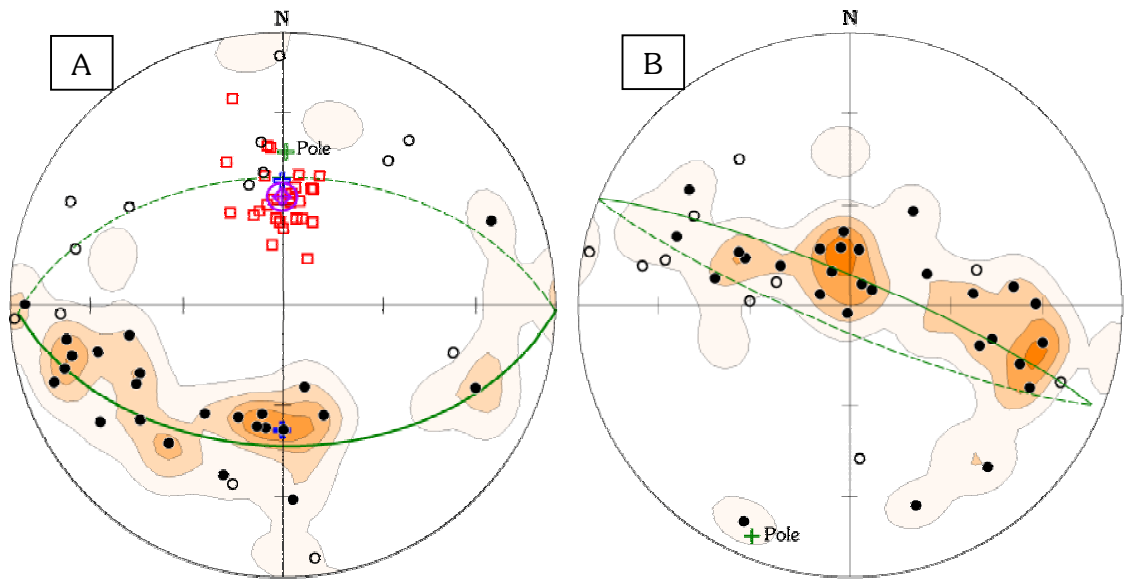


Figure 5.7: Direction of components obtained from the dolomites at Mt Arrowsmith (locality ARR). **Blue crosses** show the present-day field direction. **Red squares** represent single sample components C_1 , and the corresponding mean direction is shown with the **violet diamond** and its confidence cone (α_{95}). **Black dots** are single sample components C_2 . They lie on a great circle (**green**), which has a **pole** marked by a green cross. **A-** *in situ*. The density peak is of reverse polarity (positive reversal test R_C) from the mean direction of C_1 , and is computed from the **orange** density contours (Gaussian counting model; $K=100$). **B-** after bedding correction; only C_2 components are represented. Schmidt equal area projection. **Open** symbols are negative inclination values (upper hemisphere); **closed** symbols, positive inclination values (lower hemisphere).

5.3. The Funeral Creek Limestone (FUN)

5.3.1. Presentation

The limestone exposed close to the Funeral Creek is unnamed, but probably belongs to the Kayrunnera Group (Stevens *et al.*, 2000) and is Late Cambrian in age (conodonts). They are referred here to as the Funeral Creek Limestone; locality FUN. The small outcrop studied (photo 4) is situated SW of Pugamurtie, along the Koonenberry fault, the major fault separating the Wertago terrane to the West from the Kayrunnera terrane to the East (figure 5.2).

This limestone is well-bedded and forms a syncline. The north-western flank dips 45° SE (shown in photo 4) and the south-eastern flank dips 80° - 90° NW, the hinge being affected by a sub-vertical cleavage.

Six sites (30 cores) have been drilled in this limestone on both side of the syncline.



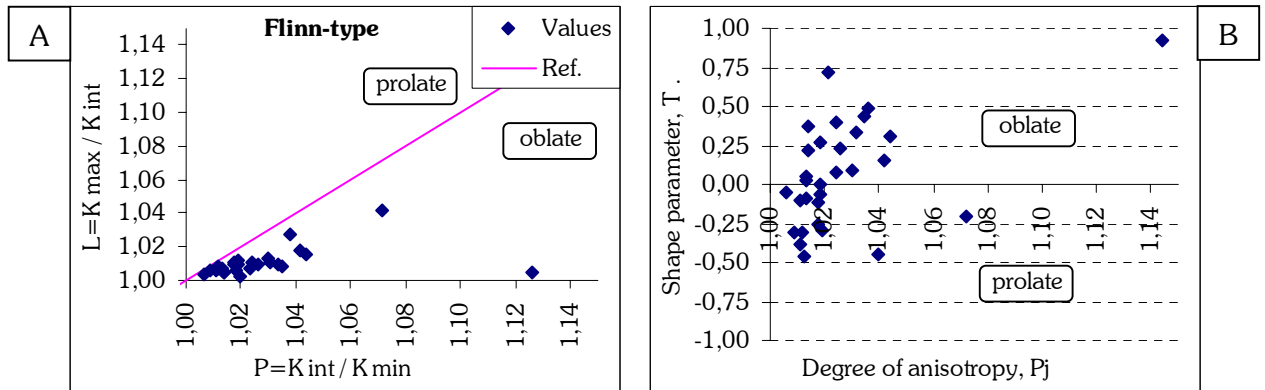
Photo 4: Late Cambrian limestone near the Funeral Creek in the vicinity of Pugamurtie. The 30-50 cm thick beds dip about 45° to the South-East on the picture but reappear with a sub-vertical bedding about 20 meters further South East (*i.e.* left hand side off picture).

5.3.2. Anisotropy of magnetic susceptibility (AMS)

Although the degree of anisotropy is rather low ($P_j = 1.03 \pm 0.03$), the Flinn-type diagram shows clear tendency of the ellipsoid of magnetic susceptibility to be oblate (figure 5.8-A). It is not that pronounced when looking at the shape parameter as $T = 0.07 \pm 0.34$ (figure 5.8-B).

However, despite the close vicinity of the Koonenberry fault and the cleavage affecting part of the outcrop, this limestone does not appear to be affected by internal strain ($Q_K@80^\circ\text{C}=1,88\pm2,38$ discarding also any lightning effects).

The density contours help visualising that the orientations of the principal axes of magnetic susceptibility are scattered, probably in relation with the low degree of anisotropy, but not randomised *in situ* (figure 5.9-A). This is apparently not the case after bedding correction (figure 5.9-B).



Figures 5.8: **A-** Flinn-type diagram (Flinn, 1962, 1965-a, 1965-b) and **B-** $\{T\}$ versus $\{P_j\}$ diagram (Jelinek, 1981; Hrouda, 1982) for the Late Cambrian Funeral Creek Limestone of locality FUN.

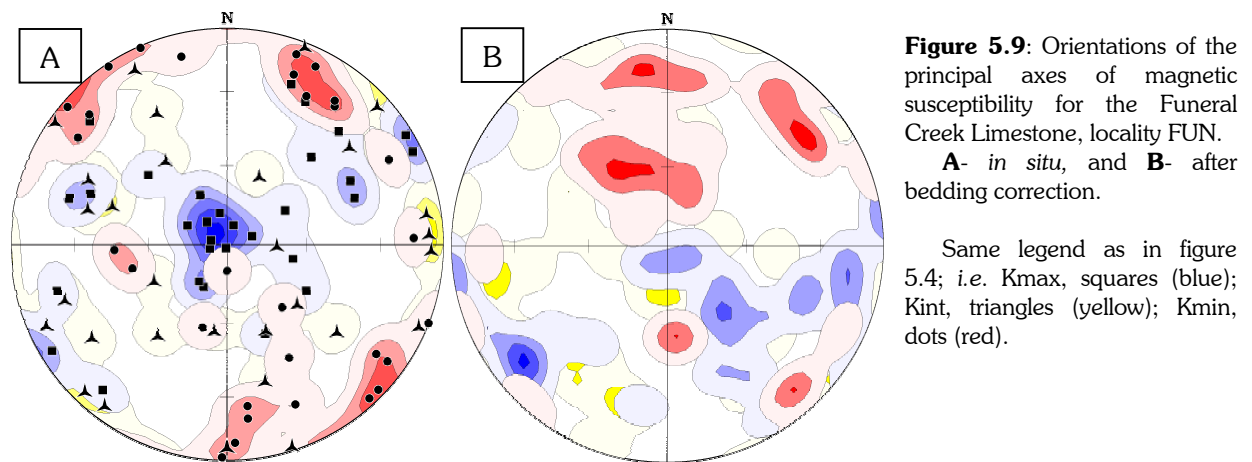


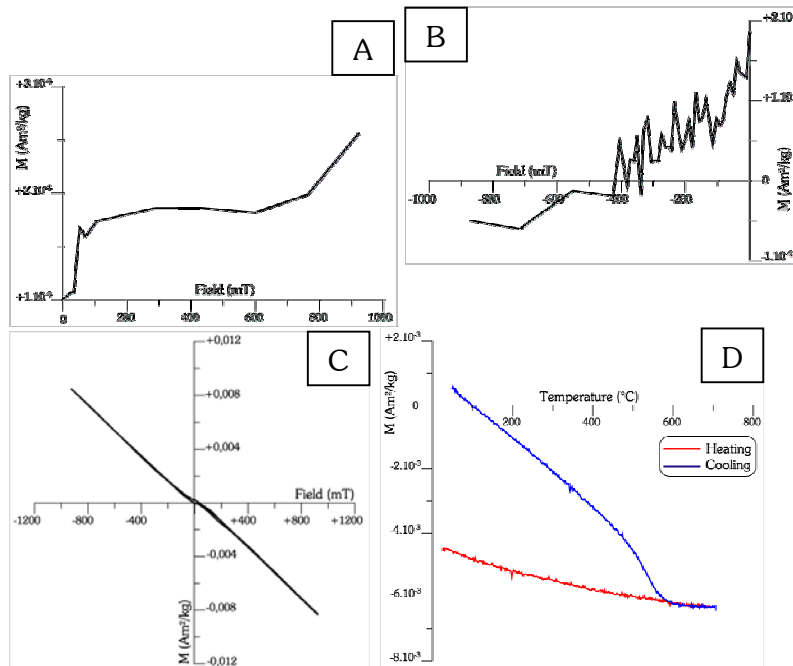
Figure 5.9: Orientations of the principal axes of magnetic susceptibility for the Funeral Creek Limestone, locality FUN.

A- *in situ*, and **B-** after bedding correction.

Same legend as in figure 5.4; i.e. Kmax, squares (blue); Kint, triangles (yellow); Kmin, dots (red).

The three axes of magnetic susceptibility are predominantly positioned on horizontal and vertical plan *in situ*, whereas they appear to be oblique after bedding correction. This is clearly in favour of a magnetic fabric acquired after folding. Kmin situated on horizontal plan and Kmax about vertical represent a tectonic magnetic fabric. Two main directions emerge from the distribution of Kmin: a NW-SE direction (also perpendicular to a vertical great circle containing most of Kmax), and a poorly defined $\sim N.15^\circ$ direction. The first direction is parallel to the main-trend orientation of the Koonenberry fault and may be associated to strike-slip movement along it. The second is rather perpendicular to another fault oriented $\sim N.115^\circ$ (figure 5.2). This fault is similar to a series of faults along the Koonenberry fault, which resemble to Riedel faults associated with dextral strike-slip movement. A direction of Kmin perpendicular to this Riedel fault may be the recording of compression during reactivation of the Koonenberry fault.

5.2.3. Rock magnetism



Figures 5.10: Example of rock magnetic measurements in the Funeral Creek Limestone (locality FUN): specimen FUN3-3.

A- IRM curve; **B-** Back field curve (coercivity); **C-** Hysteresis loop; and **D-** IST curve, in red while heating and in blue while cooling ($B=535$ mT).

$H_C=17,3$ mT; $H_{CR}=406,4$ mT.

$M_S=47,4 \cdot 10^{-5}$ Am²/kg; $M_{RS}=13,8 \cdot 10^{-5}$ Am²/kg.

dolomites from the Wydjah Formation. A little amount of goethite may be present, explaining that IRM and back field curves are not totally saturated, but not in sufficient quantity to overcome the diamagnetic response shown by the hysteresis loop. The existence of siderite or some phyllosilicates can be responsible for the formation of magnetite while cooling. Magnetite is however already present in the limestone as shown by the rapid increase of magnetisation of the IRM curve, and value of the coercive force ($H_C=17,3$ mT).

5.2.4. Palaeomagnetic results

- Demagnetisation

Thermal demagnetisation reveals two main components in the Funeral Creek Limestone. The first, component C_1 , is sometimes overprinted by a viscous or drill-induced magnetisation, but is defined up to 120°C (figure 5.11-B) although more than 60% of the remanence is removed before 80°C (figure 5.11-A). The intensity, however, keeps on decreasing up to 220°C, illustrated by the higher values of the first derivatives (boxes in figure 5.11-A). This suggests goethite as main but not unique magnetic carrier for component C_1 . This was suspected by rock magnetic measurements.

The last component, C_2 , can be demagnetised up to 550°C, and is probably carried by magnetite (which is moreover common in limestone).

- Interpretation

The direction of magnetisation of C_1 , which are not overprinted by viscous magnetisation, correspond clearly to the present-day field (red squares in figure 5.12). The overall mean direction is D.006,5°/I.-60,0° ($N=18$; $R=17,8$; $\alpha_{95}=3,8^\circ$; $\kappa=83,3$; *in situ*).

The hysteresis loop shows a strong contribution of diamagnetic minerals, certainly calcite (figure 5.10-C). This also explains the negative values on the IST curve (figure 5.10-D).

The IRM and back field curves (figures 5.10-A & B) are noisy, but seems to show the presence of both relatively low coercivity minerals and some high coercivity minerals.

The decrease in magnetisation looks rather constant while heating on the IST curve, but the increase by 500°-575°C while cooling most probably depicts the formation of magnetite. This behaviour is very similar to that observed in the dolomites of the Wadjah Formation, near Mt Arrowsmith.

It is possible, therefore, that magnetic minerals present in the Funeral Creek Limestone are analogous to that of the

Concerning components C_2 , a few seem to plot randomly but a majority shows two orientations of inverse polarity (figure 5.12). The overall mean direction is $D.180,8^\circ/I.+53,3^\circ$ ($N=16$; $R=15,8$; $\alpha_{95}=4,2^\circ$; $\kappa=80,2$; *in situ*). This direction corresponds again to the present-day field, and it is confirmed by a positive reversal test classified B *in situ*, and by a significant negative fold test (McElhinny, 1964). It must be pointed out here that this fold test is labelled “significantly negative”, as it becomes positive at only 2,6% confidence level, i.e. below 5% (see related equations in Chapter 4; §.4.1.2).

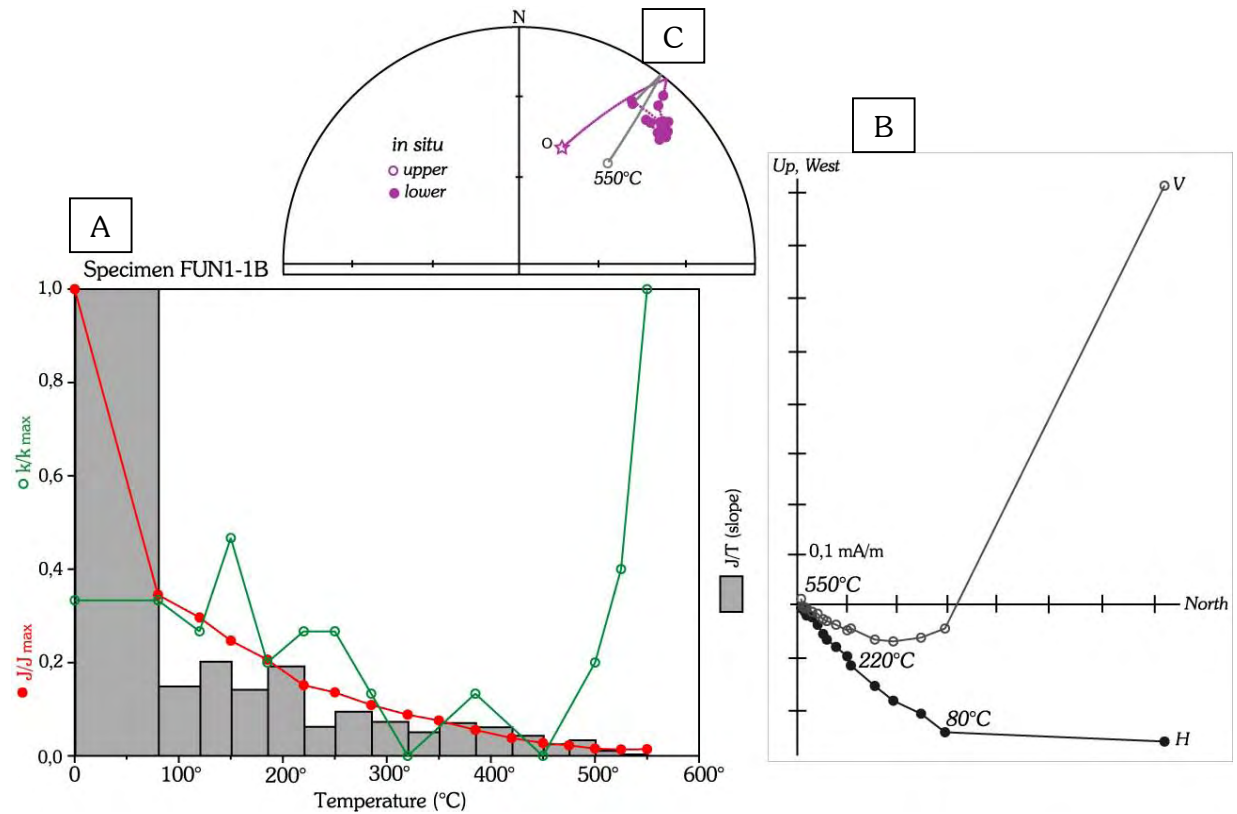


Figure 5.11: Example of palaeomagnetic results obtained by thermal demagnetisation from the Funeral Creek Limestone (locality FUN). $NRM@RT=1,11$ mA/m; $NRM@80^\circ C=3,83 \cdot 10^{-1}$ mA/m. Same legend as in figure 5.6 (all *in situ*); i.e. **A**- Demagnetisation curve with red closed circles, normalised intensity; green open circles, susceptibility; grey boxes, slope of intensity. **B**- Zijderveld diagram with open circles, projection on the vertical plane [V]; closed circles, on the horizontal plane [H]. **C**- Stereogram; “Schmidt” equal area polar projection.

Some component C_2 finally, defined by a clear rectilinear vector such as per specimen FUN1-1 (example shown in figure 5.11), point to another direction (green triangles in figure 5.12). It reflects a composite direction of magnetisation as they can be linked by a great circle having a pole orientated $D.316^\circ/I.+21^\circ$ ($\alpha_{95}=12,1^\circ$).

These results from the Late Cambrian Funeral Creek Limestone are very similar to that obtained in the Late Cambrian dolomites of the Wydjah Formation at Mount Arrowsmith. In this case, however, the negative fold test confirms the post-folding acquisition of magnetisation, and favours the hypothesis that the directions of magnetisation of component C_2 correspond indeed to the present-day field although two polarities exist and are in turn confirmed by a positive reversal test (R_B). Moreover, it is well in agreement with the significant proportion of oxidised minerals, usually carrying more than 50% of the remanence at room temperature. It demonstrates the strong weathering affecting Australian rocks.

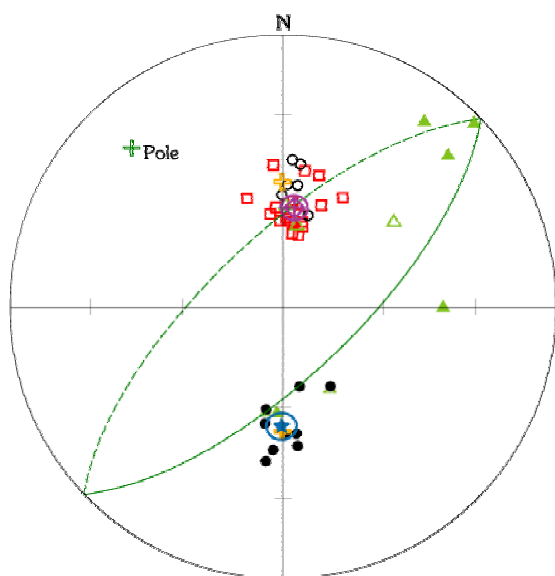


Figure 5.12: *In situ* directions of components obtained from the Funeral Creek Limestone (locality FUN).

Red squares represent single sample components C_1 , and the corresponding mean direction is shown with the **violet diamond** and its confidence cone (α_{95}).

Black dots are single sample components C_2 of dual polarities. The corresponding overall mean is the **blue star** with its 95% confidence cone (α_{95}). Other components C_2 (**green triangles**) have intermediate orientations and lie on a great circle (green), which has a **pole** marked by a green cross.

Orange crosses represent the present-day field direction.

Open symbols are negative inclination values (upper hemisphere); **closed** symbols, positive inclination values (lower hemisphere). Schmidt equal area polar projection.

5.4. The Cupala Creek sandstones (CUP)

5.4.1. Presentation



Photo 5: Photo taken from the hill where the Late Cambrian red sandstone from the Cupala Creek Formation are exposed. The ridge to the South West (right hand side of the picture) is made up with the late Early to early Middle Devonian quartzose sandstone and quartzites of the Snake Cave sandstone, unconformably overlying the Cupala Creek Formation. The underlying Early – Middle Cambrian Teltawongee beds outcrop in a creek just before the hill visible to the East (left hand side of the picture).

The studied locality (CUP) is situated in the Kayrunnera terrane (figure 5.2; photo 5). Rocks sampled are part of the Cupala Creek Formation, which consists of well-laminated red quartzose sandstones, poorly fossiliferous with only Mindyallan (early Late Cambrian) trilobites remaining at the base (Stevens *et al.*, 2000). The Kandie Tank Limestone, exposed about 15km to the North however (see below), appears to correspond to a latitudinal change in facies near the top of the Cupala Creek Formation, and yielded conodonts of latest Cambrian age (Mills, *pers. comm.*, 2002). Hence, the Cupala Creek Formation is considered Late Cambrian in age.

The Teltawongee beds, unconformably underlying the Cupala Creek Formation, are made up of tight upright folded turbidite facies sandstone of Early to Middle Cambrian age. They were deformed by the Delamerian orogeny, which is there believed to be centred around 510 Ma and probably lasted not more than 10 Ma (Mills, *pers. comm.*, 2002). Conversely, the Cupala Creek Formation is a post-Delamerian sequence, and forms a broad syncline where samples have been collected. This gentle folding is interpreted to be either Late Ordovician or Early Devonian in age (Mills, *pers. comm.*, 2002).

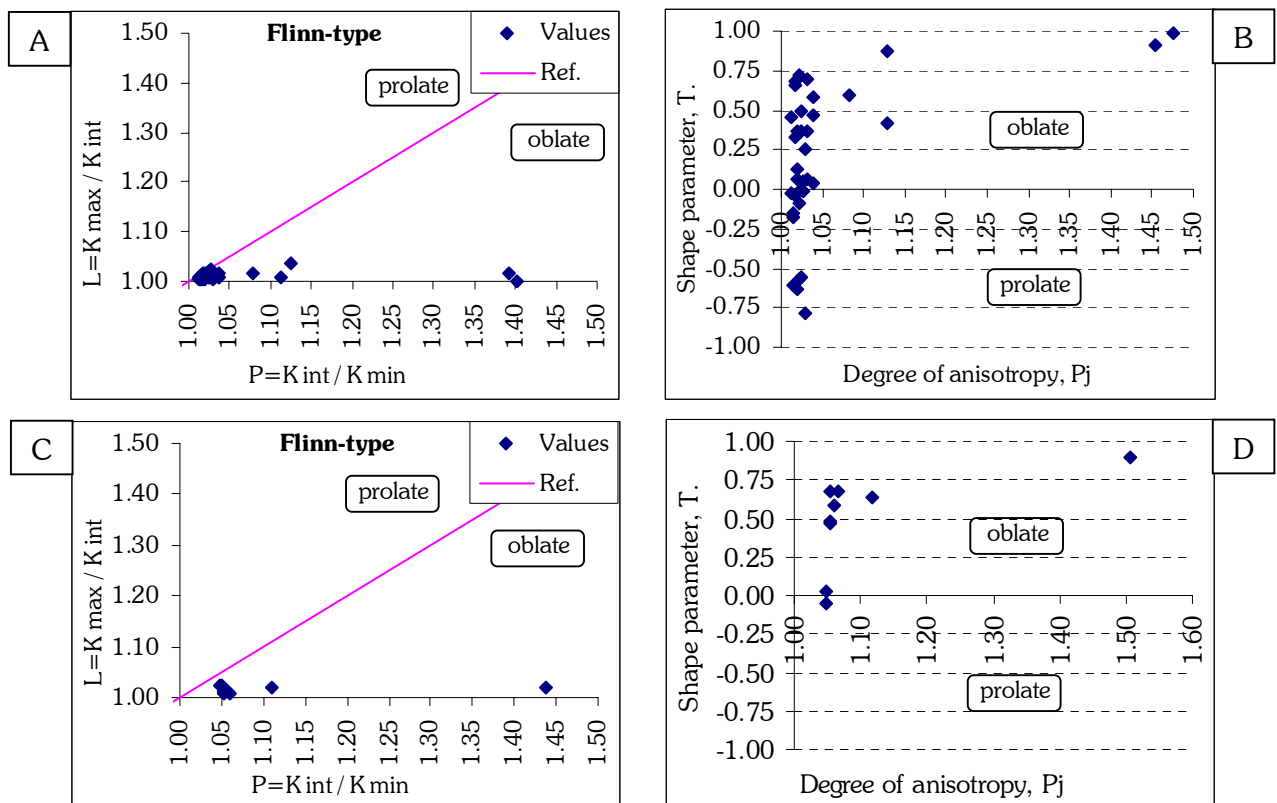
Seven sites (37 cores) have been drilled on one limb only of the poorly exposed syncline (bottom part of photo 5). As it was not possible to get a fold test, an extra site (10 cores) has been drilled in the underlying Teltawongee beds exposed in a creek situated in front of the hill on the left of photo 5 in order to perform an unconformity test.

5.4.2. Anisotropy of magnetic susceptibility (AMS)

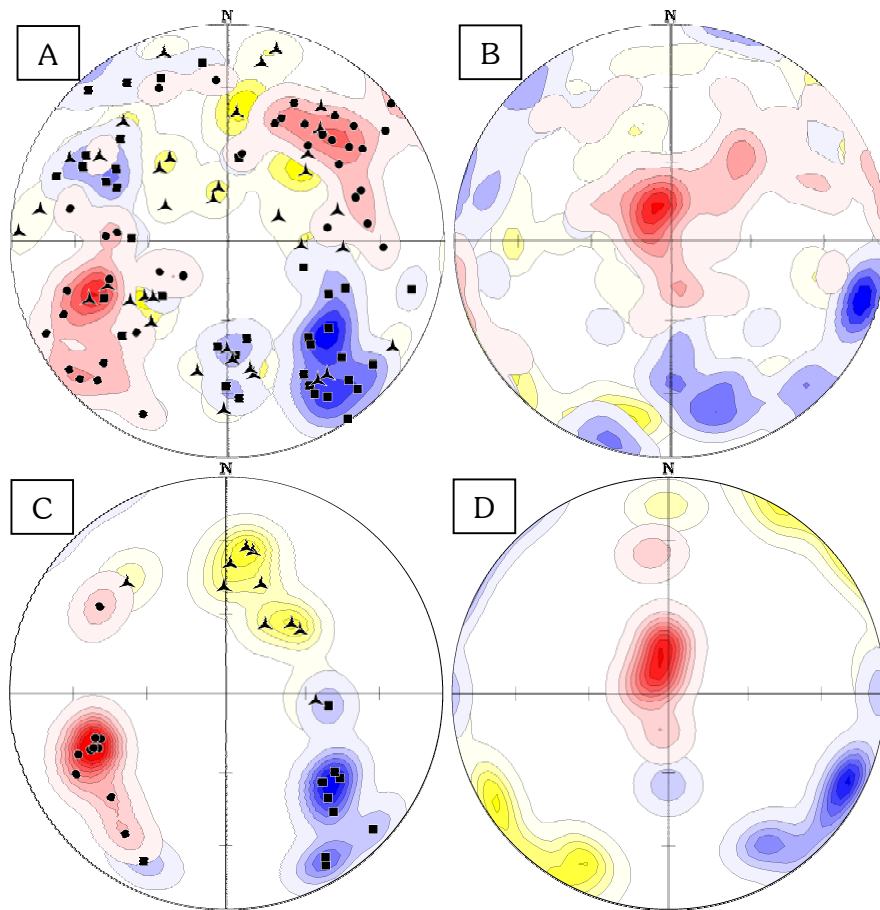
Although a particular attention was given to the structural control, bedding can be considered as monoclinial where sampling has been carried out in the Cupala Creek Formation.

AMS measurements have been performed on one specimen of every core prior to demagnetisation. The AMS parameters (figure 5.13-A & B) show that the internal strain is negligible as the degree of anisotropy $\{P_j\}$ is less than 5% in average ($P_j = 1.03 \pm 0.02$). The shape parameter $\{T\}$ indicates a slight tendency to an oblate shape of the ellipsoid of magnetic susceptibility, although it is close to isotropy given the errors bars about the mean value. This oblate shape, however, is confirmed by the Flinn-type diagram.

When the principal axes of magnetic susceptibility (K_{max} , K_{int} and K_{min}) are plotted on a stereogram (figures 5.14-A & B), their orientations are quite scattered as it can be expected for low degrees of anisotropy. After bedding correction, however, the density contours help visualising a better cluster of K_{min} about the vertical and this corresponds to a sedimentary magnetic fabric. This is in agreement with the oblate shape of the ellipsoid of magnetic susceptibility. No magnetic lineation can be clearly interpreted, albeit the better ESE to SSE grouping of K_{max} according to density contours. It is worthwhile noting that this direction is not parallel to the fold axis, but parallel to the series of Riedel faults along the Koonenberry fault as described at locality FUN (§.5.3.2; see also figure 5.2).



Figures 5.13: **A-** Flinn-type diagram (Flinn, 1962, 1965-a, 1965-b) and **B-** $\{T\}$ versus $\{P_j\}$ diagram (Jelinek, 1981; Hrouda, 1982) for the Late Cambrian Cupala Creek sandstone (locality CUP); **C-** Flinn-type diagram and **D-** $\{T\}$ vs $\{P_j\}$ diagram for the underlying Early – Middle Cambrian Teltawongee Beds (Unconformity test).



Figures 5.14: Orientations of the principal axes of magnetic susceptibility for the Cupala Creek sandstone, locality CUP.

A- *in situ*, and **B-** after bedding correction.

Orientations of the principal axes of magnetic susceptibility for the underlying Teltawongee beds, Unconformity test.

C- *in situ*, and **D-** after bedding correction.

Same legend as in figure 5.4; i.e. Kmax, squares (blue); Kint, triangles (yellow); Kmin, dots (red).

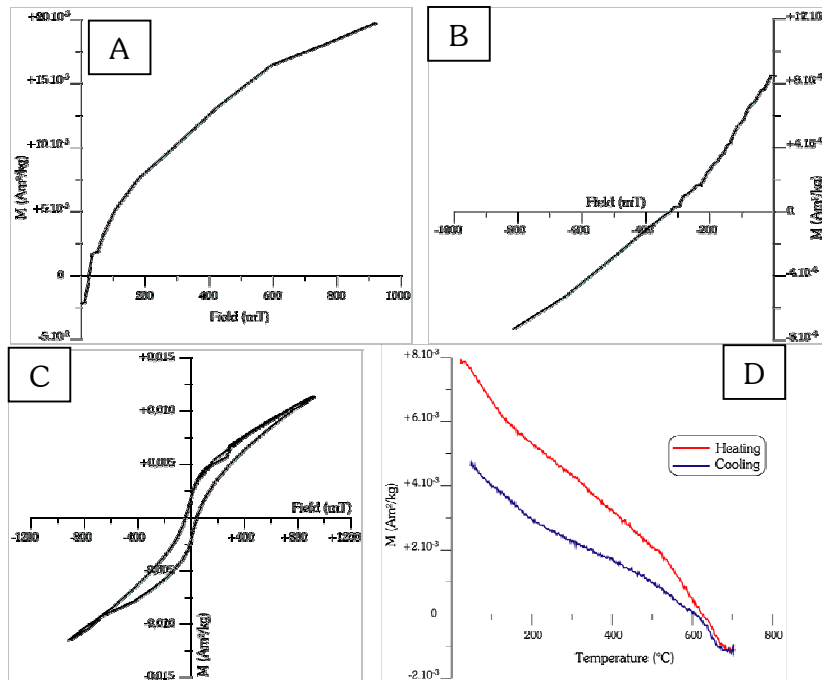
For the underlying Teltawongee beds, most of the data show also a low degree of internal strain (figures 5.13-C & D) even if the degree of anisotropy is slightly higher than in the sandstone of the Cupala Creek Formation ($P_J = 1.06 \pm 0.02$; when the highest value is excluded). The grouping of principal axes of magnetic susceptibility (figures 5.14-C & D) is also better marked, but the position of Kmin about the vertical after bedding correction still represents a sedimentary magnetic fabric. The Kmax however, are here well-clustered and aligned with the fold axis direction.

From these data, it is excluded that palaeomagnetic results can be deviated due to strain or lightning effects. Indeed, all Königsberger ratios are between 0 and 1,5 at room temperature (in average, $Q_K = 0.48 \pm 0.44$ @RT for the Cupala Creek sandstones).

5.4.3. Rock magnetism

Both IRM and back field curves show clearly the presence of high coercivity minerals as saturation is not reached (figures 5.15-A & B). The hysteresis loop however, reveals the existence of several types of mineral represented by the wasp-wasted shape of the loop, and an important contribution of paramagnetic minerals (figure 5.15-C). This shape is responsible for the high values of H_{CR}/H_R ratio (~ 4 to 4,5) and shift data in the range of MD grain on a Day plot, whereas the M_{RS}/M_S ratio corresponds to the boundary between SD and PSD grains (~ 0.5). The IST curve (figure 5.15-D) shows an important decrease in intensity up to 120°C, probably corresponding to the presence of goethite due to weathering. A second small inflexion at 550° and 600°C indicates the presence of magnetite (or perhaps minerals from the titanomagnetite family), and is more apparent on the cooling curve. The heating curve keeps on decreasing up to $\sim 650^\circ$ -700°C and is probably indicative of haematite.

Rock magnetism in the Teltawongee beds reveals the same type of magnetic carriers with the apparent presence of goethite, magnetite and haematite ($H_{CR}=196,3$ mT; $H_C=24,4$ mT; $M_S=7,5 \cdot 10^{-4}$ Am²/kg; and $M_{RS}=5,0 \cdot 10^{-4}$ Am²/kg).



Figures 5.15: Example of rock magnetic measurements in the Cupala Creek sandstones (locality CUP): specimen CUP3-3.

A- IRM curve; **B-** Back field curve (coercivity); **C-** Hysteresis loop; and **D-** IST curve, in red while heating and in blue while cooling ($B=535$ mT).

$H_C=54,7$ mT; $H_{CR}=236,4$ mT.
 $M_S=4,1 \cdot 10^{-3}$ Am²/kg; $M_{RS}=1,2 \cdot 10^{-3}$ Am²/kg.

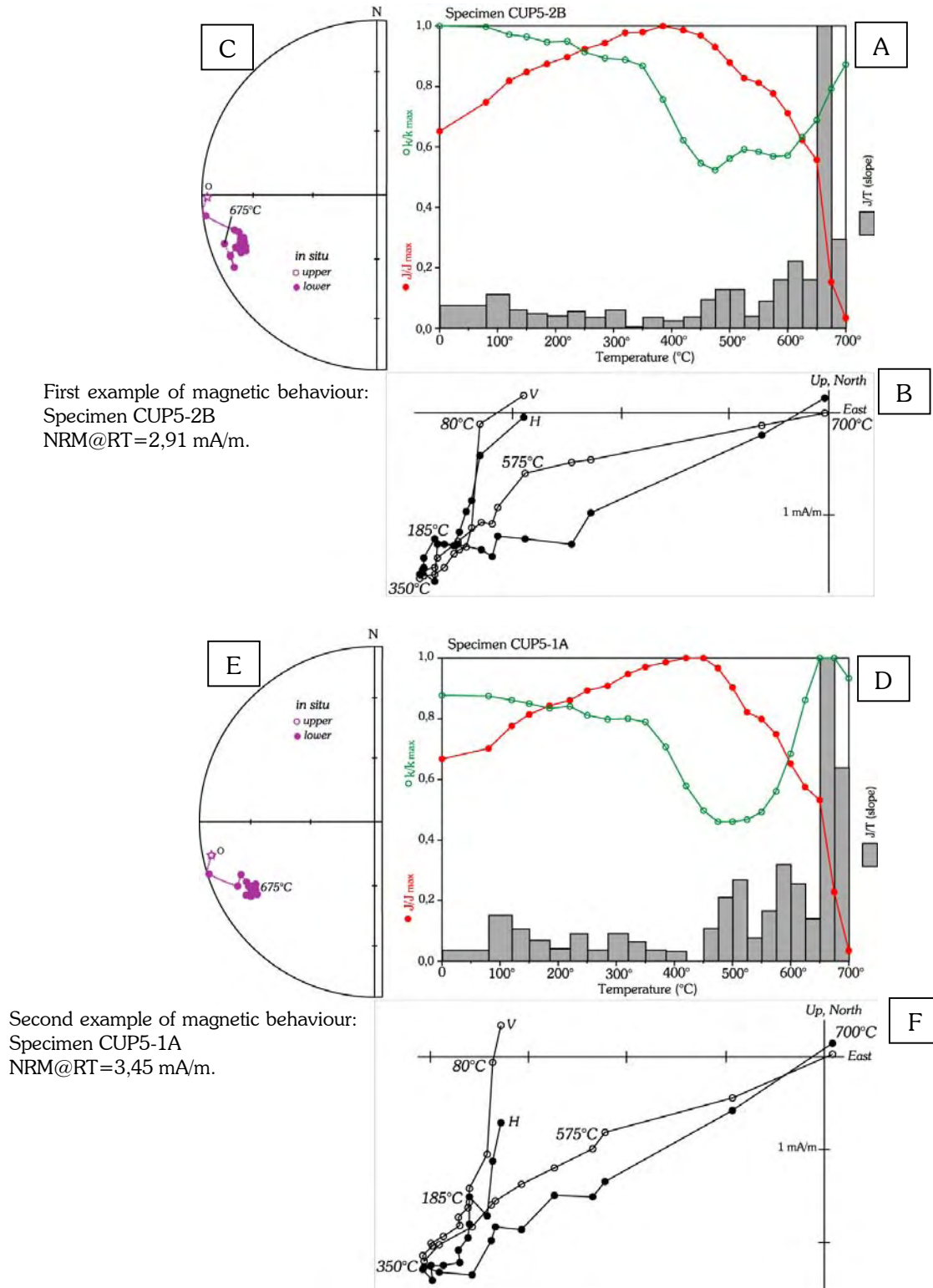
5.4.4- Palaeomagnetic results

- Demagnetisation

The 47 samples (37 of the Cupala Creek Formation and 10 from the Teltawongee beds) have been thermally demagnetised (23 steps).

In the best example (figures 5.16-A to C), four components can be distinguished after removal of a viscous or drilling-induced magnetisation below 80°C. The first, component C_1 , is demagnetised from 80° to ~185°C, and its direction corresponds well to the present-day field. Most of it, however, appears to be carried by goethite and is removed as soon as 120°C, which is in agreement with rock magnetic results. Component C_2 is demagnetised between 185° and 350°C. This component is a bit noisy but corresponds exactly to the reverse direction of component C_3 , which is removed up to 575°C, close to the Curie temperature of magnetite. Presence of magnetite (or magnetite-like mineral) was suggested by rock magnetism given the inflexion in the IST curve by 550°-600°C and the wasp-wasted shape of the hysteresis loop. Nevertheless, component C_3 does not point to the origin (particularly in inclination in figure 5.16-B), and a high temperature component C_4 is clearly visible up to 680°C, Curie temperature of haematite. This last component carries here (figure 5.16-A) about 50% of the remanence.

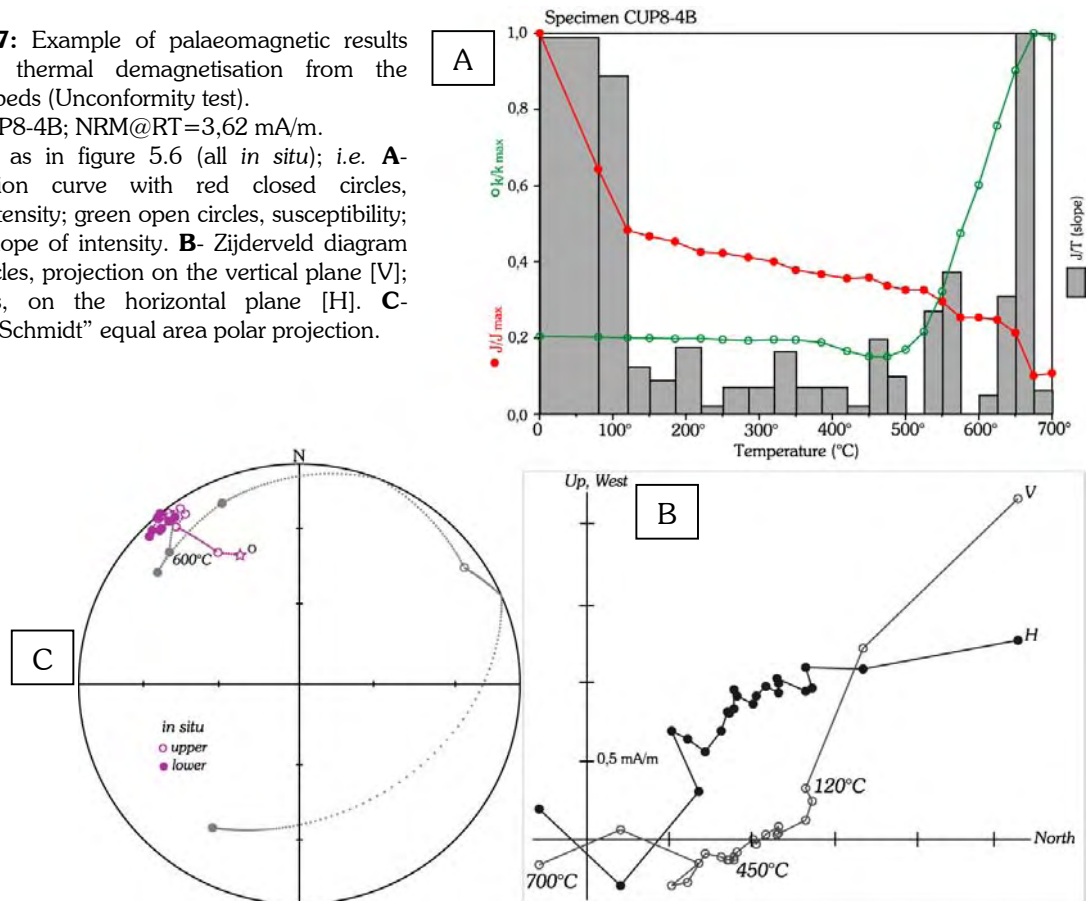
In the second example (figures 5.16-D to F), even if the transition between C_1 and C_2 is not as sharp as in the previous example, the three low to mid-temperature components are present. In this case however, the direction of magnetisation of component C_4 is not clearly distinguishable from that of component C_3 , although one can argue this latter still does not really point toward the origin. It must be noticed also that, although component C_4 still carry about 50% of the remanence (figure 5.16-D), there is an important increase in susceptibility from 550°-575°C, which may explain that component C_4 cannot be well defined.



Figures 5.16: Examples of demagnetisation of the Cupala Creek Formation. **A, B & C** correspond to the first example of magnetic behaviour with four magnetic components: specimen CUP5-2B. **D, E & F** correspond to the second example of magnetic behaviour, where component C_4 is not clearly distinguishable from component C_3 : specimen CUP5-1A.

Same legend as in figure 5.6 (all *in situ*); i.e. **A & D**- Demagnetisation curve with red closed circles, normalised intensity; green open circles, susceptibility; grey boxes, slope of intensity. **B & E**- Zijderveld diagram with open circles, projection on the vertical plane [V]; closed circles, on the horizontal plane [H]. **C & F**- Stereogram; "Schmidt" equal area polar projection.

Figures 5.17: Example of palaeomagnetic results obtained by thermal demagnetisation from the Teltawongee beds (Unconformity test). Specimen CUP8-4B; NRM@RT=3,62 mA/m. Same legend as in figure 5.6 (all *in situ*); i.e. **A**- Demagnetisation curve with red closed circles, normalised intensity; green open circles, susceptibility; grey boxes, slope of intensity. **B**- Zijderveld diagram with open circles, projection on the vertical plane [V]; closed circles, on the horizontal plane [H]. **C**- Stereogram; “Schmidt” equal area polar projection.



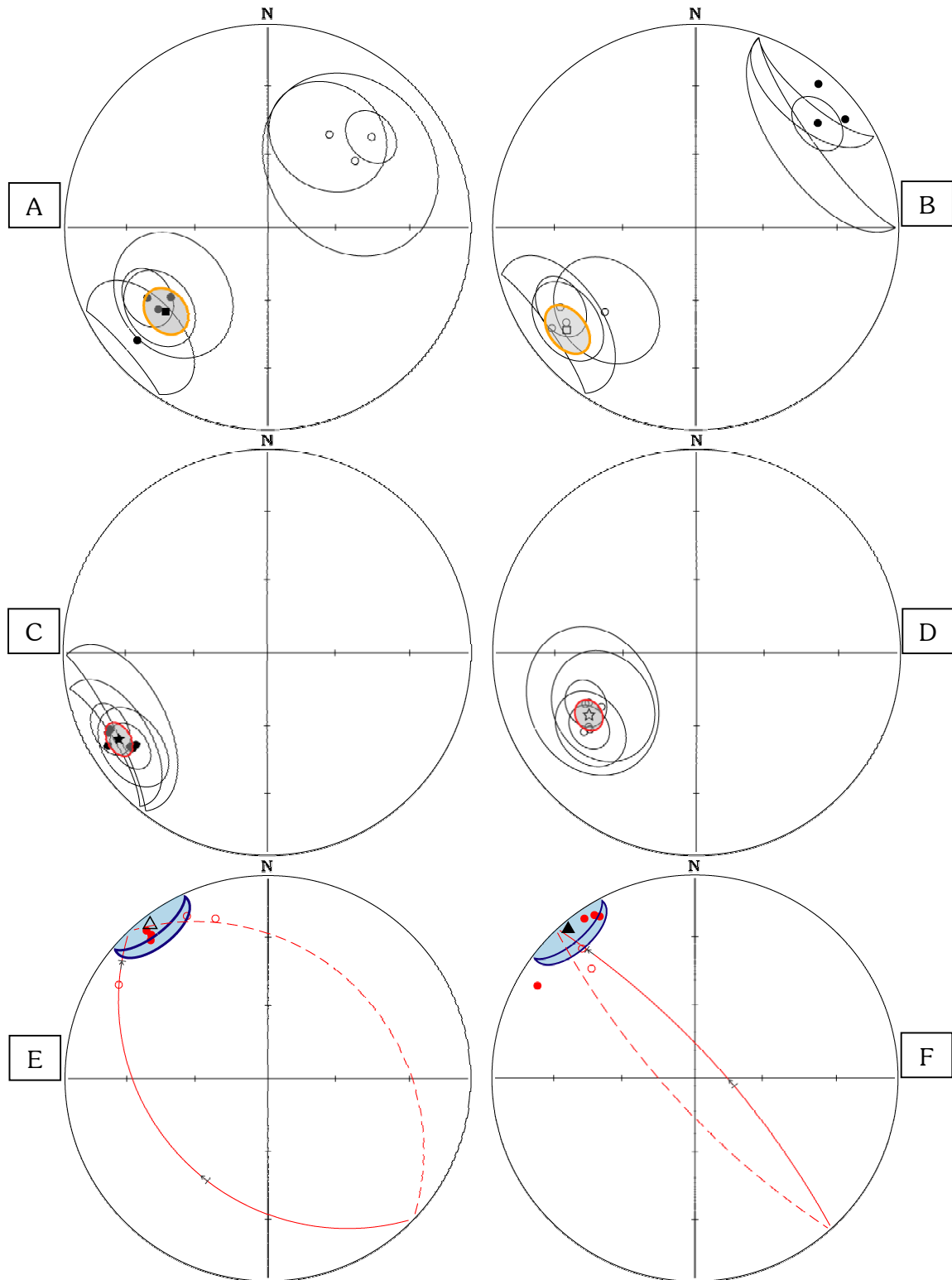
Stepwise demagnetisation of samples of the Teltawongee beds shows basically two components only (figures 5.17-A to C). A first component can be defined up to 450°C and is close to the present-day field. A high temperature one is removed from 450° to 680°C and appears to be mainly carried by haematite even if magnetite seems to present as well (figure 5.17-A). The strong increase in susceptibility from 500°-550°C obscures the magnetic signal.

- Interpretation

Mean magnetic directions per site for components C_2 show large cones calculated at the 95% confidence level, because of the tendency in overlapping between C_1 and C_2 and because of the noisy signal of C_2 . Nevertheless, site mean directions obtained from components C_2 are of reverse polarity from those from component C_3 as a positive reversal test classified C can be obtained. The overall mean direction (figures 5.18-A & B; and table 4) for the Cupala Creek Formation from site mean directions of both polarities is D.230°/I.+34° ($\alpha_{95}=9,1^\circ$ / $\kappa=44,7$) *in situ*, and D.231°/I.-18° after bedding correction ($\alpha_{95}=9,1^\circ$ / $\kappa=44,7$; same statistics as the bedding is regarded as monoclin).

Concerning component C_4 (figures 5.18-C & D; table 4), 95% confidence cones for each site are also relatively large because of the difficulty to clearly distinct components C_4 from C_3 , and that is why cones overlap those obtained from C_3 . The overall mean direction for the locality however, is clearly distinguishable from the overall mean for the mid temperature components (C_2 and C_3). *In situ*, it is D.239°/I.+15° ($\alpha_{95}=5,9^\circ$ / $\kappa=129,1$), and becomes D.240°/I.-38° ($\alpha_{95}=5,9^\circ$ / $\kappa=129,1$) after bedding correction.

The mean component obtained from the high temperature components for the unconformity test (i.e. in the underlying Teltawongee beds) is D.323°/I.-03° ($n=7$; $\alpha_{95}=13,1^\circ$ / $\kappa=22,7$) *in situ* and D.320°/I.+03° ($\alpha_{95}=13,1^\circ$ / $\kappa=22,7$) after bedding correction (figures 5.18-E & F; table 4).



Figures 5.18: Mean directions for the Cupala Creek sandstones, locality CUP.

Black circles are site mean directions with their associated 95% confidence cones.

A- *in situ*, and **B-** after bedding correction overall mean direction (**square**) for the mid temperature component (C_2 & C_3), with its α_{95} cone (orange).

C- *in situ*, and **D-** after bedding correction overall mean direction (**star**) for the high temperature component (C_4), with its α_{95} cone (red).

Unconformity test: **E-** *in situ*, and **F-** after bedding correction mean direction (**triangle**) with its α_{95} cone (blue) from single specimen high temperature components (**red circles**).

Open symbols are negative inclination values; **closed** symbols, positive inclination values. Schmidt equal area polar projection.

Table 4: Site mean directions and overall mean directions for locality CUP

Name	N	R	D.InS	I.InS	D.Bed	I.Bed	α_{95}	κ	DipDir	Dip
<i>Component C₂ per site:</i>										
Cup-04	5	4,7	033,6	-43,8	040,6	+06,2	23,1	11,9	238,2	53,0
Cup-05	3	3,0	048,7	-31,6	049,6	+20,8	10,3	143,1	238,2	53,0
Cup-06	3	2,8	052,7	-44,3	054,2	+08,6	36,7	12,3	238,2	53,0
<i>Component C₃ per site:</i>										
Cup-04	5	4,7	228,9	+14,5	226,8	-37,8	21,5	13,6	238,2	53,0
Cup-05	5	4,9	239,4	+30,6	239,4	-22,4	11,0	49,0	238,2	53,0
Cup-06	3	3,0	233,0	+32,1	233,5	-20,7	14,9	69,9	238,2	53,0
Cup-07	4	3,8	234,0	+40,0	234,9	-12,9	24,9	14,6	238,2	53,0
<i>Component C₄ per site:</i>										
Cup-01	5	5,0	243,8	+13,7	244,4	-35,5	8,9	95,7	238,2	53,0
Cup-02	4	3,8	239,5	+08,6	231,6	-36,2	21,8	18,8	238,2	53,0
Cup-04	5	4,9	234,6	+18,4	232,6	-25,3	14,7	28,2	238,2	53,0
Cup-05	5	5,0	235,5	+18,1	232,6	-26,9	8,4	83,0	238,2	53,0
Cup-06	3	2,9	243,3	+12,2	237,7	-34,8	28,6	19,7	238,2	53,0
Cup-07	5	4,6	234,7	+21,0	234,1	-23,1	33,4	10,0	238,2	53,0
<i>Unconformity test, high temperature component:</i>										
Telta	7	6,8	322,8	-03,1	319,6	-02,6	13,1	22,7	051,7	59,1
Name	B	N	R	D.InS	I.InS	D.Bed	I.Bed	α_{95}	κ	
<i>Mean direction for the mid-temperature component (C₂ & C₃):</i>										
Cup-mT	7	28	6,9	230,3	+34,1	231,3	-18,5	9,5	44,7	
<i>Mean direction for the high-temperature component (C₄):</i>										
Cup-HT	6	27	6,0	239,5	+15,2	239,7	-37,8	5,9	129,1	
<i>Unconformity test, high temperature component:</i>										
Telta	1	7	6,8	322,8	-03,1	319,6	-02,6	13,1	22,7	

N: number of samples; **B:** number of sites; α_{95} : cone calculated at the 95% confidence level; κ : precision parameter; **R:** resultant vector; **D.InS/I.InS:** declination/inclination *in situ* (geographic coordinates); **D.Bed/I.Bed:** declination/inclination after bedding correction; **DipDir/Dip:** direction of dip and dip of the bedding.

The overall mean directions from components C₄ is distinct from that of mid-temperature components, particularly in term of inclination. It cannot be due to shallowing effect, sometimes invoked concerning red beds (*e.g.* Gilder *et al.*, 2003), as the inclinations for C₄ are steeper than for C₃ after bedding correction.

Anisotropy of magnetic susceptibility measurements show that deviation due to strain effects can be discarded in these rocks and no perturbation caused by lightning is expected. Yet, the mean direction yielded by the Teltawongee beds, unconformably underlying the Cupala Creek Formation, is completely different from overall mean directions of both the mid and the high temperature components of the Late Cambrian formation, although both formations contain the same type of magnetic carriers (magnetite and in particular haematite). Hence, it can be considered that the unconformity test is positive.

Table 5: Corresponding palaeopoles for the Cupala Creek Formation

Name	B	N	<u>Australian coord.</u>		<u>African coord.</u>		dp	dm
			PLong.	Plat.	PLong.	Plat.		
<i>For mid-temperature component in situ:</i>								
Cup-mT ₁	7	28	049,8	-43,1	024,0	+06,7	6,0	10,4
<i>For mid-temperature component after bedding correction:</i>								
Cup-mT ₂	7	28	201,9	+26,4	359,9	+22,0	4,9	9,5
<i>For high-temperature component after bedding correction:</i>								
Cup-HT	6	27	198,3	+12,6	351,5	+35,0	6,1	7,0

N: number of samples; **B:** number of sites; **PLong./Plat.:** palaeopole longitude/latitude in Australian and in African coordinates. **dp/dm** : semi-axis of the ellipse of confidence.

Table 6: Comparable published Late Cambrian palaeopoles for Gondwana. The 95% confidence ellipses of the following palaeopoles overlap the ellipse of pole from the Cupala Creek Formation.

Name, place	Age	B	N	κ	α ₉₅	Q	Australian coordinates.		dp	dm	Authors
							P	Long. Plat.			
<u>Africa:</u>											
Ntonya Ring Structure, Malawi	522±13	7	27	999,9	1,9	3	010,1	-16,9	1,4	2,3	Briden, 1968
Dedza Moutain Syenite, Malawi	520±25	ng	1	ng	ng	2	006,0	-16,9	nc	nc	McElhinny <i>et al.</i> , 1968
<u>Antarctica:</u>											
Wright Valley granite, E-Ant	500±43	ng	16	ng	8,1	3	023,0	-15,4	4,1	8,2	Funaki, 1984
GH Pink granite, SVL	498±4	3	21	16,0	8,3	4	020,4	-14,6	4,3	8,5	Grunow, 1995
GH Mafic dyke, SVL	498±3	5	27	80,0	8,6	4	016,7	-11,8	7,5	7,5	Grunow, 1995
GH Grey granite, SVL	498±3	5	34	146,0	6,4	4	024,8	-12,4	4,3	4,3	Grunow, 1995
Killer Ridge/Mt Loke diorites, SVL	499±3	6	40	32,0	12,0	4	026,4	-15,4	7,7	7,7	Grunow, 2000
Lake Vanda Bonny pluton, SVL	499±3	4	28	50,0	13,1	4	032,8	-13,1	11,9	11,9	Grunow, 1995
Charnockites, M. st. E-Ant	520±24	5	37	24,3	15,6	3	028,2	-04,4	8,3	16,1	McQueen <i>et al.</i> , 1972
<u>Australia:</u>											
NW Tasmanian sed., Tasmania	503±3	11	71	20,2	10,4	4	028,9	-19,4	5,3	10,5	Li <i>et al.</i> , 1997
Upper Lake Frome Group, SA	500±5	ng	20	5,4	ng	2	025,0	-16,0	12,5	12,5	E. & G., 1974*
Jinduckin Formation, NT	483±13	7	20	7,7	13,0	3	025,0	-13,0	11,0	11,0	Luck, 1972
Hawker Group, Flinder Ranges, SA	538±8	15	89	12,3	11,4	3	014,9	-21,3	6,8	12,5	Klootwijk, 1980
<u>South America:</u>											
Salta & Juju redbeds, Argentina	508±38	ng	18	23,7	30,0	2	026,2	-18,1	28,5	41,3	Creer, 1970
Sierra de las Animas Complex, SU	510±10	7	33	12,0	18,1	4	035,4	-27,0	19,6	26,7	S-B. & R., 2002*

* **E. & G.:** Embleton & Giddings; **S-B. & R.:** Sanchez-Bettucci & Rapalini.

E-Ant: East Antarctica; **SVL:** South Victoria Land; **SA:** South Australia; **NT:** Northern Territories; **SU:** Southern Uruguay; and **GH:** Granite Harbour; **M.st.:** Mirny station.

N: number of samples; **B:** number of sites; **κ :** precision parameter; **α_{95} :** 95% confidence cone; **Q:** quality level, corresponding to the “demag-code” in the palaeomagnetic database; **PLong./Plat.:** palaeopole longitude/latitude in Australian coordinates. **dp/dm:** semi-axis of the ellipse of confidence; **Ages** and their uncertainties correspond to the average between the high and the low magnetisation ages given in the database; **ng:** not given.

Data from the I.A.G.A. palaeomagnetic database, Version 4-4 (2003), and references therein (first version published by McElhinny & Lock, 1996).

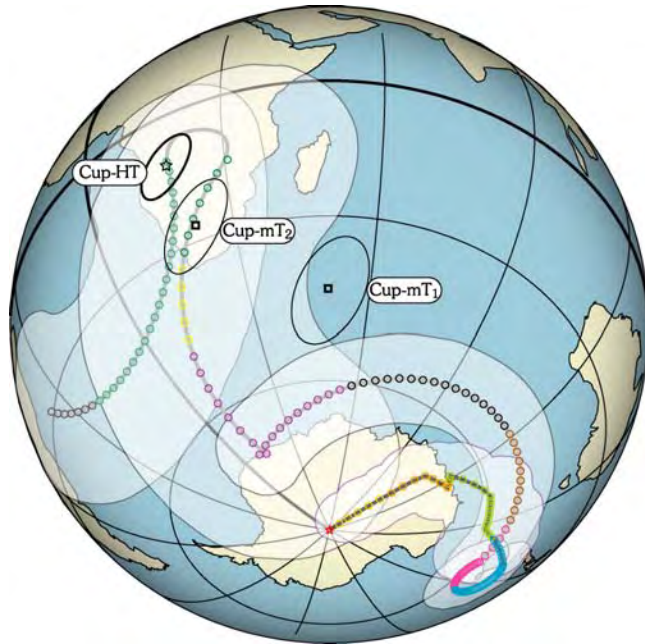


Figure 5.19: Corresponding palaeopoles in Australian coordinates. The possible APW path for Australia-Gondwana from the present-day to 570 Ma based on Small Circle Fit is shown for comparison purposes.

Same legend as in figure 2.19-A, Chapter 2 (§.2.7).

Cup-HT is the pole corresponding to component C_4 after bedding correction; **Cup-mT₁**, corresponding to C_2 & C_3 *in situ*; and **Cup-mT₂**, to C_2 & C_3 after bedding correction.

The palaeopole (Cup-HT: figure 5.19; table 5) corresponding to the mean direction of components C_4 after bedding correction is PLong.351,5° / Plat.+35,0° (dp=4,1°; dm=7,0°) and is very consistent with other poles from Gondwana (table 6; from the I.A.G.A. palaeomagnetic database, McElhinny & Lock, 1996 [Version 4-4; 2003]) as it intersects their 95% confidence ellipses. This means that components C_4 can be regarded as primary, and probably results from a

detrital remanence magnetisation (DRM). It implies also that no rotation or movement relative to the rest of the craton of Gondwana is recorded in these rocks, which means that this area of the Delamerian Orogen can be considered fixed since the Late Cambrian.

On the contrary, the mid-temperature components (C_2 and C_3) probably correspond to a remagnetisation. The presence of a reversal favours the hypothesis of a chemical overprint, which lasted long enough to record it. Unfortunately, it is not possible to constrain the age of this overprint, although it must be Early – Mid Palaeozoic.

- **Conclusions**

The red sandstones of the Late Cambrian Cupala Creek Formation show a complex magnetisation. The present-day field is almost always present at low temperatures, and mainly carried by goethite, which probably results from the strong weathering occurring in Australia. A mid-temperature direction of magnetisation can be considered as a remagnetisation of chemical origin, which lasted long enough to record a reversal carried by a component C_2 of normal polarity and a component C_3 of reverse polarity. This magnetisation passes the reversal test classified C. It seems that the magnetic carrier of C_3 is magnetite, but the carrier of C_2 is not determined. The age of remagnetisation cannot be constrained but must be Early – Mid Palaeozoic. The high temperature component is carried by haematite and may correspond to a DRM. The primary origin of this magnetisation is confirmed by the positive unconformity test performed on the tightly folded underlying Early – Mid Cambrian Teltawongee beds, and by the good correspondence with other pole of same age published for Gondwana.

It implies that this locality of the Delamerian Orogen did not record any movement or rotation since the Late Cambrian and that it can be considered as stable relative to the craton of Gondwana.

5.5. The Kandie Tank Limestone (KAN) and the Gum Creek sandstones (GUM)

5.5.1. Presentation

These two localities are important to try to confirm the previous results. Indeed, the Kandie Tank Limestone is supposed to correspond to a lateral change in facies at the top of the Cupala Creek Formation, and to have a different bedding orientation compared to that of locality CUP. The sandstones near the Gum creek is the only accessible Middle – Late Cambrian locality situated south to the apparent bending in fault and cleavage trend, changing from NNW-SSE in the northern two thirds of the map to NNE-SSW in the southern third (figure 5.2).

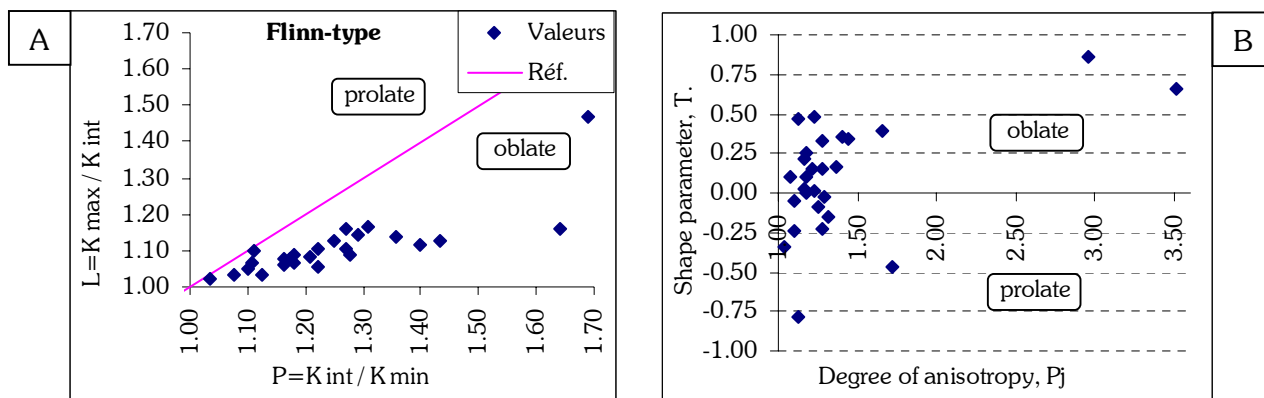
The Kandie Tank Limestone (locality KAN) is Late Cambrian in age (conodonts; Stevens *et al.*, 2000). It is exposed about 10-15 km to the North-East of locality CUP, along the Koonenberry fault (figure 5.2). It consists of a couple of hundreds of meter long outcrop of massive limestone, but no bedding has been found and the contact between the limestone and the sandstones is hidden. Mills (*personal communication*, 2002) suggested it sub-horizontally cap a hill of sandstones, which bedding appears to be close to the horizontal in the vicinity of the limestone. Six sites (30 cores) have been drilled in this rock.

The sandstones along the Gum Creek in the vicinity of Bilpa are very poorly exposed and belong to the Scope Ranges Red beds. It consists of medium-grained quartz sandstone of red bed character. Only two sites (10 cores) could be drilled just above the base of the sequence, which shows conglomerates, shallow marine quartz sandstones, quartzites and siltstones containing glauconite beds, trace fossils and trilobite exoskeletons. Where samples have been collected, the locality (GUM) – called here the Gum Creek sandstones – is believed to be

Late Cambrian in age, although the whole formation is not clearly dated and may range from Late Cambrian to Ordovician (Stevens *et al.*, 2000).

5.5.2. Anisotropy of magnetic susceptibility (AMS)

In the Kandie Tank Limestone, the degree of anisotropy is weak but well-marked ($P_j = 1.48 \pm 0.67$). On the contrary, the shape parameter $\{T\}$ does not yield a clear result ($T = -0.06 \pm 0.90$), although the Flinn-type diagram shows a clear trend in the oblate side of the diagram (figures 5.20-A & B). The Königsberger ratio suggests the existence of relative small grain size and discards lightning effects ($Q_K = 2.54 \pm 4.35 @ 80^\circ\text{C}$).



Figures 5.20: A- Flinn-type diagram (Flinn, 1962, 1965-a, 1965-b) and B- $\{T\}$ versus $\{P_j\}$ diagram (Jelinek, 1981; Hrouda, 1982) for the Late Cambrian Kandie Tank Limestone (locality KAN).

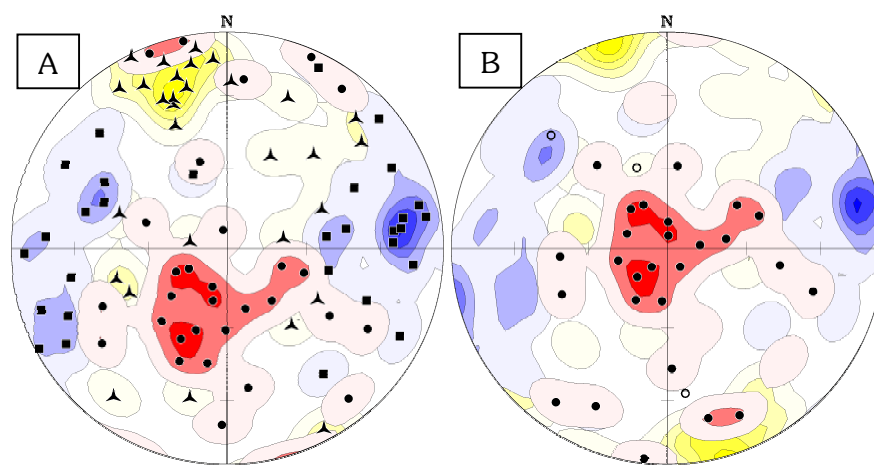


Figure 5.21: Orientations of the principal axes of magnetic susceptibility for the Kandie Tank Limestone, locality KAN.

A- *in situ*, and **B-** after the proposed correction consisting in bringing the mean value of K_{min} to the vertical.

Same legend as in figure 5.4; i.e. K_{max} , squares (blue); K_{int} , triangles (yellow); K_{min} , dots (red).

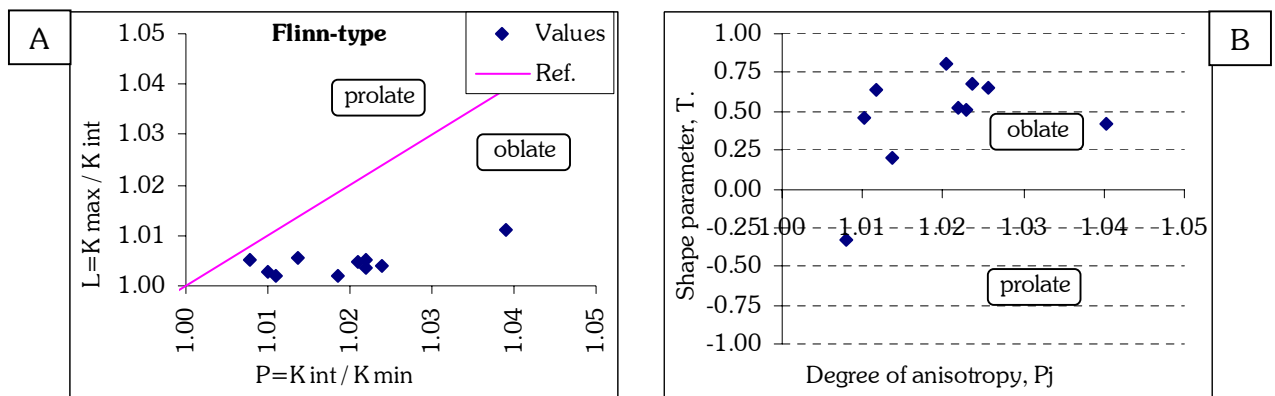
The orientations of the principal axes of magnetic susceptibility are scattered but the density contours highlight clearly three preferred directions *in situ* (figure 5.21-A). Surprisingly, K_{min} axes are not about the vertical, and the mean direction is actually orientated $\text{Dec.}194^\circ / \text{Inc.}65^\circ$ ($\alpha_{95} = 20.4^\circ$). It is proposed therefore that this result is representative of a “sedimentary” magnetic fabric, and that Kandie Tank Limestone are not sub-horizontal but have been tilted of about 25° . When this correction is applied (figure 5.21-B), K_{min} axes are obviously close to the vertical, but K_{max} and K_{int} axes are also closer to the horizontal, which is in good agreement with this tilt hypothesis.

It must be noticed also that the magnetic lineation (K_{max}) is oriented nearly E-W. It is not established whether it represents a sedimentary or a tectonic feature, but this orientation is perpendicular to the Koonenberry fault. It may correspond to a \sim N-S compression.

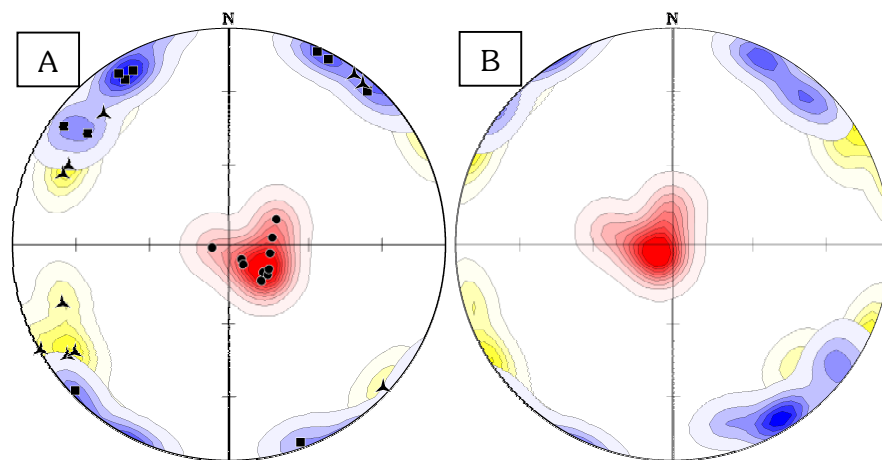
Concerning the Gum Creek sandstones, the degree of anisotropy is very weak ($P_j = 1.02 \pm 0.01$) but both the shape parameter $\{T\}$ ($T = 0.46 \pm 0.32$) and Flinn-type diagram show a clear oblate shape of the ellipsoid of magnetic susceptibility (figures 5.22-A & B).

The Königsberger ratio is small and suggests the presence of relative large magnetic grain size but discards lightning effects ($Q_K = 0.36 \pm 0.25 @ RT$).

The orientations of the principal axes of magnetic susceptibility are well-defined (figure 5.23-A & B). Kmin axes oriented about the vertical are representative of a “sedimentary” magnetic fabric. Kmax axes however, seems to group along two perpendicular directions. One, NW-SE, looks parallel to the fault trend occurring in the North of the Broken Hill area, whereas the second, NE-SW, parallels that of the South of the area.



Figures 5.22: A- Flinn-type diagram (Flinn, 1962, 1965-a, 1965-b) and B- $\{T\}$ versus $\{P_j\}$ diagram (Jelinek, 1981; Hrouda, 1982) for the Late Cambrian Gum Creek sandstones (locality GUM).



Figures 5.23: Orientations of the principal axes of magnetic susceptibility for the Gum Creek sandstones, locality GUM.

A- *in situ*, and B- after bedding correction.

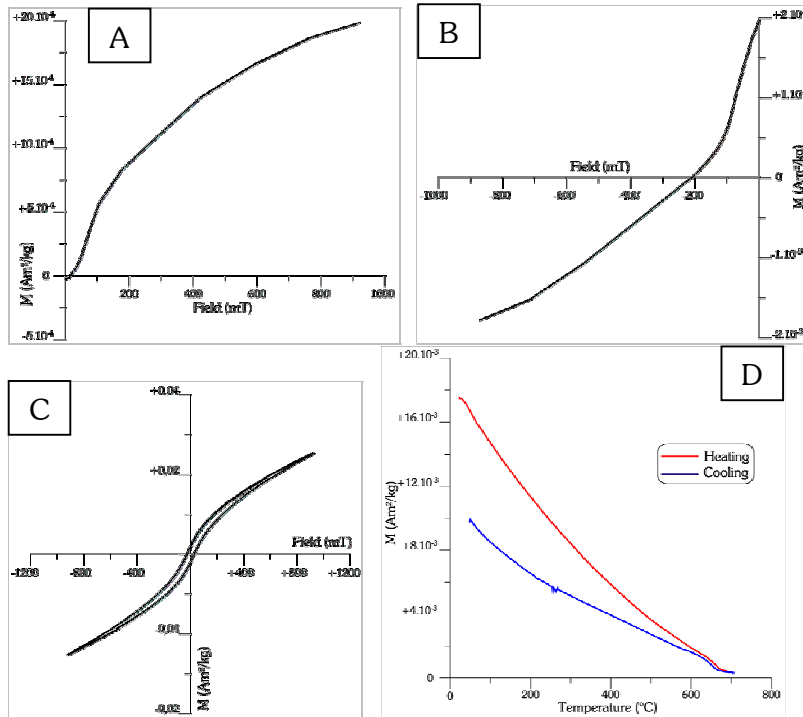
Same legend as in figure 5.4; i.e. Kmax, squares (blue); Kint, triangles (yellow); Kmin, dots (red).

This may correspond to two phases of compressions. If this is the case and if the southern part of the Broken Hill area rotated relative to the northern part, these compressions have to be posterior to this tectonic event.

5.5.3. Rock magnetism

Rock magnetic measurements have not been carried out on the Kandie Tank Limestone. The unblocking temperatures show however that the main magnetic carrier is probably magnetite, and it is likely to observe the same kind of behaviour than in the Funeral Creek Limestone (locality FUN) and the dolomites of Mt Arrowsmith (locality ARR), as suggested by thermal demagnetisation (see below).

For the Gum Creek sandstones, the IST curve reveals clearly the presence of haematite (figure 5.24-D). It is also shown by the back field and IRM curves (figures 5.24-A & B), which are not saturated. This behaviour however, seems to be also due to the presence of goethite. Finally, the wasp-wasted shape of the hysteresis loop (figure 5.24-C) and in particular, the change in slope of the back field curve (figure 5.24-B) signifies the existence of magnetite as well.



Figures 5.24: Example of rock magnetic measurements in the Gum Creek sandstones (locality GUM): specimen GUM3-3.

A- IRM curve; **B-** Back field curve (coercivity); **C-** Hysteresis loop; and **D-** IST curve, in red while heating and in blue while cooling (B=535 mT).

$H_C = 36,6$ mT; $H_{CR} = 211,8$ mT.
 $M_S = 9,1 \cdot 10^{-3}$ Am²/kg; $M_{RS} = 2,0 \cdot 10^{-3}$ Am²/kg.

The presence of both magnetite and haematite leads to a high H_{CR}/H_C ratio ($=5,8$) shifting to the range of multi-domain grains on a Day plot. Nevertheless, the M_{RS}/M_S ratio ($=0,22$) plots in the pseudo-single domain range. In any cases, as suggested by the Königsberger ratio, the grain sizes of the magnetic carriers are probably relatively large, as one could expect from medium-grained sandstones.

5.5.4. Palaeomagnetic results

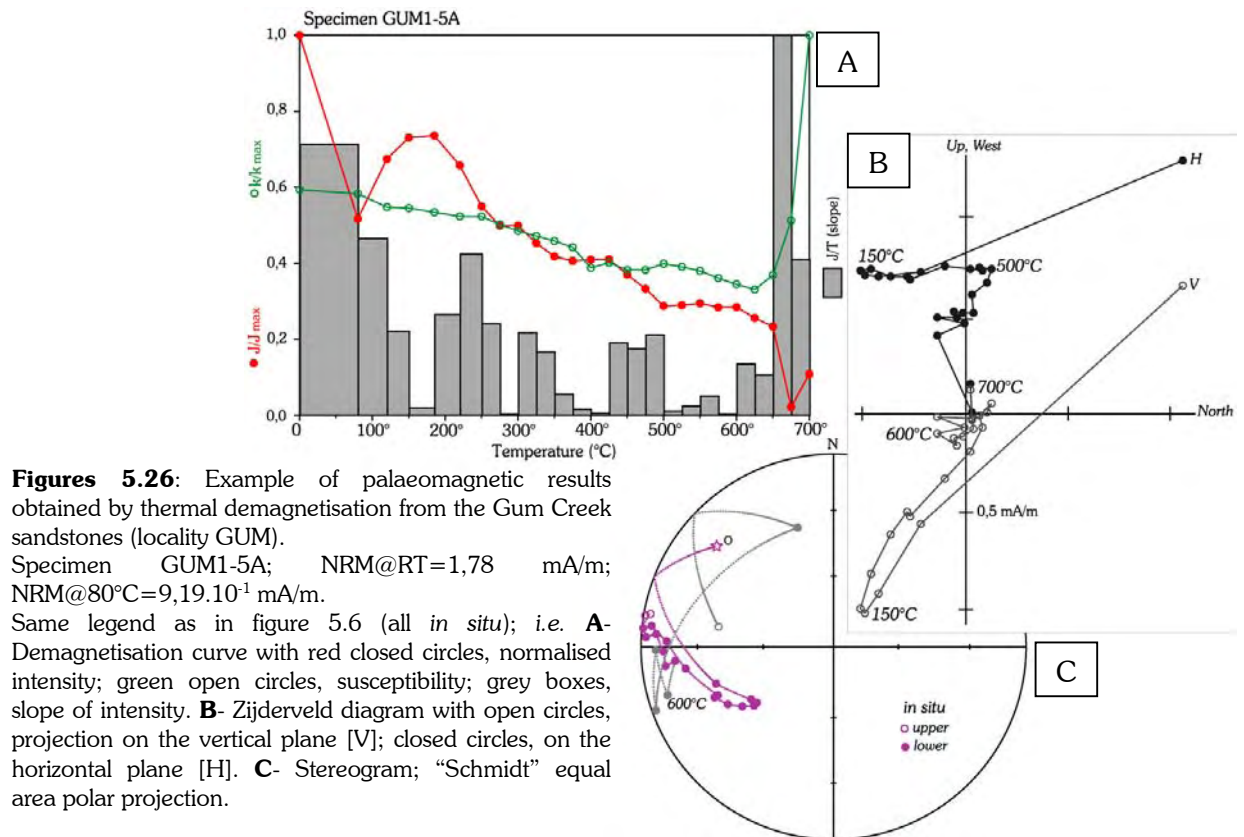
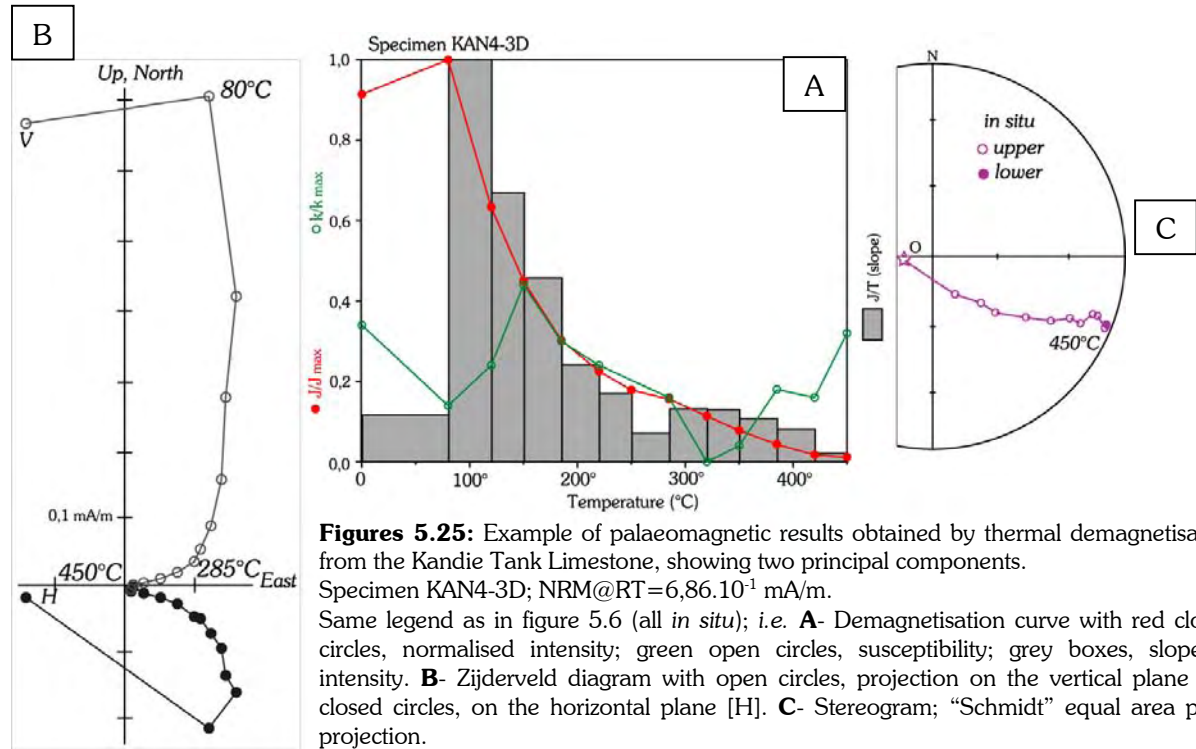
- Demagnetisation

The 30 samples from the Kandie Tank Limestone and the 10 from the Gum Creek sandstones have been thermally demagnetised.

The Kandie Tank Limestone shows two or three components. The first is a viscous magnetisation, sometimes close to the orientation of the present-day field but often deviated perhaps by a drilling-induced magnetisation. The second is removed between 80°-120°C and 250°C, and the last between 285° and 500°C, but it is common that these two ranges of temperatures show one orientation only. The magnetic carrier of the second component is not identified but magnetite is probably the magnetic carrier of the last one (figures 5.25).

Concerning the Gum Creek sandstones (figures 5.26), a first component is demagnetised up to 150°C, which direction corresponds to the present-day field. It seems to be essentially carried by goethite as expected from rock magnetic measurements. The second component is identified from 185° to 500°C and possibly carried by relatively large grains of magnetite. Finally, a last component carried by haematite and representing about 20 to 30% of

the total remanence (figure 5.16-A), is removed up to 675°C. This last component is noisy and the susceptibility increases strongly from 650°C.



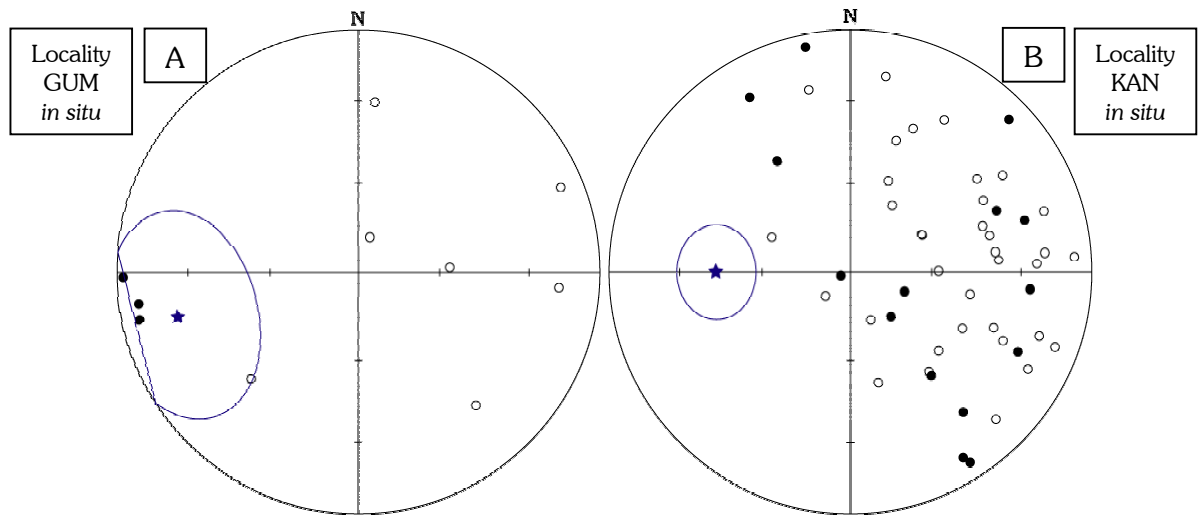
- Interpretation

Although components are usually well determined, their directions of magnetisation look randomised both *in situ* and after bedding correction.

The single specimen directions for the high temperature components only are shown here to illustrate this distribution (figure 5.27-A), but the result is the same for the mid temperature components. This may be explained by the weathering affecting these rocks but probably also by the relatively large grain size of magnetic carriers, as rock magnetic measurements suggest pseudo-single or multi-domain grains.

The distribution of components carried by magnetite in the Kandie Tank Limestone are also useless for palaeomagnetic purposes. However, *in situ* (figure 5.27-B), it seems that these direction are preferentially oriented to the Eastern hemisphere of the stereogram. This result may perhaps stem from a mixture of components demagnetised simultaneously.

In any cases, these localities cannot confirm results obtained at locality CUP.



Figures 5.27: Single specimen high temperature components (**black circles**) *in situ* for **A-** the Gum Creek sandstones, and **B-** the Kandie Tank Limestone. The overall mean directions (**blue star** and α_{95}) are not significant even if the orientation in the Kandie Tank Limestone seem to be preferentially oriented in the Eastern hemisphere of the stereogram. **Open** symbols are negative inclination values; **closed** symbols, positive inclination values. Schmidt equal area polar projection.

5.6. The Mount Daubeny Formation (DAU)

5.6.1. Presentation



Photo 6: A (left)- Conglomerate of the base of the Mt Daubeny Formation outcropping along a dried creek. This picture shows also the well-defined bedding.

B (right)- Mafic dyke intruding the red sandstones. The hat gives the scale.



The studied locality (DAU) is situated South-East of the Wertago property (figure 5.2; table 3) within the Wertago terrane. There, the Mt Daubeny Formation fills up a basin bounded by the Koonenberry Fault to the East and the largely concealed Gap Range Fault to the West. This basin is believed to be a pull-apart basin, which opened probably in the (Late?) Silurian (Buckeley, *personal communication*, 2001). Subsequently, an inversion occurred, probably in the late Early to early Middle Devonian, as the Mt Daubeny Formation forms a syncline but the Early or Middle Devonian rhyolitic to dacitic rocks intruding this formation do not appear to be folded (Mills, *personal communication*, 2001).

Where sampling has been carried out, the Mt Daubeny Formation consists of well-bedded fine-grained red-purple sandstones of Gedinnian age (Neef & Bottrill, 1991). The base of the formation is conglomeratic (photo 6-A), and mafic dykes have intruded the top of the sampled section (photo 6-B). These dykes are not dated but are post-inversion of the basin. It has been proposed that they are Early or Middle Devonian, associated with the other rhyolitic to dacitic intrusions (see locality SIS, below). It must be noticed however that dyke intrusions of probably

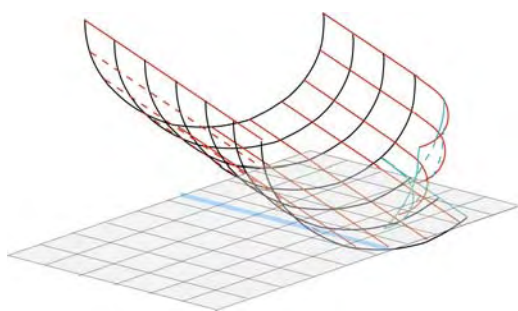


Figure 5.28: Sketch showing the geometry of the syncline of the Mt Daubeny Formation. The limb where sampling has been carried out is complicated by a fold of second generation.

Jurassic age exists to the North-East of the Broken Hill area. Eighteen cores were collected in order to perform a conglomerate test, and 14 in two dykes for a contact test. In the sandstones of the Mt Daubeny Formation itself, 46 cores (7 sites) have been collected.

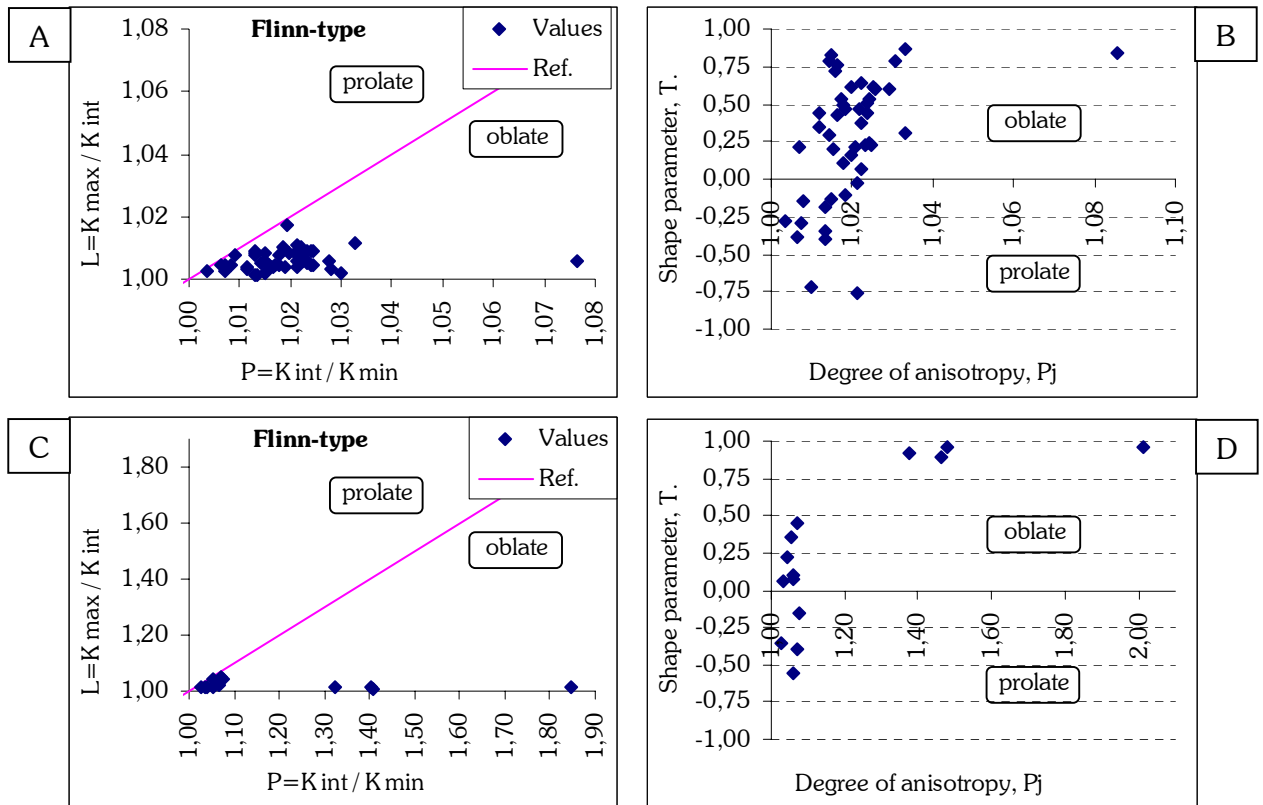
The locality is situated on one limb of the large syncline but it is there complicated by a fold of second generation (figure 5.28). The bedding correction has thus consisted in rotating data around the axis of the second fold until the bedding coincides with the bedding of the limb of the syncline. Then, data have been untilted and unfolded as usual around the plunging axis of the first fold, as in both cases (fold 1 and 2), folds can be considered as cylindrical. Within the locality, however, the bedding varies little only.

5.6.2. Anisotropy of magnetic susceptibility (AMS)

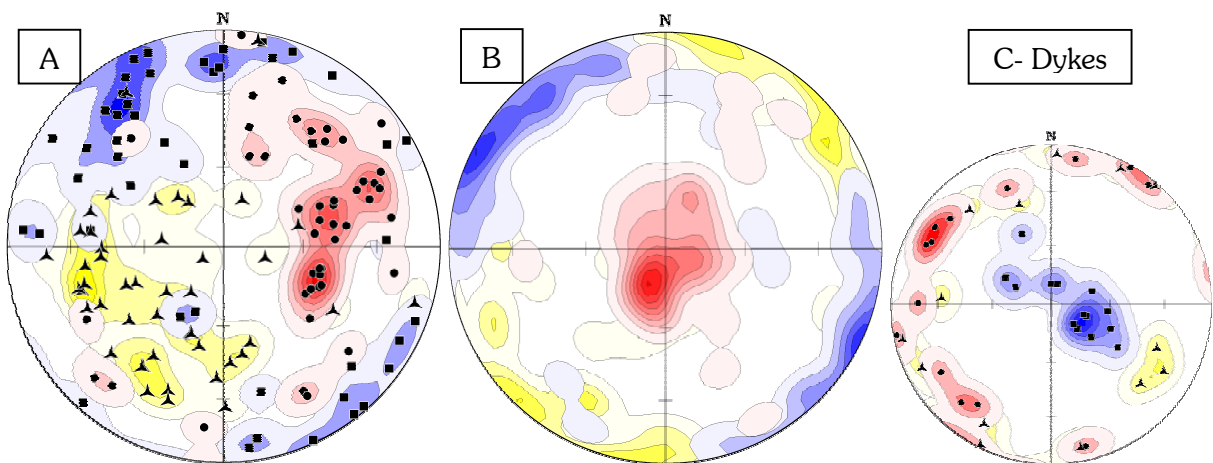
Both the Flinn-type diagram (figure 5.29-A) and the $\{T\}$ vs. $\{P_j\}$ diagram (figure 5.29-B) yield the same result. The degree of anisotropy in these sandstones is very weak ($P_j=1,02\pm0,01$) and the ellipsoid of magnetic susceptibility tends to be slightly oblate ($T=0,25\pm0,41$). Moreover, the Parés test (Parés & Van der Pluijm, 2002) shows a degree of alignment calculated for phyllosilicates always lower than 10%. The Königsberger ratio is about 1 ($Q_K=0,85\pm0,30$), so that it can be considered that both internal strain and lightning effects are absent from these rocks.

In the mafic dykes (figures 5.30-C), ten out of fourteen specimens show also a weak degree of anisotropy ($P_j=1,06\pm0,02$) and the shape of the ellipsoid of magnetic anisotropy is close to a sphere in average as the parameter $\{T\}$ is close to zero ($T=-0,02\pm0,34$). The four other specimens probably simply reflect environmental magnetic perturbation during measurements.

The directions of the principal axes of magnetic susceptibility show clearly a sedimentary magnetic fabric in the sandstones with K_{min} about the vertical and K_{int} & K_{max} about the horizontal after bedding correction (figure 5.30-B). The K_{min} , better grouped after bedding correction than *in situ*, confirm the structural control involving two folds. The directions of K_{max} are NW-SE with a slight better cluster about $\sim N.115^\circ$. It is in good agreement with the direction of the Koonenberry Fault, even if the slight better cluster of K_{max} seems to form an angle that may be attributed to a local strain resulting from a strike-slip movement on the fault.



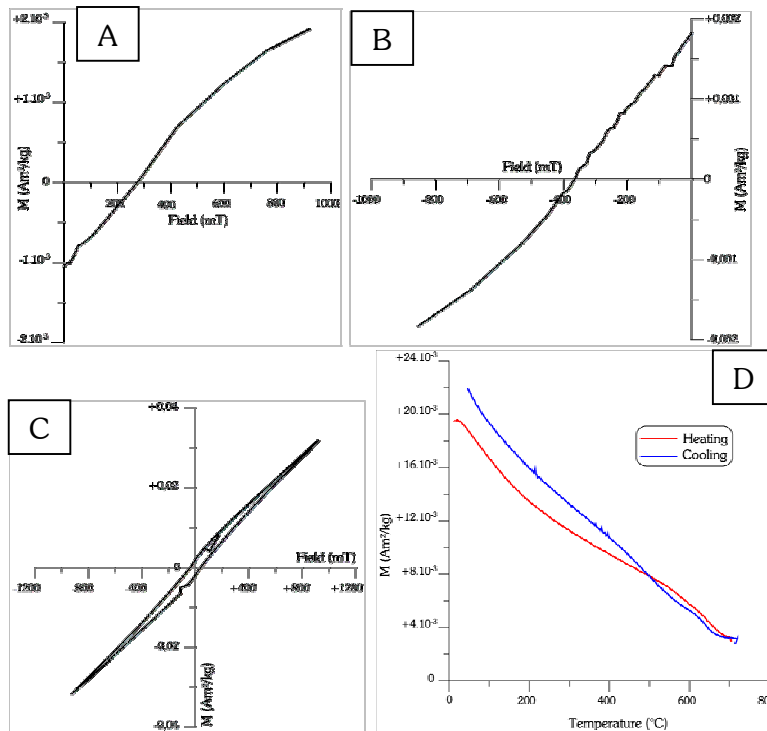
Figures 5.29: **A-** Flinn-type diagram (Flinn, 1962, 1965-a, 1965-b) and **B-** $\{T\}$ versus $\{P_j\}$ diagram (Jelinek, 1981; Hrouda, 1982) for the Gedinnian sandstones of the Mount Daubeny Formation; **C-** Flinn-type diagram and **B-** $\{T\}$ vs. $\{P_j\}$ diagram for the post-folding mafic dykes intruding the Mount Daubeny Formation (locality DAU).



Figures 5.30: Orientations of the principal axes of magnetic susceptibility for the Mount Daubeny Formation, locality DAU. For the Gedinnian sandstones **A-** *in situ*, and **B-** after bedding correction; and **C-** for the mafic dykes intruding them, *in situ* as they are post-folding. Same legend as in figure 5.4; i.e. K_{\max} , squares (blue); K_{int} , triangles (yellow); K_{\min} , dots (red).

The magnetic lineation K_{\max} in the dykes is very steep and corresponds precisely to the orientation of the dykes. It reflects therefore the magmatic flow. K_{\min} are distributed along a great circle and no preferred direction is recorded. It signifies that no strain capable of affecting the magnetic fabric of the dykes existed after their intrusion.

5.6.3. Rock magnetism



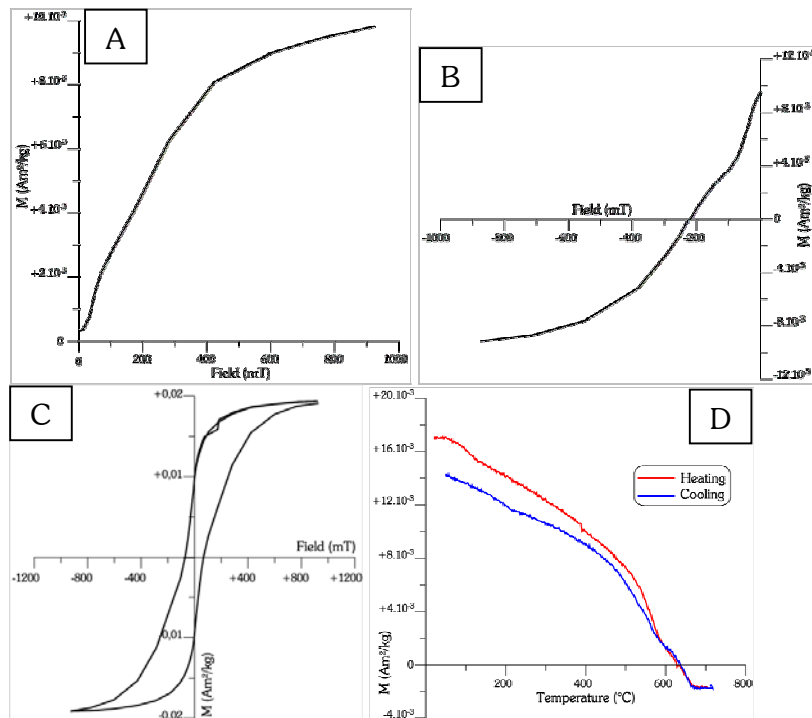
Figures 5.31: Example of rock magnetic measurements in the sandstones of the Mt Daubeny Formation (locality DAU): specimen DAU3-3.

A- IRM curve; **B-** Back field curve (coercivity); **C-** Hysteresis loop; and **D-** IST curve, in red while heating and in blue while cooling ($B=535$ mT).

$H_C=171.8$ mT; $H_{CR}=366.7$ mT.

$M_S=2.7 \cdot 10^{-3}$ Am²/kg; $M_{RS}=1.9 \cdot 10^{-3}$ Am²/kg.

The IRM and back field curves (figures 5.31-A & B) show clearly the existence of high coercivity minerals in these sandstones ($H_C=171.8$ mT). The IST curve (figure 5.31-D) suggests the presence of goethite, but in particular of haematite with a Curie temperature close to 680°C. It reveals in addition the presence of magnetite visible on the heating curve and more clearly on the cooling one. The existence of both magnetite and haematite shift the H_{CR}/H_C ratio to the range of PSD grain on the Day plot although the M_{RS}/M_S ratio stays in the SD domain. The slope of the hysteresis loop (figure 5.31-C) and the positive values at about 700°C on the IST curve witnesses the significant contribution of para-magnetic material.



Figures 5.32: Example of rock magnetic measurements from a volcanic pebble of the basal conglomerate of the Mt Daubeny Formation (locality DAU): specimen DAU1-16.

A- IRM curve; **B-** Back field curve (coercivity); **C-** Hysteresis loop; and **D-** IST curve, in red while heating and in blue while cooling ($B=535$ mT).

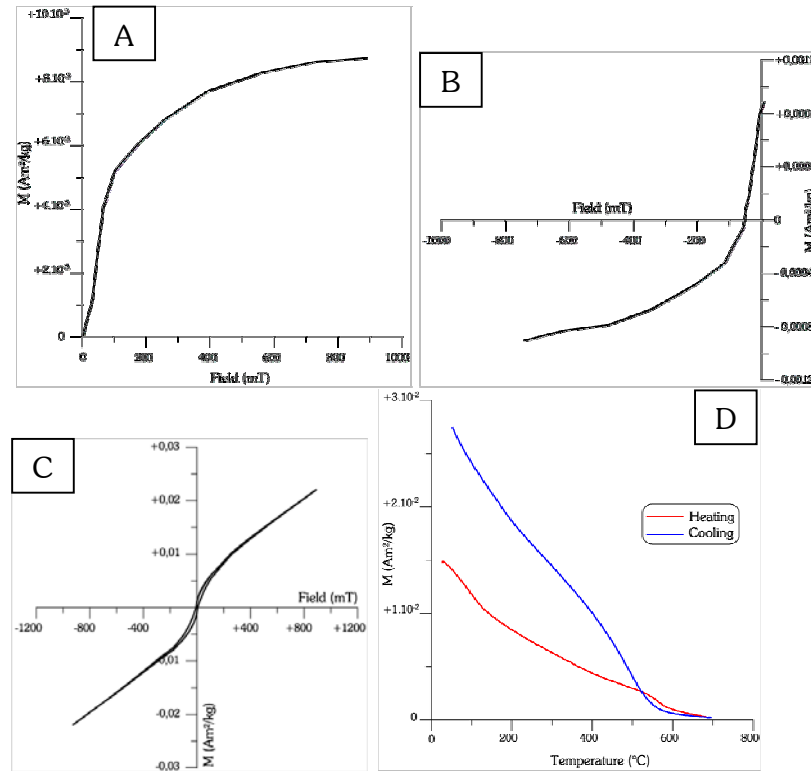
$H_C=70.4$ mT; $H_{CR}=221.1$ mT.

$M_S=17.8 \cdot 10^{-3}$ Am²/kg; $M_{RS}=9.7 \cdot 10^{-3}$ Am²/kg.

The conglomerate at the base of the Mount Daubeny Formation (photo 6-A) contains two types of pebbles, volcanic or grey sandstones, coming from the Cambrian Gnalta and

Mootwingee Groups. Rock magnetic measurements, shown here for the volcanic pebble (figures 5.32-A to D), demonstrate clearly that both types of pebbles contain and magnetite and haematite.

Conversely, measurements in the dykes (figures 5.33-A to D) suggest minerals from the titanomagnetite family (probably some low titanium titanomagnetite) as main magnetic carrier ($H_C=7,60$ mT). However, some oxidised mineral seems to exist as well, because the IRM and back field curves are not fully saturated (figures 5.33-A & B). This was expected from field observations as these dykes looks sometimes quite altered with occurrence of chlorite in particular.



Figures 5.33: Example of rock magnetic measurements in the mafic dykes intruding the Mt Daubeny Formation (locality DAU): specimen DAU7-15.

A- IRM curve; **B-** Back field curve (coercivity); **C-** Hysteresis loop; and **D-** IST curve, in red while heating and in blue while cooling ($B=504$ mT). $H_C=7,6$ mT; $H_{CR}=65,8$ mT. $M_S=5,3 \cdot 10^{-3} \text{ Am}^2/\text{kg}$; $M_{RS}=9,6 \cdot 10^{-4} \text{ Am}^2/\text{kg}$.

5.6.4. Palaeomagnetic results

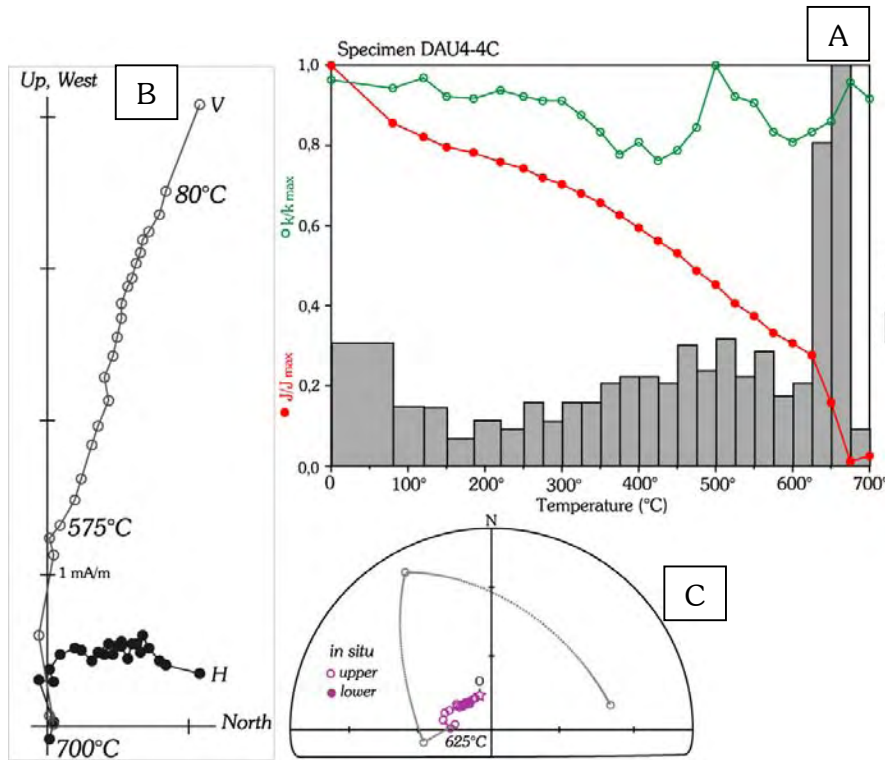
- Demagnetisation

Detailed thermal demagnetisation (26 steps), carried out on the sandstones of the Mt Daubeny Formation, isolated two components after removal of a viscous or drilling-induced magnetisation below 80° or 120°C . One, named component C_M , is fully demagnetised by 575°C , and the second, named component C_H , is removed at 675°C . These unblocking temperatures associated with rock magnetism analysis show that C_M is carried by magnetite, and C_H , by haematite.

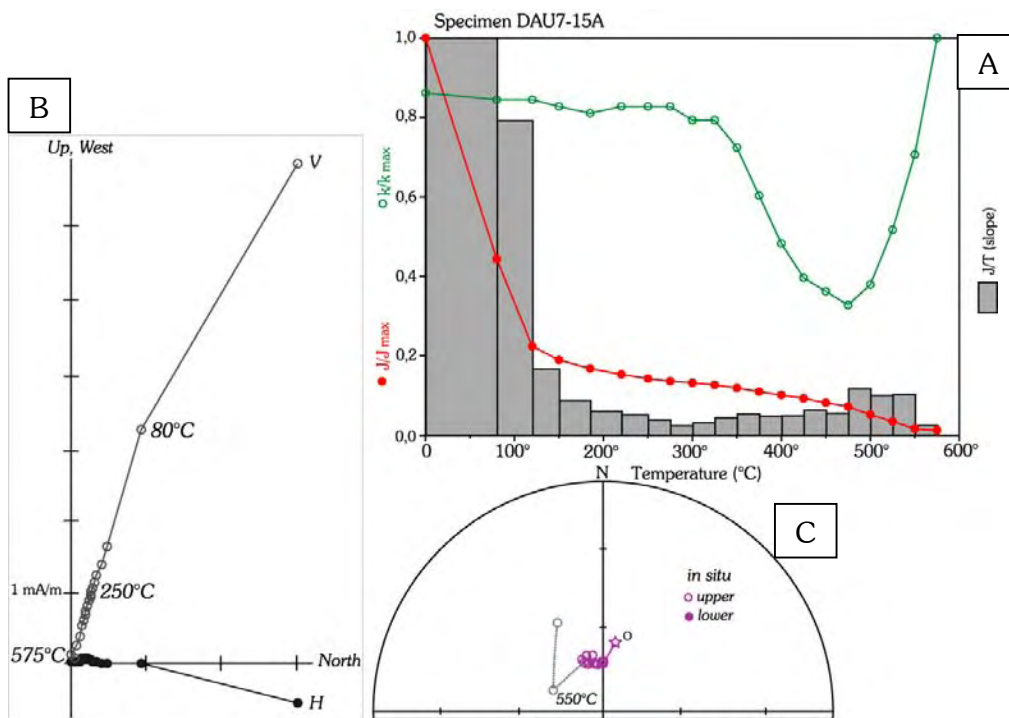
In the example shown here (figures 5.34), the two directions of magnetisation are clearly distinct, but this not the case for every specimen, and distinction between components cannot be always firmly established.

- Interpretation

Site mean directions from component C_M are plotted on a stereogram *in situ* and after bedding correction (figures 5.36-A & B; table 7). The overall mean direction *in situ* for the locality is: $D.342^\circ / I.-67^\circ$ ($\alpha_{95} = 7,2^\circ / \kappa = 72,1$), and becomes after bedding correction: $D.023^\circ / I.-36^\circ$ ($\alpha_{95} = 11,3^\circ / \kappa = 29,3$). The classic fold test (McElhinny, 1964) is negative with a κ -ratio=0,41 (it becomes positive at the 6,5% confidence level only). This suggests a post-folding remagnetisation. The *in situ* orientation corresponds by the way to a Late Jurassic or Early Cretaceous position (see below).



Figures 5.34: Example of palaeomagnetic results obtained by thermal demagnetisation from the sandstones of the Mt Daubeny Formation (locality DAU). NRM@RT=4,31 mA/m. Same legend as in figure 5.6 (all *in situ*); i.e. **A**-Demagnetisation curve with red closed circles, normalised intensity; green open circles, susceptibility; grey boxes, slope of intensity. **B**-Zijderveld diagram with open circles, projection on the vertical plane [V]; closed circles, on the horizontal plane [H]. **C**- Stereogram; "Schmidt" equal area polar projection.



Figures 5.35: Example of palaeomagnetic results obtained by thermal demagnetisation from the mafic dykes intruding the Mt Daubeny Formation (locality DAU). NRM@RT=7,50 mA/m. Same legend as in figure 5.6 (all *in situ*); i.e. **A**- Demagnetisation curve with red closed circles, normalised intensity; green open circles, susceptibility; grey boxes, slope of intensity. **B**- Zijderveld diagram with open circles, projection on the vertical plane [V]; closed circles, on the horizontal plane [H]. **C**- Stereogram; "Schmidt" equal area polar projection.

The overall mean direction for the component C_H (figures 5.36-C & D; table 7) is *in situ*: D.357° / I.-67° ($\alpha_{95} = 11,7^\circ$ / $\kappa = 27,6$), and D.026° / I.-32° ($\alpha_{95} = 9,3^\circ$ / $\kappa = 43,0$) after bedding correction. The classic fold test is not significant at the 95% confidence level with a κ -ratio= 1,6. Commonly used fold tests (e.g. bootstrap analysis of Tauxe, 1998; Enkin & Watson, 1996; McFadden, 1990) are here inadequate, because a bias is introduced when the two cylindrical folds

are unfolded. However, the classic fold test becomes positive at the 77% confidence level suggesting an improvement in grouping. It is an indication to think it can be acquired prior to folding, although the *in situ* orientation resembles to that of C_M . It must be noticed that the two sites with the larger confidence cones (in blue on figures 5.36-C & D) are situated at the base of the section where grain size is coarser.

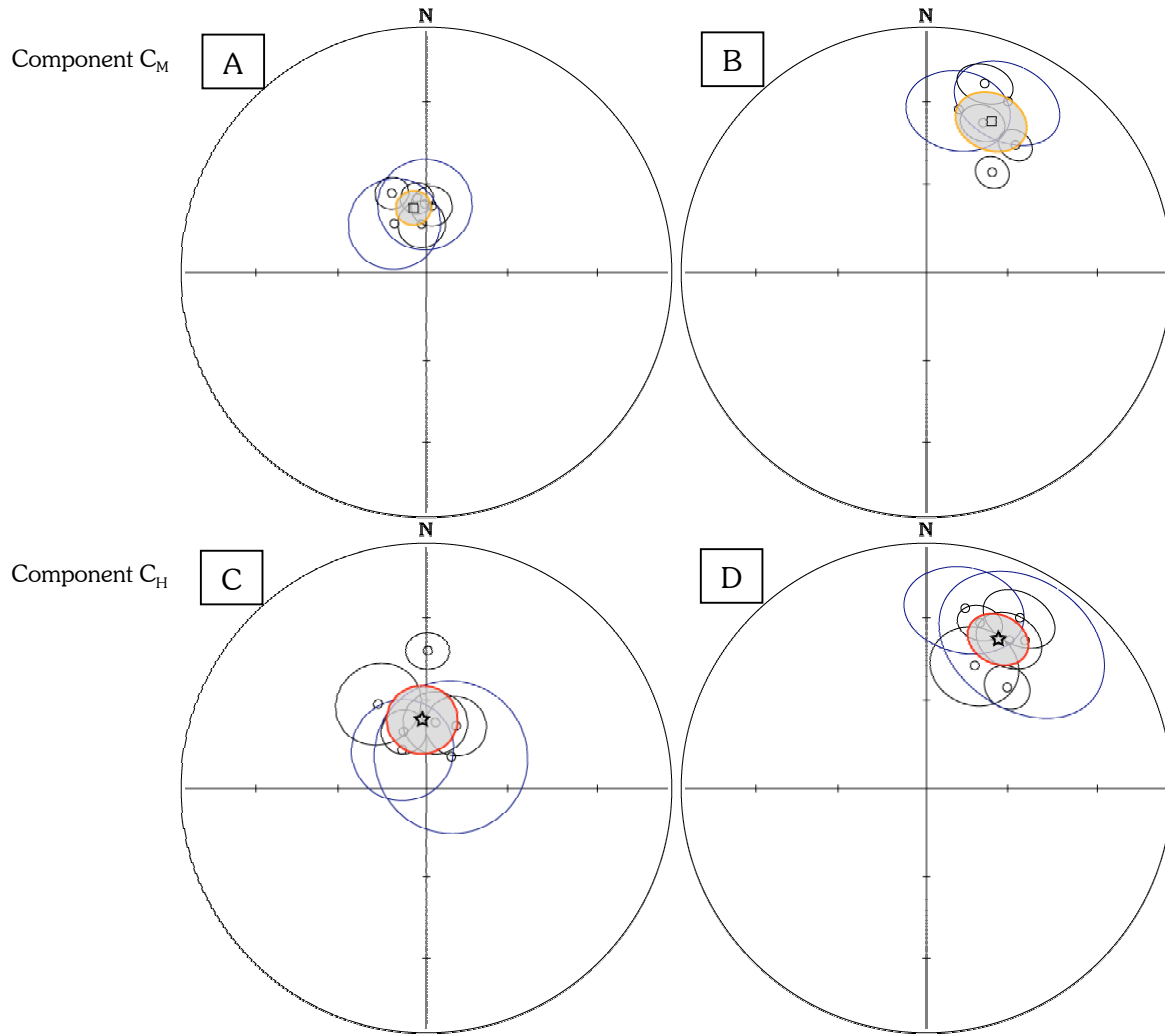


Figure 5.36: Orientation of components obtained from the sandstones of the Mt Daubeny Formation (locality DAU). **Black circles** are site mean directions with their associated 95% confidence cones (α_{95}).

A- *in situ* and **B-** after bedding correction, overall mean direction (**square**) with its 95% confidence cones (**orange**) for components C_M . **C-** *in situ* and **D-** after bedding correction, overall mean direction (**star**) with its 95% confidence cones (**red**) for components C_H . **Open** symbols are negative inclination values; **closed** symbols, positive inclination values. Schmidt equal area polar projection.

- **Conglomerate test**

Due to the different petrography in pebbles, the palaeomagnetic response is obviously different. After removal of the viscous or drilling-induced magnetisation, the volcanic pebbles show one component of magnetisation, whereas the sandstones show two directions.

In the pebbles of grey sandstone, the first component is carried by magnetite and can be compared to component C_M . The second is carried by haematite and comparable to component C_H .

In the volcanic pebbles however, both magnetite and haematite carry the same direction of magnetisation in a specimen. This component will be compared to component C_H .

The orientations of C_H look to be randomly distributed. This is confirmed by the Rayleigh and the Beran/Giné statistics, which accept uniformity at the 95% confidence level.

Conversely, orientations of C_M seem to show a slight grouping about the mean direction and statistical tests reject uniformity (figure 5.37-A; shown *in situ* only as the distribution is the same after bedding correction because the stratigraphy is monoclinical within the site).

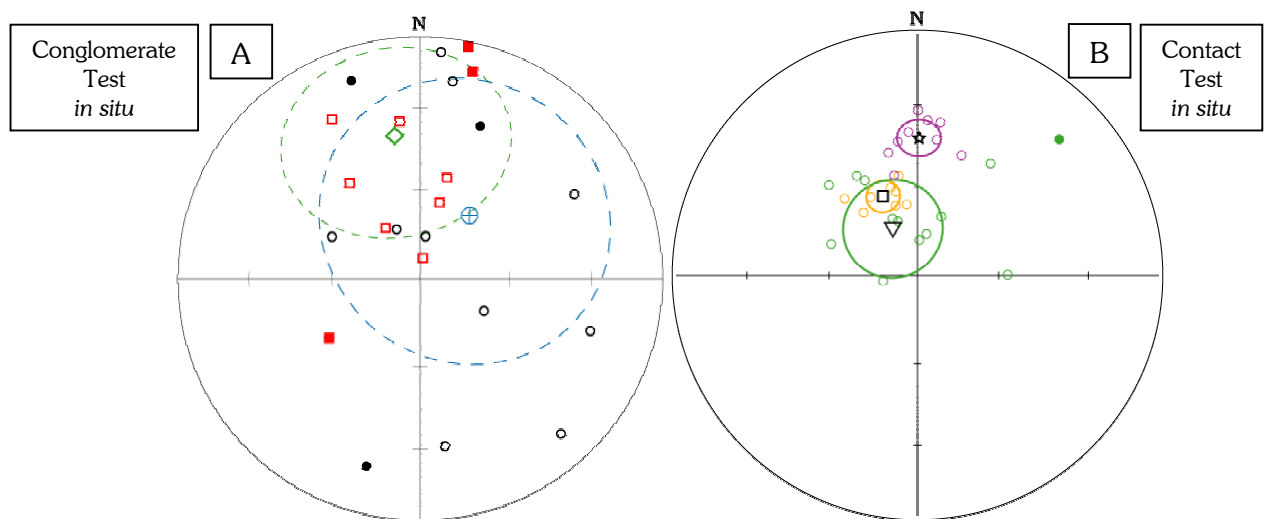
Theoretically, a conglomerate test should involve pebbles of same nature than the rocks studied, in order to avoid difference simply due to different petrography. However, as the magnetic carriers are similar and the unblocking temperatures defining components in the volcanic pebbles range from as low as 120°C to 675°C, it means at least that no important thermal remagnetisation affected this zone. From this point of view, it can be regarded as a negative conglomerate test concerning the components C_M but a positive test concerning C_H .

- **Contact test**

Two dykes have been drilled. One is about 1,5 metres wide, and the second is narrower (photo 6-B). Macroscopically, the presence of chlorite attests a certain alteration. The contact between the dykes and the red sandstones of the Mt Daubeny Formation is sharp, and the first one or two centimetres in the sandstone is pale, almost white. Ten cores have been drilled in the sandstones for the contact test at 2, 5, 10, 20, 32, 74, 152, 238, 310 & 412 cm from the edge of one dyke.

These dykes have a viscous magnetisation up to 80°-120°C but contain basically one component of magnetisation with unblocking temperatures reaching 550°C (figures 5.35, above). It is carried by some low titanium titanomagnetite and can be named component C_M . Orientations yielded by this component are very scattered (green circles in figure 5.36-B; shown *in situ* only, because these dykes are regarded as post-folding intrusions). This is probably due to alteration visible in these rocks.

However, when compared with directions from the red beds (figure 5.37-B), the mean direction obtained from the dykes (triangle) is not statistically different from the direction of the component C_M (square), which lies within the confidence cone (orange α_{95}). Conversely it is



Figures 5.37: A- Conglomerate Test. Single specimen orientations for components C_M (red squares) are scattered but not randomly distributed as they tend to group around their mean direction (green diamond and its dashed α_{95}). On the contrary, orientations of C_H (black circles) show a uniform distribution and their mean direction (blue star) has no significance.

B- Contact test. Single specimen orientations for C_M from the dykes (green circles) are scattered but their mean direction (triangle with green α_{95}) is not distinguishable from the mean direction (square and orange α_{95}) obtained from components C_M (orange circles) of the surrounding sandstones. On the contrary, it is distinct from the mean direction (star and violet α_{95}) obtained from components C_H (violet circles) of the sandstones.

Open symbols are negative inclination values (upper hemisphere); **closed** symbols, positive inclination values (lower hemisphere). Schmidt equal area polar projection; *in situ*.

distinct from the direction yielded by the component C_H (star) of the sandstones, as confidence cones from the two directions are clearly separated (green α_{95} for the dykes and violet α_{95} for components C_H of the sandstones).

Although there is no deviation in magnetisation, directions from the high temperature component C_H identified in the sandstones are statistically distinct from directions of magnetisation in the dykes, and the contact test may be considered positive.

Table 7: Site mean directions and overall mean directions for locality DAU

Name	N	R	D.InS	I.InS	D.Bed	I.Bed	α_{95}	κ	DipDir	Dip		
Component C_M per site:												
Dau-02	4	4,0	004,8	-67,5	20,6	-34,2	6,8	18,4	224,9	37,0		
Dau-03	4	3,9	358,8	-66,9	025,4	-22,7	15,6	35,8	237,6	53,4		
Dau-04	5	5,0	354,2	-73,6	017,0	-19,3	7,9	94,6	206,9	56,5		
Dau-05	1	1,0	312,8	-58,0	020,4	-56,6	∞	0,0	262,9	46,0		
Dau-06	6	6,0	353,0	-64,6	034,9	-35,9	5,4	155,1	261,9	49,0		
Dau-07	8	7,9	336,5	-60,7	033,2	-48,9	5,5	102,3	272,9	47,0		
Dau-09	4	3,9	326,7	-70,3	011,1	-31,8	15,4	36,7	215,9	49,0		
Component C_H per site:												
Dau-02	8	7,8	025,4	-66,6	029,2	-30,5	10,1	31,0	224,9	37,0		
Dau-03	6	5,9	007,9	-67,5	028,6	-20,6	10,6	40,7	237,6	53,4		
Dau-04	5	4,8	328,2	-74,7	012,0	-24,7	17,1	20,9	206,9	56,5		
Dau-05	6	5,9	338,3	-69,4	038,6	-45,5	7,5	81,2	262,9	46,0		
Dau-06	5	4,9	330,3	-56,9	021,4	-44,5	14,0	30,7	261,9	49,0		
Dau-07	9	8,9	000,6	-42,4	017,8	-28,8	6,7	60,1	272,9	47,0		
Dau-09	4	3,8	038,4	-76,3	033,6	-27,3	25,9	13,6	215,9	49,0		
Conglomerate test, component C_M :												
Dau-01	13	8,3	351,0	-24,0	003,0	-05,8	32,7	2,6	244,9	46,0		
Conglomerate test, component C_H :												
Dau-01	10	8,3	000,9	-45,7	024,2	-16,1	23,2	5,3	244,9	46,0		
Contact test (dykes), component C_M :												
Dau-08	14	11,9	344,9	-71,0	~	~	17,5	6,1	post-folding (<i>in situ</i>)			
Name	B	N	R	D.InS	I.InS	α_{95}	κ	R	D.Bed	I.Bed	α_{95}	κ
Mean direction for components M:												
Dau-M	7	32	6,9	342,2	-67,0	7,2	72,1	6,8	022,9	-35,9	11,3	29,3
Mean direction for components H:												
Dau-H	7	43	6,8	356,6	-66,6	11,7	27,6	6,9	025,6	-32,0	9,3	43,0
N: number of samples; B: number of sites; α_{95}: cone calculated at the 95% confidence level; κ: precision parameter; R: resultant vector; D.InS/I.InS: declination/inclination <i>in situ</i> (geographic coordinates); D.Bed/I.Bed: declination/inclination after bedding correction. Fold axis for the fold of first generation F1: 142° / 12°; Fold axis for the fold of second generation F2: 245° / 40°.												

- Conclusions

The mid temperature component C_M from the Mt Daubeney sandstones shows a negative fold test. Components carried by magnetite in the conglomerate are not randomly distributed, and the direction of C_M is statistically undistinguishable from mean direction obtained from the dykes. This is clearly indicative of a remagnetisation. Moreover, the corresponding palaeopole to the *in situ* orientation of C_M is: Plong.161,6° / Plat.-68,3° (dp=8,2 / dm=9,7; Australian coordinates), and falls near (*i.e.* overlap of confidence cones) the Triassic or Jurassic to Early Cretaceous segment of the APW path for Australia (figure 5.38; table 8).

It is suggested that this secondary magnetisation is linked to fluid migration related to the intrusions of dykes. Indeed, a fluid associated with the magmatic event may have circulated through the sandstones depositing magnetite throughout the formation and partly altering the dykes to form chlorite. It would explain why this magnetisation is present in the pebbles of sandstones if the fluid percolated into them but not in the volcanic ones if the fluid flowed around, as they are more coherent. Moreover, the association of pre-existing and fluid-deposited magnetite in the pebbles of sandstone can cause the observed scattering in orientations of C_M (figure 5.36-A).

This implies that the age of the dykes and this fluid migration event are Triassic or Jurassic to Early Cretaceous. A Jurassic age is favoured as it could be linked to other dyke intrusions to the North – East of the Broken Hill area (Mills, *personal communication*, 2002).

Although the high temperature component C_H can generally be distinguished from C_M , their resulting overall mean directions are quite similar. On directions of magnetisation from C_H , the fold test is positive at the 77% confidence level, but not at the 95% confidence level. This is at least partly due to the slight difference in bedding orientation between the lower and the upper section. The conglomerate test for the high temperature component is considered positive. The dyke test shows a statistically distinct orientation of components C_M from the dykes relative to component C_H of the red beds, despite scattering due alteration in the dykes.

All together, these indications lead to the conclusion that the high temperature component C_H is pre-folding. As the Mt Daubeny Formation is Gedinian in age, and folding occurred shortly after deposition (because it does not fundamentally affect the late Early to Middle Devonian rhyolitic intrusions, the “Sisters”; see below), this direction can be considered as primary magnetisation. The corresponding palaeopole (figure 5.38; table 8) is: Plong.028,7° / Plat.-62,8° (dp=5,9 / dm=10,5; Australian coordinates).

Table 8: Corresponding palaeopoles for the Mount Daubeny Formation

Name	B	N	<u>Australian coord.</u>		<u>African coord.</u>		dp	dm
			PLong.	Plat.	PLong.	Plat.		
<i>For mid-temperature component M in situ:</i>								
Dau-M	7	32	173,1	-67,0	043,4	-52,7	9,9	11,9
<i>For high-temperature component H after bedding correction:</i>								
Dau-H	7	43	028,2	-63,1	011,2	-12,8	5,9	10,5

N: number of samples; **B:** number of sites; **PLong./Plat.:** palaeopole longitude/latitude in Australian and in African coordinates. **dp/dm** : semi-axis of the ellipse of confidence.

This Early Devonian pole is similar to several Late Devonian published poles (like for Africa: the Beni-Zireg Limestone, Aïfa *et al.*, 1990; Griotte Limestone, Aïfa, 1993; for Australia: Hervey Group, Li *et al.*, 1988; Worange Point Formation, Thrupp *et al.*, 1991; Canning Basin Reef Complexes, Chen *et al.*, 1995; Canning Basin Reef Complexes, Hurley & Van der Voo, 1987) and also to Silurian – Early Devonian ones (table 9). It could signify that the movement of Gondwana in the Devonian is slow (but see discussion in Chapter 8).

It must be noticed in particular that this pole is not similar to the Snowy River Volcanics (Schmidt *et al.*, 1987) of equivalent age and largely used to draw APW paths for Gondwana.

Table 9: Comparable published Silurian – Early Devonian palaeopoles for Gondwana. The 95% confidence ellipses of the following palaeopoles overlap the ellipse of pole from the Mount Daubeny Formation.

Name, place	Age	B	N	κ	α_{95}	Q	<u>Australian coordinates.</u>				Authors
							PLong.	Plat.	dp	dm	
<u>Australia:</u>											
Bowning Group Volcanics, NSW	415±3	7	25	36,8	10,0	2	045,1	-64,0	9,0	9,0	Luck, 1973
Mugga Mugga Porphyry, ACT	422±1	nc	17	29,0	7,0	2	007,9	-63,3	6,0	9,0	Briden, 1966
Ainslie Volcanics, ACT	425±2	7	24	33,4	11,0	2	352,9	-71,0	10,0	10,0	Luck, 1973
<u>South America:</u>											
Picos & Passagem Series, Brazil	397±20	ng	12	nc	32,0	2	028,4	-70,1	36,0	36,0	Creer, 1970

NSW: New South Wales; **ACT:** Canberra

N: number of samples; **B:** number of sites; **κ :** precision parameter; **α_{95} :** 95% confidence cone; **Q:** quality level, corresponding to the “demag-code” in the palaeomagnetic database; **PLong./Plat.:** palaeopole longitude/latitude in Australian coordinates. **dp/dm** : semi-axis of the ellipse of confidence; **Ages** and their uncertainties correspond to the average between the high and the low magnetisation ages given in the database; **ng:** not given.

Data from the I.A.G.A. palaeomagnetic database, Version 4-4 (2003), and references therein (first version published by McElhinny & Lock, 1996).



Figure 5.38: Corresponding palaeopoles in Australian coordinates. The possible APW path for Australia-Gondwana from the present-day to 570 Ma based on Small Circle Fit is shown for comparison purposes.

Same legend as in figure 2.19-A, Chapter 2 (§.2.7).

Dau-H is the pole corresponding to component C_H after bedding correction; **Dau-M**, corresponding to C_M *in situ*.

5.7. The Mount Daubeny Formation from the Churinga Property (CHU)

5.7.1. Presentation

These sandstones (locality CHU) are not precisely dated. They are grey in colour, thin bedded, and are considered to be the south equivalent of the red sandstones of the Mt Daubeny Formation (photo 7). Their position is strategic, because they are exposed just South of the change in fault and cleavage trend, which turns from a North West direction in the northern part of the Broken Hill area to South East in the southern part (see map in figure 5.2). It is not known whether this change is imputable to terrane rotation. These sandstones also form a large syncline with a plunging axis. Metre-scale second-order folds exist on each limb of this syncline and have been used for fold tests, as only small zones are suitable for palaeomagnetic purposes and one limb of the large syncline is drillable.

Twenty-eight cores (5 sites) have been collected in a dried creek at the Churinga Property (figure 5.2; table 3).

5.7.2. Anisotropy of magnetic susceptibility (AMS)

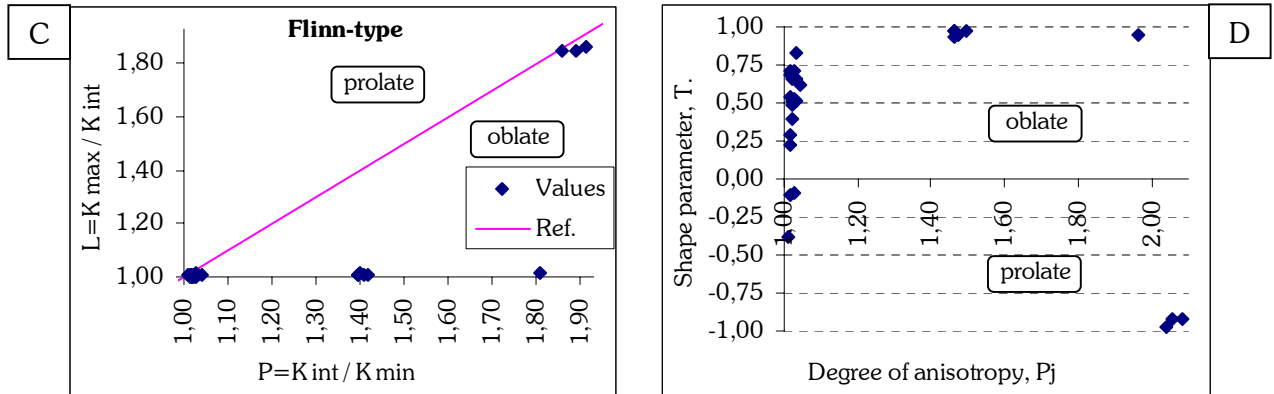
Nine specimens show a strong degree of anisotropy and marked shape of their ellipsoid of magnetic susceptibility, yielding to a relatively high $\{P_J\}$ in average for the locality ($P_J=1,25\pm0,37$). The Parés Test (Parés & Van der Pluijm, 2002) for these samples reaches 100% alignment. The fact that these values stem from high internal strain near the hinge of the meter-scale fold cannot be ruled out but it is most likely due to magnetic perturbation while measurements (figures 5.39-A & B).



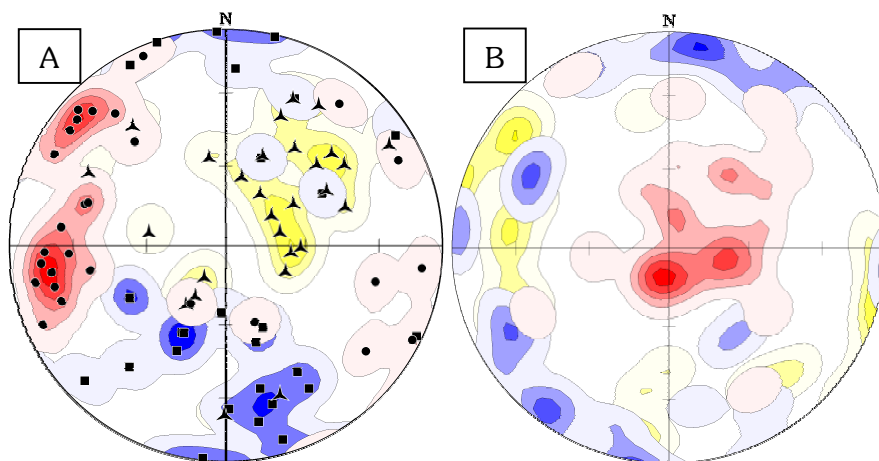
Photo 7: Meter-scale fold in the grey sandstones of the Mount Daubeny Formation from the Churinga Property. The hat gives the scale.

Indeed, the 67,9% left of the locality show a very low degree of anisotropy ($P_j = 1,02 \pm 0,01$) and tends to have an oblate shape of the ellipsoid of magnetic susceptibility ($T = 0,44 \pm 0,33$). Internal strain is therefore probably negligible in the whole locality.

The Königsberger ratio ($Q_K = 0,26 \pm 0,10$) is low probably signifying the presence of relatively large sizes of magnetic particles and in particular that no lightning effects are expected.



Figures 5.39: A- Flinn-type diagram (Flinn, 1962, 1965-a, 1965-b) and B- {T} versus {P_j} diagram (Jelinek, 1981; Hrouda, 1982) for the grey sandstones of the Mount Daubeny Formation at the Churinga Property (locality CHU).



Figures 5.40: Orientations of the principal axes of magnetic susceptibility for the sandstones of the Mt Daubeny Formation at the Churinga Property, locality CHU.

A- *in situ*, and B- after bedding correction.

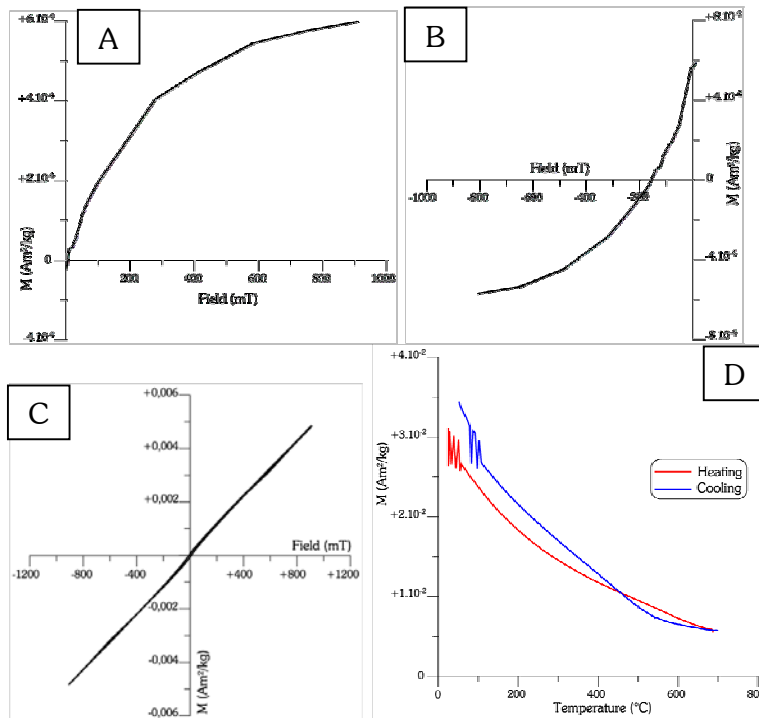
Same legend as in figure 5.4; i.e. K_{max}, squares (blue); K_{int}, triangles (yellow); K_{min}, dots (red).

The directions of the principal axes of magnetic susceptibility (figures 5.40-A & B) show two clusters of K_{min} *in situ* corresponding to the two limbs of the second folds whereas after bedding correction, they are better grouped about the vertical. This is representative of a sedimentary magnetic fabric, in good agreement with the oblate shape of the ellipsoid of magnetic susceptibility.

However, K_{min} after bedding correction are still a bit scattered. This might correspond either to perturbations during measurements or a not fully accurate bedding correction, as bedding is difficult to precisely assess on the field. No magnetic lineation can be clearly determined although the maximum density is directed ~N-S after bedding correction.

5.7.3. Rock magnetism

The slope of the hysteresis loop (figure 5.41-C) and the positive values at 700°C of the IST curve (figure 5.41-D) are representative of the strong paramagnetic contribution in these rocks. In detail, the back field curve (figure 5.41-B) show the presence of two magnetic carriers, probably magnetite given the inflexion around 580°C on the IST curve, and haematite, as the IRM and back field curves are not fully saturated (figures 5.41-A & B).



Figures 5.41: Example of rock magnetic measurements from the grey sandstones of the Mt Daubeny Formation at the Churinga Property (locality CHU): specimen CHU2-5.

A- IRM curve; **B-** Back field curve (coercivity); **C-** Hysteresis loop; and **D-** IST curve, in red while heating and in blue while cooling ($B=523$ mT).

$H_C=34,9$ mT; $H_{CR}=156,2$ mT.

$M_S=1,4 \cdot 10^{-3}$ Am²/kg; $M_{RS}=6,1 \cdot 10^{-4}$ Am²/kg.

5.7.4. Palaeomagnetic results

- Demagnetisation

Demagnetisation process shows clearly two components after removal of a viscous or drilling-induced magnetisation (figures 5.42): a component C_M up to 550°C carried by magnetite, and a component C_H from 550° to 680°C, carried by haematite. Component C_H is not always well isolated due to acquisition of laboratory-induced magnetisation during heating process, which obscures the natural remanent magnetisation. This is illustrated by the increase of magnetic susceptibility by 500°C (figure 5.42-A).

- Interpretation

Mean directions per site for component C_M are shown together with single specimen components (figures 5.43-A & B), because orientations per site appear quite clustered (for example, in the site shown in blue), except for two sites (in pink and green) where confidence cones are very large. Conversely, the overall mean direction has a very large confidence cone because site mean directions are very scattered, both *in situ* with an overall mean direction $D.334^\circ / I.-60^\circ$ ($N=27$; $\alpha_{95}=38,2^\circ / \kappa=5,0$), and after bedding correction $D.339^\circ / I.-22^\circ$ ($\alpha_{95}=47,2^\circ / \kappa=3,6$). The fold test is thus not significant with a κ -ratio=0,72. It becomes positive at the 32,5% confidence level only, meaning it is significantly worse after correction.

By contrast, the mean directions calculated for the components C_H are much better grouped (figures 5.43-C & D; and table 10), and the overall mean direction for the locality is *in situ*: $D.173^\circ / I.-56^\circ$ ($\alpha_{95}=15,7^\circ / \kappa=24,8$) and after bedding correction: $D.261^\circ / I.-13^\circ$ ($\alpha_{95}=22,0^\circ / \kappa=13,0$). However, the classic fold test (McElhinny, 1964) is not significant with a κ -ratio=0,52. The grouping is significantly worse after bedding correction, as the fold test becomes positive at the 18,5% confidence level.

No clear explanation has been found to interpret the behaviour of component C_M . However, as the AMS shows that internal strain is not strong enough to be responsible of deviation of the remanence, the only solution is that several directions of magnetisation are removed simultaneously. Albeit its large confidence cone, the overall mean direction remains consistent with the direction of remagnetisation observed in the Mt Daubeny Formation to the

North (locality DAU). This behaviour could be understood therefore as partial remagnetisation affecting certain sites more than others.

For instance the Mesozoic overprint observed in the red sandstones of the Mt Daubeny Formation (locality DAU) could be here demagnetised together with a N-S direction (site shown in blue), rather similar to what is observed in the Sisters (locality SIS, see below). This result however cannot be used further as no reliable palaeomagnetic direction can be determined.

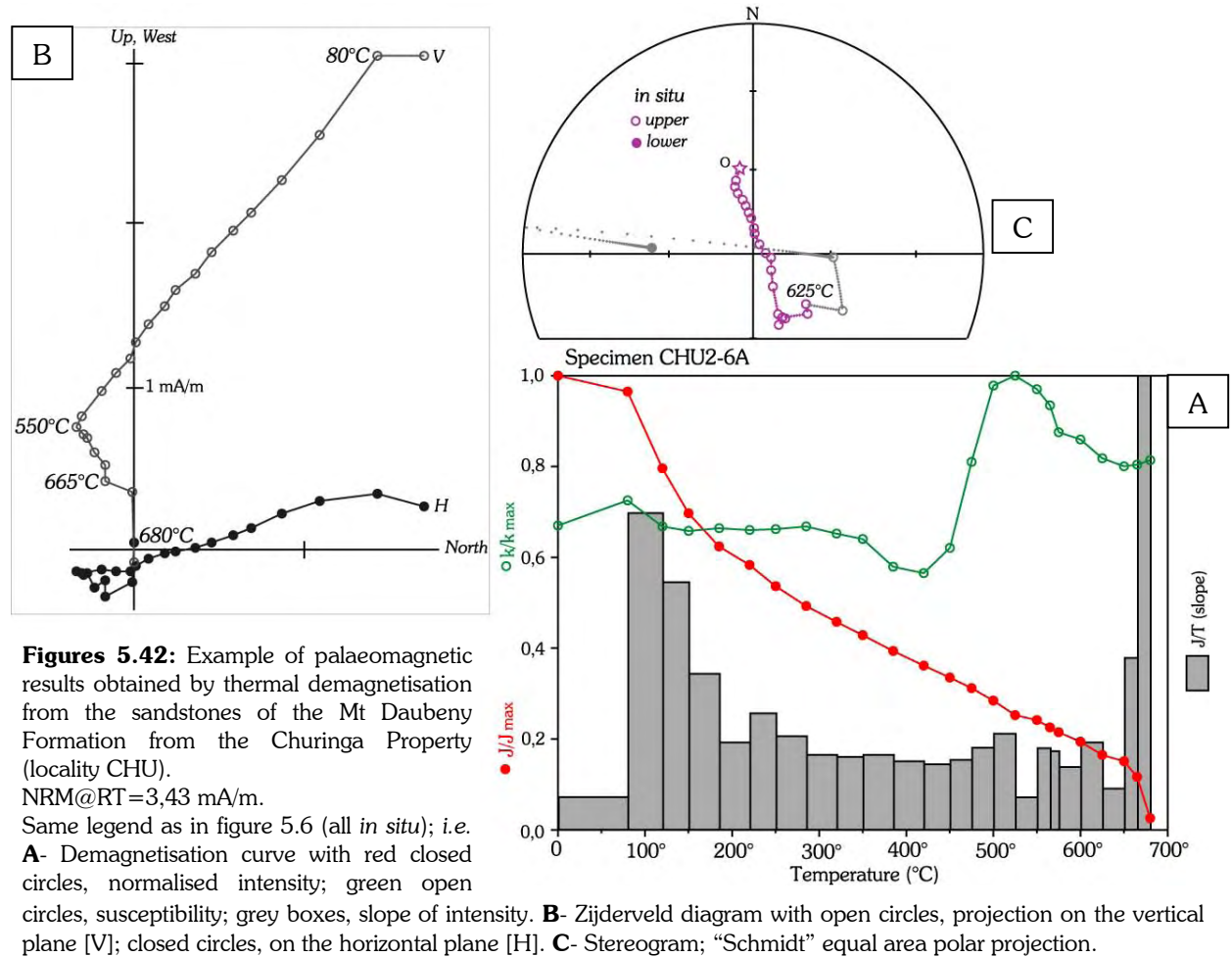


Table 10: Site mean directions and overall mean directions for locality CHU

Name	N	R	D.InS	I.InS	α_{95}	κ	R	D.Bed	I.Bed	α_{95}	κ	DipDir	Dip
<i>Component C_H per site:</i>													
Chu-1	4	3,9	138,2	-60,6	18,2	26,3	3,9	268,4	-29,4	17,3	29,1	variable	
Chu-2	5	4,7	150,4	-58,9	28,7	11,2	4,7	277,4	-38,3	19,5	23,2	variable	
Chu-3	4	3,9	190,0	-48,2	19,9	22,3	3,9	252,9	+04,4	16,8	30,9	variable	
Chu-4	5	4,9	168,0	-49,5	10,5	54,1	4,9	069,0	+07,5	11,3	46,5	variable	
Chu-5	4	3,9	204,6	-52,4	18,2	26,4	3,9	263,7	+05,2	20,4	21,3	variable	
Name	B	N	R	D.InS	I.InS	α_{95}	κ	R	D.Bed	I.Bed	α_{95}	κ	
<i>Mean direction for components H:</i>													
Chu-H	5	22	4,8	172,6	-56,3	15,7	24,8	4,7	261,4	-13,2	22,0	13,0	

N: number of samples; **B:** number of sites; α_{95} : cone calculated at the 95% confidence level; κ : precision parameter; **R:** resultant vector; **D.InS/I.InS:** declination/inclination *in situ* (geographic coordinates); **D.Bed/I.Bed:** declination/inclination after bedding correction.

The direction of dip (**DipDir**) and dip (**Dip**) of the bedding orientation cannot be given since it highly varies within site (see photo 7).

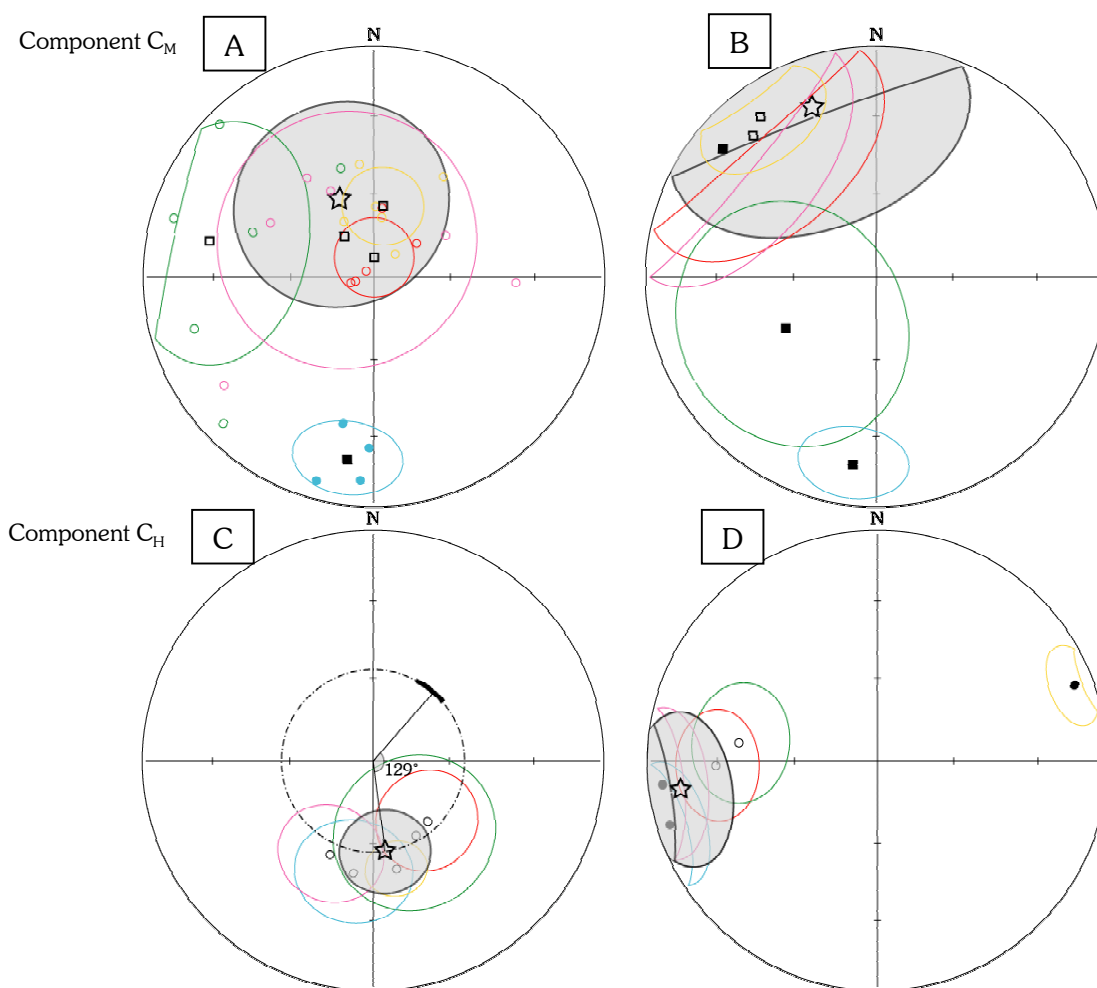


Figure 5.43: Components obtained from the sandstones of the Mt Daubeny Formation at the Churinga Property (locality CHU). **A-** *in situ* and **B-** after bedding correction, overall mean direction (**star**) with its 95% confidence cones (**shaded grey**) for components M. **Coloured circles** (shown *in situ* only) are single specimen components M and **black squares** are the corresponding site mean directions with their associated 95% confidence cones (α_{95}). **C-** *in situ* and **D-** after bedding correction, overall mean direction (**star**) with its 95% confidence cones (**shaded grey**) for components H. **Black circles** are site mean directions with their associated 95% confidence cones (α_{95}). Also shown *in situ*, possible positions (**dashed small circle**) obtained by rotation around a vertical axis, and the angle that fit the Small Circle Fit path for Australia-Gondwana as shown in figure 2.19-B (Chapter 2; §.2.7). **Open** symbols are negative inclination values; **closed** symbols, positive inclination values. Schmidt equal area polar projection.

The classic fold test of McElhinny (1964) suggests a post-folding remagnetisation for the high temperature component C_H with a κ -ratio=0,52. However, the exact geometry of the metre-scale folds, thought to be of second order of the main syncline, is rather difficult to determine precisely. It cannot be ruled out then that the low κ -ratio is just apparent and only due to inaccurate bedding correction. Yet, neither the palaeopole corresponding to the *in situ* direction (Plong.136,4°/Plat.+21,1°; $dp=16,3$ / $dm=22,6$; in Australian coordinates) nor that corresponding to the direction after bedding correction (table 11) fall close to any Early Devonian or younger segments of the AWP path expected for Australia (figure 5.44) even when the alternate polarities are considered. It is also different from the direction obtained from the Mount Daubeny Formation to the North (locality DAU).

It is based on 22 samples, so that it does not satisfy the Van der Voo's criteria, but this direction has probably a meaning. The simplest explanation appears therefore to admit that the *in situ* direction of magnetisation has been affected by a post-folding rotation. Because of its inclination, a rotation around a vertical axis can bring this direction close to a Late Devonian to Late Carboniferous segment of the APW path for Australia, although this last is not well defined.

Regardless of confidence cones, this rotation has to be about 120° - 150° relative to the Mid Carboniferous pole position deduced from the Small Circle Fit path (figure 5.43-C) and posterior to this time. It is unlikely that such rotation be younger than Mid Carboniferous, but an Early Carboniferous age, although quite surprising, can be consistent with the fact that numerous fault reactivations have been observed (Mills, personal communication). Moreover, it is in particular in good agreement with the $\sim 120^{\circ}$ change in direction observed for the cleavage and fault trend in the Broken Hill area (Mills, *personal communication*, 2002; see also map in figure 5.2).

Table 11: Corresponding palaeopoles for the Mount Daubeny Formation

Table 11: Corresponding palaeopoles for the Austral-Euroasy Formation.								
Name	B	N	<u>Australian coord.</u>		<u>African coord.</u>		dp	dm
			PLong.	Plat.	PLong.	Plat.		
For high-temperature component C_H in situ:								
Chu-InS	5	22	136,4	+21,1	127,2	+07,5	16,3	22,6
For high-temperature component C_H after bedding correction:								
Chu-Bed	5	22	222,5	+03,7	201,7	-46,8	11,4	22,4
N: number of samples; B: number of sites; PLong./Plat.: palaeopole longitude/latitude in Australian and in African coordinates. dp/dm : semi-axis of the ellipse of confidence.								

N: number of samples; **B:** number of sites; **PLong./Plat.:** palaeopole longitude/latitude in Australian and in African coordinates. **dp/dm** : semi-axis of the ellipse of confidence.

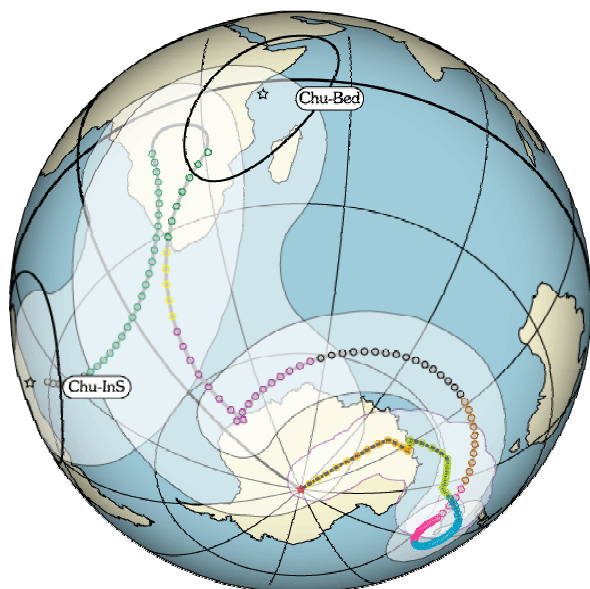


Figure 5.44: Alternate polarities for the corresponding palaeopoles in Australian coordinates. The possible APW path for Australia-Gondwana from the present-day to 570 Ma based on Small Circle Fit is shown for comparison purposes.

Same legend as in figure 2.19-A, Chapter 2 (§.2.7).

Chu-Bed is the pole corresponding to component C_H after bedding correction; **Chu-InS**, corresponding to C_H *in situ*.

5.8. Rhyolitic to dacitic intrusions – The Sisters (SIS)

5.8.1. Presentation

The Sisters (locality SIS; figure 5.2) are the names of hills made up of rhyolitic and dacitic dykes, sills and domes, which intrude the Mt Daubeny Formation near the locality DAU (described above). These intrusions are kilometre-scale and are considered as Early to Middle Devonian in age (Stevens *et al.*, 2002).

Photo 8: One of the Sisters. A sill showing columnar jointing of Early – Middle Devonian rhyolites forms this hill in the vicinity of the Wertago Property.



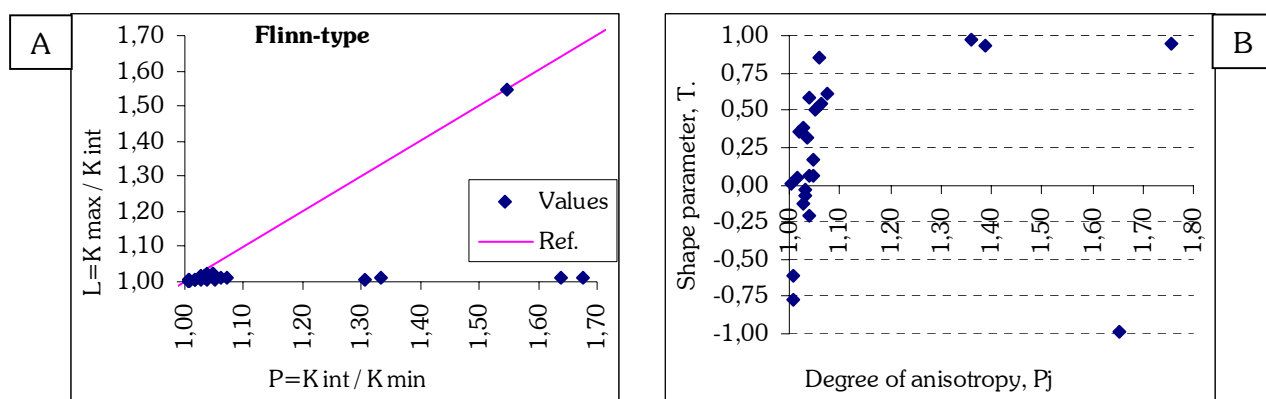
Twenty-five cores (5 sites) have been drilled in these very hard rocks. Sampling has been carried out on two hills showing jointing columns. Penetrative cleavage exists between those two hills, but does not look in the field to affect the sampled sites.

These intrusions are post-main phase of deformation, but they appear to be gently folded and tilted ($\sim 15^\circ$).

5.8.2. Anisotropy of magnetic susceptibility (AMS)

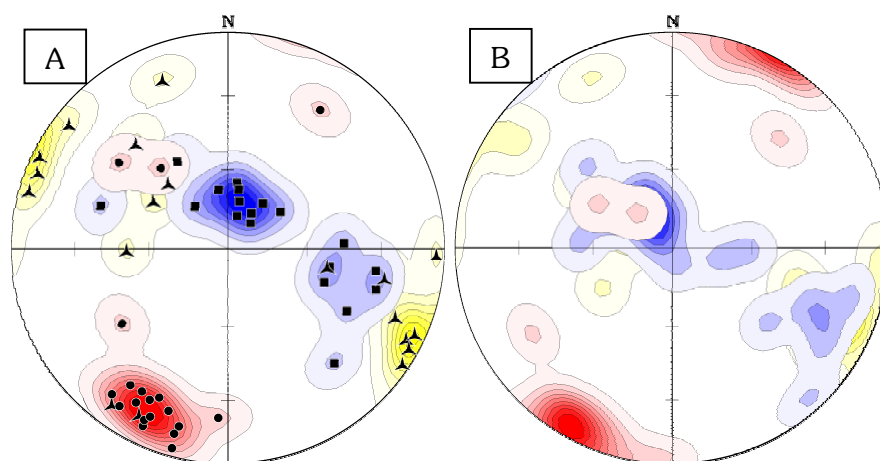
Except for five specimens, the locality shows a very weak degree of anisotropy ($P_J = 1,04 \pm 0,02$; when the five specimens are excluded) and an oblate shape of the ellipsoid of magnetic anisotropy ($T = 0,14 \pm 0,41$), illustrated by both the Flinn-type and the $\{P_J\}$ vs. $\{T\}$ diagrams (figures 5.45-A & B). This means that the cleavage observed between the two hills does not affect these samples and the internal strain is negligible.

The five other specimens yield very high Königsberger ratio (up to $Q_K = 84,6$ in one case). It appears they have been then struck by lightning. This effect seems to be recorded in site Sis-04 and the beginning of site Sis-05, and that is why $Q_K = 9,44 \pm 19,72$ in average for the locality.



Figures 5.45: **A-** Flinn-type diagram (Flinn, 1962, 1965-a, 1965-b) and **B-** $\{T\}$ versus $\{P_J\}$ diagram (Jelinek, 1981; Hrouda, 1982) for the rhyolitic sills forming hills named the Sisters (locality SIS).

Density contours show however three good clusters, even if K_{max} and K_{int} tend to be distributed along a vertical plane, resulting in an oblate tendency of the ellipsoid of magnetic susceptibility. The vertical lineation can mark either a vertical flow or a slight vertical extrusion due to horizontal compression (figures 5.46-A & B). The K_{min} is indeed orientated in the same direction as K_{int} in the sandstones of the Mt Daubeny Formation. As the ellipsoid is nearly a sphere, a slight compression may turn a horizontal axis into K_{min} , and a vertical into K_{max} .



Figures 5.46: Orientations of the principal axes of magnetic susceptibility for the Sisters, locality SIS.

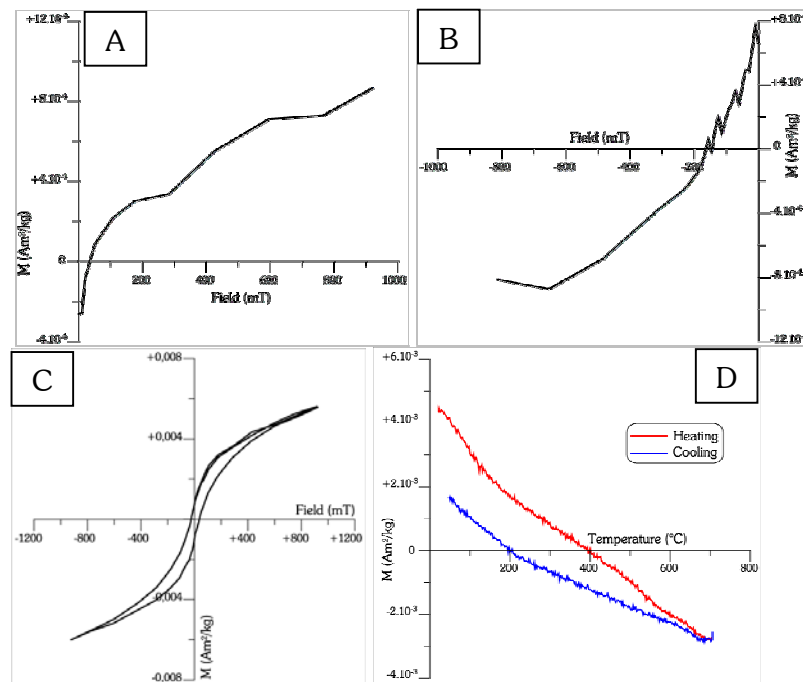
A- *in situ*, and **B-** after bedding correction.

Same legend as in figure 5.4; i.e. K_{max} , squares (blue); K_{int} , triangles (yellow); K_{min} , dots (red).

If the orientation of K_{min} has the same origin as K_{int} and K_{max} in the sandstones of the Mt Daubeny Formation, it would imply that the inferred dextral strike-slip movement on the Koonenberry fault is syn- or post-Middle Devonian, and that the rhyolitic intrusions were at shallow level to record a (slight) vertical extrusion.

It must be noticed finally that a gentle tilt occurred afterwards, because bedding measured on intercalated sedimentary layers dips to the South, and this is confirmed by the better horizontal and vertical positions of the principal axes of magnetic susceptibility after correction.

5.8.3. Rock magnetism



Figures 5.47: Example of rock magnetic measurements from the rhyolitic intrusions of the Sisters (locality SIS): specimen SIS2-4.

A- IRM curve; **B-** Back field curve (coercivity); **C-** Hysteresis loop; and **D-** IST curve, in red while heating and in blue while cooling ($B=535$ mT).

$H_C=33,6$ mT; $H_{CR}=145,0$ mT.

$M_S=3,1 \cdot 10^{-3}$ Am²/kg; $M_{RS}=8,6 \cdot 10^{-4}$ Am²/kg.

The IST curve (figure 5.47-D) shows three inflexions while heating: a first about 150°C representative of the existence of oxidised minerals, and probably mainly goethite, a second around 580°C and a third around 680°C, the Curie temperatures of magnetite and haematite respectively. The existence of high coercivity material like haematite and goethite is also visible on the IRM and back field curves, which are not saturated, although these curves are noisy (figures 5.47-A & B). The hysteresis loop has a slightly wasp-wasted shape probably associated with the coexistence of magnetite and haematite in these rocks, and that is the reason why the H_{CR}/H_C ratio is shifted to the multi-domain range in a Day plot whereas the M_{RS}/M_S ratio stays in the pseudo-single domain range.

5.8.4. Palaeomagnetic results

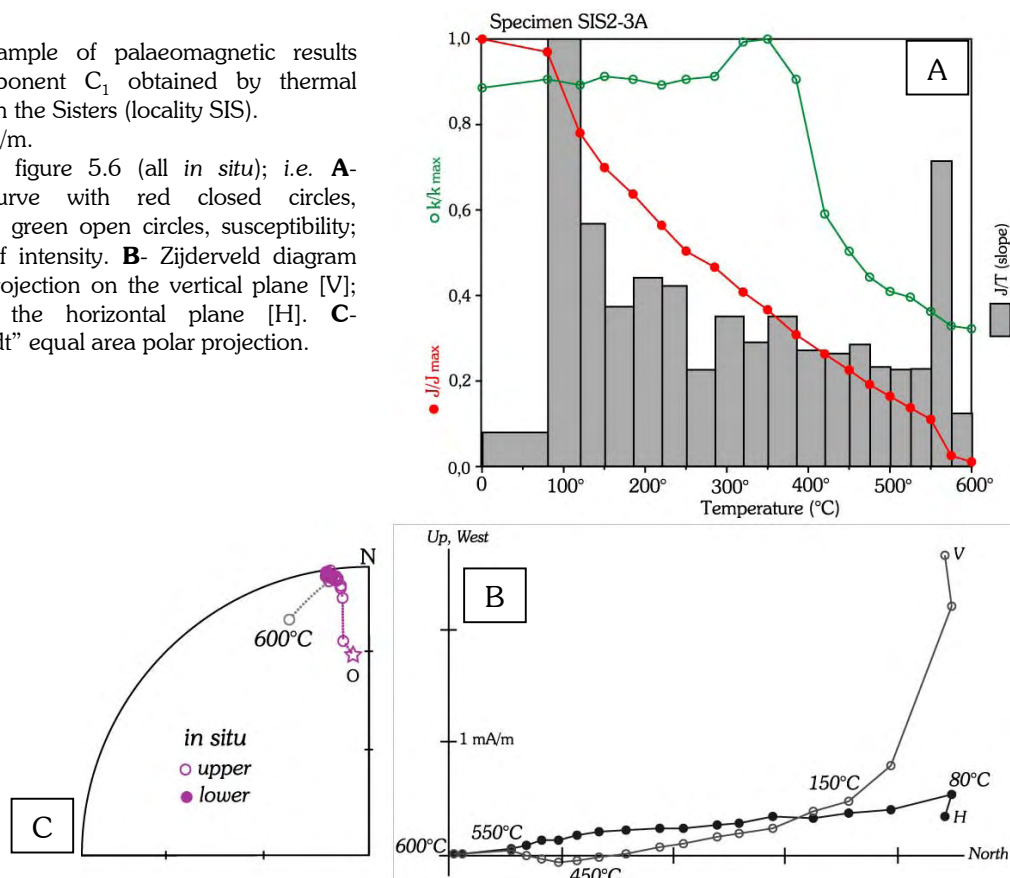
- Demagnetisation

After removal of a present-day field overprint up to 150°C, two kinds of mid temperature component, C_1 and C_2 , can be defined on a linear segment between 200° and 450°C, but occasionally persist up to 575°C (figures 5.48). It is therefore carried by magnetite. In some cases, a high temperature component C_3 can in addition be readily identified between 575° and 680°C, Curie temperature of haematite (figures 5.49).

The mid temperature components are either N-S shallow or E-W shallow, corresponding to C_1 and C_2 respectively. The component C_3 is found in seven specimens only and most of the time, it is not well defined because of its weakness (figure 5.50). For three samples, no linear segment could be sufficiently well determined and great circle analysis has been used (figure 5.50).

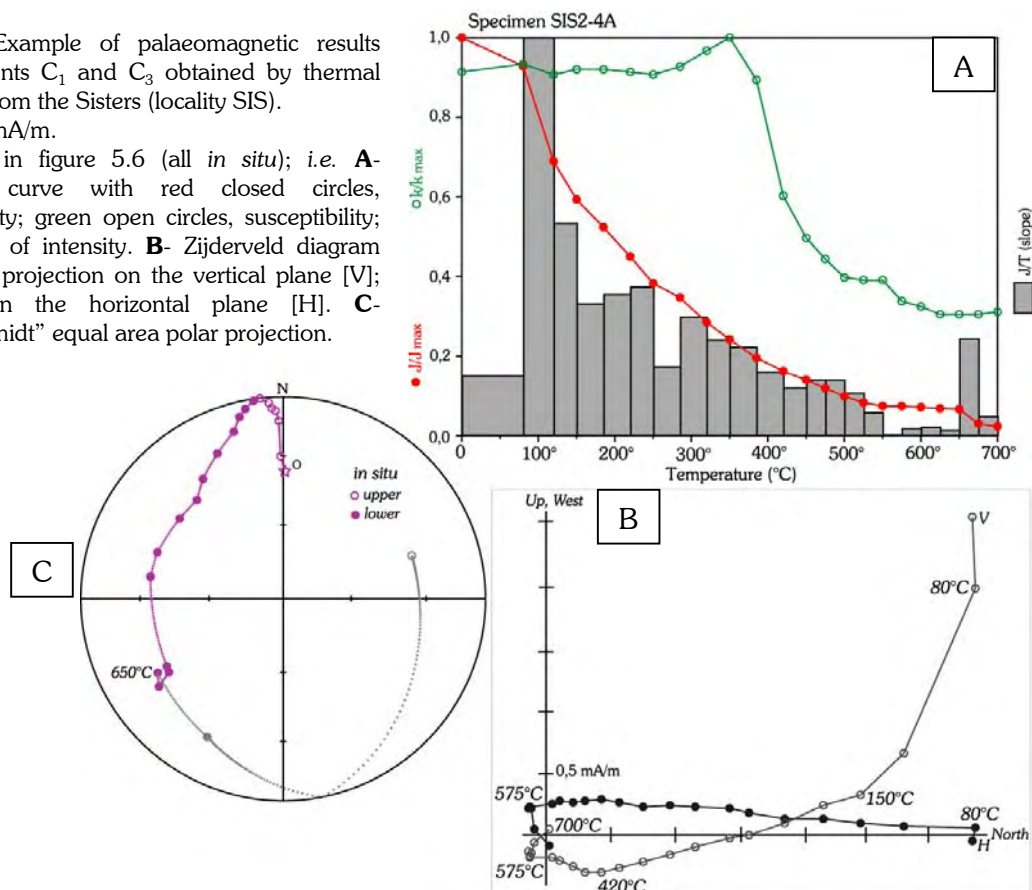
Figures 5.48: Example of palaeomagnetic results showing only component C_1 obtained by thermal demagnetisation from the Sisters (locality SIS). $NRM@RT=5,32$ mA/m.

Same legend as in figure 5.6 (all *in situ*); i.e. **A**- Demagnetisation curve with red closed circles, normalised intensity; green open circles, susceptibility; grey boxes, slope of intensity. **B**- Zijderveld diagram with open circles, projection on the vertical plane [V]; closed circles, on the horizontal plane [H]. **C**- Stereogram; “Schmidt” equal area polar projection.



Figures 5.49: Example of palaeomagnetic results showing components C_1 and C_3 obtained by thermal demagnetisation from the Sisters (locality SIS). $NRM@RT=4,18$ mA/m.

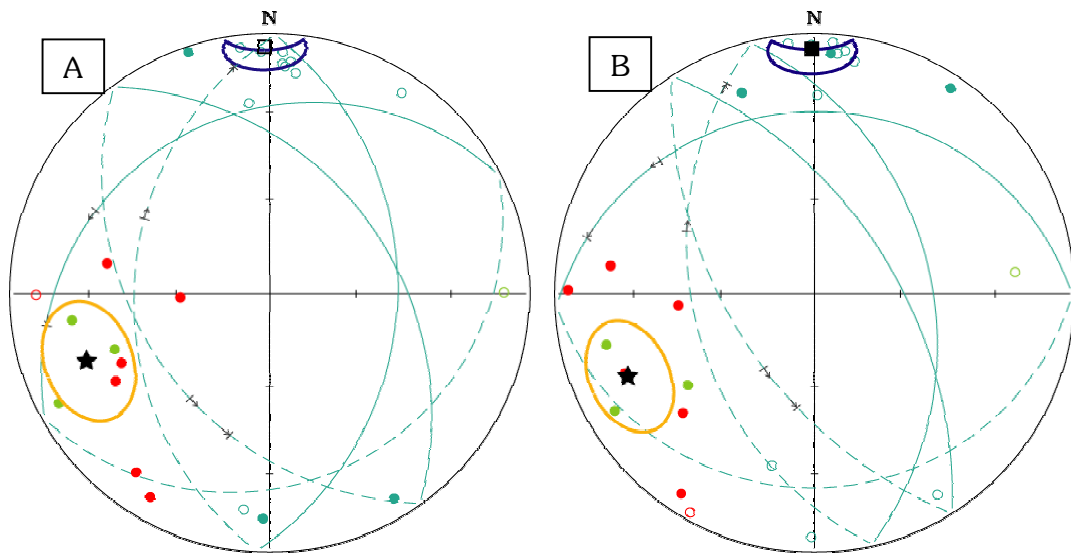
Same legend as in figure 5.6 (all *in situ*); i.e. **A**- Demagnetisation curve with red closed circles, normalised intensity; green open circles, susceptibility; grey boxes, slope of intensity. **B**- Zijderveld diagram with open circles, projection on the vertical plane [V]; closed circles, on the horizontal plane [H]. **C**- Stereogram; “Schmidt” equal area polar projection.



- Interpretation

The apparent duality in orientation for the mid components C_1 and C_2 (figure 5.50) is not understood yet. The segment between 450° and 550°C probably represents an overlap in demagnetisation spectra. It is possible then that two generations of magnetite are present in these rhyolites.

When only the N-S direction carried by magnetite is considered (C_1), the overall mean direction calculated from single specimen components (shown in turquoise in figures 5.50; table 12) is D.359°/I.-04° ($\alpha_{95}=9,6$ / $\kappa=15,8$) *in situ*, and becomes D.000°/I.+05° ($\alpha_{95}=10,3$ / $\kappa=13,9$) after bedding correction. A slight variation in bedding orientation between the two hills influences the statistical parameters. That is the reason why the classic fold test (McElhinny, 1964) is positive at the 36,0% confidence level only and favours a post-folding acquisition of magnetisation (κ -ratio=0,9). The palaeopole corresponding to this very shallow direction however does not resemble to any expected for this age or any younger ages (figure 5.51; table 13). In addition, it appears unlikely that a post-Devonian orientation of magnetisation be so shallow. This direction could thus represent a late Early to early Middle Devonian remagnetisation but seems to be then in contradiction with the pole obtained from the Mount Daubeny Formation (locality DAU), which might be in agreement with other Early Devonian poles whereas this one is not. From specimen SIS2-3A (figure 5.48) and SIS2-4A (figure 5.49), it seems however that the direction of magnetisation might move from the position of C_1 to the position of C_3 . A mixture of several components, demagnetised simultaneously therefore, could be an explanation for such a striking result. Nevertheless, this link between C_1 and C_3 is not systematic at all. In particular, directions obtained from great circles (figures 5.50) show a link with other directions of magnetisation that cannot be defined with the present data. However, the existence of alteration and lighting effects, determined from rock magnetic measurements, can be considered as a probable cause for this multiplicity of orientations.



Figures 5.50: Components obtained from the rhyolites of the Sisters intruding the Mt Daubeny Formation (locality SIS). **A-** *in situ* and **B-** after bedding correction.

Blue circles (and curved lines) are single specimen component C_1 (lines are components obtained by great circle analysis) oriented ~N-S; **green**, components C_2 oriented ~E-W; and **red**, components C_3 . The overall N-S mean direction (**square**) is shown with its 95% confidence cones (α_{95} ; **dark blue**) for N-S components C_1 . The overall E-W mean direction (**star**) is shown with its α_{95} (**orange**) for E-W components C_2 and components C_3 .

Open symbols are negative inclination values (upper hemisphere); **closed** symbols, positive inclination values (lower hemisphere). Schmidt equal area polar projection.

Table 12: Overall mean directions for the locality SIS obtained from single specimen orientations

Name	N	R	D.InS	I.InS	α_{95}	κ	R	D.Bed	I.Bed	α_{95}	κ
<i>Mean direction for components M directed North-South:</i>											
Sis-NS	16	15,1	358,9	-04,1	9,6	15,8	15,0	359,5	+05,1	10,3	13,9
<i>Mean direction for components H & M directed East-West:</i>											
Sis-EW	11	9,8	249,5	+24,2	16,6	8,5	10,0	245,3	+20,9	15,4	9,8

N: number of samples; **B:** number of sites; α_{95} : cone calculated at the 95% confidence level; κ : precision parameter; **R:** resultant vector; **D.InS/I.InS:** declination/inclination *in situ* (geographic coordinates); **D.Bed/I.Bed:** declination/inclination after bedding correction.

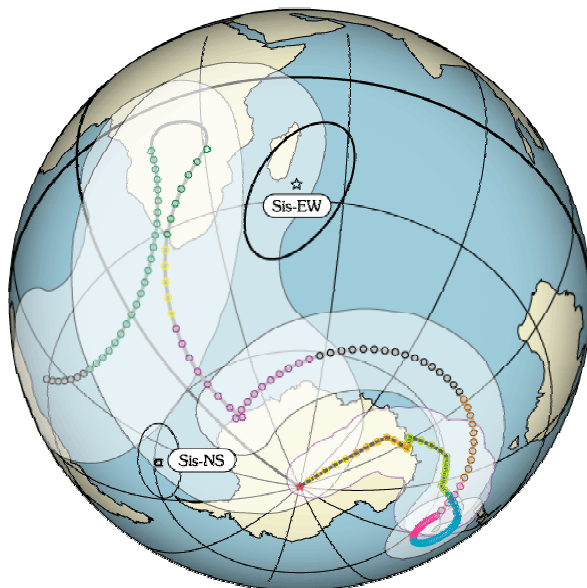
Component C_3 is apparent only in seven specimens (shown in red in figures 5.50) and shows a great scattering. In four cases (shown in green in figures 5.50), magnetite seems to carry the same ~E-W orientation (C_2). The overall mean direction calculated from these single specimen components (figures 5.50; table 12) is D.250°/I.+24° ($\alpha_{95}=16,6$ / $\kappa=8,5$) *in situ*, and becomes D.245°/I.+21° ($\alpha_{95}=15,4$ / $\kappa=9,8$) after bedding correction. The κ parameter seems to increase a little bit after bedding correction (κ -ratio=1,1) but it cannot be considered as a significant improvement as the classic fold test is positive only at the 62,0% confidence level. The palaeopole (figure 5.51; table 13) corresponding to this direction after bedding correction however, would be better consistent with the X-type APW path proposed for Gondwana by Bachtadse & Briden (1991) for instance, but difficult to link to the Y-type APW path of Schmidt *et al.* (1990).

In conclusion, it appears from these data, that several directions of magnetisation with low inclination values are recorded in these Early – Middle Devonian magmatic rocks, but too few data are as yet available to draw any conclusions. More work on these volcanics is then needed to define these magnetisations.

Table 13: Corresponding palaeopoles for the Sisters

Name	N	<u>Australian coord.</u>		<u>African coord.</u>		dp	dm
		PLong.	Plat.	PLong.	Plat.		
<i>For the North-South component (C_1) in situ:</i>							
Sis-NS	16	320,4	-61,1	343,3	-28,6	4,8	9,6
<i>For the East-West component (C_2 & C_3) after bedding correction:</i>							
Sis-EW	11	049,4	-26,6	026,4	+23,3	8,5	16,2

N: number of samples; **B:** number of sites; **PLong./Plat.:** palaeopole longitude/latitude in Australian and in African coordinates. **dp/dm** : semi-axis of the ellipse of confidence.

**Figure 5.51:** Alternate polarities for the corresponding palaeopoles in Australian coordinates. The possible APW path for Australia-Gondwana from the present-day to 570 Ma based on Small Circle Fit is shown for comparison purposes.

Same legend as in figure 2.19-A, Chapter 2 (§.2.7).

Sis-EW is the pole corresponding to components H & M~E-W after bedding correction; **Sis-NS**, corresponding to M~N-S *in situ*.

5.9. Conclusions about the Broken Hill area

5.9.1. Palaeomagnetic results

Palaeomagnetic studies in the Broken Hill area are difficult because rocks are usually poorly exposed, and because the history of magnetisation appears to be complex.

A majority of localities shows an important weathering effect, which totally overprints previous magnetic signals in some cases such as for localities ARR and FUN. In localities KAN and GUM the magnetic signal consists of an unstable magnetisation and/or a mixture of several components simultaneously demagnetised.

At locality CUP however, it seems that a primary magnetisation can be isolated, confirmed by a positive unconformity test. The pole obtained is consistent with many other poles for Gondwana, and this implies that locality CUP has not undergone any movement or rotation over palaeomagnetic resolution since the Late Cambrian. Locality DAU does not really yield significant field tests, but the fold test, the contact test and conglomerate test all indicate a pre-folding age of magnetisation and are good arguments to favour a primary origin. If the locality CUP is stable since the Late Cambrian, it is possible that the pole obtained from locality DAU is also representative of cratonic Gondwana. The Mount Daubeny Formation however fills up a pull-apart basin, which may have tectonically behaved differently than the surrounding terranes. This could be confirmed by a more complete study of the rhyolitic to dacitic volcanics, which intrude the Mount Daubeny Formation such as the Sisters (locality SIS). The results obtained here are statistically not reliable but the pole Sis-EW could be consistent with the hypothesis that the pull-apart basin moved independently from the craton of Gondwana. These rocks are then a key locality for further studies.

The locality CHU seems to indicate that the southern part of the Broken Hill area, and subsequently the Delamerian Orogen, is not stable until the Devonian or Carboniferous. Indeed the directions shown by the components C_H are in any cases difficult to explain without invoking a remagnetisation acquired prior to a $\sim 110\text{--}140^\circ$ clockwise rotation (or $\sim 220\text{--}250^\circ$ anticlockwise), which looks similar to the $\sim 120^\circ$ change in cleavage and fault trend direction between the northern and southern part of the Broken Hill area. Unfortunately, this is the only results from this part and, according to the Van der Voo's criteria, it cannot be considered statistically reliable.

5.9.2. Regional magnetic fabric

It is clear that the AMS is a good tool to evaluate the internal strain in rocks, and to give indications about tectonic history in a locality. On a gross scale, the magnetic fabric can help understanding the regional tectonic evolution.

Magnetic fabrics in the Broken Hill area (figure 5.52) are generally very weakly developed. However, magnetic lineation tends to parallel the general fault trend at Mount Arrowsmith (ARO & ARR; north-west of the map), in the Cupala Creek Formation (CUP) and perhaps in the Mt Daubeny Formation of the Churinga Property (CHU).

In the Funeral Creek Formation (FUN) as well as rocks from the Gum Creek near Bilpa (GUM; to the south of the map), it seems that two fabrics are superimposed. In the Gum Creek, the first lineation tends to parallel the NW-SE fault trend of the North of the map, and the second fabric, the NE-SW fault trend of the South of the map. At Funeral Creek, the first fabric is rather parallel to the Koonenberry Fault, whereas the second seems to be perpendicular to it. This perpendicular fabric can be found also in the Kandie Tank Limestone, which lies just west of the Koonenberry Fault as well. This fabric is difficult to explain, but it is probably linked to a series of faults, which resemble to Riedel faults developed along the Koonenberry Fault.

Finally, it has been suggested that fabrics in the vicinity of the Mount Daubeny (DAU and SIS) forming an angle of about 30° with the Koonenberry Fault, can be coherent with a dextral strike-slip movement.

AMS results indicate then that NE-SW compression with strike-slip movement on the Koonenberry Fault occurred, but other directions of strain have also affected these rocks. This is in good agreement with geological observations (Mills, *personal communications*).

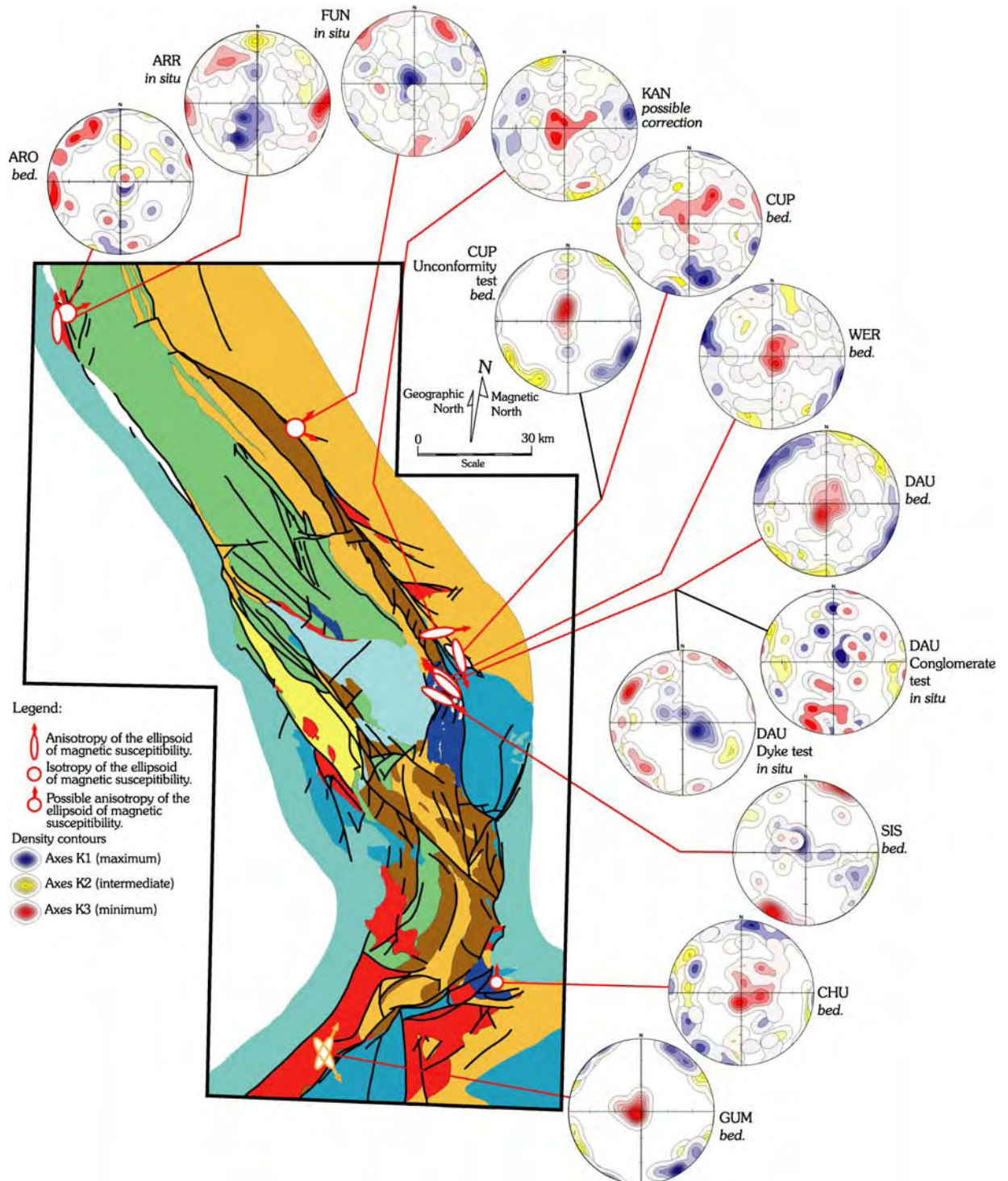


Figure 5.52: Regional magnetic fabric of the Broken Hill area.

Density contours clearly highlights that magnetic lineation are controlled by fault orientations. Small ellipses indicate the directions of elongation of the ellipsoids of magnetic susceptibility deduced from density contours (Gaussian model, $K=100$). Same simplified geological map as per figure 5.2.

Summary of chapter 5

The Broken Hill area is situated in far western New South Wales, and ten localities were there targeted. Nevertheless, only a few are revealed suitable to yield useful palaeomagnetic indications.

Late Cambrian to Early Ordovician rocks at Mt Arrowsmith (localities ARR & ARO) and from the Funeral Creek Limestone (FUN) reflect the particularly strong weathering affecting Australia. The directions of magnetisation are that of the present-day field, but with both the normal and reverse polarity. Intermediate directions of magnetisation are also common explaining why components are often deviated from mean directions. It results in a great scattering in directions of magnetisation. The results obtained from the Late Cambrian Kandie Tank Limestone (KAN) or the Gum Creek Sandstones near Bilpa (GUM) illustrate also this difficulty in determining correct site means directions although components appear to be relatively well defined.

The Late Cambrian red sandstones from the Cupala Creek Formation however show a coherent signal despite a complex magnetisation. After removal of a component corresponding to the present-day field, a mid temperature component involving a reversal is interpreted as an Early Palaeozoic chemical remagnetisation, and a high temperature component is regarded as primary since it is confirmed by a positive unconformity test. Moreover, the corresponding palaeopole matches a large number of Late Cambrian poles published for Gondwana and suggests therefore that locality CUP underwent no palaeomagnetically detectable translation or rotation relative to the craton since the Late Cambrian. The Early Devonian (Gedinnian) sandstones from the Mt Daubeny Formation (DAU) show also two main directions of magnetisation. One is interpreted as post-folding overprint, apparently Jurassic in age, associated to fluid migration probably caused by magmatic event leading to dyke intrusions. The second is believed to be pre-folding and consequently probably primary. In spite of the little change in bedding orientation, the classic fold test (McElhinny, 1964) is positive at the 77% confidence level. In addition, the conglomerate test is considered positive for components H since uniformity is accepted at the 95% confidence level, and the contact test shows a statistically distinct directions of magnetisation in the dykes and in the sandstones, so that it may be considered to some positive. The supposed equivalent rocks from the Mt Daubeny Formation at the Churinga property (CHU) reveal an unclear component M, interpreted as a possible mixture between a Jurassic overprint and an unknown direction of magnetisation. Component H is more consistent and suggests a 129° clockwise rotation of the locality in good agreement with the regional 120° change in fault and cleavage trend. Results from the Early to Middle Devonian rhyolitic intrusions (locality SIS) are probably key to confirm or invalidate most of the hypothesis put forward in this study. So far however, the mean direction Sis-EW seems to be based on scattered end points consistent with the Early – Middle segment of the X-type APW path proposed by Bachtadse & Briden (1991), whereas Sis-NS is not clearly understood but could be simply an intermediate direction of magnetisation.

Chapter 6

Palaeomagnetic results from the Mount Bowen area

6.1. Presentation of the Mount Bowen area

6.1.1. Sampling coverage

The Mount Bowen area is located at the boundary between the Central and the Western Lachlan Orogen (figure 6.1). Every localities (table 14) are considered Devonian in age (figure 6.2), although the Ural Volcanics, in the South of the map, are in fact latest Silurian to earliest Devonian. The Geological Survey of New South Wales currently carries out a detailed mapping of these volcanics, which are exposed near Mount Bowen, name chosen herein for this area.

Only the rocks sampled in the syncline at the Bulgoo Property (locality BUL) correspond actually to rocks from the Western Belt of the Lachlan Orogen.

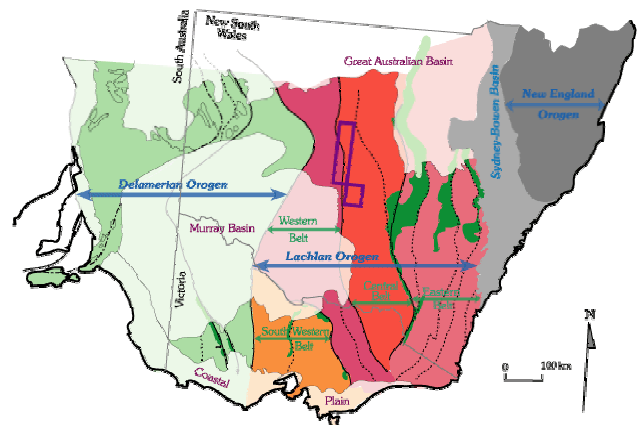


Figure 6.1: Inset recalls the position the Mount Bowen area in the Southern Tasmanides as presented on the map of figure 4.7 (Chapter 4). The corresponding simplified geological map is shown in figure 6.2.

6.1.2 – Geological features

The simplified map shows in particular a North-South fault and thrust trend, along which granites and volcanics were emplaced from the Silurian to Early Devonian (figure 6.2). The NW direction of the fold axis at the locality BUL, and other structural features such as the ENE lineament West of the Mount Hope Township suggest that transverse structures probably exist as well.

Hence, it makes terrane rotation not impossible in this area.

Table 14: List of localities in the Mount Bowen area

Mnemonics	Names coming from	Location (Long. /lat.)
BOW	Mount Bowen	146,2155 / -33,3657
BUL	Bulgoo property	145,5473 / -31,8684
HOP	Mount Hope	145,8554 / -32,8475
MER	Merrie Abba property	146,0951 / -33,3649
NOM	Nombiginni Quarry	145,9073 / -32,4713
SHE	Shepherds Hill Quarry	146,2469 / -33,0470
TAR	Tarilta property (quarry)	146,2432 / -33,4030

Mnemonics refer to table 1, Chapter 4; §.4.3.

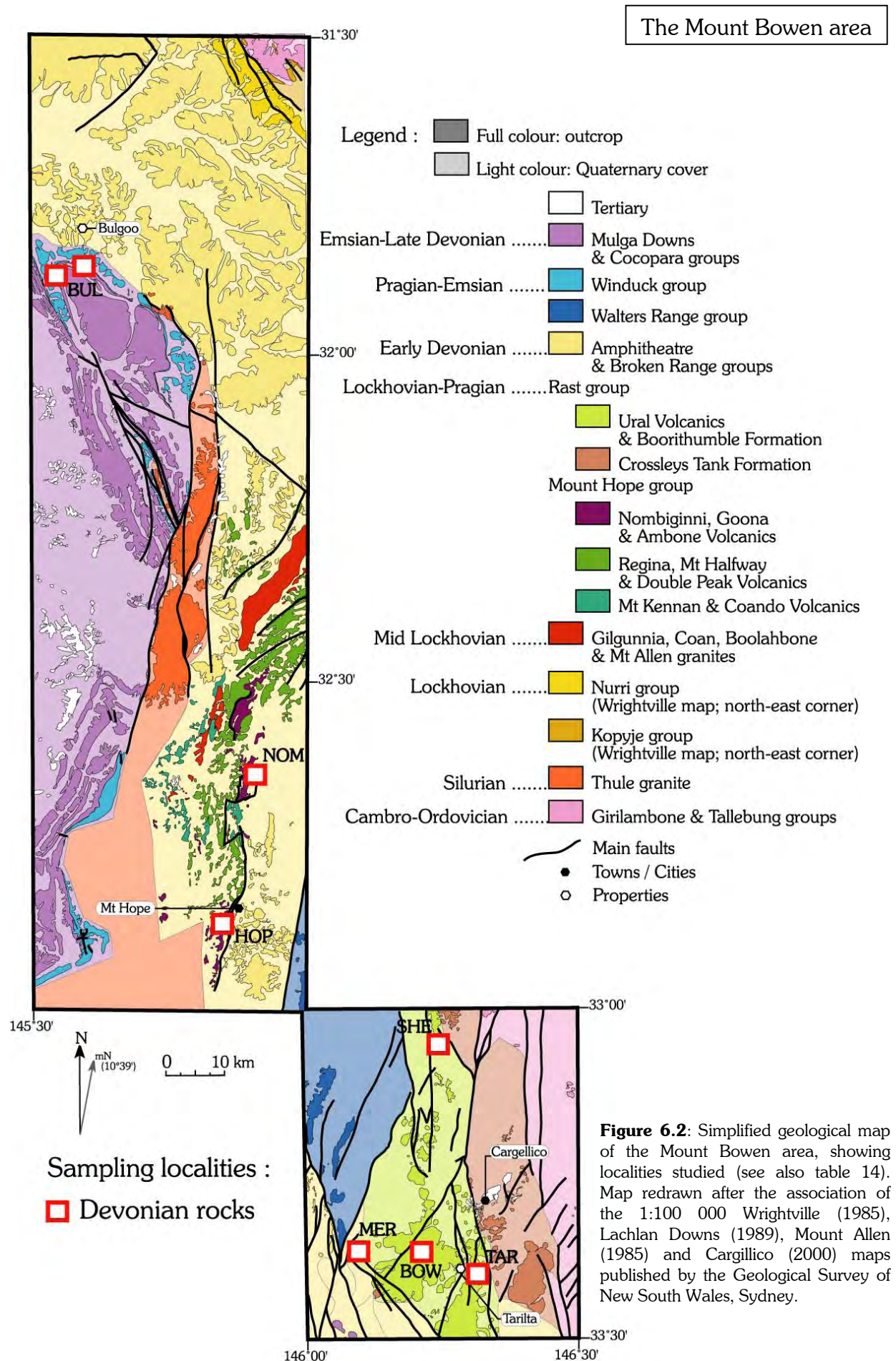


Figure 6.2: Simplified geological map of the Mount Bowen area, showing localities studied (see also table 14). Map redrawn after the association of the 1:100 000 Wrightville (1985), Lachlan Downs (1989), Mount Allen (1985) and Cargillico (2000) maps published by the Geological Survey of New South Wales, Sydney.

Localities sampled are at most gently folded and not affected by metamorphism. There is a regionally pervasive to moderately spaced steep to vertical cleavage, associated with shear fabric. The degree of strain seems to be domainal. These are thought to be related to a NE-SW directed extension in the Mid Devonian time, which caused opening of the Rast Basin (Ural Volcanics) and the Mount Hope Basin. It is followed by a later compression and inversion of the basin, thought to be Tabberaberan in age. Shear-faults accompanied both events, according to Glen *et al.* (1996), Scheibner (1998), and also Glen *et al.* (1992-a).

6.2. The Gundaroo sandstones from the Bulgoo Property (BUL)

6.2.1. Presentation

Sampling has been carried out in the Unit A2 of the Gundaroo sandstones, where they are fine-grained. These pink quartz-rich rocks belong to the Winduck Group and are Late Pragian in age (Glen, 1986; Glen, *personal communication*, 2001). Seven sites (39 cores) have been drilled on both limbs of a syncline. This locality is in the vicinity of the hinge of the fold, but where samples have been collected, this last can be considered as cylindrical, with shallow plunging axis.

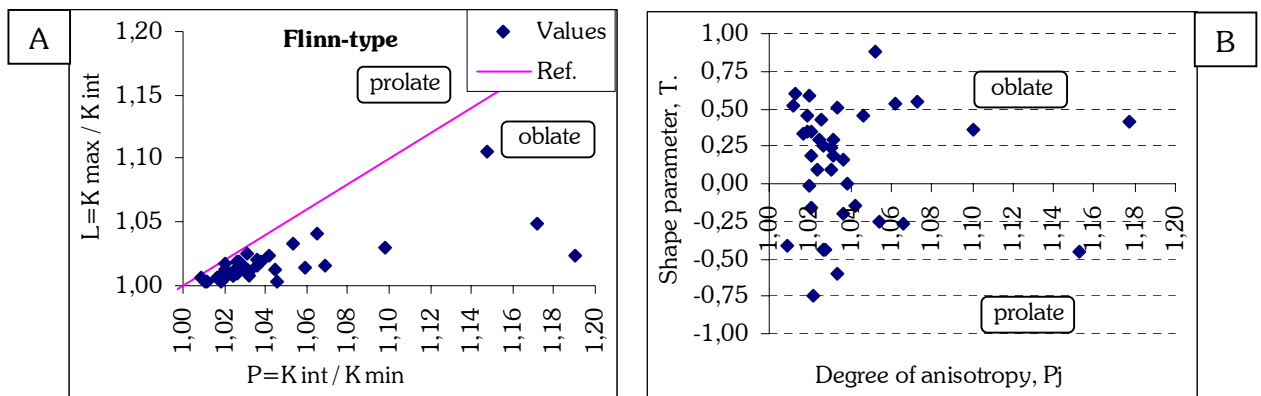
This syncline has a surprising North West trend, which contrasts with the rather N-S regional trend. On closer examination to the geological map (Wrightville 1:100 000 map sheet; Geological Survey of New South Wales), secondary folds with E-W axes affect this syncline.

6.2.2. Anisotropy of magnetic susceptibility (AMS)

Measurements of the AMS in these silicic sandstones reveal that the degree of anisotropy is weak ($P_j = 1,04 \pm 0,04$; figure 6.3-B) but relatively marked. The internal strain however can be considered as negligible. Both the Flinn-type and the $\{T\}$ vs. $\{P_j\}$ diagrams show that the ellipsoid of magnetic susceptibility tends to be oblate in shape (figures 6.3).

The Königsberger ratio is low in six sites ($Q_K @ RT = 0,98 \pm 5,50$), but high in site BUL-07 where $Q_K @ RT = 27,66$ in average and reaches 95,18 for the last core BUL7-6. This last site therefore might have been struck by lightning, but the presence of patch of oxidised material on cores probably reflects alteration, which might be also the explanation of such values of Q_K .

The directions of the principal axes of magnetic susceptibility show that the magnetic fabric has been acquired prior to folding (figures 6.4). Density contours highlight that K_{min} form two groups *in situ*, which are brought close to the vertical after bedding correction. This is representative of a sedimentary magnetic fabric. The magnetic lineation (K_{max}) however is better grouped along an E-W direction, which is not aligned with the axis of the Bulgoo syncline, but with secondary fold axes, suggesting that a latter N-S compression is recorded.



Figures 6.3: **A-** Flinn-type diagram (Flinn, 1962, 1965-a, 1965-b) and **B-** $\{T\}$ versus $\{P_j\}$ diagram (Jelinek, 1981; Hrouda, 1982) for the Late Pragian Gundaroo sandstones of the Bulgoo Property (locality BUL).

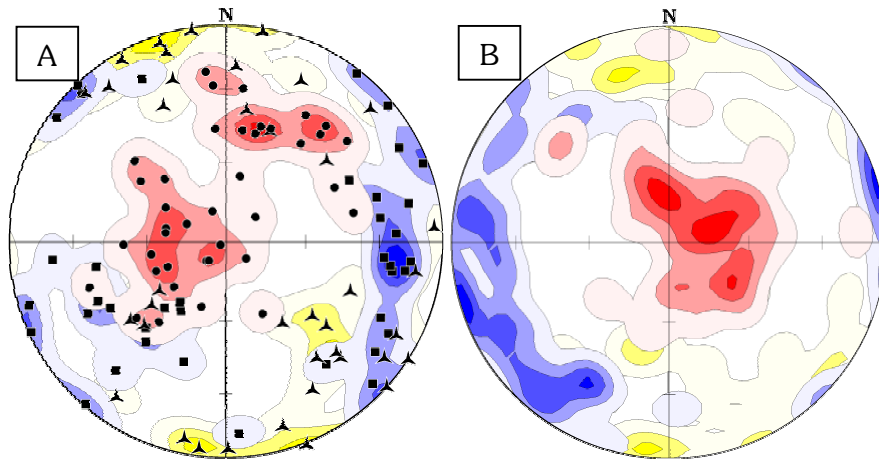


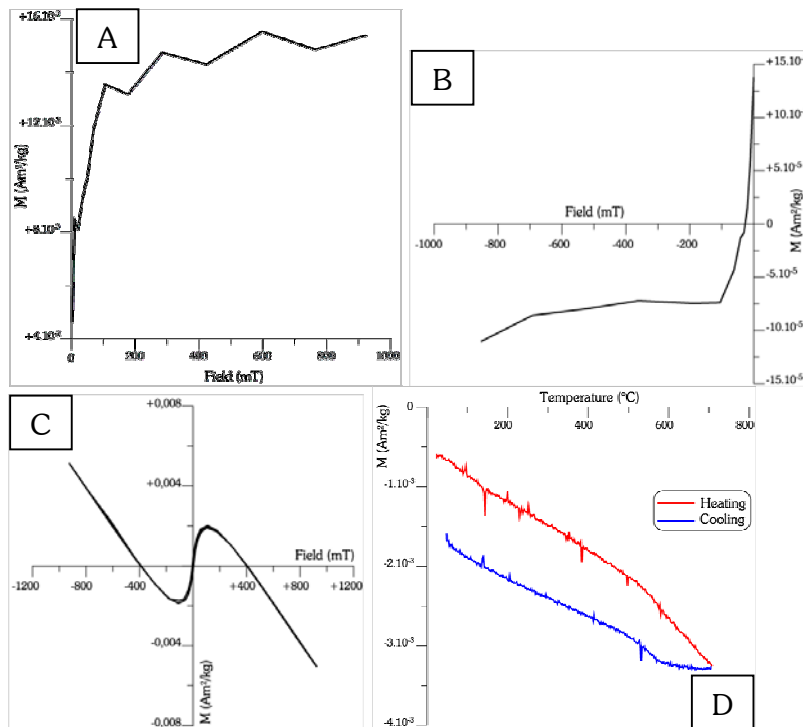
Figure 6.4: Orientations of the principal axes of magnetic susceptibility for the Gundaroo sandstones of the Bulgoo Property, locality BUL.

A- *in situ*, and **B-** after bedding correction.

Same legend as in figure 5.4 (Chapter 5; §.5.2.2); i.e. Kmax, squares (blue); Kint, triangles (yellow); Kmin, dots (red).

6.2.3. Rock magnetism

Two kinds of magnetic properties are observed in this locality, according to the presence or not of oxidised minerals.



Figures 6.5: First example of rock magnetic measurements from the Gundaroo sandstones at the Bulgoo Property (locality BUL): specimen BUL3-3.

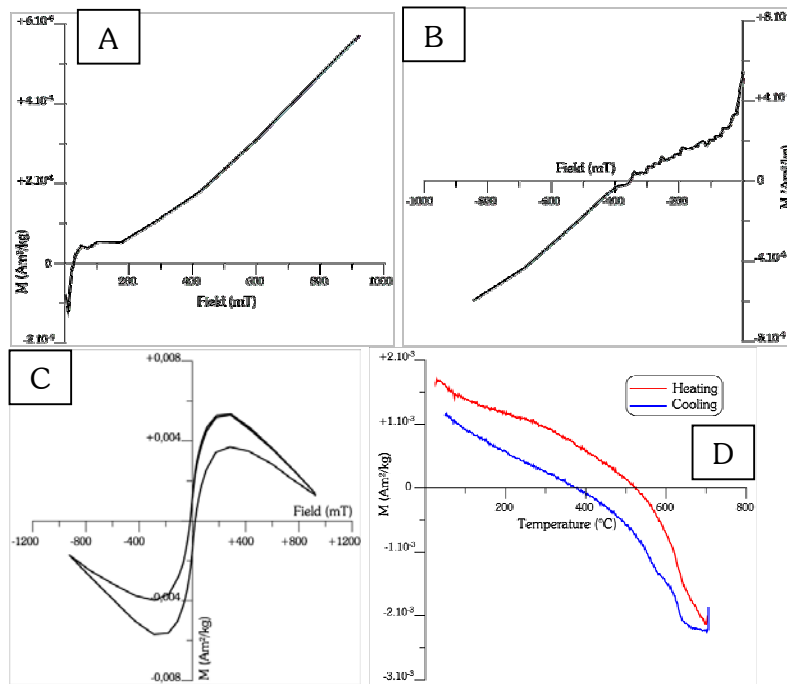
A- IRM curve; **B-** Back field curve (coercivity); **C-** Hysteresis loop; and **D-** IST curve, in red while heating and in blue while cooling ($B=535$ mT).

$H_C=3,67$ mT; $H_{CR}=26,54$ mT.

$M_S=1,9 \cdot 10^{-3}$ Am²/kg; $M_{RS}=1,4 \cdot 10^{-4}$ Am²/kg.

The slope of the hysteresis loop (figure 6.5-C) and the negative values at 700°C of the IST curve (figure 6.5-D) are representative of the strong diamagnetic contribution in this first example of magnetic behaviour. The constant decay of the IST curve up to ~550°C indicates also the presence of paramagnetic minerals, but the inflexion by 550°-580°C and the rapid saturation observed in the IRM and back field curves (figures 6.5-A & B) witnesses that magnetite is the main magnetic carrier in this sample.

Diamagnetic contribution is also strong in the second example. The IRM and back field curves however (figures 6.6-A & B) show clearly in this case the existence of both low and high coercivity minerals, also expressed by the wasp-wasted shape of the hysteresis loop (figure 6.6-C). The low coercivity mineral is identified as magnetite like in the first example. The high coercivity mineral is related to the patch of oxidation macroscopically observed, and is made up of haematite as the Curie temperature reaches 680°C (figure 6.6-D).



Figures 6.6: Second example of rock magnetic measurements from the Gundaroo sandstones at the Bulgoo Property (locality BUL): specimen BUL7-1.

A- IRM curve; **B-** Back field curve (coercivity); **C-** Hysteresis loop; and **D-** IST curve, in red while heating and in blue while cooling ($B=535$ mT).

$H_C=17,12$ mT; $H_{CR}=353,95$ mT.

$M_S=3,5 \cdot 10^{-3}$ Am²/kg; $M_{RS}=6,6 \cdot 10^{-4}$ Am²/kg.

The presence of haematite is spatially limited and appears to be aligned to a second order ~E-W fault cross-cutting one limb of the syncline. It is likely that this oxidation event is linked to fluid migration along this discontinuity.

6.2.4. Palaeomagnetic results

- Demagnetisation

Thermal demagnetisation yields two kinds of behaviour as well.

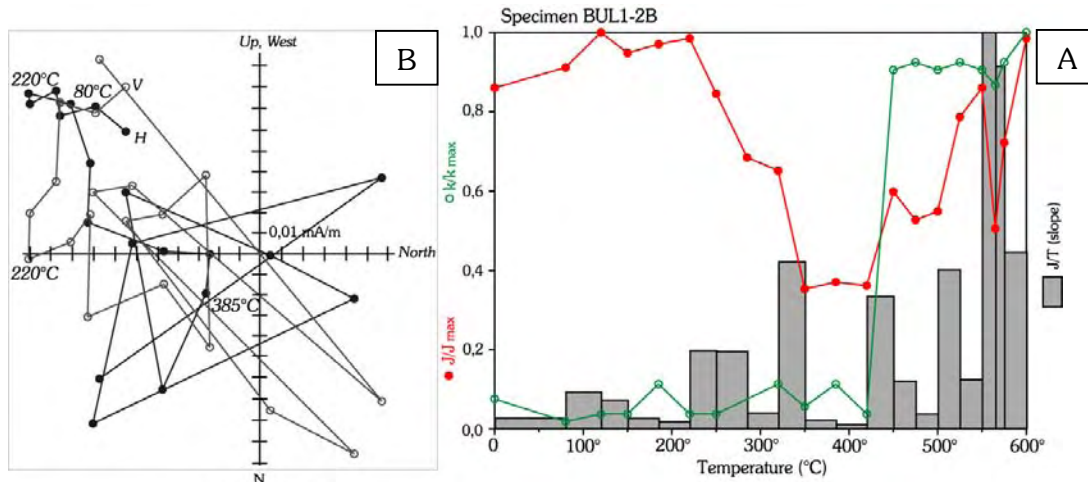
In samples from four sites (out of 7), a component C_1 can sometimes be identified after removal of a viscous or drilling-induced magnetisation, although the magnetic signal is noisy. C_1 seems to persist up to 220°C. From 220° to 350°C, about 60% of the remanence is removed with a component C_2 , which orientation can only be roughly determined when present. As a peak in the first derivative (grey boxes of figure 6.7-A) occurs around 320°C, it is possible that some pyrrhotite is also present in these rocks and carries C_2 . Above this temperature, the susceptibility increases drastically and the NRM is lost.

In samples from the three other sites (sites Bul-02 & Bul-03 on one limb and Bul-07 on the other limb), the viscous or drilling-induced magnetisation is easily removed and a component C_3 is clearly visible from 80° to 575°C (figures 6.8), close to the Curie temperature of magnetite. A slight inflexion in the intensity curve and a peak in the corresponding first derivative are also present by 320°C (figure 6.8-A), and may be explained by the existence of pyrrhotite. However, if pyrrhotite is really present, it carries here the same component C_3 as magnetite. Finally, a last component C_4 is carried by haematite resulting from oxidation, and is demagnetised from 600° to 680°C.

- Interpretation

The presence of pyrrhotite can be responsible for the noisy magnetic behaviour of some samples as magnetisation in iron-sulphides is complex. It can be due also to unstable grains of magnetite as the H_{CR}/H_C ratio ($=7,22$ for the example BUL3-3) obtained by rock magnetic measurements plot in the multi-domain range. However, the orientation of C_1 corresponds to the present-day field direction, and is D.000°/I.-57° ($\alpha_{95}=5,9^\circ$ / $\kappa=50,6$; table 15).

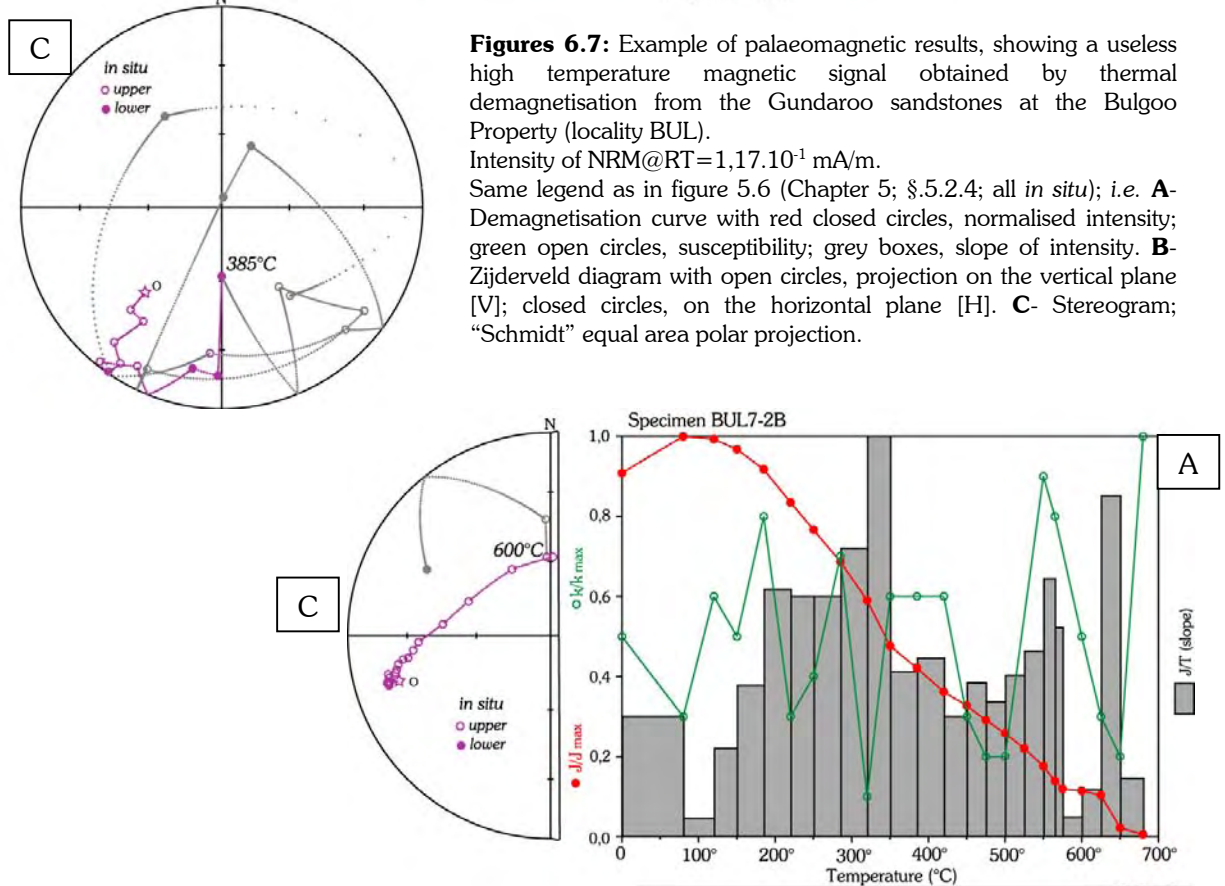
Component C_2 , which appears to be mainly carried by pyrrhotite, is not well determined.



Figures 6.7: Example of palaeomagnetic results, showing a useless high temperature magnetic signal obtained by thermal demagnetisation from the Gundaroo sandstones at the Bulgoo Property (locality BUL).

Intensity of NRM@RT = $1,17 \cdot 10^{-1}$ mA/m.

Same legend as in figure 5.6 (Chapter 5; §.5.2.4; all *in situ*); i.e. **A**- Demagnetisation curve with red closed circles, normalised intensity; green open circles, susceptibility; grey boxes, slope of intensity. **B**- Zijderveld diagram with open circles, projection on the vertical plane [V]; closed circles, on the horizontal plane [H]. **C**- Stereogram; “Schmidt” equal area polar projection.



Figures 6.8: Example of palaeomagnetic results, showing an interesting high temperature magnetic signal obtained by thermal demagnetisation from the Gundaroo sandstones at the Bulgoo Property (locality BUL).

NRM@RT = $1,17 \cdot 10^{-1}$ mA/m.

Same legend as in figure 5.6 (Chapter 5; §.5.2.4; all *in situ*); i.e. **A**- Demagnetisation curve with red closed circles, normalised intensity; green open circles, susceptibility; grey boxes, slope of intensity. **B**- Zijderveld diagram with open circles, projection on the vertical plane [V]; closed circles, on the horizontal plane [H]. **C**- Stereogram; “Schmidt” equal area polar projection.

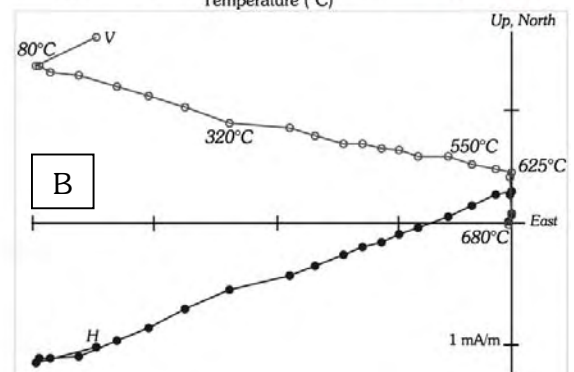
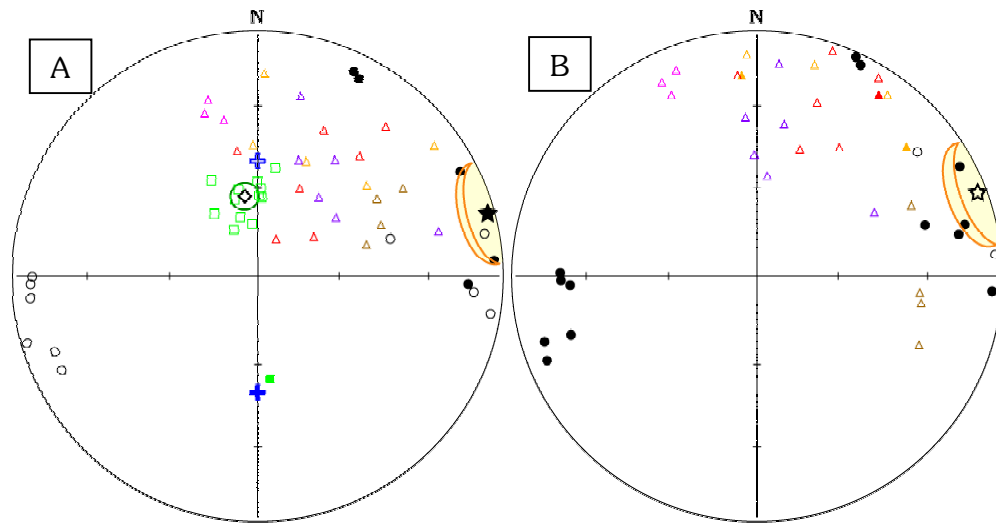


Table 15: Overall mean directions for the locality BUL obtained from single specimen orientations

Name	N	R	D.InS	I.InS	α_{95}	κ	R	D.Bed	I.Bed	α_{95}	κ
<i>Mean direction for components C_1:</i>											
Bul- C_1	13	12,8	359,8	-54,4	5,9	50,6	12,7	326,2	-39,1	6,5	41,1
<i>Mean direction for components C_2:</i>											
Bul- C_2	25	22,4	029,5	-43,9	10,0	9,4	20,0	021,8	-26,2	14,9	4,8
<i>Mean direction for components C_3:</i>											
Bul- C_3	15	13,6	074,6	+01,7	12,7	10,0	13,5	069,3	-02,8	13,2	9,3
<i>Mean direction for components C_4:</i>											
Bul- C_4	13	12,9	350,9	-62,5	4,6	80,5	12,2	339,9	-35,1	10,7	16,0

N: number of samples; **B:** number of sites; α_{95} : cone calculated at the 95% confidence level; κ : precision parameter; **R:** resultant vector; **D.InS/I.InS:** declination/inclination *in situ* (geographic coordinates); **D.Bed/I.Bed:** declination/inclination after bedding correction.

**Figures 6.9:** Orientation of components obtained from the Gundaroo sandstones of the Bulgoo Property (locality BUL). **A-** *in situ* and **B-** after bedding correction.

Coloured triangles are single components C_2 (red: site Bul-01; orange: site Bul-02; brown: Bul-03; pink: Bul-04; violet: Bul-07); **black circles** are single components C_3 with their corresponding overall mean direction (**star**) and associated **orange** confidence cone (α_{95}); **green squares** are single specimen components C_4 shown *in situ* only with their overall mean direction (**diamond**) and **dark green** α_{95} . **Blue crosses** show the present-day field direction.

Open symbols are negative inclination values (upper hemisphere); **closed** symbols, positive inclination values (lower hemisphere). Schmidt equal area polar projection.

The directions of magnetisation of component C_2 are very scattered (triangles in figures 6.9; table 15) and the overall mean direction has no great meaning, but they resemble to a post-folding remagnetisation with a κ -ratio of 0,5 only (Positive fold test obtained at the 1,0% confidence level). However, it is believed that C_2 simply correspond to intermediate directions between the present-day field (C_1) and component C_3 (figures 6.9; table 15).

Component C_3 is carried by magnetite and are usually well defined on Zijdeveld diagrams (figures 6.8) but their directions are also scattered (black circles in figures 6.9; table 15). The overall mean direction calculated from single specimen components is D.075°/I.+02° (α_{95} =12,7° / κ =10,0) *in situ* and D.069°/I.-03° (α_{95} =13,2° / κ =9,3) after bedding correction. These directions, both *in situ* and after bedding correction, are very shallow in inclination and do not match those expected for Gondwana for Late Pragian or younger ages (see also table 16; figure 6.10). It has been mentioned above that site Bul-07 can be affected by lightning strike, but these directions are also seen in sites Bul-02 and Bul-03, which are situated on the other flank of the syncline. It is therefore hardly conceivable that this can be the cause of such shallow E-W orientation. The classic fold test (McElhinny, 1964) yields a κ -ratio below one (=0,9) but this is no significant worsening as it is positive at the 42,0% confidence level. These directions of magnetisation could thus be Mid Palaeozoic in age. Terrane rotation or perhaps shallowing effects

might be therefore an explanation. Nevertheless, this result is statistically much too poor to be reliable. However, the corresponding palaeopoles (from results obtained *in situ* and after bedding correction) are shown for indication (figure 6.10; table 16).

Finally, component C_4 (red squares in figure 6.9-A; table 15) is carried by haematite and the overall mean direction (from single specimens) is $D.351^\circ/I.-63^\circ$ ($\alpha_{95}=4,6^\circ / \kappa=80,5$) *in situ* and $D.340^\circ/I.-35^\circ$ ($\alpha_{95}=10,7^\circ / \kappa=16,0$) after bedding correction. This is clearly a post-folding remagnetisation as the classic fold test is significantly negative (fold test positive below the 0,1% confidence level; κ -ratio=0,2). Besides, one opposite polarity allows the reversal test to be positive and classified *C in situ*. As already noticed, haematite probably results from fluid migration, which triggered oxidation along a fault. The overall mean direction obtained is very close to a mid Cainozoic (~ 30 -35 Ma) direction of magnetisation. It will be shown in Chapter 7 (in the Molong area) that directions corresponding to these ages are common. However, in this case, this direction cannot be clearly distinguished from the present-day geomagnetic dipole field either.

Table 16: Corresponding palaeopoles for the Gundaroo sandstones of the Bulgoo Property (locality BUL)

Name	B	N	<u>Australian coord.</u>		<u>African coord.</u>		dp	dm
			PLong.	Plat.	PLong.	Plat.		
For component C_3 in situ:								
Bul-InS	~	15	226,5	+12,6	205,7	-37,6	6,4	12,7
For component C_3 after bedding correction:								
Bul-Bed	~	15	045,5	-18,2	023,7	+32,1	6,6	13,2

N: number of samples; **B**: number of sites; **PLong./Plat.**: palaeopole longitude/latitude in Australian and in African coordinates. **dp/dm**: semi-axis of the ellipse of confidence.

N: number of samples; **B:** number of sites; **PLong./Plat.:** palaeopole longitude/latitude in Australian and in African coordinates. **dp/dm:** semi-axis of the ellipse of confidence.

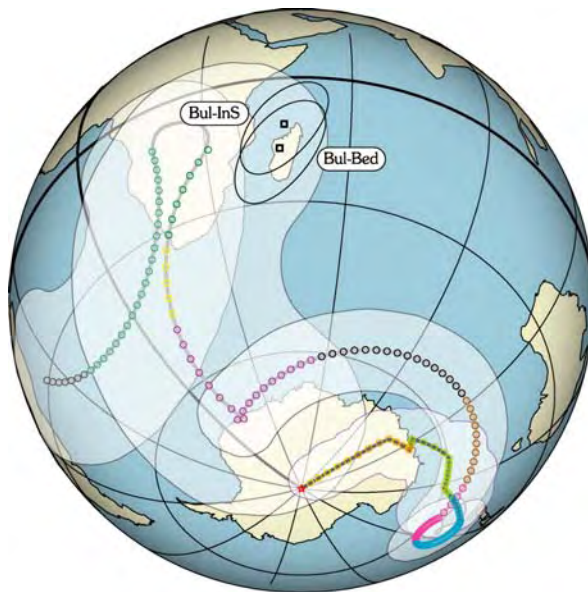


Figure 6.10: Corresponding palaeopoles in Australian coordinates. The possible APW path for Australia-Gondwana from the present-day to 570 Ma based on Small Circle Fit is shown for comparison purposes.

Same legend as in figure 2.19-A, Chapter 2 (§.2.7).

Bul-InS is the pole corresponding to component C_3 *in situ* and **Bul-Bed**, corresponding to C_3 after bedding correction.

6.3. The Ambone Volcanics from Mount Hope (HOP)

6.3.1. Presentation

The Ambone Volcanics consist of two massive lava flow units separated by partly turbiditic sediments. Lava units show columnar jointing well developed nearly everywhere. Those sampled (photo 9) are 4 to 6 metres long and about 50 cm in diameter. Petrographically, the rocks are rhyodacite porphyries, and are thought to have been emplaced as extensive submarine lava flows, although large sills origin cannot be ruled out. These volcanics are latest Pragian in age (Scheibner, 1987).

These rocks are folded along a N-S axis, but only one limb has been drilled as the other one is relatively strongly cleaved because of the presence of a fault.

Bedding measurements show that the columns are precisely perpendicular to the palaeohorizontal, and that the fold can be regarded as cylindrical with a horizontal axis.

Six sites (30 cores) have been drilled on a hill just West of the Mount Hope Township.

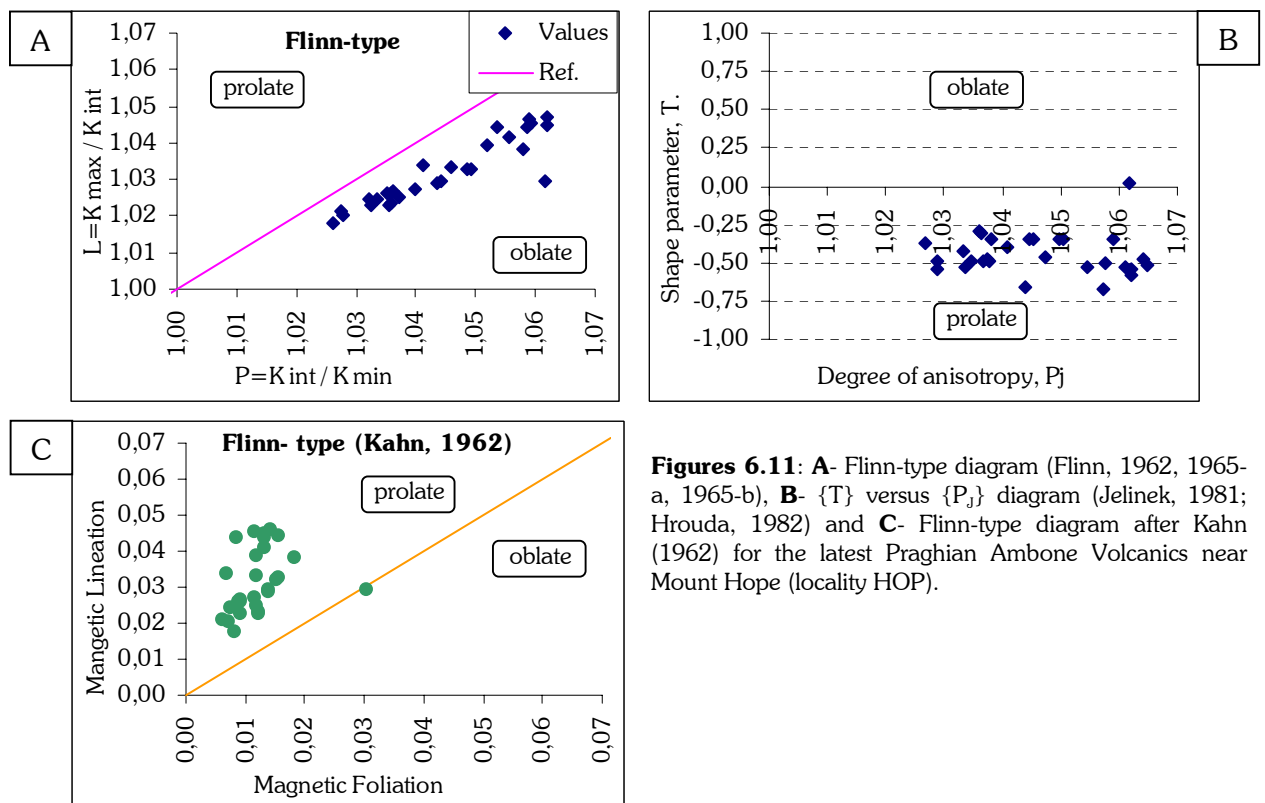


Photo 9: Columnar jointings in the rhyodacite porphyries of the latest Praghian Ambone Volcanics near the Mt Hope township. The hat gives the scale.

6.3.2. Anisotropy of magnetic susceptibility (AMS)

The results obtained by AMS from these rocks are remarkable. The degree of anisotropy is well marked ($P_j = 1,05 \pm 0,01$; figure 6.11-B) but weak (figures 6.11-A to C). The shape of the ellipsoid of magnetic susceptibility is also very consistent in the whole locality. The $\{T\}$ parameter indicates clearly a prolate shape ($T = -0,44 \pm 0,13$). This is not case for the Flinn-type diagram (figure 6.11-A), which shows there its limit to determine the shape of the ellipsoid. Indeed, the Flinn-type diagram proposed by Kahn (1962) is in this case much more appropriate and illustrates clearly the prolate tendency revealed by the $\{T\}$ parameter (figure 6.11-C).

The Königsberger ratio shows for some samples a relatively high value, but the average for the locality remains low ($Q_K @ RT = 1,77 \pm 5,83$). It can be concluded from these values that the nearby strong cleavage does not affect the internal strain in the sampled rocks and lightning effects seem to be absent.



Figures 6.11: A- Flinn-type diagram (Flinn, 1962, 1965-a, 1965-b), B- $\{T\}$ versus $\{P_j\}$ diagram (Jelinek, 1981; Hrouda, 1982) and C- Flinn-type diagram after Kahn (1962) for the latest Praghian Ambone Volcanics near Mount Hope (locality HOP).

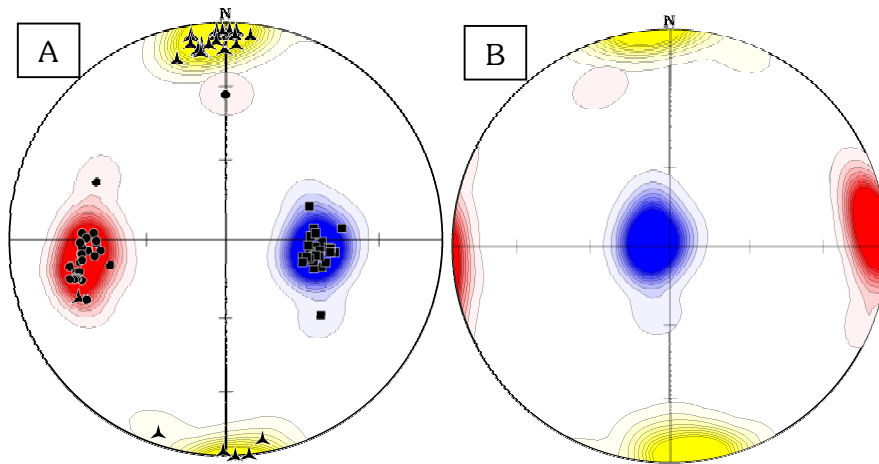


Figure 6.12: Orientations of the principal axes of magnetic susceptibility for the Ambone Volcanics near Mt Hope, locality HOP.

A- *in situ*, and **B-** after bedding correction.

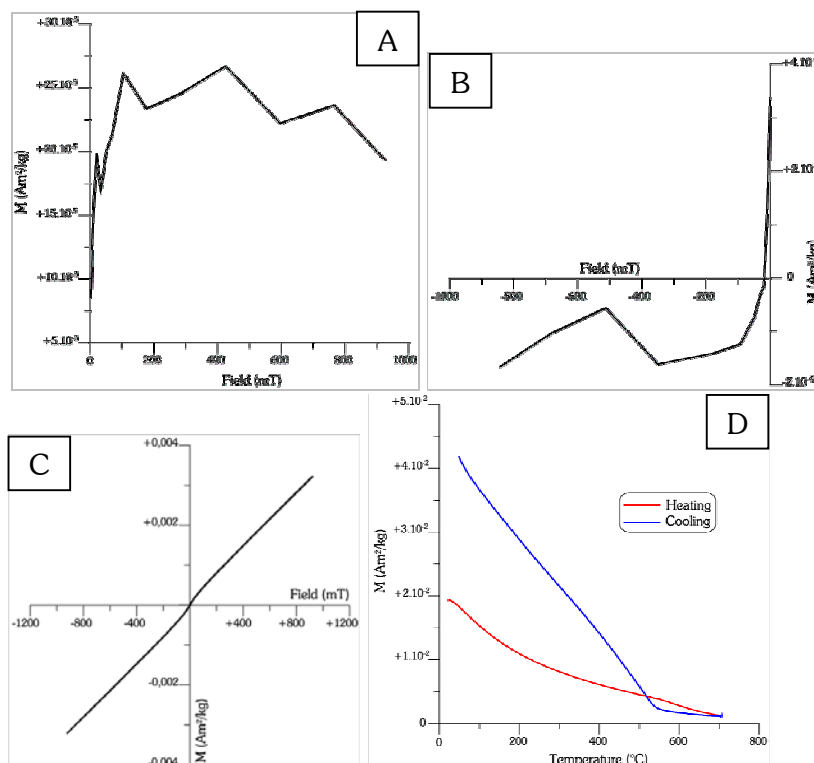
Same legend as in figure 5.4 (Chapter 5; §.5.2.2); i.e. Kmax, squares (blue); Kint, triangles (yellow); Kmin, dots (red).

The thirty directions of the principal axes of magnetic susceptibility are perfectly clustered and coincide very well with the bedding as they are in horizontal and vertical positions after bedding correction (figure 6.12-B). Hence, this magnetic fabric has been acquired prior to folding.

Nevertheless, the positions of Kmin on the horizontal and Kmax on the vertical is surprising. The vertical magnetic lineation cannot correspond to the magmatic flow, as these rocks have been emplaced as sub-horizontal lava flow. This must then corresponds to a tectonic recording. Kmin in horizontal position usually witnesses strong strain, but the AMS parameters show that this is not here the case as the degree of anisotropy is about 5% only.

The best plausible explanation is that the ellipsoid of magnetic susceptibility was nearly a sphere when the rock formed so that there is no sedimentary magnetic fabric to overcome. A slight E-W compression occurred and as these rocks were close to or at the surface, the material tended to escape with a vertical extrusion. This magnetic fabric can be thus the response of sub-surface rocks to a gentle E-W compressional event.

6.3.3. Rock magnetism



Figures 6.13: Example of rock magnetic measurements from the Ambone Volcanics near Mt Hope (locality HOP): specimen HOP3-3. **A-** IRM curve; **B-** Back field curve (coercivity); **C-** Hysteresis loop; and **D-** IST curve, in red while heating and in blue while cooling ($B=535$ mT).

$H_C=4,34$ mT; $H_{CR}=18,65$ mT.
 $M_S=1,4 \cdot 10^{-3}$ Am²/kg; $M_{RS}=1,1 \cdot 10^{-4}$ Am²/kg.

The shape of the hysteresis loop (figure 6.13-C) indicates at the same time an important contribution of paramagnetic material and a low value of magnetisation at saturation ($M_S = 1,4 \cdot 10^{-3} \text{ Am}^2/\text{kg}$). The IRM and back field curves are very noisy because the weakness of these samples reach the limit of the VFTBs. However the main features of these curves can still be recognised and they show the presence of low coercivity material (figures 6.13-A & B). Both the H_{CR}/H_C and M_{RS}/M_S ratios point to large grain sizes as they plot close to the pseudo-single to multi-domain boundary on the Day plot ($H_{CR}/H_C = 4,29$; and $M_{RS}/M_S = 7,6 \cdot 10^{-2}$). The IST curve suggests that these relatively large grains of low coercivity material are magnetite (or low titanium titanomagnetite) as an inflexion is visible around 580°C on the heating curve. By cooling, new magnetite (or titanomagnetite) is formed. This may result from the transformation of some phyllosilicates, which were probably responsible for the paramagnetic behaviour.

The presence of relatively large grains of magnetite (or titanomagnetite) can be however expected from such rhyodacite porphyries.

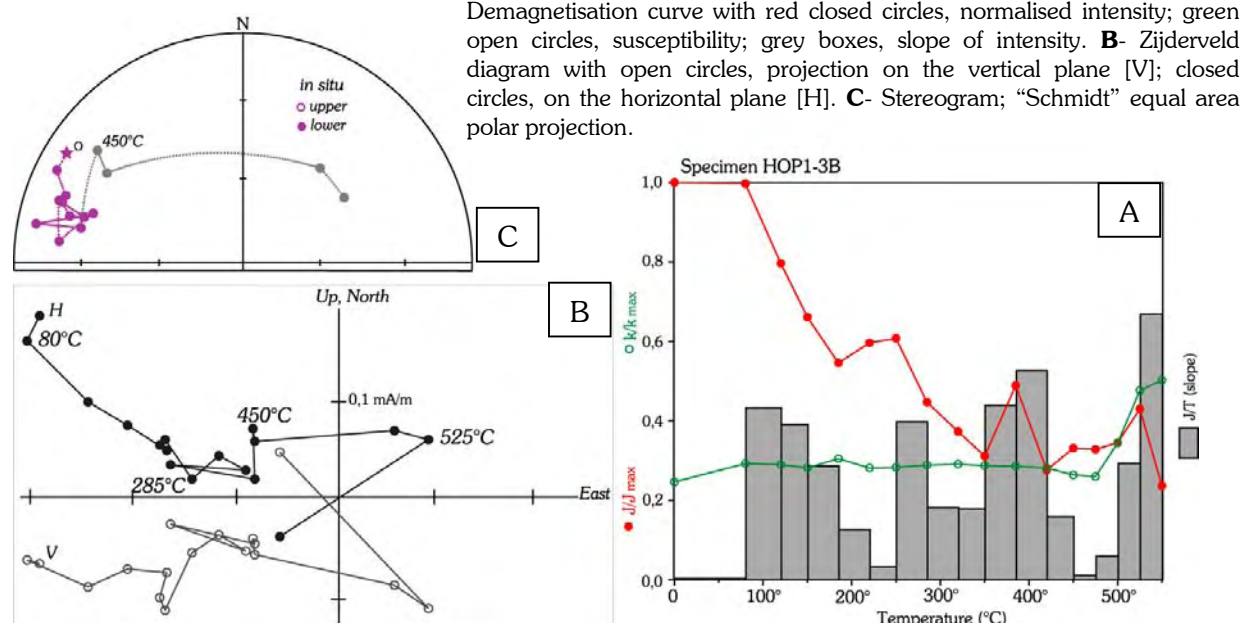
6.3.4. Palaeomagnetic results

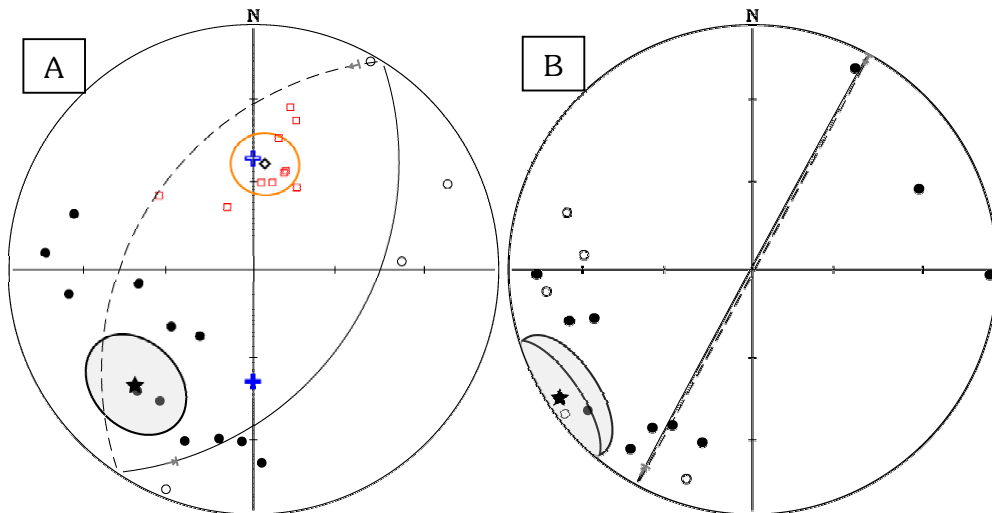
- Demagnetisation

After removal of a viscous or drilling-induced magnetisation below 80°C , two components can be defined with difficulty (figures 6.14). A noisy component C_1 is demagnetised from 80° to about 285°C , and a component C_2 seems to be present up to 575°C , but the signal is very scattered and a viscous magnetisation appears from 475°C with a strong increase in susceptibility (figure 6.14-A). It is not determined what carries C_1 , but magnetite (or titanomagnetite) is probably the main magnetic carrier of C_2 . The very noisy signal probably results from unstable magnetisation due to the grain size.

- Interpretation

Albeit noisy, the orientation of components C_1 , which can be satisfyingly defined (figure 6.15-A; table 17), corresponds to the present-day field with a direction *in situ* D.006°/I.-54° ($\alpha_{95} = 11,0/\kappa = 20,4$) and a κ -ratio of 0,9.





Figures 6.15: Orientation of components obtained from the Ambone Volcanics near Mount Hope (locality HOP). **A-** *in situ* and **B-** after bedding correction. **Red squares** are single specimen directions from component C_1 shown *in situ* only with their overall mean direction (**diamond**) and **orange** confidence cone (α_{95}); **Blue crosses** show the present-day field direction; **Black circles** (and lines, obtained from great circle analysis) are single specimen directions from component C_2 shown with their overall mean direction (**star**) and **shaded grey** α_{95} . **Open** symbols are negative inclination values (upper hemisphere); **closed** symbols, positive inclination values (lower hemisphere). Schmidt equal area polar projection.

Table 17: Overall mean directions for the locality HOP obtained from single specimen orientations

Name	N	R	D.InS	I.InS	α_{95}	κ	R	D.Bed	I.Bed	α_{95}	κ
<i>Mean direction for component C_1:</i>											
Hop- C_1	10	9,6	006,3	-53,8	11,0	20,4	9,5	050,7	-38,8	11,4	19,1
<i>Mean direction for component C_2:</i>											
Hop- C_2	17	14,2	225,3	+31,5	16,7	5,5	14,1	236,1	+03,9	17,0	5,3

N: number of samples; **B:** number of sites; **α_{95} :** cone calculated at the 95% confidence level; **κ :** precision parameter; **R:** resultant vector; **D.InS/I.InS:** declination/inclination *in situ* (geographic coordinates); **D.Bed/I.Bed:** declination/inclination after bedding correction.

Orientations of C_2 are very scattered and the overall mean direction has no real meaning (black star in figures 6.15; table 17). All orientations of C_2 however are of reverse polarity of directions plotting in the N-E quadrant of the stereogram with negative inclination values, which can be expected for Devonian times. The classic fold test does not help constraining the age magnetisation, as it is positive at the 45,5% confidence level (κ -ratio=1). It must be pointed out however that these kinds of direction are quite similar to those observed in the rhyolitic intrusions of the Sisters in the Broken Hill area (locality SIS), and to a certain extent, similar to directions of the Mt Daubeny Formation of the Churinga Property (locality CHU in the Broken Hill area) and the Gundaroo sandstones at the Bulgoo Property (locality BUL, above) after bedding correction.

Nevertheless, no conclusion can be drawn about the palaeoposition from these rocks, although these similarities exist.

6.4. The Ural Volcanics (localities BOW, TAR, SHE, MER)

6.4.1. Presentation

The Ural Volcanics (volcanics and associated volcanoclastics) were deposited during the Siluro-Devonian in the Rast Trough of the Central Lachlan Orogen. The sequence is interpreted as syn-rift to rift fill (Colquhoun *et al.*, 2000). Overlying sag deposits were presumably removed by erosion, possibly only now preserved on the adjacent shelves as the shallow marine Walters Range Group (southern part of the map in figure 6.2). Isotopic and fossil evidence indicates that volcanism probably spanned the latest Silurian to Early Devonian, with the upper

limit poorly constrained. A fossil assemblage found in volcanoclastic breccia horizons provides evidence of marine conditions, with debris sourced from a shallow marine shelf of limited extent and indicates an Early Devonian age (most likely Pragian to Emsian). This is generally consistent with new SHRIMP U/Pb zircon dates, which have been obtained by Meakin *et al.* (2002) for coherent volcanic facies within the sequence: 410 ± 8 , 414 ± 13 , 413 ± 5 and 424 ± 6 Ma, the last age probably reflecting inheritance of zircons (see below). Geochemical data analysis reveals that the volcanics are dominantly rhyolitic to dacitic in composition but range to andesitic and basaltic in small volumes. The Ural Volcanics have been interpreted by Colquhoun *et al.* (2000) as forming a large syncline. Bedding is usually very difficult to determine and the main argument for this fold is the presence of leaning columnar jointings in particular near the Merri Abba Property (locality MER). This interpretation is refuted by Katharine Bull (University of Tasmania) who is currently mapping this region in detail, and argues on the basis of parallel lavas and sills to clastic contacts that no large-scale fold exist (Bull, *personal communications*).

Four different localities have been studied in the Ural Volcanics.

- The Ural Volcanics from the Mount Bowen (BOW)

The mainly dacitic rocks from the top of the Mount Bowen yielded a SHRIMP age of 424 ± 6 Ma. They have been then selected as palaeomagnetic target and six sites (29 cores) have been sampled (figure 6.2; table 14).

There is a pervasive steep cleavage present in this rocks (as well as regionally, see also locality HOP above), more visible in the interbedded sediments, which are less competent than the volcanics, especially if they are silicic and possibly silicified, such as the Ural Volcanics (Bull, *personal communication*, 2002). However, the degree of strain seems to be low, and the bedding is regarded as horizontal.



Photo 10: View from the top of the Mount Bowen, showing that it is the last relief before the Delamerian Orogen to the West.

- The Ural Volcanics from the quarry near the Tarilta Property (TAR)

This quarry shows spectacular alteration facies. The cause and age of this alteration are still unresolved. Four cores (one site) have been collected as pilot investigation to try to see if palaeomagnetism could bracket a possible period for this event. The results are unfortunately totally randomised and this locality is therefore not considered further (locality TAR; figure 6.2, table 14).

- The Ural Volcanics from the Shepherds Hill quarry (SHE)

The Ural Volcanics are very well exposed in the quarry at Shepherds Hill (photo 11), where the deepest pits are filled up with water. A SHRIMP dating have been also obtained there and yields an age of 410 ± 8 Ma. The rhyolitic rocks also show the steep regional shear fabric, but the “apparent folds” seen are the result of flow banding. It is impossible to know what their original



Photo 11: Abandoned quarry at Shepherds Hill where rocks have been collected (locality SHE). View to the South.

orientations were, as bedding is not visible. A $\sim N.20^\circ$ steep fault cross-cuts the quarry (back ground in the right hand side of photo 11; part in the shadow) and indicates a sinistral strike-slip movement.

Seven sites (35 cores) have been drilled all over the quarry (locality SHE).

- The Ural Volcanics from the small quarry at the Merri Abba Property (MER)

Polygonal columnar jointings (photo 12) dated by SHRIMP at 413 ± 5 Ma are also easily accessible at the Merri Abba Property (figure 6.2; table 14). These rocks are more andesitic and the columns are leaning to the East (the column axes are oriented $D.300^\circ/I.+55^\circ$ in average; $\alpha_{95}=2,4^\circ$).

Colquhoun *et al.* (2000) based the existence of a syncline in the Ural Volcanics on such observation, but whether these columns result from folding (or tilting) or non-vertical thermal gradient while cooling is still not firmly establish.

It can be seen on the picture that the soil is about 50 cm deep, and underlying rocks look very fresh.

Six sites (30 cores) have been drilled all along this quarry (locality MER).



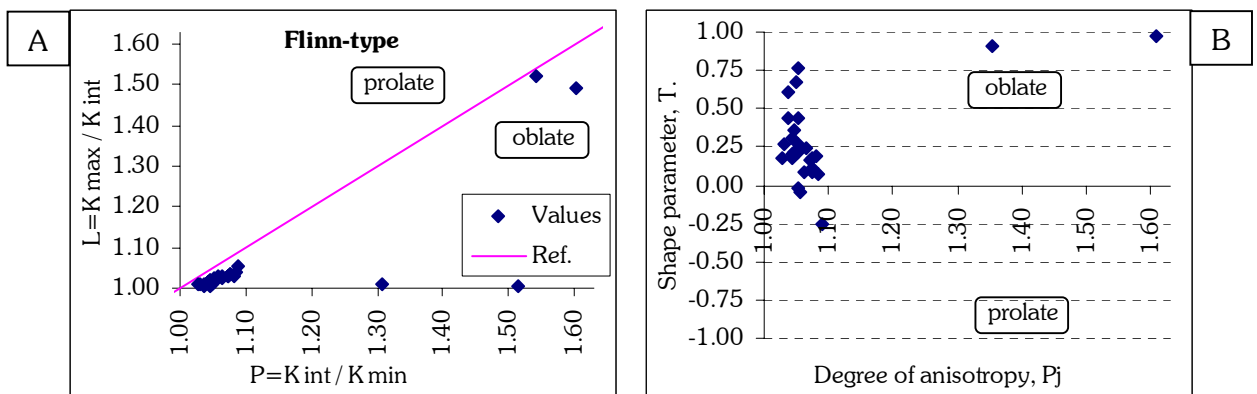
Photo 12: Leaning polygonal columnar jointings of andesitic rocks exposed in the small quarry belonging to the Merri Abba Property (locality MER).

6.4.2. Anisotropy of magnetic susceptibility (AMS)

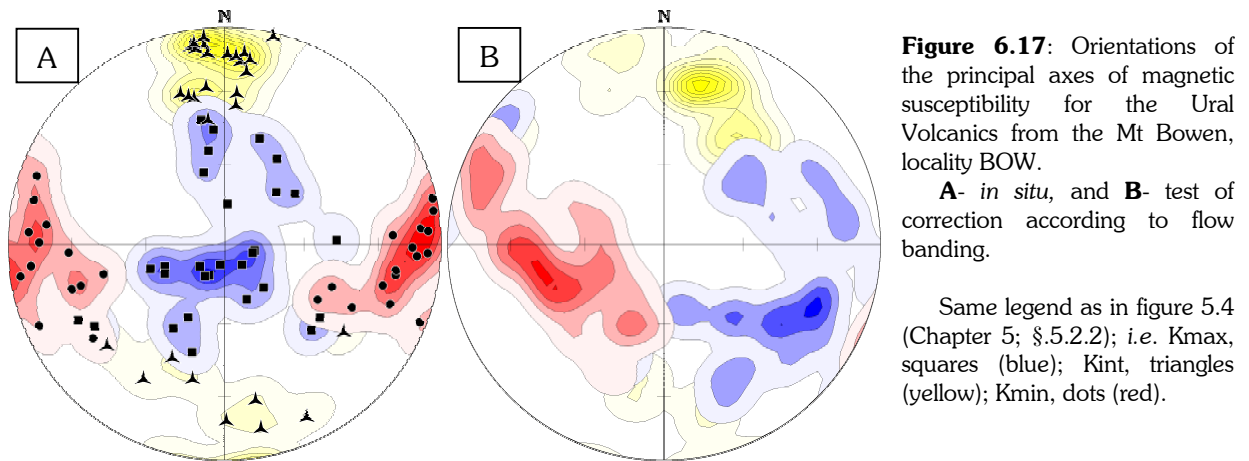
- The Ural Volcanics from the Mount Bowen (BOW)

The degree of anisotropy is low but marked ($P_j=1,07 \pm 0,06$ when the highest values are excluded since they probably stem from magnetic disturbances during measurement; figure 6.16-B) and the test of Parés & Van der Pluijm (2002) shows a degree of alignment around 20%.

The shape parameter $\{T\}$ as well as the Flinn-type diagram indicates a relatively well-pronounced oblate shape of the ellipsoid of magnetic susceptibility ($T=0,26 \pm 0,26$ when high values are excluded). Nevertheless, the internal strain is not strong enough to be able to deviate palaeomagnetic results in these rocks ($Q_K@RT=1,55 \pm 2,26$; discarding also the possibility of lightning effects).



Figures 6.16: **A-** Flinn-type diagram (Flinn, 1962, 1965-a, 1965-b) and **B-** $\{T\}$ versus $\{P_j\}$ diagram (Jelinek, 1981; Hrouda, 1982) for the Ural Volcanics from the Mount Bowen (424 ± 6 Ma; locality BOW).



The principal axes of magnetic susceptibility are relatively well grouped even if a distribution along great circles tends to arise. It can be shown that flow banding is not representative of the bedding, as directions corrected from them lead to oblique magnetic fabric (figure 6.17-B). On the contrary, *in situ* (figure 6.17-A) Kmax, Kint and Kmin are situated on horizontal and vertical plan, which confirm the assumption that no bedding correction is needed for these rocks.

The E-W horizontal position of the pole to the magnetic foliation (Kmin) and the vertical position of the magnetic lineation (Kmax) however are surprising as the Ural Volcanics at Mount Bowen are believed to be a lava flow or an emergent sill (Bull, *personal communication*, 2002). This vertical lineation cannot therefore represent the magmatic flow.

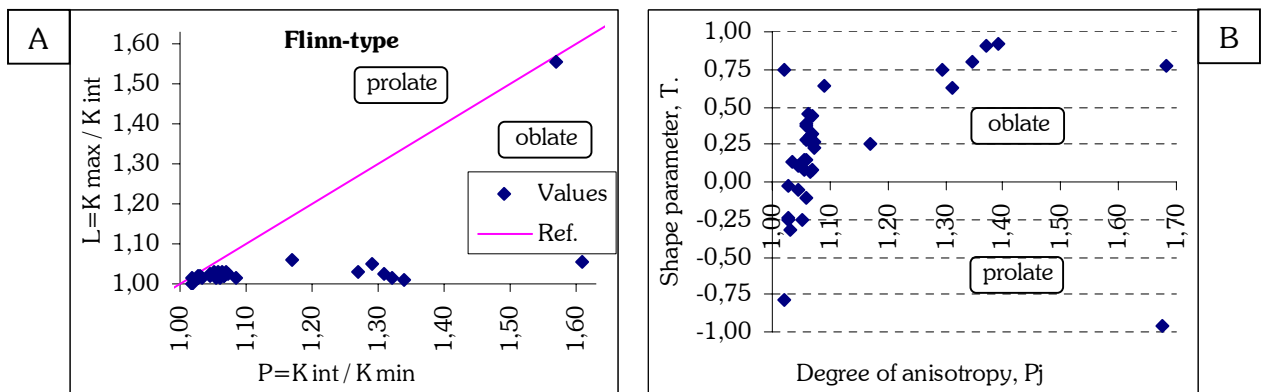
Like for locality HOP, the most plausible explanation is to invoke an E-W compression, which leads to the recording of vertical extrusion by the magnetic fabric.

- The Ural Volcanics from the Shepherds Hill quarry (SHE)

Similarly, the degree of anisotropy in the rhyolitic rocks of the quarry is relatively pronounced ($P_j = 1,13 \pm 0,17$; figure 6.18-B) and the test of Parés & Van der Pluijm (2002) shows a maximum of degree of alignment around 20%.

Both the Flinn-type and the $\{T\}$ vs. $\{P_j\}$ diagrams better point to an oblate shape of the ellipsoid of magnetic susceptibility ($T = 0,21 \pm 0,43$), but internal strain cannot deviate palaeomagnetic results.

The Königsberger ratio has a low value and this may indicate the presence of relatively large magnetic grain sizes ($Q_K @ RT = 0,16 \pm 0,36$).



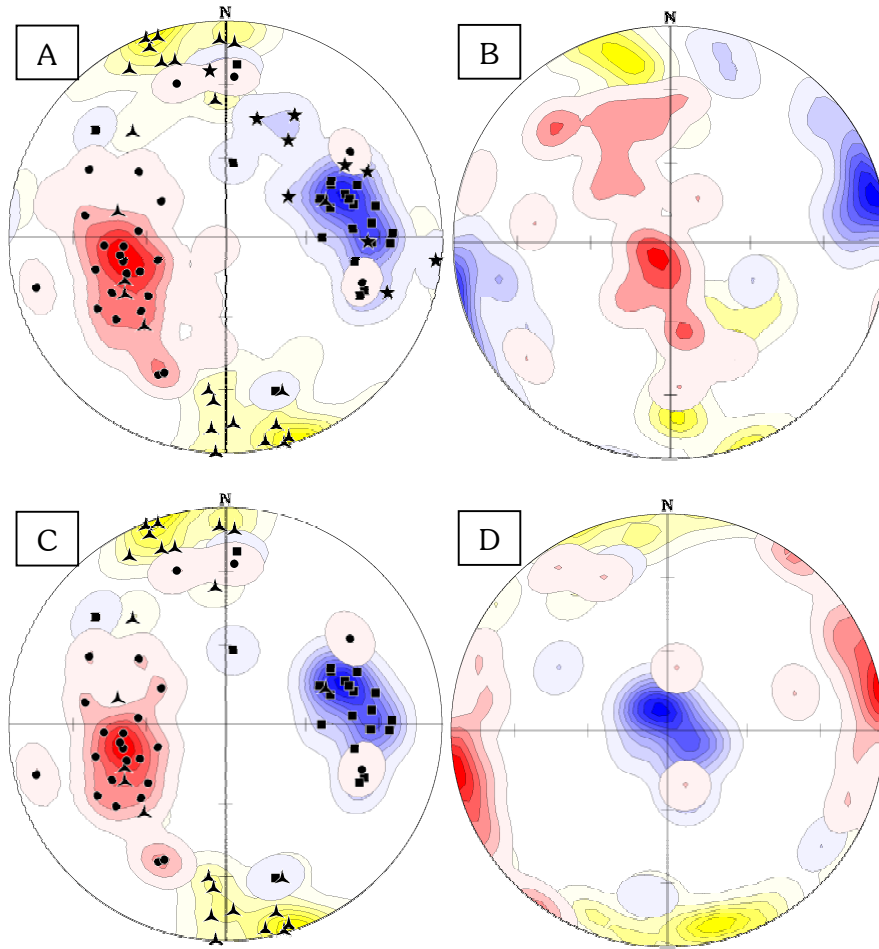


Figure 6.19: Orientations of the principal axes of magnetic susceptibility for the Ural Volcanics from the Shepherds Hill quarry, locality SHE.

A- All data shown *in situ*; stars correspond to Kmax from sites She-03 & She-05; and **B-** Correction consisting in bringing Kmin to the vertical. Data from sites She-03 & She-05 are not included.

C- Data excluding sites She-03 & She-05 and shown *in situ*; and **D-** Correction consisting in bringing Kmax to the vertical. Data from sites She-03 & She-05 are not included.

Same legend as in figure 5.4 (Chapter 5; §.5.2.2); i.e. Kmax, squares (blue); Kint, triangles (yellow); Kmin, dots (red).

The directions of the principal axes of magnetic susceptibility are oblique *in situ* (figure 6.19-A). They are however well clustered, except for data coming from the sites She-03 and She-05. It is particularly visible that Kmax from these two sites are distributed on a great circle (stars in figure 6.19-A), whereas it is not the case for Kmax from the other sites (figure 6.19-C).

When we look at the position of these two specific sites (She-03 and She-05), it can be seen that they are aligned more or less parallel with the fault observed at the south-eastern wall of the quarry (black dashed line in figure 6.20), and also with an exposure of sediments to the South West. Hence, it can be suggested that the deviation of magnetic lineation in these sites are caused by a cryptic fault or shear zone (orange dashed line in figure 6.20), possibly parallel to the fault observed.

Because of the presence of these faults, it is possible that the oblique magnetic fabric is due to block tilting, even if a magmatic origin (flow) cannot be ruled out. It is likely however that, as per localities BOW and HOP, the original shape of the ellipsoid of magnetic susceptibility was close to a sphere and the magnetic fabric

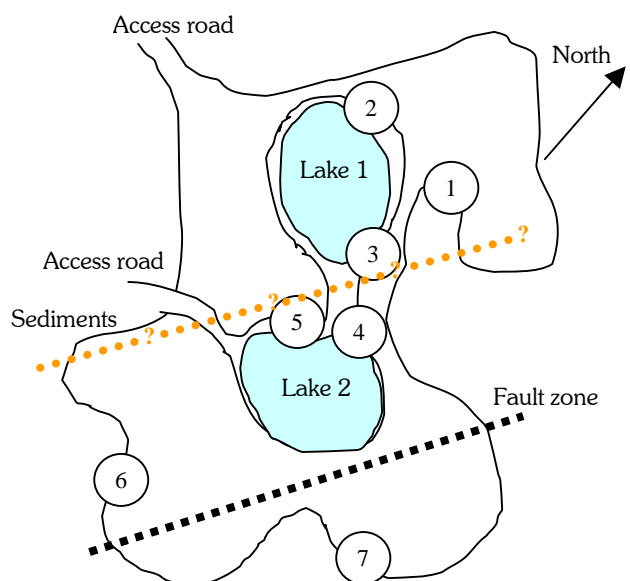


Figure 6.20: Sketch map of the Shepherds Hill quarry with numbers referring to drilled sites.

observed has a tectonic origin. The oblique directions could not be acquired under a thrust, because such structures have not been reported and the directions of the principal axes are not compatible with the observed fault. Moreover, it is likely that the degree of anisotropy would be then much higher. A tectonic tilting appears then to be the best explanation, as folding can be discarded over the quarry since the directions are similar from sites She-01 to She-07.

A tilt correction may consist in bringing K_{min} to the vertical (figure 6.19-B) to obtain a fabric similar to a sedimentary magnetic fabric. The magnetic lineation would be then sub-parallel the fault direction. This could results therefore from a slight compression against it.

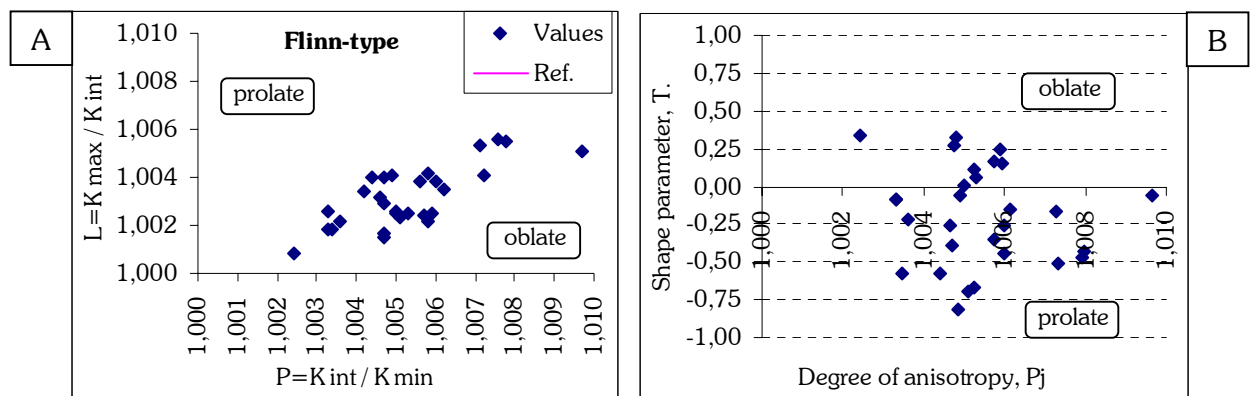
The second possible correction would consist in bringing the K_{max} to the vertical (figure 6.19-D). In this case, K_{min} is directed \sim E-W and remarkably resemble to the magnetic fabric observed in localities BOW and HOP. This second option is favoured as the magnetic fabric would be more consistent throughout the Ural Volcanics on the one hand, and could give an explanation for some palaeomagnetic results observed (see below).

- The Ural Volcanics from the Merri Abba Property (MER)

Anisotropy of magnetic susceptibility (figures 6.21) is much more weaker in these andesitic rocks from the small quarry at the Merri Abba Property (locality MER).

The degree of anisotropy is about 0,5% ($P_j = 1,005 \pm 0,002$) and the uncertainty around the shape parameter covers largely both side of the $\{T\}$ vs. $\{P_j\}$ diagram (figure 6.21-B). This means that the shape is not clear, although the mean value points to a prolate shape of the ellipsoid of magnetic susceptibility ($T = -0,19 \pm 0,33$). The Flinn-type diagram (figure 6.21-A) shows conversely an oblate shape, but the alternative Flinn-type diagram proposed by Kahn (1962) points to a slight tendency for a prolate shape.

These results imply in conclusion, that the magnetic fabric is very close to isotropy.



Figures 6.21: **A-** Flinn-type diagram (Flinn, 1962, 1965-a, 1965-b) and **B-** $\{T\}$ versus $\{P_j\}$ diagram (Jelinek, 1981; Hrouda, 1982) for the Ural Volcanics from the Merri Abba Property (413 ± 5 Ma; locality MER).

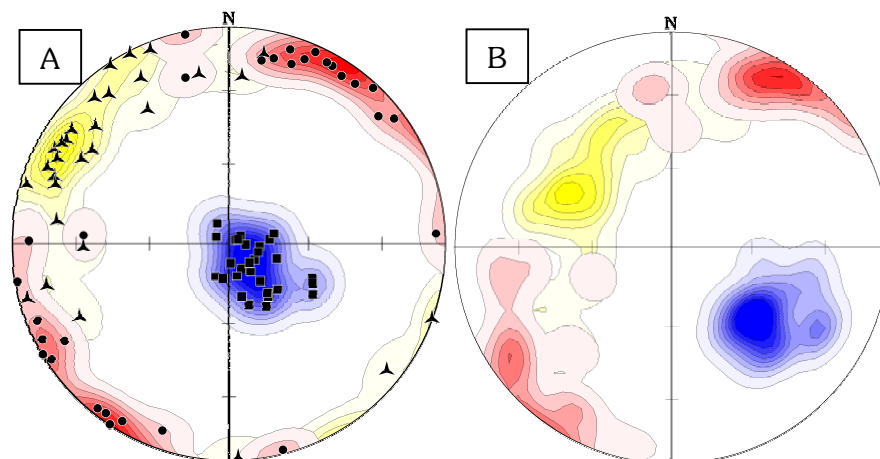


Figure 6.22: Orientations of the principal axes of magnetic susceptibility for the Ural Volcanics from the Merri Abba Property, locality MER.

A- *in situ*, and **B-** test of correction consisting in bringing the columnar jointings to the vertical.

Same legend as in figure 5.4 (Chapter 5; §.5.2.2); i.e. K_{max} , squares (blue); K_{int} , triangles (yellow); K_{min} , dots (red).

It is clear that lightning effects are very unlikely down in a quarry. However the Königsberger ratio is interesting as it is also very low ($Q_K@RT=0,06\pm0,04$). This may signify that relatively large magnetic particles are present in these rocks.

It is striking to see that, although the magnetic fabric is close to isotropy, the three axes of magnetic susceptibility are well grouped (figures 6.22). Moreover, the magnetic lineation (K_{max}) is in this case again close to the vertical *in situ* (figure 6.22-A). It can be proved here that, assuming that the columnar jointings are perpendicular to the bedding and are representative of a fold as proposed by Colquhoun *et al.* (2000) is erroneous, since the directions of the principal axes become oblique when the columns are brought to the vertical (figure 6.22-B).

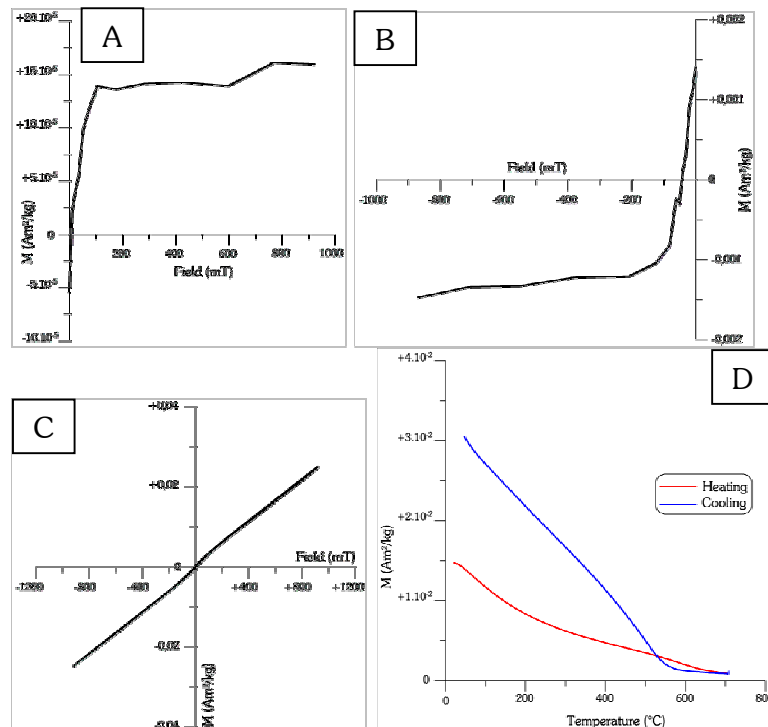
It can be inferred from these results that no bedding correction appears necessary for locality MER, although a slight tilt ($\sim 5-10^\circ$) cannot be ruled out. A NE-SW compression seems to have caused here a tendency to vertical extrusion.

- AMS measurements after thermal demagnetisation

AMS has been measured again after thermal demagnetisation, in particular for the localities HOP and MER. This has been carried out in order to test the hypothesis that the vertical magnetic lineation results from vertical extrusion. Such response could indeed arise from particular magnetic condition where a swap in principal axes of magnetic susceptibility might be observed. Thermal demagnetisation, however, does not modify at all the magnetic fabric obtained before heating, and this implies that it results from petrofabric features.

6.4.3. Rock magnetism

Rock magnetic measurements are shown for the locality MER only, as palaeomagnetic results are really interesting only for this locality (see below). However, the magnetic composition in the Ural Volcanics seems to be quite homogeneous.



Figures 6.23: Example of rock magnetic measurements from the Ural Volcanics at the Merri Abba Property (locality MER): specimen MER1-1.

A- IRM curve; **B-** Back field curve (coercivity); **C-** Hysteresis loop; and **D-** IST curve, in red while heating and in blue while cooling ($B=535$ mT).

$H_C=12,7$ mT; $H_{CR}=43,8$ mT.
 $M_S=1,0 \cdot 10^{-3}$ Am²/kg; $M_{RS}=1,7 \cdot 10^{-4}$ Am²/kg.

The IRM and back field curves show the presence of low coercivity material (figures 6.23-A & B). The slope of the hysteresis loop (figure 6.23-C) witnesses the strong contribution of paramagnetic minerals. They are likely to be phyllosilicates as new magnetite is formed when cooling, and may results from the transformation of such minerals (figure 6.23-D). The IST curve shows however that magnetite (or low titanium titano-magnetite) was already present before this transformation as a slight inflexion is visible around 580°C on the heating curve. It appears also that some oxidised minerals are present in this specimen coming from the first site, which is the closest to the surface in the quarry, as the IST curve shows a steeper slope up to 150°-200°C, and the IRM and back field curves are not very fully saturated. The reduced hysteresis loop finally, has a slight wasp-wasted shape, which may be caused by the presence of these oxidised materials together with magnetite (or low titanium titano-magnetite) or may indicate the existence several sizes of magnetic particles.

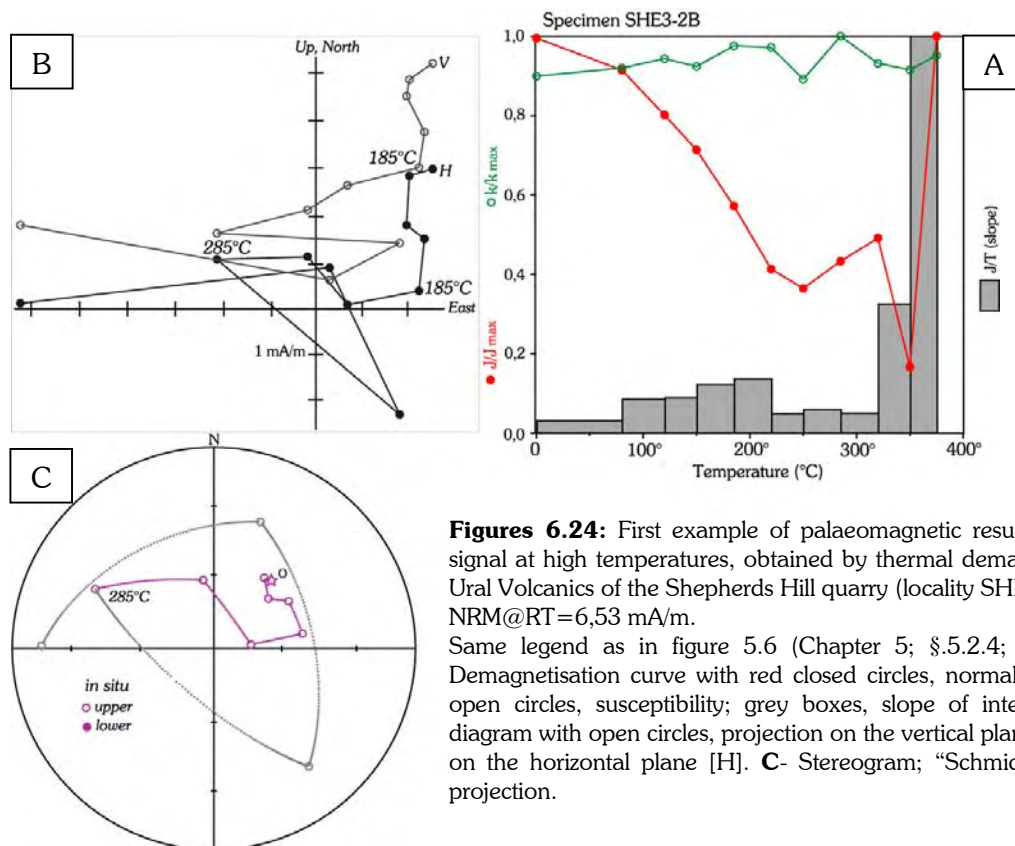
6.4.4. Palaeomagnetic results

- Demagnetisation in localities BOW and SHE

All specimens of locality BOW and most of locality SHE show a demagnetisation analogous to that of Specimen SHE3-2 (figures 6.24).

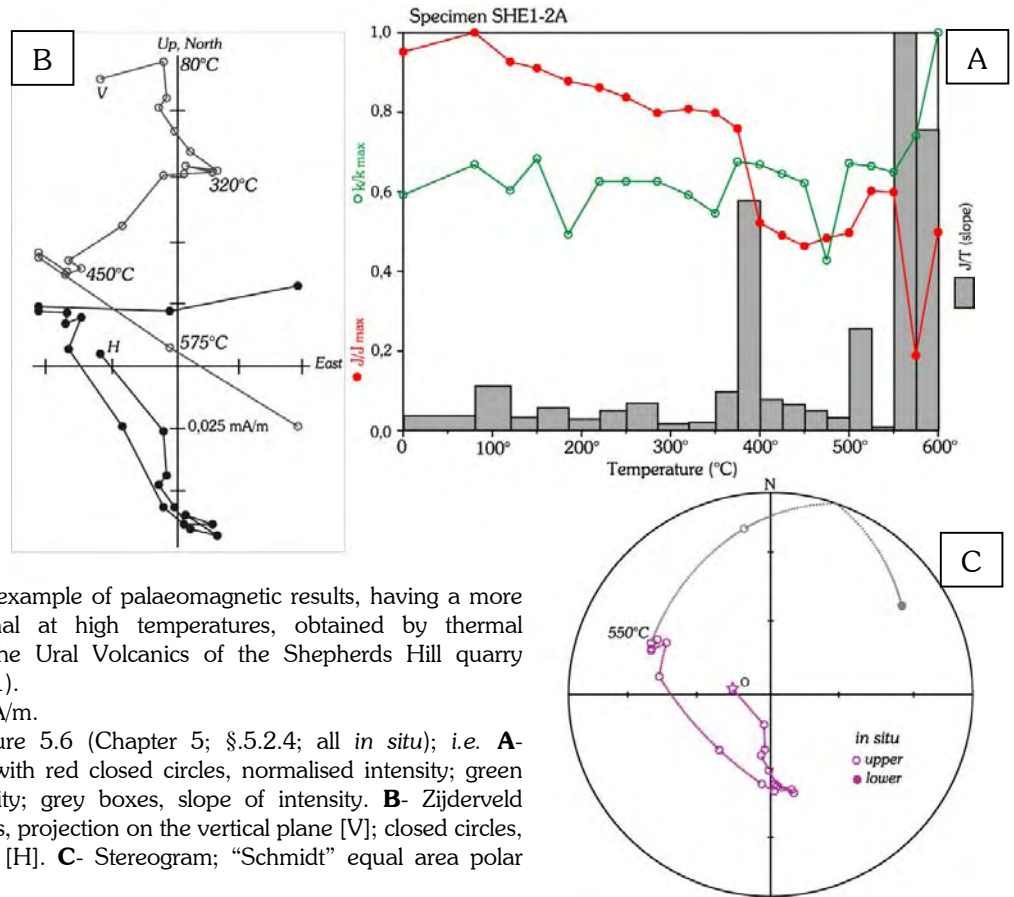
After removal of a viscous or drilling-induced magnetisation, a noisy component C_1 is identified from 80° to 185°C. The magnetic carrier of this component is not determined but could be some oxidised mineral. Its direction corresponds generally relatively well with the present-day field.

In many cases, a component C_2 seems to exist but is lost very rapidly as the magnetic signal becomes completely scattered. C_2 may be observed from 185° up to 285°-320°C (figure 6.24). It must be pointed out that the susceptibility appears to remain stable, which suggests that the scattering is perhaps not associated with important mineralogical changes.



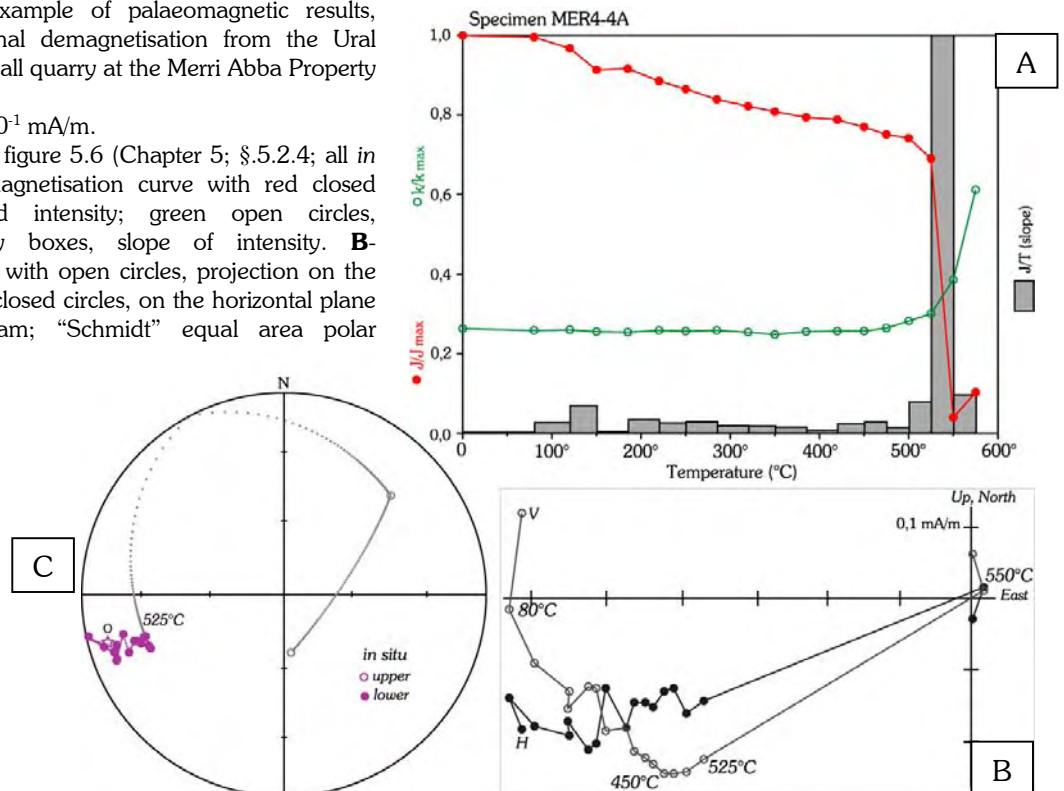
Figures 6.24: First example of palaeomagnetic results, showing a noisy signal at high temperatures, obtained by thermal demagnetisation from the Ural Volcanics of the Shepherds Hill quarry (locality SHE; site She-03). NRM@RT=6,53 mA/m.

Same legend as in figure 5.6 (Chapter 5; §.5.2.4; all *in situ*); i.e. **A**- Demagnetisation curve with red closed circles, normalised intensity; green open circles, susceptibility; grey boxes, slope of intensity. **B**- Zijderveld diagram with open circles, projection on the vertical plane [V]; closed circles, on the horizontal plane [H]. **C**- Stereogram; “Schmidt” equal area polar projection.



Figures 6.25: Second example of palaeomagnetic results, having a more coherent magnetic signal at high temperatures, obtained by thermal demagnetisation from the Ural Volcanics of the Shepherds Hill quarry (locality SHE; site She-01). $NRM@RT = 1,17 \cdot 10^{-1}$ mA/m. Same legend as in figure 5.6 (Chapter 5; §.5.2.4; all *in situ*); i.e. **A-** Demagnetisation curve with red closed circles, normalised intensity; green open circles, susceptibility; grey boxes, slope of intensity. **B-** Zijderveld diagram with open circles, projection on the vertical plane [V]; closed circles, on the horizontal plane [H]. **C-** Stereogram; “Schmidt” equal area polar projection.

Figures 6.26: Example of palaeomagnetic results, obtained by thermal demagnetisation from the Ural Volcanics of the small quarry at the Merri Abba Property (locality MER). $NRM@RT = 6,46 \cdot 10^{-1}$ mA/m. Same legend as in figure 5.6 (Chapter 5; §.5.2.4; all *in situ*); i.e. **A-** Demagnetisation curve with red closed circles, normalised intensity; green open circles, susceptibility; grey boxes, slope of intensity. **B-** Zijderveld diagram with open circles, projection on the vertical plane [V]; closed circles, on the horizontal plane [H]. **C-** Stereogram; “Schmidt” equal area polar projection.



In three sites of locality SHE however (sites She-01, She-02 & She-07), several specimens show a more stable magnetic behaviour while demagnetising (figures 6.25).

Component C_1 is identifiable from 80° to 220°C, then C_2 from 320° to ~475°C. From this temperature, the susceptibility increases and obscures a component C_3 probably up to 575°C.

- Demagnetisation in locality MER

After removal of the viscous or drilling-induced magnetisation at 80°C, two different components can be much clearly identified in the rocks of locality MER (figures 6.26). The first, called C_{MT} , is a rather noisy component demagnetised from 80° to 450°C. The last component C_{HT} carries about 75% of the remanence and shows a sharp decay in intensity between 525° and 550°C and a strong increase of the susceptibility from these temperatures. The thirty specimens from this locality yield all the same response.

- Interpretation of results from the localities BOW, SHE & MER

At Mount Bowen (locality BOW), directions of magnetisation of components C_1 correspond to the present-day field, but the orientation of C_2 is revealed completely randomised.

For rocks from the Shepherds Hill quarry (locality SHE; figures 6.27 and table 18), the orientation of component C_1 represents also the present-day field, but C_1 from site She-07 appear to be of reverse polarity. It results in a positive reversal test classified C for this component which is D.355°/I.-45° (N=19; $\alpha_{95}=5,9^\circ/\kappa=33,7$; *in situ*). The recording of the present-day field so deep in the quarry and the existence of this dual polarity are not understood yet. However, the presence of faults (see figure 6.20) might have played a role if this magnetisation is associated to some fluid migration.

The magnetic carrier of component C_2 is not established and its orientation cannot be determined since directions of magnetisation from single specimen seem to be randomly distributed. As for locality BOW therefore, the significance of this magnetisation remains unresolved.

The overall mean direction (triangle in figure 6.27) obtained from single specimen component C_3 from three sites is D.274°/I.-47° (N=12; $\alpha_{95}=8,5^\circ/\kappa=27,2$) *in situ*. Two polarities are present but the reversal test is intermediate and consequently not significant. This direction does not resemble any expected for Australia or Gondwana. When corrected from the proposed tilt determined by AMS analysis and consisting in bringing K_{max} to the vertical, this direction becomes similar to that of the mid temperature component C_{MT} determined at Merri Abba (locality MER) and is D.007°/I.-75° ($\alpha_{95}=8,5^\circ/\kappa=27,2$). The mid temperature direction at Merri Abba could be Carboniferous in age and this would imply that the tectonic tilt occurred after this age.

In the small quarry indeed (locality MER; figures 6.28 and table 19), the overall mean direction *in situ* for C_{MT} is D.026°/I.-60° ($\alpha_{95}=15,2^\circ/\kappa=26,3$) and becomes D.345°/I.-44° ($\alpha_{95}=16,0^\circ/\kappa=23,7$) if the columnar jointings are brought to the vertical as proposed by Colquhoun *et al.* (2000). This result shows as well that this correction appears to be erroneous, because the only direction encompassed by the confidence cone is the present-day field and it is excluded that the tectonic tilt occurred in recent times. In addition, it seems to worsen the κ parameter as the columns are not exactly parallel one another and a non-vertical thermal gradient appears much more likely to be the cause of such a feature. Conversely, when data are regarded *in situ*, the confidence cone overlap with Carboniferous and Early Permian orientations and Late Cretaceous to Cainozoic orientations expected for Australia-Gondwana. However, a Carboniferous age of remagnetisation can be favoured, because it can be related to the end of the Tabberabberan or Kanimblan orogenic events that have been tectonically recorded in this region.

The overall mean direction for C_{HT} is D.252°/I.+34° ($\alpha_{95}=7,1^\circ/\kappa=88,9$) *in situ*, and the direction D.223°/I.+48° ($\alpha_{95}=8,7^\circ/\kappa=60,1$) after the correction proposed by Colquhoun *et al.*

(2000) is thus considered irrelevant (the classic fold is positive at the 27% confidence level only). The *in situ* direction nevertheless does look like any expected directions expected for this age or younger ages. One site, Mer-01, has a larger confidence cone (shown in blue in figure 6.28-B), but it is not discarded since it still largely overlaps the other site mean directions. This site is the closest to the surface in the quarry, and this deviation is likely to be due to weathering effect, as some oxidised minerals seem to be present there (see rock magnetism carried out in one specimen from this site; §.6.4.3, figure 6.23, above). This means that weathering may have an important influence as deep as 1,5 metre in very coherent rocks, and may be then (partly) responsible for results obtained at Mount Bowen (locality BOW) or Mount Hope (locality HOP) for instance. The site mean directions from the five other sites are very well clustered with a κ parameter reaching 1172,7 ($D.251^\circ/I.+31^\circ$ [$\alpha_{95}=2,2^\circ/\kappa=1172,7$] without site Mer-01 *in situ*). Given this value and the fact that sampling has been carried out in one lava flow only, it seems very likely that secular variation has not been averaged out and not a palaeopole but a virtual geomagnetic pole (VGP) has been here recorded. If a 30° cone, corresponding to the largest plausible deviation of a VGP to a specific pole position is drawn, the position corresponding to this direction might be compatible to an earliest Devonian position suggested by the X-type of the APW path for Gondwana but not to the Y-type path. In conclusion, except for the very peculiar case of a VGP recorded during a reversal, this result is very different from the Y-type APW path and in particular from the Snowy River Volcanics pole of Schmidt *et al.* (1987) of equivalent age. This means that one of these two results at least has been rotated. It implies also that this rotation is post-Early Devonian and that the Lachlan Orogen is not stable until that time.

Only data from the small quarry of the Merri Abba Property (locality MER) are calculated from a sufficient number of samples to have reliable statistical parameter, but the corresponding palaeopole (for C_3 & C_{MT}) and VGP (for C_{HT}) are shown however for the localities SHE and MER for indication (figure 6.29 and table 20).

Table 19: Site mean directions and overall mean directions for the locality MER

Name	N	R	D.InS	I.InS	α_{95}	κ
Component C_{MT} per site:						
Mer-01	4	4,0	037,2	-39,1	11,4	66,2
Mer-02	5	4,8	044,1	-58,9	16,5	22,6
Mer-03	5	4,8	025,8	-62,5	17,0	21,3
Mer-05	3	2,9	015,6	-63,3	20,8	36,3
Mer-06	4	3,9	343,8	-70,3	19,1	24,2
Component C_{HT} per site:						
Mer-01	5	4,8	255,0	+51,2	16,6	22,1
Mer-02	5	4,9	252,2	+32,3	10,2	60,7
Mer-03	5	5,0	253,5	+32,7	4,7	267,4
Mer-04	5	5,0	250,0	+29,6	3,3	529,7
Mer-05	5	5,0	248,3	+30,0	4,1	350,0
Mer-06	5	4,9	252,8	+29,9	8,7	78,2

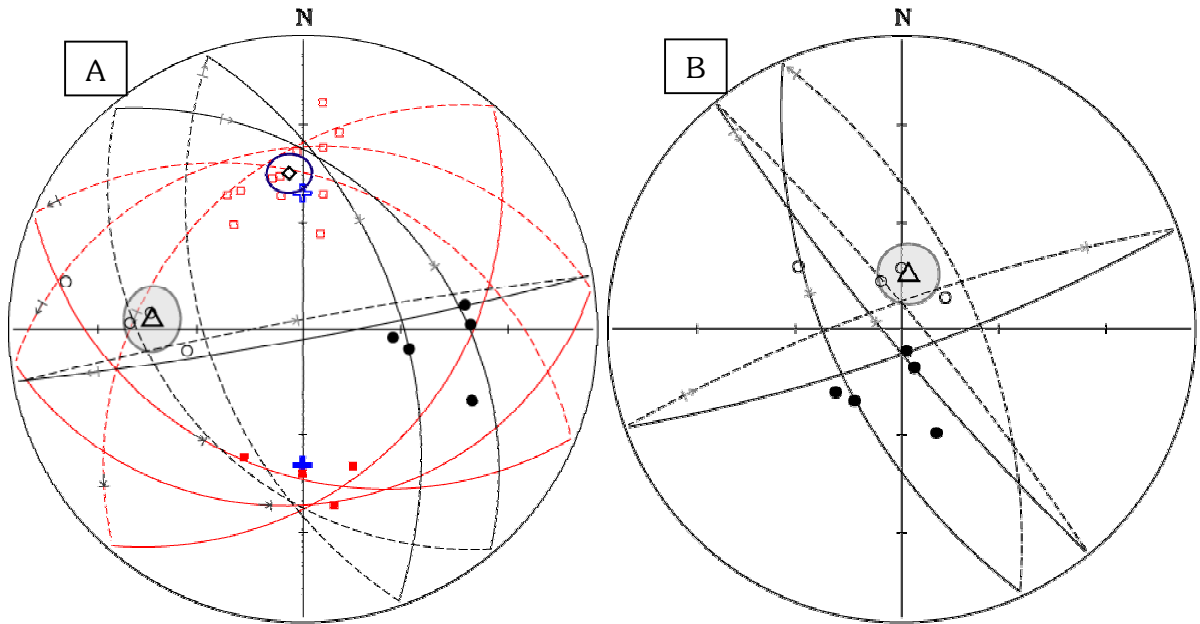
Name	B	N	R	D.InS	I.InS	α_{95}	κ
Mean direction for the mid-temperature component (C_{MT}):							
MER-mT	5	21	4,8	026,0	-60,2	15,2	26,3
Mean direction for the high-temperature component (C_{HT}):							
MER-HT	6	30	5,9	251,8	+34,3	7,1	88,9

N: number of samples; **B:** number of sites; α_{95} : cone calculated at the 95% confidence level; κ : precision parameter; **R:** resultant vector; **D.Ins/I.InS:** declination/inclination *in situ* (geographic coordinates). It is considered that no bedding correction is needed for these rocks.

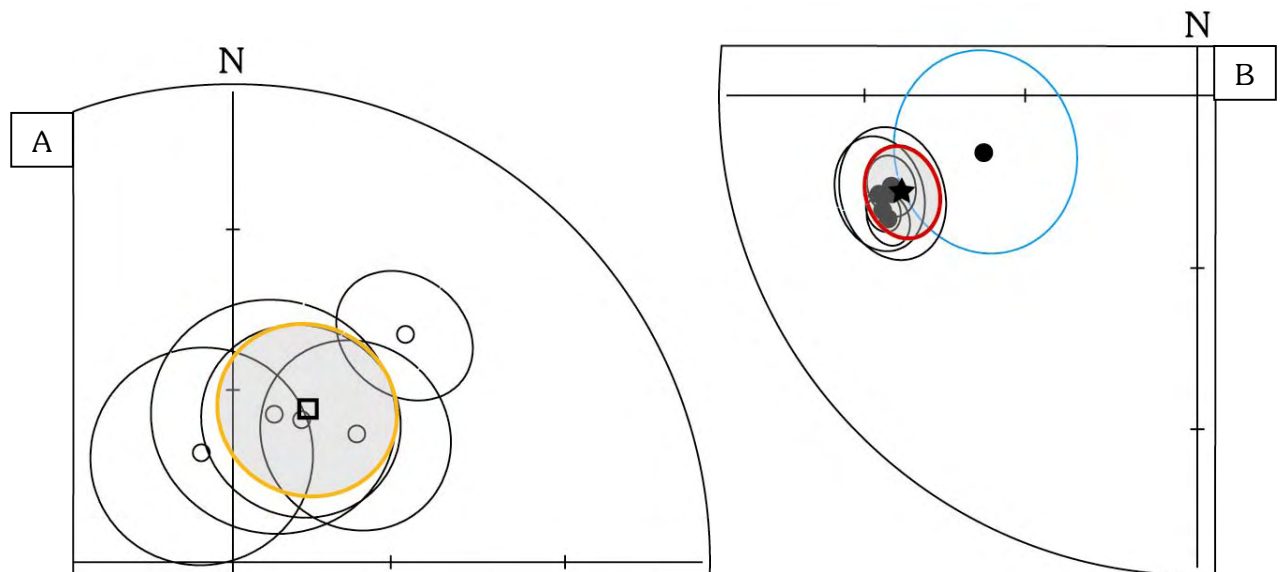
Table 18: Overall mean directions for the locality SHE obtained from single specimen orientations

Name	N	R	D.InS	I.InS	α_{95}	κ	R	D.Bed	I.Bed	α_{95}	κ
<i>Mean direction from single specimen component C_1 obtained at the Sherpherds Hill quarry (locality SHE):</i>											
She- C_1	19	18,5	354,9	-45,1	5,9	33,9	18,5	025,1	-21,5	5,9	33,7
<i>Mean direction from single specimen component C_3 obtained at the Sherpherds Hill quarry (locality SHE):</i>											
She- C_3	12	11,7	273,8	-46,6	8,5	27,2	11,7	007,3	-74,5	8,5	27,2

N: number of samples; α_{95} : cone calculated at the 95% confidence level; κ : precision parameter; **R:** resultant vector; **D.InS/I.InS:** declination/inclination *in situ* (geographic coordinates); **D.Bed/I.Bed:** declination/inclination after bedding correction.



Figures 6.27: Orientation of components obtained from the Ural Volcanics at the Shepherds Hill quarry (locality SHE). **A-** *in situ* and **B-** after bedding correction deduced from AMS, *i.e.* correction consisting in bringing Kmax to the vertical. **Red squares** (and lines, obtained from great circle analysis) are directions of single specimen component C_1 shown *in situ* only with their overall mean direction (**diamond**) and **dark blue** confidence cone (α_{95}); **Black circles** (and lines, obtained from great circle analysis) are directions of single specimen component C_3 shown with their overall mean direction (**triangle**) and **shaded grey** α_{95} . **Open** symbols are negative inclination values (upper hemisphere); **closed** symbols, positive inclination values (lower hemisphere). Schmidt equal area polar projection.



Figures 6.28: Orientation of components obtained from the Ural Volcanics of the small quarry at the Merri Abba Property (locality MER), shown *in situ* only, since it is considered that no bedding is needed.

A- Mid temperature component C_{MT} *in situ*. **Black circles** and associated confidence cones (α_{95}) are site mean directions used to calculate the overall mean direction (**square**) and its α_{95} (shaded grey with **orange** limit).

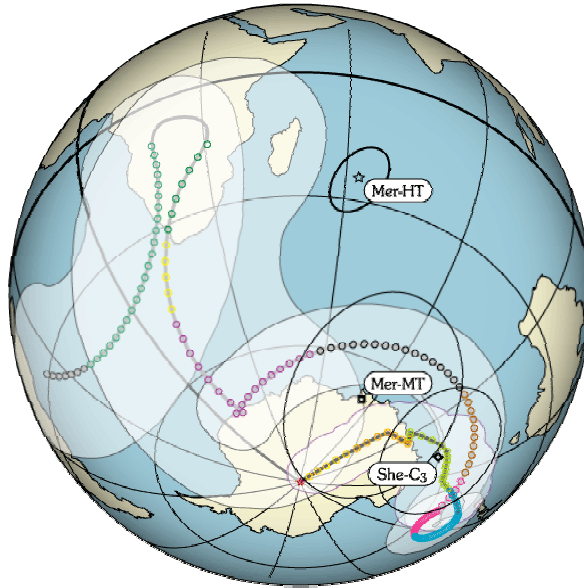
B- High temperature component C_{HT} *in situ*. **Black circles** and associated confidence cones (α_{95}) are site mean directions used to calculate the overall mean direction (**star**) and its α_{95} (shaded grey with **red** limit). The site mean direction with a blue α_{95} corresponds to site Mer-01, and is thought to be affected by weathering.

Open symbols are negative inclination values (upper hemisphere); **closed** symbols, positive inclination values (lower hemisphere). Schmidt equal area polar projection.

Table 20: Corresponding palaeopoles for the Ural Volcanics

B	n	Australian coord.		African coord.		dp	dm
		Plat	PLong	Plat	PLong		
<i>Locality SHE, last components (C_3):</i>							
~	12	-61,7	138,8	-38,5	052,7	14,1	15,5
<i>Locality MER, mid temperature components (C_{MT}):</i>							
5	21	-67,9	084,4	-22,6	032,6	17,5	23,1
<i>Locality MER, high temperature components (C_{HT}):</i>							
6	30	-25,1	062,9	+21,7	039,6	4,7	8,2

N: number of samples; **B**: number of sites; **PLong./Plat.**: palaeopole longitude/latitude in Australian and in African coordinates. **dp/dm** : semi-axis of the ellipse of confidence.

**Figure 6.29:** Corresponding palaeopoles in Australian coordinates. The possible APW path for Australia-Gondwana from the present-day to 570 Ma based on Small Circle Fit is shown for comparison purposes.

Same legend as in figure 2.19-A, Chapter 2 (§.2.7).

Mer-HT is the VGP corresponding to component C_{HT} *in situ*; **Mer-MT**, corresponding to C_{MT} *in situ*; and **She- C_3** , to C_3 after bedding correction, deduced from AMS measurements (Kmax brought to the vertical).

6.5. Conclusions about the Mount Bowen area

6.5.1. Palaeomagnetic results

Palaeomagnetic results from the Mount Bowen area are of poor quality except for the locality MER.

At locality BUL, the E-W shallow direction (C_3) is difficult to interpret, because it resembles to a Palaeozoic orientation due to its shallow inclination, but it seems that the bedding correction does not really improve the grouping. This would imply that it corresponds to a remagnetisation post-dating the folding, which is thought to have taken place in the Early Carboniferous, although there is some isotopic evidence suggesting that the main deformation occurred in the Early Devonian (Glen, 1986). This inclination appears to be too shallow to correspond to post-Early Carboniferous age of magnetisation. Hence, either this results from a mixture of components demagnetised simultaneously, or a tectonic explanation should be found. A third possibility consists in invoking shallowing effects sometimes observed in sedimentary rocks (e.g. Gilder *et al.*, 2003), because the palaeopole obtained after bedding correction from C_3 may correspond to the X-path of Bachtadse & Briden (1991) if a 10°-15° correction is applied on the mean inclination value. However, too few data are available to draw any firm conclusions.

In addition, post-Early Carboniferous large tectonic movement and rotation are quite in contradiction with the fact that a Carboniferous overprint seem to be present at localities SHE and MER, even if block tilting is believed to occurred after this remagnetisation at locality SHE. Nevertheless, it cannot be ruled out that these remagnetisations are Late Cretaceous or even Cainozoic in age, so that it would give no constraint on the tectonic setting during the Carboniferous.

However, even if the secular variation does not seem to be averaged out at locality MER, the VGP obtained plots quite far from any proposed paths, although a cone of 30° drawn around it overlap the X-type APW path published by Bachtadse & Briden (1991) for instance. Although it can be always argued that this VGP has been recorded during an Earth field reversal, the important result from this VGP position is that it does not correspond to the pole from Snowy River Volcanics of equivalent age (Schmidt *et al.*, 1987). This implies that one of the two localities of the Lachlan Orogen, or maybe the two, were rotated after the Early Devonian, which means that the southern Tasmanides are not cratonised in the Early – Mid Palaeozoic.

6.5.2. Regional magnetic fabric

The AMS is of paramount importance in this area to test hypothesis concerning bedding control.

In volcanic rocks studied, the striking feature is the vertical position of the magnetic lineation since the degree of internal strain is generally low. The best explanation found is a tendency of these rocks to vertical extrusion caused by an E-W compression. This direction of the pole to the magnetic foliation is found in most of the area (figure 6.30) and is perpendicular to the main fault trend. It is believed that this magnetic fabric has been acquired because of the shallow (sub-surface) emplacement of these volcanics.

The exception of locality BUL however, showing an E-W direction of magnetic lineation apparently parallel to secondary fold axes, and the post-Late Devonian tilting inferred from locality SHE, witnesses the complex tectonic history of this area.

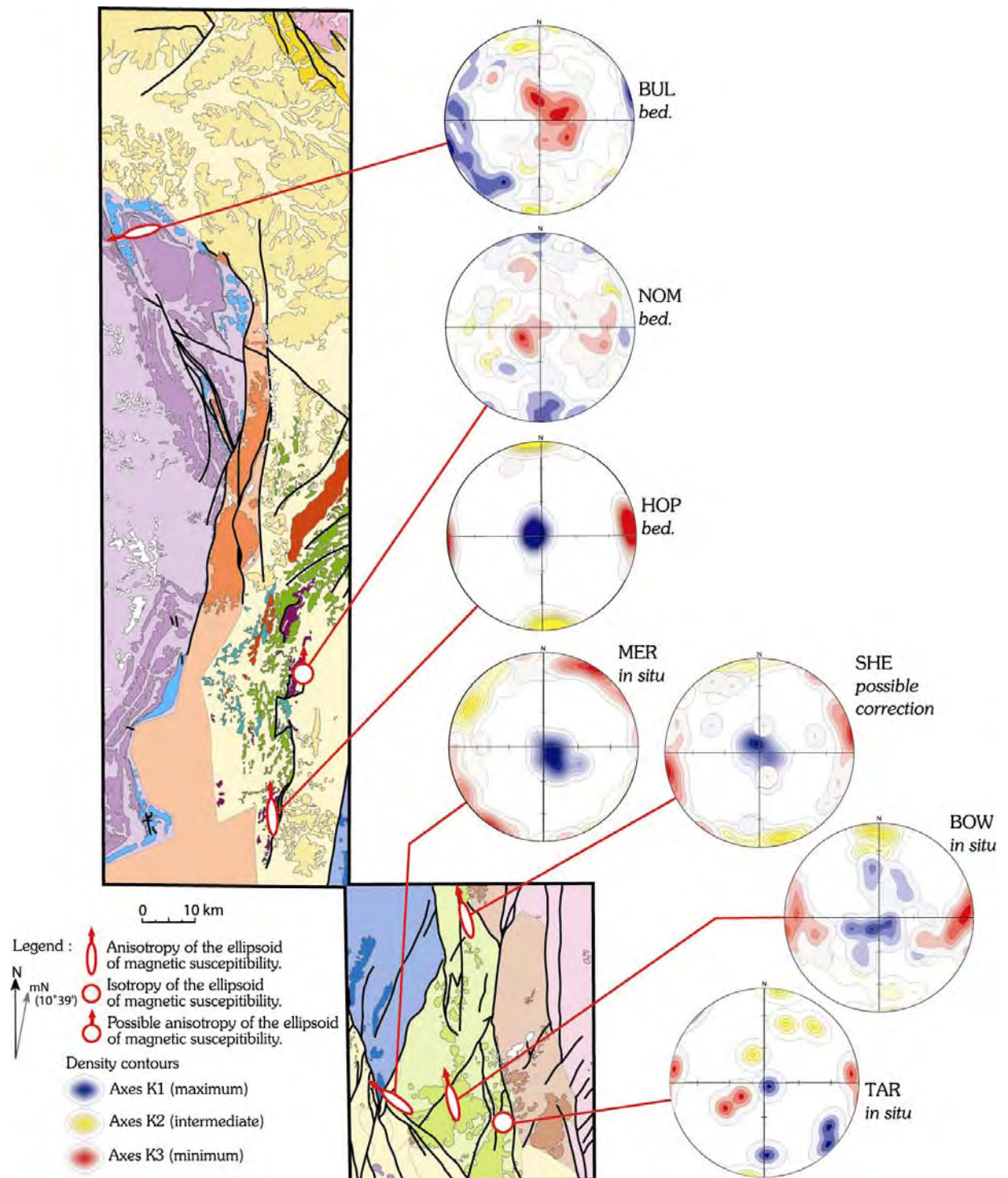


Figure 6.30: Regional magnetic fabric of the Mount Bowen area.

Density contours clearly highlights that magnetic lineation are controlled by fault orientations. Small ellipses indicate the directions of elongation of the ellipsoids of magnetic susceptibility deduced from density contours (Gaussian model, $K=100$). Same simplified geological map as per figure 6.2.

Summary of chapter 6

The Mount Bowen area covers the boundary between the Central and the Western Belt of the Lachlan Orogen, and seven localities were there targeted, among which four belongs to the Early Devonian Ural Volcanics. Nevertheless, only a few are revealed suitable to yield useful palaeomagnetic indications.

The AMS plays an important role in the structural control since it confirms the assumption that the Ural Volcanics from localities BOW and MER do not need bedding correction, whereas block tilting apparently occurred at locality SHE after the beginning of the Carboniferous. These results are also in agreement with the suggestion that these volcanic rocks were emplaced at the sub-surface, because the magnetic fabric is interpreted as representing vertical extrusion caused by a general E-W compression.

Palaeomagnetically, the very silicic rocks from locality BOW yield only scattered results. At locality SHE, only two sites seem to show the existence of a pre-tilting Carboniferous overprint. This would be in agreement with the Carboniferous remagnetisation inferred from component C_{MT} at locality MER. There, the more andesitic lava flow dated by SHRIMP at 413 ± 5 Ma by Meakin *et al.* (2002), shows in addition a clear and systematic component C_{HT} , which carries about 75% of the remanence and shows a sharp decay in intensity between 525° and 550° C. When the first site slightly affected by weathering is discarded, the κ parameter reaches 1172,7 and lead to think that this result is more likely to represent a VGP than a palaeopole. However, even when a 30° cone around this VGP is considered to take secular variations into account, it is clearly distinct from the pole obtained by Schmidt *et al.* (1987) from the Snowy River Volcanics of similar age. This means that one of the two localities at least has been rotated. Further North, the latest Pragian Ambone Volcanics yield very scattered results as well, probably due to relative large grain sizes. Nevertheless, the directions of magnetisation plot in the N-E quadrant of a stereogram with negative inclination values, and this corresponds to what can be expected for Devonian times. Thus, these directions are possibly deviated from a primary magnetisation. At the Bulgoo Property finally (locality BUL), the pink quartz-rich rocks of the Late Pragian Gundaroo Sandstones are probably too weak to yield a stable magnetic signal. In some cases however, a Tertiary overprint carried by pyrrhotite is present. This could correspond to a component largely observed in the Molong area. In three sites, it seems that site mean directions can be calculated for component C_3 but the overall mean direction do not match Late Pragian segments of any published APW path for Gondwana, although the pole "Bul-Bed" is relatively close to the Early Devonian segment of the X-path of Bachtadse & Briden (1991). This mismatch could be due to partially composite directions of magnetisation, as it appears to be the case for components C_2 , or perhaps to shallowing effects sometimes encountered in red beds. In any cases, it is believed that this result is statistically too poor to be reliable.

Chapter 7

Palaeomagnetic results from the Molong area

7.1. Presentation of the Molong area

7.1.1. Sampling coverage

The Molong area focuses on the Northern part of the Eastern Lachlan Orogen, where the Ordovician Volcanics of the Macquarie Arc (dark green zones in figure 7.1) are particularly exposed.

Most of our localities (table 21) are located in this area (figure 7.1). This has several main reasons. First, the landscape is not as flat as to the West, and opportunities are greater to find sufficiently good outcrops for drilling purposes. Secondly, recent new mapping has been undertaken by the Geological Survey of New South Wales in this area, which yields many new results and good age and structural controls on rock targeted. Thirdly, attempt has been made to detect possible differential movements between the three Ordovician belts of the Macquarie Volcanic Arc, which are believed to be pre-Lachlan Orogeny (see below). Unfortunately, the western volcanic belt (the Junee-Naroomine high) is not sufficiently exposed for a correct coverage, and the eastern belt (the Rockley-Gulgong high) has been subject to metamorphism, at least in part, up to actinolite / biotite grade (Barron, 1998). Thus, the greater number of localities comes from the central belt (the Molong high).

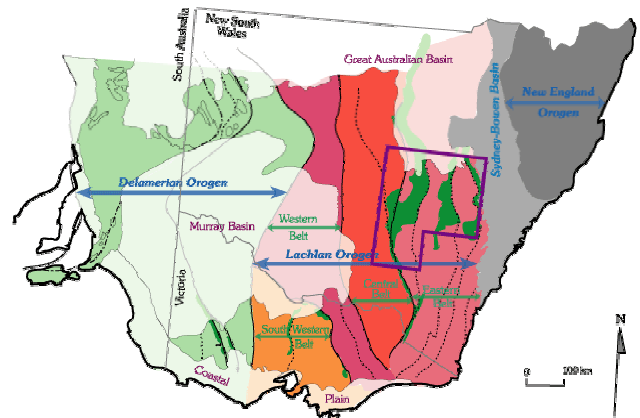


Figure 7.1: Inset recalls the position the Molong area in the Southern Tasmanides as presented on the map of figure 4.7 (Chapter 4). The corresponding simplified geological map is shown in figure 7.2.

Table 21: List of localities in the Molong area

Mnemonics	Names coming from	Location (Long. /lat.)
ANG	Angullong Formation	148,8717 / -33,5933
ASQ	Asqui property	148,8668 / -33,1521
BOG	Bogan Gates	147,7894 / -33,0876
BOO	Little Boonderoo property	148,8819 / -33,6064
CAT	Catombal Group	148,8283 / -33,0075
DUL	Dulladery Volcanics	148,4959 / -33,1936
GAM	Gamboola property	148,8731 / -33,1029
GRE	Grega Group	148,6692 / -33,2396
GRO	Grove property	148,7103 / -33,5094
HER	Hervey Group	148,5638 / -33,3698
KOO-O	Koonoona property (Ordovician volcanics)	148,8734 / -33,5491
KOO-S	Koonoona property (Silurian limestone)	148,8860 / -33,5393

Mnemonics refer to table 1, Chapter 4; §.4.3.

Continues on next page.

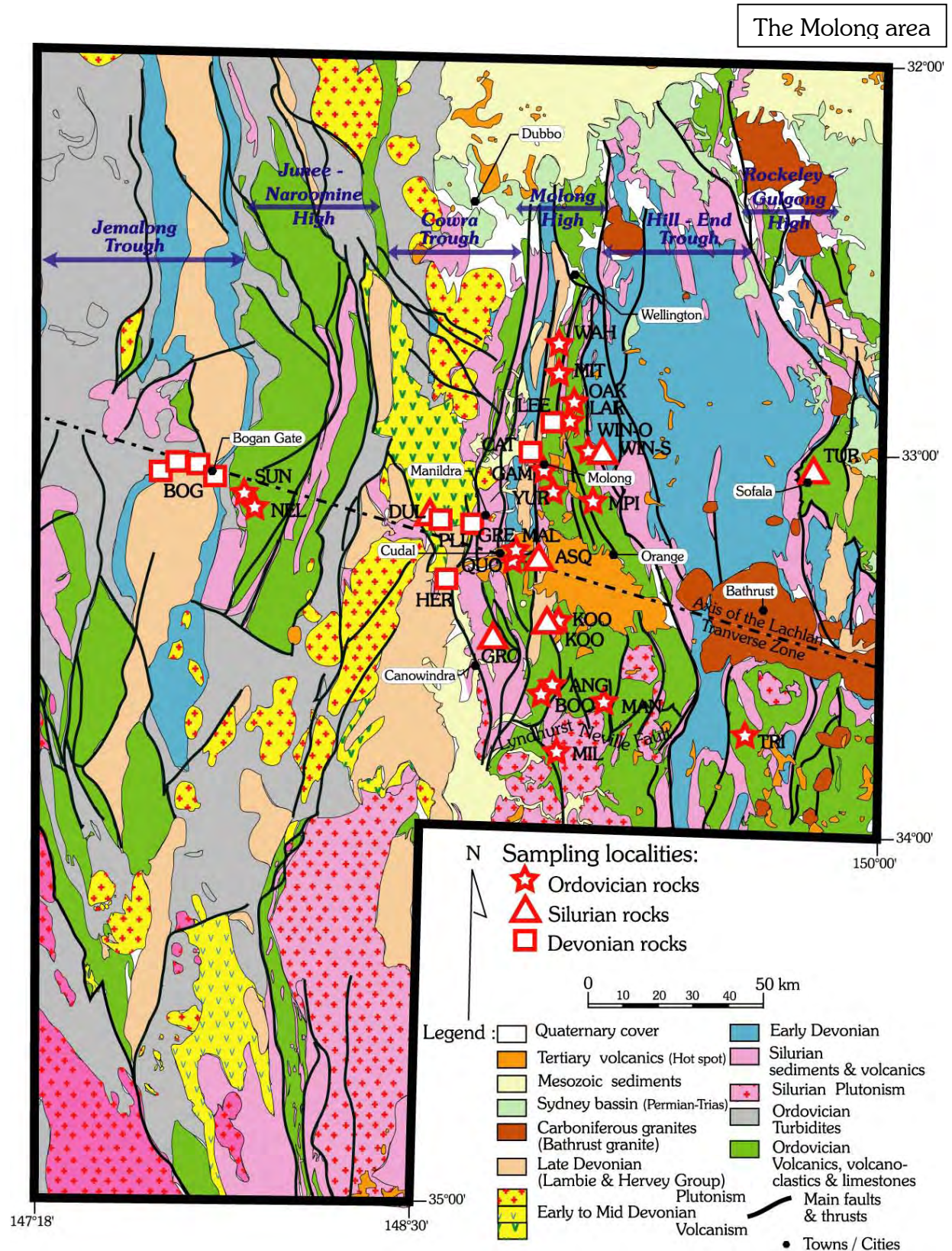


Figure 7.2: Simplified geological map of the Molong area focussing on the Ordovician Macquarie Volcanic Arc (green), showing localities studied (see also table 21). The axis of the Lachlan Transverse Zone of Glen & Wyborn (1997) is also indicated. Map redrawn after the 1:500 000 sytheses maps Central – Eastern New South Wales: 1 – Geology (Glen & Zhang, 2001), published by the Geological Survey of New South Wales, Sydney.

7.1.2. Geological features

The Molong area is classically subdivided in Highs and Troughs, the Ordovician Volcanics of the Macquarie Arc forming the heart of the Highs and Silurian – Devonian sediments filling up the Troughs.

From West to East, they are called the Jemalong Trough, the Junee-Naroomine High, the Cowra Trough, the Molong High, the Hill-End Trough, and the Rockley-Gulgong High. It is not firmly established yet whether these highs form one or more volcanic arcs. Indeed, it has been suggested that these highs are part of a single volcanic arc related to a subduction zone, which would have been folded probably during the Early Devonian (Bowning orogenic event), or that it is the results of hot spot volcanism. Currently however, the prevailing hypothesis is that the

Ordovician Volcanic arc has been split in three during the Silurian (Quidongan orogenic event) caused by extension due to slab roll-back. Extensional structures have been interpreted from seismic profiles (Glen *et al.*, 1998; Glen *et al.*, 2002), although most of them were inverted during the Early Devonian compression (Glen *et al.*, 1999).

Nevertheless, the degree of metamorphism is usually relatively low (prehnite / pumpellyite grade; Barron, 1998), and the general trend of faults, thrusts and fold axes is ~N-S. This is not true, however, for the Rockley-Gulgong High and Hill-End Trough to the East, which have undergone higher grades of metamorphism (biotite / actinolite; Barron, 1998), probably associated with the Early Carboniferous Kanimblan orogenic event. In addition, at smaller scale throughout the Molong area, strong cleavage and complex folding such as conical folds are common. Glen & Wyborn (1997) and Glen & Walsche (1999) argued also that apparent structures, such as the elongation of the Carboniferous Bathrust granitoids intrusions and Tertiary Hot Spot Volcanism, the change in direction of the axis of the Devonian syncline near Manildra or at Bogan Gates, and in particular the abrupt change between the three Ordovician Macquarie Volcanic Arcs to the single Kiandra Volcanic Belt, is due to cross-structures in the Lachlan Orogen. Hence, those authors suggested the existence of the Lachlan Transverse Zone (which axis is shown in figure 7.2). These structures would allow differential movements and/or rotations, and could help explaining curious observations such as the presence of Ordovician turbidites in both fore-arc position (East of the Rockley-Gulgong High) and back-arc position Jemalong Trough and Central Lachlan Orogen, whereas their source is the Delamerian – Ross Orogeny to the West (Fergusson & Tye, 1999; Colquhoun *et al.*, 1999).

Therefore, it is possible that first, these volcanic arcs of the Eastern Lachlan Orogen were far offshore in the Ordovician, and secondly, that they undergone differential movements and/or rotations prior to or during the Lachlan Orogeny. As Ordovician rocks are the oldest exposed in this area and as they may show the largest block movement or rotation, they were believed to be the best target. Unfortunately, sampling was only possible in the Molong High, because the Rockley-Gulgong High is too metamorphosed and the Junee-Naroomine too poorly exposed. It will be shown that the magnetisation and tectonic history is however very complex, such as in particular, the widespread occurrence of a Tertiary overprint carried by pyrrhotite.

Table 21: List of localities; continued...

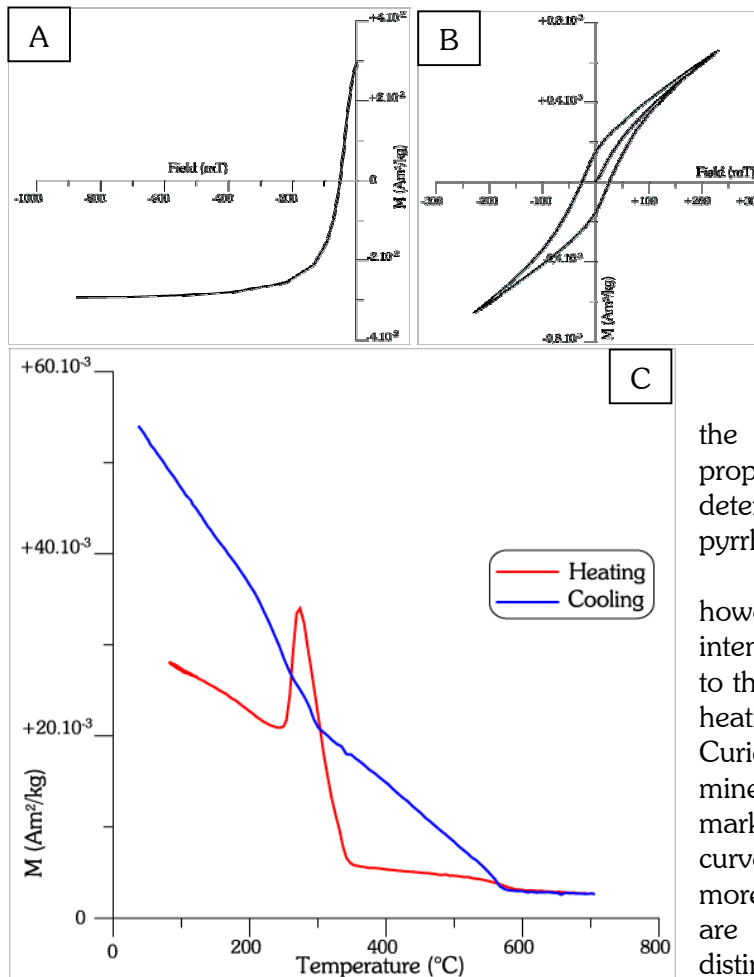
Mnemonics	Names coming from	Location (Long. /lat.)
LAR	Laras Lee property	148,8664 / -33,0005
LEE	Laras Lee property	148,8668 / -33,1521
MAL	Malachi Hill	148,7877 / -33,3036
MIL	Milburn Creek	148,9311 / -33,8342
MIT	Mitchell Formation	148,9136 / -32,7964
MPI	Mitchell – Pillow lavas	148,9161 / -33,1241
NEL	Nelangaloo property	147,9523 / -33,1647
OAK	Oakdale Formation (old*)	148,9029 / -32,9097
PLI	Pli replissé (Hervey group)	148,5134 / -33,2268
QUO	Quondong Quarry	148,7724 / -33,3261
SUN	Sunny Side property	147,9249 / -33,1293
TRI	Triangle Creek Formation	149,5465 / -33,7453
TUR	Turon River	149,7258 / -33,1008
WAH	Wahringa Limestone	148,9084 / -32,7743
WIN-O	Winchester property (Ordovician turbidites)	148,7971 / -33,0514
WIN-S	Winchester property (Silurian limestone)	148,9471 / -33,0418
YUR	Yuranigh Limestone	148,8777 / -33,1295

*Old name, since it is now mapped as the Fairbridge Volcanics.
Mnemonics refer to table 1, Chapter 4; §.4.3.

7.2. The Tertiary Overprint

7.2.1. Presentation and rock magnetism

Most of the localities presented above (figure 7.2; table 21) show a systematic component, called C_p , which can be removed at 300°-320°C. This is close to the Curie temperature of pyrrhotite, and that is why this mineral is favoured as being the magnetic carrier of C_p . Greigite could be another candidate since its Curie temperature is about 330°C (e.g. Dunlop & Özdemir, 1997), but this mineral is believed to be not stable enough through time to carry C_p (Heunemann, *personal communication*). Rock magnetic measurements however, can hardly bring the magnetic carrier of C_p to the fore. The only case where pyrrhotite can be readily seen is at the Grove Property (locality GRO) to the North-West of Canowindra (figures 7.3). Unfortunately, these Silurian shale and siltstones are exposed on the top of a hill, and it seems that they have been struck by lightning. The Königsberger ratio is indeed very high ($Q_K@RT=48,54\pm70,12$) and reaches 247,40 for one specimen. Moreover, these rocks look quite weathered and a penetrative cleavage affects them. This can probably explain why the different palaeomagnetic components obtained are completely randomised, and why the component carried by pyrrhotite does not yield a similar orientation as in the other localities.



Figures 7.3: Example of rock magnetic measurements identifying the presence of pyrrhotite. Early Wenlock Gospel Oak Shale formation of the Grove Property (locality GRO): specimen GRO1-5.

A- Back field curve; **B-** Hysteresis loop; and **C-** IST curve, in red while heating and in blue while cooling ($B=523$ mT).

$H_C=38,88$ mT; $H_{CR}=51,8$ mT.

$M_S=2,1 \cdot 10^{-2}$ Am²/kg; $M_{RS}=1,5 \cdot 10^{-2}$ Am²/kg.

As in many localities, the back field curve and hysteresis properties (figures 7.3-A & B) are not determining in recognising the presence of pyrrhotite.

The IST curve (figure 7.3-C), however, shows here a clear increase in intensity around 270-300°C corresponding to the alteration of sulphide minerals while heating, and a strong decay at 320°C, Curie temperature of pyrrhotite. Sulphide minerals are formed again while cooling as marked by an inflexion in the cooling curve at 300°C. It is being understood that more magnetic mineralogy experiments are needed, in particular to firmly distinguish between pyrrhotite and greigite (see for instance Torii *et al.* 1996).

The IRM curve is not shown here, but it can be mentioned as information that these rocks also carry magnetite (Curie temperature of 580°C visible on the IST curve) and some oxidised mineral, perhaps goethite, as the both IRM and back field curve are not fully saturated and haematite does not seem to be present. The paramagnetic behaviour is relatively strong and probably due to phyllosilicates as one can expect from shale and siltstones.

7.2.2. Palaeomagnetic results

The overall mean directions for component C_p are listed below (table 22) and the regional overall mean direction (figure 7.4-A) is $D.004^\circ/I.-63^\circ$ ($\alpha_{95}=2,6^\circ/\kappa=320,8$; *in situ*). These directions are given *in situ* only since fold tests both at the scale of localities and at regional scale are clearly negative (the classic fold test [McElhinny, 1964] can be positive only below the 0,1% confidence level at regional scale).

This direction is difficult to distinguish from the present-day field (Geographic North), which is $D.000^\circ/I.-52,4^\circ$ for a locality situated at Glat:-33°/GLong:150°. However, the inclination appears to be systematically steeper, and the corresponding palaeopole for C_p at the same locality [150°/-33°] is PLong.136,2°/Plat.-78,0° ($dp=3,2^\circ$; $dm=4,1^\circ$).

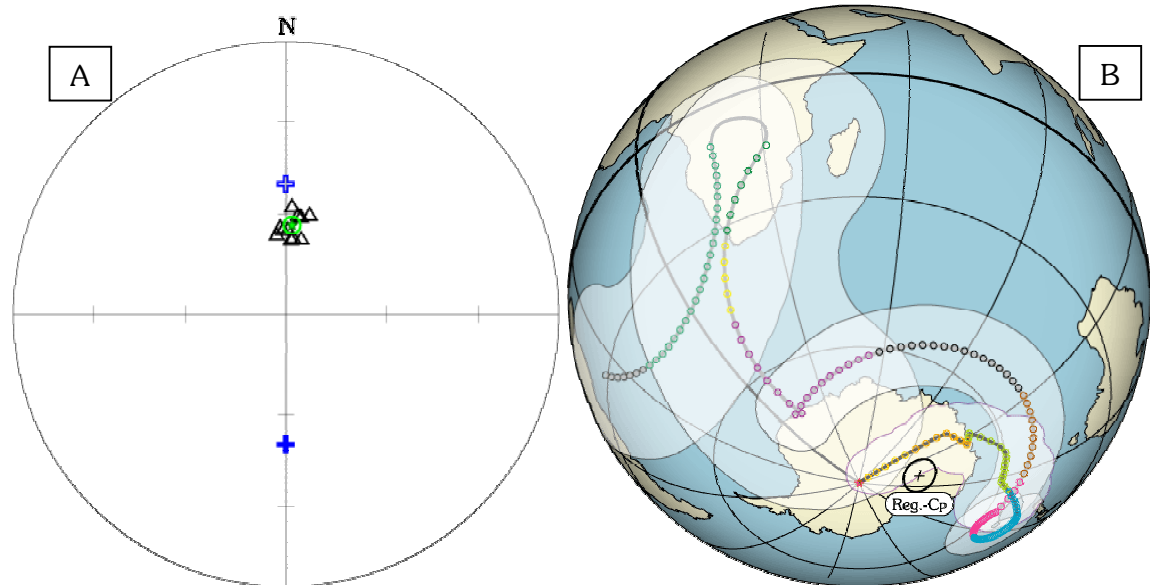
The confidence ellipse intersects almost all ellipses for the Cainozoic, but is compatible only with mean directions ranging from 20 to 35 Ma in age (figure 7.4-B).

Table 22: Overall mean directions per locality obtained for component C_p

Name	N	B	R	D.InS	I.InS	α_{95}	κ	Comments
Locality ASQ	16	3	2,9	338,6	-63,8	30,9	17,0	* too large confidence cone
Locality BOO	56	12	11,9	358,1	-64,2	4,3	101,5	positive reversal test classified C
Locality GAM	32	7	6,8	003,8	-67,1	10,2	35,7	intermediate reversal test
Locality LEE	43	9	8,9	353,5	-65,6	4,3	141,6	
Locality MAL	25	5	4,9	013,2	-58,8	10,3	55,7	intermediate reversal test
Locality MAN	21	4	4,0	006,8	-59,6	5,2	307,4	
Locality MIT	40	6	6,0	003,2	-57,0	3,2	431,2	
Locality NEL	22	6	5,9	008,6	-59,9	7,3	85,6	
Locality OAK	21	4	4,0	011,3	-66,6	10,6	76,4	
Locality QUO	64	14	13,8	001,2	-64,2	5,4	55,6	
Locality KOO	14	3	2,9	004,2	-60,2	20,3	37,9	* too large confidence cone
Locality WAH	25	5	4,9	356,3	-63,4	9,6	64,7	
Locality WIN	41	9	9,0	005,2	-66,6	2,4	471,5	
Regional C_p	420	11	11,0	004,0	-63,1	2,6	320,8	

N: number of samples; **B:** number of sites; **α_{95} :** cone calculated at the 95% confidence level; **κ :** precision parameter; **R:** resultant vector; **D.InS/I.InS:** declination/inclination *in situ* (geographic coordinates).

* when confidence cones are too large (*i.e.* superior to $16,0^\circ$), the mean direction is not used for the calculation of the regional overall mean direction.

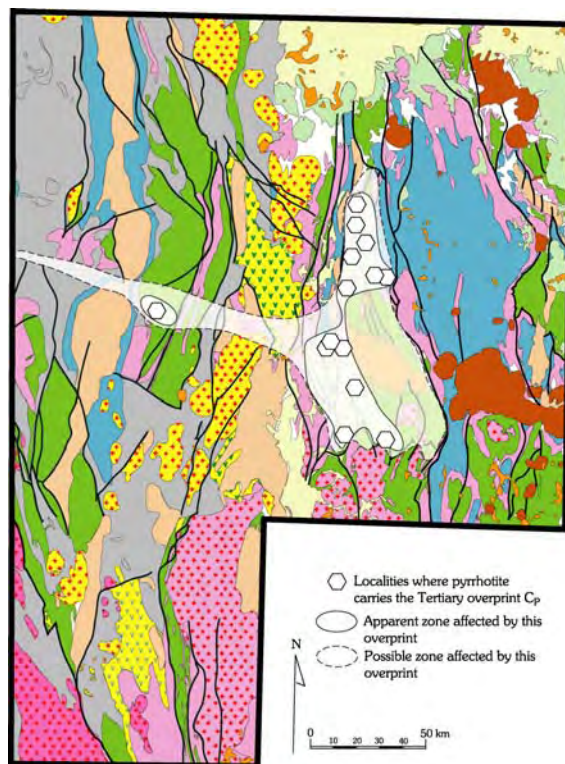


Figures 7.4: **A-** Regional overall mean direction (**green star**) and its associated confidence cone (α_{95} ; **green**) for components C_p carried by pyrrhotite throughout the Molong area. **Triangles** are overall mean direction from localities listed in table 22; **Blue stars** represent the direction of the present-day dipole field. **Open** symbols are negative inclination values (upper hemisphere); **Closed** symbols, positive inclination values (lower hemisphere); Schmidt equal area polar projection. **B-** Corresponding palaeopoles **Reg.- C_p** in Australian coordinates. The possible APW path for Australia-Gondwana from the present-day to 570 Ma based on Small Circle Fit is shown for comparison purposes.

This component C_p is therefore believed to be effectively a Tertiary overprint, probably Oligocene in age. It can be related to the Tertiary Hot Spot Volcanism, which occurred in the Early – Middle Miocene (Pogson & Watkins, 1998). Indeed, it seems that C_p is more obviously present where faults and fracture zones are more important. The nature of the rocks seems also to play a major role since for example, C_p is not observed in the very coherent pillow lavas from the Mitchell Formation (locality MPI). This leads to think that fluid migration containing sulphides and triggered by an increase in thermal gradient could have preceded the magmatic event and could explain the regional extent of this remagnetisation. It must be pointed out also, that C_p seems to have been observed along a fault in the Gundaroo sandstones of the Bulgoo Property (locality BUL) in the Mount Bowen area (Central Lachlan Orogen; see Chapter 6, §.6.2).

The regional extent (figure 7.5) of this remagnetisation is difficult to assess, because the sampling coverage is not uniformly distributed and because C_p is sometimes itself overprinted by the present-day field or some viscous magnetisation. This is the case for example in the Cudgelbar Sandstone Member drilled in the vicinity of Bogan Gates (locality BOG). Nevertheless, the Lachlan Transverse Zone proposed by Glen & Wyborn (1997) and Glen & Walsche (1999) might have played a major role concerning the drainage of such fluids.

Finally, it must be pointed out that if pyrrhotite was purely thermally overprinted, it would imply that denudation in the Molong area exceeded 10 kilometres since the Oligocene with a thermal gradient of 30°/km. If we assume a thermal gradient of 60°/km because of the Hot Spot volcanism, and a magnetisation occurring at 150°C for instance because C_p is thought to result from a thermo-chemical overprint, a denudation of 2,5 kilometres is still needed. This is in good agreement with the kilometre-scale denudation claimed by O'Sullivan *et al.* (2000-b).



Figures 7.5: Possible regional extent of the occurrence of components C_p carried by pyrrhotite (**hexagons**). The white zone with **solid line** represent the area, which appears to have pyrrhotite, even if this last does not necessarily show C_p such as in locality GRO (see text). White zone with **dashed line** is a possible zone affected by the postulated fluids containing sulphides. It can be then controlled by structural boundaries and perhaps in particular by the Lachlan Transverse Zone of Glen & Wyborn (1997) and Glen & Walsche (1999), since C_p seems to have been found also to the West, in the Central Lachlan Orogen.

7.3. The Ordovician Oakdale Formation (WIN-O) and the Silurian Nandillyan Formation (WIN-S) from the Winchester Property (WIN)

7.3.1. Presentation

Two localities will be treated together here. At the Winchester property, in the north-east of Molong (figure 7.2), the Silurian limestone of the Nandillyan Formation (locality WIN-S) overlies unconformably the Ordovician turbidites of the Oakdale Formation (locality WIN-O). It is then interesting to compare the two magnetic signatures.

The Ordovician turbidites there consist of quartz-rich sandstones of red-bed character. They range in age from Eastonian to Bolindian (Late Ordovician. Pogson & Watkins, 1998;

Percival, *personal communication*, 2000). They are folded and the bedding is sub-vertical where sampling has been carried out.

The overlying Silurian rocks (photo 14) belong to the Nandillyan Limestone. These 30 to 50 cm thick beds have been deposited with an angular unconformity after the Early Silurian gap of sedimentation of the Molong area. This limestone is dark grey, quite fossiliferous and rich in organic matter. Its age is early Early Wenlock to basal Ludlow (Pogson & Watkins, 1998; Percival, *personal communication*, 2000).

Five sites (25 cores) have been drilled in the Ordovician turbidites and five others (25 cores as well) in the overlying Silurian Limestone.

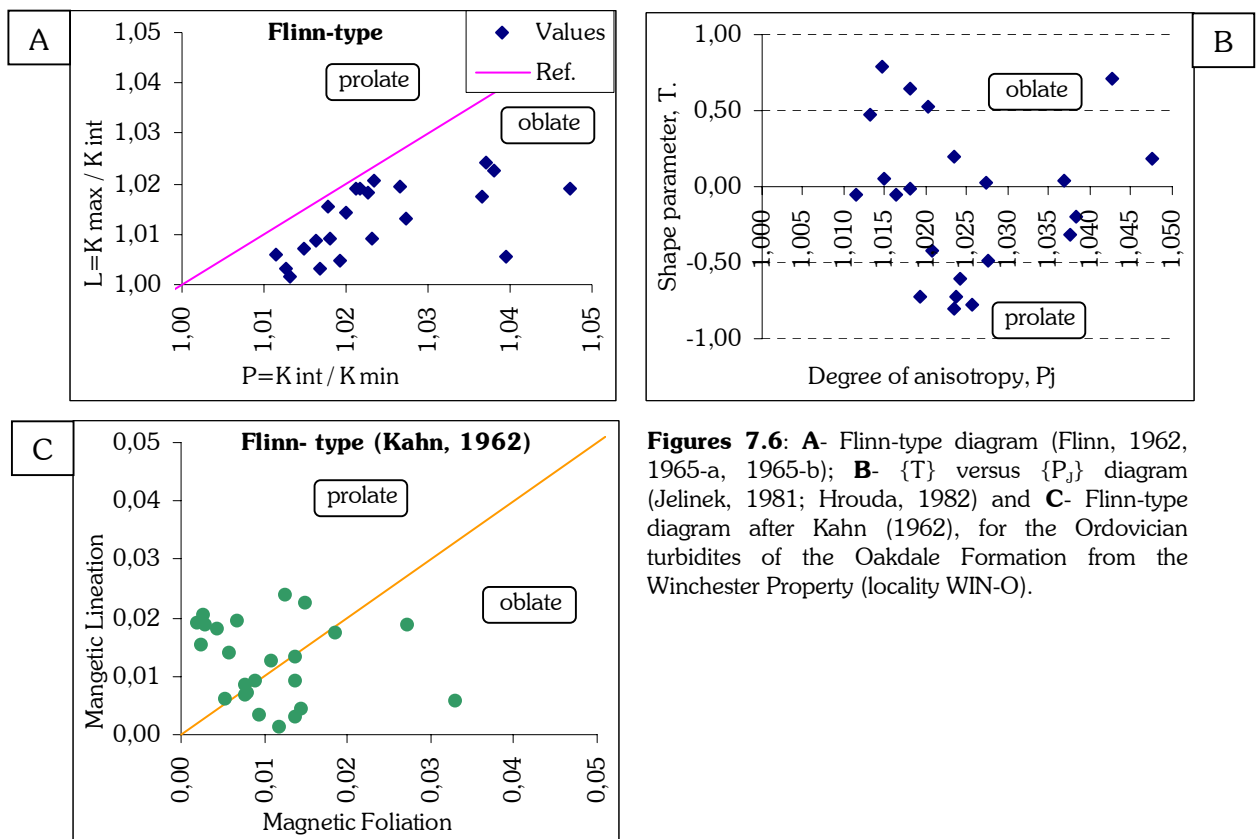


Photo 14: Kangaroos (tiny points above the outcrop in the middle of the picture) hopping over the Silurian Nandillyan Limestones of the Winchester Property (locality WIN-S).

7.3.2. Anisotropy of magnetic susceptibility (AMS)

- AMS parameters in the Ordovician turbidites of the Oakdale Formation (WIN-O)

The degree of anisotropy in these rocks is very weak ($P_j = 1,02 \pm 0,01$) and the magnetic fabric is close to isotropy as the shape of the ellipsoid of magnetic susceptibility cannot be well determined. The $\{T\}$ parameter (figure 7.6-B) tends to show a slight tendency for a prolate shape of the ellipsoid of magnetic susceptibility but the uncertainty around the mean value is relatively large ($T = -0,07 \pm 0,50$). In this condition, the Flinn-type diagram looks not appropriate.

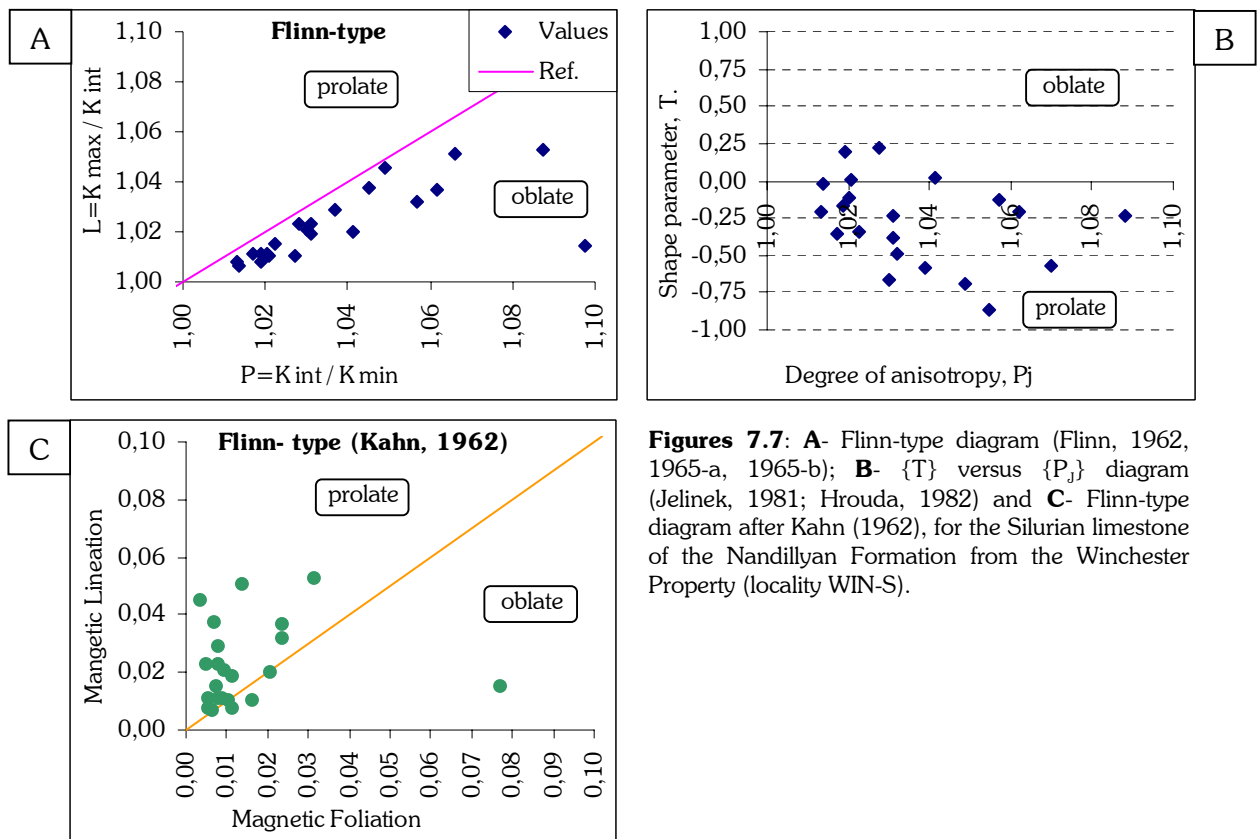


Figures 7.6: **A-** Flinn-type diagram (Flinn, 1962, 1965-a, 1965-b); **B-** $\{T\}$ versus $\{P_j\}$ diagram (Jelinek, 1981; Hrouda, 1982) and **C-** Flinn-type diagram after Kahn (1962), for the Ordovician turbidites of the Oakdale Formation from the Winchester Property (locality WIN-O).

Indeed, the Flinn-type diagram (figure 7.6-A) expresses an oblate shape but the alternative Flinn-type diagram proposed by Kahn (1962) is probably more relevant (figure 7.6-C) for such low values. The mean value plots in the prolate side, although the error bars cover both sides of the diagram ($\text{Lineation}=0,013\pm0,007$; $\text{Foliation}=0,011\pm0,008$). In conclusion, the ellipsoid of magnetic susceptibility is close to a sphere and the magnetic fabric can be regarded as almost isotropic.

- AMS parameters in the Silurian limestone of the Nandillyan Formation (WIN-S)

Not surprisingly, the situation is very similar in the overlying limestone. The degree of anisotropy is very low ($P_j=1,04\pm0,02$) and the ellipsoid of magnetic susceptibility is close to a sphere ($T=-0,23\pm0,35$) although a prolate shape arises (figure 7.7-B). The shape is also not correctly expressed by the Flinn-type diagram from Flinn (figure 7.7-A), but this tendency is confirmed by the Flinn-type diagram of Kahn (1962) with a mean value plotting perhaps more clearly in the prolate side of the diagram (figure 7.7-C) than observed in the Ordovician turbidites ($\text{Lineation}=0,023\pm0,014$; $\text{Foliation}=0,015\pm0,016$).



Figures 7.7: **A-** Flinn-type diagram (Flinn, 1962, 1965-a, 1965-b); **B-** $\{T\}$ versus $\{P_j\}$ diagram (Jelinek, 1981; Hrouda, 1982) and **C-** Flinn-type diagram after Kahn (1962), for the Silurian limestone of the Nandillyan Formation from the Winchester Property (locality WIN-S).

- AMS parameters for the locality WIN

Although the folding is important with bedding orientations close to the vertical and the locality WIN is situated near the fault that separates the Molong High from the Hill-End Trough, which is believed to be relatively highly metamorphosed (up to biotite / actinolite in some places according to Barron, 1998), the magnetic fabric is nearly isotropic and the degree of internal strain negligible. The Königsberger ratios are moderate, meaning that the size of the magnetic particles can be relatively small, and in particular that lightning effects are absent ($Q_K@RT=1,54\pm1,48$ for the Ordovician turbidites of locality WIN-O; $Q_K@RT=1,23\pm0,90$ for the Silurian limestone of locality WIN-S).

- Directions of the principal axes of magnetic susceptibility (WIN)

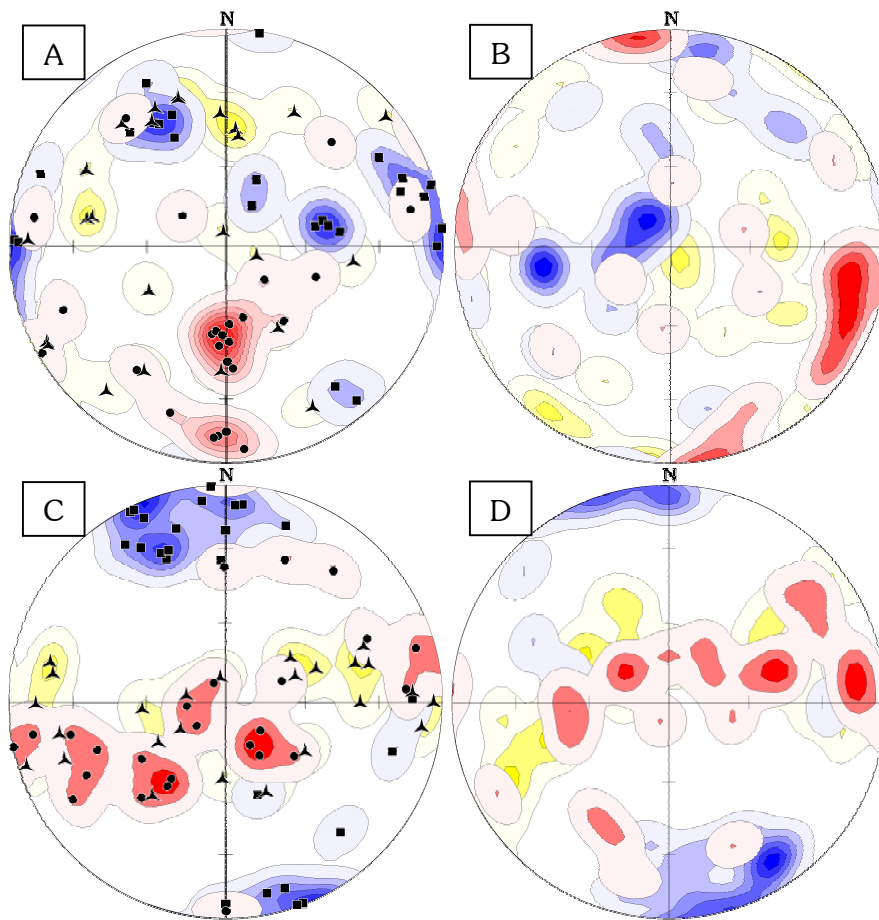


Figure 7.8: Orientations of the principal axes of magnetic susceptibility for the Ordovician turbidites of the Oakdale Formation (A & B; WIN-O), and for the Silurian limestone of the Nandillyan Formation (C & D; WIN-S).

A- *in situ*, and **B-** after bedding correction; locality WIN-O.

C- *in situ*, and **D-** after bedding correction; locality WIN-S.

Same legend as in figure 5.4 (Chapter 5; §.5.2.2); i.e. Kmax, squares (blue); Kint, triangles (yellow); Kmin, dots (red).

The magnetic fabrics are in any cases different in the turbidites and the limestone (figures 7.8), and are relatively well marked given the very low degree of anisotropy. It is very likely that this difference stems from the petrography, since the Ordovician quartz-rich sandstone is much harder than the Silurian limestone.

In the turbidites, the principal directions are very scattered, as one can expect given the nearly spherical shape of the ellipsoid of magnetic susceptibility. However, the density contours are here very helpful to highlight that the directions appear to be oblique *in situ* (figure 7.8-A). Kmax, Kint and Kmin are better positioned on vertical and horizontal plans after bedding correction. This indicates that the magnetic fabric was probably acquired prior to folding, which is quite in agreement with the very low degree of anisotropy in these rocks. The poles to the magnetic foliation (Kmin) however, are sub-horizontal and the magnetic lineation (Kmax), sub-vertical (figure 7.8-B). This cannot be caused by a relatively high level of compression given the degree of anisotropy even if such fabric are generally found in strongly deformed rocks, but the same problem has been encountered in the Ural Volcanics of the Mount Bowen area (Chapter 6; §.6.4). These silicic turbidites here, possibly silicified, are probably very coherent rocks, which may behave in a similar way to the dacite – rhyolites of the Ural Volcanics. A plausible explanation is therefore that this fabric expresses as well a vertical extrusion, in response to a horizontal stress. This would imply that the original magnetic fabric was close to isotropy and a sedimentary magnetic fabric has not been recorded. This is possible if diagenesis, and possibly silification, occurred soon after deposition. It implies also that these rocks were relatively close to the surface when compression happened. It seems also that there are two clusters of Kmin, one E-W and a second N-S. As only an E-W direction of Kmin is visible in the Silurian limestone (figures 7.8-C & D), it can be suggested that a N-S direction of strain affected the turbidites prior to the deposition of the limestone, say between the Bolindian (late Late Ordovician) and the Early Wenlock (late

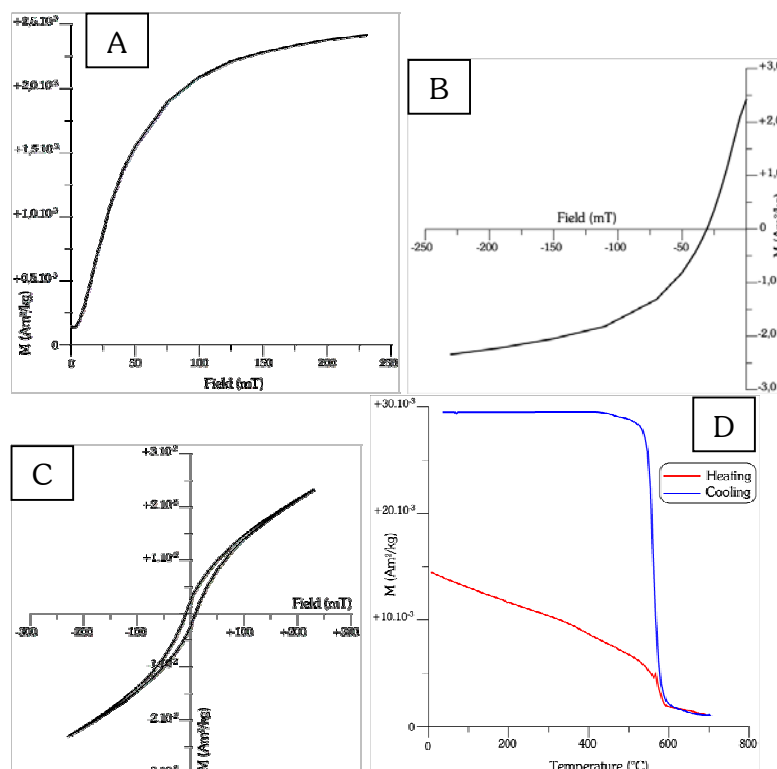
Early Silurian). Nevertheless, it cannot be excluded that the N-S direction is posterior to the E-W direction and that it has not been recorded in the limestone because it was not strong enough to overprint the previous magnetic fabric. In this case however, it would be expected that the magnetic lineation in the limestone be more deviated.

As the Silurian limestone unconformably overlies the turbidites, it is hardly conceivable that the limestone recorded a post-folding magnetic fabric whereas the turbidites kept its pre-folding one. In any cases, the interpretations would not be fundamentally changed, as the directions are analogous *in situ* and after bedding correction (figures 7.8-C & D). K_{min} are distributed along an E-W sub-vertical plan, whereas K_{max} are relatively well clustered in a N-S direction. This is very coherent with the prolate shape of the ellipsoid of magnetic susceptibility deduced from AMS parameters. It is probably the result of an intermediate magnetic fabric where the sedimentary magnetic fabric with a vertical K_{min} is overprinted by a tectonic magnetic fabric, which tends to bring K_{min} to the horizontal plan. It witnesses therefore an E-W direction of strain. The magnetic lineation is aligned with the fold axis (that is why the bedding correction does not change its direction), and it is very likely that the fold result from this E-W compression.

7.3.3. Rock magnetism

- Ordovician turbidites of the Oakdale Formation (WIN-O)

The predominant magnetic carrier seems to be magnetite as illustrated by the relatively low coercivity on the back field curve (figure 7.9-B) and in particular by the marked decay in intensity by 580°C on the IST curve while heating (figure 7.9-D). The slope of the hysteresis loop as well as the quite constant decay on the IST curve while heating, show the important contribution of paramagnetic minerals. They may be at the origin of the new formation of magnetite while cooling (figure 7.9-D). The IRM and back field curves are not saturated (figures 7.9-A & B) and a slight inflexion seems to exist on the IST curve around 680°C. Haematite appears therefore to be present, but probably in little quantity, as it is not well marked on the IST curve and has no apparent influence on the hysteresis loop. It will be shown below that pyrrhotite is also present in these rocks but rock magnetic measurements do not yield any indication of its existence.



Figures 7.9: Example of rock magnetic measurements from the Ordovician turbidites of the Oakdale Formation at the Winchester Property (locality WIN-O): specimen WIN4-3.

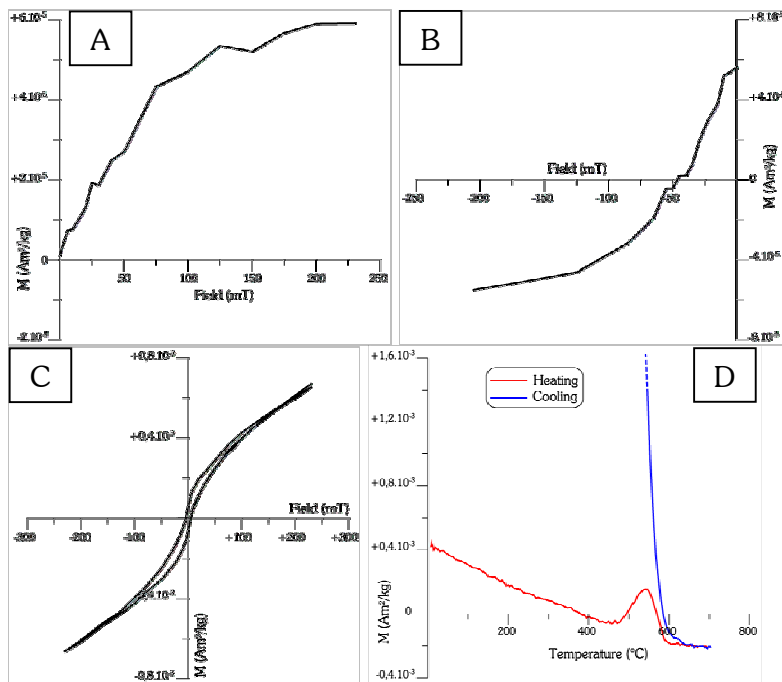
A- IRM curve; **B-** Back field curve (coercivity); **C-** Hysteresis loop; and **D-** IST curve, in red while heating and in blue while cooling ($B=100$ mT).

$H_C=11,66$ mT; $H_{CR}=30,75$ mT.

$M_S=8,8 \cdot 10^{-3}$ Am²/kg; $M_{RS}=2,4 \cdot 10^{-3}$ Am²/kg.

- Silurian limestone of the Nandillyan Formation (WIN-S)

The IRM and back field curves (figures 7.10-A & B) are a bit noisy but it can be seen that two minerals seem to be predominant, a relatively low coercivity one and a higher coercivity one which leads to not fully saturated curves. This duality is confirmed by the wasp-wasted shape of the hysteresis loop (figure 7.10-C). These measurements, however, do not allow determining further the nature of these minerals. The IST curve shows clearly the formation of new magnetite while heating and in particular when cooling (figure 7.10-D), but the original mineralogy remains unclear. Palaeomagnetic investigations using thermal demagnetisation better indicate that these two phases are probably magnetite and haematite. The presence of pyrrhotite is also inferred from palaeomagnetism but is not visible on these curves. Nevertheless, the paramagnetic contribution is obvious from the slope of the hysteresis loop and the quite linear decay in intensity of the IST curve while cooling.



Figures 7.10: Example of rock magnetic measurements from the Silurian limestone of the Nandillyan Formation at the Winchester Property (locality WIN-S): specimen WIN7-5.

A- IRM curve; **B-** Back field curve (coercivity); **C-** Hysteresis loop; and **D-** IST curve, in red while heating and in blue while cooling, being cut to zoom on features of the heating curve ($B=100$ mT).

$H_C=5,27$ mT; $H_{CR}=46,46$ mT.

$M_S=2,3 \cdot 10^{-4}$ Am²/kg; $M_{RS}=6,1 \cdot 10^{-5}$ Am²/kg.

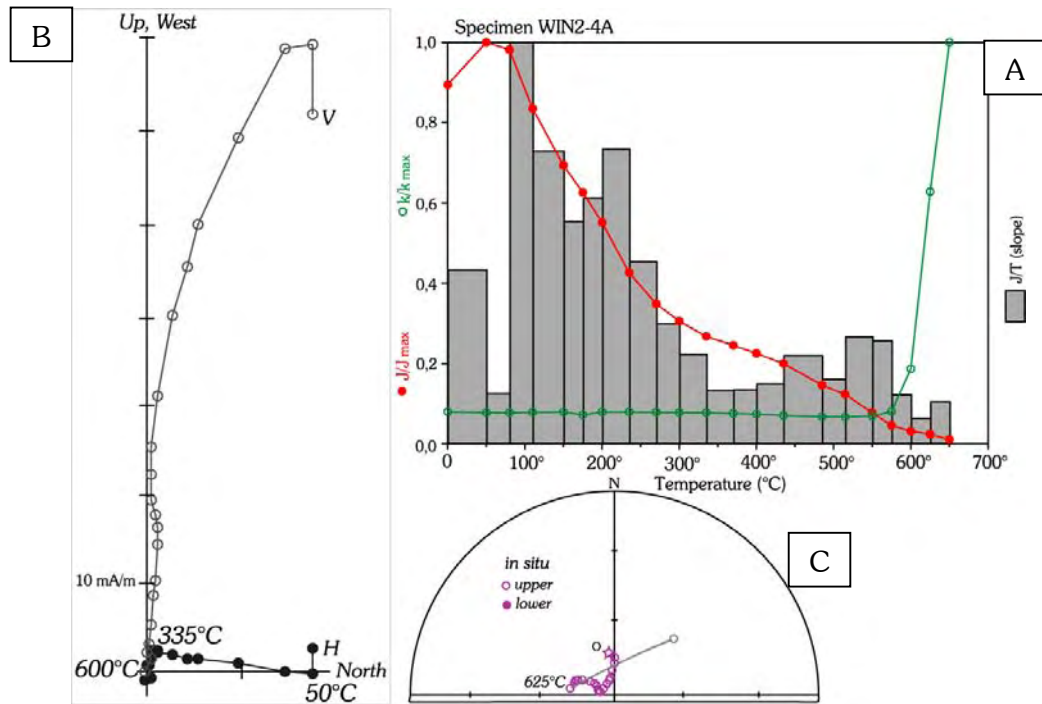
7.3.4. Palaeomagnetic results

- Demagnetisation of the Ordovician turbidites (WIN-O)

A drilling-induced or viscous magnetisation is easily removed at 50°C, and two components can be subsequently determined (figures 7.11). A lower temperature component C_p is demagnetised up to 300°C. The second, component C_{HT-O} is identified from 335°C to about 600°C. The demagnetisation curve (figure 7.11-A) shows that this component seems to be fully demagnetised at around 650°C, which means that some haematite can carry it but the main magnetic carrier of C_{HT-O} is magnetite with an unblocking temperature around 575°C. The susceptibility is very stable up to 575°C and increases suddenly from this temperature. It witnesses then mineralogical changes and it is also possible that haematite stems from this alteration.

- Demagnetisation of the Silurian limestone (WIN-S)

The magnetic behaviour while demagnetising is analogous with two main components (figures 7.12). C_p removed from 50° – 80°C to ~310°C, and C_{HT-S} from ~310°C to ~530°C. In this case however, C_p carries almost entirely the NRM, and C_{HT-S} corresponds only to 2,6% of the remanence at 385°C ($NRM@385^\circ C=5,29 \cdot 10^{-2}$ mA/m). It is so weak that it can be often seen that C_p does not point really to the origin but the identification of C_{HT} is very difficult, even using a great circle analysis. C_{HT-S} is actually defined with difficulty in two sites only.



Figures 7.11: Example of palaeomagnetic results obtained by thermal demagnetisation from the Ordovician turbidites of the Oakdale Formation at the Winchester Property (locality WIN-O).

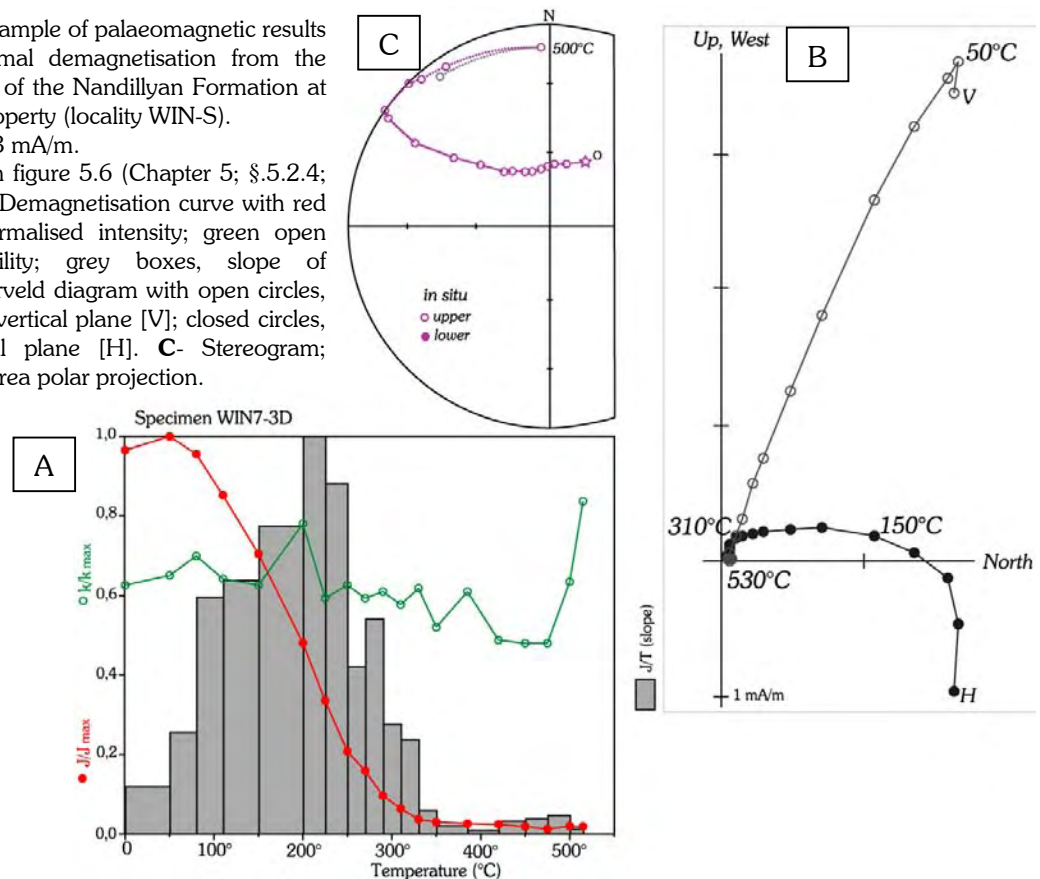
$\text{NRM}@50^\circ\text{C}=7,11 \cdot 10^{-1} \text{ mA/m}$.

Same legend as in figure 5.6 (Chapter 5; §.5.2.4; all *in situ*); i.e. **A**- Demagnetisation curve with red closed circles, normalised intensity; green open circles, susceptibility; grey boxes, slope of intensity. **B**- Zijderveld diagram with open circles, projection on the vertical plane [V]; closed circles, on the horizontal plane [H]. **C**- Stereogram; “Schmidt” equal area polar projection.

Figures 7.12: Example of palaeomagnetic results obtained by thermal demagnetisation from the Silurian limestone of the Nandillyan Formation at the Winchester Property (locality WIN-S).

$\text{NRM}@50^\circ\text{C}=2,03 \text{ mA/m}$.

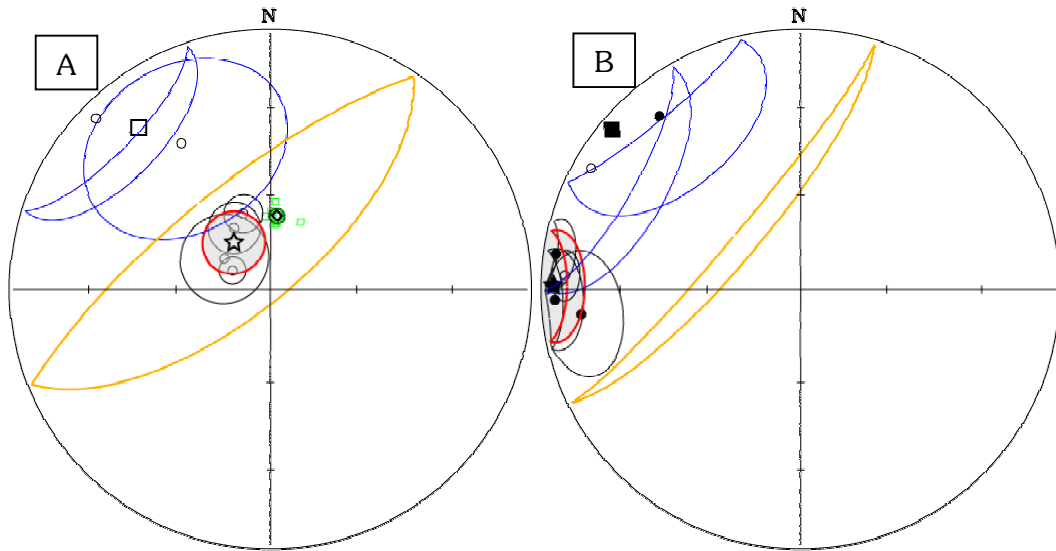
Same legend as in figure 5.6 (Chapter 5; §.5.2.4; all *in situ*); i.e. **A**- Demagnetisation curve with red closed circles, normalised intensity; green open circles, susceptibility; grey boxes, slope of intensity. **B**- Zijderveld diagram with open circles, projection on the vertical plane [V]; closed circles, on the horizontal plane [H]. **C**- Stereogram; “Schmidt” equal area polar projection.



- Interpretation for the Ordovician and Silurian rocks (WIN)

Components C_p , revealed in both localities (WIN-O & WIN-S), correspond very well with the Tertiary overprint presented above (§.7.2). The overall mean direction (figure 7.13-A; table 23) obtained from site means of both localities is $D.005^\circ/I.-67^\circ$ ($\alpha_{95}=2,4^\circ/\kappa=477,5$) *in situ*, and it is apparently carried by pyrrhotite as the unblocking temperature is close to 320°C , the Curie temperature of pyrrhotite.

Concerning components C_{HT-O} & C_{HT-S} , they appear to be carried in both cases by magnetite, but the overall mean directions in the turbidites is steep *in situ* and E-W very shallow after bedding correction, which looks different from the nearly constant NW shallow direction in the limestone in the two coordinate systems (figures 7.13; table 23). The overall mean direction of the turbidites *in situ* is compatible with directions of magnetisation ranging from Triassic to Early Cretaceous in age as it is $D.322^\circ/I.-71^\circ$ ($\alpha_{95}=9,9^\circ/\kappa=87,5$). The bedding correction worsens the κ parameter as it leads to $D.276^\circ/I.+03^\circ$ ($\alpha_{95}=11,0^\circ/\kappa=70,1$) but this change is considered not significant as the classic fold test becomes positive at the 39,5% confidence level. Nevertheless, given this κ -ratio ($=0,8$) and the fact that the direction of magnetisation after bedding correction does not resemble to any expected for Gondwana, the *in situ* mean direction corresponding to C_{HT-O} is more likely to represent an Early Mesozoic remagnetisation. How then this overprint can be recorded in the turbidites but not in the limestone? This paradox can be explained if it is assumed that the remagnetisation is localised along fault/thrust, because the locality WIN-O is geographically closer to the boundary between the Molong High and the Hill-End Trough. Moreover, C_{HT-S} is poorly defined and probably not well isolated from C_p , but it can be partially affected by an Early Mesozoic remagnetisation as well. The scattering obtained could result then from a mixture between an undetermined pre- or post-folding NW shallow direction and the Early Mesozoic overprint.



Figures 7.13: Direction of components obtained from the Ordovician turbidites and the Silurian limestone at the Winchester Property (locality WIN), **A-** *in situ* and **B-** after bedding correction.

Green squares are site mean directions for C_p shown *in situ* only with their overall mean direction (**diamond**) and **dark green** confidence cone (α_{95}); **Black circles** are site mean directions C_{HT} shown with **black** α_{95} for C_{HT-O} and **blue** α_{95} for the two C_{HT-S} . Their respective overall mean directions (**star** for C_{HT-O} & **square** for C_{HT-S}) and associated α_{95} (**shaded red** for C_{HT-O} & **orange** for C_{HT-S}) are shown on the same stereograms for comparison purposes.

Open symbols are negative inclination values (upper hemisphere); **closed** symbols, positive inclination values (lower hemisphere). Schmidt equal area polar projection.

Table 23: Site mean directions and overall mean directions for the locality WIN

Name	N	R	D.InS	I.InS	α_{95}	κ	R	D.Bed	I.Bed	α_{95}	κ	DipDir	Dip
Component C_{HT-O} per site:													
WinO-01	2	2,0	303,7	-72,4	14,0	319,2	2,0	263,5	+14,7	16,0	247,2	090,7	86,0
WinO-02	4	4,0	296,6	-76,7	4,3	464,6	4,0	267,6	+04,2	11,9	60,8	081,9	84,4
WinO-04	4	4,0	340,3	-64,4	6,1	231,1	4,0	273,4	-08,4	6,1	231,1	067,5	82,0
WinO-05	2	2,0	329,3	-67,3	8,2	937,9	2,0	278,2	+03,7	8,2	937,9	078,9	85,2
Component C_{HT-S} per site:													
WinS-07	5	4,6	314,5	-05,6	27,3	9,2	4,6	320,7	+13,7	29,1	8,2	059,6	79,6
WinS-10	5	4,8	328,7	-33,8	30,3	10,6	4,8	299,9	-06,0	30,7	10,3	063,8	71,6
Name	B	N	R	D.InS	I.InS	α_{95}	κ	R	D.Bed	I.Bed	α_{95}	κ	
Mean direction for the component C_p :													
WIN- C_p	9	41	9,0	005,2	-66,6	2,4	471,5	8,7	272,0	-21,2	9,9	27,8	
Mean direction for the component C_{HT-O} :													
WIN- C_{HT-O}	4	10	4,0	321,6	-71,0	9,9	87,5	4,0	275,8	+02,7	11,0	70,1	
Mean direction for the component C_{HT-S} :													
WIN- C_{HT-S}	2	10	1,9	321,0	-19,8	73,9	13,6	1,9	310,5	+03,9	67,3	16,0	

N: number of samples; **B:** number of sites; α_{95} : cone calculated at the 95% confidence level; κ : precision parameter; **R:** resultant vector; **D.InS/I.InS:** declination/inclination *in situ* (geographic coordinates); **D.Bed/I.Bed:** declination/inclination after bedding correction; **DipDir/Dip:** Direction of dip and dip for the bedding.

However, it is being understood that these results cannot be considered as a significantly reliable given the number of samples (10 only in each localities) and in particular the size of the confidence cone for the locality WIN-S, but it witnesses at least that an Early Mesozoic magnetic event may have occurred. The corresponding palaeopole for WIN- C_{HT-O} *in situ* is PLong.187,0°/Plat.-55,3° (dp=15,0°; dm=17,2°), but it is interesting to see that the confidence ellipse in Australian coordinates is smaller for the palaeopole calculated from C_{HT-O} after bedding correction (figure 7.14; table 24). Results from locality WIN-S are shown for indication but are not considered further.

Table 24: Palaeopoles obtained from the locality WIN

B	N	Australian coord.		African coord.		dp	dm	Coordinates system
		Plat	PLong	Plat	PLong			
Locality WIN-S, components C_{HT-S} :								
2	10	-47,5	262,4	-57,7	315,2	40,4	77,3	from <i>in situ</i> orientation
2	10	+31,7	085,7	+51,4	109,5	33,8	67,4	after bedding correction
Locality WIN-O, components C_{HT-O} :								
4	10	-55,3	187,0	-63,7	058,4	15,0	17,2	from <i>in situ</i> orientation
4	10	+04,1	063,1	+48,4	054,4	5,5	11,0	after bedding correction

N: number of samples; **B**: number of sites; **PLong./Plat.**: palaeopole longitude/latitude in Australian and in African coordinates. **dp/dm** : semi-axis of the ellipse of confidence.

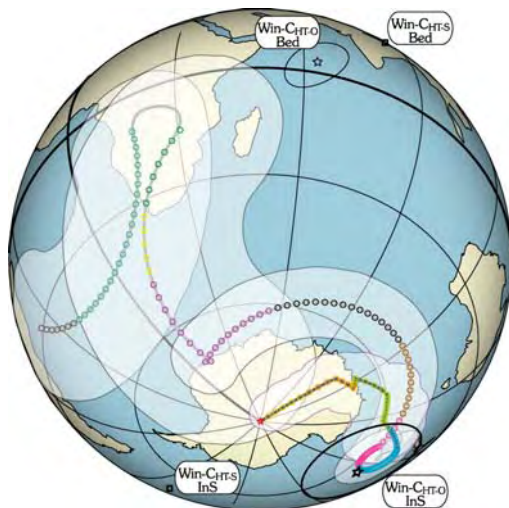


Figure 7.14: Corresponding palaeopoles in Australian coordinates. The possible APW path for Australia-Gondwana from the present-day to 570 Ma based on Small Circle Fit is shown for comparison purposes. Same legend as in figure 2.19-A, Chapter 2 (§.2.7).

Win- C_{HT-O} InS is the palaeopole (star) corresponding to component C_{HT-O} *in situ*, and **Win- C_{HT-O} Bed**, to C_{HT-O} after bedding correction; **Win- C_{HT-S} InS** corresponding to C_{HT-O} *in situ*, and **Win- C_{HT-S} Bed**, to C_{HT-S} after bedding correction (squares) are shown for indication only as they cannot be considered as significantly reliable. Their confidence ellipses are by the way not drawn given their size.

7.4. The Mitchell Formation (MIT)

7.4.1. Presentation

These Early Ordovician rocks comprise fine-grained volcanoclastics beds, and are exposed in a road-cut along the Mitchell Highway between Molong and Dubbo and behind a hill, about 500 metres West of the highway (figure 7.2). They belong to the Hensleigh Group and are Bendigonian in age (probably Be-3 [late Early Ordovician] where sampling has been carried out; Percival, *personal communication*, 2000).

This rocks are folded by a cylindrical fold having a rather N-S horizontal axis. Thirty-six cores (7 sites) have been collected.

7.4.2. Anisotropy of magnetic susceptibility (AMS)

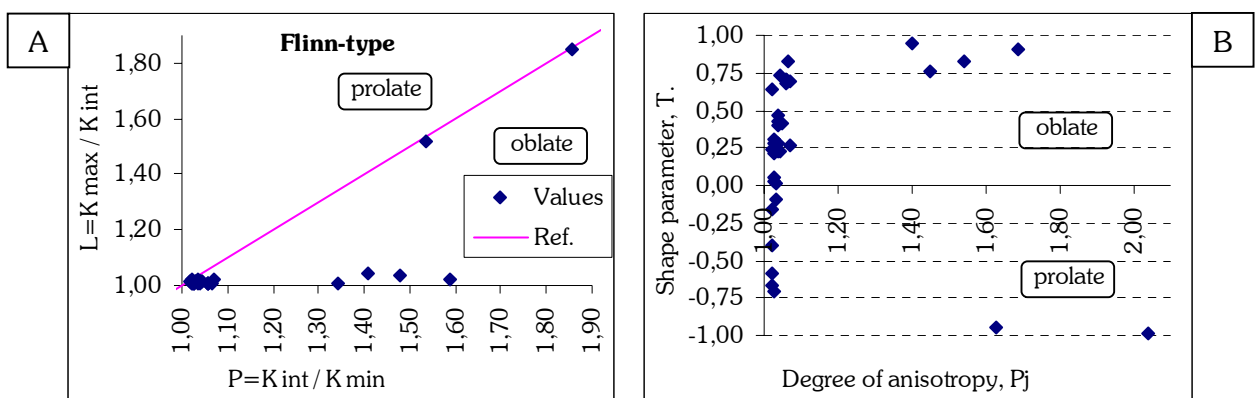
The degree of anisotropy is marked ($P_j = 1,14 \pm 0,24$) because of high values obtained for six specimens (figures 7.15). It is probable that it results from magnetic perturbations during measurements. When they are excluded, $\{P_j\}$ drops to a very low value in average ($P_j = 1,04 \pm 0,02$) and it can be considered that it is representative of the locality as it concerns 87% of the specimens. It is believed therefore that internal strain is negligible in these volcanoclastic rocks.

These six specimens have no real influence on the average of the $\{T\}$ parameter as some plot in the prolate field and others in the oblate one. However, when they are excluded, $\{T\}$ indicates that the ellipsoid of magnetic susceptibility is rather oblate ($T = 0,22 \pm 0,42$), although the error bars cover both sides of the diagram.

The Königsberger ratio probably does not bring much information about the grain size, but confirms that lightning is unlikely to be the cause of palaeomagnetic deviation in this locality ($Q_K @ RT = 0,25 \pm 0,11$).

The orientations of the principal axes of magnetic susceptibility are well grouped (figures 7.16). It is obvious here that the magnetic fabric was acquired after folding. The different axes are well positioned on sub-vertical and sub-horizontal plans *in situ* and becomes oblique after bedding correction on the one hand, and over all, the density contours highlight that K_{min} split in two groups and K_{max} are not anti-symmetrical anymore when the correction is applied (figure 7.16-B).

The poles to the magnetic foliation (K_{min}) are sub-horizontal. It means that the sedimentary magnetic fabric has been overcome and a tectonic fabric took place instead. In addition, the magnetic lineation is aligned with the fold axis, which means that it records probably a pure shear strain reflecting an E-W direction of compression.



Figures 7.15: **A-** Flinn-type diagram (Flinn, 1962, 1965-a, 1965-b); and **B-** $\{T\}$ versus $\{P_j\}$ diagram (Jelinek, 1981; Hrouda, 1982) for the volcanoclastic rocks of the Mitchell Formation (locality MIT).

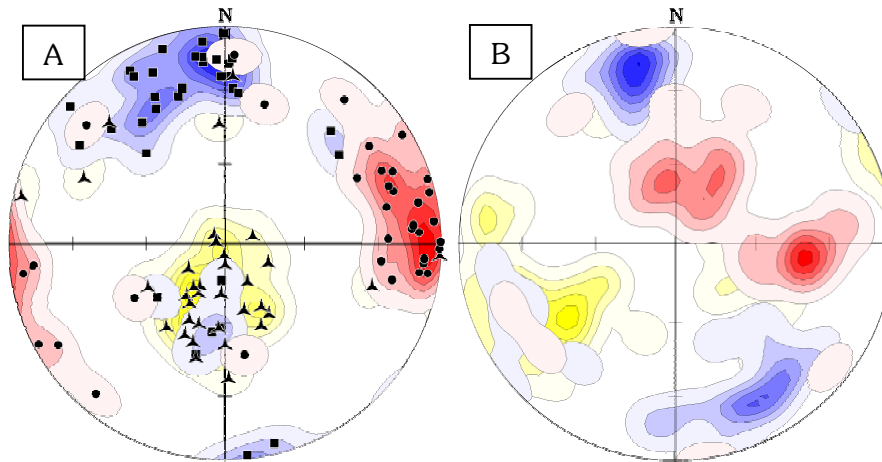


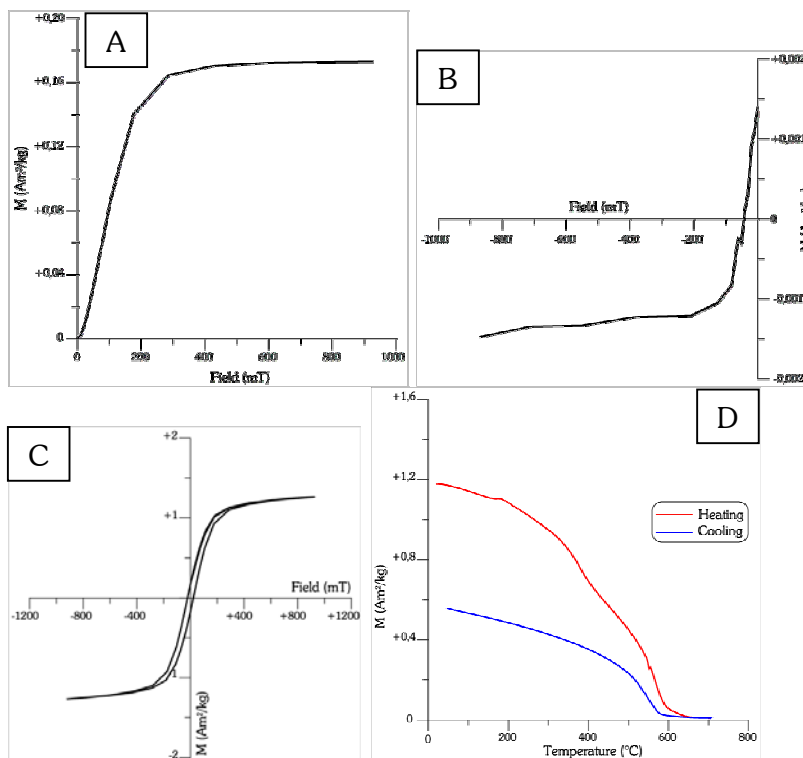
Figure 7.16: Orientations of the principal axes of magnetic susceptibility for the volcaniclastic rocks from the Mitchell Formation, locality MIT.

A- *in situ*, and **B-** test of correction.

Same legend as in figure 5.4 (Chapter 5; §.5.2.2); i.e. K_{max}, squares (blue); K_{int}, triangles (yellow); K_{min}, dots (red).

7.4.3. Rock magnetism

The IRM and back field curves show the presence of a relatively low coercivity mineral (figures 7.17-A & B), and the decay around 580°C on the IST curve when cooling, suggests it is due to magnetite (figure 7.17-D). Since the IRM and back field curves reach saturation and the IST curve is close to zero above 600°C, haematite is probably in very minor quantity and oxidation minerals such as goethite or maghaemite have probably not an important influence if they exist. There is apparently a minor contribution of paramagnetic material since the slope of the hysteresis loop is not pronounced. The presence of several inflexions on the heating part of the IST curve around 200°C and 400°C at least suggests the existence of other phases. It can be due to grain of titano-magnetite, but it will be show below that pyrrhotite seems to be present in these rocks.



Figures 7.17: Example of rock magnetic measurements from the volcanoclastic rocks of the Mitchell Formation (locality MIT): specimen MIT2-3.

A- IRM curve; **B-** Back field curve (coercivity); **C-** Hysteresis loop; and **D-** IST curve, in red while heating and in blue while cooling (being cut to zoom on features (B=535 mT).

$H_C = 22,23 \text{ mT}$; $H_{CR} = 89,08 \text{ mT}$.
 $M_S = 1,13 \text{ Am}^2/\text{kg}$; $M_{RS} = 0,17 \text{ Am}^2/\text{kg}$.

7.4.4. Palaeomagnetic results

- Demagnetisation

After removal of a drilling-induced or viscous magnetisation up to 120°C, two main components can be observed. A clear linear segment defines component C_p from 120° to 220°C, when it begins to be slightly deviated up to 320°C. This last temperature corresponds to the Curie temperature of pyrrhotite, and it will be shown below that C_p carries the Tertiary magnetisation presented in §.7.2. The deviation occurring from 220°C is thought to be related to an overlap of unblocking temperature spectra between C_p and a second component C_{HT} . This latter is usually isolated up to 565° – 575°C, even if the demagnetisation curve shows that a magnetisation remains up to 700°C. The direction of magnetisation of C_{HT} varies between two extreme positions.

In the first case, the end-point is oriented to South-East with a very shallow inclination value (figures 7.18). C_{HT} is mainly carried by magnetite (or some low titanium titano-magnetite) but a little amount of material with higher unblocking temperature is also present, since the sample is only fully demagnetised at 700°C. The magnetic signal is however not stable above 575°C.

In the second case (figures 7.19), component C_{HT} is stable from 350° to 565°C and is oriented in this example D.359°/I.-49° (MAD=2,5°), which corresponds very well to the present-day field which is here D.000°/I.-52° (geographic North). This component seems also to be carried by magnetite (or some low titanium titano-magnetite), but about 20% of the remanence is still present and persists up to 700°C. It is likely that weathering caused the oxidation of magnetite and formed some mineral such as haematite or maghaemite, which carries C_{HT} . However, above 565°C, a viscous magnetisation is acquired and the magnetic signal is lost as illustrated by the scattered data on the orthogonal projection (figure 7.19-B).

- Interpretation

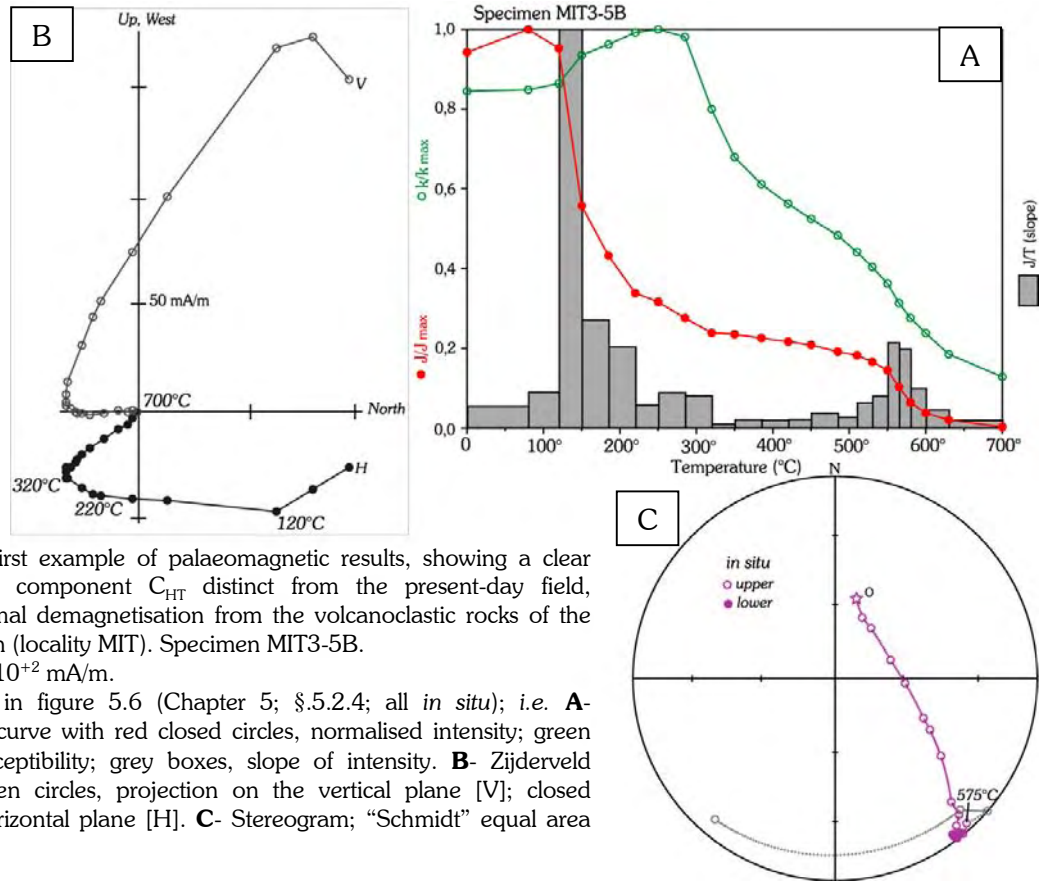
The overall mean direction for components C_p corresponds then very well with the Tertiary overprint (figure 7.20-A; table 25). It is clearly an overprint because the classic fold test is significantly negative (it is positive only below the 0,1% confidence level).

When single specimen components C_{HT} are plotted on a stereogram (figures 7.20), they are distributed on a great circle, which has a pole oriented D.050°/I.+33°. This great circle represents all possible orientations between the present-day field as shown in the second example of demagnetisation (figures 7.19) and an unknown SE direction represented by the first example of demagnetisation (figures 7.18). When components C_{HT} of SE direction are well isolated (as per figures 7.18), site mean directions have been calculated (table 24). This is possible for two sites only, but the overall mean direction obtained from them is D.143°/I.+00° ($\alpha_{95}=12,8^\circ/\kappa=381,3$) *in situ* and D.172°/I.+39° ($\alpha_{95}=21,8^\circ/\kappa=133,8$) after bedding correction. This means that the grouping appears to be much worse when the bedding correction is applied. The classic fold test is not possible with two data only, but when it is performed on the eight single data, the fold test becomes positive at the 11% confidence level only.

Table 25: Site mean directions and overall mean directions for the locality MIT

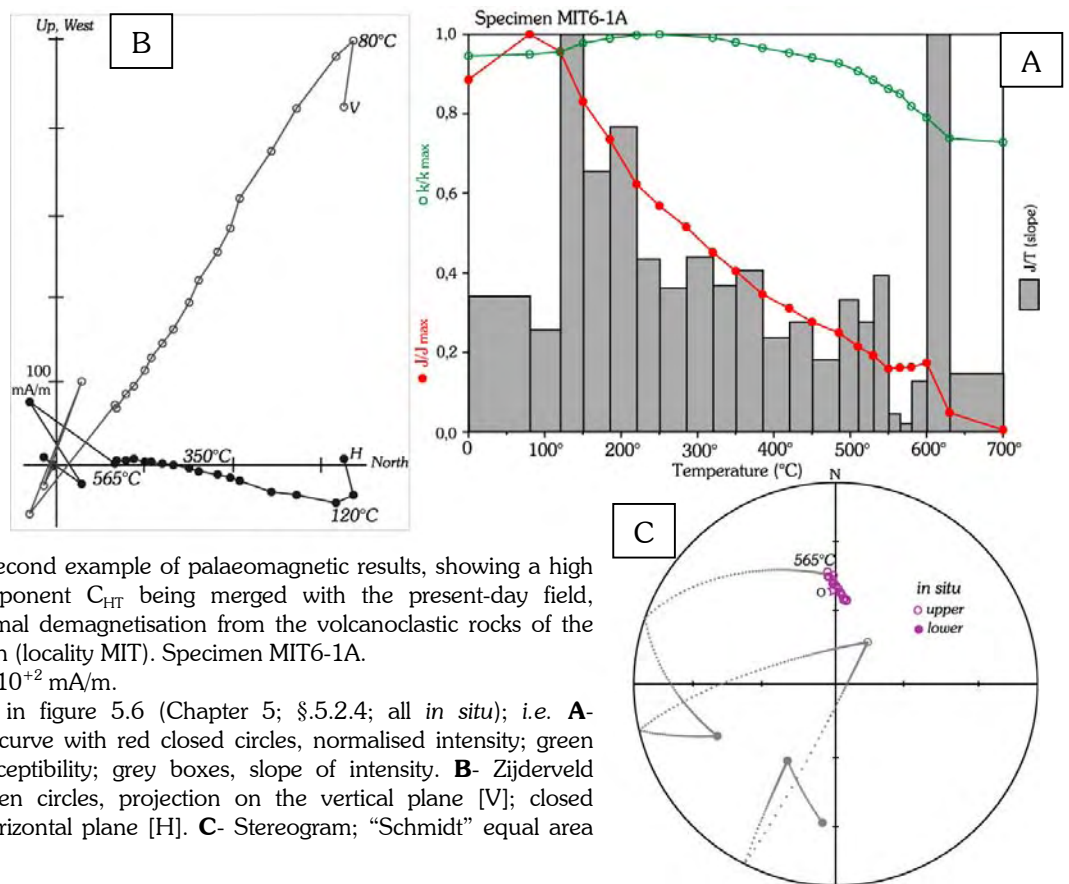
Name	N	R	D.InS	I.InS	α_{95}	κ	R	D.Bed	I.Bed	α_{95}	κ	DipDir	Dip
Component C_{HT} per site:													
Mit-01	3	3,0	143,7	-02,5	5,7	465,1	3,0	165,0	+28,8	5,7	465,1	270,5	77,0
Mit-03	5	4,9	142,8	+03,3	9,2	69,8	4,9	176,0	+42,8	9,2	69,8	276,5	74,0
Name	B	N	R	D.InS	I.InS	α_{95}	κ	R	D.Bed	I.Bed	α_{95}	κ	
Mean direction for the component C_p :													
MIT- C_p	6	40	6,0	003,2	-57,0	3,2	431,2	5,8	055,9	-23,1	14,8	21,5	
Mean direction for the component C_{HT} :													
MIT- C_{HT}	2	8	2,0	143,3	+00,4	12,8	381,3	2,0	171,8	+38,9	21,8	133,8	

N: number of samples; B: number of sites; α_{95} : cone calculated at the 95% confidence level; κ : precision parameter; R: resultant vector; D.Ins/I.InS: declination/inclination *in situ* (geographic coordinates); D.Bed/I.Bed: declination/inclination after bedding correction; DipDir/Dip: Direction of dip and dip for the bedding.



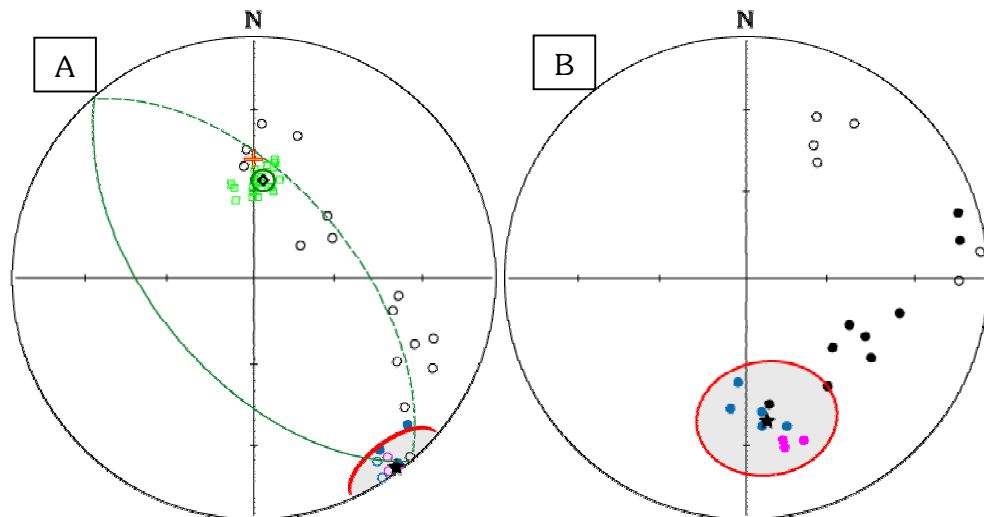
Figures 7.18: First example of palaeomagnetic results, showing a clear high temperature component C_{HT} distinct from the present-day field, obtained by thermal demagnetisation from the volcanoclastic rocks of the Mitchell Formation (locality MIT). Specimen MIT3-5B. $NRM@RT = 1,81.10^{+2}$ mA/m.

Same legend as in figure 5.6 (Chapter 5; §.5.2.4; all *in situ*); i.e. **A**- Demagnetisation curve with red closed circles, normalised intensity; green open circles, susceptibility; grey boxes, slope of intensity. **B**- Zijderveld diagram with open circles, projection on the vertical plane [V]; closed circles, on the horizontal plane [H]. **C**- Stereogram; “Schmidt” equal area



Figures 7.19: Second example of palaeomagnetic results, showing a high temperature component C_{HT} being merged with the present-day field, obtained by thermal demagnetisation from the volcanoclastic rocks of the Mitchell Formation (locality MIT). Specimen MIT6-1A. $NRM@RT = 5,36.10^{+2}$ mA/m.

Same legend as in figure 5.6 (Chapter 5; §.5.2.4; all *in situ*); i.e. **A**- Demagnetisation curve with red closed circles, normalised intensity; green open circles, susceptibility; grey boxes, slope of intensity. **B**- Zijderveld diagram with open circles, projection on the vertical plane [V]; closed circles, on the horizontal plane [H]. **C**- Stereogram; “Schmidt” equal area polar projection.



Figures 7.20: Direction of components obtained from the Late Ordovician volcanoclastic rocks of the Mitchell Formation (locality MIT), **A-** *in situ* and **B-** after bedding correction.

Green squares are single specimen orientations for C_p shown *in situ* only with their overall mean direction (**diamond**) and **green** confidence cone (α_{95}) calculated from site mean directions; the **red cross**, shown *in situ* only, represent the present-day field orientation (geographic North) at locality MIT. **Circles** are single specimen orientations for C_{HT} shown in **black** when they represent an intermediate direction and are distributed along a great circle (**dark green**) and shown in colour when they have been used to calculate site mean directions (**pink** for site Mit-01 & **blue** for site Mit-03). The overall mean directions (**star**) and associated α_{95} (**red**) have been obtained from sites Mer-01 & Mer-03 only.

Open symbols are negative inclination values (upper hemisphere); **closed** symbols, positive inclination values (lower hemisphere). Schmidt equal area polar projection.

It is believed therefore that this SE and horizontal orientation is a post-folding remagnetisation. The directions of magnetisation obtained from C_{HT} vary therefore between a position corresponding to an overprint (case of figure 7.18) and a position corresponding to the present-day field (case of figure 7.19; *i.e.* a fully weathered sample). Nevertheless, the SE direction does not correspond to any expected for Australia – Gondwana, as they should plot in the NE quadrant of the stereogram. Although this result is based on eight data only, such a shallow inclination should correspond to an Early – Mid Palaeozoic age of magnetisation.

The corresponding palaeopole from the *in situ* overall mean direction is PLong.274,7°/Plat.-42,5° ($dp=6,4^\circ$; $dm=12,8^\circ$) in Australian coordinates (figure 7.21; table 26) and plot far from any proposed paths. The most plausible explanation is to admit that the sampled Mitchell Formation was rotated and/or translated after folding, which is believed here to be Silurian or Early Devonian. This would represent thus a syn-/post-Silurian age of magnetisation.

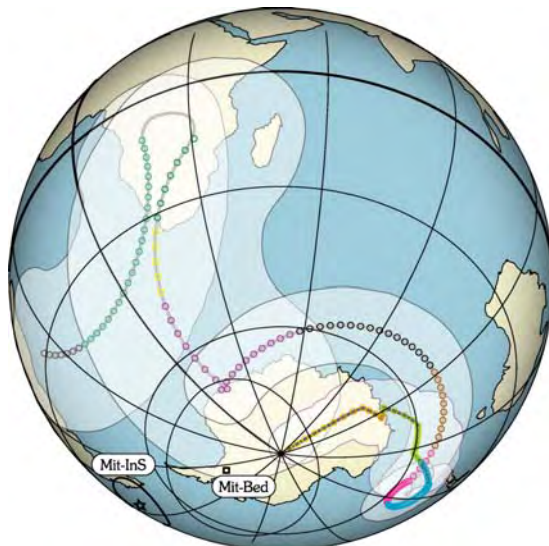


Figure 7.21: Corresponding palaeopoles in Australian coordinates. The possible APW path for Australia-Gondwana from the present-day to 570 Ma based on Small Circle Fit is shown for comparison purposes. Same legend as in figure 2.19-A, Chapter 2 (§.2.7).

Mit-InS is the palaeopole (**star**) corresponding to component C_{HT} *in situ*, and **Mit-Bed**, to C_{HT} after bedding correction (**square**). This last, however, is shown for indication purposes only as fold tests suggest this direction of magnetisation corresponds to a post-folding overprint. It must be pointed out that **Mit-InS** plots far away from any published APW path (here from the Small Circle Fit path as well). This suggests the existence of post-folding rotation and/or translation of locality MIT.

Table 26: Palaeopoles obtained from the volcanoclastic rocks of the Mitchell Formation (locality MIT)

B	N	<i>Australian coord.</i>		<i>African coord.</i>		dp	dm	Coordinates system
		<u>Plat</u>	<u>Plong</u>	<u>Plat</u>	<u>PLong</u>			
<i>Locality MIT, components C_{HT}:</i>								
2	8	-42,5	274,7	-48,3	309,2	6,4	12,8	from <i>in situ</i> orientation
2	8	-77,0	293,0	-41,7	359,1	15,5	26,0	after bedding correction

N: number of samples; **B:** number of sites; **PLong./Plat.:** palaeopole longitude/latitude in Australian and in African coordinates. **dp/dm** : semi-axis of the ellipse of confidence.

7.5. The Fairbridge Volcanics (OAK)

7.5.1. Presentation

Unit 1 of the Fairbridge Volcanics was formerly associated to the Oakdale Formation, which has given the mnemonic “OAK” for the locality, but recent mapping (Glen, *personal communication*, 2003; Meffre *et al.*, *in preparation*) changed this nomenclature. However, they consist of fine-grained volcanoclastic sandstones (photos 15), which are exposed along the Bell River, North East of Molong (figure 7.2). The fossil biota contained in the formation range from Late Darriwillian to Late Gisbornian (*i.e.* late Middle to early Late Ordovician; Pogson & Watkins, 1998), and the rocks of Unit 1 are believed to be Gisbornian in age (Glen, *personal communication*, 2003; Meffre *et al.*, *in preparation*).

Sixty nine cores (13 sites) have been drilled in these rocks among which eleven sites on one limb of a fold and only two on the second limb as this last looks very altered. The bedding on the best side of the fold is sub-vertical (photo 15-A) and even slightly overturned for some sites. Fining-up grain facies allowed the determination of the facing (photo 15-B).

Nine sites have been obtained in 2002, and four sites during a previous field trip in 2000. For an unresolved reason yet, rock collected in 2002 yielded bad results whereas the 20 cores obtained in 2000 had all a identical clear magnetic signal. It is possible that an error occurred while collecting or measuring the new set of samples or that a problem happened during rock transport. However, only samples from the four sites (20 cores) obtained in 2000 are presented here for their palaeomagnetic results.

7.5.2. Anisotropy of magnetic susceptibility (AMS)

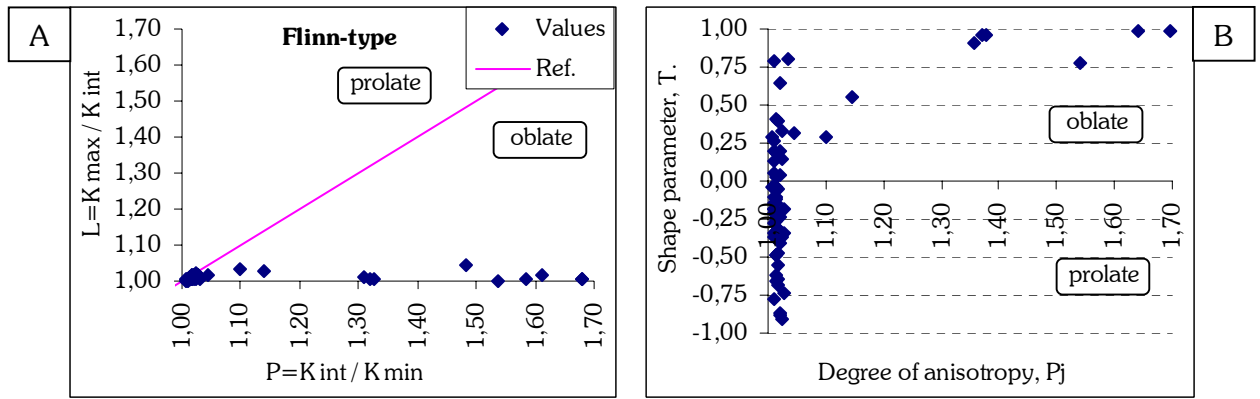
All the 69 cores have been measured for AMS and the averaged degree of anisotropy is pronounced ($P_j = 1,09 \pm 0,21$). This is due to the high values of ten specimens (figures 7.22). When they are excluded, $\{P_j\}$ drops to very low values ($P_j = 1,02 \pm 0,01$). As this last average represents 85,5% of the locality, it is believed that the degree of internal strain is very low, and that the measurement of these ten specimens may have suffer environmental perturbation.



Photo 15-A: Sub-vertical beds of volcanoclastic sandstones from the Fairbridge Volcanics (locality OAK).



Photo 15-B: Grain size fining-up and determining the facing of the sandstones of the Fairbridge Volcanics (locality OAK).



Figures 7.22: **A-** Flinn-type diagram (Flinn, 1962, 1965-a, 1965-b); and **B-** $\{T\}$ versus $\{P_j\}$ diagram (Jelinek, 1981; Hrouda, 1982) for every cores from the volcanoclastic sandstones of the Fairbridge Volcanics (locality OAK).

Although error bars cover both side of the diagram, the shape parameter (figure 7.22-B) indicates that the ellipsoid of magnetic susceptibility is prolate in average ($T = -0.16 \pm 0.39$; when the ten specimens are excluded), and lightning effects can be discarded ($Q_K @ RT = 0.17 \pm 0.09$).

The directions of the principal axes of magnetic susceptibility are a bit scattered (figures 7.23), but the density contours help seeing that the magnetic fabric is not fundamentally different *in situ* and after bedding correction. The magnetic lineation is N-S and the magnetic foliation consists in a sub-vertical E-W plan. Slight differences, however, are important.

The K_{\min} appear to be slightly better grouped around the vertical after bedding correction (figure 7.23-B). This can express that the sedimentary magnetic fabric is still predominant but is partly overprinted by a tectonic fabric caused by an ~E-W direction of strain. The magnetic lineation is aligned with the fold axis, but the fact that they are dispersed on the horizontal plan might signify either that the sedimentary lineation is not fully overprinted or that the direction of strain was not or not always obtained by pure shear stresses.

On the other hand, it is possible that the magnetic fabric has been acquired after folding. The K_{\min} grouped horizontally around an E-W direction *in situ* (figure 7.23) would mark then a tectonic magnetic fabric acquired after an E-W direction of strain. The maximum density for the K_{\max} is in this case also aligned with the fold axis, but the dispersion occurs along a vertical plan. This could express the penchant of the magnetic lineation to be vertical and record thus the tendency of the magnetic fabric to show a vertical extrusion. This possibility is generally encounter in strongly deformed rocks, which is not the case here given the AMS parameters. A pre-folding acquisition of the magnetic fabric is therefore favoured.

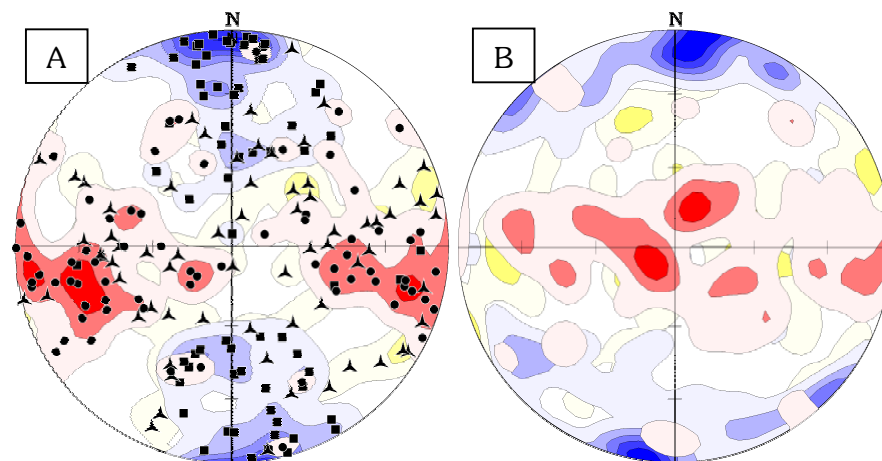


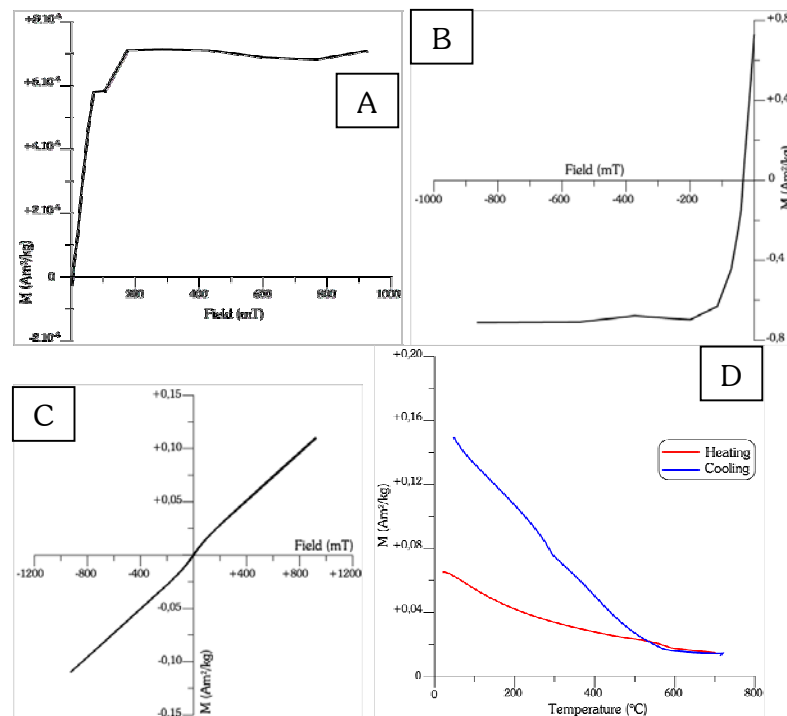
Figure 7.23: Orientations of the principal axes of magnetic susceptibility for the volcanoclastic rocks from the Fairbridge Volcanics, locality OAK.

A- *in situ*, and **B-** test of correction.

Same legend as in figure 5.4 (Chapter 5; §.5.2.2); i.e. K_{\max} , squares (blue); K_{int} , triangles (yellow); K_{\min} , dots (red).

7.5.3. Rock magnetism

The IRM and back field curves show the existence of a relatively low coercivity mineral (figures 7.24-A & B), and these curves reach saturation. The decay around 580°C on the IST curve when cooling (figure 7.24-D) suggests magnetite (or some low titanium titanomagnetite) to be the main magnetic carrier and the responsible of the behaviour seen on the IRM and back field curves. The decrease in intensity below 200°C on the heating part of the IST curve is unlikely to be due to some oxidised material, except perhaps maghaemite, but can be the expression of the existence of pyrrhotite, as it is revealed by thermal demagnetisation (see below). Its presence, however, is probably marked here by an inflexion on the cooling curve around 300°C. Finally, it must be noticed that there is a major contribution of paramagnetic material given the slope of the hysteresis loop. It is also revealed by the positive values of magnetisation at 700°C on the IST curve.



Figures 7.24: Example of rock magnetic measurements from the volcanoclastic rocks of the Fairbridge Volcanics (locality OAK): specimen OAK3-1.

A- IRM curve; **B-** Back field curve (coercivity); **C-** Hysteresis loop; and **D-** IST curve, in red while heating and in blue while cooling ($B=535$ mT).

$H_C=10,32$ mT; $H_{CR}=34,30$ mT.

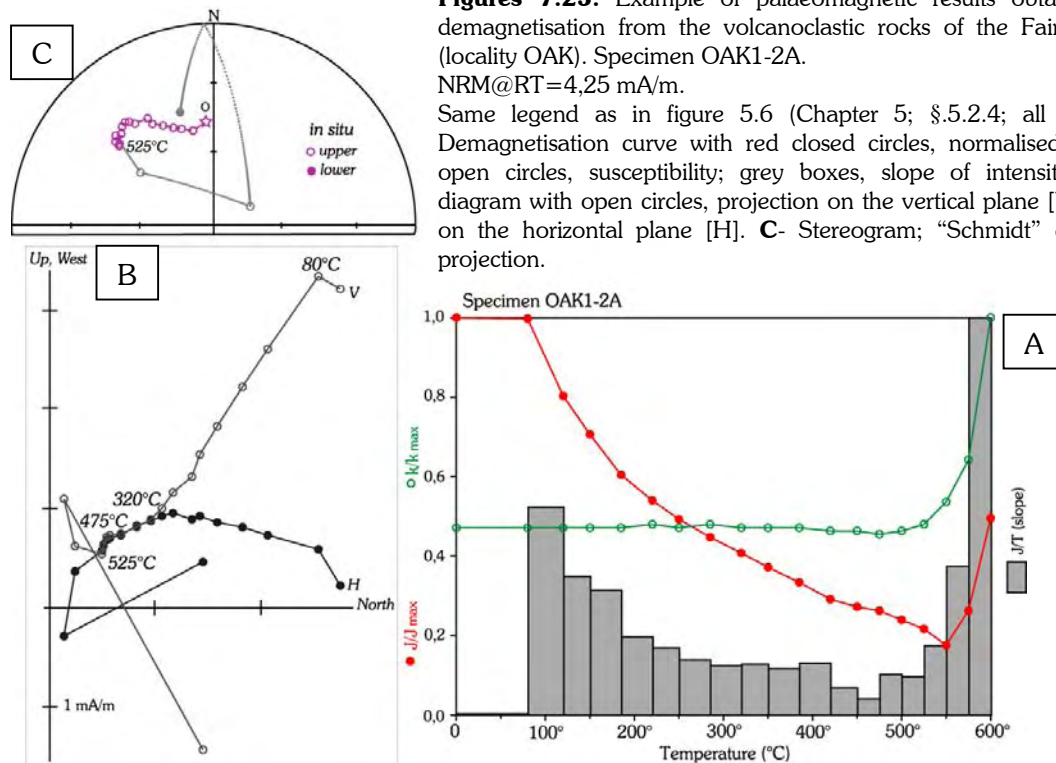
$M_S=5,3 \cdot 10^{-3}$ Am²/kg; $M_{RS}=7,3 \cdot 10^{-4}$ Am²/kg.

7.5.4. Palaeomagnetic results

- Demagnetisation

During thermal demagnetisation of the 20 cores collected in 2000, up to three main components can be identified (figures 7.25).

The first, component C_1 , is removed between 80° and 320°C. It is probably carried by pyrrhotite. The second, C_2 , is demagnetised from 320° to ~475°C, but still do not point to the origin (figure 7.25-B). Its magnetic carrier is undetermined. It can be some large grain of magnetite, some titanomagnetite, or perhaps even some maghaemite, although no haematite often caused by the alteration of maghaemite has been observed in these rocks. Finally, a component C_3 seems to point to the origin but is not fully isolated as a viscous magnetisation is acquired from 525° – 550°C with a strong increase in susceptibility (figure 7.25-A). The original magnetic signal is then lost.



- Interpretation

The directions plotted on stereogram (figures 7.26) correspond to single specimen components in order to show the consistency of the results obtained, although it concerns only twenty cores. The overall mean directions presented, however, are calculated from site mean directions (table 27).

The overall mean direction from components C_1 is $D.012^\circ/I.-66^\circ$ ($\alpha_{95}=10,5^\circ/\kappa=76,9$) *in situ*. It seems to be carried by pyrrhotite and corresponds very well with the Tertiary remagnetisation presented in §.7.2.

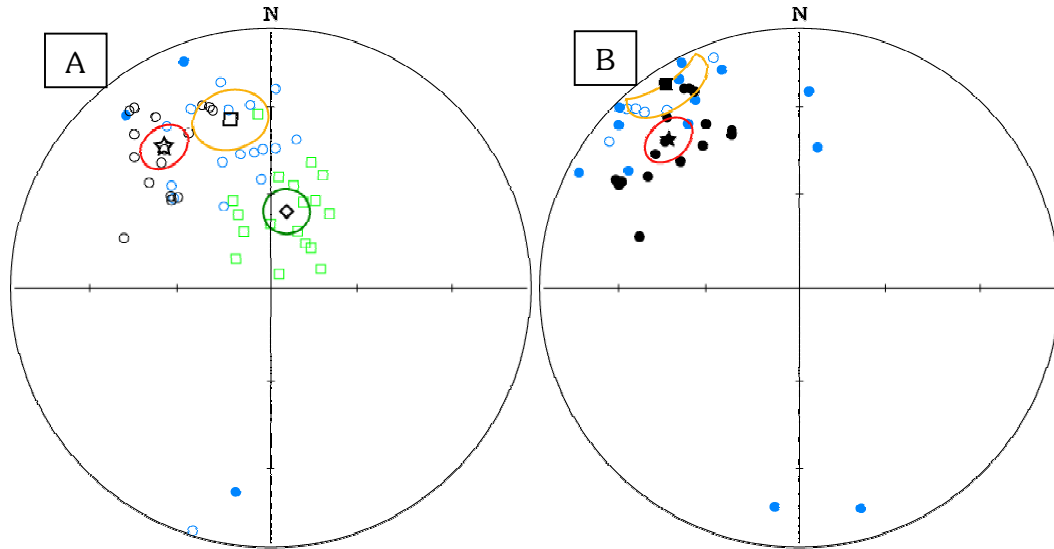
The overall mean direction from C_2 is $D.347^\circ/I.-33^\circ$ ($\alpha_{95}=10,7^\circ/\kappa=75,2$) *in situ* and $D.323^\circ/I.-31^\circ$ ($\alpha_{95}=7,1^\circ/\kappa=167,1$) *in situ* for C_3 . They become $D.327^\circ/I.+05^\circ$ ($\alpha_{95}=10,7^\circ/\kappa=74,6$) and $D.319^\circ/I.+24^\circ$ ($\alpha_{95}=7,1^\circ/\kappa=166,3$) after bedding correction respectively. These orientations are different from any possibly expected for the Ordovician or for any younger ages, as they should plot in the NE quadrant of the stereogram. Terrane rotation appears therefore to be the most plausible explanation for such results. Nevertheless, the age of magnetisations cannot be constrained because of the lack of any field tests. The slight change of the κ parameter is not statistically significant. However, inclination values, both *in situ* and after bedding correction, are consistent with Early to Mid Palaeozoic magnetisation events.

When the *in situ* orientations are considered, components C_2 and C_3 have the same inclination values. This could be understood as two times of remagnetisation events acquired during terrane rotation around a vertical axis. It will be shown in the following chapter that such a rotation can match Devonian segments of some proposed APW paths for Gondwana. This possibility would be thus consistent with the fact that the main phase of deformation occurred in the Early Devonian in this area.

On the other hand, the overall mean direction of C_2 after bedding correction can be compared to that obtained *in situ* from the Mitchell Formation (locality MIT). This similarity is perhaps a coincidence, but could be regarded as the same remagnetisation event affecting both localities, one (locality OAK) prior to folding and the second (locality MIT) post-folding. The mean direction obtained from the C_3 components after bedding correction has a positive inclination value, which is close to what is expected for the Ordovician. This direction of magnetisation could

be then consistent with a pre-folding or even a primary magnetisation, but a counter-clockwise rotation of 90° or more around a vertical axis and prior to folding is necessary.

All the different possibilities are shown here (figure 7.27, table 28; Note that Oak-C₃-InS and Oak-C₃-Bed are shown with their alternate polarity to make them visible), and a discussion of the most plausible solution is given in the following chapter.



Figures 7.26: Components obtained from the Late Ordovician volcanoclastic rocks of the Fairbridge Volcanics (locality OAK), **A-** *in situ* and **B-** after bedding correction.

Green squares are single specimen orientations for component C₁ shown *in situ* only with their overall mean direction (**diamond**) and **dark green** confidence cone (α_{95}) calculated from site mean directions. **Blue** and **black circles** are single specimen orientations for components C₂ and C₃ respectively shown with their overall mean directions (**black squares** and **stars**) and **orange & red** confidence cone (α_{95}) calculated from site mean directions, as given in table 26. **Open** symbols are negative inclination values (upper hemisphere); **closed** symbols, positive inclination values (lower hemisphere). Schmidt equal area polar projection.

Table 27: Site mean directions and overall mean directions for the locality OAK

Name	N	R	D.InS	I.InS	α_{95}	κ	R	D.Bed	I.Bed	α_{95}	κ	DipDir	Dip
<i>Components C₂ per site:</i>													
Oak-01	5	4,2	342,0	-25,7	9,8	62,4	4,2	332,1	+11,8	9,8	62,4	090,1	76,2
Oak-02	5	4,4	353,9	-36,3	31,9	6,7	4,4	325,3	-01,4	31,9	6,7	096,5	80,6
Oak-03	5	4,8	349,6	-42,2	18,6	17,8	4,8	318,7	+00,0	18,6	17,8	096,5	81,0
Oak-04	5	4,3	342,3	-26,5	35,9	5,5	4,3	331,4	+11,1	35,9	5,5	096,5	81,0
<i>Components C₃ per site:</i>													
Oak-01	5	4,8	315,2	-33,8	15,8	24,5	4,8	311,9	+27,4	15,8	24,5	090,1	76,2
Oak-02	2	2,0	327,3	-32,3	17,6	203,4	2,0	319,9	+20,2	17,6	203,4	096,5	80,6
Oak-03	4	3,9	329,8	-31,3	19,8	22,5	3,9	322,0	+18,9	19,8	22,5	096,5	81,0
Oak-04	5	4,8	319,7	-27,8	17,6	19,9	4,8	319,9	+28,2	17,6	19,9	096,5	81,0
Name	B	N	R	D.InS	I.InS	α_{95}	κ	R	D.Bed	I.Bed	α_{95}	κ	
<i>Mean direction for the components C₁:</i>													
OAK-C ₁	4	18	4,0	011,7	-66,4	10,5	76,9	4,0	296,8	-16,3	10,6	76,6	
<i>Mean direction for the components C₂:</i>													
OAK-C ₂	4	20	4,0	346,6	-32,8	10,7	75,2	4,0	326,8	+05,4	10,7	74,6	
<i>Mean direction for the components C₃:</i>													
OAK-C ₃	4	16	4,0	323,0	-31,4	7,1	167,1	4,0	318,5	+23,7	7,1	166,3	

N: number of samples; **B:** number of sites; α_{95} : cone calculated at the 95% confidence level; κ : precision parameter; **R:** resultant vector; **D.InS/I.InS:** declination/inclination *in situ* (geographic coordinates); **D.Bed/I.Bed:** declination/inclination after bedding correction; **DipDir/Dip:** direction of dip and dip of the bedding.

Table 28: Palaeopoles obtained from the volcanoclastic rocks of the Fairbridge Volcanics (locality OAK)

B	N	<i>Australian coord.</i>		<i>African coord.</i>		dp	dm	Coordinates system
		<u>Plat</u>	<u>PLong</u>	<u>Plat</u>	<u>PLong</u>			
<i>Components C₂:</i>								
4	20	-70,7	287,0	-43,9	350,8	6,9	12,1	from <i>in situ</i> orientation
4	20	+42,5	101,0	+42,9	133,2	5,4	10,7	after bedding correction
<i>Components C₃:</i>								
4	16	-53,1	255,4	-61,6	327,1	4,5	8,0	from <i>in situ</i> orientation
4	16	+29,8	100,6	+39,1	115,4	4,0	7,6	after bedding correction
N : number of samples; B : number of sites; PLong/Plat. : palaeopole longitude/latitude in Australian and in African coordinates. dp/dm : semi-axis of the ellipse of confidence.								

N: number of samples; **B:** number of sites; **PLong./Plat.:** palaeopole longitude/latitude in Australian and in African coordinates. **dp/dm** : semi-axis of the ellipse of confidence.

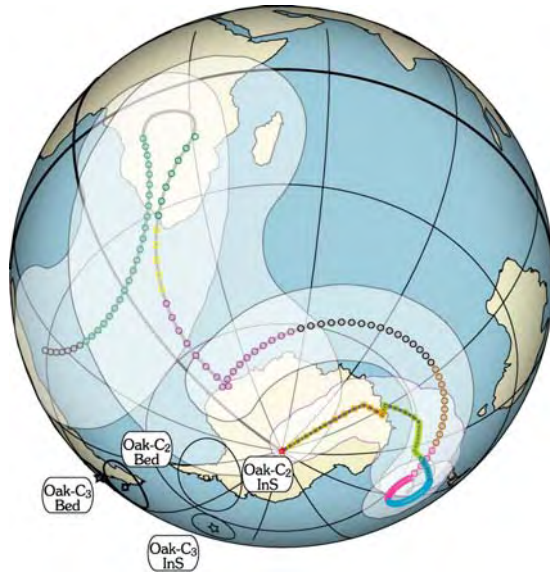


Figure 7.27: Corresponding palaeopoles in Australian coordinates. The possible APW path for Australia-Gondwana from the present-day to 570 Ma based on Small Circle Fit is shown for comparison purposes. Same legend as in figure 2.19-A, Chapter 2 (§.2.7).

Oak-C₂ InS and **Oak-C₂ Bed** are the palaeopoles (**squares**) corresponding to component C_2 *in situ* and after bedding correction respectively. Similarly, **Oak-C₃ InS** and **Oak-C₃ Bed** are the palaeopoles (**stars**) corresponding to component C_3 *in situ* and after bedding correction respectively. These last poles are shown with their alternative polarity in order to make them visible.

7.6. The Bowan Park Limestone Subgroup from the Quondong quarry (QUO)

7.6.1. Presentation

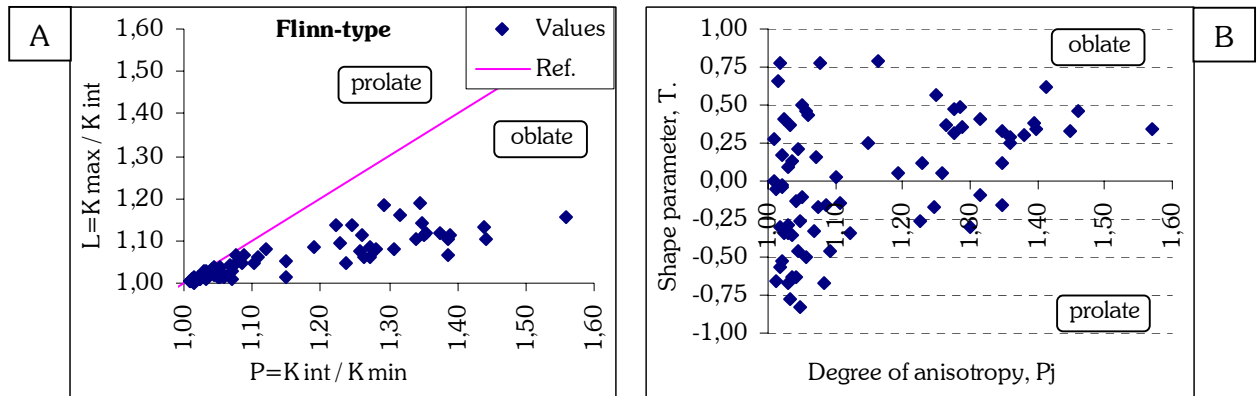
The rocks targeted are located in an active quarry near Cudal (figure 7.2). In this quarry, the limestone is dark grey in colour, thickly bedded to massive, and has non-negligible quartz content. The bedding is nearly monoclinical, so that fold tests are not possible. The Bowan Park Limestone Subgroup unconformably overlies the Fairbridge Volcanics and belongs to the Barrajin Group. It contains a rich fauna and is Eastonian (middle Late Ordovician) in age (Pogson & Watkins, 1998; Percival, *personal communication*, 2000).

Fourteen sites (70 cores) have been obtained at this locality (QUO).

7.6.2. Anisotropy of magnetic susceptibility (AMS)

A great number of specimens shows a relatively high degree of anisotropy ($P_j = 1,15 \pm 0,15$), but the shape of the ellipsoid of magnetic susceptibility is not well pronounced ($T = 0,02 \pm 0,41$). The average of $\{T\}$ points hardly in the oblate part of the $\{T\}$ vs. $\{P_j\}$ diagram (figure 7.28-B). This oblate shape however, is clearly outlined by the Flinn-type diagram (figure 7.28-A). In any cases, these values of degree of anisotropy cannot be regarded as high enough to induce a significant deviation of the palaeomagnetic record (Cogné, 1987).

Lightning strikes cannot affect the collected cores since they were drilled deep in the Quondong quarry. The Königsberger ratio however, is some cases relatively high ($Q_K @ 80^\circ C = 1,08 \pm 10,90$). This means that the susceptibility can be “anomalously” high.



Figures 7.28: **A-** Flinn-type diagram (Flinn, 1962, 1965-a, 1965-b); and **B-** $\{T\}$ versus $\{P_j\}$ diagram (Jelinek, 1981; Hrouda, 1982) for the Bowan Park Limestone of the Quondong quarry (locality QUO).

The information yielded by the AMS parameters, leads to think that the relatively high degree of anisotropy is not caused by tectonic effects, but more probably by the magnetic mineralogy of the limestone. The existence of very small single domain grains and/or superparamagnetic minerals in particular could lead to high values of susceptibility and apparent high values of $\{P_j\}$ without clearly developing a shape for the ellipsoid of magnetic susceptibility.

The direction of the principal axes of magnetic susceptibility could be viewed as randomised if the density contours did not reveal slight density peaks (figures 7.29-A & B). Concerning K_{min} , for instance, density contours highlight the confusion of some direction with K_{max} and K_{min} . This is in agreement with the hypothesis that the degree of anisotropy is not only related to tectonic strain. However, the highest density peak coincides well with the bedding since it is close to the vertical after bedding correction (figure 7.29-B). It represents a “sedimentary” magnetic fabric acquired prior to folding.

Although hidden by density contours of “confused” K_{min} , the peak density of K_{max} is directed E-W. This magnetic lineation is rather considered as a tectonic feature even if a sedimentary cause cannot be ruled out (see below, paragraph about the regional magnetic fabric in the Molong area).

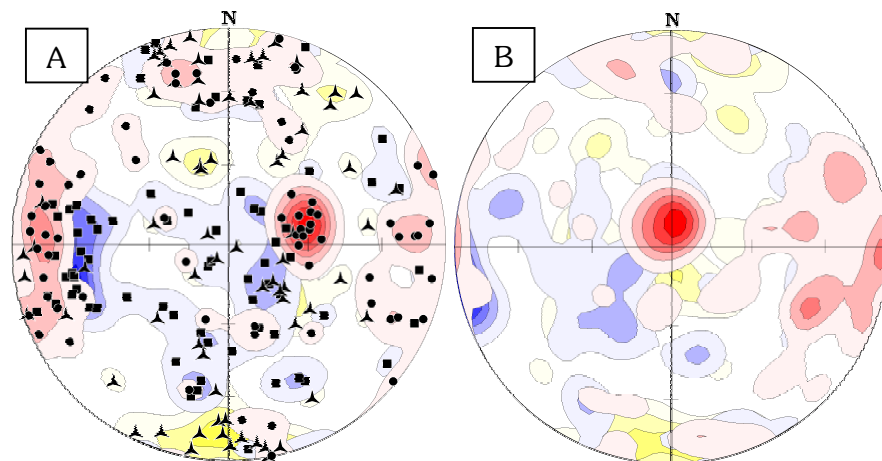


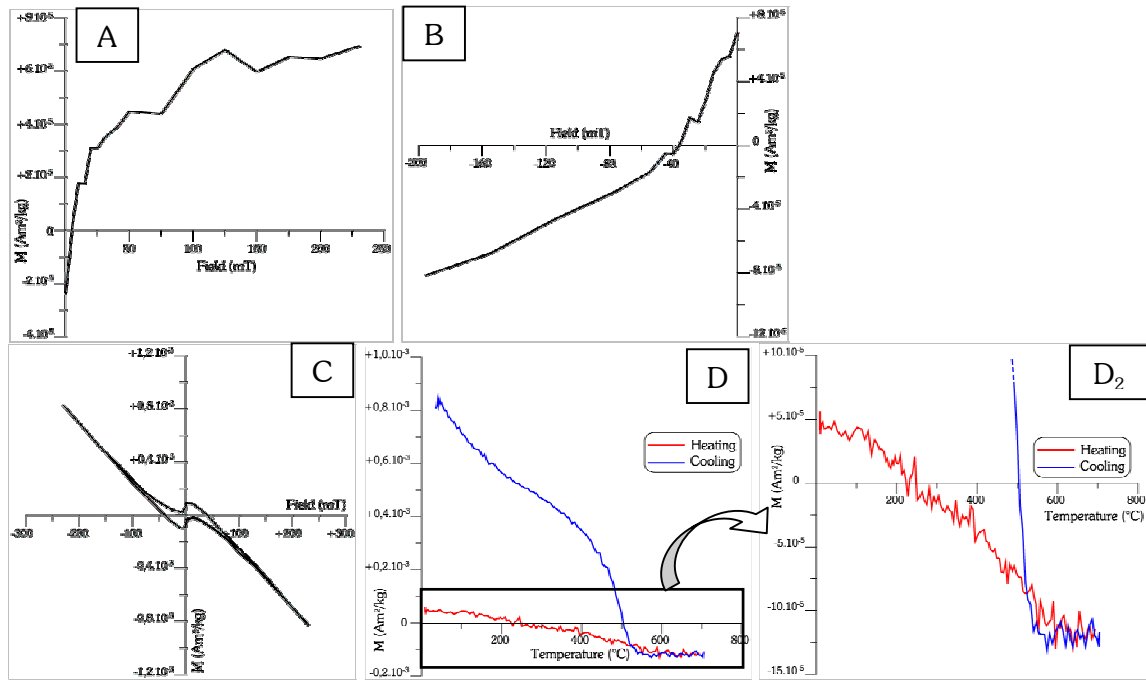
Figure 7.29: Orientations of the principal axes of magnetic susceptibility for the Bowan Park Limestone from the Quondong quarry, locality QUO.

A- *in situ*, and **B-** test of correction.

Same legend as in figure 5.4 (Chapter 5; §.5.2.2); i.e. K_{max} , squares (blue); K_{int} , triangles (yellow); K_{min} , dots (red).

7.6.3. Rock magnetism

Thermal demagnetisation process reveals two kinds of high temperature components (see below). Rock magnetic measurements are therefore shown for the two specimens chosen as example for thermal demagnetisation. However, it must be noticed that these curves are noisy because intensities are very weak and reach the limit of the VFTB.

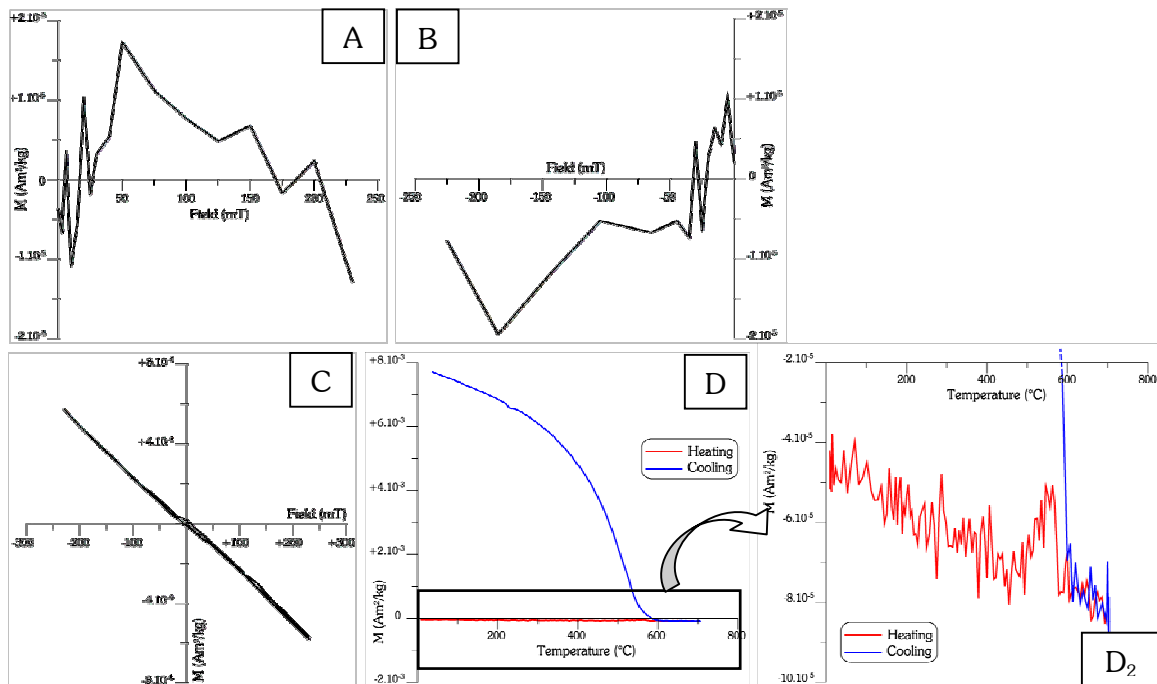


Figures 7.30: First example of rock magnetic measurements from the Bowan Park Limestone of the Quondong quarry (locality QUO): specimen QUO8-1.

A- IRM curve; **B-** Back field curve (coercivity); **C-** Hysteresis loop; and **D-** IST curve, in red while heating and in blue while cooling & **D₂**- Zoom on features of the heating curve (B=25 mT).

$$H_C = 7,03 \text{ mT}; H_{CR} = 36,75 \text{ mT}.$$

$$M_S = 2,1 \cdot 10^{-4} \text{ Am}^2/\text{kg}; M_{RS} = 6,7 \cdot 10^{-5} \text{ Am}^2/\text{kg}.$$



Figures 7.31: Second example of rock magnetic measurements from the Bowan Park Limestone of the Quondong quarry (locality QUO): specimen QUO12-1 (B=25 mT).

A- IRM curve; **B-** Back field curve (coercivity). Note that the weak intensity of this specimen reaches the limit of the VFTBs, and these curves are shown as indication for the general trend only: abscissae-axis is crossed between 10 and 30 mT indicating the presence of low coercivity material. **C-** Hysteresis loop; and **D-** IST curve, in red while heating and in blue while cooling & **D₂**- Zoom on features of the heating curve.

$$H_C = 9,96 \text{ mT}; H_{CR} = 21,48 \text{ mT}.$$

$$M_S = 2,9 \cdot 10^{-5} \text{ Am}^2/\text{kg}; M_{RS} = 1,4 \cdot 10^{-5} \text{ Am}^2/\text{kg}.$$

In the first example, IRM and back field curves show the existence of relatively low coercivity mineral (figures 7.30-A & B) since $H_c = 7,03$ mT, and higher coercivity material because the curves do not reach saturation. However, the IST curve shows an important inflexion around 580°C (figure 7.30-D & D₂), which means that magnetite is the main magnetic carrier. It seems that no mineral has a Curie temperature higher than magnetite in these rocks, which implies that material with higher coercivity can be due to oxidised material such as goethite or maghaemite for instance. Concerning, the origin of the formation of new magnetite visible on the cooling part of the IST curve is not clear, but might be caused by minor phyllosilicates. Albeit the noise in the zoom on the heating part of the IST curve (figure 7.30-D₂), it seems that an inflexion is also present around 300°C. This is probably the illustration of the occurrence of pyrrhotite, which is more clearly outlined by thermal demagnetisation (see below). The hysteresis loop shows clearly that the diamagnetic contribution is strong, but it must be pointed out that it is possible because other magnetic contributions (*i.e.* para- and ferromagnetism [*s.l.*]) are also very weak.

The second example (figures 7.31) is much noisier, and also weaker in intensity. It reaches the limit of the VFTBs, but some general trend can be observed. It seems the magnetic mineralogy is analogous, with the presence of low coercivity mineral (figures 7.31-A & B) probably due to magnetite and an important contribution of diamagnetism (figure 7.31-C). It appears however that high coercivity material is here absent or in too little quantity to be detectable, since the IRM and back field curves are probably saturated. On the zoom of the heating part of the IST curve (figure 7.31-D₂), a small peak is visible between 500 and 600°C and mark the formation of magnetite, which becomes much more visible with the cooling curve. As for the first example, the origin of this transformation is not resolved.

7.6.4. Palaeomagnetic results

- Demagnetisation

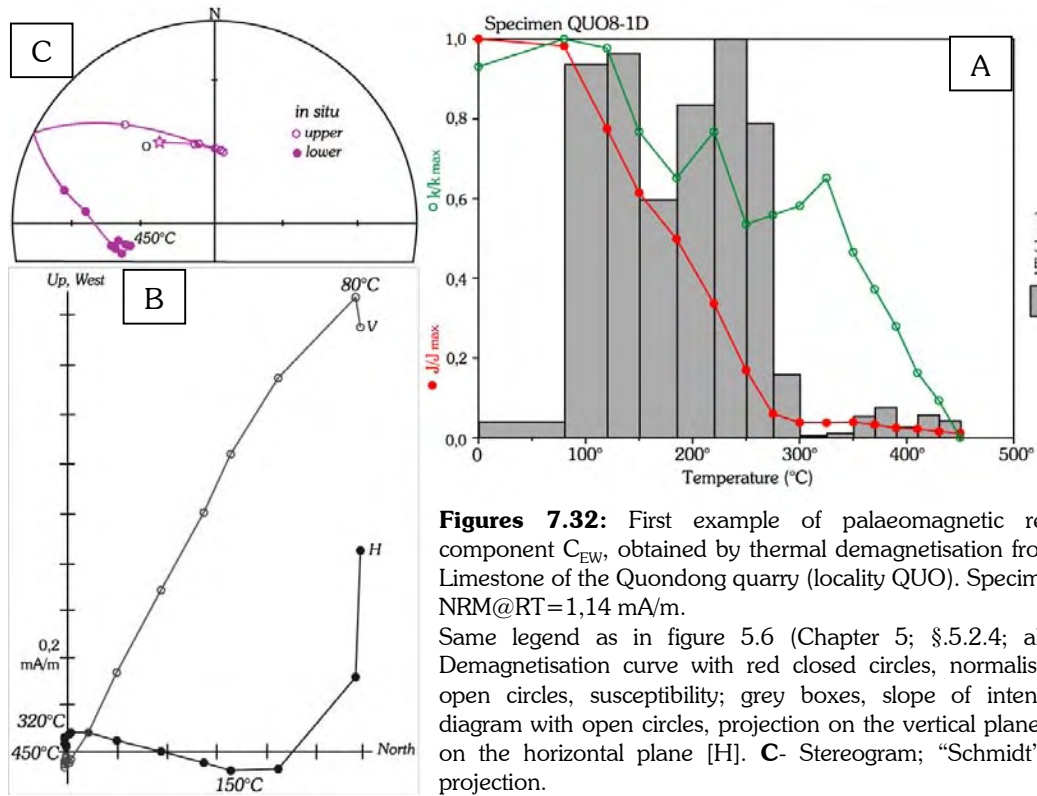
The Bowan Park Limestone reveals two main components after removal of a viscous component C_0 up to 120° – 150°C (figures 7.32 & 7.33), which shows generally the present-day field orientation (table 29).

The first, C_1 , can be isolated from 150°C to 300° – 320°C. It is therefore believed to be carried here as well by pyrrhotite since the direction of magnetisation corresponds to the Tertiary overprint presented in §.7.2 (table 28). This component carries also most of the remanence.

The second is fully demagnetised at 450° – 500°C. It generally carries just about 5 – 10% of the NRM. Rock magnetic measurements suggest magnetite as principal magnetic carrier, but two directions of magnetisation are observed. One, called component C_{EW} , is directed E-W (figures 7.32), whereas the second, C_{NS} , has a N-S direction of magnetisation (figures 7.33). Both, however, are weak, since intensities of the NRM at 300°C equal $4,343.10^{-2}$ mA/m for C_{EW} and $5,878.10^{-2}$ mA/m for C_{NS} , but are here relatively well defined. Unfortunately, this is not true for all sites, and great circle analysis has been largely used. C_{EW} can be satisfyingly isolated in sites Quo-08, Quo-09, Quo-10, and rather poorly in site Quo-05. As for C_{NS} , it is determined in sites Quo-11, Quo-12, Quo-13, and possibly in sites Quo-04 and Quo-06. An apparent intermediate direction between C_{EW} and C_{NS} seems to be present in site Quo-14, and perhaps in sites Quo-01, Quo-02 and Quo-07.

- Interpretation

As the magnetisation of the high temperature components C_{EW} and C_{NS} can be identified satisfyingly in some sites only, the overall mean directions are presented after calculations on single specimen components (figures 7.34), but calculations on site mean directions are also given in table 29.



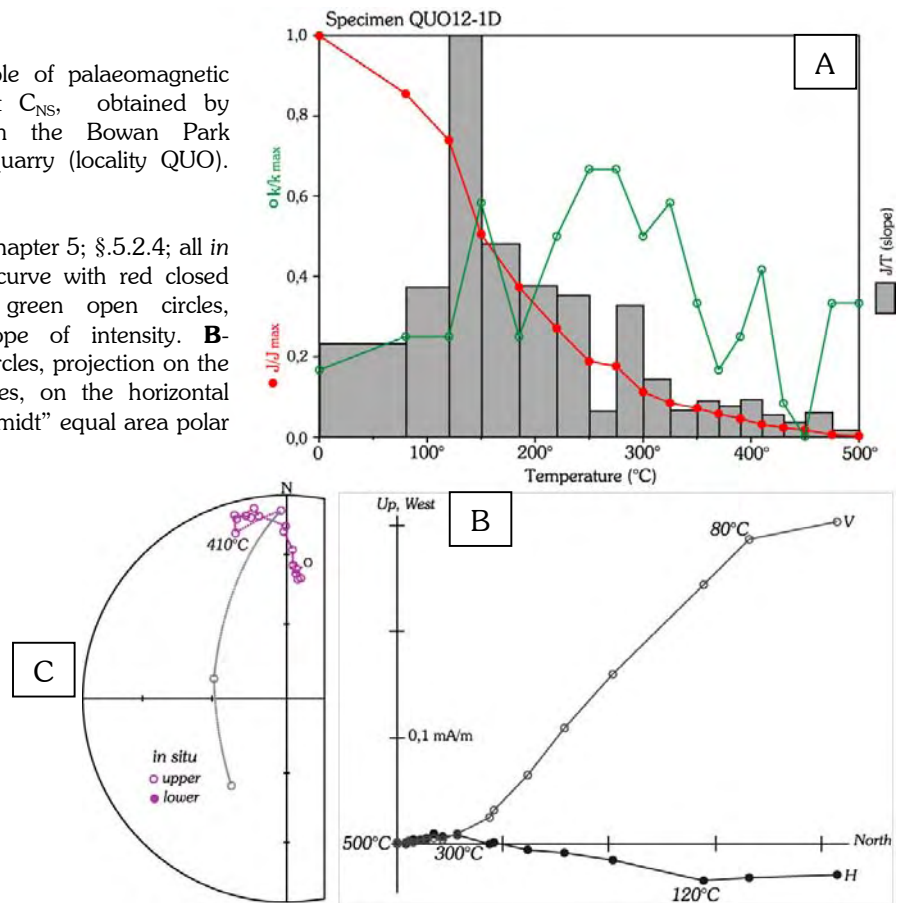
Figures 7.32: First example of palaeomagnetic results, showing a component C_{EW} , obtained by thermal demagnetisation from the Bowan Park Limestone of the Quondong quarry (locality QUO). Specimen QUO8-1D. NRM@RT=1,14 mA/m.

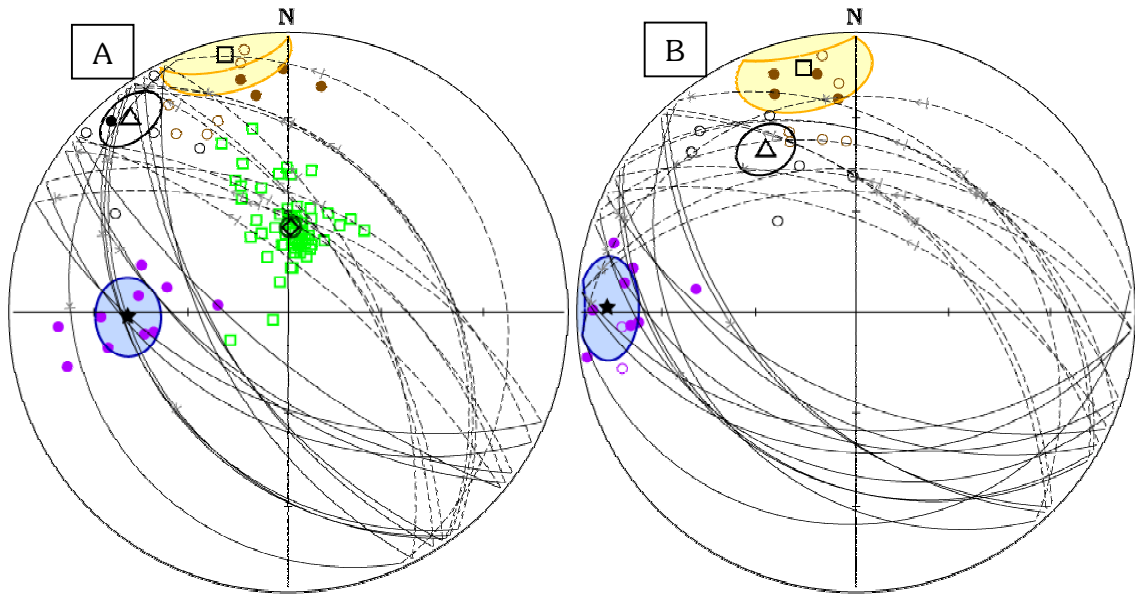
Same legend as in figure 5.6 (Chapter 5; §.5.2.4; all *in situ*); i.e. **A**- Demagnetisation curve with red closed circles, normalised intensity; green open circles, susceptibility; grey boxes, slope of intensity. **B**- Zijderveld diagram with open circles, projection on the vertical plane [V]; closed circles, on the horizontal plane [H]. **C**- Stereogram; “Schmidt” equal area polar projection.

Figures 7.33: Second example of palaeomagnetic results, showing a component C_{NS} , obtained by thermal demagnetisation from the Bowan Park Limestone of the Quondong quarry (locality QUO). Specimen QUO12-1D.

NRM@RT=5,25.10⁻¹ mA/m.

Same legend as in figure 5.6 (Chapter 5; §.5.2.4; all *in situ*); i.e. **A**- Demagnetisation curve with red closed circles, normalised intensity; green open circles, susceptibility; grey boxes, slope of intensity. **B**- Zijderveld diagram with open circles, projection on the vertical plane [V]; closed circles, on the horizontal plane [H]. **C**- Stereogram; “Schmidt” equal area polar projection.





Figures 7.34: Direction of components obtained from the Late Ordovician (Eastonian) Bowan Park Limestone of the Quondong quarry (locality QUO), **A-** *in situ* and **B-** after bedding correction.

Green squares are single specimen orientations of component C_1 shown *in situ* only with their overall mean direction (**diamond**) and **dark green** confidence cone (α_{95}) calculated from single specimen directions. **Brown circles** are orientations of single specimen component C_{NS} , **black circles** (and black lines are components defined by great circles analysis) are orientations of single specimen components of intermediate direction, and **violet circles** are single specimen orientations of component C_{EW} . They are shown with their overall mean directions: **squares** and **orange** confidence cone (α_{95}) for C_{NS} , **stars** and **blue** confidence cone (α_{95}) for C_{EW} , **triangle** (of no real significance) and **black** confidence cone (α_{95}) for intermediate directions. These mean directions are calculated from the single specimen directions, but overall mean direction obtained from site means are given in table 28.

Open symbols are negative inclination values (upper hemisphere); **closed** symbols, positive inclination values (lower hemisphere). Schmidt equal area polar projection.

Table 29: Site mean directions and overall mean directions for the locality QUO

Name	N	R	D.InS	I.InS	α_{95}	κ	R	D.Bed	I.Bed	α_{95}	κ	DipDir	Dip
<i>Components C_{EW} per site:</i>													
Quo-08	5	4,9	268,1	+48,3	13,4	33,7	4,9	271,8	+20,5	13,4	33,7	280,6	28,2
Quo-09	3	3,0	260,6	+23,2	15,9	60,9	4,9	261,1	-09,5	15,9	60,9	268,4	33,0
Quo-10	2	2,0	285,1	+48,2	22,8	122,4	2,0	283,7	+13,9	22,8	122,4	280,6	34,4
<i>Components C_{NS} per site:</i>													
Quo-11	4	3,8	331,3	-15,5	24,8	14,7	3,8	338,5	-24,5	24,8	14,7	269,4	21,4
Quo-12	3	2,9	339,8	-16,8	20,2	38,3	2,9	350,7	-29,0	20,2	38,3	280,6	28,0
Quo-13	4	4,0	356,8	+17,0	10,6	76,1	4,0	346,5	+15,8	10,6	76,1	263,6	34,0
Name	B	N	R	D.InS	I.InS	α_{95}	κ	R	D.Bed	I.Bed	α_{95}	κ	
<i>Mean direction for the components C_0:</i>													
QUO- C_0	13	60	12,7	359,7	-53,7	6,4	42,4	31,2	033,9	-51,7	7,5	31,2	site means
QUO- C_0	~	60	58,7	359,2	-51,9	3,6	27,1	58,4	030,6	-50,7	3,9	23,3	single sp.
<i>Mean direction for the components C_1:</i>													
QUO- C_1	14	62	13,8	001,2	-64,2	5,4	55,6	13,6	049,1	-57,9	7,4	29,7	site means
QUO- C_1	~	62	60,4	001,7	-64,8	3,0	38,3	59,5	049,6	-58,6	3,7	24,65	single sp.
<i>Mean direction for the components C_{EW}:</i>													
QUO- C_{EW}	3	10	2,9	270,0	+40,4	26,9	22,1	2,9	272,1	+08,5	30,2	17,7	site means
QUO- C_{EW}	~	10	9,6	268,4	+41,1	10,6	21,6	9,5	270,9	+10,3	11,8	17,8	single sp.
<i>Mean direction for the components C_{NS}:</i>													
QUO- C_{NS}	3	10	2,8	345,0	-06,7	35,9	12,8	2,8	348,0	-13,4	40,0	10,6	site means
QUO- C_{NS}	~	10	9,3	346,2	-04,2	14,4	12,2	9,1	347,8	-10,2	15,6	10,5	single sp.

N: number of samples; **B:** number of sites; α_{95} : cone calculated at the 95% confidence level; κ : precision parameter; **R:** resultant vector; **D.InS/I.InS:** declination/inclination *in situ* (geographic coordinates); **D.Bed/I.Bed:** declination/inclination after bedding correction; **DipDir/Dip:** direction of dip and dip of the bedding.

For the locality, the first line (**site means**) gives the overall mean direction for each component calculated from site mean directions, and the second line (**single sp.**), the overall mean direction calculated from single specimen directions.

Albeit their dispersion, the high temperatures components can be thus separated in two principal groups: the N-S cluster and the E-W cluster.

If only the N-S cluster is considered (brown dots in figures 7.34), the orientation *in situ* is D.346° / I.-04° ($\alpha_{95}=12,2^\circ$ / $\kappa=14,4$) and D.348° / I.-10° ($\alpha_{95}=15,6^\circ$ / $\kappa=10,5$) after bedding correction. Although the change in bedding orientation is very small, there is a decrease in the precision parameter κ since the classic fold test is positive only at the 25,0% confidence level.

The E-W cluster (violet dots in figure 5.27) yields D.268° / I.+41° ($\alpha_{95}=10,6^\circ$ / $\kappa=21,6$) *in situ*, and D.271° / I.+10° ($\alpha_{95}=11,8^\circ$ / $\kappa=17,8$) after bedding correction. Similarly, the κ parameter decreases when the bedding correction is applied and the fold test becomes positive at the 34,0% confidence level.

When the last component is too weak to be well isolated, great circles analysis has been used. For some components, there is a connection between components C_1 and C_{EW} . For others however, this connection seems to exist between C_{EW} and C_{NS} . It means that the two orientations are demagnetised in the same range of temperatures, and some intermediate directions also exists (black dots in figures 7.34). The mean direction on these components (back triangle in figure 7.34) has therefore no real meaning.

The age of magnetisation cannot be constrained here, but it is likely that both C_{EW} and C_{NS} are post-folding remagnetisations. It is striking to see that these two directions are very similar to those obtained in the Early – Middle rhyolitic intrusions of the Sisters (Broken Hill area). Nevertheless, the *in situ* E-W direction is relatively close to that observed in the Early Devonian Ural Volcanics of the Merri Abba property, whereas after bedding correction, it seems more similar to the poorly defined orientations of the Mt Daubeny Formation of the Churinga property (Broken Hill area), or the Gundaroo sandstones of the Bulgoo property (Mt Bowen area).

It is therefore speculative to try to draw any conclusions from similarities at this stage, in particular between localities distant from several hundreds kilometres one another. However, both C_{EW} and C_{NS} have low inclination values, which imply an Early – Middle Palaeozoic age of magnetisation, and probably post-Early Devonian as the main folding phase is believed to be Early Devonian (Bowling orogenic event). The duality in orientation apparently contained in the same type of magnetic carrier within the same rocks is however not understood.

The palaeopoles corresponding to the overall mean direction calculated on single specimen directions (figures 7.34; table 29) for C_{EW} and C_{NS} plot apart from any expected positions for Gondwana (figure 7.35; table 30). Hence, it can be concluded that, although the ages and origins of these magnetisations are not understood, the most plausible explanation for the positions of these palaeopoles is that terrane rotation and/or movement occurred.

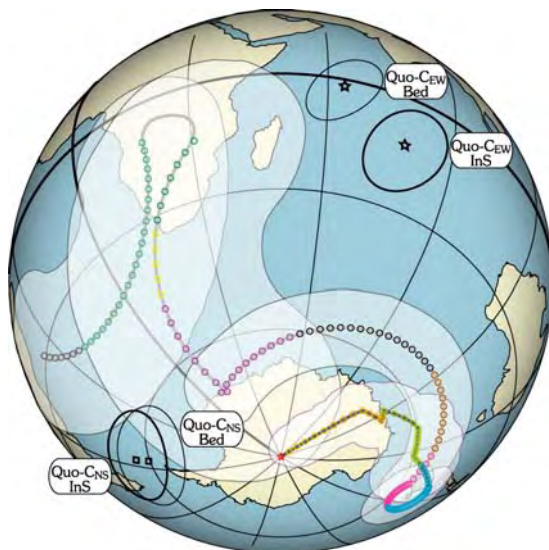


Figure 7.35: Corresponding palaeopoles in Australian coordinates. The possible APW path for Australia-Gondwana from the present-day to 570 Ma based on Small Circle Fit is shown for comparison purposes. Same legend as in figure 2.19-A, Chapter 2 (§.2.7).

Quo- C_{EW} InS and **Quo- C_{EW} Bed** are the palaeopoles (**stars**) corresponding to component C_{EW} *in situ* and after bedding correction respectively. Similarly, **Quo- C_{NS} InS** and **Quo- C_{NS} Bed** are the palaeopoles (**squares**) corresponding to component C_{NS} *in situ* and after bedding correction respectively.

Table 30: Palaeopoles obtained from the Bowan Park Limestone of the Quondong quarry (locality QUO)

B	N	Australian coord.		African coord.		dp	dm	Coordinates system
		Plat	PLong	Plat	PLong			
<i>Components C_{EW}:</i>								
~	10	-13,9	078,0	+25,3	058,9	7,8	12,9	from <i>in situ</i> orientation
~	10	-02,1	063,6	+42,6	051,0	6,0	11,9	after bedding correction
<i>Components C_{NS}:</i>								
~	10	-56,2	303,4	-34,5	333,8	7,2	14,4	from <i>in situ</i> orientation
~	10	-57,3	003,1	-35,3	337,8	8,0	15,8	after bedding correction

N: number of samples; **B**: number of sites; **PLong/Plat.**: palaeopole longitude/latitude in Australian and in African coordinates. **dp/dm** : semi-axis of the ellipse of confidence. Poles obtained from overall direction calculated from single component directions (see table 28).

N: number of samples; **B:** number of sites; **PLong./Plat.:** palaeopole longitude/latitude in Australian and in African coordinates. **dp/dm** : semi-axis of the ellipse of confidence. Poles obtained from overall direction calculated from single component directions (see table 28).

7.7. The Yuranigh Limestone Member (YUR)

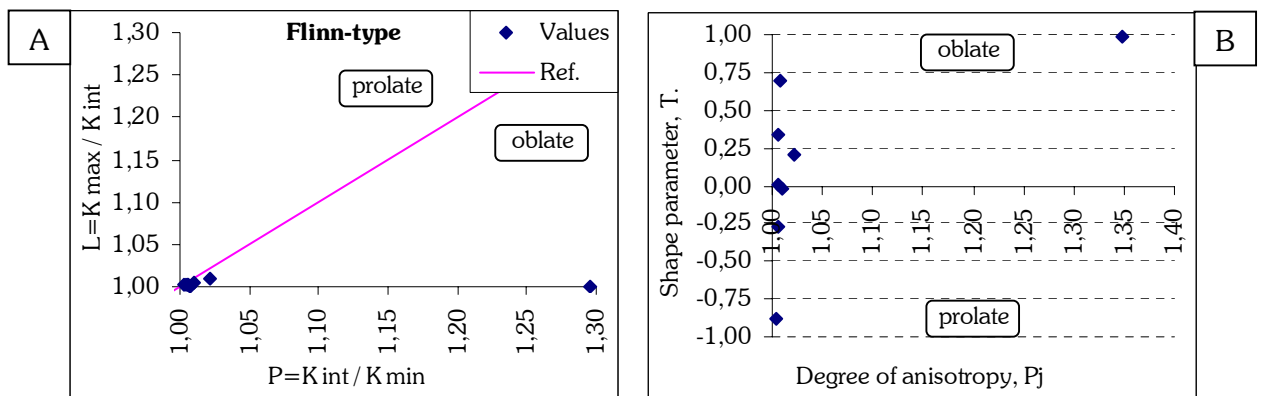
7.7.1. Presentation

The unit is named after the neighbouring Yuranigh Creek, which is situated about 3 km south of Molong (figure 7.2). The Yuranigh Limestone Member consists of massive and bedded limestone, calcareous siltstone and lithic sandstone and includes an interbedded weathered trachyandesite flow. The main limestone body referable to the Yuranigh Limestone Member (locality YUR) is up to 180 metres thick, and lies conformably within the Fairbridge Volcanics. On the field however, the limestone sufficiently exposed to be drilled represent about 50 metres long and 10 meters wide only. The Yuranigh Limestone Member contains a sparse biota, which indicates a likely Late Gisorbian age (Gi-2; early Late Ordovician) and supports a very shallow water depositional environment deepening upwards through the unit (Percival, *personal communication*, 2000; Pogson & Watkins, 1998).

Two sites (10 cores) have been obtained in the limestone and one (4 cores) has been drilled in the volcanic flow. This last however is revealed too weathered, and no stable magnetic response could have been obtained from this rock. Hence, only results from the limestone are presented below.

7.7.2. Anisotropy of magnetic susceptibility (AMS)

The degree of magnetic anisotropy is very low ($P_j = 1,05 \pm 0,12$) and the shape of the ellipsoid of magnetic anisotropy is not clearly marked ($T = 0,13 \pm 0,56$), although the mean value of $\{T\}$ plots in the oblate part of the $\{T\}$ vs. $\{P_j\}$ diagram (figure 7.36-B). This shape and the low values of $\{L\}$ & $\{P\}$ on the Flinn-type diagram (figure 7.36-A) confirm this information. It can be stated hence that the degree of internal strain is negligible and cannot cause deviations.



Figures 7.36: **A-** Flinn-type diagram (Flinn, 1962, 1965-a, 1965-b); and **B-** $\{T\}$ versus $\{P_j\}$ diagram (Jelinek, 1981; Hrouda, 1982) for the Yuranigh Limestone Member (locality YUR).

The Königsberger ratio has relatively elevated values ($Q_K@RT=2,63\pm1,11$) leading to think that the size of the magnetic particles may be small. It seems to exclude, however, the possibility that these rocks have been struck by lightning.

The direction of the principal axes of magnetic susceptibility are regarded as randomised both *in situ* and after bedding correction (figures 7.37) giving no specific information about the fabric of the rock. This is in relative good agreement with the very low degree of anisotropy. It could be possible however that a magnetic fabric arises if the number of samples was larger.

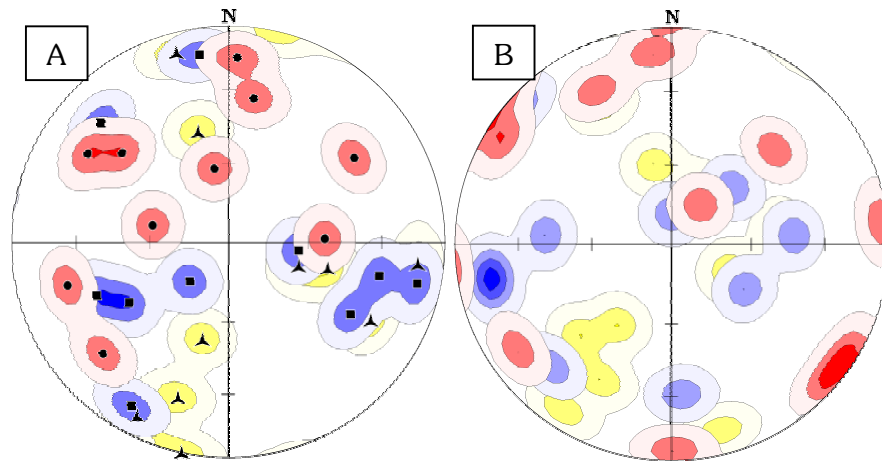
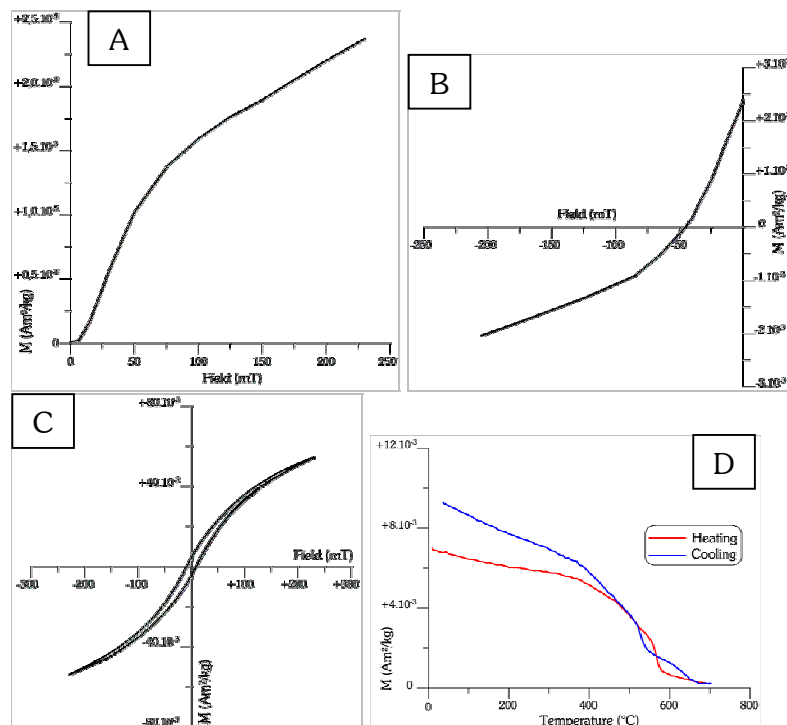


Figure 7.37: Orientations of the principal axes of magnetic susceptibility for the Yuranigh Limestone Member, locality YUR.

A- *in situ*, and **B-** test of correction.

Same legend as in figure 5.4 (Chapter 5; §.5.2.2); i.e. Kmax, squares (blue); Kint, triangles (yellow); Kmin, dots (red).

7.7.3. Rock magnetism



Figures 7.38: Example of rock magnetic measurements from Yuranigh Limestone (locality YUR): specimen YUR3-1.

A- IRM curve; **B-** Back field curve (coercivity); **C-** Hysteresis loop; and **D-** IST curve, in red while heating and in blue while cooling ($B=25$ mT).

$H_C=11,63$ mT; $H_{CR}=45,61$ mT.
 $M_S=1,4 \cdot 10^{-2}$ Am²/kg; $M_{RS}=2,3 \cdot 10^{-3}$ Am²/kg.

The IRM and back field curves show the presence of a relatively low coercivity mineral (figures 7.38-A & B), but the curves are not saturated. The IST curve (figure 7.38-D) shows that this low coercivity material can correspond to magnetite as an important decrease in magnetisation occurs around 580°C. As a slight decay is visible below 200°C and a magnetisation persists up to 650° – 700°C, it is possible that oxidation of magnetite gave rise to the existence of

some maghaemite, haematite and/or goethite. However, these decreases are confused by the contribution of paramagnetic mineral, clearly revealed by the slope of the hysteresis loop (figure 7.38-C). Finally, the cooling curve shows clearly that haematite and magnetite are newly formed.

In any cases, magnetite can be considered as the main magnetic carrier in these rocks.

7.7.4. Palaeomagnetic results

- Demagnetisation

The demagnetisation curve (figure 7.39-A) shows clearly two principal ranges of unblocking temperatures. The first occurs between 300° and 350°C and the second, between 525° and 575°C. In terms of directions, the orthogonal projection (figure 7.39-B) reveals an unclear first component from room temperature to 120°C apparently corresponding to the present-day field. It may be carried therefore by a few amount of goethite. Then, only one direction of magnetisation seems to be present up to 575°C, close to the Curie temperature of magnetite. It define then a single component C_s . Above, if haematite or maghaemite exists, it is too weak to be measured. The strong increase in susceptibility reflects some thermo-chemical alteration, also illustrated by the apparition of a noisy signal.

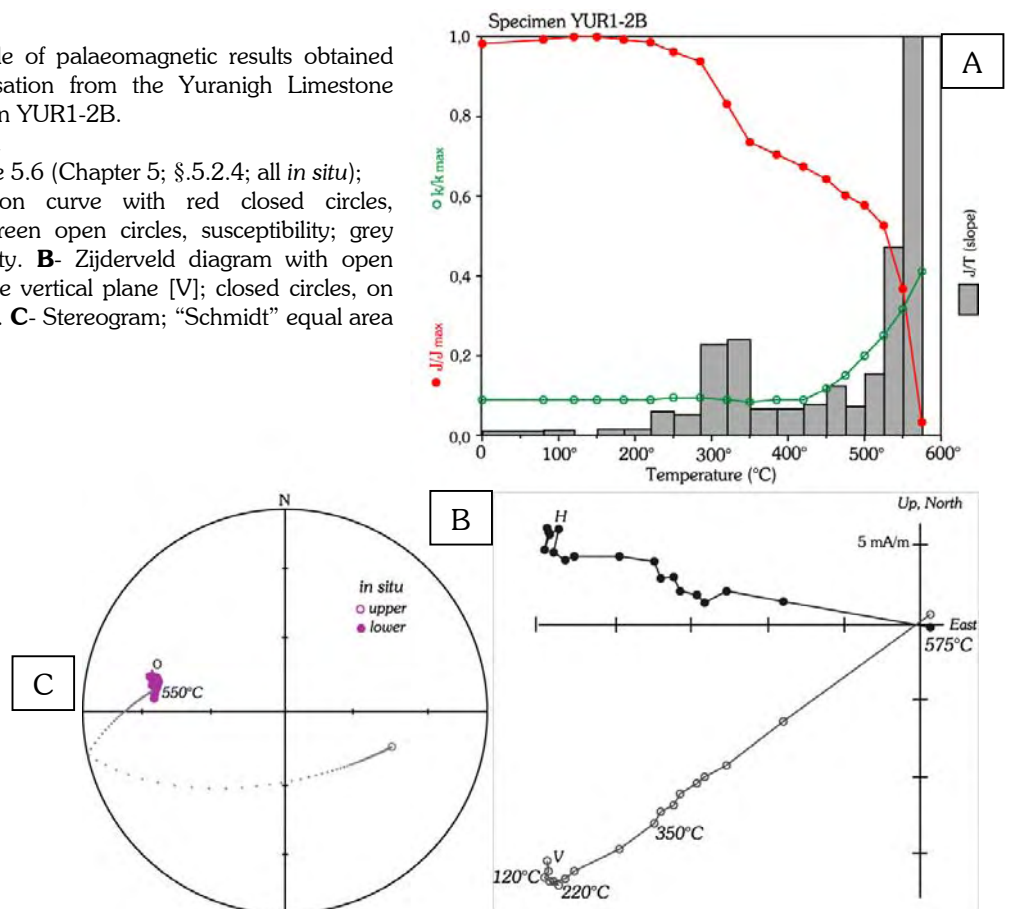
- Interpretation

The material demagnetised between 300° and 350°C has the same direction of magnetisation than magnetite. This mid unblocking temperature spectrum is probably the fact of some sulphides such as pyrrhotite or greigite, but does not appears to be related with the Tertiary overprint found in several other localities. Conversely, the presence of sulphide might be due to anoxic conditions in the very shallow water environment when the limestone formed (see §.7.7.1).

Figures 7.39: Example of palaeomagnetic results obtained by thermal demagnetisation from the Yuranigh Limestone (locality YUR). Specimen YUR1-2B.

NRM@RT=4,25 mA/m.

Same legend as in figure 5.6 (Chapter 5; §.5.2.4; all *in situ*); i.e. **A-** Demagnetisation curve with red closed circles, normalised intensity; green open circles, susceptibility; grey boxes, slope of intensity. **B-** Zijderveld diagram with open circles, projection on the vertical plane [V]; closed circles, on the horizontal plane [H]. **C-** Stereogram; “Schmidt” equal area polar projection.



Since only ten cores have been collected in this limestone, the overall mean direction calculated from just two sites is regarded as less significant as the overall mean direction calculated from single specimen components. However, the two are shown in table 31.

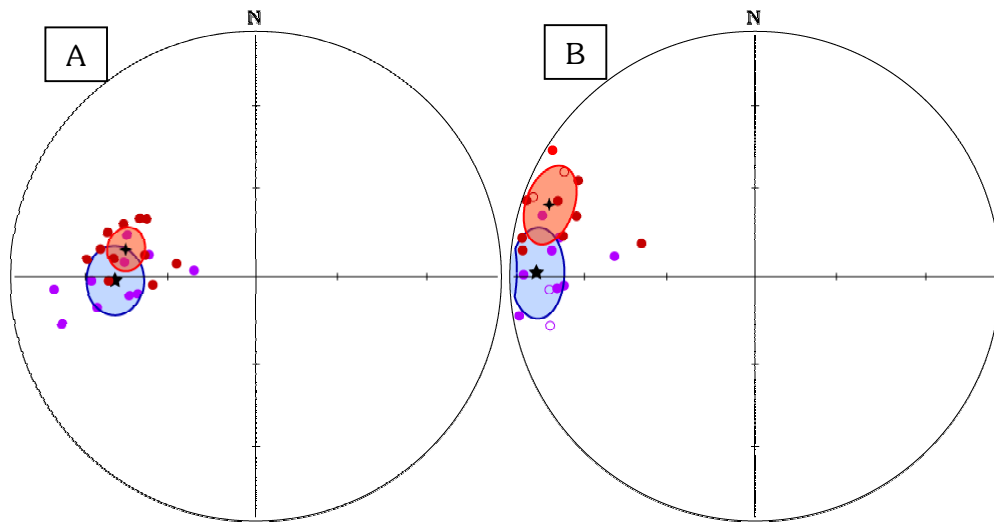
The overall mean direction calculated from single specimen components, C_s , is indeed interesting because all the ten specimens have a very similar magnetic behaviour, and the directions are well consistent one another (figures 7.40). The mean direction is oriented D.282° / I.+44° ($\alpha_{95}=7,5^\circ$ / $\kappa=42,4$) *in situ*, and D.290° / I.+09° ($\alpha_{95}=11,5^\circ$ / $\kappa=18,7$) after bedding correction. The similarity with the mean direction of C_{EW} at locality QUO is striking (figures 7.40), and is believed to be here more relevant than other similarities noticed, since localities QUO and YUR are separated by only a couple of tens of kilometres (see figure 7.2). In addition, as in locality QUO, the grouping in palaeomagnetic direction is significantly worse after bedding correction since the classic fold test is positive only at the 4,5% confidence level. This suggests a post-folding remagnetisation, which is also confirmed if the fold test is performed at regional scale encompassing the three sites from locality QUO and the two from locality YUR (table 31). The classic fold test is in this case positive at the 20% confidence level.

Table 31: Site mean directions and overall mean directions for the locality YUR

Name	N	R	D.InS	I.InS	α_{95}	κ	R	D.Bed	I.Bed	α_{95}	κ	DipDir	Dip
<i>Components C_s per site:</i>													
Yur-01	6	5,9	282,3	+42,5	9,6	49,3	5,9	291,2	+00,9	10,0	45,9	314,0	46,1
Yur-02	4	3,9	282,5	+45,8	17,7	28,0	3,8	286,6	+22,5	24,7	14,8	298,9	24,0
Name	B	N	R	D.InS	I.InS	α_{95}	κ	R	D.Bed	I.Bed	α_{95}	κ	
<i>Mean direction for the components C_s:</i>													
YUR- C_s	2	10	2,0	282,4	+44,2	7,2	1203,7	2,0	289,0	+11,7	50,0	27,1	site means
YUR- C_s	~	10	9,8	282,4	+43,8	7,5	42,4	9,5	289,5	+09,3	11,5	18,7	single sp.
<i>Mean direction combining the components C_{EW} from locality QUO and C_{YUR} from locality YUR:</i>													
QUO-YUR	5	20	4,9	274,9	+42,1	12,8	36,7	4,8	278,9	+09,9	17,6	19,9	site means

N: number of samples; **B:** number of sites; α_{95} : cone calculated at the 95% confidence level; κ : precision parameter; **R:** resultant vector; **D.InS/I.InS:** declination/inclination *in situ* (geographic coordinates); **D.Bed/I.Bed:** declination/inclination after bedding correction; **DipDir/Dip:** direction of dip and dip of the bedding.

For the locality, the first line (**site means**) gives the overall mean direction for each component calculated from site mean directions, and the second line (**single sp.**), the overall mean direction calculated from single specimen directions.



Figures 7.40: Direction of components obtained from the Late Gisbornian (early Late Ordovician) Yuranigh Limestone Member (locality YUR), **A**- *in situ* and **B**- after bedding correction.

Bordeaux circles are single specimen orientations of component C_s , and the **black star** (4 branches) is the corresponding mean direction with its associated 95% confidence cone (**red**); **violet circles** correspond to orientations of component C_{EW} from locality QUO shown for comparison with their mean direction (**star**, 5 branches) and **blue** α_{95} as per figures 7.34.

Open symbols are negative inclination values (upper hemisphere); **closed** symbols, positive inclination values (lower hemisphere). Schmidt equal area polar projection.

Table 32: Palaeopoles obtained from the Yuranigh Limestone (locality YUR)

B	N	<i>Australian coord.</i>		<i>African coord.</i>		dp	dm	Coordinates system
		<u>Plat</u>	<u>Plong</u>	<u>Plat</u>	<u>PLong</u>			
<i>Components C_s:</i>								
~	10	-04,3	086,9	+27,8	073,2	5,9	9,4	from <i>in situ</i> orientation
~	10	+13,5	073,8	+49,7	076,0	5,9	11,6	after bedding correction

N: number of samples; **B**: number of sites; **PLong./Plat.**: palaeopole longitude/latitude in Australian and in African coordinates. **dp/dm** : semi-axis of the ellipse of confidence. Poles obtained from overall direction calculated from single component directions (see table 30).

These results are again based on few data only, and must therefore be regarded with caution. However, the good consistency in the directions observed within the locality YUR and the similarity with C_{EW} from locality QUO leads to think that this direction of magnetisation has a real palaeomagnetic meaning.

The palaeopoles corresponding to the overall mean direction calculated on single specimen directions (figures 7.40; table 31) for C_s plot far away from any expected positions for Gondwana (figure 7.41; table 32), no matter the coordinates system considered. Given the negative fold test however (although it is based on 10 data only), it is likely that C_s has to be considered *in situ*, and the position of corresponding palaeopole, shown with heavy line for its confidence cone (figure 7.41), is favoured.

Still, the ages and origins of this magnetisation remains unresolved, although it should represent a post-Early Devonian pole position since the major folding phase is believed to be caused by Bowring orogenic event (Early Devonian). In any cases however, and like for locality QUO, the most plausible explanation for these positions (*in situ* and after bedding correction) is that terrane rotation and/or movement occurred.

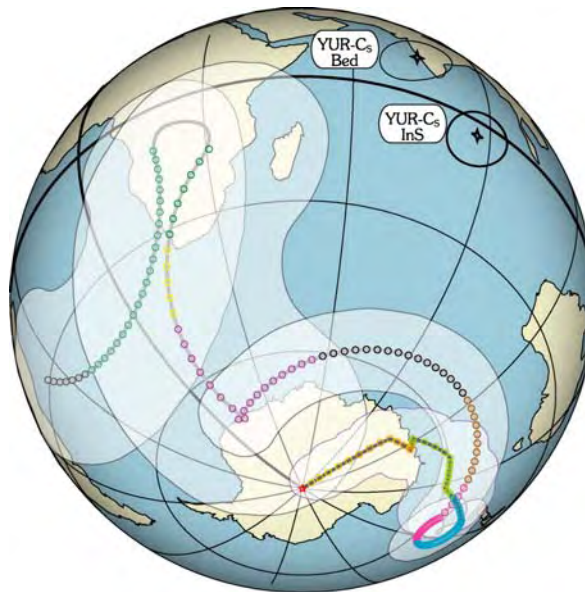


Figure 7.41: Corresponding palaeopoles in Australian coordinates. The possible APW path for Australia-Gondwana from the present-day to 570 Ma based on Small Circle Fit is shown for comparison purposes.

Same legend as in figure 2.19-A, Chapter 2 (§.2.7).

YUR- C_s InS and **YUR- C_s Bed** are the palaeopoles (**stars, 4 branches**) corresponding to component C_s *in situ* and after bedding correction respectively.

7.8. The Cliefden Caves Limestone from the Little Boonderoo Property (BOO)

7.8.1. Presentation

The main body of the Cliefden Caves Limestone Subgroup forms an irregular, arcuate, strongly block-faulted belt, 500 to 1000 metres wide, which extends from 2 km to the North of the Cliefden Caves to about 8 km to the South-East and 8 km to the South-West of the

Cliefden Caves. The sampled locality (BOO) itself is situated in the vicinity of the Little Boonderoo Property, about 40 km to the East of Canowindra (figure 7.2).

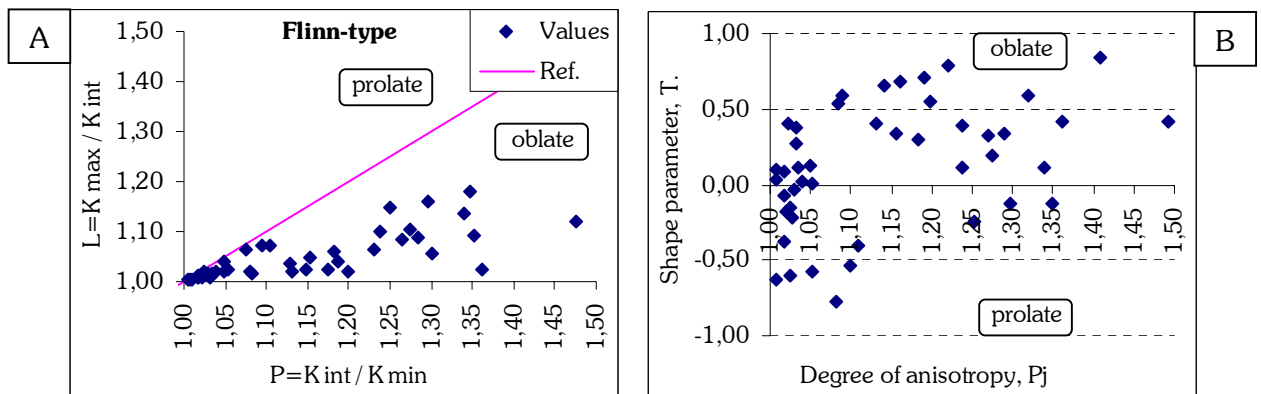
The Cliefden Caves Limestone Subgroup, belonging to the Barrajin Group, is thought to disconformably overlie the Walli Volcanics, and the contact with the overlying Malongulli Formation is abrupt and erosional. This relationship has been interpreted by Webby (1992) to be due to an episode of submarine scouring during subsidence. The sedimentology and palaeoecology of the unit reflect carbonate deposition in a mostly shallow but fluctuating marine environment due to tectonically induced sea level changes.

The main unit constituting the sampled locality is the Belubula Limestone, which is composed of massively bedded (0,1 – 1 metre), gently folded (where sampling has been carried out), grey lime, mudstone, and skeletal wackestone. It appears to have accumulated in quiet conditions, possibly analogous to those of a shelf lagoon (Webby, 1992). The diverse biotas contained in the limestone suggest an Early Eastonian (early – middle Late Ordovician) age (Percival, *personal communication*, 2000; Pogson & Watkins, 1998).

Forty-nine cores have been collected in nine sites.

7.8.2. Anisotropy of magnetic susceptibility (AMS)

Both the $\{T\}$ vs. $\{P_j\}$ and the Flinn-type diagrams (figures 7.42) reflect a relatively high degree of anisotropy ($P_j = 1,14 \pm 0,13$). The shape of the ellipsoid of magnetic susceptibility is clearly oblate according to the Flinn-type diagram (figure 7.42-A), but, although the mean value tends to confirm this shape, the $\{T\}$ parameter has error bars covering both sides of the $\{T\}$ vs. $\{P_j\}$ diagram (figure 7.42-B). It is unlikely however, that such values of degree of anisotropy can induce a significant deviation of the palaeomagnetic results (Cogné, 1987).



Figures 7.42: **A-** Flinn-type diagram (Flinn, 1962, 1965-a, 1965-b); and **B-** $\{T\}$ versus $\{P_j\}$ diagram (Jelinek, 1981; Hrouda, 1982) for the Cliefden Caves Limestone Member from the Little Boonderoo Property (locality BOO).

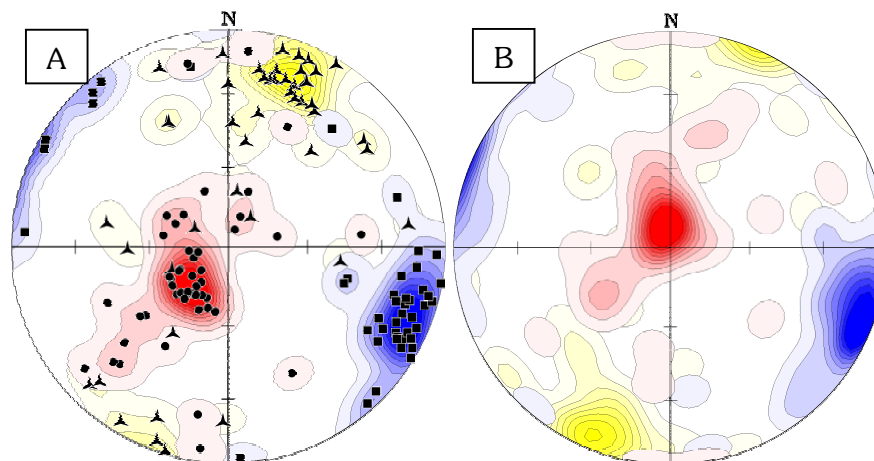


Figure 7.43: Orientations of the principal axes of magnetic susceptibility for the Cliefden Caves Limestone, locality BOO.

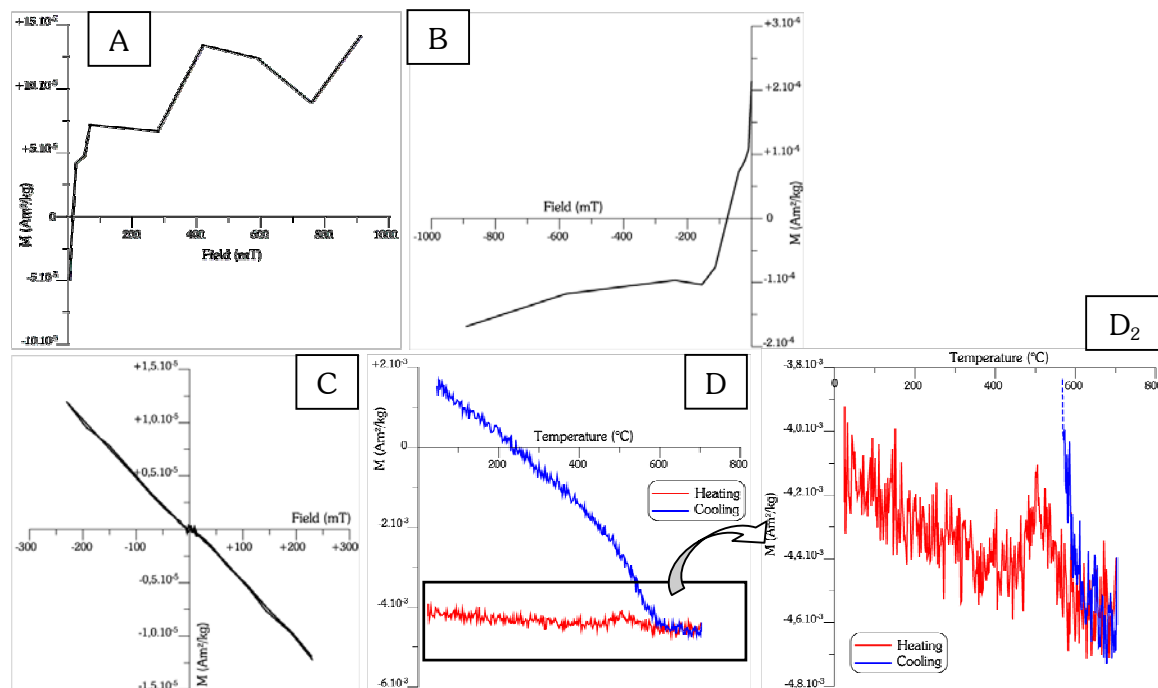
A- *in situ*, and **B-** test of correction.

Same legend as in figure 5.4 (Chapter 5; §.5.2.2); i.e. Kmax, squares (blue); Kint, triangles (yellow); Kmin, dots (red).

It is possible that the degree of anisotropy has not only tectonic causes. As it was apparently the case for the Bowan Park Limestone of locality QUO (§7.6), it is also possible that relative high values of susceptibility stems from very small magnetic grains. Indeed, the mean value of the Königsberger ratio ($Q_K@RT=1,82\pm6,17$) is compatible with the possible existence of small magnetic particles. The values of Q_K , however, never exceed 15 and it excludes lightning strikes effects.

On the contrary to locality QUO, the directions of the principal axes of magnetic susceptibility are well grouped (figures 7.43). K_{min} correspond well with the pole to the bedding since they are situated near a vertical position after bedding correction (figures 7.43-B). The sedimentary magnetic fabric is therefore preserved in these rocks, which is in good agreement with the oblate shape of the ellipsoid of magnetic susceptibility revealed by AMS parameters. Some K_{min} however appears to show a significant deviation from the mean value (or density peak) and tends to be aligned along a great circle linked to the density peak of K_{int} . It is believed that this corresponds to a moderately developed tectonic magnetic fabric superimposed to the sedimentary one. It is perpendicular to the magnetic lineation, and probably reflects a NNE-SSW direction of strain.

7.8.3. Rock magnetism



Figures 7.44: Example of rock magnetic measurements from the Cliefden Caves Limestone (locality BOO): specimen BOO1-1. **A-** IRM curve; **B-** Back field curve (coercivity); **C-** Hysteresis loop; and **D-** IST curve, in red while heating and in blue while cooling & **D₂**- Zoom on features of the heating curve ($B=535$ mT).

$$H_C=9,86 \text{ mT}; H_{CR}=41,30 \text{ mT}.$$

$$M_S=4,9 \cdot 10^{-4} \text{ Am}^2/\text{kg}; M_{RS}=1,9 \cdot 10^{-4} \text{ Am}^2/\text{kg}.$$

The intensity of magnetisation is very low, and it explains why the curves obtained are so noisy. Albeit their bad shape, the IRM and back field curves (figures 7.44-A & B) show the presence of low coercivity material (a theoretical curve fitted on the back field curve gives the value for H_{CR} : $H_{CR}=41,3$ mT) and look saturated, probably signifying the absence of high coercivity material such as oxidised minerals. The hysteresis loop indicates a nearly pure diamagnetic behaviour of this limestone (figure 7.44-C), confirmed by the strongly negative values on the IST curve around 700°C (figure 7.44-D). The contribution of ferromagnetic [s.l.] material is

minor. Nevertheless, the heating part of the IST curve is not exactly horizontal and this slope denotes a weak contribution of paramagnetic material as well. This last can be caused by some phyllosilicates for instance, and can explain the formation of new magnetite marked by a peak on the heating curve around 500°C and a clear magnetisation recorded from ~580°C on the cooling curve (figure 7.44-D₂). Magnetite was however probably present before this mineralogical change, and is believed to be the main magnetic carrier having the low coercivity observed. Magnetite is furthermore very common in carbonates.

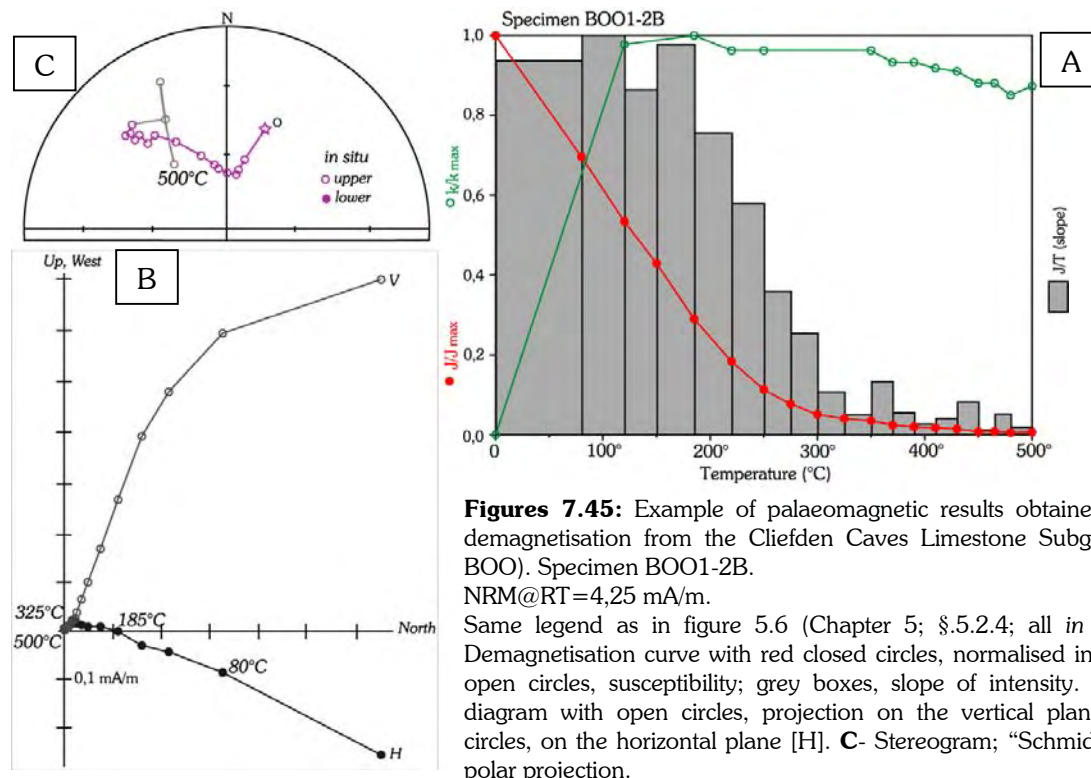
7.8.4. Palaeomagnetic results

- Demagnetisation

Most of the remanence is removed around 300°C (figure 7.45-A), and the specimen shown here is fully demagnetised by 450° – 500°C. In this case, three components are visible. The first, up to 150°C, is a viscous magnetisation, showing randomised direction of magnetisation or a tendency to align the present-day field orientation. Nevertheless, it carries about 50% of the NRM at room temperature. The second, component C_p, is isolated between 150° – 185°C and 325°C. This is close to the Curie temperature of pyrrhotite, and the direction of magnetisation corresponds here also to the Tertiary overprint presented in §.7.2. The third component, C_M is very weak and can be hardly isolated. It is sufficiently distinguishable, however, (figure 7.45-B) to define a component in five of the nine sites obtained in this limestone. It is believed to be carried by magnetite as suggested from rock magnetic measurements.

- Interpretation

Components C_p is found in the nine sites drilled (table 33), but in some cases, this component can be apparently determined up to a higher temperature than 320°C. In site Boo-06 in addition, this component seems to be of reverse polarity. If these components of higher unblocking temperature are included, the overall mean direction is D.358°/I.-64° ($\alpha_{95}=4,3^\circ/\kappa=101,5$) *in situ*, and a positive reversal test classified C is obtained.



The fact that this last component appears to match C_p could mean that the Tertiary overprint is not a chemical remagnetisation only but more probably a thermo-chemical magnetisation event. The classic fold test (McElhinny, 1964) is significantly negative (it becomes positive at the 5,0% confidence level only), and proves in this locality as well that C_p is really a post-folding overprint.

Concerning component C_M , the different fold tests performed (McElhinny, 1964; McFadden, 1990; Enkin & Watson, 1996; Tauxe, 1998) yield a non-significant result (both with stepwise or at 100% unfolding), certainly because the change in bedding orientation is too small. The mean direction is oriented D.319°/I.-47° ($\alpha_{95}=11,9^\circ/\kappa=42,0$) *in situ*, and D.293°/I.-51° ($\alpha_{95}=10,5^\circ/\kappa=54,1$) after bedding correction. The classic fold test is positive at the 63,5% confidence level, which is the limit fixed herein to assess whether it can be considered that a possible improvement in grouping exist or not. No fold test seems therefore to be able to give an indication concerning a possible age of magnetisation.

Goleby (1980) also studied the Belubula Limestone and found a direction of magnetisation D.358°/I.-64° (B=4; N=66 but apparently from 26 cores; $\alpha_{95}=2,9^\circ/\kappa=38,5$) *in situ*. He considered this direction as primary, but this interpretation is strongly questioned here since it is strikingly close to our component C_p . In addition, Goleby (1980) studied several localities of different age in the same area as our locality BOO, and in particular the Malongulli Formation (siliceous and calcareous siltstone and marl) and the Angullong Tuff (predominantly volcanic breccias) overlying the Cliefden Caves Limestone Subgroup. His results are listed in table 34.

Table 33: Site mean directions and overall mean directions for the locality BOO

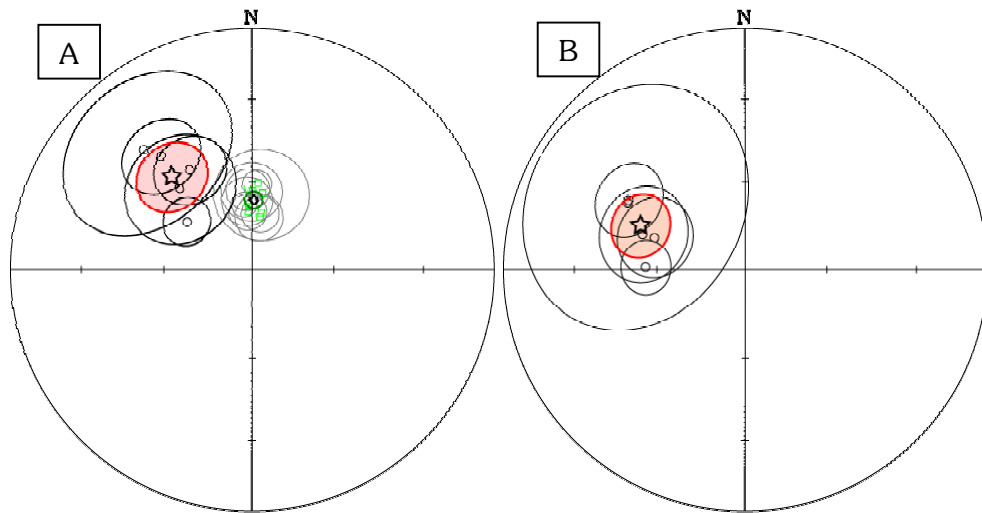
Name	N	R	D.InS	I.InS	α_{95}	κ	R	D.Bed	I.Bed	α_{95}	κ	DipDir	Dir
<i>Components C_M per site:</i>													
Boo-01	3	2,9	318,0	-32,6	28,1	20,2	2,8	299,7	-42,6	40,7	10,2	006,9	17,6
Boo-02	4	4,0	306,4	-62,1	8,2	127,4	4,0	271,4	-55,5	8,9	107,0	036,3	21,4
Boo-03	5	4,9	321,2	-38,7	13,0	35,7	4,9	300,9	-42,3	12,0	41,8	032,7	23,4
Boo-04	4	3,9	318,3	-52,2	18,8	27,7	3,9	289,2	-52,3	15,8	38,9	032,7	23,2
Boo-09	6	5,8	328,0	-49,1	12,1	31,9	5,8	289,7	-56,7	13,3	26,1	025,0	28,6
Name	B	N	R	D.InS	I.InS	α_{95}	κ	R	D.Bed	I.Bed	α_{95}	κ	
<i>Mean direction for the components C_p:</i>													
BOO- C_p	9	45	9,0	001,4	-66,2	2,9	314,7	8,9	281,2	-79,5	4,4	135,7	
<i>Mean direction for the components C_M:</i>													
BOO- C_M	5	22	4,9	319,1	-47,1	11,9	42,0	4,9	292,7	-50,5	10,5	54,1	

N: number of samples; **B:** number of sites; α_{95} : cone calculated at the 95% confidence level; κ : precision parameter; **R:** resultant vector; **D.InS/I.InS:** declination/inclination *in situ* (geographic coordinates); **D.Bed/I.Bed:** declination/inclination after bedding correction.

Table 34: Overall mean directions for several localities studied by Goleby (1980)

Name	B	N	n	D.InS	I.InS	α_{95}	κ	D.Bed	I.Bed	α_{95}	κ
<i>The Late Eastonian (late middle Late Ordovician) Malongulli Formation:</i>											
MG	7	22	61	326,9	-60,0	17,6	12,7	255,8	-50,7	4,6	173,6
<i>The Bolindian (late Late Ordovician) Angullong Tuff:</i>											
AT	4	20	32	322,6	-55,5	6,1	18,2	259,7	-51,4	5,7	21,1
<i>The Late Wenlock – Early Llundlow Tenandra Formation:</i>											
TF	2	6	11	324,0	-16,9	57,8	20,8	334,6	-41,9	9,0	26,7
<i>The Late Llundlow Cowra Granodiorite:</i>											
CG	1	6	8	302,5	-31,6	10,4	30,2	328,6	-27,0	10,3	30,1
<i>The Late Silurian to Early Devonian Dolerite Intrusions:</i>											
D	1	4	6	335,9	-63,9	6,6	103,7	301,2	-34,0	6,6	103,6

N: number of cores and **n:** number of specimens apparently used, since Goleby measured several specimens from the same core; **B:** number of sites; α_{95} : cone calculated at the 95% confidence level; κ : precision parameter; **R:** resultant vector; **D.InS/I.InS:** declination/inclination *in situ* (geographic coordinates); **D.Bed/I.Bed:** declination/inclination after bedding correction.



Figures 7.46: Direction of components obtained from the Eastonian (middle Late Ordovician) Cliefden Caves Limestone (locality BOO), **A-** *in situ* and **B-** after bedding correction.

Green squares (with their associated grey 95% confidence cones) are site mean directions for components C_p , shown *in situ* only. **Black diamond** and green α_{95} is the corresponding overall mean direction. **Black circles** and black α_{95} are site mean directions for components C_M , and the **star** with its red α_{95} is the overall mean direction of the locality.

Open symbols are negative inclination values; **closed** symbols, positive inclination values. Schmidt equal area polar projection.

For Goleby (1980), all these directions (table 34) represented primary magnetisations, and most of them have a positive fold test. The reliability of the results from these fold tests are however questionable, because first, it is believed that some components have been confused such as in the Cliefden Caves Limestone, and secondly, because a strong bias is introduced when several specimens of the same core are used for the calculations of means.

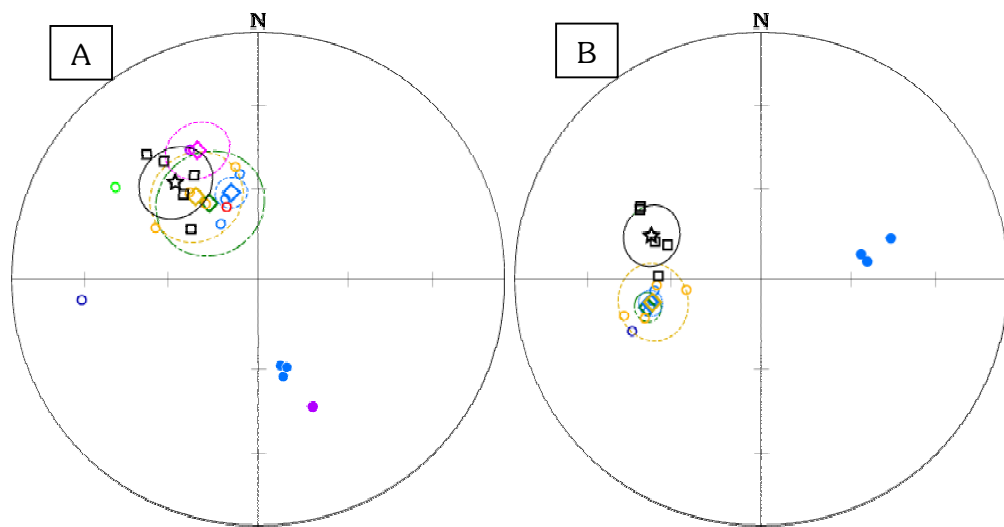
In any cases, the directions obtained by Goleby in the overlying units (Malongulli Formation & Angullong Tuff) are relatively close to those obtained at locality BOO. The fold test performed by Goleby on the Malongulli Formation (in blue in figures 7.47) is positive at more than the 99,9% confidence level (classic fold test of McElhinny, 1964), but is obtained thanks to one site only (dark blue circle in figures 7.47), which can let the reader sceptical. If this particular site is excluded, the overall mean direction *in situ* is interestingly positioned between our components C_p and C_M (blue diamond and dashed line in figure 7.47-A). This leads to think that component C_p might not have been fully removed and site mean directions could represent intermediate directions of magnetisation. Besides, the site that allows the positive test is situated to the East of the profile used for the other sites. The geological structure in this zone is complex with different orientations of fold axes. At kilometre scale, the general structure of the Cliefden Caves Limestone and neighbouring formations is a conical fold with a plunging axis. Goleby has apparently not taken this fact into account for the bedding correction. On the results from the Angullong Tuff, the classic fold test is not positive at the 95% confidence level but at the 92%. As the results from locality BOO are just at the limit to recognise a possible improvement in grouping (63,5% positive fold test), it could mean indeed that the magnetisation is pre-folding in origin. Nevertheless, when compared one another, the overall mean directions from locality BOO, the Malongulli Formation and the Angullong Tuff are better grouped *in situ* than after bedding correction (figures 7.47). This might also stem from the fact that the structural control in the different localities has been differently appreciated, since bedding orientation is difficult to assess in this arcuate, block-faulted belt.

On the other hand, the directions obtained *in situ* in these three Late Ordovician localities look similar to directions obtained by Goleby in Silurian rocks: the Cowra Granodiorite (red circle in figure 7.47-A) and the Dolerite Intrusions (light green circle in figure 7.47-A), considering their confidence cone (see table 34). They are obtained from a little number of data,

but are statistically undistinguishable from the Late Ordovician results. The mid Silurian Tenandra Formation (Pogson & Watkins, 1998; thought to be Siluro-Devonian by Goleby, 1980) has a positive fold test and reversal test after bedding correction. The corresponding orientation (shown after bedding correction in pink in figure 7.47-A, whereas the other results are *in situ* in this figure) is also statistically undistinguishable from the other directions, although one has to be cautious with this result based on two sites only. It is quite confusing because, if the positive fold test inferred from the two sites of the Tenandra Formation is believed, the direction of magnetisation in the Ordovician rocks are pre-mid Silurian in age, and perhaps indeed primary. The problem is that the Silurian results after bedding correction are not analogous one another. Conversely, if the good correspondence of all these directions *in situ* is regarded as not coincidental, a post-mid Silurian remagnetisation can be suspected, but the positive tests of the Tenandra Formation should be questioned. It must be pointed out in addition that these directions *in situ* are equivalent to the Siluro-Devonian direction of magnetisation reported by Schmidt *et al.* (1987) for the Snowy River Volcanics, which is D.341°/I.-56° ($\alpha_{95}=9,7^\circ/\kappa=25,6$) in the coordinates of locality BOO.

In conclusion, the age of magnetisation for locality BOO cannot be in definitive constrained.

Concerning the corresponding palaeopole for locality BOO (figure 7.48; table 35), the pole calculated from C_M *in situ* is comparable to the pole from the Snowy River Volcanics (Schmidt *et al.*, 1987) and therefore to the Y-type APW path of Schmidt *et al.* (1990), but the pole corresponding to C_M after bedding correction is away from any position expected for Gondwana.



Figures 7.47: Comparison between the directions obtained from the Cliefden Caves Limestone (locality BOO) and results reported by Goleby (1980).

A- **Black squares** are site mean directions and **black star**, the overall mean direction (and its **black** 95% confidence cone, α_{95}) for locality BOO *in situ*. **Blue circles** are site mean directions from Goleby for the Malongulli Formation; **green diamond** (and **green dashed lines** for the α_{95}) is the overall mean direction as given by Goleby, but the **blue diamond** (and **blue dashed line** for the α_{95}) is the overall mean direction if the isolated “E-W”-directed site (**dark blue circle**) is excluded. It looks then it could also correspond to an intermediate direction between our components C_p and C_M (see figure 7.46-A). **Orange circles** for site mean directions and **orange diamond** (and **orange dashed line** for the α_{95}) for the overall mean direction correspond to results given by Goleby for the Angullong Tuff *in situ*. The **red** and the **light green circles** are the mean directions *in situ* for the Cowra Granodiorite and the Dolerite Intrusions respectively. Finally, the **violet circles** are the two site mean directions and the **pink diamond** (and **pink dashed line** for the α_{95}), the overall mean direction obtained **after** bedding correction for the Tenandra Formation.

B- Locality BOO, Malongulli Formation and Angullong Tuff shown after bedding correction; same colour coding, i.e. black for locality BOO, blue for the Malongulli Formation and orange for the Angullong Tuff.

Open symbols are negative inclination values (upper hemisphere); **closed** symbols, positive inclination values (lower hemisphere). Schmidt equal area polar projection.

Table 35: Palaeopoles obtained from the Cliefden Caves Limestone Subgroup (locality BOO)

B	N	<i>Australian coord.</i>		<i>African coord.</i>		dp	dm	Coordinates system
		<u>Plat</u>	<u>PLong</u>	<u>Plat</u>	<u>PLong</u>			
<i>Components C_S:</i>								
5	22	-54,7	236,3	-70,6	344,3	10,0	15,4	from <i>in situ</i> orientation
5	22	-34,2	221,3	-84,4	219,4	9,5	14,1	after bedding correction

N: number of samples; **B**: number of sites; **PLong./Plat.**: palaeopole longitude/latitude in Australian and in African coordinates. **dp/dm** : semi-axis of the ellipse of confidence.

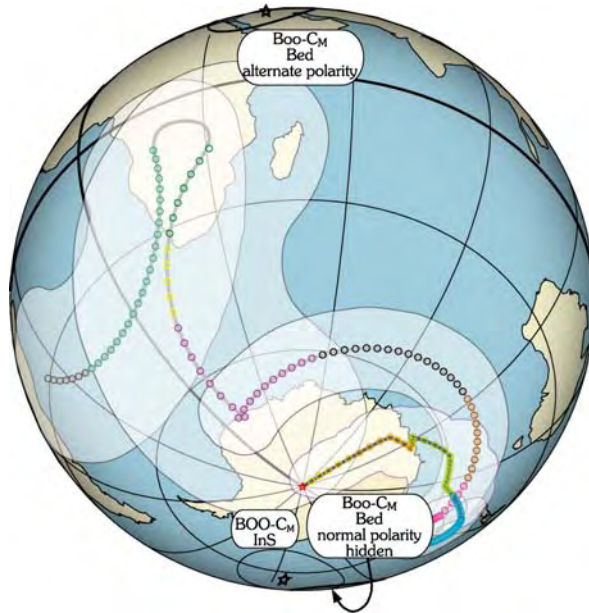


Figure 7.48: Corresponding palaeopoles in Australian coordinates. The possible APW path for Australia-Gondwana from the present-day to 570 Ma based on Small Circle Fit is shown for comparison purposes.

Same legend as in figure 2.19-A, Chapter 2 (§.2.7).

BOO- C_M InS and **BOO- C_M Bed** are the palaeopoles (**stars**) corresponding to component C_M *in situ* and after bedding correction respectively. This last, is shown with its two possible polarities as polarity directly inferred from C_M after bedding correction plots on the hidden side of the Earth.

The confidence ellipse of the pole BOO- C_M InS overlaps that of the pole from the Snowy River Volcanics (Schmidt *et al.*, 1987), but this not the case for BOO- C_M Bed, which does not correspond to any position expected for Gondwana (here shown with the Small Circle Fit path), regardless the polarity considered.

7.9. Conclusions about the Molong area

7.9.1. Palaeomagnetic results

At regional scale, the widespread occurrence of component C_p is the most striking feature of the Molong area. This component is believed to be carried by sulphide and probably by pyrrhotite since C_p is almost always fully demagnetised about 320°C, Curie temperature of pyrrhotite. The mean direction calculated from all localities showing C_p is very compatible with an Oligocene age and can be related to the hot spot volcanism event that affected the Molong area. This overprint is thought to be due to a thermo-chemical magnetisation event, possibly caused by migration of hot fluid triggered by the change in thermal gradient in the Lachlan Orogen. The spatial extent of this overprint is not clearly established yet, but may be not only limited to the Molong area. It appears, however, that structural boundaries and petrology played an important role in the presence of component C_p , since faults and thrusts seems to control more or less its occurrence. It is in agreement with the hypothesis of fluid migration, which could preferentially guide and favour crystallisation of sulphides. The regional distribution of C_p is also possibly in favour of structures cross-cutting the North-South general fault and thrust trend. Indeed, C_p has not been found at locality MIL (figure 7.2), South of the Lyndhurst – Neville fault proposed by Glen & Wyborn (1997), but seems to more concentrated along the Lachlan Transverse Zone also inferred by these authors.

Concerning the other components isolated, none of the localities meet the statistical level to satisfy the Van der Voo's criteria (Van der Voo, 1993). However, most of them are believed to be sufficiently well determined to give an indication concerning palaeopole positions. The major problem usually is to constrain the age of magnetisation and in particular to assess whether they are pre- or post-folding magnetisations. For locality MIT, the classic fold test (McElhinny, 1964),

positive at the 11% confidence level only, is a good argument to think it is a post-folding magnetisation. Similarly, this test is positive at the 34% and the 4,5% confidence level only for localities QUO and YUR respectively. These two localities show analogous component orientation *in situ* and favour a post-folding remagnetisation event. For these three localities (MIT, QUO and YUR), the directions of magnetisation observed do not correspond to any expected by any authors for Gondwana – Australia. The most plausible explanation is therefore to admit that terrane rotation and/or translation occurred after these magnetisations. As the orogenic events that have mainly affected the Eastern Lachlan Orogen are Silurian and Early Devonian, it implies that the Lachlan Orogen is not cratonised until then.

The use of palaeomagnetic data from this region of Gondwana to draw an APW path appears thus to be erroneous. This will be however discussed in the following Chapter.

7.9.2. Regional magnetic fabric

The AMS measured for this study yields one of the first maps of the regional fabric in the Molong area.

The most important result is the good alignment of the magnetic lineation with the fault and thrust trend and in particular the progressive change in direction from a North-South trend to an East-West trend to the South (figure 7.49). This change corresponds very well with the proposed Lyndhurst – Neville Fault inferred from field indications by Glen & Wyborn (1997). It constitutes so far one of best independent arguments for the existence of this fault. It also implies that cross-cutting structures do exist, and is in agreement therefore with the existence of the Lachlan Transverse Zone (Glen & Wyborn, 1997).



Density contours clearly highlights that magnetic lineation are controlled by fault orientations. Small ellipses indicate the directions of elongation of the ellipsoids of magnetic susceptibility deduced from density contours (Gaussian model, $K=100$). Note in particular the change in direction of the magnetic lineation in the vicinity of the Lyndhurst – Neville Fault (Glen & Wyborn, 1997), to the South of the Molong High. Same simplified geological map as per figure 7.2.

Summary of chapter 7

The Molong area focuses on the Eastern Belt of the Lachlan Orogen, and in particular on the Ordovician Macquarie Volcanic Arc. Most of the localities targeted (29) come from this area. The AMS measured for this study yields one of the first maps of the regional fabric in the Molong area, and constitutes so far one of the best independent arguments for the existence of the Lyndhurst – Neville Fault (Glen & Wyborn, 1997).

The most striking palaeomagnetic result is the widespread occurrence of a Tertiary overprint, which is interpreted to be probably Oligocene in age and carried by pyrrhotite. It can result from a thermo-chemical remagnetisation associated to the Tertiary Hot Spot volcanism, and more localised along structural boundary such as in particular the Lachlan Transverse Zone of Glen & Wyborn (1997).

The Ordovician turbidites of the Winchester Property (locality WIN-O) show also that other localised post-Palaeozoic overprints probably occurred, since a Jurassic remagnetisation appears to be there recorded. The magnetic signal measured in the Silurian Nandyllian Formation (WIN-S) is too weak to be satisfyingly determined. On the contrary, the Bendigonian Mitchell Formation (MIT) is a good example of problems encountered in the Southern Tasmanides even when the last component is clearly isolated. In this locality indeed, two sites are believed to show a well-defined post-folding magnetisation $Mit-C_{HT}$, but in other sites, this direction is affected by all degree of weathering until entire overprint. However, whatever the APW path considered for Gondwana, the pole corresponding to $Mit-C_{HT}$ does not resemble to any directions expected. The most plausible explanation is to admit that the sampled Mitchell Formation was rotated and/or translated after folding. In the Gisbornian volcanoclastic rocks of locality OAK, two components of magnetisation are also well determined but do not match any segments of APW path. It is not clear whether these magnetisations are pre- or post-folding, but rotation and/or translation must be invoked to account for these results. The directions of magnetisation observed in the Eastonian Bowan Park Limestone (QUO) are more difficult to interpret, because it appears that magnetite is the principal carrier of two different components, C_{NS} and C_{EW} , which can be consequently demagnetised simultaneously. Both components however, are likely to represent mid Palaeozoic overprints. The idea that C_{EW} is a remagnetisation is also comforted by the similarity with the direction of magnetisation systematically obtained from the Late Gisbornian Yuranigh Limestone (locality YUR). Localities QUO and YUR must be regarded as rotated and/or translated. The last results presented are the directions of magnetisation obtained from the Early Eastonian Cliefden Caves Limestone of the Little Boonderoo Property (BOO). A very weak component C_M is sufficiently distinguishable to be clearly defined in five of the nine sites obtained in this limestone. This result is consistent with those reported by Goleby (1980) for the overlying Malongulli Formation and the Angullong Tuff, and probably also to the Silurian Tenandra Formation. It corresponds well to the result obtained by Schmidt *et al.* (1987) in the Snowy River Volcanics. By contrast to Goleby's conclusions, C_M is interpreted here as representing an overprint.

Chapter 8

Discussion and conclusions

8.1. Summary of the presented results

Numerous palaeomagnetic data have been presented in the previous chapters, but most of them have a complex magnetisation and the corresponding palaeopoles are usually defined on a limited number of samples. Their statistical significance cannot therefore be considered satisfying. Nevertheless, it is believed that the different components are in general sufficiently well isolated to be indicative of possible palaeopositions. When the poles obtained (table 36) are plotted on a reconstruction of Gondwana (in African coordinates; figures 8.1), the majority does not correspond to any positions expected from APW paths published by many authors (see Chapter 2; here shown with the X- and Y-paths from Bachtades & Briden [1991] and Schmidt *et al.* [1990] respectively, and also to the Small Circles Fit path introduced in Chapter 2).

Several hypotheses can be put forward to explain this phenomenon, but assumptions must be made in particular regarding the age of magnetisation. Two extreme cases are discussed below before suggesting a plausible synthetic solution.

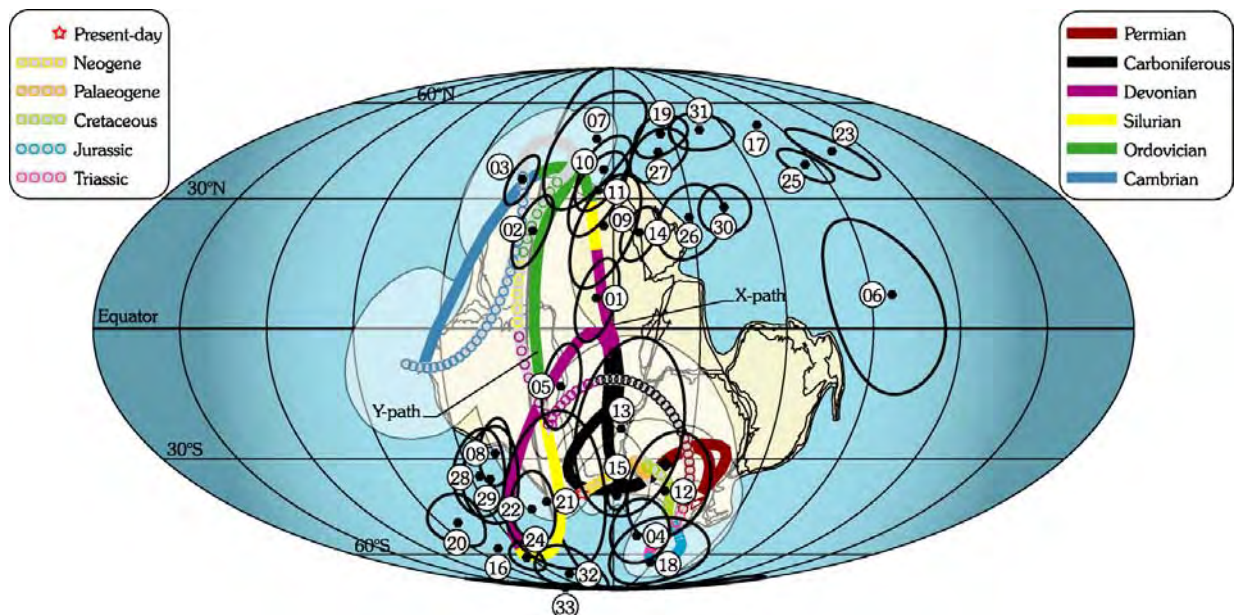


Figure 8.1: Palaeopoles presented in the previous chapters, and shown on a reconstruction of Gondwana in African coordinates. Numbers refer to table 36. They are compared to the X-path of Bachtadse & Briden (1991) and the Y-path of Schmidt *et al.* (1990); also shown the Small Circle Fit path (coloured circles) and its 95% confidence envelope. Mollweide projection; centred on longitude 030°E.

Table 36: Localities presented in the previous chapters and corresponding palaeopoles

Name	B	N	<u>Australian coord.</u>		<u>African coord.</u>		dp	dm	InS/Bed	N°
			PLong.	Plat.	PLong.	Plat.				
Broken Hill area:										
Arr/Aro	is considered to represent the present-day field (weathering)									
Fun	is considered to represent the present-day field (weathering)									
Cup-mT ₁	7	28	049,8	-43,1	024,0	+06,7	6,0	10,4	InS	1
Cup-mT ₂	7	28	201,9	+26,4	359,9	+22,0	4,9	9,5	Bed	2
Cup-HT	6	27	198,3	+12,6	351,5	+35,0	6,1	7,0	Bed	3
Kan	is considered to scattered to be used									
Gum	is considered to scattered to be used									
Dau-M	7	32	173,1	-67,0	043,4	-52,7	9,9	11,9	InS	4
Dau-H	7	43	028,2	-63,1	011,2	-12,8	5,9	10,5	Bed	5
Chu-InS	5	22	136,4	+21,1	127,2	+07,5	16,3	22,6	InS	6
Chu-Bed	5	22	222,5	+03,7	201,7	-46,8	11,4	22,4	Bed	7
Sis-NS	~	16	320,4	-61,1	343,3	-28,6	4,8	9,6	InS	8
Sis-EW	~	11	049,4	-26,6	026,4	+23,3	8,5	16,2	Bed	9
Mount Bowen area:										
Bul-InS	~	15	226,5	-18,2	205,7	-37,6	6,4	12,7	InS	10
Bul-Bed	~	15	045,5	-18,2	023,7	+32,1	6,6	13,2	Bed	11
Hop	is considered to scattered to be used									
She-C ₃	~	12	138,8	-61,7	052,7	-38,5	14,1	15,5	Bed	12
Mer-MT	5	21	084,4	-67,9	032,6	-22,6	17,5	23,1	InS	13
Mer-HT	6	30	062,9	-25,1	039,6	+21,7	4,7	8,2	InS	14
Molong area:										
Ill overp. C _p	11	420	136,2	-78,0	031,6	-39,9	3,2	4,1	InS	15
Win-C _{HT-S}	2	10	262,4	-47,5	315,2	-57,7	40,4	77,3	InS	16
Win-C _{HT-S}	2	10	085,7	+31,7	109,5	+51,4	33,8	67,4	Bed	17
Win-C _{HT-O}	4	10	187,0	-55,3	058,4	-63,7	15,0	17,2	InS	18
Win-C _{HT-O}	4	10	063,1	+04,1	054,4	+48,4	5,5	11,0	Bed	19
Mit-InS	2	8	274,7	-42,5	309,2	-48,3	6,4	12,8	InS	20
Mit-Bed	2	8	293,0	-77,0	359,1	-41,7	15,5	26,0	Bed	21
Oak-C ₂	4	20	287,0	-70,7	350,8	-43,9	6,9	12,1	InS	22
Oak-C ₂	4	20	101,0	+42,5	133,2	+42,9	5,4	10,7	Bed	23
Oak-C ₃	4	16	255,4	-53,1	327,1	-61,6	4,5	8,0	InS	24
Oak-C ₃	4	16	100,6	+29,8	115,4	+39,1	4,0	7,6	Bed	25
Quo-C _{EW}	~	10	078,0	-13,9	058,9	+25,3	7,8	12,9	InS	26
Quo-C _{EW}	~	10	063,6	-02,1	051,0	+42,6	6,0	11,9	Bed	27
Quo-C _{NS}	~	10	303,4	-56,2	333,8	-34,5	7,2	14,4	InS	28
Quo-C _{NS}	~	10	003,1	-57,3	337,8	-35,3	8,0	15,8	Bed	29
Yur-C _S	~	10	086,9	-04,3	073,2	+27,8	5,9	9,4	InS	30
Yur-C _S	~	10	073,8	+13,5	076,0	+49,7	5,9	11,6	Bed	31
Boo-C _M	5	22	236,3	-54,7	344,3	-70,6	10,0	15,4	InS	32
Boo-C _M	5	22	221,3	-34,2	219,4	-84,4	9,5	14,1	Bed	33

N: number of samples; B: number of sites; PLong./Plat.: palaeopole longitude/latitude in Australian and in African coordinates. dp/dm: semi-axis of the ellipse of confidence. InS/Bed: palaeopole calculated from component considered *in situ* (InS) or after bedding correction (Bed). N°: number corresponding to figure 8.1.

8.2. Signification and reliability of the presented results

8.2.1. Three key localities

From these results, the poles from three localities can be used to anchor the basis of different hypotheses. They are regarded as the most important since they are based on sufficient number of samples ($N \geq 24$ & $B \geq 5$) to be statistically reliable (according to Van der Voo's criteria, 1993), and two are supported by field tests, which are regarded as positive. All three are believed to carry a primary magnetisation giving the best possible constraint on the age.

The poles obtained from the Cupala Creek Formation are in agreement with the hypothesis of a (para-)autochthonous origin for the terranes of the southern Tasmanides. Cup-

HT is interpreted as probably primary in origin thanks to a positive unconformity test, and corresponds very well to both the X- and Y-paths as well as the Small Circle Fit path (Number 3 in figure 8.1). This implies that this zone did not undergo any palaeomagnetically detectable displacement or rotation since the Late Cambrian. Cup-mT, thought to be caused by a chemical remagnetisation, must also correspond to a segment of an APW path. Unfortunately, it cannot be directly determined whether this secondary magnetisation has been acquired prior or after folding, and both options are possible. Indeed, the corresponding palaeopoles match many of the APW paths presented in Chapter 2, and in particular, the distinction between the two schools of thought (*i.e.* the X- & Y-paths) cannot be done. Cup-mT₁ (Number 1), inferred from components considered *in situ*, corresponds very well with the Devonian segment of the X-path, whereas Cup-mT₂ (Number 2), obtained after bedding correction, matches the Ordovician segment of the Y-path and also the Small Circle Fit path. It is therefore not possible to favour yet one of these paths, but it comforts at least the idea that one of them is close to the true APW path for Gondwana. In other words, it appears very unlikely that the APW path runs 60° East of Arabia for example (see figure 8.2).

Although setting in an apparent pull-apart basin, the poles from the Mt Daubeny Formation Dau-H & -M may also represent Gondwana, since locality DAU lies just East of locality CUP. Given the confidence ellipses of the pole and the path, Dau-M (Number 4) can correspond to a remagnetisation ranging in age from Late Permian to Cretaceous and even perhaps Early Cretaceous, but a Late Jurassic – Early Cretaceous age seems more plausible. Concerning Dau-H (Number 5), the classic fold test (McElhinny, 1964) positive at the 77% confidence level associated with the conglomerate test and the contact test also considered positive lead to think that this magnetisation is primary in origin and consequently Early Devonian in age. The pole position favours the Small Circle Fit path. It might look not totally in agreement in terms of age, but the confidence ellipses are largely overlapping. In any cases, this pole is in disagreement with both the X-path of Bachtadse & Briden (1991) anchored on the Givetian Gilif Hill Volcanics pole (Bachtadse & Briden, 1991) and the Y-path of Schmidt *et al.* (1990) anchored on the Snowy River Volcanics pole (Schmidt *et al.*, 1987). In addition to the Small Circle Fit path, it does match also pole positions proposed by Smith (1999) and Torsvik & Van der Voo (2002) for the Early Devonian (figure 8.2; compare figure 8.1 to figures 2.4, Chapter 2).

Besides these two results from the Broken Hill area, only one other locality meet the Van der Voo's criteria: the Ural Volcanics from the Merri Abba Property (locality MER). However, Mer-HT (Number 14) is not believed to represent a pole but a VGP. This means that the magnetisation is primary of course and thus dated at 413 ± 5 Ma, but also that a significant deviation from the true palaeopole position can be expected. The likelihood that this VGP has been recorded precisely during an Earth magnetic reversal is not null but very small. Nevertheless, the deviation of a VGP from the pole can be large and is thought to have a maximum angle of about 30° (see for instance Soffel, 1991). In other words, it is very likely that the Gedinian palaeopole position for locality MER lies within a 30° cone around the VGP (dashed line in figure 8.2). Under these conditions, Grunow's path (1999) and the X-paths of Morel & Irving (1978) and Bachtadse & Briden (1991) are the only published paths (among the eleven presented in Chapter 2) that can match this result. This is therefore in contradiction with the pole obtained from the Mt Daubeny Formation (Dau-H) and even more with the pole from the Snowy River Volcanics (Schmidt *et al.*, 1987).

At this point, it must be noticed that two reliable results of similar age obtained in this study, Dau-H and Mer-HT, are very different in position one another. Both results however seem to contradict the existence of a Siluro-Devonian loop reaching south South America. It favours therefore an X-type APW path for Gondwana rather than a Y-type path.

These two Early Devonian results will be used as basis of the following hypotheses.

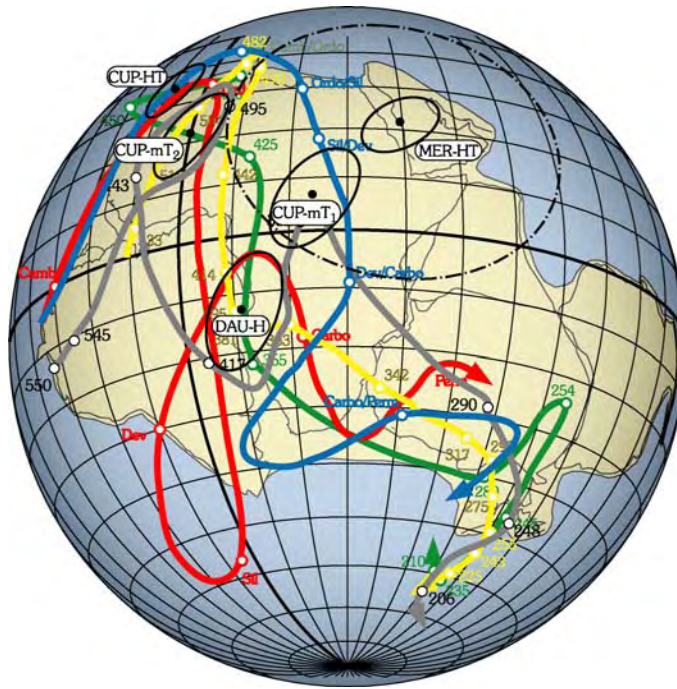


Figure 8.2: The three localities yielding statistically reliable results since they meet the Van der Voo's criteria, and in particular a sufficient number of samples. They can be used to anchor different subsequent hypotheses.

Mnemonics refer to table 36. The dashed line represent a 30° cone around the VGP obtained at locality MER.

These results are comparable to several APW paths: in **blue**, the X-path of Bachtadse & Briden (1991); **red**, the Y-path of Schmidt *et al.* (1990); and also in **green**, the path after Grunow (1999); **yellow**, after Smith (1999); **grey**, after Torsvik & Van der Voo (2002).

Orthogonal projection; grid spacing 10°.

8.2.2. Other results

Concerning the other results, they do not satisfy the statistical reliability criteria as defined by Van der Voo (1993). However, there is two ways in dealing with such data.

On the one hand, it can be considered that these results cannot be representative of a palaeoposition and must be ignored. Indeed, it can be argued for example that a larger number of data would show a distribution on a great circle as those observed in localities ARR and FUN for instance. If this option is retained, the discussion is restricted to the three key localities: CUP, DAU and MER. This constitutes the first hypothesis for a possible palaeo-reconstruction (see below).

On the other hand, one can consider these data carry a real palaeomagnetic signal. Every well-isolated component therefore can be regarded as indicator of a palaeoposition. Moreover, these poles do not satisfy the Van der Voo's criteria, but several are very close to meet them. Chu-H for example fails only because two components are missing ($B=5$; $N=22$; κ and α_{95} being correct). The situation is the same for Boo- C_M . For Oak- C_2 & - C_3 , the number of samples is smaller, but all of them show an analogous behaviour while demagnetising. This probably confers a greater reliability for this kind of results. The similar results, Yur- C_S & Quo- C_{EW} , obtained from two formations of equivalent petrography and geographically close one another, can be regarded as an indication of the possibly good reliability of these data. Combining these data into a discussion of the possible palaeogeography of the Southern Tasmanides and Gondwana constitutes the second hypothesis presented below. However, in this case, the problem consists mainly in assigning an age of magnetisation. Fold tests are often inefficient in choosing between pre- and post-folding magnetisation for these rocks, and even when they allow it, the possibilities remain numerous. Two options, to take this problem of age of magnetisation into account, are thus presented in a following paragraph.

8.3. Palaeoreconstruction based on key localities

For sake of clarity, let us consider here three reference paths only, *i.e.* the X-path of Bachtadse & Briden (1991), the Y-path of Schmidt *et al.* (1987), and the Small Circle Fit path, which can be regarded as a sort of compromise between the two lasts.

If only data having satisfying statistical parameters are examined, only the three key localities (CUP, DAU, MER) should be taken into account. The Late Cambrian pole Cup-HT match the three paths (figure 8.3). From this point of view, the Delamerian Orogen can be considered as part of the craton of Gondwana. The problem bears on the Early Devonian poles.

8.3.1. Hypothesis 1: data favour the X-path

As Dau-H has been obtained in an apparent pull-apart basin, it is conceivable that, despite the careful bedding correction involving two folds, the whole basin be rotated. However, it would be a local tectonic effect, meaning that anyhow the Southern Tasmanides can be part of the craton of Gondwana. If it is assumed that the VGP Mer-HT is deviated within a 30° cone around the true Early Devonian pole, it can be in agreement with the Gilif Hill Volcanics pole upon which is mainly based the X-path of Bachtadse & Briden (1991). Hence, it can be suggested that the craton of Gondwana extended eastwards to the Central Lachlan Orogen at least from the Early Devonian. Nevertheless, the Snowy River Volcanics, exposed further East, has to be thereupon rotated. The loop of the Y-path of Schmidt *et al.* (1987) anchored on this pole is consequently an artefact.

A rotation of the pole Dau-H around a vertical axis at locality DAU corresponds well with the Early Devonian segment of the X-path. The rotation of the whole Mt Daubeny basin would be therefore of about 25° to 30° counter-clockwise (figure 8.3). It is also in agreement with the inferred Silurian?-Early Devonian sinistral strike-slip movement along the Koonenberry Fault.

If the X-path is favoured, the overprint Cup-mT in the Cupala Creek Formation cannot correspond anymore to an Ordovician remagnetisation, and must be then regarded as Early – Mid Devonian in age (figure 8.3). This would give a new Early – Mid Devonian pole for Gondwana. In addition, this option looks favourable since Early – Mid Devonian tectonism and magmatism can be the cause of this remagnetisation.

Nevertheless, concerning the Late Devonian, two poles from the Lachlan Orogen are available (see Chapter 4; §.4.4): the Hervey Group [HG] obtained by Li *et al.* (1988) and the Worange Point Formation [WPF] by Thrupp *et al.* (1991). These rocks consist mainly in continental sediments disconformably overlying older rocks. They were folded during the Early Carboniferous Kanimblan orogenic event, but the generally constant North-South trend in fold axes in particular lead to think that no large terrane rotation occurred after their deposition. The Kanimblan event is the last major tectonic event affecting this region (see Chapter 3), and the Lachlan Orogen is believed to be cratonised from this time.

Nevertheless, the Hervey Group and Worange Point Formation poles do not correspond to the X-path of Bachtadse & Briden (1991). On the contrary, they well match the Late Devonian segment of the Small Circles Fit path (figure 8.3). If the X-path is favoured, these poles have to be also rotated. It is still conceivable that compressions due to the last orogenic event (Kanimblan) triggered a large scale (at the scale of the Eastern Lachlan Orogen) counter-clockwise rotation, since a ~20° clockwise rotation is needed to match the HG and WPF poles to the X-path of Bachtadse & Briden (1991).

8.3.2. Hypothesis 2: data favour the Small Circles Fit path

A majority of Late Devonian pole from Cratonic Australia and from Africa plots close to the corresponding Angola and Gabon, like the Hervey Group and the Worange Point Formation poles (see Chapter 2; and in particular figure 2.6). Therefore, Dau-H possibly corresponds to the Small Circles Fit path, and this last can be a better approximation for the APW path for Gondwana. Cup-mT₂ could be then a pre-folding Ordovician remagnetisation of the Cupala Creek Formation. Mer-HT however, must have undergone a clockwise rotation of about 25° to 30°. This would imply that the whole Lachlan Orogen is not stable up to the Devonian.

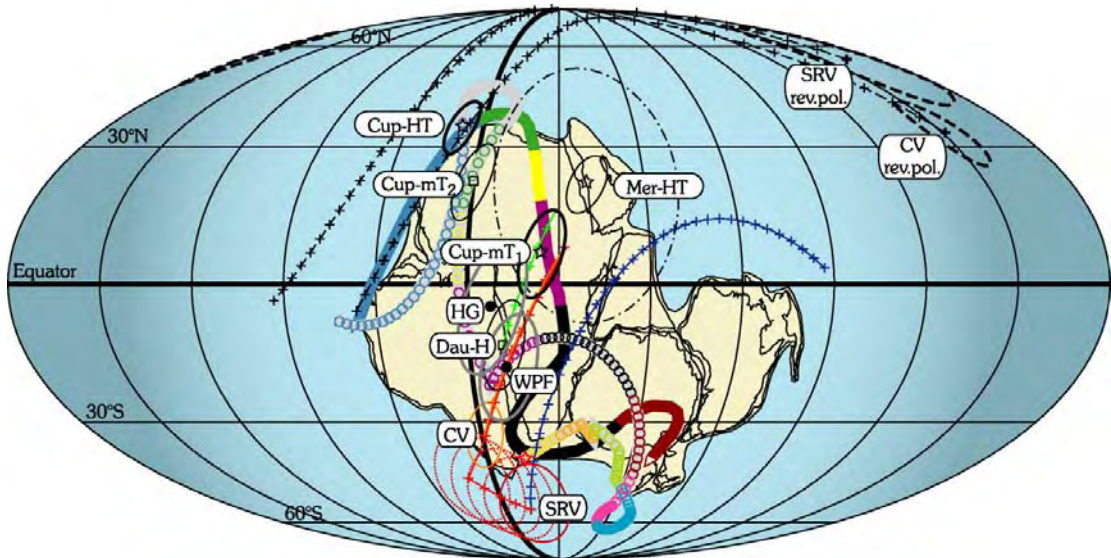


Figure 8.3: Hypotheses based on key localities only.

The poles corresponding to the key localities (CUP, DAU, MER) as per figure 8.2 on a Mollweide projection (centred on longitude 030°E). **Crosses** represent 5° rotation around a vertical axis at the locality. DAU-H must undergo a 25°/30° clockwise rotation (**green**) to fit the Early Devonian segment of the X-path of Bachtadse & Briden (1991). The Comerong Volcanics pole (CV; Schmidt *et al.*, 1986) has to be rotated 45°/50° clockwise to fit the Mid – Late Devonian segment of the X-path (**orange**). A rotation around a vertical axis at the locality corresponding to the Snowy River Volcanics (SRV) is not sufficient to match one of the Early Devonian segments of APW paths (blue). A displacement must be therefore involved before rotating this data (**red**; 95% confidence ellipses, **red dotted** lines, are left along the track corresponding to the displacement). **SRV rev.pol.** and **CV rev.pol.** are the poles and their possible positions after rotation around a vertical axis if the reverse polarity is chosen (**black dashed** lines). HG and WPF are the Late Devonian Hervey Group and Worange Point Formation poles (**black** dots and **grey** ellipses).

The Carboniferous hairpin of the X-path has been mainly drawn by Bachtadse & Briden (1991) to take into account the supposed Carboniferous overprint of the Gilif Hills Volcanics and poles like the Snowy River Volcanics and the Comerong Volcanics, which were thereupon suggested to be also overprinted. This cannot be the case however, since the Snowy River Volcanics have a convincing positive fold test at the 95% confidence level and the folding is likely to be Early Devonian in age (Bowning orogenic event). This hairpin is therefore based on this single overprint, which complicates this path. The Small Circles Fit path is simpler and could be thus a better approximation.

The problem is that a good explanation must be found as well for the positions of the Givetian Gilif Hill Volcanics pole of Bachtadse & Briden (1991) and its supposed Carboniferous overprint.

8.3.3. Synthetic hypothesis

Although the previous hypotheses are possible, it is believed that a synthetic solution may better explain all these data. Indeed, hypothesis 1 appears more convincing concerning the Early Devonian since it can account for Mer-HT, Cup-mT₁ and the Givetian Gilif Hills Volcanics pole, and the possibility of rotation of Dau-H has geological grounds. By contrast, the Small Circles Fit path seems to be a better approximation from the Late Devonian. Hence, no rotation is needed to account for several poles, among which the poles from the Hervey Group and Worange Point Formation. The only problem of this synthetic hypothesis is to explain the position of the overprint observed in the Gilif Hills Volcanics, but it can be argued that the age constraint on overprints are usually poor and this may represent another event.

Another question has not been touched on yet. How the Snowy River Volcanics can then match the X-path of Bachtadse & Briden (1991)? A simple rotation around a

vertical axis situated at the sampled locality cannot explain this pole, since it can only match latest Devonian to Mid Carboniferous parts of the X-path or even the Small Circle Fit path (blue line and crosses in figure 8.3). Choosing the reverse polarity does not help solving the problem (black dashed line and crosses on figure 8.3).

A displacement of the locality, where the Snowy River Volcanics were drilled, appears therefore needed. In Australian coordinates, a translation of the locality to the West would be the shortest solution, but it would entail an overlap with the Australian craton. By contrast, a translation to the South is conceivable. Moreover, this displacement is in agreement with the sinistral strike-slip movement recorded on faults separating the Central and Eastern Lachlan Orogen. The amount of translation to bring the Snowy River Volcanics pole close to the Comerong Volcanics (Schmidt *et al.*, 1986) mean pole position is about 20°, which means around 2220 km. This displacement would have occurred between 404 Ma (± 13 Ma, according to the “Low Age”/“High Age” of the palaeomagnetic database; McElhinny & Lock, 1996), age of the Snowy River Volcanics, and 374,5 Ma ($\pm 4,5$ Ma), age of the Comerong Volcanics, that is to say from the latest Silurian to the early Middle Devonian.

A clockwise rotation of 45°/50° for the Comerong Volcanics and 50°/55° for the Snowy River Volcanics can then make these poles corresponding to the Early and Middle Devonian segments of the X-path. This can be best related to the Tabberabberan orogenic event.

If the synthetic hypothesis is retained, the connection between the X-path of Bachtadse & Briden (1991) and the Small Circles Fit path concerns the Middle Devonian times. It does not contradict the previous proposed rotations, but it is possible that the rotation angle given for the Comerong Volcanics be smaller (perhaps 35°/40° instead of 45°/50°).

If only data from the three key localities (CUP, DAU, MER) are considered, it could be suggested that the craton of Gondwana extended to the East to the Central Lachlan Orogen as early as the Siluro-Devonian boundary. It appears it cannot be the case for the Eastern Lachlan Orogen at least up to the end of the Tabberabberan orogenic event (*i.e.* from the Late Devonian). If the other results are taken into account for this discussion, it will be shown that the tectonic formation of the southern Tasmanides may be more complicated (see §.8.4).

8.4. Palaeoreconstruction based on all results

As stated above, it is thought that the other results presented herein are in general sufficiently well isolated to be indicative of palaeopositions, although their statistical parameters do not meet the most important (*i.e.* the three first) Van der Voo's criteria (1993). The discussion can be divided in three parts.

8.4.1. Localities from the southern Molong area

The Cliefdens Caves Limestone (BOO) is situated the most to the South of the Molong area. The statistical parameters are close to meet the three first Van der Voo's criteria, and it has been shown that the pole obtained from the *in situ* overall mean direction in particular, is analogous to that reported by Goleby (1980) in the overlying Malongulli and Angullong formations, and even perhaps in the Silurian Tenandra Formation. However, both the poles obtained from *in situ* components (Boo-InS; number 32 in figure 8.1) or from directions calculated after bedding correction (Boo-Bed; number 33 in figure 8.1) plot far from any paths. A rotation at least must be therefore admitted. A rotation around a vertical axis at the locality BOO brings both Boo-InS (about 75° to 85° rotation) and Boo-Bed (about 100° to 110° rotation) at the Devonian-Carboniferous boundary of both the X- and the Small Circles Fit paths (blue for Boo-InS and black for Boo-Bed in figure 8.4). Although the confidence cones are large enough to make it unnecessary, it is suggested that a translation, similar to that inferred for the Snowy River Volcanics, would better explain these pole positions. The reverse polarity option (blue and black dashed lines in figures 8.4) would not simplify the problem since rotation and translation are also

needed. In addition, the good correspondence between Boo-InS and the Snowy River Volcanics in terms of pole position, sense of translation and sense of rotation lead to think that Boo-InS corresponds indeed to a post-folding remagnetisation. Similarly to the Snowy River Volcanics, the Cliefden Caves Limestone would have moved (northward in Australian coordinates) along the margin of Gondwana in the late Early to early Middle Devonian, and the counter-clockwise rotation of the terrane could be related to the Tabberabbearan orogenic event (mostly Givetian).

The alternative polarities (green and violet dashed lines in figure 8.4) of Quo-C_{EW} and Yur-C_S can only match Cambrian or Early Ordovician segments of the X- and Small Circles Fit paths after rotation around a vertical axis at their localities. This option is therefore discarded. A 40°/55° rotation of the mean pole for Quo-C_{EW} and a 55°/70° rotation for Yur-C_S can match a Middle – Late Devonian segment of the paths, but these rotations must be clockwise, that is to say opposite to that of the Cliefden Caves Limestone. As no translation seems to be here needed, it can be understood as an induced rotation in response to the movement of the terrane carrying the Cliefden Caves Limestone. The problem is to interpret the second direction of magnetisation, Quo-C_{NS}, observed in the Bowan Park Limestone at locality QUO. Both the normal and reverse polarities (orange and brown in figure 8.4) appear to better correspond to a Silurian age of magnetisation after rotation. This rotation has to be about 100°/105° counter-clockwise for the alternate polarity and about 75° clockwise for the normal polarity, but as a ~55° rotation is needed in the Mid Devonian, the angular rotation of the terrane carrying locality QUO would be for the Silurian about 130° for Quo-C_{NS} and only 45°/50° for the alternate polarity. The choice of polarity is correlated to the other results from the northern Molong area.

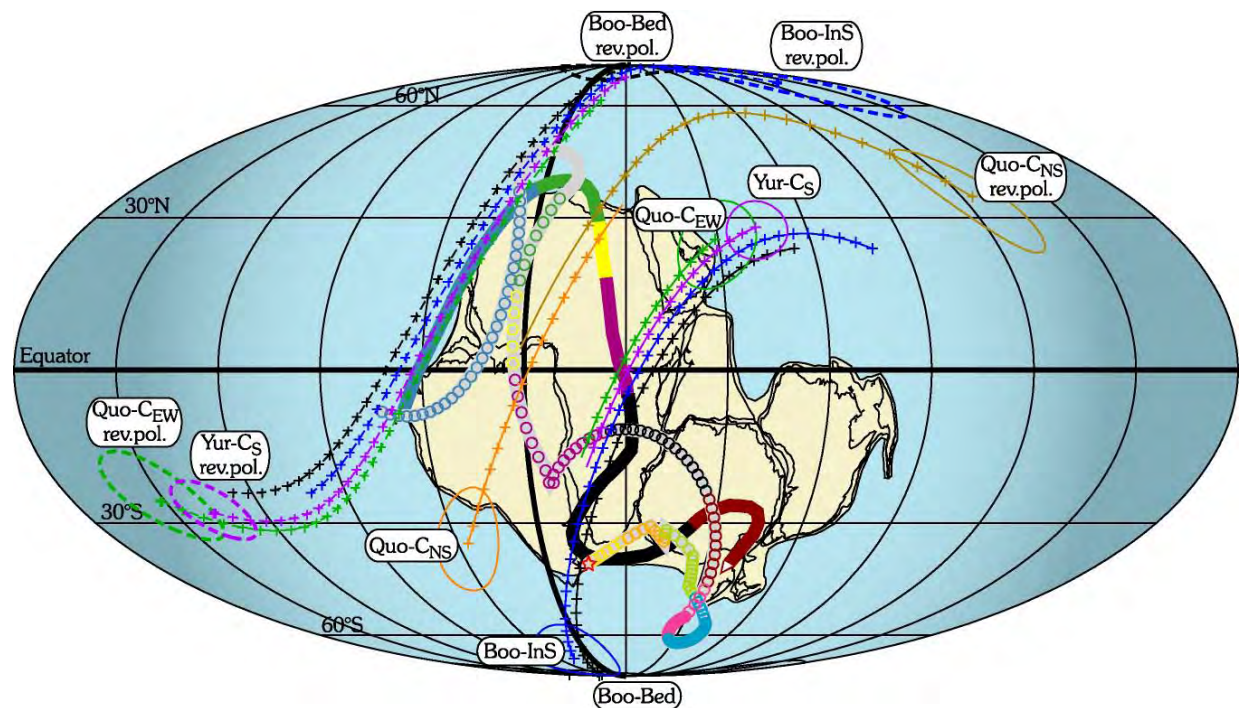


Figure 8.4: Localities from the southern Molong area.

Poles corresponding to localities BOO, QUO, YUR on a Mollweide projection (centred on longitude 030°E). **Crosses** represent 5° rotation around a vertical axis at the locality. When Boo-InS (**blue**) or Boo-Bed (**black**) is rotated clockwise, it matches the Devonian-Carboniferous boundary of the X- or Small Circles Fit paths. A translation of locality Boo can therefore probably better explain these results. By contrast, Boo-C_{EW} (**green**) and Yur-C_S (**violet**) must undergo a counter-clockwise rotation to match the paths. The reverse polarities option cannot give a simpler explanation (**dashed** lines; blue for Boo-InS; black for Boo-Bed; green for Quo-C_{EW}; and violet for Yur-C_S). The second direction of magnetisation obtained at locality QUO implies also rotation, which can be clockwise for Quo-C_{NS} (**orange**) or counter-clockwise when the reverse polarity option is retained (**brown**).

8.4.2. Localities from the northern Molong area

North of the Lachlan Transverse Zone of Glen & Wyborn (1997), localities WIN, MIT and OAK yield interesting results. Whatever the options retained, large rotations are needed to explain the palaeopole positions obtained. As these rotations have relatively similar angular values, it is suggested that the terranes carrying these localities did not fundamentally behaved independently, and a relatively large block probably rotated as one entity. The sense of rotation should be thereupon the same. By contrast to the South however (i.e. for the Snowy River Volcanics and locality BOO), no translation seems to be here necessary.

Win- C_{HT-O} (Number 18 in figure 8.1; table 36) is very consistent with an Early Jurassic age of magnetisation, and is therefore thought to be an overprint possibly related to fault reactivation and/or fluid migration along these structures. These events may be correlated with the Triassic to Early Jurassic volcanism that affected South Eastern Australia, or even movements associated with the beginning of the separation between Australia and Antarctica in the Late Jurassic (see §3.3.4; Chapter 3). Concerning Win- C_{HT-S} (Number 16 & 17 in figure 8.1; table 36), the pole positions obtained from *in situ* and after bedding correction directions appear similar to possible pole positions inferred from localities MIT and OAK, but the confidence ellipses are too large to favour an age of magnetisation and a sense of rotation. Consequently, this pole cannot be considered further.

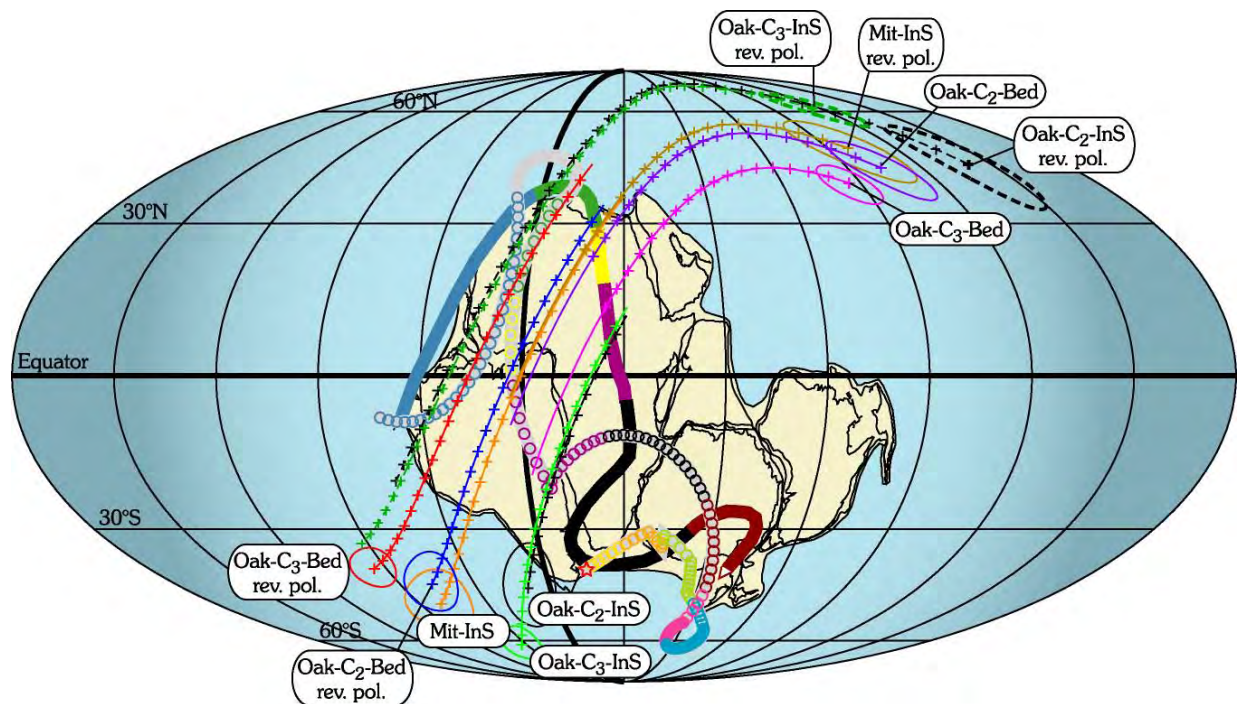


Figure 8.5: Localities from the northern Molong area.

Poles corresponding to localities MIT and OAK on a Mollweide projection (centred on longitude 030°E). **Crosses** represent 5° rotation around a vertical axis at the locality. Both Mit-InS (**orange**) and its alternate polarity (**brown**) correspond to the Silurian segment of the X-path after clockwise and counter-clockwise rotation respectively. The age of magnetisation relative to folding is not constrained for Oak-C₂ and Oak-C₃, and polarity options give numerous possibilities. Oak-C₂-InS (light **green**) & Oak-C₃-InS (**black**) can match the Middle Devonian segment of the X- and Small Circles Fit paths, whereas their alternate polarities (green and black **dashed** lines respectively) can be discarded. Oak-C₂-Bed (**violet**) can be consistent with an Early Silurian age of remagnetisation and its alternate polarity (**blue**) could be slightly older with an Ordovician-Silurian age. Oak-C₃-Bed (**pink**) can correspond to a pre-folding and pre-rotation Early Devonian age of magnetisation, and finally, its alternate polarity (**red**) could be also a primary magnetisation since it matches well an early Late Ordovician age after rotation.

At locality MIT, the classic fold test (McElhinny, 1964) is positive at the 11% confidence level only and witnesses a secondary origin of magnetisation. After rotation (100° clockwise for Mit-InS, orange in figure 8.5; 80° counter-clockwise for the alternate polarity, brown in figure 8.5), both polarity options match the same Early Silurian segment of the X-path. This remagnetisation is thus believed to be Early Silurian in age and associated with the Benambran/Quidongan orogenic events but the sense of rotation remains unresolved.

Hence, the determination of this sense of rotation of the northern Molong area is dependent of poles obtained at locality OAK. Unfortunately, no fold test is available and the magnetisation may have been acquired prior or after folding. After rotation, Oak-C₂-InS (black in figure 8.5) and Oak-C₃-InS (green in figure 8.5) correspond to the same Early to Middle Devonian segment, and can therefore reflect two times of remagnetisation during rotation. This option would date when the northern Molong area block rotated counter-clockwise since Oak-C₂-InS needs a 60°/65° clockwise rotation and Oak-C₃-InS, an 85°/90° clockwise rotation. Alternate polarities can be discarded as they only match the Early Ordovician segment of the X-path (black and green dashed lines in figure 8.5). By contrast, the alternate polarities for Oak-C₂-Bed (blue in figure 8.5) and Oak-C₃-Bed (red in figure 8.5) are possible options. Indeed, a 105°/110° clockwise rotation for Oak-C₃-Bed [rev.pol.] corresponds well to the early Late Ordovician segment of the X-path and could consequently represent a primary magnetisation. Oak-C₂-Bed [rev. pol.] needs a 95° clockwise rotation to match the Ordovician – Silurian boundary of the X-path. Given the confidence ellipse, this pole position could be related to the beginning of the Lachlan orogeny, *i.e.* the Benambran orogenic event. The normal polarities of these poles, Oak-C₂-Bed (violet in figure 8.5) and Oak-C₃-Bed (pink in figure 8.5), would correspond by rotation to an Early Silurian and Early Devonian age of magnetisation respectively. However, Oak-C₃-Bed would be younger than Oak-C₂-Bed. Although this possibility cannot be ruled out, the likelihood that a component with an unblocking temperature spectrum between 320°C and 475°C is more stable than a component with a spectrum between 475° and 550°C, is very low. In other words, Oak-C₃ is likely to be older than or contemporaneous to Oak-C₂, which means that either Oak-C₃-Bed [rev.pol.] is probably primary and Oak-C₂-Bed [rev.pol.] a pre-folding remagnetisation corresponding to the beginning of the Lachlan orogeny or Oak-C₃-InS and Oak-C₂-InS are syn-rotation overprints acquired in the Early – Middle Devonian. In any cases, this entails that the sense of rotation is clockwise.

The hypothesis of syn-rotation overprints at locality OAK is favoured for two main reasons. First, despite the formation studied are different, both localities MIT and OAK are composed of volcanoclastic rocks with magnetite (or low titanium titanomagnetite) as main magnetic carrier. There is little chance to find a primary magnetisation (or acquired soon after deposition) at locality OAK when it appears that all the other localities (MIT, but also BOO, QUO, YUR), having the same kind of magnetic material (~magnetite), are remagnetised. Secondly, the pole from the Snowy River Volcanics (SRV) after translation and the pole from the Comerong Volcanics (CV) are particularly consistent with Oak-C₃-InS and Oak-C₂-InS (compare figures 8.3 and 8.5), supporting the idea of syn-rotation remagnetisations. It can be suggested therefore that the southern Eastern Lachlan Orogen carrying the Snowy River Volcanics and locality BOO was perhaps one entity moving northward (in Australian coordinates) along the margin of Gondwana in the Silurian(?)–Early Devonian until it amalgamated to the northern Molong block. Both blocks rotated then counter-clockwise in the Early – Middle Devonian during the Bowring/Bindian orogenic events or even the Tabberabberan orogenic event. The northern block possibly rotated more (~100°) than the southern one (~60°). This differential rotation could have been accommodated by the Transverse Lachlan Zone (Glen & Wyborn, 1997) and could subsequently give an explanation for the clockwise (*i.e.* opposite) rotation observed at localities QUO and YUR. Indeed, these localities are situated just on this inferred structure and could have recorded a local tectonic effect due to the greater movement of the northern block against the southern one.

Although movements are described for blocks, it is thought that palaeomagnetically undetectable translations and/or rotations of single terrane within each block are possible.

8.4.3. Localities from the Mt Bowen and Broken Hill areas

It has been shown that Mer-HT can be explained without any rotation as long as the X-path of Bachtadse & Briden (1991) is retained as reference path for Gondwana. Consequently, the Central Lachlan Orogen is regarded as fixed relative to the craton. In this configuration, Mer-MT (Number 13 in figure 8.1; table 36) corresponds to a Late Devonian or Early Carboniferous age of magnetisation, which can be related either to the end of the Tabberabberan orogenic event or to the Kanimblan orogenic event (§.6.4; Chapter 4).

The poles, Bul-InS (Number 10 in figure 8.1; table 36) and Bul-Bed (Number 11 in figure 8.1; table 36), obtained from the Gundaroo Sandstone at locality BUL, are problematic. These rocks are Early Devonian in age but the corresponding palaeopoles look Late Ordovician or Silurian. The fold axis at locality BUL has a surprising NW-SE trend, which contrasts with the rather N-S regional trend (see §.6.2; Chapter 6). It has been suggested that this could be a consequence of the Lachlan Transverse Zone (Glen & Walsche, 1999). A 20°/25° counter-clockwise rotation of Bul-Bed (black in figure 8.6) around a vertical axis situated at locality BUL can make the confidence ellipse tangent to the Early Devonian segment of the X-path but not overlapping it. Moreover, the rotation expected to obtain a NW-SE fold axis trend from a ~N-S trend is clockwise. The alternate polarity, Bul-Bed [rev.pol.], does not give any satisfying solution (red in figure 8.6). Rotation does not appear therefore to be the cause of this pole position. On the contrary, shallowing effects, sometimes observed in red beds, could be responsible for this apparent offset. A 15° change in inclination value is sufficient for the 95% confidence ellipse to overlap the beginning of the Devonian segment of the X-path (in pink in figure 8.6). However, it must be pointed out that this pole is rather poorly constrained, and lightning effects and/or composite directions of magnetisation cannot entirely be ruled out.

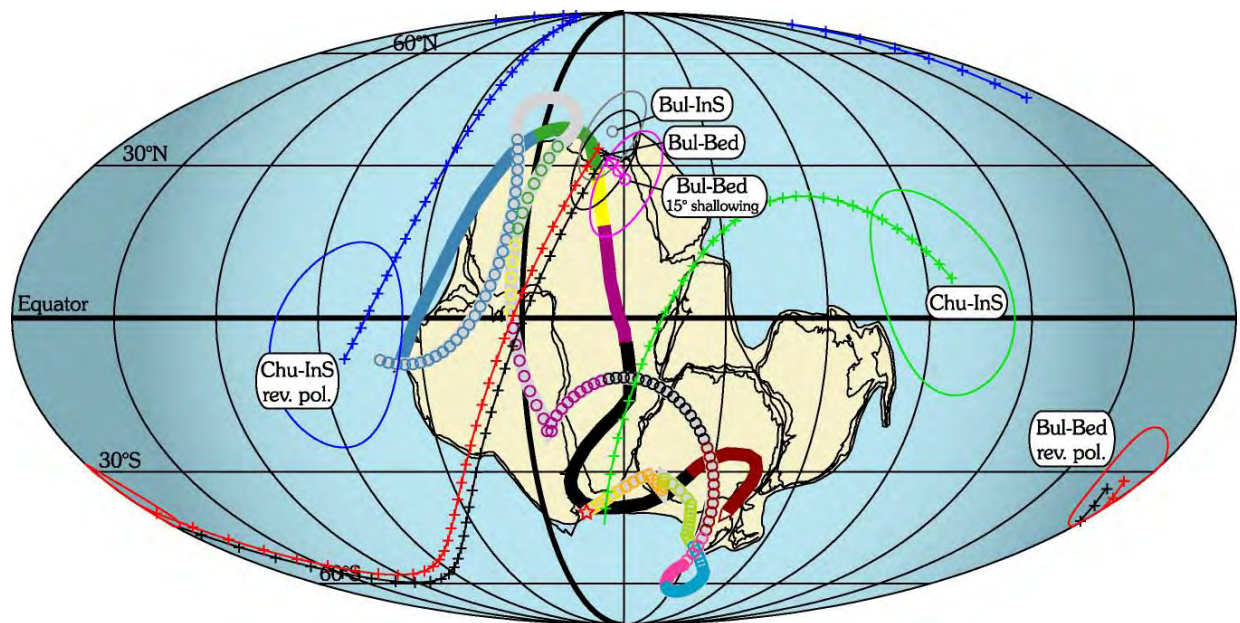


Figure 8.6: Localities from the Mt Bowen and Broken Hill areas.

Poles corresponding to localities BUL and CHU on a Mollweide projection (centred on longitude 030°E). **Crosses** represent 5° rotation around a vertical axis at the locality. Given the change in fold axis trend at locality BUL, a ~40° clockwise rotation of Bul-Bed could be expected. However, only a 20°/25° counter-clockwise rotation of Bul-Bed (**black**) can make the confidence ellipse tangent to the Early Devonian segment of the X-path. A ~180° counter-clockwise rotation is needed for the alternate polarity (Bul-Bed [rev.pol.]) to obtain a similar result (**red**). Hence, rotation is not believed to be the solution in the Central Lachlan Orogen. Shallowing effect in these red beds however could be the cause of this pole position (**pink**; Bul-Bed [15° shallowing], an open circle is drawn at 5°, 10° and 15°). On the contrary, after a 130° counter-clockwise rotation, Chu-InS (green) corresponds well with a Late Devonian to Early Carboniferous age of magnetisation. Within the confidence ellipse, it is in good agreement with the 120° change in fault and cleavage trend observed on the field. The alternate polarity option, Chu-InS [rev.pol.], can be discarded (**blue**).

However, results from locality BUL are in agreement with those from locality MER since no rotation appears to be needed. This suggests that the Central Lachlan Orogen is stable relative to the craton of Gondwana.

Dau-M is considered to be an overprint and its corresponding palaeopole matches segments of the Small Circles Fit path ranging from Triassic to Early Cretaceous (Number 4 in figure 8.1; table 36). A Jurassic age of magnetisation is suggested on the basis of volcanic dykes intruding the Broken Hill area at that time (Mills, *personal communication*, 2002; see also §.5.6, Chapter 5).

The grouping after bedding correction for components H at the Churinga Property (locality CHU) is significantly worse than *in situ* since the classic fold test (McElhinny, 1964) is positive at the 18,5% confidence level only. Chu-InS however, does not match any segment of the proposed paths for Gondwana. Rotation around a vertical axis at locality CHU of the alternate polarity Chu-InS [rev.pol.] yields no interesting solution (blue in figure 8.6). Alternatively, a 130° counter-clockwise rotation of Chu-InS (green in figure 8.6) well matches the Late Devonian to Early Carboniferous segments of both the X-path of Bachtadse & Briden (1991) and the Small Circles Fit path. Given the confidence ellipse, this result is in good agreement with the suggested 120° clockwise rotation of the southern part of the Broken Hill area, inferred from change in fault and cleavage trend (see Chapter 5). This magnetisation could be therefore interpreted as a Late Devonian overprint, possibly related to the end of the Tabberabberan orogenic event and recorded before a Late Devonian to Early Carboniferous rotation. It is suggested here that this rotation is associated either to the setting up of the Melbourne – Mathinna Terrane as proposed by Glen *et al.* (1992-b) or to much more important fault reactivations than previously thought, involving major terrane movements related to the intra-plate Early Carboniferous Alice Spring Orogeny in Central Australia. The hypothesis put forward by Glen *et al.* (1992-b) is however favoured, because major movements due to the Alice Spring Orogeny would have probably affected the northern part of the Broken Hill area as well, which is not observed (cf. locality CUP). This result is of paramount importance since it implies that the South-Western Belt of the Lachlan Orogen was probably not entirely stable until the Early Carboniferous.

Finally, the pole Sis-EW (Number 9 in figure 8.1; table 36) is in agreement with the assumption that the northern Broken Hill area was fixed relative to the craton. Indeed, despite the poor quality of this pole due to the scattering of components Sis-EW, the 95% confidence ellipse of Sis-EW matches well the Early Devonian segment of the X-path. Hence, it confirms the idea that these rhyolites intruded the Mount Daubeny Formation just after folding, and agrees with the proposed middle to late Early Devonian age for these rocks. Nevertheless, a serious doubt can be cast on all these results if the pole Sis-NS is confirmed. This position (Number 8 in figure 8.1; table 36) is incoherent with all other results from this area. The only explanation would be therefore to rotate this data by around 75° clockwise. It is believed however that this direction of magnetisation corresponds to a composite direction due to overlap of unblocking temperature spectra (see §.5.8; Chapter 5). Hence, it is suggested that this result should be ignored.

For all these results, the lack of field tests is a serious handicap. Most of the results presented here are deeply complicated by remagnetisations, and finding adequate rocks for palaeomagnetic purposes is revealed difficult. Among all the localities studied for this work, a careful study of the rhyolites at locality SIS, however, appears to be the best possible check of all these results and should be able to confirm or invalidate all hypotheses put forward in this discussion. It is therefore of paramount importance to re-investigate with a larger number of sites and samples these intrusions, which can provide good palaeomagnetic results and could be isotopically dated.

As conclusion, one of the numerous possibilities of Early – Middle Palaeozoic palinspastic reconstructions of the Southern Tasmanides is provided below to illustrate the combination of all these results.

8.5. Conclusions

The palaeoposition of Gondwana remains largely enigmatic for most of the Palaeozoic Era. It looks contradictory with the fact that this huge landmass encompassed about the two thirds of the present-day continents. Moreover, understanding its drift history has great implications for many disciplines in Earth Sciences. The break-off of Rodinia, the possible existence of Pannotia, the Pangea configurations, the supercontinent cycles, the palaeoclimatic changes, the Cambrian explosion of life and the bio-diversification at least are all directly linked to the palaeopositions of Gondwana.

In terms of palaeomagnetism, the determination of an APW path for Gondwana appears to be the major difficulty. Among the numerous published paths, results obtained for this study seems to favour an X-type path such as that proposed by Bachtadse & Briden (1991) for the Early Palaeozoic, whereas the Late Palaeozoic part is probably better approached so far by a rough approximation such as the Small Circles Fit path. It is believed that details of the APW path for Gondwana should be considered only once the general pattern of the path can be firmly established. In any cases, the Y-type path involving a Silurian – Devonian loop such as the path proposed by Schmidt *et al.* (1990) appears to be erroneous due to the use of data from the Southern Tasmanides.

Concerning the tectonic history of this region, many authors (e.g. Schmidt & Morris, 1977; Morel & Irving, 1978; Goleby, 1980; Schmidt *et al.*, 1986, and 1987; Hargraves *et al.*, 1987; Van Houten & Hargraves, 1987; Van der Voo, 1988; Offler *et al.*, 1998) believed that the terranes of the Lachlan Orogen were amalgamated – if ever allochthonous – to the craton of Gondwana at least since the Early Silurian, age of the first orogenic event (Benambran), and probably since the Cambrian. Results presented herein indicate it cannot be the case since several rocks of similar ages show different pole positions. The best explanation for all these directions of magnetisation is to admit that terrane translations and rotations occurred in the Silurian – Devonian times, and perhaps even until the Early Carboniferous concerning the South-Western Belt of the Lachlan Orogen. This is in good agreement with the hypotheses proposed by Glen *et al.* (1992-b) for terranes accretion and tectonic setting of this part of the Tasmanides.

The following palaeogeographic reconstructions are based on these arguments, but it is understood that it is only one of the numerous possibilities to make coincide all information available.

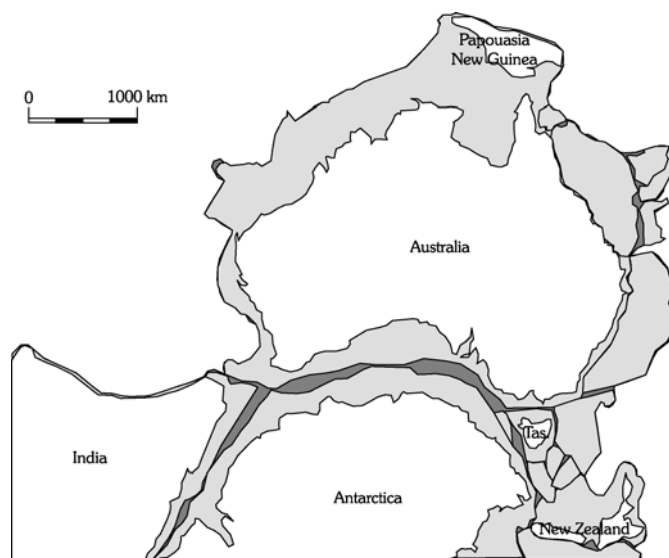


Figure 8.7: Reconstruction of the Australia-Antarctica-New Zealand region at anomaly M0 (120,8 Ma), redrawn after Müller *et al.* (2000).

Details of the palaeogeography of the Tasmanides are shown on a reconstruction redrawn after Müller *et al.* (2000) of the Australia-Antarctica-New Zealand region at anomaly M0 (figure 8.7), i.e. 120,8 Ma ago. The choice of a reconstruction has great implications in terranes association and possible tectonic regime (§.1.2.2, Chapter 1). By contrast to the reconstruction between Australia and Antarctica suggested by Stump *et al.* (1987) or Borg & De Paolo (1991) for instance, Tasmania is here placed at higher latitude than Northern Victoria Land, and allows the determination of possible tectonic blocks. Terranes association between the Tasmanides and New Zealand in particular are also largely based on reconstruction proposed by Sutherland (1999).

- Ordovician and Silurian

No data from the Southern Tasmanides is available for these periods, but the best approximation of the APW path for Gondwana appears to be the X-path from Bachtadse & Briden (1991). The South Pole should be then to the “North” of Africa (in present-day coordinates) in the Ordovician (figure 8.8-A) and at the level of Tchad or Sudan in the Silurian (figure 8.8-B).

The pole obtained from the Late Cambrian Cupala Creek Formation (locality CUP) implies that the northern Broken Hill area is fixed relative to the craton. Li *et al.* (1997) published the same result for Late Cambrian rocks of North-West Tasmania. It is considered also that the Central Belt of the Lachlan Orogen did not undergo palaeomagnetically detectable displacement, so that all these areas from the Southern Tasmanides are left in their present-day position relative to the craton.

The Ordovician Macquarie Volcanic arc witnesses the presence of a subduction zone by the North Eastern Belt block [N.E.B.]. It has been shown that no translation is needed for this block, but a $\sim 100^\circ$ counter-clockwise rotation probably occurred in the mid Devonian. The N.E.B. block is therefore left adjacent to the Central Belt of the Lachlan Orogen, considered fixed relative to the craton. The position of the subduction zone almost perpendicular to the Central Belt and the Delamerian – Ross Orogen could solve the problem of the presence of Ordovician turbidites both in the fore-arc and in the back-arc basins.

The positions of the other blocks are unknown, but the South Eastern Belt block [S.E.B.] should be close to the South Western Belt block [S.W.B.] to account for stratigraphic similarities between them (see Chapter 3). The Narooma Terrane [N.T.] was partially subducted in the Late Ordovician, to be subsequently thrust back over the S.E.B. (Adaminaby Terrane) in the Early Silurian (Glen & Percival, *personal communication*, 2002). A subduction zone is therefore represented between the S.E.B. and N.T. in the Ordovician (figure 8.8-A), and these blocks are considered already amalgamated one another in the Silurian (figure 8.8-B).

No clear information exists concerning the tectonic setting and palaeoposition of the Thomson Orogen, and Hodgkinson – Broken Ridge Orogen. These areas are thus left fixed relative to the craton of Gondwana.

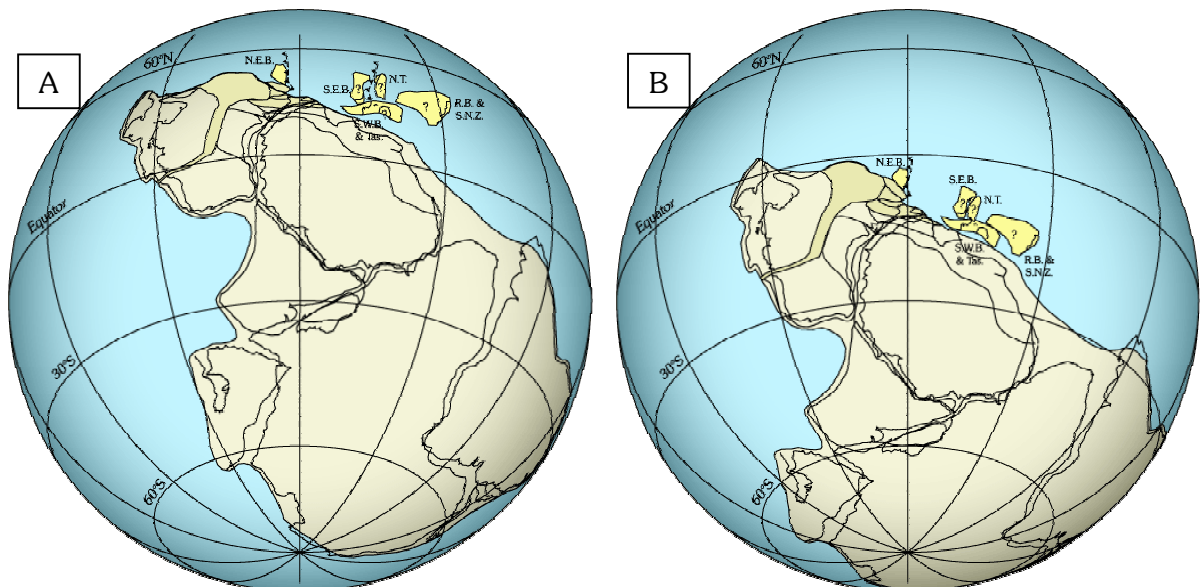


Figure 8.8: A- Ordovician and B- Silurian palaeogeographic reconstruction of Gondwana.

The position of Gondwana is deduced from the X-type APW path of Bachtadse & Briden (1991). N.E.B. is the North Eastern Belt block of the Lachlan Orogen; S.E.B., the South Eastern Belt block; N.T., the Narooma Terrane; S.W.B. & Tas., the South Western Belt and Eastern Tasmania block; R.B. & S.N.Z., the Robertson Bay and South New Zealand block. Their positions are unknown since no palaeomagnetic data is available for them. Orthogonal projections.

- Silurian – Devonian boundary

The Silurian – Devonian position of the S.E.B. block is inferred from the pole obtained by Schmidt *et al.* (1987) in the Snowy River Volcanics, which needs a large translation (figures 8.9). Obviously, the distance between this palaeoposition and the present-day position relative to the craton can significantly vary given the confidence ellipse of this pole and also the accuracy of the X-path chosen as reference. However, the Narooma Terrane was probably accreted to the S.E.B. block, and they probably moved rapidly northward (in Australian coordinates). The Central Belt of the Lachlan Orogen forms a promontory, which is particularly subject to strong deformation and metamorphism. This can also explain the transpressional movements observed along major faults of the Lachlan Orogen.

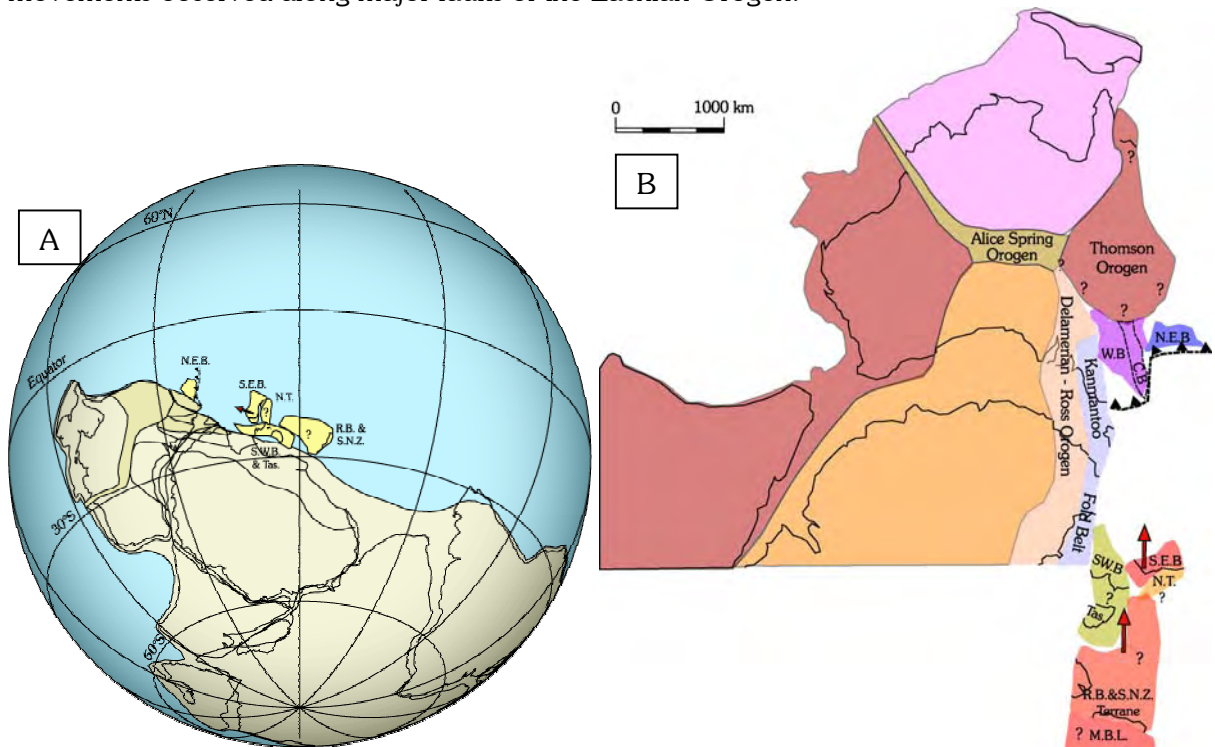


Figure 8.9: Early Devonian palinspastic reconstruction.

A- Global view, and **B-** Zoom on the different elements of the Southern Tasmanides.

W.B., Western Belt of the Lachlan Orogen; C.B., Central Belt; N.E.B., North Eastern Belt block; S.E.B., the South Eastern Belt block; N.T., the Narooma Terrane; S.W.B. & Tas., the South Western Belt and Eastern Tasmania block; R.B. & S.N.Z., the Robertson Bay and South New Zealand block; M.B.L., Marie Byrd Land.

- late Early to Middle Devonian

The different blocks must have reached already their present-day latitude relative to the craton (figures 8.10). As proposed by Glen *et al.* (1992-b), it is suggested that the South Western Belt indented between the Central/Western Belt and the Kanmantoo Fold Belt shifting most of the deformation to the South West. It is possible that terranes rotation occurred during this collision in the northern part of the S.W.B. block. Western Tasmania was probably part of this block since strong correlation exists between the South Western Belt and Western Tasmania, whereas a big contrast is observed between Eastern and Western Tasmania (see Glen *et al.*, 1992-b). This scenario can relatively simply explain also the apparent double vergence of subduction in this area. Indeed, the S.W.B. block would have also indented the former subduction zone and the tectonically complex triple subductions proposed by Gray & Foster (1997) is not necessary anymore. This is also in good agreement with the new tectonic evolution of Victoria and the shape of the South Western Belt recently proposed by Willman *et al.* (2002, see below).

To the East, the subduction zone must have jump outboard these newly amalgamated blocks, but a strong transpressional component led to the counter-clockwise rotation of the N.E.B. and the S.E.B. blocks, according to palaeomagnetic records measured for this study.

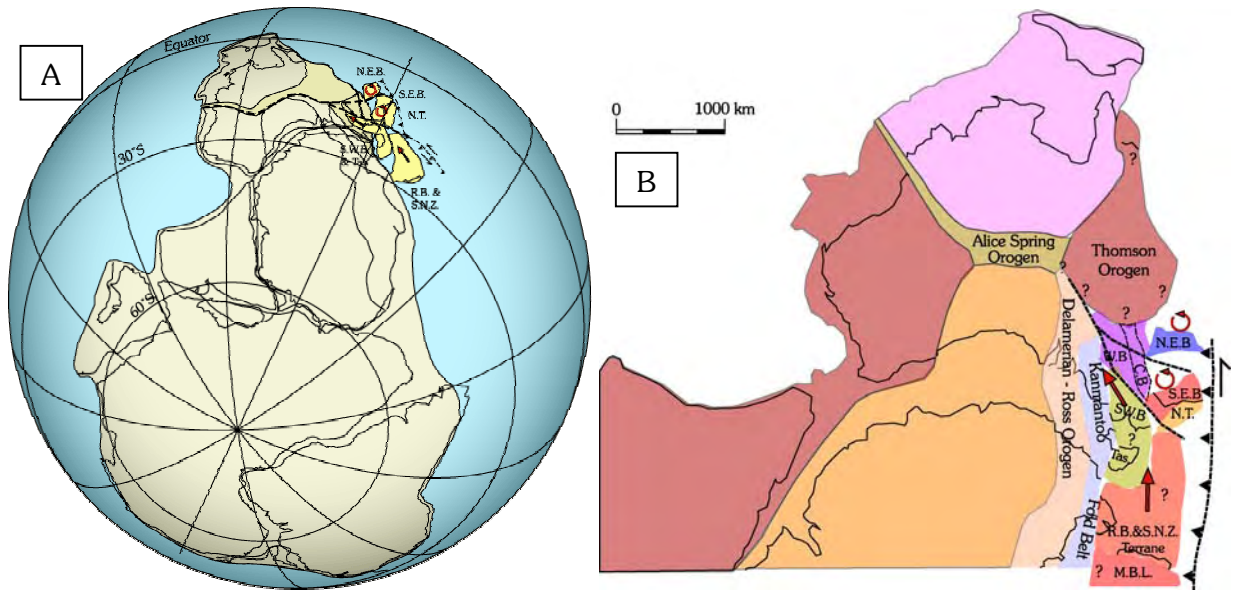


Figure 8.10: late Early to Middle Devonian palinspastic reconstruction.

A- Global view, and **B-** Zoom on the different elements of the Southern Tasmanides.

Same abbreviations as in figure 8.9. Block rotations inferred from palaeomagnetic records measured for this study probably occurred at that time.

The junction between these two blocks would correspond to the Lachlan Transverse Zone of Glen & Wyborn (1997). The counter-clockwise rotation of the N.E.B. block against the S.E.B. block probably provoked also clockwise rotation of terranes situated in the close vicinity of the Transverse Lachlan Zone, such as the 55° rotation observed in the Bowan Park Limestone (locality QUO) and the Yuranigh Limestone (locality YUR).

- Late Devonian

Poles obtained from the Late Devonian Hervey Group (Li *et al.*, 1988) and the Worange Point Formation (Thrupp *et al.*, 1991) indicate that rotations to the East are complete.

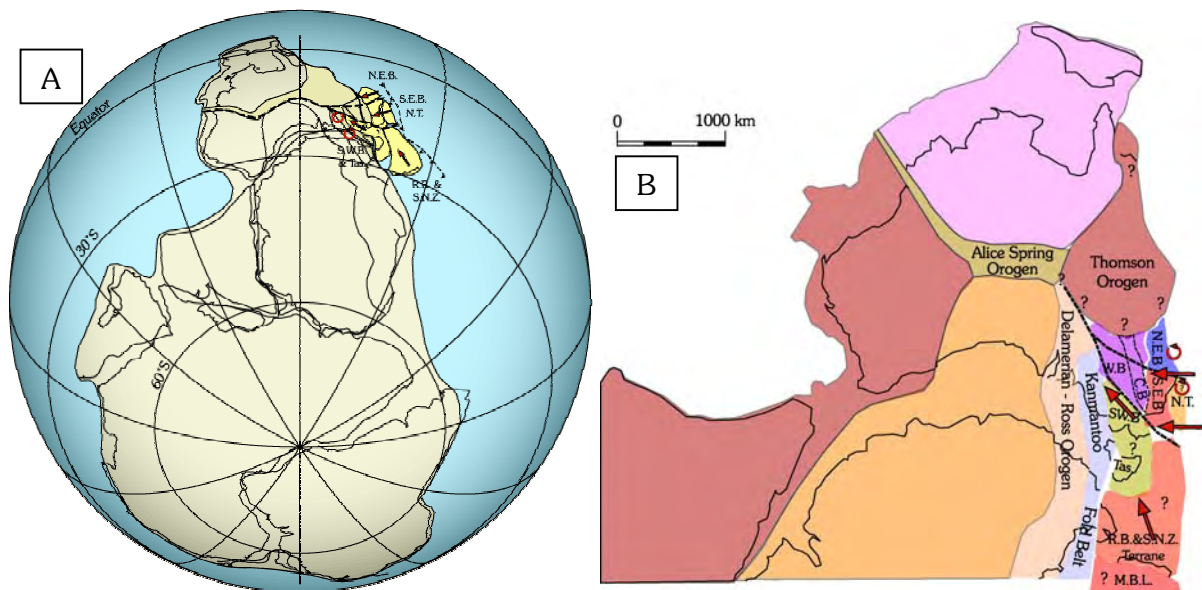


Figure 8.11: Late Devonian palinspastic reconstruction.

A- Global view, and **B-** Zoom on the different elements of the Southern Tasmanides.

Same abbreviations as in figure 8.9. Rotations to the East are complete, but compression is still present, and the wedge formed by the S.W.B. block can be still active.

Nevertheless, East – West compression is still important since Late Devonian formations are tightly folded along North – South fold axis. Moreover, the wedge formed by the S.W.B. block is perhaps not yet fully in place, and the Southern Tasmanides cannot be considered stable (figures 8.11).

- Early Carboniferous

The rotation inferred from the Mt Daubeny Formation at the Churinga Property (locality CHU) and the change in fault and cleavage trend in the Southern part of the Broken Hill area is here thought to be a consequence of the punching of the S.W.B. block in the Kanmantoo Fold Belt. It is particularly conceivable if the South Western Belt of the Lachlan Orogen is extended from the green stone belt of the Gouvernor Fault, East of the Melbourne terrane, to that of the Moyston Fault, west of the Stawell terrane, as proposed by Willman *et al.* (2002). These ultra mafic rocks could be some relicts of the subduction zone that has been indented, and the S.W.B. block would be close enough to the southern part of the Broken Hill area to induce this rotation. It is not clear whether this happened in the Late Devonian or in the Early Carboniferous, but it is likely then to observe in the Kanmantoo Fold Belt clockwise rotation North of the S.W.B. block and counter-clockwise rotation South of it.

The setting up of the rest of the Lachlan Orogen is probably complete with, however, slight late reactivation of the Lachlan Transverse Zone and granite intrusion along it (cf. Bathurst Granite). The accretion of the New England Orogen begins to the East with also the formation of the Sydney – Bowen Basin, while the Northern Australian craton moved southward and begin to form the intra-plate Alice Spring Orogeny.

It is considered that the Southern Tasmanides are fully cratonised only after the complete positioning of the South Western Belt. It seems thus that palaeomagnetic data from this region older than Early Carboniferous should not be used or used with extreme caution for the determination of the APW path of Gondwana.

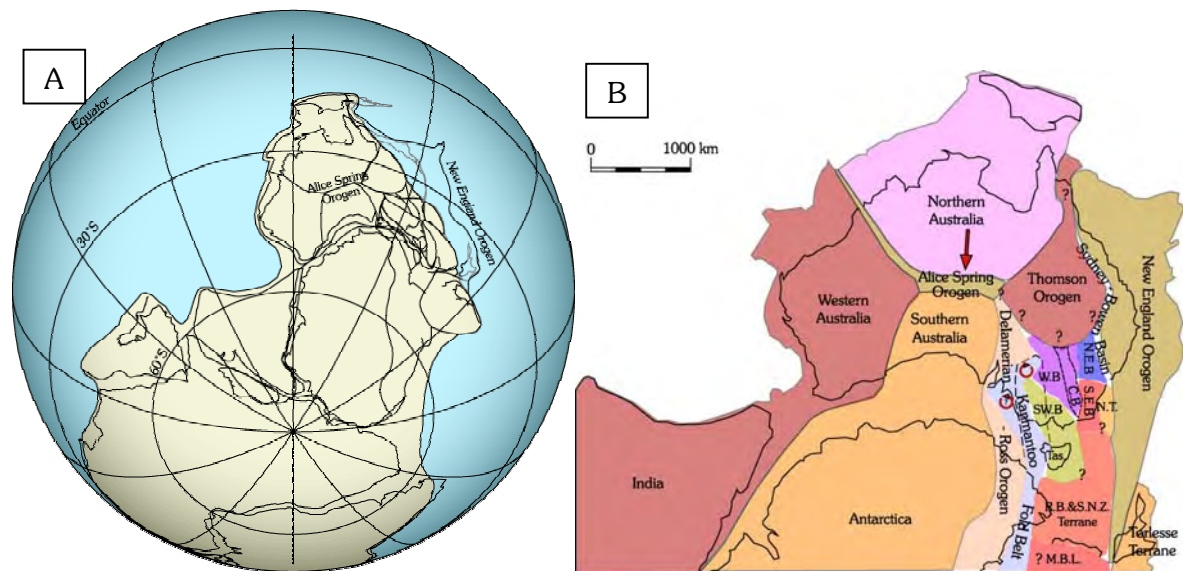


Figure 8.12: Early Carboniferous palinspastic reconstruction.

A- Global view based on the Small Circle Fit path, and **B-** Zoom on the different elements of the Southern Tasmanides. Same abbreviations as in figure 8.9. The tectonic onset of the Southern Tasmanides is complete. The S.W.B. block has wedged the northern part of the Kanmantoo Fold Belt in the Late Devonian or Early Carboniferous and entailed local rotations. The Early Carboniferous is the time of the accretion of the New England Orogen to the East and the formation of the intra-plate Alice Spring Orogeny in central Australia.

A great number of localities have been studied for this work. Unfortunately, only a few are revealed suitable for reliable palaeomagnetic analysis, and in particular the lack of positive field tests is a fundamental problem in constraining the age of magnetisation. This is mainly due to strong weathering effects in Australia and also to the fact that most of the rocks were remagnetised during orogenic events in the Silurian and Devonian. Nevertheless, AMS measurements are revealed a powerful structural tool since stress and strain regimes are poorly known in this region and difficult to assess with other methods.

Concerning palaeomagnetic results, it is believed that several are sufficiently representative to allow proposing a plausible scenario about the tectonic setting of the Southern Tasmanides. It must be pointed out however that this scenario is strongly linked to the choice of a reference APW path for Gondwana. The timing and the amount of displacement and rotation can be significantly modified if another reference path is used.

It is therefore of crucial importance to firmly established the shape of this APW path. This can be done only by adding a significant number of results from clear cratonic regions (from Africa for example) in the palaeomagnetic database.

From then on, a more detailed study of the Southern Tasmanides should be carried out. A detailed re-investigation involving a large number of sites of the rhyolite from the Sisters (locality SIS) and from fresh rocks of the Ural Volcanics (such as at locality MER) can probably confirm or invalidate immediately the scenario proposed herein. However, for the understanding of this region, the best solution is probably to study first Early Carboniferous and Late Devonian rocks to determine more precisely when terranes can be considered cratonised. Then only, older rocks will help refining the complex tectonic history of this region.

References

- Aifa T.** (1993)- Different styles of remagnetisation in Devonian sediments from the north-western Sahara (Algeria). *Geophysical Journal International*, **115**, n°2, 529-537.
- Aifa T., Feinberg H. & Pozzi J.-P.** (1990)- Devonian – Carboniferous palaeopoles for Africa: consequences for Hercynian geodynamics. *Tectonophysics*, **179**, n° 3-4, 287-304.
- Bachtadse V. & Briden J.** (1990)- Paleomagnetic constraints on the position of Gondwana during Ordovician to Devonian times. In McKerrow & Scotese (Ed.), *Palaeozoic Palaeogeography and Biogeography*, Geological Society Memoir, **12**, 43-48.
- Bachtadse V. & Briden J.** (1991)- Palaeomagnetism of Devonian ring complexes from the Bayuda Desert – new constraints on the Apparent Polar Wander path for Gondwanaland. *Geophysical Journal International*, **104**, 635-646.
- Barron L.** (1998)- Metamorphism, Bathurst, NSW. Geological Survey of New South Wales 1:250000 Geological Series Explanatory Notes, pages 284-286.
- Besse J. & Courtillot V.** (1991)- Revised and Synthetic Apparent Polar Wander Paths of the African, Eurasian, North American and Indian Plates, and True Polar Wander since 200 Ma. *Journal of Geophysical Research*, **96**, n°B3, 4029-4050.
- Blevin P., Ellis D. & Warren R.** (1996)- Metallogenic implications of granite tectonics: the Lachlan Fold Belt as a case study. From <http://www.es.mq.edu.au/gemoc/annrep97/abs96/Blev396.html>
- Borg S. & De Paolo D.** (1991)- A tectonic model of the Antarctic Gondwana margin with implications for southeastern Australia: isotopic and geochemical evidence. In Hatcher & Zonenshain (Ed.), *Accretionary Tectonics and Composite Continents*, *Tectonophysics*, **196**, 339-358.
- Bowring S. & Erwin D.** (1998)- A new look at evolutionary rates in deep time: uniting paleontology and high-precision geochronology. *GSA Today*, September, **8**, n°9, 1-8.
- Browne W.** (1947)- A short history of the Tasman geosyncline of eastern Australia. *Science Progress*, **35**, 623-637.
- Bullard E., Everett J. & Smith G.** (1965)- The fit of the continents around the Atlantic. *Philosophical Transactions Royal Society London*, **A258**, 41-51.
- Burrett C., Long J. & Stait B.** (1990)- Early-Middle Palaeozoic biogeography of Asian terranes derived from Gondwana. In McKerrow & Scotese (Ed.), *Palaeozoic palaeogeography and biogeography*, Geological Society Memoir, **12**, 163-174.
- Butler R.** (1992)- Paleomagnetism: magnetic domains to geologic terranes. Blackwell Scientific Publications, USA, 319 pages.
- Chen Z., Li Z.-X. & Powell C.** (1995)- Paleomagnetism of the Upper Devonian Reef Complexes, Canning Basin, Western Australia. *Tectonics*, **14**, n°1, 154-167.
- Cocks L. & Fortrey R.** (1990)- Biogeography of Ordovician and Silurian faunas. In McKerrow & Scotese (Ed.), *Palaeozoic palaeogeography and biogeography*, Geological Society Memoir, **12**, 97-104.
- Cogné J.-P.** (1987)- Contribution à l'étude paléomagnétiques de roches déformées. Mémoires et Documents du Centre Armoricaïn d'Etude Structurale des Socles, n°17 (Thèse d'état), Rennes, 204 pages.
- Collins W.** (1991)- A reassessment of the "Hunter-Bowen Orogeny": tectonic implication for the southern New England Fold Belt. *Australian Journal of Earth Sciences*, **38**, 409-423.
- Collinson D.** (1983)- Methods in palaeomagnetism and rock magnetism, techniques and instrumentation. Chapman and Hall, London, 503 pages.
- Colquhoun G., Cameron R. & Meakin S.** (2000)- Provisional Cargellico 1:100 000 Geological Sheet. Geological Survey of New South Wales, Sydney.

- Colquhoun G., Fergusson C. & Tye S.** (1999)- Provenance of early Palaeozoic sandstones, southern Australia, Part 2: cratonic to arc switching. *Sedimentary Geology*, **125**, 153-163.
- Coney P.** (1992)- The Lachlan Belt of eastern Australia and circum-Pacific tectonic evolution. In Fergusson & Glen (Ed.), *The Palaeozoic Eastern Margin of Gondwanaland: tectonics of the Lachlan Fold Belt, southeastern Australia and related orogens*. Tectonophysics, **214**, 1-25.
- Courtilot V., Davaille A., Besse J. & Stock J.** (2003)- Three distinct types of hotspots in the Earth's mantle. *Earth and Planetary Science Letters*, **205**, 295-308.
- Crook K., Bein J., Hughes R. & Scott P.** (1973)- Ordovician and Silurian history of the southeastern part of the Lachlan geosyncline. *Journal of Geological Society of Australia*, **20**, 113-138.
- Dalziel I. & Pankhurst R.** (1987)- Joint U.K. – U.S. West Antarctic tectonics project: an introduction. In McKenzie (Ed.), *Gondwana Six: structure, tectonics, and geophysics*, American Geophysical Union, Geophysical Monograph, **40**, 173-182.
- Dalziel I.** (1991)- Pacific margins of Laurentia and East Antarctica – Australia as a conjugate rift pair: evidence and implications for an Eocambrian supercontinent. *Geology*, **19**, 598-601.
- Dalziel I.** (1992-a)- Antarctica: a tale of two supercontinents? *Annual Reviews of Earth and Planetary Sciences*, **20**, 501-526.
- Dalziel I.** (1992-b)- On the organisation of the American plates in the Neoproterozoic and the breakout of Laurentia. *GSA Today*, **2**, 240-241.
- Dalziel I.** (1997)- Neoproterozoic-Palaeozoic geography and tectonics: review, hypothesis, environmental speculation. *Geological Society of America Bulletin*, **108**, 16-42.
- Dalziel I., Lawver L., Coffin M. & Gahagan L.** (1999)- From Texas to Antarctica. PLATES project, University of Texas Institute for Geophysics – PowerPoint Animation available at: <http://www.ig.utexas.edu/research/projects/paltes/plates.htm>.
- Direen N. & Crawford** (2003)- The Tasman Line: where is it, what is it, and is it Australia's Rodinian breakup boundary? *Australian Journal of Earth Sciences*, **50**, 491-502.
- DiVenere V. & Kent D.** (1999)- Are the Pacific and Indo-Atlantic hotspots fixed? Testing the plate circuit though Antarctica. *Earth and Planetary Science Letters*, **170**, 105-117.
- Du Toit A.** (1937)- *Our wandering continents*. Oliver & Boyd, Edinburgh, 366 pages.
- Duggan M., Lyons P., Raymond O., Scott M., Sherwin L., Wallace D., Krynen J., Young G., Wyborn D., Glen R. & Leys M.** (1999)- Forbes preliminary edition – 1:250 000 geological map (SI55-7). Australian Geological Survey Organisation, Canberra / Geological Survey of New South Wales, Sydney.
- Dunlop D. & Özdemir Ö.** (1997)- *Rock magnetism – Fundamentals and frontiers*. Cambridge Studies in Magnetism, Cambridge Press University, Cambridge United Kingdom, 573 pages.
- Embleton B., McEhlinny M., Crawford A. & Luck G.** (1974)- Palaeomagnetism and the tectonic evolution of the Tasman Orogenic Zone. *J. Geol. Soc. Australia*, **21**, 187-194.
- Enkin R. & Watson G.** (1996)- Statistical analysis of palaeomagnetic inclination data. *Geophysical Journal International*, **126**, 495-504.
- Fergusson C. & Coney P.** (1992)- Convergence and intraplate deformation in the Lachlan Fold Belt of southeastern Australia. In Fergusson & Glen (Ed.), *The Palaeozoic Eastern Margin of Gondwanaland: tectonics of the Lachlan Fold Belt, southeastern Australia and related orogens*. Tectonophysics, **214**, 417-439.
- Fergusson C. & Tye S.** (1999)- Provenance of early Palaeozoic sandstones, southern Australia, Part 1: vertical changes through the Bangal fan-type deposit. *Sedimentary Geology*, **125**, 135-151.
- Finney S. & Xu C.** (1990)- The relationship of Ordovician graptolite provincialism to palaeogeography. In McKerrow & Scotese (Ed.), *Palaeozoic palaeogeography and biogeography*, Geological Society Memoir, **12**, 123-128.
- Fisher R.** (1953)- Dispersion on a sphere. *Proc. Roy. Soc. London*, **A217**, 295-305.
- Flinn D.** (1962)- On folding during three dimensional progressive deformation. *Q. J. Geol. Soc. London*, **118**, 385-428.
- Flinn D.** (1965-a)- On the symmetry principle and the deformation ellipsoid. *Geol. Mag.*, **102**, 36-45.
- Flinn D.** (1965-b)- Deformation in metamorphism. In Pitcher & Flinn (Ed.), *Controls of Metamorphism*, Oliver & Boyd, Edinburgh, 46-72.
- Gahagan L., Lawver L. & Dalziel I.** (1999)- Antarctica, Keystone of Gondwana. **PLATES Project**, University of Texas Institute for Geophysics.

- Gaina C., Müller R., Royer J.-Y., Stock J., Hardebeck J. & Symonds P.** (1998)- The tectonic history of the Tasman Sea: a puzzle with 13 pieces. *Journal of Geophysical Research B: Solid Earth*, **103**, n°B6, 12413-12433.
- Geeve R., Schmidt P. & Roberts J.** (2002)- Palaeomagnetic results indicate pre-Permian counter-clockwise rotation of the southern Tamworth Belt, southern New England Orogen, Australia. *Journal of Geophysical Research*, **107**, n°B9, 1-16.
- Gilder S., Chen Y., Cogné J.-P., Tan X., Courtillot V., Sun D. & Li Y.** (2003)- Paleomagnetism of Upper Jurassic to Lower Cretaceous volcanic and sedimentary rocks from the western Tarim Basin and implications for inclination shallowing and absolute dating of the M-0 (ISEA?) chron. *Earth and Planetary Science Letters*, **206**, 587-600.
- Glen R. & Walsche J.** (1999)- Cross-structures in the Lachlan Orogen: the Lachlan Transverse Zone example. *Australian Journal of Earth Sciences*, **46**, 641-658.
- Glen R. & Wyborn D.** (1997)- Inferred thrust imbrication, deformation gradients and the Lachlan Transverse Zone in the Eastern Belt of the Lachlan Orogen. *Australian Journal of Earth Sciences*, **44**, 49-68.
- Glen R. & Zhang W.** (2001)- Syntheses maps central-eastern New South Wales: 1 – Geology 1:500 000. Geological Survey of New South Wales, Department of Mineral Ressources, Sydney.
- Glen R.** (1986)- Geology of the Wrightville 1:100 000 sheet 8034. Explanatory Notes, Geological Survey of New South Wales, Sydney.
- Glen R.** (1988)- Basin inversion, thrusts, and ore deposits at Cobar, New South Wales; preliminary report. *Quarterly Notes – Geological Survey of New South Wales*, **73**, 21-26.
- Glen R.** (1992)- Thrust, extensional and strike-slip tectonics in an evolving Palaeozoic orogen: a structural synthesis of the Lachlan Orogen of southeastern Australia. In Fergusson & Glen (Ed.), *The Palaeozoic Eastern Margin of Gondwanaland: tectonics of the Lachlan Fold Belt, southeastern Australia and related orogens*. *Tectonophysics*, **214**, 341-380.
- Glen R., Clare A. & Spencer R.** (1996)- Extrapolating the Cobar Basin model to the regional scale; Devonian basin-formation and inversion in western New South Wales. In G. Cook Warren *et al.* (Eds), *The Cobar mineral field; a 1996 perspective*. Spectrum Series - Australasian Institute of Mining and Metallurgy. Australasian Institute of Mining and Metallurgy, Carlton, Victoria, Australia, 43-83.
- Glen R., Dallmeyer R. & Black L.** (1992-a)- Isotopic dating of basin inversion – The Palaeozoic Cobar Basin, Lachlan Orogen, Australia. In Fergusson & Glen (Ed.), *The Palaeozoic Eastern Margin of Gondwanaland: tectonics of the Lachlan Fold Belt, southeastern Australia and related orogens*. *Tectonophysics*, **214**, 249-268.
- Glen R., Felton E. & Brown R.** (1985)- Wrightville 1:100 000 Geological Sheet 8034. Geological Survey of New South Wales, Sydney.
- Glen R., Korsch R., Direen N., Jones L., Johnstone D., Lawrie K., Finlayson D. & Shaw R.** (2002)- Crustal structure of the Ordovician Macquarie Arc, Eastern Lachlan Orogen, based on seismic-reflection profiling. *Australian Journal of Earth Sciences*, **49**, 323-348.
- Glen R., Korsch R., Finlayson D., Johnstone D. & Walshe J.** (1998)- New data on the Ordovician intraoceanic Macquarie Arc: preliminary interpretation of seismic refraction and reflection profiling along and across the Molong Volcanic Belt, Lachlan Orogen, New South Wales. *Australian Institute of Geoscientists, Bulletin*, **23**, 93-96.
- Glen R., Lennox P. & Foster D.** (1999)- $^{40}\text{Ar}/^{39}\text{Ar}$ dating of deformations west of the Hill End Trough, Lachlan Orogen, New South Wales. *Quaternary Notes* 110, 13-22.
- Glen R., Scheibner E. & Van den Berg A.** (1992-b)- Paleozoic intraplate escape tectonics in Gondwanaland and major strike-slip duplication in the Lachlan Orogen of southeastern Australia. *Geology*, **20**, 795-798.
- Goleby B.** (1980)- Early Palaeozoic palaeomagnetism of South East Australia. Thesis of Master of Science in the Australian National University, Canberra, 162 pages.
- Gray D. & Foster D.** (1997)- Orogenic concepts – Application and definition: Lachlan Fold Belt, eastern Australia. *American Journal of Science*, **297**, 859-891.
- Gray D., Foster D. & Bucher M.** (1997)- Recognition and definition of orogenic events in the Lachlan Fold Belt. *Australian Journal of Earth Sciences*, **44**, 489-501.
- Grunow A. & Encoarnación J.** (2000)- Cambro-Ordovician palaeomagnetic and geochronologic data from southern Victoria Land, Antarctica: revision of the Gondwana apparent polar wander path. *Geophysical Journal International*, **141**, 391-400.

- Grunow A.** (1995)- Implications for Gondwana of new Ordovician paleomagnetic data from igneous rocks in southern Victoria Land, East Antarctica. *Journal of Geophysical Research*, **100**, n°B7, 12589-12603.
- Grunow A.** (1999)- Gondwana events and palaeogeography: a palaeomagnetic review. *Journal of African Earth Sciences*, **28**, 53-69.
- Hargraves R., Dawson E. & Van Houten F.** (1987)- Palaeomagnetism and age of mid-Palaeozoic ring complexes in Niger, Western Africa, and tectonic implications. *Geophys. J. R. Astron. Soc.*, **90**, 705-729.
- Havliček V.** (1989)- Climatic changes and development of benthic communities through the Mediterranean Ordovician. *Sub. Geol. Ved., Geol.*, **44**, 79-116.
- Hoffman P.** (1991)- Did the breakout of Laurentia turn Gondwanaland inside-out? *Science*, **252**, 1409-1412.
- Hoffman P.** (1999)- The break-up of Rodinia, birth of Gondwana, true polar wander and the snowball Earth. *Journal of African Earth Sciences*, **28**, n°1, 17-33.
- Hrouda F.** (1982)- Magnetic anisotropy of rocks and its application in geology and geophysics. *Geophysical Surveys*, **5**, 37-82.
- Hurley N. & Van der Voo R.** (1987)- Paleomagnetism of the Upper Devonian Reefal Limestone, Canning Basin, Western Australia. *Geological Society of America Bulletin*, **98**, n°2, 138-146.
- Jefferson C.** (1978)- Correlation of middle and upper Proterozoic strata between north-western Canada and Central Australia. *Geological Society America Abstracts Programs*, **7**, 429.
- Jelinek V.** (1981)- Characterization of the magnetic fabric of rocks. *Tectonophysics*, **79**, 63-70.
- Jenkins R., Landenberger B. & Collins W.** (2002)- Late Palaeozoic retreating and advancing subduction boundary in the New England Fold Belt, New South Wales. *Australian Journal of Earth Sciences*, **49**, 467-489.
- Kent D. & Van der Voo R.** (1990)- Palaeozoic palaeogeography from palaeomagnetism of the Atlantic-bordering continents. In McKerrow & Scotese (Ed.), *Palaeozoic palaeogeography and biogeography*, Geological Society Memoir, **12**, 49-56.
- Khan A.** (1962)- The anisotropy of magnetic susceptibility in some igneous and metamorphic rocks. *Journal of Geophysical Research*, **67**, 2873-2885.
- Khattach D., Robardet M. & Perroud H.** (1995)- A Cambrian pole for the Moroccan coastal meseta. *Geophysical Journal International*, **120**, n°1, 132-144.
- Kirschvink J.** (1980)- The least-squares line and plane and the analysis of palaeomagnetic data. *Geophysical Journal of the Royal Society*, **62**, 699-718.
- Kirschvink J., Ripperdan R. & Evans D.** (1997)- Evidence for a large-scale Early Cambrian reorganization of continental masses by inertial interchange true polar wander. *Science*, **277**, 541-545.
- Klootwijk C.** (1980)- Early Palaeozoic palaeomagnetism in Australia. *Tectonophysics*, **64**, 249-332.
- Klootwijk C.** (2002)- Carboniferous palaeomagnetism of the Rocky Creek Block, northern Tamworth Belt, and the New England pole path. *Australian Journal of Earth Sciences*, **49**, 375-405.
- Königsberger J.** (1938)- Natural residual magnetism in eruptive rocks. *Terr. Magn. Atm. Electr.*, **43**, 119-299.
- Korsch R., Barton T., Gray D., Owen A. & Foster D.** (2002)- Geological interpretation of a deep seismic-reflection transect across the boundary between the Delamerian and Lachlan Orogens, in the vicinity of the Grampians, western Victoria. *Australian Journal of Earth Sciences*, **49**, 1057-1075.
- Korsch R., Wake-Dyster K. & Johnstone D.** (1992)- Seismic imaging of Late Palaeozoic-Early Mesozoic extensional and contractional structures in the Bowen and Surat basins, eastern Australia. *Tectonophysics*, **215**, 273-294.
- Lawver L. & Scotese C.** (1987)- A revised reconstruction of Gondwanaland. In McKenzie (Ed.) *Gondwana Six: structure, tectonics and geophysics*. American Geophysical Union, Geophysical Monograph, **40**, 17-23.
- Lawver L., Gahagan L. & Dalziel I.** (1999)- A tight fit-Early Mesozoic Gondwana _ A plate reconstruction perspective. In Motoyoshi & Shiraishi (Ed.), *Origin and evolution of continents: proceedings of the International Symposium "Origin and Evolution Continents", 13-14 October 1997, Tokyo*, Memoirs of National Institute of Polar Research, Special Issue, **53**, 214-229.

- Leitch E. & Scheibner E.** (1987)- Stratotectonic terranes of the eastern Australian Tasmanides. In Leitch & Scheibner (Ed.), *Terrane Accretion and Orogenic Belts*. American Geophysical Union, Geodynamic series **19**, 1-19.
- Li Z.-X. & Powell C.** (2001)- An outline of the palaeogeographic evolution of the Australasian region since the beginning of the Neoproterozoic. *Earth-Science Reviews*, **53**, 237-277.
- Li Z.-X., Baillie P. & Powell C.** (1997)- Relationship between northwestern Tasmania and East Gondwanaland in the Late Cambrian/Early Ordovician: paleomagnetic evidence. *Tectonics*, **16**, n°1, 161-171.
- Li Z.-X., Schmidt P. & Embleton B.** (1988)- Paleomagnetism of the Hervey Group, Central New South Wales and its tectonic implications. *Tectonics*, **7**, n°3, 351-367.
- Livermore R., Smith A. & Briden J.** (1985)- Palaeomagnetic constraints on the distribution of continents in the Late Silurian and Early Devonian. *Philos. Trans. R. Soc. London, Serie B*, **309**, 29-56.
- McElhinny M. & Embleton B.** (1974)- Australian palaeomagnetism and the Phanerozoic plate tectonics of eastern Gondwanaland. *Tectonophysics*, **22**, 1-29.
- McElhinny M. & Lock J.** (1996)- I.A.G.A. palaeomagnetic databases with access (Version 4.3, 2002). *Surveys in Geophysics*, **17**, 575-591.
- McElhinny M.** (1964)- Statistical significance of the Fold Test in palaeomagnetism. *Research Note; Geophysical Journal of the Royal Astronomical Society*, **8**, n°3, 338-340.
- McElhinny M., Powell C. & Pisarevsky S.** (2003)- Paleozoic terranes of eastern Australia and the drift history of Gondwana. *Tectonophysics*, **362**, n°1-4, 41-65.
- McFadden P.** (1990)- A new fold test for paleomagnetic studies. *Geophysical Journal International*, **103**, 163-169.
- McKerrow W., Mac Niocaill C., Ahlberg P., Clayton G., Cleal C. & Eagar R.** (2000)- The Late Paleozoic relations between Gondwana and Laurussia. In Franke W., Haak V., Oncken O. & Tanner D. (eds.)- *Orogenic processes: Quantification and modelling in the Variscan Belt*, Geological Society London, Special Publications, **179**, 9-20.
- McMenamin M. & McMenamin D.** (1990)- The emergence of animals. *The Cambrian breakthrough*, New York, Columbia University Press, 217 pages.
- McRae G.** (1989)- Lachlan Downs 1:100 000 Geological Sheet 8033. Geological Survey of New South Wales, Sydney.
- Meakin S., Cameron R., Colquhoun G., Simpson C., Barron L. & Wilde S.** (2002)- The Ural Volcanics: a Siluro-Devonian felsic volcanic succession in Central NSW. In Preiss, V. (editor), 2002. *Geoscience 2002: Expanding Horizons. Abstracts of the 16th Australian Geological Convention*, Adelaide Convention Centre, Adelaide, SA, Australia. July 1-5 2002, No. 67, page 244.
- Meert J. & Van der Voo R.** (1997)- The assembly of Gondwana 800-550 Ma. *Journal of Geodynamics*, **23**, n°3/4, 223-235.
- Meffre S., Crawford T., Scott R., Simpson C., Boulton S.** (in preparation)- Stratigraphy, geochemistry, and alteration in the Molong section of the Ordovician Volcanics. NSW Ordovician SPIRT – 1999 Work Program report.
- Moore E.** (1991)- Southwest U.S. – East Antarctica (SWEAT) connection: a hypothesis. *Geology*, **19**, 425-428.
- Morel P. & Irving E.** (1978)- Tentative paleocontinental maps for the Early Phanerozoic and Proterozoic. *Journal of Geology*, **86**, n°5, 535-561.
- Morel P. & Irving E.** (1981)- Paleomagnetism and evolution of Pangea. *Journal of Geophysical Research*, **86**, n°3, 1858-1872.
- Müller R., Gaina C. & Clark S.** (2000)- Seafloor spreading around Australia. In Veevers (ed.), *Billion-year earth history of Australia and neighbours in Gondwanaland*. ARC National Key Centre for Geochemical Evolution and Metallogeny of Continents (GEMOC), GEMOC Press, Sydney, pages 18-28.
- Müller R., Roest W., Royer J.-Y., Gahagan L. & Sclater J.** (1997)- Digital isochrones of the world's ocean floor. *Journal of Geophysical Research*, **102**, n°B2, 3211-3214.
- Neef G. & Bottrill R.** (1991)- Early Devonian (Gedinnian) nonmarine strata present in a rapidly subsiding basin in far western New South Wales, Australia. *Sedimentary Geology*, **71**, 195-212.

- O'Sullivan P., Belton D. & Orr M.** (2000-b)- Post-orogenic thermotectonic history of the Mount Buffalo region, Lachlan Fold Belt, Australia: evidence for Mesozoic to Cenozoic wrench-fault reactivation? *Tectonophysics*, **317**, 1-26.
- O'Sullivan P., Gibson D., Kohn B., Pillans B. & Pain C.** (2000-a)- Long-term landscape evolution of the Northparkes Region of the Lachlan Fold Belt, Australia: constraints from fission track and paleomagnetic data. *Journal of Geology*, **108**, 1-16.
- O'Sullivan P., Kohn B., Foster D. & Gleadow A.** (1996)- Mesozoic and Cainozoic thermotectonic history of the Lachlan Fold Belt, New South Wales, Australia. *Geological Society of Australia, Abstracts*, **41**, 327.
- Offler R., Miller J., Gray D., Foster D. & Bale R.** (1998)- Crystallinity and b_0 spacing of K-white micas in a Paleozoic accretionary complex, Eastern Australia: metamorphism, paleogeotherms, and structural style of an underplated sequence. *Journal of Geology*, **106**, 495-509.
- Packham G.** (1969)- The geology of New South Wales. *Journal of the Geological Society of Australia*, **16**, Part 1, 1-271.
- Palmer A. & Geissman J.** (1999)- Geological time scale. The Geological Society of America, *Palmer & Geissman compilers*, Product code CTS004.
- Parés J. & Van der Pluijm B.** (2002)- Evaluating magnetic lineations (AMS) in deformed rocks. *Tectonophysics*, **350**, 283-298.
- Pedder A. & Oliver W._{JR}** (1990)- Rugose coral distribution as a test of Devonian palaeogeography models. In McKerrow & Scotese (Ed.), *Palaeozoic palaeogeography and biogeography*, Geological Society Memoir, **12**, 267-275.
- Perroud H., Van der Voo R. & Bonhommet N.** (1984)- Paleozoic evolution of the Armorica plate on the basis of paleomagnetic data. *Geology*, **12**, 579-582.
- Pogson D. & Watkins J.** (1998)- Bathurst 1:250 000 Geological sheet. Explanatory Notes, Geological Survey of New South Wales, 430 pages.
- Powell C.** (1995)- Are Neoproterozoic glacial deposits preserved on the margins of Laurentia related to the fragmentation of two supercontinents? – Comment, *Geology*, **23**, 1053-1054.
- Powell C., Li Z.-X., Thrupp G. & Schmidt P.** (1990)- Australian Palaeozoic palaeomagnetism and tectonics, tectonostratigraphic terrane constraints from the Tasman Fold Belt. In Grady *et al.* (Ed.), *Australian Tectonics*. *Journal of Structural Geology*, **12**, 553-565.
- Powell C., McElhinny M., Meert J. & Park J.** (1993)- Paleomagnetic constraints on timing of the Neoproterozoic break-up of Rodinia and the Cambrian formation of Gondwana. *Geology*, **21**, 223-235.
- Pueyo E., Parés J., Millán H. & Pocovi A.** (2003)- Conical folds and apparent rotations in paleomagnetism (a case study in the Southern Pyrenees). *Tectonophysics*, **362**, 345-366.
- Rakotosolofo N.** (1999)- Geology, carbon isotope stratigraphy, and palaeomagnetism of the Karoo sequences of the southern Morondava Basin, SW Madagascar. Master of Science, Faculty of Natural Science, Rand Afrikaans University, 162 pages.
- Rees A.** (1966)- The effects of depositional slopes on the anisotropy of magnetic susceptibility of laboratory deposited sands. *Journal of Geology*, **74**, 856-867.
- Robardet M.** (2003)- The Armorica 'microplate': fact or fiction? Critical review of the concept and contradictory palaeobiogeographical data. *Palaeogeography, Palaeoclimatology, Palaeoecology*, **195**, 125-148.
- Royer J.-Y., Müller R., Gahagan L., Lawver L., Mayes C., Nürnberg D. & Sclater J.** (1992)- A global isochron chart. Technical report n°117, University of Texas Institute for Geophysics, 19 pages.
- Scheibner E.** (1985)- Mount Allen 1:100 000 Geological Sheet 8032. Geological Survey of New South Wales, Sydney.
- Scheibner E.** (1987)- Geology of the Mount Allen 1:100 000 sheet 8032. Explanatory Notes, Geological Survey of New South Wales, Sydney.
- Scheibner E.** (1996)- Geology of New South Wales – Synthesis. Volume 1; Structural Framework. Erwin Scheibner & Helena Basden (Ed.), *Department of Mineral Resources, Geological Survey of New South Wales, Memoir Geology 13/1*, 295 pages.
- Scheibner E.** (1998)- Geology of New South Wales – Synthesis. Volume 2; Geological evolution. Erwin Scheibner & Helena Basden (Ed.), *Department of Mineral Resources, Geological Survey of New South Wales, Memoir Geology 13/2*, 359 pages.

- Schmidt P. & Morris W.** (1977)- An alternative view of the Gondwana Paleozoic apparent polar wander path. *Canadian Journal of Earth Sciences*, **14**, 2674-2678.
- Schmidt P., Embleton B. & Palmer H.** (1987)- Devonian magnetization of the Snowy River Volcanics. *Geophysical Journal of Royal Astronomical Society*, **91**, 171-199.
- Schmidt P., Embleton B., Cudahy T. & Powell C.** (1986)- Prefolding and pre-megakinking magnetization from the Devonian Comerong Volcanics, New South Wales, Australia, and their bearing on the Gondwana Pole Path. *Tectonics*, **5**, 135-150.
- Schmidt P., Powell C., Li Z.-X. & Thrupp G.** (1990)- Reliability of Palaeozoic palaeomagnetic poles and APWP of Gondwanaland. In Schmidt & Van der Voo (Ed.), *Reliability of Palaeomagnetic Data*, *Tectonophysics*, **184**, 87-100.
- Scotese C. & Barrett S.** (1990)- Gondwana's movement over the South Pole during the Palaeozoic: evidence from lithological indicators of climate. In McKerrow & Scotese (Ed.), *Palaeozoic palaeogeography and biogeography*, *Geological Society Memoir*, **12**, 75-85.
- Scotese C. & McKerrow W.** (1990)- Revised world maps and introduction. In McKerrow & Scotese (Ed.), *Palaeozoic palaeogeography and biogeography*, *Geological Society Memoir*, **12**, 1-21.
- Scotese C., Van der Voo R. & Barrett S.** (1985)- Silurian and Devonian base maps. *Philos. Trans. R. Soc. London, Serie B*, **309**, 57-77.
- Smith A.** (1999)- Gondwana: its shape, size and position from Cambrian to Triassic times. *Journal of African Earth Sciences*, **28**, n°1, 71-97.
- Smith G. & Hallam A.** (1970)- The fit of the southern continents. *Nature*, **225**, 139-149.
- Smith G. & Livermore R.** (1991)- Pangea in Permian to Jurassic time. *Tectonophysics*, **187**, 135-179.
- Soffel H.** (1991)- *Pläomagnetismus und archäomagnetismus*. Springer-Verlag, Berlin Heidelberg, Germany, 276 pages.
- Stevens B., Mills K., Direen N., Buckley P. & Cooper I.** (2000)- Koonenberry pre-Permian interpretation map. Geological Survey of New South Wales, Sydney.
- Stump E.** (1987)- Construction of the Pacific margin of Gondwana during the Pannotios cycle. In McKenzie (Ed.), *Gondwana Six: structure, tectonics, and geophysics*, *American Geophysical Union, Geophysical Monograph*, **40**, 77-87.
- Stump E., White A. & Borg S.** (1986)- Reconstruction of Australia and Antarctica: evidence from granites and recent mapping. *Earth and Planetary Science Letters*, **79**, 348-360.
- Süßmilch C.** (1914)- *Geology of New South Wales*. Angus & Robertson, Sydney.
- Sutherland R.** (1999)- Basement geology and tectonic development of the greater New Zealand region: an interpretation from regional magnetic data. *Tectonophysics*, **308**, 341-362.
- Tait J., Bachtadse V. & Soffel H.** (1994)- New Palaeomagnetic constraints on the position of central Bohemia during Early Ordovician times. *Geophysical Journal International*, **116**, 131-140.
- Tait J., Bachtadse V. & Soffel H.** (1995)- Upper Ordovician palaeogeography of the Bohemian Massif: implications for Armorica. *Geophysical Journal International*, **122**, 211-218.
- Talent J.** (1959)- Notes on middle Palaeozoic stratigraphy and diastrophism in eastern Victoria. *Mining and Geological Journal*, **6**, n°3, 57-58.
- Talent J.** (1965)- The stratigraphic and diastrophic evolution of central and eastern Victoria in Middle Paleozoic times. *Proceeding of the Royal Society of Victoria*, **79**, 179-195.
- Tauxe L.** (1998)- Paleomagnetic principles and practice. *Modern approaches in geophysics*, **17**, Monograph title, Kluwer Academic Publishers, Dordrecht, Netherlands, 299 pages.
- Thrupp G., Kent D., Schmidt P. & Powell C.** (1991)- Paleomagnetism of red beds of the Late Devonian Worange Point Formation, SE Australia. *Geophysical Journal International*, **104**, n°1, 179-201.
- Torii M., Fukuma K., Horng C.-S. & Lee T.-Q.** (1996)- Magnetic discrimination of pyrrhotite – and greigite-bearing sediment samples. *Geophysical Research Letters*, **23**, n°14, 1813-1816.
- Torsvik T. & Smethrust M.** (1999)- Plate tectonic modelling: virtual reality with GMAP. *Computers & Geosciences*, **25**, 395-402.
- Torsvik T. & Van der Voo R.** (2002)- Refining Gondwana and Pangea palaeogeography: estimates of Phanerozoic non-dipole (octupole) fields. *Geophysical Journal International*, **151**, 771-794.
- Torsvik T., Carter L., Ashwal L., Bhushan S., Pandit M. & Jamtveit M.** (2001-a)- Rodinia refined or obscured: palaeomagnetism of the Malani igneous suite (NW India). *Precambrian Research*, **108**, 319-333.
- Torsvik T., Løvlie R. & Storetvedt K.** (1993)- Multicomponent magnetization in the Helmsdale Granite, North Scotland; geotectonic implications. *Tectonophysics*, **98**, 111-129.

- Torsvik T., Smethrust M., Meert J., Van der Voo R., Mckerrow W., Brasier M., Sturt B. & Walderhaug H.** (1996)- Continental break-up and collision in the Neoproterozoic and Palaeozoic – a tale of Baltica and Laurentia. *Earth Science Reviews*, **40**, 229-258.
- Torsvik T., Van der Voo R., Meert J., Mosar J. & Walderhaug H.** (2001-b)- Reconstructions of the continents around the North Atlantic at about the 60th parallel. *Earth and Planetary Science Letters*, **187**, 55-69.
- Turner S., Kelley S., Van den Berg A., Foden J., Sandiford M. & Flöttmann T.** (1996)- Source of the Lachlan Fold Belt flysch linked to convective removal of the lithospheric mantle and rapid exhumation of the Delamerian – Ross Fold Belt. *Geology*, **24**, n°10, 941-944.
- Van den Berg A. & Wilkinson H.** (1982)- Victoria. In Cooper & Grindley (Eds.), *Late Proterozoic to Devonian sequences of southeastern Australia, Antarctica and New Zealand and their correlation*, Geological Society of Australia Special Publication **9**, pages 36-47.
- Van der Voo R. & Torsvik T.** (2001)- Evidence for Late Paleozoic and Mesozoic non-dipole fields provides an explanation for the Pangea reconstruction problems. *Earth and Planetary Science Letters*, **187**, 71-81.
- Van der Voo R.** (1988)- Paleozoic paleogeography of North America, Gondwana, and intervening displaced terranes: comparisons of paleomagnetism with paleoclimatology and biogeography patterns. *Geological Society of American Bulletin*, **100**, 311-324.
- Van der Voo R.** (1993)- Palaeomagnetism of the Atlantic, Tethys, and Iapetus oceans. *Cambridge University Press*, 411 pages.
- Van Houten F. & Hargraves R.** (1987)- Palaeozoic drift of Gondwana: palaeomagnetic and stratigraphic constraints. *Geol. J.*, **22**, 341-359.
- Veevers J.** (1984) [Editor]- Phanerozoic Earth History of Australia. *Clarendon Press, Oxford*, 418 pages.
- Veevers J.** (2000)- Billion-year earth history of Australia and neighbours in Gondwanaland. ARC National Key Centre for Geochemical Evolution and Metallogeny of Continents (GEMOC), GEMOC Press, Sydney, 388 pages.
- Veevers J.** (2001)- Atlas of billion-year earth history of Australia and neighbours in Gondwanaland. ARC National Key Centre for Geochemical Evolution and Metallogeny of Continents (GEMOC), GEMOC Press, Sydney, 76 pages.
- Webby B.** (1992)- Ordovician island biotas: New South Wales record and global implications. *Royal Society of New South Wales, Journal and Proceedings*, **125**, 51-77.
- Wegener A.** (1912)- Die Entstehung der Kontinente. *Geologische Rundschau*, **2**, 276-292.
- Wegener A.** (1915)- Die Entstehung der Kontinente und Ozeane. Braunschweig, Friedrich Vieweg und Sohn.
- Weil A., Van der Voo R., Niocaill C. & Meert J.** (1998)- The Proterozoic supercontinent Rodinia: paleomagnetically derived reconstructions for 1100 to 800 Ma. *Earth and Planetary Science Letters*, **154**, 13-24.
- Willman C., Van den Berg A. & Morand V.** (2002)- Evolution of the South-eastern Lachlan Fold Belt in Victoria. *Australian Journal of Earth Sciences*, **49**, n°2, 271-289.
- Wilson C., Grunow A. & Hanson R.** (1997)- Gondwana assembly: the view from southern Africa and East Antarctica. *Journal of Geodynamics*, **23**, n°3/4, 263-286.
- Young G., Moody J. & Casas J.** (2000)- New discoveries of Devonian vertebrates from South America, and implications for Gondwana – Eurasia contact. *Palaeontology/Paléontologie*, C. R. Acad. Sciences Paris, **331**, 755-761.
- Zijderveld J.** (1967)- A.C. demagnetisation of rocks. In Collinson, Créer & Runcorn (Ed.), *Methods in Palaeomagnetism*, Elsevier Science, New York, pages 254-286.

Annexe I: Palaeomagnetic database and level of selection

N°	ROCKNAME	Level	PLAT	PLONG	N	K	α_{95}	Age average	+/-	ϵ	Authors	Year
Af	~Africa											
1	Nuanetsi Lavas	Base	29.00	247.50	6	8.1	25.0	202.0	+/-	13.0	Brock	1968
2	Shawa Ijolite	Base	64.20	265.60	52	46.0	12.0	205.0	+/-	16.0	Gough & Brock	1964
3	Zarzaitine Formation	Low	70.90	235.10	68	353.0	2.6	206.5	+/-	28.5	Kies <i>et al.</i>	1995
4	Nusab el Balgum Complex	Base	64.10	230.70	50	81.2	5.4	216.0	+/-	5.0	Saradeth <i>et al.</i>	1989
5	Red Sandstone Formation	Base	68.00	230.50	32	208.0	4.6	221.5	+/-	13.5	Opdyke	1964
6	Argana Redbeds	Base	50.60	251.40	22	7.5	12.0	221.5	+/-	13.5	Martin <i>et al.</i>	1978
7	Upper Triassic Sediments	Base	54.90	223.30	14	36.7	11.5	221.5	+/-	13.5	Ghorabi & Henry	1991
8	Al Aziza Formation	Mid	59.30	214.10	40	36.0	3.8	231.0	+/-	8.0	Muttoni <i>et al.</i>	2001
9	Al Aziza Formation	Base	54.50	225.80	20	36.0	5.5	231.0	+/-	8.0	Muttoni <i>et al.</i>	2001
10	Volcanics and sediments combined	Base	69.00	250.90	54	44.3	11.6	238.0	+/-	3.0	Daly & Pozzi	1976
11	Ait-Aadel Dolerites	Base	72.00	254.50	62	27.0	7.5	238.0	+/-	3.0	Hailwood	1975
12	Issaldain Dolerites	Base	77.30	140.60	45	88.0	6.0	238.0	+/-	3.0	Hailwood	1975
13	Titchka Sandstone	Base	68.50	266.80	30		21.8	238.0	+/-	3.0	Hailwood	1975
14	Jwaneng Kimberlite	Base	72.00	219.20	6	176.0	5.1	242.5	+/-	7.5	Hargraves	1989
15	Gebel Farsh El Azraq	Base	22.20	252.90	39	5.9	24.8	243.0	+/-	8.0	Wassif	1991
16	Maji-ya-Chumvi Beds	Base	67.00	269.00	32	13.9		248.5	+/-	7.5	McElhinny & Brock	1975
17	Cassanje Series	Base	54.00	260.00	25	21.0	6.0	248.5	+/-	7.5	Valencio <i>et al.</i>	1978
18	K5 Red Sandstones	Base	75.00	144.00	5	23.0	9.8	250.0	+/-	2.0	Nairn	1964
19	Permian Redbeds	High	26.90	265.10	81	84.2	5.3	254.0	+/-	6.0	Nyblade <i>et al.</i>	1993
20	K3 Beds, Songwe-Ketewaka coalfields	Mid	27.60	269.80	27	59.8	12.0	257.0	+/-	3.0	Opdyke	1964
21	K3 Beds, Galula coalfield	Mid	46.00	220.00	34	227.0	5.0	257.0	+/-	3.0	Opdyke	1964
22	K3 Beds, Songwe-Kiwira coalfield	Base	58.00	254.00	8		7.1	257.0	+/-	3.0	Nairn	1964
23	Sediments, Tunisia	Base	49.40	199.80	24	18.0	22.0	257.5	+/-	12.5	Abou-Deeb & Tarling	1984
24	Chougrane Redbeds	Low	32.20	244.10	45	20.0	4.7	273.0	+/-	17.0	Daly & Pozzi	1976
25	Serie d'Abadla, Upper Unit	Low	29.00	240.00		59.0	6.0	273.0	+/-	17.0	Morel <i>et al.</i>	1981
26	Djebel Tarhat Redbeds	Base	24.00	243.80	30	34.6	7.8	273.0	+/-	17.0	Martin <i>et al.</i>	1978
27	Taztot Trachyandesite	Base	38.70	236.80	12	80.0	4.6	273.0	+/-	17.0	Daly & Pozzi	1976
28	Abadla Formation Lower Unit	Mid	29.10	237.80	96	138.0	3.6	275.0	+/-	15.0	Merabet <i>et al.</i>	1998
29	Jebel Nehoud Ring Complex	Mid	40.80	251.30	62	78.1	6.0	280.0	+/-	2.0	Bachtadse <i>et al.</i>	2002
30	Volcanics, Morocco	Base	36.00	238.00	24	20.2	20.9	280.5	+/-	24.5	Westphal <i>et al.</i>	1979
31	Upper El Adeb Larache Formation	Low	38.50	237.50	34	837.0	2.8	286.5	+/-	16.5	Henry <i>et al.</i>	1992
32	Lower Tiguentourine Formation	Mid	33.80	241.40	28	170.0	4.1	290.0	+/-	10.0	Derder <i>et al.</i>	1994
33	Abu Durba Sediments	Low	25.60	244.00	66	53.0	7.2	306.5	+/-	16.5	Abdeldayem <i>et al.</i>	1994
34	Edjeleh Fold	High	28.30	238.90	49	130.0	4.6	307.0	+/-	4.0	Derder <i>et al.</i>	2001
35	Lower El Adeb Larache Formation	Mid	28.70	235.80	61	161.0	3.5	307.0	+/-	4.0	Henry <i>et al.</i>	1992
36	Dwyka System Combined	Mid	25.00	247.00	104			315.0	+/-	25.0	Opdyke <i>et al.</i>	2001
37	Ain Ech Chebbi, Hassi Bachir Formations	Base	25.40	234.80	43	127.8	4.1	316.0	+/-	9.0	Daly & Irving	1983
38	Oubarakat and El-Adeb Larache Formations	Mid	28.20	235.50	72	118.0	4.5	317.0	+/-	6.0	Derder <i>et al.</i>	2001
39	Sediments, Algeria	Base	26.70	237.90	30	38.5	12.5	319.0	+/-	14.0	Abou-Deeb & Tarling	1984
40	Reggane sediments	High	26.60	224.70	64	297.0	5.3	320.0	+/-	13.0	Derder <i>et al.</i>	2001
41	Ain-Ech-Chebbi Formation	Base	25.00	225.00	20	21.0		325.5	+/-	7.5	Conrad & Westphal	1975
42	Oued Draa Aftez Limestone	Base	7.60	232.50	8	24.1	11.4	341.5	+/-	8.5	Martin <i>et al.</i>	1978
43	Djebel Hadid Redbeds	Base	0.10	56.40	12	26.4	8.6	341.5	+/-	8.5	Martin <i>et al.</i>	1978
44	Basalts, diorite and contact	Low	16.10	242.50	19	17.8	22.3	348.0	+/-	15.0	Martin <i>et al.</i>	1978
45	Beni-Zireg Limestones	High	19.20	199.80	54	24.0	3.7	365.0	+/-	2.0	Aifa <i>et al.</i>	1990
46	Griotte Limestones	High	21.00	199.90	54	24.0	3.7	365.0	+/-	2.0	Aifa	1993
47	Gilif Hills Volcanics	Mid	-25.90	191.60	39	18.7	10.8	377.0	+/-	5.0	Bachtadse & Briden	1991

Annexe I: Palaeomagnetic database and level of selection (continued)

48	Hazzel Matti Formation	High	16.20	241.70	53	378.0	6.3	379.0	+/-	2.0	Smith <i>et al.</i> 1994
49	Gneiguira Supergroup	Low	35.50	224.00	44	89.0	5.1	397.0	+/-	20.0	Kent <i>et al.</i> 1984
50	Bokkeveld Group	Base	10.00	15.00	13	33.0	7.0	398.5	+/-	18.5	Bachtadse <i>et al.</i> 1987
51	Air intrusives	Mid	43.40	188.60	53	44.7	6.6	407.0	+/-	8.0	Hargraves <i>et al.</i> 1987
52	Pakhuis, Cedarberg Formations	Base	25.00	343.00	9	9.0	18.0	446.5	+/-	11.5	Bachtadse <i>et al.</i> 1987
53	Salala Ring Complex	Mid	-39.60	149.50	49	39.6	9.2	463.0	+/-	3.0	Bachtadse & Briden 1989
54	Graafwater Formation	Mid	28.00	14.00	28	25.0	9.0	482.5	+/-	12.5	Bachtadse <i>et al.</i> 1987
55	Group des Plateau d'Oujeff	Base	44.80	43.80	11	41.0	40.0	487.5	+/-	17.5	Morris & Carmichael 1978
56	Hasi-Messaud Sediments	Base	53.00	26.00	30		3.0	487.5	+/-	17.5	Bucur 1971
57	Hook Intrusives	Base	14.00	336.50	10	15.9	32.0	500.0	+/-	17.0	Brock 1967
58	Qena-Safaga dykes	Low	-87.30	124.20	126	36.0	4.8	503.5	+/-	23.5	Davies <i>et al.</i> 1980
59	Um Rus dykes	Low	85.10	165.70	88	48.3	5.7	503.5	+/-	23.5	Davies <i>et al.</i> 1980
60	Sidi-Said-Maachou Volcanics	High	14.00	231.00	66	70.0	6.0	511.5	+/-	6.5	Khattach <i>et al.</i> 1995
61	Sidi-Said-Maachou Volcanics	Mid	18.00	235.00	101	33.0	6.0	511.5	+/-	6.5	Khattach <i>et al.</i> 1995
62	Dedza Mountain Syenite	Base	26.00	341.00	1			520.0	+/-	25.0	McElhinny <i>et al.</i> 1968
63	Esh El Mellaha Dykes	Base	87.30	25.90	18		10.9	520.0	+/-	25.0	Abdullah <i>et al.</i> 1984
64	Esh El Mellaha Dykes	Low	81.60	120.80	49		4.1	520.0	+/-	25.0	Abdullah <i>et al.</i> 1984
65	Esh El Mellaha Dykes	Low	82.70	273.50	62		7.5	520.0	+/-	25.0	Abdullah <i>et al.</i> 1984
66	Atar Cliff Group, Units CO7 & 8	Base	0.30	69.30	23	9.0	11.0	520.0	+/-	25.0	Perrin <i>et al.</i> 1988
67	Ntonya Ring Structure	Mid	27.80	344.90	27	999.9	1.9	522.0	+/-	13.0	Briden 1968
68	Sediments and Volcanics	Base	46.90	42.30	64	181.6	6.8	530.0	+/-	18.0	Daly <i>et al.</i> 1977
69	Abu Durba Sandstones	Base	18.00	341.20	16	43.6	38.8	531.5	+/-	13.5	Abdeldayem <i>et al.</i> 1994
70	Volcanics and sediments	Low	46.90	42.20	64	182.0	6.8	532.0	+/-	18.0	Daly & Pozzi 1977
Ant ~Antarctica											
1	Mt. Keinath Monzogranite	Base	31.00	209.00	7	17.0	14.1	450.0	+/-	4.0	Lanza & Tonarini 1998
2	Vanda lamprophyre and porphyry	Mid	2.50	203.80	58		5.2	471.5	+/-	8.5	Funaki 1984
3	Teall Nunatak	Mid	11.00	201.00	58	163.0	7.2	479.0	+/-	4.0	Lanza & Tonarini 1998
4	Lake Vanda Feldspar Porphyry Dykes	Mid	3.90	207.20	38	51.0	8.5	484.0	+/-	7.0	Grunow 1995
5	Lamprophyre Dykes	Base	9.30	206.70	16		10.9	484.0	+/-	7.0	Manzoni & Nanni 1977
6	Sor Rondane Intrusives	Base	28.50	189.50	16		4.5	489.0	+/-	7.0	Zijderveld 1968
7	Granite Harbour Pink Granite	Low	3.40	196.70	21	16.0	8.3	498.0	+/-	4.0	Grunow 1995
8	Granite Harbour Mafic Dykes	Mid	-0.80	195.00	27	80.0	8.6	498.0	+/-	3.0	Grunow 1995
9	Granite Harbour Grey Granite	Mid	3.60	201.60	34	146.0	6.4	498.0	+/-	3.0	Grunow 1995
10	Killer Ridge/Mt Loke Diorites	Mid	7.00	201.40	40	32.0	12.0	499.0	+/-	3.0	Grunow & Encarnacion 2000
11	Lake Vanda Bonny Pluton	Mid	8.30	207.90	28	50.0	13.1	499.0	+/-	3.0	Grunow 1995
12	Granitic rocks, Wright Valley	Base	5.40	198.50	16		8.1	500.0	+/-	43.0	Funaki 1984
13	Briggs Hill Bonny Pluton	Base	-2.70	221.40	8	16.0	14.5	505.0	+/-	2.0	Grunow 1995
14	Charnockites, Mirnyy Station	Low	1.50	28.50	37	24.3	15.6	520.0	+/-	24.0	McQueen <i>et al.</i> 1972
15	Zanuck Granite	Mid	-7.30	36.20	54	23.7	10.8	521.0	+/-	2.0	Grunow & Encarnacion 2000
16	Wyatt and Akerman Formations	High	1.30	39.80	69	34.7	7.9	525.0	+/-	3.0	Grunow & Encarnacion 2000
Asia ~India											
1	Pachmarhi Beds	Low	10.10	310.10	31	32.8	4.6	206.5	+/-	28.5	Wensink 1968
2	Jomosom Quartzite	Mid	22.00	298.50	32	11.0	8.0	209.0	+/-	1.0	Klootwijk & Bingham 1980
3	Parsora Formation	High	21.00	312.50	30	121.6	8.4	209.0	+/-	1.0	Agarwal 1980
4	Parsora Sandstone	Mid	30.00	305.00	49	200.0	5.7	221.5	+/-	13.5	Bhalla & Verma 1969
5	Wardha Valley (Kamthi?) Sediments	Mid	-21.00	309.60	57	62.8	2.4	221.5	+/-	13.5	Wensink 1968
6	Tiki Formation	Mid	20.00	323.60	30	28.9	7.8	226.5	+/-	8.5	Agarwal 1980
7	Limestones, Kashmir	Low	-20.20	305.10	96	104.3	9.0	226.5	+/-	18.5	Klootwijk <i>et al.</i> 1983
8	Thinigoan Limestone	Mid	26.10	296.80	57	503.1	11.2	231.5	+/-	8.5	Klootwijk & Bingham 1980

Annexe I: Palaeomagnetic database and level of selection (continued)

9	Mukut Limestone	High	22.40	286.70	40	30.2	4.2	232.0	+/-	3.0	Appel <i>et al.</i> 1991
	Godavary Valley (Kamthi?)										
10	Sediments	Low	18.00	307.00	52	85.0	2.0	232.0	+/-	24.0	Verma & Bhalla 1968
11	Mangli Beds	Base	-7.30	304.30	23	43.3	4.6	243.0	+/-	2.0	Wensink 1968
12	Panchet clays	Base	7.50	120.50	13	49.0	6.0	248.5	+/-	7.5	Klootwijk 1974
13	Krol-A Limestone	Base	-3.50	289.50	14	8.0	15.0	249.0	+/-	41.0	Klootwijk <i>et al.</i> 1982
	Wargal and Chhidru										
14	Formations	High	-2.20	305.80	113	10.7	4.3	250.5	+/-	5.5	Haag & Heller 1991
15	Kamthi(?) Beds	Base	-4.10	282.80	17	411.1	1.8	250.5	+/-	5.5	Wensink 1968
16	Chhidru Formation	Base	24.00	280.50	7	10.0	20.0	250.5	+/-	5.5	Klootwijk <i>et al.</i> 1986
17	Zewan Beds	Mid	-28.10	309.90	83	69.3	14.9	250.5	+/-	5.5	Klootwijk <i>et al.</i> 1983
	Kamthi Redbeds, Wardha										
18	Valley	Mid	4.00	129.00	105	24.0	6.5	250.5	+/-	5.5	Klootwijk 1975
19	Bhimtal(Bhowali) volcanics	Base	10.00	138.00	13	25.4	25.0	267.5	+/-	22.5	Athavale <i>et al.</i> 1980
20	Thini Chu Formation	Low	-6.50	305.00	41	10.0	7.5	267.5	+/-	22.5	Klootwijk & Bingham 1980
21	Speckled Sandstones	Low	13.00	137.50	86	50.0	7.3	273.0	+/-	17.0	Wensink 1975
22	Alozai Formation	Base	-18.10	291.00	36	6.1	12.1	289.5	+/-	33.5	Klootwijk <i>et al.</i> 1981
23	Blaini Limestone	Base	-26.50	291.00	62	7.0	7.5	289.5	+/-	33.5	Klootwijk <i>et al.</i> 1982
24	Lower Blaini Diamictite	Base	2.50	261.50	23	7.0	12.0	289.5	+/-	33.5	Klootwijk <i>et al.</i> 1982
25	Talchir Series	Base	31.50	134.30	23	109.4	2.9	306.5	+/-	16.5	Wensink & Klootwijk 1968
26	Syringotheris Limestone	Base	28.50	238.00	18	8.0	13.0	358.5	+/-	4.5	Klootwijk <i>et al.</i> 1983
27	Rudraprayag volcanics	Low	30.00	168.00	28	26.4	15.2	403.0	+/-	40.0	Athavale <i>et al.</i> 1980
28	Marhaum Formation	Base	-11.50	200.00	18	12.5	10.0	437.5	+/-	20.5	Klootwijk <i>et al.</i> 1983
29	Trahagaum Formation	Low	-79.00	173.00	53	22.5	4.0	476.5	+/-	18.5	Klootwijk <i>et al.</i> 1983
30	Salt Pseudomorph Beds	Base	26.60	213.50	43	129.0	5.9	511.5	+/-	6.5	Wensink 1972
31	Jutana Formation	Base	20.50	231.00	21	9.0	11.0	520.5	+/-	4.5	Klootwijk <i>et al.</i> 1986
32	Khewra Sandstone	Base	36.00	223.50	9	40.5	8.0	531.5	+/-	13.5	Klootwijk <i>et al.</i> 1986
33	Purple Sandstone	Base	28.00	212.00	11	15.0	12.0	535.0	+/-	10.0	McElhinny 1970
Au	~Australia										
1	Kiama Dykes	Mid	55.00	350.60	24	102.0	7.6	200.0	+/-	10.0	Schmidt 1990
2	Brown Clays	Base	32.30	349.90	6	26.3		221.5	+/-	13.5	Schmidt <i>et al.</i> 1976
3	Knapp Head Dyke	Base	39.40	339.10	7	145.7	5.0	226.5	+/-	18.5	Harris & Li 1995
4	Milton Monzonite	Mid	15.80	351.80	69	77.0	5.0	237.5	+/-	7.5	Dunlop <i>et al.</i> 1997
5	Narrabeen Chocolate Shales	Base	49.00	340.00	32	100.0	7.0	243.0	+/-	2.0	Irving 1963
	Munmorah Conglomerate,										Embleton &
6	Patonga Claystone	High	30.40	326.90	94	230.8	3.9	243.0	+/-	2.0	McDonnell 1980
	Illawarra Coal Measures and										
7	Narrabeen Group	Base	36.00	327.60	7	31.6	16.6	248.5	+/-	7.5	Facer 1981
8	Gerringong Volcanics	Mid	44.00	312.00	43	26.0	6.0	253.0	+/-	4.0	Irving & Parry 1963
	Mount Leyshon Intrusive										
9	Complex	High	43.20	317.30	70	53.5	3.4	286.0	+/-	6.0	Clark 1996
10	Tuckers Igneous Complex	Mid	47.50	323.00	85	40.9	3.6	287.5	+/-	3.5	Clark 1996
11	Long Point Dyke	Base	21.50	284.20	5	38.9	12.4	289.5	+/-	33.5	Harris & Li 1995
12	Stirling Range Drive Dyke	Base	49.40	254.00	4	14.4	25.0	289.5	+/-	33.5	Harris & Li 1995
13	Featherbed Volcanics	Mid	43.00	311.70	166	170.6	5.1	292.5	+/-	12.5	Klootwijk <i>et al.</i> 1993
14	Bulgonunna Volcanics	Mid	40.40	315.50	27	21.0	9.6	299.0	+/-	6.0	Lackie <i>et al.</i> 1992
15	Newcastle Range Volcanics	Low	65.70	307.10	59	109.8	4.6	306.5	+/-	23.5	Anderson 2000
16	Yetholme Adamellite	Base	84.00	141.00	34	62.7	9.7	318.0	+/-	17.0	Facer 1976
17	Bathurst Batholith	Mid	45.30	251.90	198		7.6	325.5	+/-	6.5	Wahyono 1992
18	Percy Creek Volcanics	Base	23.30	317.20	5	19.7	18.2	331.0	+/-	14.0	Chamalaun 1968
	Star of Hope Formation										
19	Volcanics	Base	66.90	127.50	6	14.3	18.4	343.0	+/-	20.0	Klootwijk <i>et al.</i> 1993
20	Mount Eclipse Sandstone	High	37.60	232.60	69	32.2	8.6	344.5	+/-	5.5	Chen <i>et al.</i> 1994
21	Silver Hills Volcanics	Base	63.10	203.80	11	76.2	5.3	360.0	+/-	17.0	Klootwijk <i>et al.</i> 1993
22	Brewer Conglomerate	High	47.10	221.00	33	86.7	6.0	365.0	+/-	2.0	Chen <i>et al.</i> 1993
23	Worange Point Formation	High	67.90	208.60	63	15.9	10.7	365.0	+/-	2.0	Thrupp <i>et al.</i> 1991
24	Hervey Group	Mid	54.40	204.10	56	13.8	15.5	365.0	+/-	2.0	Li <i>et al.</i> 1988
25	Canning Basin Reef Complex	High	62.00	203.20	52	11.0	15.2	368.5	+/-	4.5	Chen <i>et al.</i> 1995

Annexe I: Palaeomagnetic database and level of selection (continued)

26	Catombal Group	Base	49.00	132.00	66	33.0	10.0	370.0	+/-	7.0	Williamson & Robertson 1976
27	Lochiel Formation	Base	28.00	92.00	25	18.1	18.5	370.0	+/-	7.0	Embleton & Shepherd 1977
28	Reef Complex, Canning Basin	Mid	49.10	218.00	89	61.6	7.8	370.0	+/-	7.0	Hurley & Van der Voo 1987
29	Mulga Downs Group	Base	54.00	276.00	12	17.7	8.0	374.0	+/-	7.0	Embleton 1977
30	Hermannsburg Sandstone	Base	61.00	180.90	24	35.6	21.0	374.0	+/-	7.0	Li <i>et al.</i> 1991
31	Comerong Volcanics	High	76.90	150.70	52	38.8	7.4	374.5	+/-	4.5	Schmidt <i>et al.</i> 1986
32	Parke Siltstone	Base	60.90	138.10	9	12.9	14.9	384.0	+/-	7.0	Li <i>et al.</i> 1991
33	Wellington-Cowra Area Sediments and Intrusions	Base	42.20	71.80	42	10.0	30.6	397.0	+/-	20.0	Goleby 1980
34	Mount Leyshon Devonian Dykes	Low	78.00	18.80	25	46.1	7.6	398.5	+/-	16.5	Clark 1996
35	Snowy River Volcanics	High	74.30	42.70	47	25.6	9.7	404.0	+/-	13.0	Schmidt <i>et al.</i> 1987
36	Bowling Group Volcanics	Base	64.00	225.00	25	36.8	10.0	414.5	+/-	2.5	Luck 1973
37	Mugga Mugga Porphyry	Base	63.20	187.90	17	29.0	7.0	422.0	+/-	1.0	Briden 1966
38	Cowra Trough-Molong High Sediments	High	44.50	174.00	154	29.3	17.3	422.5	+/-	5.5	Goleby 1980
39	Laidlaw and Douro Volcanics	Base	54.00	91.00	35	18.4	10.0	423.5	+/-	4.5	Luck 1973
40	Ainslie Volcanics	Base	71.00	173.00	24	33.4	11.0	424.5	+/-	1.5	Luck 1973
41	Mereenie Sandstone	Base	15.70	62.70	51	7.8	25.6	424.5	+/-	33.5	Li <i>et al.</i> 1991
42	Mt Leyshon Silurian Dykes	Base	-21.70	231.90	14	39.1	8.3	425.0	+/-	3.0	Clark 1996
43	Ravenswood Batholith and Aureole	High	-17.50	232.70	51	20.0	7.1	425.0	+/-	3.0	Clark 1996
44	Cowra Trough-Molong High Sediments	High	40.00	211.70	74	45.7	13.7	433.0	+/-	10.0	Goleby 1980
45	Molong High Formations	Base	9.60	23.90	161	402.1	6.2	456.5	+/-	13.5	Goleby 1980
46	Stairway Sandstone	Base	2.00	230.50	10	24.7	10.0	462.5	+/-	4.5	Embleton 1972
47	Tumblagooda Sandstone	Low	-26.70	33.70	34	555.6	3.0	469.0	+/-	26.0	Schmidt & Embleton 1990
48	Walli and Mt Pleasant Andesites	Mid	12.20	183.30	30	551.4	10.7	482.5	+/-	12.5	Goleby 1980
49	Jinduckin Formation	Base	13.00	205.00	20	7.7	13.0	482.5	+/-	12.5	Luck 1972
50	Chatswood Limestone and Ninmaroo Formation	Base	-3.10	234.10	64	6.7	7.4	492.5	+/-	7.5	Ripperdan & Kirschvink 1992
51	Black Hill Norite	Base	37.50	214.40	22	67.5	3.8	494.0	+/-	7.0	Schmidt <i>et al.</i> 1993
52	Upper Lake Frome Group	Base	16.00	205.00	20	5.4		500.0	+/-	5.0	Embleton & Giddings 1974
53	NW Tasmanian Sediments	High	19.40	208.90	71	20.2	10.4	502.5	+/-	2.5	Li <i>et al.</i> 1997
54	Basal Lake Frome Group	Mid	31.40	206.90	80	16.6	10.1	509.5	+/-	4.5	Klootwijk 1980
55	Upper Shannon Formation, Ross River	Base	14.90	34.90	9	28.0	10.6	511.5	+/-	6.5	Klootwijk 1980
56	Giles Creek dolomite, Ross River	Mid	38.30	204.50	33	38.5	10.4	511.5	+/-	6.5	Klootwijk 1980
57	Aroona Dam sediments	Base	36.00	213.00	11	7.0		515.0	+/-	10.0	Embleton & Giddings 1974
58	Billy Creek Formation, Aroona Creek and Wirrealpa Limestone	Mid	37.40	200.10	78	11.0	14.4	518.5	+/-	6.5	Klootwijk 1980
59	Hudson Formation	Base	18.00	19.00	17	7.0	14.0	520.0	+/-	15.0	Luck 1972
60	Hugh River Shales	Base	11.00	37.00	7	43.5	9.0	520.0	+/-	15.0	Embleton 1972
61	Lower Cambrian sediments, Kangaroo Island	Base	33.80	195.10	77	9.4	12.3	521.5	+/-	3.5	Klootwijk 1980
62	Pertaoorta Group, Areyonga Gorge	Low	32.70	191.50	136	84.5	7.3	525.0	+/-	20.0	Klootwijk 1980
63	Todd River Dolomite	High	43.20	159.90	34	14.7	6.7	531.5	+/-	13.5	Kirschvink 1978
64	Hawker Group	Mid	21.30	194.90	89	12.3	11.4	537.5	+/-	7.5	Klootwijk 1980
IndO ~Madagascar											
1	Isalo Group	Low	74.00	277.10	32	89.4	5.9	206.5	+/-	28.5	Embleton & McElhinny 1975
2	Sakamena Group, Overall Result	Base	65.80	291.60	31			248.5	+/-	7.5	McElhinny <i>et al.</i> 1976
3	Lower Sakamena Group	Mid	86.80	268.70	27	31.3	12.2	250.5	+/-	5.5	Rakotosolofa <i>et al.</i> 1999
4	Sakoa Group, Overall Result	Low	52.80	260.70	33			290.0	+/-	20.0	McElhinny <i>et al.</i> 1976

Annexe I: Palaeomagnetic database and level of selection (conitnued)

5	Sakoa Group	Base	68.70	210.80	31	33.6	13.4	290.0	+/-	20.0	Rakotosolofo <i>et al.</i> 1999
6	Carion Granite	Low	6.80	181.00	100	31.0	9.0	507.5	+/-	29.5	Meert <i>et al.</i> 2001
MidE ~Arabia											
1	Saharonim Formation	Base	48.60	179.70		2.4		226.5	+/-	18.5	Freund & Tarling 1979
	SHD1 Permo-Triassic										
2	Borehole	Base	53.20	250.20	16	6.4	15.9	244.5	+/-	3.5	Torcq <i>et al.</i> 1997
3	Um Bogma Formation	Mid	-22.00	97.00	76	30.1	7.5	341.5	+/-	8.5	ElAgami <i>et al.</i> 2000
4	Red Sandstones	Base	36.70	323.40	20		7.5	487.5	+/-	17.5	Burek 1969
	Hornblende diorite porphyry										
5	stock	Base	25.80	332.20	12	14.5	11.8	525.0	+/-	20.0	Kellogg & Beckmann 1983
6	Dykes	Base	26.00	161.00	12	26.3	8.6	535.0	+/-	10.0	Sallomy & Krs 1980
SAm ~South America											
1	Motuca Formation	Base	81.00	116.00	7	51.6	35.5	226.5	+/-	18.5	Creer 1970
2	Dolerite Dykes	Mid	82.00	140.00	90	25.0	10.0	232.0	+/-	5.0	Veldkamp <i>et al.</i> 1971
	Corumbatai Formation, Passa										
3	Dois Group	Base	86.00	114.00	17	8.4	13.1	245.5	+/-	10.5	Valencio <i>et al.</i> 1975
4	Guyana Dykes	Base	63.80	28.90	33	20.6	13.6	248.5	+/-	7.5	Hargraves 1978
5	Sierra de la Ventana Redbeds	Base	78.00	39.00	9		14.0	250.5	+/-	5.5	Creer <i>et al.</i> 1970
6	Iratí Formation	Base	82.70	234.70	14	225.0	14.5	250.5	+/-	5.5	Pascholati <i>et al.</i> 1976
7	Choiqúe Mahuida Formation	Base	75.00	164.00	25	30.3	10.2	260.0	+/-	10.0	Conti & Rapalini 1990
8	Tunas Formation	Low	74.10	205.90	254	38.7	4.8	270.0	+/-	20.0	Tomezzoli 2001
9	Tunas Formation	High	63.00	193.90	197	47.3	4.8	275.0	+/-	15.0	Tomezzoli & Vilas 1999
	Itararé Subgroup, Tubarao										
10	Group	Base	57.00	177.00	12		11.2	306.5	+/-	16.5	Valencio <i>et al.</i> 1975
11	Piauí Formation	Base	50.00	165.00	15		16.0	311.5	+/-	11.5	Creer 1970
12	Picos and Passagem Series	Base	30.00	133.00	12		32.0	397.0	+/-	20.0	Creer 1970
	Herrada Member, Sierra										
13	Grande Formation	Base	42.00	103.50	10	23.0	10.3	407.0	+/-	16.0	Rapalini & Vilas 1991
	Rosales Horizon, Sierra										
14	Grande Formation	Base	-3.40	58.00	14	11.9	12.0	425.5	+/-	2.5	Rapalini & Vilas 1991
15	Urucum Formation	Base	34.00	344.00	23		9.0	430.0	+/-	13.0	Creer 1965
16	Urucum Formation	Base	17.40	346.80	10	22.6	10.5	456.0	+/-	39.0	Creer 1972
	Sierra de las Animas Complex,										
17	upper part	Base	5.90	338.10	33	12.0	18.1	510.0	+/-	10.0	Sanchez-Bettucci & Rapalini 2002
	Acampamento Velho										
18	Formation	Base	61.00	158.00	8		17.0	520.0	+/-	10.0	D'Agrella-Filho & Pacca 1988
	Acampamento Velho										
19	Formation	Base	44.00	345.00	7		42.0	520.0	+/-	10.0	D'Agrella-Filho & Pacca 1988

200-543 Ma palaeomagnetic data listed in **black** for cratonic data, and in **grey** for data coming from “suspect” regions.

Levels of selection are defined in Chapter 2, §.2.5.1. **Plat/PLong** are pole latitude/longitude in their location coordinates; **N** is the number of samples; **κ** , the precision parameter; **α_{95}** , the cone at the 95% confidence level associated to the pole; **Age \pm s** is the age average and its corresponding uncertainty calculated from the age window of magnetisation (High Mag Age/Low Mag Age) provided in the palaeomagnetic database [I.A.G.A. palaeomagnetic database, McElhinny & Lock (1996); Version 4-4]. When this window refers to a geological period, absolute ages are based on the geological time scale presented in Chapter 1, §1.1.2 (figure 1.3).

Annexe II: Palaeomagnetic data between 175 and 560 Ma coming from the Delamerian or Lachlan Orogen

N°	Mnemo	ROCKNAME	Level	PLAT	PLONG	N	κ	α ₉₅	Age average	+/-	ε	Authors	Year
1	GmS	Gibraltar Microsyenite	Base	54,20	337,70	13	25,30	25,10	178,0	+/-	5,0	Thomas <i>et al.</i>	2000
2	SBD	Sydney Basin Dykes	High	52,30	358,30	29	999,90	2,70	180,0	+/-	10,0	Robertson	1979
3	GI	Glenrowan Intrusives	Base	45,20	20,00	4	?	?	181,0	+/-	5,0	Schmidt	1976
4	WVBB	Western Victoria Basalt Belt	Base	47,00	358,00	36	37,60	11,10	194,0	+/-	5,0	Schmidt	1976
5	GVME	Garrawilla Volcanics and Moonbi Extrusives	Base	46,10	355,20	36	52,00	?	197,0	+/-	10,0	Schmidt	1976
6	KD	Kiama Dykes	Mid	55,00	350,60	24	102,00	7,60	200,0	+/-	10,0	Schmidt	1990
7	SBC	Brown Clays	Base	32,30	349,90	6	26,30	?	221,5	+/-	13,5	Schmidt <i>et al.</i>	1976
8	MM	Milton Monzonite	Mid	15,80	351,80	69	77,00	5,00	237,5	+/-	7,5	Dunlop <i>et al.</i>	1997
9	NCS	Narrabeen Chocolate Shales	Base	49,00	340,00	32	100,00	7,00	243,0	+/-	2,0	Irving	1963
10	MCPC	Munmorah Conglomerate, Patonga Claystone	High	30,40	326,90	94	230,80	3,90	243,0	+/-	2,0	Embleton & McDonnell	1980
11	ICM	Illawarra Coal Measures and Narrabeen Group	Base	36,00	327,60	7	31,60	16,60	248,5	+/-	7,5	Facer	1981
12	GgV	Gerrigong Volcanics	Mid	44,00	312,00	43	26,00	6,00	253,0	+/-	4,0	Irving & Parry	1963
13	YA	Yetholme Adamellite	Base	84,00	141,00	34	62,70	9,70	318,0	+/-	17,0	Facer	1976
14	BB	Bathurst Batholith	Mid	45,30	251,90	198	?	7,60	325,5	+/-	6,5	Wahyono	1992
15	WPF	Worrange Point Formation	High	67,90	208,60	63	15,90	10,70	365,0	+/-	2,0	Thrupp <i>et al.</i>	1991
16	HG	Hervey Group	Mid	54,40	204,10	56	13,80	15,50	365,0	+/-	2,0	Li <i>et al.</i>	1988
17	CG	Catombal Group	Base	49,00	132,00	66	33,00	10,00	370,0	+/-	7,0	Williamson & Robertson	1976
18	LF	Lochiel Formation	Base	28,00	92,00	25	18,10	18,50	370,0	+/-	7,0	Embleton & Shepherd	1977
19	MDG	Mulga Downs Group	Base	54,00	276,00	12	17,70	8,00	374,0	+/-	7,0	Embleton	1977
20	CV	Comerong Volcanics	High	76,90	150,70	52	38,80	7,40	374,5	+/-	4,5	Schmidt <i>et al.</i>	1986
21	WCSI	Wellington-Cowra Area Sediments and Intrusions	Base	42,20	71,80	42	10,00	30,60	397,0	+/-	20,0	Goleby	1980
22	SRV	Snowy River Volcanics	High	74,30	42,70	47	25,60	9,70	404,0	+/-	13,0	Schmidt <i>et al.</i>	1987
23	BGV	Bowling Group Volcanics	Base	64,00	225,00	25	36,80	10,00	414,5	+/-	2,5	Luck	1973
24	MMP	Mugga Mugga Porphyry	Base	63,20	187,90	17	29,00	7,00	422,0	+/-	1,0	Briden	1966
25	CMS2	Cowra Trough-Molong High Sediments	Base	44,50	174,00	154	29,30	17,30	422,5	+/-	5,5	Goleby	1980
26	LDV	Laidlaw and Douro Volcanics	Base	54,00	91,00	35	18,40	10,00	423,5	+/-	4,5	Luck	1973
27	AV	Ainslie Volcanics	Base	71,00	173,00	24	33,40	11,00	424,5	+/-	1,5	Luck	1973
28	CMS1	Cowra Trough-Molong High Sediments	High	40,00	211,70	74	45,70	13,70	433,0	+/-	10,0	Goleby	1980
29	MhF	Molong High Formations	High	9,60	23,90	161	402,10	6,20	456,5	+/-	13,5	Goleby	1980
30	WMtPA	Walli and Mt Pleasant Andesites	Mid	12,20	183,30	30	551,40	10,70	482,5	+/-	12,5	Goleby	1980
31	BHN	Black Hill Norite	Base	37,50	214,40	22	67,50	3,80	494,0	+/-	7,0	Schmidt <i>et al.</i>	1993
32	ULFG	Upper Lake Frome Group	Base	16,00	205,00	20	5,40	?	500,0	+/-	5,0	Embleton & Giddings	1974
33	NWTas	NW Tasmanian Sediments	High	19,40	208,90	71	20,20	10,40	502,5	+/-	2,5	Li <i>et al.</i>	1997
34	BLFG	Basal Lake Frome Group	Mid	31,40	206,90	80	16,60	10,10	509,5	+/-	4,5	Klootwijk	1980

Annexe II: Palaeomagnetic data from the Delamerian or Lachlan Orogen (continued)

35	ADS	Aroona Dam sediments Billy Creek Formation, Aroona Creek and	Base	36,00	213,00	11	7,00	?	515,0	+/-	10,0	Embleton & Giddings	1974
36	BCF	Wirrealpa Limestone Lower Cambrian sediments, Kangaroo Island	Mid	37,40	200,10	78	11,00	14,40	518,5	+/-	6,5	Klootwijk	1980
37	KI		Base	33,80	195,10	77	9,40	12,30	521,5	+/-	3,5	Klootwijk	1980
38	HkG	Hawker Group	Mid	21,30	194,90	89	12,30	11,40	537,5	+/-	7,5	Klootwijk	1980
39	PQ	Pound Quartzite	Base	60,00	186,00	10	4,70	?	550,0	+/-	5,0	Embleton & Giddings	1974

175 – 560 Ma palaeomagnetic data coming from the southern Tasmanides (except from the New England Orogen) and plotted in figure 4.7 (Chapter 4; §.4.4). Mnemonics (**Mnemo**) are the same as in figure 4.7.

Levels of selection are defined in Chapter 2, §.2.5.1. **Plat/PLong** are pole latitude/longitude in their location coordinates; **N** is the number of samples; **κ** , the precision parameter; **α_{95}** , the cone at the 95% confidence level associated to the pole; **Age $\pm\epsilon$** is the age average and its corresponding uncertainty calculated from the age window of magnetisation (High Mag Age/Low Mag Age) provided in the palaeomagnetic database [I.A.G.A. palaeomagnetic database, McElhinny & Lock (1996); Version 4-4]. When this window refers to a geological period, absolute ages are based on the geological time scale presented in Chapter 1, §1.1.2 (figure 1.3).

* The NW Tasmanian sediments [NW Tas] are not pointed in figure 4.7.

Lebenslauf

Name: Christian V  rard
Geburtsdatum: 07 Juni 1974
Geburtsort: Annecy, Frankreich
Familienstand: Ledig
Staatsangeh  rigkeit: Franz  sisch

Schulbildung

1980-1985 Grundschule in Epagny, Frankreich
1985-1989 „Coll  ge“ in Meythet, Frankreich
1989 Abschlu   „Brevet des Coll  ges“
1989-1993 Gymnasium „Lyc  e Gabriel Faur  “ in Annecy, Frankreich
1993 Abschlu   „Baccalaur  at C“ (Abitur)

Universit  re Ausbildung

1993-1996 Studium der Geologie und Biologie an der Universit   de Savoie in Chamb  ry, Frankreich
1996 Abschlu   „Dipl  me d’  tude Universitaire G  n  ral (DEUG) B“ (mit Auszeichnung)
1996-1997 Studium der Geologie an der Universit   Joseph Fourier in Grenoble, Frankreich
1997 Abschlu   „Licence“ (mit Auszeichnung)
1997-1998 Studium der Geologie an der Universit   Joseph Fourier in Grenoble, Frankreich
1998 Abschlu   „Ma  trise“ (mit Auszeichnung)
Titel der Abschlu  sarbeit: *„Die magnetische Struktur der Longobucco-Bocchigliero Deckenbau (Italien): Untersuchung der strukturelle Inversion vom Rand der Tethys in Kalabrien“*; Betreuer Dr. Jean-Pierre Bouillin (CR1, CNRS)
1998-1999 Studium der Geologie an der Universit   Joseph Fourier in Grenoble, Frankreich
1999 Abschlu   „Dipl  me d’  tude Approfondie (DEA)“ (mit Auszeichnung)
Titel der Abschlu  sarbeit: *„Numerische Modellierung glazialer Erosion“*; Betreuer Dr. Peter Van der Beek (MC, UJF Grenoble 1)
1999 „Test of English as a Foreign Language“ (TOEFL)
2000-heute wissenschaftlicher Angestellter an der Ludwig-Maximilians-Universit  t M  nchen (LMU), Department f  r Geo- und Umweltwissenschaften, Sektion Geophysik, im Rahmen des Projektes „Gondwana“ gef  rdert von der VW-Stiftung
Titel der Doktorarbeit: *„Pal  omagnetismus des Pal  ozoikums von s  d  stlichem Australien: Implikationen f  r die Scheinbare Polwanderungskurve von Gondwana“*; Betreuer Dr. Jennifer Tait (LMU M  nchen).